

# **Dissertation**

submitted to the  
Combined Faculty of Natural Sciences and Mathematics  
of the  
Ruperto Carola University Heidelberg, Germany  
for the degree of  
Doctor of Natural Sciences

Presented by  
**Marten Meyer, M.Sc.**  
born in El Paso, Texas, USA

Oral examination:  
13.07.2020



Development of the T-Plex Assay:  
A novel multiplex method to detect antigen-specific  
T cell responses *in vitro* using bead array-based artificial  
antigen-presenting cells

**Referees:**

PD Dr. Ralf Bischoff  
PD Dr. Frank Momburg

*Für Ansas, Hinnerk und Martin*

## Acknowledgements

This dissertation was accomplished with the contribution of many wonderful people in the period of October 2015 to May 2020 in the “Antigen Presentation and T/NK Cell Activation Group” headed by PD Dr. Frank Momburg within the Clinical Cooperation Unit “Applied Tumor Immunity” (Head of Department: Prof. Dr. Dirk Jäger) at the German Cancer Research Center (Deutsches Krebsforschungszentrum (DKFZ)), Heidelberg.

First and foremost, I like to thank Prof. Dr. Dirk Jäger for providing me with the opportunity and resources to work on this exciting PhD project. In the same breath, I would like to express my deepest gratitude to my excellent supervisors PD Dr. Frank Momburg (DKFZ) and Dr. Inka Zörnig (Department of Medical Oncology, National Center for Tumor Diseases (NCT)). Both have initiated this project to work on and have supported me constantly with stimulating ideas and guidance throughout this study. Moreover, I thank them both for their continuous trust in my work and abilities.

I am very thankful to PD Dr. Ralf Bischoff (Division of Functional Genome Analysis, DKFZ) for agreeing to be the 1<sup>st</sup> referee of this dissertation. Ralf Bischoff, Frank Momburg and Inka Zörnig have all contributed their valuable time and vital input during my thesis advisory committees (TAC) for which I am very grateful. I would also like to kindly thank Prof. Dr. Suat Özbek and Prof. Dr. Viktor Umansky for becoming members of the examination commission of this dissertation.

Furthermore, I am greatly indebted to Frank Momburg for our innumerable and invaluable scientific discussions and who enabled this study by vigorously designing all necessary protein expression constructs, as well as to Nadja Bulbuc, who carried out the majority of construct cloning procedures. Likewise, I would like to thank Dr. Katharina Billian-Frey and Philipp Fieger (former Hi-STEM lab members, Heidelberg) for introducing me to various protein production and purification systems. Furthermore, I am also greatly indebted to, Anna Lena Eck, Nina Böttcher and especially Susanne Knabe, who have supported me with dedication to produce and purify all recombinant proteins. Moreover, a very special thank you goes to Susanne Knabe for her constant support on a professional and personal level as well as for her help to achieve a stimulating working environment.

I am very thankful to the group of highly talented former students including Magdalena Rausch, Sarah Schott, Javad Assazardeh and Gordon Karolus, who accomplished their master thesis under PD Dr. Frank Momburg’s and my supervision and especially made my time as PhD student definitely more colorful. Further, I would like to thank my other lab members including Dr. Alexander Rölle and Márcia Gonçalves for stimulating scientific and personal discussions. Moreover, I would like to highly acknowledge Dr. Inka Zörnig, Dr. Zeynep Koşaloğlu, Dr. Zhiqin Huang and Iris Kaiser of the Department of Medical Oncology, NCT, for providing invaluable patient material as well as for their *in silico* predictions of putative cancer neoepitopes. Likewise, I would like to thank Claudia Ziegelmeier and Claudia Luckner-Minden (both NCT) for their additional construct cloning efforts. Further, I kindly thank Sabrina Purr and Giovanni Mastrogiulio (both DKFZ) as well as Prof. Dr. Frits Koning and Yvonne Kooy-Winkelaar (both Leiden University Medical Center) for providing exquisite T cell lines.

A very special thank you goes to Ann-Kathrin Mehnert for her unforgotten encouragement and love during my entire time as a PhD student. Finally, I would like to deeply thank my dear brother Anas Meyer and best friends Martin Ehlers and Hinnerk Rohwedder for their selfless and constant support during all periods of my life. Despite being far away, they have always offered the strongest personal support I could have wished for.



## Summary

Assessment of T cell responses towards disease-associated antigens is of key interest in order to develop and monitor immunotherapeutic interventions. Patient sample material, however, is usually highly limited, which hinders comprehensive screening of putative novel antigens by conventional methods such as the enzyme-linked immunospot (ELISPOT) or peptide major histocompatibility complex (pMHC) multimer staining. To overcome this issue, several alternative assays have recently been proposed that allow simultaneous measurement (i.e. multiplex) of a larger pool of T cell specificities within a single assay reaction. However, these technological approaches are currently not well suited for a broad and routine laboratory usage. Therefore, we have developed a novel sensitive method called T-Plex Assay for the multiplex detection of antigen-specific T cell responses using flow cytometry, which can be implemented easily into routine laboratory practice.

The elaborated T-Plex Assay concept is based on cell-sized, fluorescently color-coded magnetic polystyrene beads such as the Luminex xMAP MagPlex<sup>®</sup> microspheres, which we have conjugated to defined recombinant pMHC-I or pMHC-II molecules. This pMHC conjugation in turn converts the beads into barcoded, artificial antigen-presenting cells (aAPCs) with the capacity to drive antigen-specific T cell activation. In addition, on the same pMHC-coated bead surface we co-immobilized monoclonal antibodies specific for various T cell effector cytokines such as interferon- $\gamma$  that are released upon T cell activation. These assembled barcoded aAPCs with cytokine capture capacity serve ultimately as cell contact-dependent biosensors for cognate T cell populations. Executing the T-Plex Assay concept, we developed an easy-to-use and profoundly optimized T-Plex Assay protocol facilitating highly reproducible as well as simultaneous measurement of theoretically up to 80 antigen-specific T cell responses within a single reaction, while allowing for complete recovery of the viable T cell sample post analysis. As a proof of concept, we demonstrated the T-Plex Assay-based detection of various HLA-A\*02:01-restricted viral antigen-specific T cell populations within healthy donor peripheral blood-derived T cells. Here, the T-Plex Assay displayed a similar sensitivity compared to conventional standard assays such as the pMHC multimer staining. Moreover, we used the T-Plex Assay in a small pilot study of four cancer patients to validate the immunogenicity of several *in silico* predicted HLA-A\*02:01-restricted tumor neoantigens. Unfortunately, analysis of cancer patient-derived peripheral blood by the T-Plex Assay or corresponding pMHC multimer staining did not reveal any T cell population specifically responding to the tested putative neoantigens.

In an interlinked study aspect, we established a novel manufacturing strategy for efficient and easily parallelized small-scale production of correctly folded and ready-to-use soluble pMHC-I and pMHC-II molecules based on various mammalian cell transient gene expression systems. Here, we elaborated several expression constructs encoding for covalently assembled pMHC-I as well as pMHC-II Fc-fusion proteins. These pMHC-Fc proteins were successfully produced and notably bound in an antigen-specific manner to their cognate T cell populations.

Although the true potential of the T-Plex Assay remains to be further analyzed, we think that the T-Plex Assay including our soluble pMHC production strategy holds great promise for clinical applications aiming for the routine discovery and validation of novel disease-associated T cell antigens particularly in cases where cell material is limited.



## Zusammenfassung

Das Erfassen von T-Zell-Antworten, die gegen krankheitsassoziierte Antigene gerichtet sind, ist von größtem Interesse, um immuntherapeutische Behandlungen zu entwickeln und zu überwachen. Probenmaterial von Patienten ist jedoch häufig stark limitiert, was in der Regel ein umfassendes Screening von neuen potenziellen Antigenen erschwert, wenn konventionelle Methoden wie der ELISPOT (enzyme-linked immunospot) oder die Peptid-MHC-Multimer (pMHC-Multimer) Färbung angewendet werden. Um dieses Problem zu lösen, wurden bereits mehrere alternative Methoden vorgeschlagen, welche das simultane (d.h. multiplexierte) Messen von einer größeren Anzahl von T-Zell-Spezifitäten in einer einzelnen Testreaktion ermöglichen. Diese Ansätze sind jedoch derzeit für eine breite und routinemäßige Laboranwendung wenig geeignet. Aus diesem Grund haben wir eine neue multiplexfähige Methode namens T-Plex Assay für die Detektion von antigenspezifischen T-Zell-Antworten mittels Durchflusszytometrie entwickelt, welche leicht in die gängige Laborpraxis eingebettet werden kann.

Das erarbeitete T-Plex Assay-Konzept basiert auf etwa zellgroßen, fluoreszenz-kodierten, magnetischen Polystyrol-Mikrosphären („beads“), wie dem Luminex xMAP MagPlex® System. Auf der Mikrosphären-Oberfläche haben wir definierte rekombinante pMHC-I und -II Moleküle immobilisiert. Die Verknüpfung mit pMHC verwandelt die *beads* in artifizielle antigenpräsentierende Zellen (aAPC) mit der Fähigkeit, eine antigenspezifische T-Zell-Aktivierung auszulösen. Zusätzlich zu den pMHC-Molekülen haben wir auf den *beads* monoklonale Antikörper immobilisiert, die spezifisch für Zytokine sind, welche von aktivierten T-Zellen sezerniert werden – hierzu zählt insbesondere Interferon- $\gamma$ . Letztendlich dienen diese aAPCs, welche die Fähigkeit haben, Zytokine zu binden, als zellkontaktabhängige Biosensoren für antigenspezifische T-Zell-Populationen. Begleitend zum T-Plex-Assay-Konzept haben wir ein einfach zu verwendendes und gründlich optimiertes T-Plex-Assay-Ablaufprotokoll entwickelt, welches ein sehr gut reproduzierbares und simultanes Messen von theoretisch bis zu 80 antigenspezifischen T-Zell-Antworten innerhalb einer einzelnen Testreaktion ermöglicht und gleichzeitig erlaubt, die komplette, noch lebende T-Zell-Probe nach der Analyse zurück zu gewinnen, um sie weiter zu kultivieren. Als konzeptionellen Beweis haben wir die T-Plex Assay basierte Detektion von verschiedenen HLA-A\*02:01-restringierten virusantigen-spezifischen T-Zell-Populationen gezeigt, die sich innerhalb der Gesamtmenge von T-Zellen im peripheren Blut von mehreren gesunden Spendern befindet. Hier zeigte der T-Plex Assay eine Sensitivität, die sehr ähnlich zu konventionellen Methoden ist. Darüber hinaus haben wir den T-Plex Assay in einer Pilotstudie mit vier Krebspatienten eingesetzt, um die Immunogenität von mehreren, *in silico* vorhergesagten HLA-A\*02:01-restringierten Tumor-Neoantigenen zu validieren. Leider konnten wir in diesen Experimenten weder mit dem T-Plex-Assay noch mit einer entsprechende pMHC-Multimer-Färbung eine Neoantigen-spezifische T-Zell-Population für die getesteten Peptidantigene im peripheren Blut dieser Patienten detektieren.

In einem weiteren Studienaspekt haben wir zusätzlich ein neues Herstellungsverfahren für die effiziente und leicht parallelisierbare Produktion von korrekt gefalteten, löslichen pMHC-I und pMHC-II Molekülen im kleinen Maßstab etabliert, welches auf dem Einsatz von transienten Genexpressionssystemen in verschiedenen Säugerzellen beruht. Hierzu haben wir zahlreiche Expressionskonstrukte etabliert, welche für hochstabile, kovalent assemblierte pMHC-I-Fc und pMHC-II-Fc Fusionsproteine kodieren. Diese löslichen pMHC-I-Fc und pMHC-II-Fc Konstrukte wurden erfolgreich produziert und zeigten die erwartete spezifische Bindung an T-Zell-Populationen mit passender Antigen-spezifität. Auch wenn das wahre Potential des T-Plex Assays noch weiter evaluiert

## Zusammenfassung

werden muss, sind wir überzeugt, dass der T-Plex Assay zusammen mit unserem neuen Produktionsverfahren für rekombinante lösliche pMHC-Fc-Moleküle ein großer Gewinn für klinische Anwendungen sind, die zum Ziel haben, neue krankheitsassoziierte T-Zellantigene routinemäßig zu entdecken und zu validieren, insbesondere, wenn Zellmaterial nur begrenzt verfügbar ist.

# Table of contents

Acknowledgements .....	v
Summary .....	vii
Zusammenfassung.....	ix
Table of contents .....	xi
List of figures and tables.....	xvii
Abbreviations.....	xxi
<b>1  Introduction .....</b>	<b>- 1 -</b>
1.1 The adaptive immune system and its central dogmata in a nutshell .....	- 1 -
1.2 From antigen processing to T cell activation .....	- 3 -
1.2.1 Structural and genetic aspects of peptide-MHC class I and II complexes .....	- 3 -
1.2.2 Classical MHC class I and II antigen presentation pathways .....	- 5 -
<b>1.2.2.1 Classical MHC-I presentation pathway .....</b>	<b>- 6 -</b>
<b>1.2.2.2 Classical MHC-II presentation pathway .....</b>	<b>- 7 -</b>
1.2.3 Molecular clues required for T cell activation .....	- 8 -
<b>1.2.3.1 Structure of T cell receptor complex and early signaling events (signal 1) .....</b>	<b>- 8 -</b>
<b>1.2.3.2 Role of co-stimulatory and co-inhibitory receptors during T cell activation (signal 2) .....</b>	<b>- 10 -</b>
<b>1.2.3.3 The role of inflammatory cytokines during T cell activation (signal 3) .....</b>	<b>- 11 -</b>
<b>1.2.3.4 The immunological synapse – The interface between T cell and APC .....</b>	<b>- 12 -</b>
1.3 The interplay of heterogeneous subsets of T cells and APCs .....	- 14 -
1.3.1 Dendritic cells – Unique and highly specialized professional antigen-presenting cells.....	- 14 -
1.3.2 CD4 <sup>+</sup> T cells – Essential helpers and regulators of adaptive immune responses .....	- 15 -
1.3.3 CD8 <sup>+</sup> T cells – Highly trained and precise cell killers.....	- 18 -
<b>1.3.3.1 Dynamics of a CD8<sup>+</sup> T cell response and CD8<sup>+</sup> T cell memory differentiation .....</b>	<b>- 19 -</b>
<b>1.3.3.2 CD8<sup>+</sup> T cell exhaustion as a consequence of chronic viral infections or cancer .....</b>	<b>- 20 -</b>
1.4 Tumor-specific T cells – Central agents for cancer immunotherapy .....	- 21 -
1.4.1 From cancer immunosurveillance to cancer immunotherapy .....	- 21 -
1.4.2 Tumor antigens – Cornerstones for multiple cancer immunotherapy approaches .....	- 23 -
<b>1.4.2.1 Tumor-associated antigens .....</b>	<b>- 23 -</b>
<b>1.4.2.2 Tumor-specific antigens with a focus on mutated neoantigens.....</b>	<b>- 24 -</b>
1.5 Methods to detect antigen-specific T cells .....	- 27 -
1.5.1 Methods for analyzing the effector response of an antigen-specific T cell population .....	- 30 -
<b>1.5.1.1 Conventional cytokine expression-based assays for antigen-specific T cell detection.....</b>	<b>- 30 -</b>
<b>1.5.1.2 Analysis of activation marker expression by antigen-specific stimulated T cells .....</b>	<b>- 32 -</b>
<b>1.5.1.3 Lack of simple and sensitive assays for antigen-specific multiplex detection of T cell responses .....</b>	<b>- 32 -</b>
1.5.2 pMHC multimers – Tools for direct visualization of antigen-specific T cell populations.....	- 34 -
<b>1.5.2.1 Evolution of pMHC-I multimer design and production .....</b>	<b>- 35 -</b>
<b>1.5.2.2 Evolution of multiplex detection of antigen-specific T cells by pMHC-I multimers.....</b>	<b>- 37 -</b>
<b>1.5.2.3 Aspects of pMHC-II multimers regarding production, design and usage .....</b>	<b>- 38 -</b>
1.6 Expression of covalent assembled pMHC-I – The single-chain trimer concept.....	- 40 -
1.7 Artificial antigen-presenting cells – Flexible systems for cognate T cell activation.....	- 42 -
1.8 Aim of the study .....	- 43 -

<b>2  Material and methods.....</b>	<b>- 45 -</b>
2.1 Maintenance cell culture .....	- 45 -
2.1.1 T2 cell line culture .....	- 45 -
2.1.2 Mammalian cell lines for recombinant protein production .....	- 46 -
2.1.3 T cell line culture .....	- 47 -
<b>2.1.3.1 Survivin/HLA-A2-specific CD8<sup>+</sup> T cell line maintenance culture .....</b>	<b>- 48 -</b>
<b>2.1.3.2 Virus-specific CD8<sup>+</sup> T cell line maintenance culture .....</b>	<b>- 48 -</b>
<b>2.1.3.3 MTB/HLA-DR3-specific CD4<sup>+</sup> T cell line expansion and maintenance culture .....</b>	<b>- 48 -</b>
2.1.4 Culture and preparation of human peripheral blood mononuclear cells (PBMC) .....	- 48 -
2.2 Molecular biology related work.....	- 50 -
2.2.1 Cloning of various disulfide-trapped (dt) pMHC-I single-chain trimer (SCT) Fc-fusion constructs..	- 50 -
<b>2.2.1.1 Cloning of a heterodimeric pMHC-I-Fc construct with a single AviTag (pMHC-I-pCC-Fc).....</b>	<b>- 50 -</b>
<b>2.2.1.2 Cloning of homodimeric pMHC-I-Fc construct with an optionally cleavable Fc (pMHC-I-*Fc).....</b>	<b>- 51 -</b>
<b>2.2.1.3 Cloning of a Fc-free monomeric pMHC-I construct .....</b>	<b>- 51 -</b>
<b>2.2.1.4 Cloning of pMHC-I-Fc with HLA-I <math>\alpha</math>2-domain Q115E mutation and pMHC-I-CH1-Fc constructs.....</b>	<b>- 51 -</b>
2.2.2 Cloning of a heterodimeric monovalent pMHC-II-pCC-Fc construct .....	- 52 -
<b>2.2.2.1 Cloning of a pMHC-II-pCC-Fc construct as a two-vectors system .....</b>	<b>- 52 -</b>
<b>2.2.2.2 Cloning of a peptide-exchangeable (px) MHC-II-pCC-Fc construct .....</b>	<b>- 52 -</b>
<b>2.2.2.3 Cloning of a pMHC-II-pCC-Fc constructs as an one-vector system.....</b>	<b>- 53 -</b>
2.2.3 Cloning of a heterodimeric HLA-DM-pCC-Fc construct .....	- 53 -
2.2.4 Cloning of an ER-retained enzyme biotin ligase (BirA <sub>KDEL</sub> ).....	- 54 -
2.2.5 Recombinant DNA plasmid amplification and purification for subsequent protein productions...	- 54 -
2.3 Recombinant mammalian cell-based transient gene expression (TGE) systems .....	- 55 -
2.3.1 CHO-S/ProCHO-4/PEI system for protein production .....	- 55 -
<b>2.3.1.1 PEI-based transfection procedure for large-scale 100 mL CHO-S TGE batches .....</b>	<b>- 56 -</b>
<b>2.3.1.2 Procedure for small-scale protein-production using 2 mL CHO-S batches.....</b>	<b>- 56 -</b>
2.3.2 ExpiCHO TGE system for protein production .....	- 57 -
2.3.3 293-F TGE system for protein production .....	- 57 -
2.3.4 Expi293-F TGE system for protein production .....	- 58 -
2.3.5 <i>In vivo</i> biotinylation of AviTag-fusion proteins during mammalian cell-based TGE .....	- 59 -
2.4 Transient gene expression (TGE) validation and IgG titer quantification .....	- 59 -
2.4.1 Validation of protein expression by intracellular FACS staining.....	- 59 -
2.4.2 Mouse/human IgG titer quantification of cell supernatants by ELISA .....	- 60 -
2.5 Affinity chromatography-based protein purification.....	- 62 -
2.5.1 Strep-tag II / Strep-Tactin-based protein affinity chromatography .....	- 63 -
2.5.2 His-tag-based protein purification and Fc-cleavage of pMHC-I-*Fc molecules.....	- 64 -
<b>2.5.2.1 His-tag / Ni-NTA Sepharose-based batch affinity chromatography.....</b>	<b>- 64 -</b>
<b>2.5.2.2 His-tag / His Mag Sepharose Excel-based batch affinity chromatography .....</b>	<b>- 65 -</b>
<b>2.5.2.3 Thrombin-mediated enzymatic cleavage of pMHC-I-*Fc constructs .....</b>	<b>- 66 -</b>
2.5.3 Protein A resin-based affinity chromatography .....	- 67 -
2.5.4 SDS-PAGE analysis .....	- 67 -
2.6 pMHC multimer generation and quality control .....	- 68 -
2.6.1 Streptavidin-based multimerization of biotinylated soluble pMHC molecules .....	- 68 -
2.6.2 NativePAGE-based analysis of pMHC multimer formation .....	- 69 -

2.7	Flow cytometric analysis of T cell specificity, phenotype and activation .....	- 70 -
2.7.1	Surface staining for T cell lineage, activation, memory and exhaustion markers.....	- 71 -
2.7.2	Intracellular staining for cytokines (ICS) and CD107a degranulation assay .....	- 72 -
2.7.3	pMHC multimer and pMHC-Fc staining.....	- 74 -
2.7.3.1	<b>pMHC-I multimer and pMHC-I-Fc staining for the detection of antigen-specific CD8<sup>+</sup> T cells .....</b>	<b>- 75 -</b>
2.7.3.2	<b>pMHC-II tetramer staining for the detection of antigen-specific CD4<sup>+</sup> T cells.....</b>	<b>- 76 -</b>
2.8	Generation of virus antigen-specific HLA-A2-restricted CD8 <sup>+</sup> T cell lines.....	- 76 -
2.8.1	Peptide pulse-based antigen-specific expansion of CD8 <sup>+</sup> T cells.....	- 77 -
2.8.2	MACS-based isolation of antigen-specific CD8 <sup>+</sup> T cell populations .....	- 78 -
2.9	Conventional assays for measuring functional T cell responses.....	- 78 -
2.9.1	Assembly of various bead- and cell-based artificial antigen presenting cells (aAPCs) .....	- 78 -
2.9.1.1	<b>DynaBead Goat-anti-mouse IgG-based aAPC assembly .....</b>	<b>- 80 -</b>
2.9.1.2	<b>MACS<sup>®</sup> anti-mouse IgG microbead-based aAPC assembly.....</b>	<b>- 80 -</b>
2.9.1.3	<b>xMAP MagPlex microspheres (Luminex beads)-based aAPC assembly .....</b>	<b>- 80 -</b>
2.9.1.4	<b>Peptide pulse of T2 and T2.DR3.DM cells to generate cellular aAPCs .....</b>	<b>- 82 -</b>
2.9.2	Stimulation for 4 h or 18 h of T cell lines and PBMC using aAPCs or direct peptide pulse .....	- 82 -
2.9.3	Assessment of T cell-mediated antigen-specific killing by chromium-51 release assay .....	- 83 -
2.9.4	Measurement of antigen-specific T cell proliferation upon pMHC-based stimulation.....	- 83 -
2.9.4.1	<b>Plate immobilized pMHC-I-Fc-based induction of T cell proliferation .....</b>	<b>- 84 -</b>
2.9.4.2	<b>MACSiBead immobilized biotinylated pMHC-I-based induction of T cell proliferation.....</b>	<b>- 84 -</b>
2.9.4.3	<b>Read-out of antigen-specific T cell proliferation after a 6-day stimulation .....</b>	<b>- 85 -</b>
2.10	Exogenous peptide-exchange of biosynthetic peptide-loaded px-MHC-II-pCC-Fc.....	- 85 -
2.11	T-Plex Assay related workflows and protocols .....	- 88 -
2.11.1	Generation of T-Plex beads – Color-coded aAPCs with cytokine capture capacity.....	- 88 -
2.11.1.1	<b>Assembly of 1<sup>st</sup> generation T-Plex beads .....</b>	<b>- 89 -</b>
2.11.1.2	<b>Assembly of 2<sup>nd</sup> generation T-Plex beads and their optimization .....</b>	<b>- 89 -</b>
2.11.1.3	<b>Additional T-Plex beads assembly variations .....</b>	<b>- 90 -</b>
2.11.1.4	<b>Assembly of T-Plex<sup>2</sup> beads for the detection of multiple cytokines (pilot experiment) .....</b>	<b>- 90 -</b>
2.11.2	T-Plex Assay – Co-culture of T-Plex beads and T cells and subsequent bead read-out.....	- 90 -
2.11.2.1	<b>T-Plex Assay based on a 96-well magnet and 3D/wave shaking system.....</b>	<b>- 91 -</b>
2.11.2.2	<b>T-Plex Assay based on a “one-tube-reaction” using a tube rolling system .....</b>	<b>- 91 -</b>
2.11.2.3	<b>T-Plex bead anti-cytokine staining .....</b>	<b>- 92 -</b>
2.11.3	T cell isolation or CD14 <sup>+</sup> cells depletion from PBMC by MACS.....	- 93 -
2.11.3.1	<b>Analysis of phagocytosis of Luminex beads by CD14<sup>+</sup> monocytes and partial block by CD47 .....</b>	<b>- 94 -</b>
2.12	T-Plex Assay-based immunogenicity analysis of <i>in silico</i> predicted putative neoepitopes using cancer patient-derived peripheral blood .....	- 95 -
2.12.1	Patient material, mutation calling, <i>in silico</i> HLA typing and neoepitope prediction .....	- 95 -
2.12.2	Peptide vaccination and ELISpot follow-up analysis .....	- 95 -
2.12.3	T-Plex Assay- and pMHC-I multimer-based analysis of cancer patient-derived peripheral blood .....	- 95 -
2.12.3.1	<b>Production of putative neoepitope- or corresponding wt-peptide presenting pHLA-A2-*Fc .....</b>	<b>- 95 -</b>
2.12.3.2	<b>T-Plex Assay- and pMHC-I multimer-based analysis of patient-derived peripheral blood .....</b>	<b>- 96 -</b>
<b>3 </b>	<b>Results Part 1 – Production and validation of soluble pMHC-Fc proteins.....</b>	<b>- 97 -</b>
3.1	Establishment of pMHC-I-Fc mammalian-cell-based productions and validation.....	- 97 -
3.1.1	Successful production of pMHC-I-Fc proteins and antigen-specific binding to a T cell line.....	- 97 -
3.1.2	Validation of optimal CHO-S/ProCHO-4/PEI TGE parameters for small-scale productions .....	- 101 -
3.1.3	Cognate stimulation of Sur/A2-specific CD8 <sup>+</sup> T cells by bead-immobilized pHLA-A2-Fc (aAPCs)..	- 103 -

## Table of contents

3.2 Generation of multiple virus-specific T cell lines using pMHC-I-Fc-based magnetic enrichment.....	- 105 -
3.2.1 Detection and stimulation of PBMC-derived virus-specific CD8 <sup>+</sup> T cells using pMHC-I-Fc.....	- 105 -
3.2.2 Generation, validation and characterization of virus-specific HLA-A2-restricted CD8 <sup>+</sup> T cell lines derived from healthy donors.....	- 107 -
3.2.3 pHLA-A2-Fc-conjugated microbeads partially do not meet the T cell activation threshold .....	- 109 -
3.3 Production and validation of <i>in vivo</i> biotinylated heterodimeric pMHC-I-pCC-Fc .....	- 111 -
3.4 Production and validation of pMHC-I multimers based on <i>in vivo</i> biotinylated homodimeric dt-SCT fused to a cleavable Fc (*Fc).....	- 113 -
3.4.1 Equal staining performance of pMHC-I multimers formed by monomeric dt-SCT produced as homodimer fused to a cleavable Fc compared to commercial pMHC-I pentamers .....	- 113 -
3.4.2 Comparison of four HEK- and CHO-based TGE systems for the production of dt-pMHC-I-*Fc molecules .....	- 117 -
3.5 Usage of immobilized pMHC-I-Fc to drive antigen-specific T cell proliferation .....	- 119 -
3.6 Establishment of soluble pMHC-II-pCC-Fc production and their validation .....	- 121 -
3.6.1 Antigen-specific stimulation of bead-immobilized pHLA-DR3-pCC-Fc molecules .....	- 121 -
3.6.2 Antigen-specific binding of <i>in vivo</i> biotinylated pHLA-DR3-pCC-Fc-based multimers.....	- 122 -
3.6.3 Implementation of HLA-DM-mediated peptide-exchange of soluble px/HLA-DR3-pCC-Fc .....	- 124 -
<b>4  Results Part 2 – Development of the T-Plex Assay .....</b>	<b>- 129 -</b>
4.1 Pilot - Development of a novel multiplex assay to detect antigen-specific T cells .....	- 130 -
4.1.1 Linking T cell specificities to defined Luminex beads – The T-Plex Assay (TPA) concept .....	- 130 -
4.1.2 Proof-of-concept for a T-Plex Assay facilitated by spatially separated immobilized beads.....	- 133 -
4.1.3 Proof-of-concept for a T-Plex Assay within one constantly rotating cryotube .....	- 136 -
4.1.4 The “pilot” T-Plex Assay does detect antigen-specific T cell responses with poor sensitivity among healthy donor-derived isolated CD8 <sup>+</sup> T cells but not among unseparated PBMC.....	- 137 -
4.2 T-Plex Assay optimization phase 1 – Moving to 2 <sup>nd</sup> generation T-Plex beads .....	- 138 -
4.2.1 Optimized T-Plex bead architecture leads to a higher assay sensitivity.....	- 138 -
4.2.1.1 Validation of the 2 <sup>nd</sup> gen. T-Plex beads using the Survivin <sub>96-104</sub> /A2-specific CD8 <sup>+</sup> T cell line .....	- 138 -
4.2.1.2 Validation of 2 <sup>nd</sup> gen. T-Plex beads using isolated CD8 <sup>+</sup> T cells from healthy-donor PBMC.....	- 140 -
4.2.2 Parallel detection of multiple T cell lines by 2 <sup>nd</sup> generation T-Plex beads .....	- 142 -
4.2.3 Sensitivity and dynamic range of 2 <sup>nd</sup> gen.T-Plex beads compared to pMHC-I multimer staining. -	143 -
4.2.4 The T-Plex Assay is impaired by CD14 <sup>+</sup> cells but not by other bystander cells present in PBMC.. -	146 -
4.2.4.1 T-Plex Assay performance based on the cellular composition of the test sample .....	- 146 -
4.2.4.2 Playing with food – Phagocytosis of T-Plex beads by CD14 <sup>+</sup> monocytes .....	- 146 -
4.2.5 Sensitivity issue of the T-Plex Assay in comparison to pMHC multimer staining and ICS .....	- 148 -
4.3 T-Plex Assay optimization phase 2 – Advancing to an optimized assay protocol.....	- 150 -
4.3.1 Increased tube rotation speed, reaction duration, initial proximity of T-Plex beads and sample as well as another IFN- $\gamma$ capture mAb clone improves the T-Plex Assay .....	- 151 -
4.3.2 Increased tube filling volume and additional conjugation of co-stimulatory mAbs decrease the T-Plex Assay performance.....	- 152 -
4.3.3 Integration of optimal T-Plex Assay parameters leads to a very high sensitivity that is comparable to pMHC-I multimer stainings. ....	- 156 -
4.3.4 pHLA-A2-Fc variations harboring the mutation Q115E in the HLA-A2 $\alpha$ 2-domain or a mIgG2a-Fc with additional CH1-domain did not influenced the T-Plex Assay’s performance.....	- 159 -

4.3.5 pMHC-I-Fc immobilization on T-Plex beads via anti-IgG-Fc/IgG-Fc or biotin/streptavidin interactions leads to equal T-Plex Assay outcomes and similar T-Plex bead properties.....	161 -
4.4 Successful detection of minor T cell populations in healthy donors by the T-Plex Assay .....	163 -
4.4.1 Comparable sensitivities of an optimized T-Plex Assay and commercial pMHC-I multimer for the detection of low-frequent virus-specific CD8 <sup>+</sup> T cell populations .....	163 -
4.4.2 Antigen-specific detection by the T-Plex Assay does not alter the cognate T cell population.....	165 -
4.5 <i>In silico</i> predicted HLA-A2-restricted neopeptides of four cancer patients were not immunogenic as shown by T-Plex Assay- and pMHC-I multimer-based analysis .....	167 -
4.6 Successful detection of antigen-specific CD4 <sup>+</sup> T cell line by the T-Plex Assay.....	174 -
4.6.1 Antigen-specific detection of a CD4 <sup>+</sup> T cell line by pMHC-II-pCC-Fc-loaded T-Plex beads. ....	174 -
4.6.2 T-Plex <sup>2</sup> Assay concept – Simultaneous functional profiling of multiple antigen-specific CD4 <sup>+</sup> and CD8 <sup>+</sup> T cell responses .....	175 -
4.6.3 Proof-of-principle of a T-Plex <sup>2</sup> Assay for the antigen-specific detection of CD4 <sup>+</sup> T cells.....	177 -
<b>5   Discussion.....</b>	<b>179 -</b>
5.1 On the route to efficient and high-throughput production of correctly folded pMHC-Fc molecules ..	179 -
5.1.1 Emergence of novel productions strategies for recombinant soluble pMHC-I molecules.....	179 -
5.1.1.1 The cumbersome conventional pMHC-I production strategy .....	179 -
5.1.1.2 Efficient SCT-Fc molecules production using mammalian TGE systems.....	179 -
5.1.1.3 Further optimization of our dt-SCT-Fc construct design and production strategy .....	181 -
5.1.1.4 Advantages and disadvantages of SCTs compared to peptide exchange strategies for high-throughput production of soluble pMHC-I molecules.....	183 -
5.1.1.5 Future directions regarding pMHC-I*-Fc construct designs.....	185 -
5.2.1 Moderately efficient production of soluble peptide-linked MHC-II-Fc constructs using mammalian transient gene expression systems .....	185 -
5.3 The T-Plex Assay – A novel <i>in vitro</i> multiplex assay using color-coded beads serving as biosensors for cognate antigen-specific T cell pools .....	188 -
5.3.1 T-Plex beads – “Off-the-shelf” biosensors for cognate antigen-specific T cell pools .....	188 -
5.3.2 The T-Plex Assay – An easy-to-use multiplex assay designed for broad laboratory practice.....	189 -
5.3.3 The application scope of the T-Plex Assay and its strength as well as limitations .....	191 -
5.3.4 Novel, recently reported alternative methods to detect antigen-specific T cells without the need of next-generation sequencing (NGS) .....	192 -
5.3.5 Novel NGS-based methods to detect antigen-specific T cells or to dissect putative T cell epitopes on a genome-wide level .....	193 -
5.3.6 Open questions regarding the T-Plex Assay .....	195 -
5.3.6.1 Does the T-Plex Assay work independently of the T cells’ individual differentiation and functional status and reliably solely based on cognate pMHC-encounter? .....	195 -
5.3.6.2 What is the true nature of the interaction between cognate T cells and T-Plex beads that facilitate the unique read-out of the T-Plex Assay? .....	195 -
5.3.6.3 What are the critical parameters to move beyond an IFN- $\gamma$ -based T-Plex Assay? .....	196 -
<b>Supplementary Figures.....</b>	<b>199 -</b>
<b>Supplementary Tables .....</b>	<b>209 -</b>
<b>References .....</b>	<b>211 -</b>
<b>Appendix – Protein sequences of produced soluble pMHC molecules .....</b>	<b>227 -</b>
(i) pMHC-I [dt-SCT]-mIgG2a-Fc constructs .....	227 -
(ii) pMHC-I [dt-SCT]-CH1-mIgG2a-Fc constructs.....	227 -
(iii) pMHC-I [dt-SCT]-mIgG2a-Fc-Strep-tag II constructs .....	228 -

(iv) Heterodimeric pMHC-I [dt-SCT] <b>pCC</b> -mIgG2a-Fc constructs .....	- 229 -
(v) Homodimeric <b>pMHC-I [dt-SCT]-*mIgG2a-Fc</b> constructs .....	- 230 -
(vi) Monomeric <b>pMHC-I [dt-SCT]</b> constructs .....	- 230 -
(vii) Heterodimeric <b>pMHC-II-pCC-Fc</b> constructs .....	- 231 -
(viii) Heterodimeric <b>HLA-DM-pCC-Fc</b> constructs .....	- 234 -

## List of figures and tables

Figure 1.1   Overview of the immune system .....	- 1 -
Figure 1.2   Three-dimensional structures of peptide-bound MHC-I and MHC-II molecules.....	- 4 -
Figure 1.3   Classical MHC-I and -II antigen-presentation pathways in a highly schematic view .....	- 6 -
Figure 1.4   Overview of signals that drive T cell activation .....	- 9 -
Figure 1.5   Scheme of a mature immunological T cell synapse.....	- 12 -
Figure 1.6   The helping feature of CD4 <sup>+</sup> T cells for the priming of naïve CD8 <sup>+</sup> T cells .....	- 17 -
Figure 1.7   Linear progressive T cell differentiation model.....	- 19 -
Figure 1.8   Overview of frequently applied cancer neoantigen discovery workflows .....	- 26 -
Figure 1.9   Overview of common approaches to detected T cells in an antigen-specific manner.....	- 27 -
Figure 1.10   Cellular APCs barcoding and functional pMHC-microarray concept.....	- 33 -
Figure 1.11   Disulfide-trapped single-chain trimer design and peptide anchoring in the MHC-I F pocket .....	- 41 -
Figure 3.1   Successful mammalian cell-based production and cognate binding of pMHC-I-Fc molecules. ....	- 99 -
Figure 3.2   Long stability of dt-pHLA-A2-Fc-STag proteins and 24-deep well-based small-scale production-	102 -
Figure 3.3   Antigen-specific stimulation of Sur/A2 CD8 <sup>+</sup> T cells by bead-immobilized cognate pHLA-A2-Fc	- 104 -
Figure 3.4   Detection and stimulation of virus-specific CD8 <sup>+</sup> T cells within PBMC using pMHC-I-Fc .....	- 106 -
Figure 3.5   Generation, validation and characterization of HCMV pp65 <sub>495-503</sub> /A2 specific CD8 <sup>+</sup> T cell lines	- 108 -
Figure 3.6   Generation of three virus-specific HLA-A2 restricted CD8 <sup>+</sup> T cell lines .....	- 109 -
Figure 3.7   Stimulation of HCMV pp65 <sub>495-503</sub> / A2 specific CD8 <sup>+</sup> T cell line #416 and #5561 with aAPCs .....	- 110 -
Figure 3.8   Production and validation of pMHC-I multimers based on a biotinylated heterodimeric Fc.....	- 112 -
Figure 3.9   Unspecific binding of pMHC-I-pCC-Fc-based multimers at higher staining concentrations. ....	- 113 -
Figure 3.10   Successful production and validation of <i>in vivo</i> biotinylated pMHC-I-Fc* cleavable Fc.....	- 116 -
Figure 3.11   Comparison of different TGE systems for the production of <i>in vivo</i> biotinylated pMHC-I-*Fc.	- 118 -
Figure 3.12   Induction of antigen-specific proliferation based on plate- and bead-immobilized pMHC-I-Fc-	120 -
Figure 3.13   Direct <i>ex vivo</i> expansion of healthy donor-derived HCMV/A2-specific CD8 <sup>+</sup> T cells by aAPCs .	- 121 -
Figure 3.14   Successful production and antigen-specific stimulation of bead-immobilized pMHC-II-pCC-Fc	- 123 -
Figure 3.15   Antigen-specific binding of tethered-peptide associated MHC-II-pCC-Fc multimers.....	- 124 -
Figure 3.16   Validation of a HLA-DM-dependent peptide-exchangeable HLA-DR3-pCC-Fc construct.....	- 126 -
Figure 3.17   Production and validation of a soluble HLA-DM-pCC-Fc construct .....	- 127 -
Figure 4.1   Linking T cell specificities to defined bead colors – The T-Plex Assay core concept .....	- 131 -
Figure 4.2   Observed IFN-γ “cross-bleeding” onto control T-Plex beads using static assay conditions.....	- 132 -
Figure 4.3   Agitation during T cell stimulation by T-Plex beads as key to overcome IFN-γ cross-bleeding...	- 133 -
Figure 4.4   T-Plex Assay-based detection of a cogante T cell response facilitated by a 96-well magnet.....	- 135 -
Figure 4.5   Detection of a cognate human T cell line by a one-tube-rolling multiplex T-Plex Assay.....	- 136 -
Figure 4.6   T-Plex Assay-based detection of HCMV pp65 <sub>495-503</sub> /A2 specific T cells derived from isolated CD8 <sup>+</sup> T cells but not from unseparated PBMC. ....	- 137 -

## List of figures and tables

Figure 4.7   Optimized 2 <sup>nd</sup> generation T-Plex architecture leads to an improved assay sensitivity .....	- 139 -
Figure 4.8   2 <sup>nd</sup> generation T-Plex beads allows detection of minor T cell populations and complete cell recovery .....	- 141 -
Figure 4.9   T-Plex Assay-based antigen-specific multiplex detection of a defined set of CD8 <sup>+</sup> T cell lines ...	- 143 -
Figure 4.10   Bystander T cells do not decrease the sensitivity of the T-Plex Assay .....	- 144 -
Figure 4.11   pMHC-I multimer staining in comparison to T-Plex Assay of T cell line spiked samples.....	- 145 -
Figure 4.12   T-Plex Assay performance is impaired by CD14 <sup>+</sup> monocytes present in PBMC .....	- 147 -
Figure 4.13   Sensitivity of the T-Plex Assay in comparison to pMHC-I multimer staining and ICS.....	- 149 -
Figure 4.14   Systemic optimization of the T-Plex Assay and identification of crucial parameters – Part 1 ..	- 153 -
Figure 4.15   Optimization of the T-Plex Assay and identification of crucial parameters – Part 2.....	- 155 -
Figure 4.16   Combination of optimal parameters improved dramatically the T-Plex Assay's sensitivity .....	- 157 -
Figure 4.17   Optimized T-Plex Assay outperforms the sensitivity for the detection of HCMV/A2-specific T cells compared to a corresponding pMHC-I multimer staining but has a limited quantitative dynamic range .....	- 158 -
Figure 4.18   pHLA-A2-Fc variations harboring the $\alpha$ 2-domain Q115E mutation or a CH1-mIgG2a-Fc marginally affected T cell binding and stimulation capacity as well as T-Plex Assay performance.....	- 160 -
Figure 4.19   T-Plex bead assembly variations and impact on T-Plex Assay performance .....	- 162 -
Figure 4.20   Reliable detection of small T cell populations using the optimized T-Plex Assay .....	- 164 -
Figure 4.21   Antigen-specific T cell detection by the T-Plex Assay does not alter the original sample's phenotype.....	- 166 -
Figure 4.22   Peptide vaccination schedule and time points of blood taken from each individual patient ...	- 168 -
Figure 4.23   Analysis of cancer patient-derived peripheral blood by T-Plex beads displaying putative T cell neopeptides .....	- 171 -
Figure 4.24   Neopeptide pMHC-I multimer staining of cancer patient derived CD8 <sup>+</sup> T cells to validate corresponding T-Plex Assay-based analysis .....	- 172 -
Figure 4.25   Antigen-specific detection of the MTB/DR3 CD4 <sup>+</sup> T cell line by cognate 2 <sup>nd</sup> gen. T-Plex beads.-	- 174 -
Figure 4.26   T-Plex <sup>2</sup> Assay principle – Multiplex-based antigen-specific CD4 <sup>+</sup> and CD8 <sup>+</sup> T cell detection with parallel functional profiling.....	- 176 -
Figure 4.27   Proof-of-principle of a T-Plex <sup>2</sup> Assay for the antigen-specific detection of CD4 <sup>+</sup> T cells .....	- 178 -
Supplementary Figure S1   Characterization of the Survivin/HLA-A2-specific CD8 <sup>+</sup> T cell line .....	- 199 -
Supplementary Figure S2   Comparative binding analysis of protein A- vs. Strep-Tactin-based purified pMHC-I-Fc constructs and binding performance of complexes consisting of Strep-Tactin and pMHC-I-Fc-STag .....	- 200 -
Supplementary Figure S3   Assessment of required thrombin units for complete pMHC-I-*Fc cleavage and validation of pMHC-I multimer formation .....	- 201 -
Supplementary Figure S4   Purification of biotinylated pMHC-I-*Fc homodimers and usage for pMHC-I multimers.....	- 201 -
Supplementary Figure S5   Successful production of Fc-free biotinylated monomeric pMHC-I (dt-SCT) using the 293-F system and its subsequent binding validation .....	- 202 -
Supplementary Figure S6   Dynabead pilot experiment — Detection of an antigen-specific T cell response by analyzing IFN- $\gamma$ load on aAPCs with IFN- $\gamma$ capture capacity .....	- 203 -
Supplementary Figure S7   Healthy donor #3838 after MACS-based sample preparation .....	- 204 -

Supplementary Figure S8   Time course of the T-Plex Assay.....	- 204 -
Supplementary Figure S9   The fraction of IFN- $\gamma$ <sup>+</sup> T-Plex beads upon cognate T cell interaction is not influenced by the number of irrelevant bystander T-Plex beads.....	- 205 -
Supplementary Figure S10     Cancer patient peripheral blood immune cells composition and CD25 and PD-1 expression profile of the CD8 <sup>+</sup> T cell population one day after thawing .....	- 206 -
Supplementary Figure S11   Highly sensitive detection of CMV/A2-specific T cells by streptavidin / IFN $\gamma$ -capture mAb conjugated T-Plex beads loaded with cognate monomeric biotinylated pMHC-I .....	- 207 -
Supplementary Figure S12   Detection of an antigen-specific CD4 <sup>+</sup> T cell line using T-Plex beads with various cytokine capture capacities.....	- 208 -
Table 1.1   CD4 <sup>+</sup> T cell subsets – Inducing extrinsic cytokines and secreted effector cytokines .....	- 16 -
Table 1.2   Tumor antigen classifications .....	- 23 -
Table 1.3   Overview of selected assays for the direct visualization of antigen-specific (Ag <sup>+</sup> ) T cells or their antigen-specific response. ....	- 29 -
Table 3.1   dt-pHLA-A2-Fc-STag production efficiency across different published peptide ligands using the CHO-S/PEI/ProCHO-4 TGE system.....	- 100 -
Table 4.1   Quantitative analysis of the pMHC-I multimer staining of HD-PBMC #3838 and extrapolated cell quantities used for a corresponding T-Plex analysis (linked to Fig. 4.13) .....	- 150 -
Table 4.2   Quantitative analysis of the pMHC-I multimer staining of HD-PBMC #5561 and HD-PBMC #8595 shown in Fig. 4.20 and extrapolated cell quantities used for a corresponding optimized T-Plex Assay.....	- 165 -
Table 4.3   Quantitative analysis of the pMHC-I multimer staining of HD-#3637 PBMC shown in Fig. 4.21 and extrapolated absolute cell quantities used for a corresponding T-Plex Assay.....	- 167 -
Table 4.4   Cancer patient characteristics, used long peptides for vaccination and ELISpot results.....	- 168 -
Table 4.5   Produced neopeptide and corresponding wt-peptide-loaded HLA-A2 molecules .....	- 170 -
Table 5.1   Comparison of methods for recombinant soluble pMHC-I molecule production .....	- 180 -
Table 5.2   Comparison of methods for recombinant soluble pMHC-II molecule production .....	- 187 -
Supplementary Table S1   Production efficiencies of <i>in vivo</i> biotinylated pHLA-A2-*Fc constructs across various mammalian TGE systems .....	- 209 -
Supplementary Table S2   Production efficiencies of <i>in vivo</i> biotinylated monomeric Fc-free pHLA-A2 constructs using the 293-F TGE system .....	- 209 -
Supplementary Table S3   Production efficiencies of various peptide-HLA-II-pCC-Fc constructs across different mammalian TGE system and purification methods .....	- 210 -



## Abbreviations

<b>A2</b>	HLA allele A*02:01		
<b>aAPC</b>	Artificial antigen-presenting cell		
<b>AC</b>	Affinity chromatography	<b>dt-pHLA-A2-Fc</b>	dt-SCT of a defined peptide HLA-A*02:01 complex fused to mIgG2a-Fc
<b>ACT</b>	Adoptive cellular transfer	<b>dt-SCT</b>	Disulfide-trapped pMHC-I single-chain trimer
<b>AICD</b>	Activation-induced cell death	<b>DTT</b>	Dithiothreitol
<b>AMP</b>	Ampicillin	<b>EBV</b>	Epstein-Barr virus
<b>anti- / <math>\alpha</math>-</b>	Monoclonal mAb specific for ("anti") an indicated antigen	<b>EDTA</b>	Ethylenediaminetetraacetic acid
<b>APC</b>	Antigen presenting cells	<b>EDC</b>	1-ethyl-3-(3-dimethylaminopropyl) carbodiimide hydrochloride
<b>- APC</b>	Conjugated to allophycocyanin	<b>EGTA</b>	Ethylene glycol tetraacetic acid
<b>ATP</b>	Adenosine triphosphate	<b>ELISA</b>	Enzyme-linked immunosorbent assay
<b><math>\beta_2m</math></b>	$\beta_2$ -microglobulin	<b>ELISpot</b>	Enzyme-linked immunospot assay
<b>BCR</b>	B cell receptor	<b>ER</b>	Endoplasmic reticulum
<b>BSA</b>	Bovine serum albumin	<b>EK</b>	Enterokinase
<b><math>^{\circ}C</math></b>	Degree Celsius	<b>Fc<math>\gamma</math>R</b>	Fc receptors for immunoglobulin gamma
<b>CAR</b>	Chimeric antigen receptor	<b>Flu</b>	Influenza A virus
<b>CCL</b>	C-C motive ligand (chemokine)	<b>FMO</b>	Fluorescence-minus-one control
<b>CCR</b>	C-C motive ligand receptor	<b>FACS</b>	Fluorescence activated cell sorting
<b>CD</b>	Cluster of differentiation	<b>FBS / FCS</b>	Fetal bovine serum / calf serum
<b>cDNA</b>	Complementary DNA	<b>Fc</b>	Fragment crystallizable – here of murine immunoglobulin isotype gamma 2a (mIgG2a-Fc)
<b>CDR</b>	Complementarity-determining region	<b>*Fc</b>	Fragment crystallizable that bears a N-terminal enzymatic cleavage site
<b>CEA</b>	Carcinoembryonic antigen	<b>Fig.</b>	Figure
<b>CFSE</b>	Carboxyfluorescein diacetate succinimidyl ester	<b>FT</b>	Flow-through
<b>CH</b>	Constant heavy chain domain	<b>g / mg / <math>\mu</math>g / ng</b>	gram / milligram / microgram / nanogram
<b>CHO</b>	Chinese hamster ovary cells	<b>G<math>\alpha</math>M-IgG</b>	Goat anti-mouse IgG polyclonal serum
<b>CHO-S</b>	CHO cells growing in suspension	<b>GFP</b>	Green-fluorescent protein
<b>CLIP</b>	Class II-associated invariant chain peptide	<b>Gy</b>	Gray (1 Gy = 1 Joule / kg)
<b>CR</b>	Crude cell supernatant	<b>Gzm B</b>	Granzyme B
<b>CTL</b>	Cytotoxic T cell	<b>h</b>	Hour
<b>CTLA-4</b>	Cytotoxic T lymphocyte-associated protein 4	<b>H<sub>2</sub>O<sub>2</sub></b>	Hydrogen peroxide
<b>CTV</b>	CellTrace™ Violet	<b>HA</b>	hemagglutinin
<b>CV</b>	column-bed volume	<b>HABA</b>	Hydroxy-azophenyl-benzoic acid
<b>CyTOF</b>	Cytometry by time-of-flight	<b>HC</b>	Heavy chain
<b>Da / kDa</b>	Dalton / kilo dalton	<b>HCMV</b>	Human cytomegalovirus
<b>DAMPs</b>	danger-associated molecular patterns	<b>HCV</b>	Hepatitis C virus
<b>DC</b>	Dendritic cell	<b>HD</b>	Healthy blood donor
<b>ddH<sub>2</sub>O</b>	Double distilled laboratory-grade water		
<b>DKFZ</b>	German Cancer Research Center, Heidelberg		
<b>DMSO</b>	Dimethylsulfoxid		
<b>DNA</b>	Deoxyribonucleic acid		
<b>dt-pMHC-I-Fc</b>	Disulfide-trapped single-chain-trimer of peptide, $\beta_2$ -		

## Abbreviations

<b>HEK</b>	Human embryonic kidney cells	<b>MHC-I / -II</b>	Major histocompatibility complex class I / II
<b>HEPES</b>	2-(4-(2-Hydroxyethyl)-1-piperacynyl)-ethanesulfonic acid	<b>Mo-DC</b>	Monocyte-derived dendritic cell
<b>HBV</b>	Hepatitis B virus	<b>MP</b>	Influenza A virus matrix protein 1
<b>HIC</b>	Hydrophobic interaction chromatography	<b>MTB</b>	Mycobacterium tuberculosis
<b>HIV</b>	Human immunodeficiency virus	<b>MTOC</b>	Microtubule-organizing center
<b>HLA</b>	Human leucocyte antigen	<b>MW</b>	Molecular weight
<b>HPV</b>	Human papilloma virus	<b>MWCO</b>	Molecular weight cut-off
<b>HRP</b>	horseradish peroxidase	<b>NFAT</b>	Nuclear factor of activated T cells
<b>Hsp</b>	Heat-shock protein	<b>NGS</b>	Next-generation sequencing
<b>HT</b>	Hypoxanthine and thymidine	<b>NK(T) cells</b>	Natural killer (T) cells
<b>hTERT</b>	Human telomerase reverse transcriptase	<b>NP</b>	4-hydroxy- 3-nitrophenylacetyl
<b>HTLV-1</b>	Human T lymphotropic virus 1	<b>NSM</b>	Non-synonymous mutations
<b>ICB</b>	Immune checkpoint blocking therapy	<b>NTA</b>	Nitrilotriacetic acid
<b>ICS</b>	Intracellular cytokine staining	<b>OVA</b>	Ovalbumin
<b>IEX</b>	Ion-exchange chromatography	<b>OVN</b>	Overnight
<b>IFN</b>	Interferon	<b>pAPC</b>	Professional antigen-presenting cell
<b>Ig / IgG</b>	Immunoglobulin G (complete)	<b>PBS</b>	Phosphate buffered saline
<b>Ii</b>	Invariant chain (CD74)	<b>PBMC</b>	Peripheral blood mononuclear cells
<b>IL</b>	Interleukin	<b>pCC</b>	Amphiphilic parallel coiled-coil basic / acidic “zipper” heterodimerization domain
<b>IS</b>	Immunological synapse	<b>PD-1</b>	Programmed cell death protein-1
<b>ITAM</b>	Immune receptor tyrosine-based activation motifs	<b>PD-L1</b>	PD-ligand 1
<b>ITIM</b>	Immune receptor tyrosine-based inhibitory motifs	<b>PE</b>	Phycoerythrin
<b>K<sub>d</sub></b>	Dissociation constant	<b>PEI</b>	Polyethyleneimine
<b>KIH</b>	Knob-into-hole	<b>PES</b>	Polyethersulfone
<b>L / mL / μL</b>	Liter / milliliter / microliter	<b>PHA-L</b>	Phytohemagglutinin-L from Phaseolus vulgaris
<b>LPLC</b>	Low-pressure liquid chromatography	<b>pHLA-A2*</b>	Soluble dt-SCT comprising the HLA-A*02:01 allele that has been produced as Fc-conjugated homodimer and released from the Fc by enzymatic digestion
<b>LAG-3</b>	Lymphocyte activation gene-3	<b>PLC</b>	Peptide-loading complex
<b>LB</b>	Luria-Bertani broth medium	<b>PMA</b>	Phorbol-12-myristate-13-acetate
<b>LC</b>	Light chain	<b>pMHC-I / II</b>	Peptide-loaded MHC-I / II complex
<b>LCMV</b>	Lymphocytic choriomeningitis virus	<b>pMHC-I-Fc</b>	Homodimeric pMHC-I according to the dt-SCT design fused to a Fc
<b>LDS</b>	Lithium dodecyl sulphate	<b>pMHC-I-pCC-Fc</b>	Heterodimeric bivalent pMHC-I (dt-SCT) fused via pCC to a Fc
<b>LPS</b>	Lipopolysaccharide	<b>pMHC-II-pCC-Fc</b>	Heterodimeric monovalent peptide-tethered MHC-II fused via pCC to a Fc
<b>m / nm</b>	Meter / nanometer	<b>PRR</b>	Pattern recognition receptors
<b>M / mM / μM</b>	Molar / millimolar / micromolar	<b>PS</b>	Polystyrene
<b>mAb</b>	Monoclonal antibody	<b>PVDF</b>	Polyvinylidene difluoride
<b>MACS</b>	Magnet activated cell sorting		
<b>MART-1</b>	Melanoma antigen 1 recognized by T cells		
<b>MCR</b>	pMHC-TCR hybrid system		
<b>MDCS</b>	Myeloid-derived suppressor cells		
<b>MFI</b>	Median fluorescent intensity		
<b>MIIC</b>	MHC class II compartment		
<b>min</b>	Minute		

<b>Qdots</b>	Quantum dots	<b>WES</b>	Whole exome sequencing
<b>RNA</b>	Ribonucleic acid	<b>wt</b>	Wild type
<b>rpm</b>	Rounds per minute		
<b>RT</b>	Room temperature (i.e. 21–24°C)		
<b>rcf</b>	relative centrifugal force		
<b>Ref.</b>	Reference		
<b>SABR</b>	Signaling and antigen-presenting bifunctional receptor		
<b>SAv</b>	Streptavidin		
<b>SCT</b>	pMHC single-chain trimer comprising peptide, $\beta_2$ -microglobulin and MHC-I heavy chain		
<b>SCT-Ig</b>	pMHC single-chain trimer fused to a complete IgG		
<b>SDS-PAGE</b>	Sodium dodecyl sulfate–polyacrylamide gel electrophoresis		
<b>Sec.</b>	Section / chapter		
<b>SEC</b>	Size exclusion chromatography		
<b>SFM</b>	Serum free medium		
<b>SMAC</b>	Supramolecular activation cluster		
<b>STag</b>	Strep-tag II		
<b>Sulfo-NHS</b>	N-hydroxysulfosuccinimid		
<b>T<sub>CM</sub> / EM</b>	T cell with central memory / effector memory phenotype		
<b>Th</b>	T helper cell		
<b>Treg</b>	T regulatory cell		
<b>TAA</b>	Tumor-associated antigens		
<b>TAP</b>	Transporter associated with antigen processing		
<b>TGE</b>	Transient gene expression		
<b>TCR</b>	T cell receptor		
<b>TIGIT</b>	T cell immunoreceptor with immunoglobulin and ITIM domains		
<b>TIL</b>	Tumor infiltrating lymphocytes		
<b>TIM-3</b>	T cell immunoglobulin and mucin domain-containing protein3		
<b>TLRs</b>	Toll-like receptors		
<b>TMB</b>	3,3',5,5'-Tetramethylbenzidine		
<b>TNF</b>	Tumor necrosis factor		
<b>TNFR</b>	Tumor necrosis factor receptor		
<b>TPA</b>	T-Plex Assay		
<b>TRIS</b>	Tris(hydroxymethyl)-aminomethan		
<b>TSA</b>	Tumor-specific antigens		
<b>UV</b>	Ultra-violet		
<b>VPA</b>	Valproic acid sodium salt		
<b>v/v</b>	Volume/volume		
<b>w/v</b>	Weight/volume		



# 1 | Introduction

## 1.1 The adaptive immune system and its central dogmata in a nutshell

Our immune system has evolved to protect us from infectious diseases caused by daily encountered pathogens including viruses, bacteria, parasites and fungi (1). In the same breath, fast elimination of tumorigenic viral infections as well as defusing acute tissue inflammations by the immune system can prevent malignant cell transformation and subsequent cancer initiation and progression. Moreover, it is well established that T cells can directly recognize and eliminate cancer cells based on their antigen presentation of aberrantly expressed genes (2) as introduced in more detail in **Sections 1.2 and 1.4**. Consequently, the immune system must firstly have the capacity to differentiate “foreign” environmental agents including a variety of microorganisms as well as malignant body cells from healthy cells referred to as “self” and secondly must initiate appropriate countermeasures, which finally manifests in the word *immunity*.

From a bird’s eye view, the immune system comprises two highly interconnected arms termed innate and adaptive (also termed acquired) immunity as summarized in **Fig. 1.1**. The innate branch of the immune system utilizes a limited set of germline-encoded receptors that are triggered by molecular structures shared among microorganisms referred to as pathogen-associated molecular patterns (PAMPs) or danger-associated molecular patterns (DAMPs). These so-called pattern recognition receptors (PRR) such as toll-like receptors (TLRs) allow rapid responses against pathogens within minutes of innate immune cells like dendritic cells (DCs), macrophages and granulocytes. Moreover, natural killer (NK) cells express a defined set of inhibitory and activating receptors that among other functions in particular senses cell stress and the lack of major histocompatibility complex class I molecule (MHC-I) surface expression, which is often associated with viral infections or malignant cell transformation. In contrast, a decisive feature of the adaptive immune system is the expression of a tremendous pool of unique antigen-specific receptors that are “acquired” by somatic DNA recombination of receptor gene segments during T cell and B cell development, respectively (1).

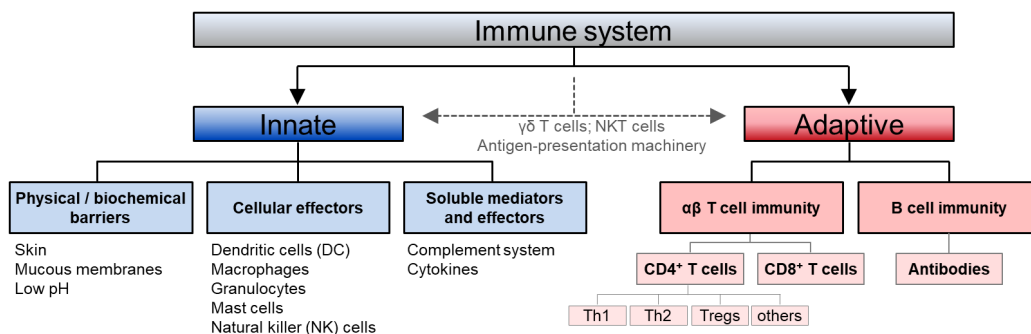


**Figure 1.1 | Overview of the immune system**

**Innate immunity** serves as first line of defense and acts immediately upon pathogen encounter. It comprises several components including epithelial barriers, soluble effector systems such as the complement system and a variety of effector immune cells like phagocytic macrophages, dendritic cells or granulocytes as well as natural killer cells. **Adaptive immunity** responds to novel antigens that have not been previously encountered by selectively expanding highly antigens-specific pools of B cells and conventional ( $\alpha\beta$ ) T cells, which usually requires days to develop. Natural killer T cells (NKT) and unconventional  $\gamma\delta$  T cells with limited antigen specificity can be seen as evolutionary bridge between innate and adaptive immunity, which has been reviewed recently by (3, 4) and will not be covered here. Moreover, the antigen presentation by professional antigen-presenting cells, in particular by DCs, is essential for an effective long-lasting adaptive immune response and thus may be seen as interphase between innate and adaptive immunity as introduced in **Section 1.3**. Modified figure was adapted from (5) with permission.

## 1 | Introduction

In more detail, each individual B or T cell expresses only a single type of B cell receptor (BCR) or T cell receptor (TCR) on their plasma membrane, respectively, whose unique genomic sequence is the result of a random and imprecise rearrangement of variable (V), diversity (D) and joining (J) genes, a process also known as V(D)J recombination. The resulting diversity referred to as the immune repertoire of BCRs and TCRs allows the binding to millions of different protein as well as non-protein structures. In fact, the entire TCR repertoire of human healthy adults comprise over 100 million different specificities as shown recently by (6). In cases a molecule is able to elicit an adaptive immune responses it is considered as a whole as antigens, whereas the antigenic determinant that is actually recognized (i.e. bound) by a BCR/TCR is referred to as epitope. Within this study the terms antigen and epitope are for simplicity often interchangeable used. Unlike BCRs, which mostly recognize antigens in their native form (i.e. the BCR binds to an epitope within the three-dimensional conformation of the protein), TCRs bind with few exceptions to linear short peptide fragments (i.e. 8–20 amino acids) derived from intracellularly processed protein-based antigens of intracellular as well as extracellular origin that are presented by peptide-loaded major histocompatibility complex (MHC) class I and class II molecules (pMHC-I/-II) on the cell surface, which will be introduced in more detail in **Sections 1.2**.

Another vital feature of the adaptive immunity termed central tolerance comprise the clonal deletion in case of TCRs (reviewed in (7)) and molecular editing as well as deletion of BCRs (reviewed in (8)) that recognize self-antigens (also referred to as auto-antigens) with high affinity during T cell and B cell development, which takes place in the thymus and bone marrow, respectively. This process is vital to delete putatively harmful TCRs/BCRs from the immune repertoire that might otherwise induce fetal autoimmune reactions. In addition, self-antigen-specific T cells that “escaped” initial central tolerance mechanism and have been released into the circulation are kept in check by various so-called peripheral tolerance mechanism. Most pronounced is the state of long-term T cell hypo-responsiveness also termed “anergy”, that is induced if a naïve (i.e. antigen-unexperienced) self-reactive T cell encounters a self-antigen (referred to as T cell activating “signal 1”) on an antigen-presenting cells (APC) in the absence of “danger-associated” co-stimulatory signals (“signal 2”). On the contrary, naïve T cells that encounter their cognate (i.e. matching) “foreign” antigen for the first time in the context of provided co-stimulatory signals and cytokines) will undergo massive clonal expansion and differentiation into effector T cells – a process referred to as T cell priming (for more details see **Section 1.3**). Upon clearance of a pathogen that initiated the T cell priming phase in the first place (primary infection), the major fraction of the corresponding antigen-specific effector T cell population contracts over-time, whereas a rather small and heterogeneous pool of antigen-experienced T cells may persist for up to a life-long and which are commonly called memory T cells. Similarly, also B cells differentiate upon initial cognate antigen encounter into antibody-secreting plasma cells and develop a long-living memory pool of cells that allows a rapid response upon pathogen re-exposure. The capacity to “memorize” an initial antigen encounter is reflected by the persistence of an antigen-experienced B cell as well as T cell pool that is yet another essential feature of the adaptive immune system (1).

In the following chapters, prior known aspects most relevant to the present study will be introduced with a strong focus on T cell biology. The subsequent sections will initially cover the principles of antigen presentation as well as their recognition by T cells leading to their subsequent activation (**Section 1.2 & 1.3**). Moreover, the pivotal role of T cells for cancer immunotherapy will be introduced with focus on tumor-antigens (**Section 1.4**). Finally, recent technologies and their limitations will be introduced that allow the detection, enumeration and isolation of T cells in an antigen-specific manner (**Section 1.5**).

## 1.2 From antigen processing to T cell activation

In the following an overview will be given regarding processes and central molecular elements that contribute to the initiation of a functional T cell response. Yet, the underlying high molecular complexity is beyond the presented study and has been described in more detail elsewhere (1). Moreover, the biology of conventional T cells expressing  $\alpha$ - and  $\beta$ -chain TCRs that interact with classical peptide-MHC complexes will be focused upon here, because they comprise the majority (95%) of the entire T cell pool. Thus, throughout the study, the term T cell refers to a mature  $\alpha\beta$  T cell of either CD4<sup>+</sup> or CD8<sup>+</sup> lineage. Natural killer T cells (NKT) and unconventional T cells expressing  $\gamma\delta$  TCRs that display a limited antigen-specificity, respectively, as well as  $\alpha\beta$  TCRs that bind to lipid-based antigens or vitamin B metabolites presented by CD1 subtypes and the MHC class I-related molecule MR1, respectively, will be not covered here (3, 4, 9).

In a very simplified view, T cell activation is the end result of a two-step process as well as of a *bona fide* interaction of a two-component system. The process starts within an antigen-presenting cell (1<sup>st</sup> component, APC) with the intracellular protein degradation of putative antigens into peptide fragments (antigen processing) and their stable association with MHC molecules leading to their surface expression (antigen presentation). Upon cognate encounter of a T cell (2<sup>nd</sup> component) with the APC via a TCR/pMHC interaction, a signaling cascade within the T cell is triggered (antigen recognition) that, depending on the overall cellular context, induces a plethora of events (T cell activation) including cellular differentiation and in the pursuit of differentiation, lineage-dependent effector functions including cytokine secretion and/or induction of cell death of the target APC, which will be described in **Section 1.3**.

### 1.2.1 Structural and genetic aspects of peptide-MHC class I and II complexes

A central hallmark of T cell biology is, that ( $\alpha\beta$ ) T cells expressing the co-receptor CD4 (CD4<sup>+</sup> T cells) are restricted to bind to surface expressed peptide-loaded (p) MHC class II molecules (pMHC-II), whereas CD8<sup>+</sup> T cells recognize pMHC class I molecules (pMHC-I). Moreover, pMHC-I molecules are expressed at different levels by all nucleated cells with few exceptions including male germ cells in the testis. In contrast, the expression and associated antigen-presentation machinery of pMHC-II is with few exceptions restricted to professional antigen-presenting cells comprising dendritic cells, B cells and macrophages (10, 11). However, MHC-II expression can be induced by interferon- $\gamma$  (IFN- $\gamma$ ) and other inflammatory molecules in non-professional APCs including mesenchymal stromal cells, fibroblasts, endothelial cells and even certain cancer cells – most notably melanoma cells (12–14).

**Genetic aspects of MHC molecules** | Both classical MHC-I and -II molecules are encoded by the major histocompatibility complex gene cluster located on chromosome 6 in humans, which overall comprises roughly 260 genes that mostly fulfill immunological functions. Most gene products within the human MHC class I and II gene region are called human leukocyte antigens (HLA). The genes coding for the classical MHC-I  $\alpha$ -chains comprise three gene loci, in humans termed HLA-A, B and C, respectively. In addition, there are non-classical, rather monomorphic MHC class I molecules termed HLA-E, F and G. Moreover, three pairs of MHC class II  $\alpha$ - and  $\beta$ -chain genes can be distinguished termed HLA-DR, -DP and -DQ. The polygenic set of classical MHC-I and -II genes is highly polymorphic, meaning that multiple variants (allelic forms) of these gene exist within the human population. This allelic polymorphism and associated variations in amino acid sequences are heavily concentrated in the part of the MHC molecules that directly interacts with putative peptide ligands. Thus, the allelic MHC polymorphism defines the peptide repertoire that is presented by any given APC (1, 15).

**Structural aspects of pMHC-I molecules** | From a structural perspective both classical MHC-I and -II molecules share an overall similar protein folding and appear as a heterotrimeric protein complex on the cell surface. The trimeric pMHC-I complex comprises an (i)  $\alpha$ -chain (also referred to as heavy chain, 43 kDa), (ii) a soluble, invariant, non-covalently associated light chain (12 kDa) called  $\beta_2$ -microglobulin ( $\beta_2m$ ), whose gene is located on chromosome 15 in humans, as well as (iii) a short peptide positioned in the peptide-binding groove formed by the  $\alpha$ -chain (**Fig. 1.2a**), (11).

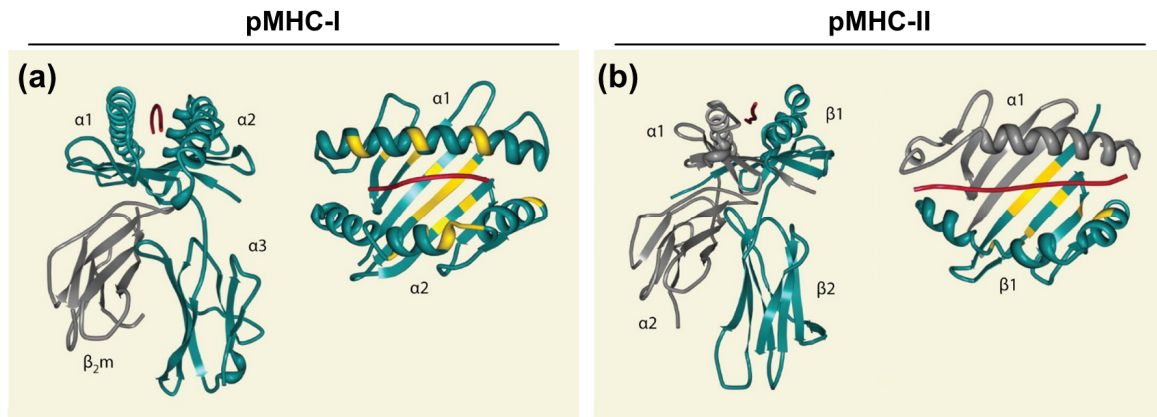


**Figure 1.2 | Three-dimensional structures of peptide-bound MHC-I and MHC-II molecules**

**(a) Structure of a peptide-loaded MHC-I molecule.** Shown is a ribbon diagram from a side view angle (**left panel**) and from a top view (**right panel**) of a HLA-A\*02:01 complex associated with a peptide (residue 58–66) derived from the influenza A (Flu) matrix protein 1 (Flu MP<sub>58–66</sub>). The MHC-I  $\alpha$ -chain comprising the  $\alpha 1$ ,  $\alpha 2$  and  $\alpha 3$  domain is shown in dark green; monomorphic  $\beta_2$ -microglobulin ( $\beta_2m$ ) in grey; Flu MP<sub>58–66</sub> peptide in red.

**(b) Structure of a peptide-loaded MHC-II molecule.** Shown is a peptide-HLA-DR1 complex comprising the  $\beta$ -chain of HLA-DRB1\*01:01 (dark green), which is associated with the monomorphic HLA-DRA\*01  $\alpha$ -chain (grey) and the peptide ligand (red) Flu hemagglutinin (HA) residue 306–318 (Flu HA<sub>306–318</sub>). **(a & b)** Highly polymorphic residues of HLA-A and HLA-DR molecules are highlighted in yellow. Modified figure was adapted from (11) with permission.

The MHC-I  $\alpha$ -chain glycoprotein consists of a transmembrane domain with a short cytoplasmic C-terminal tail and three N-terminal extracellular domains ( $\alpha 1$ ,  $\alpha 2$  and  $\alpha 3$ ) of which the  $\alpha 1$  and  $\alpha 2$  domain form the characteristic MHC-fold harboring a peptide-binding groove, whereas the  $\alpha 3$  domain contains a monomorphic immunoglobulin (Ig)-like fold. The underlying Ig-fold domains contributed by the  $\alpha 3$  domain and  $\beta_2m$  support the stability of the binding groove. Moreover, the  $\alpha 3$  domain contains interactions sites needed for the antigen-processing machinery as well as a conserved seven amino acid loop that serves as a binding site for the CD8 co-receptor (15, 16). The peptide-binding groove of MHC-I is formed by two antiparallel  $\alpha$ -helices overlaying an eight-stranded antiparallel  $\beta$ -sheet (**Fig. 1.2a**), in which the highly polymorphic  $\alpha 1$  and  $\alpha 2$  domains contribute to an  $\alpha$ -helix and four strands of the  $\beta$ -sheet each. The MHC-I peptide-binding groove is closed at both ends by conserved and bulky amino acids including tyrosine residue 84 (Y84) and tryptophan 167 (W167) leading to a size restriction of the accommodated peptides of 8–11 amino acids in length. The peptide is bound in a coordinated manner by sequence-independent as well as sequence-dependent interactions with side chains of residues of the peptide-binding groove, which contribute to the stability of the entire MHC complex. Sequence-independent peptide binding occur via a cluster of tyrosine residues, which are conserved across all MHC-I molecules and positioned near the N- as well as C-terminus of the peptide ligand's backbone. Moreover, polymorphic side-chain residues of the MHC backbone, which are protruding from the  $\alpha$ -helices and  $\beta$ -strands into the peptide-binding groove form six pockets (A–F), which are crucial for the peptide-sequence dependent interaction with the MHC molecule.

Peptide-MHC complex formation requires the stable anchoring of peptide side-chains into these specific pockets of shape and chemistry. Therefore, the MHC allele-specific shape and chemistry of these pockets imposes constraints for peptide ligand binding, which in turn is reflected by the peptide-binding motifs found in the sequence of naturally processed and presented peptide ligands. In the case of the HLA-A\*02:01 allele, the sequence-specific peptide-binding motif typically comprises two aliphatic so-called anchor residues located at position 2 (preferably leucine) and position 9 (preferably valine) of the peptide sequence, whose side chains fit into the respective pockets (i.e. A and F pocket) formed by the HLA-A\*02:01 peptide binding groove (1, 16, 17).

**Structural aspects of pMHC-II molecules** | The heterodimeric pMHC-II is composed of membrane-anchored  $\alpha$ - (35 kDa) and  $\beta$ -chain (28 kDa) containing the extracellular domains  $\alpha$ 1 and  $\alpha$ 2, and  $\beta$ 1 and  $\beta$ 2, respectively, in which the  $\alpha$ 2 and  $\beta$ 2 domain have an Ig-like fold (**Fig. 1.2b**). The  $\alpha$ 1 and  $\beta$ 1 domain form a peptide-binding groove that has an overall similar architecture as compared to MHC-I. However, in contrast to MHC-I, the MHC-II binding groove is open at both ends allowing the accommodation of peptides typically 13–25 amino acid residues in length, with the peptide usually extruding on both sides of the groove. Moreover, similar to MHC-I also side-chain residues of the  $\alpha$ -helices and  $\beta$ -sheets of the  $\alpha$ 1 and  $\beta$ 1 domains form distinct pockets (P1–P9) that define certain peptide-binding motifs (1, 16).

### 1.2.2 Classical MHC class I and II antigen presentation pathways

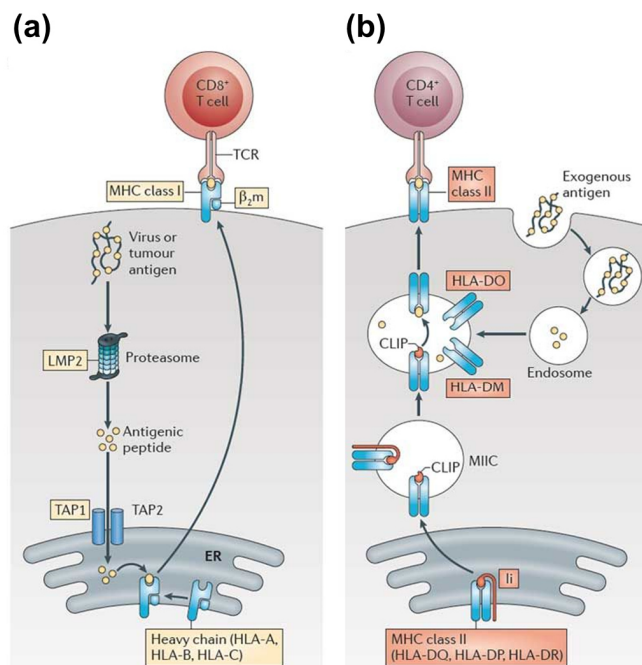
Presentation of peptides on MHC molecules termed immunopeptidome (or peptide repertoire) is a central mechanism that shapes both T cell- as well as B cell (humoral)-mediated immunity. These peptides may originate from self-proteins including certain aberrantly expressed tumor antigens (**Section 1.4.2**) or entirely “foreign” proteins derived from extracellular as well as intracellular pathogens, whose capacity to elicit an immune response is commonly called “immunogenicity”. In the following chapter, key aspects of the antigen-presentation pathways will be shortly described, whose entire complexity, however, has been explained in more detail elsewhere including (1, 10, 11, 18).

Depending on the original source of the antigen, two major antigen-presentation pathways can be distinguished, which include two different proteolytic systems summarized in (**Fig. 1.3**). Cytosolic proteins of either cellular (“self”) or “foreign” origin are primarily presented by MHC-I molecules, whereas MHC-II molecules are destined to present exogenous antigens, which have been internalized predominantly by professional antigen-presenting cells (i.e. B cells, DCs and macrophages) through various mechanism including phagocytosis, macropinocytosis or receptor-mediated endocytosis (reviewed in (10, 11)). Yet, important exceptions to the basic antigen-presentation pathways exist including the presentation of exogenous antigens by MHC-I molecules – a process also termed cross-presentation (18) – as well as the presentation of cytosolic antigens via autophagy-related mechanisms on MHC-II molecules (19).

### 1.2.2.1 Classical MHC-I presentation pathway

**From cytosolic proteins to peptides** | Within the cytosol, aged folded proteins as well as defective ribosomal products (DRiPs, i.e. unfolded polypeptides, (20)) are primarily cleaved into peptide-fragments by the multi-protein 26S proteasome complex. The 26S proteasome complex (reviewed in (21)) comprises a barrel-shaped catalytic core (20S proteasome) that is capped at each end by an additional multi-subunit complex termed 19S cap. The 19S complex recognizes and unfolds ubiquitinated proteins in an ATP-dependent manner. Moreover, the 20S proteasomes can be bound by an alternative IFN- $\gamma$ -inducible 11S capping structure (PA28) that facilitates rapid ATP-independent proteolysis of unfolded peptides but not of folded proteins. The 20S core comprises seven distinct  $\alpha$ 1 to  $\alpha$ 7 as well as seven  $\beta$ 1 to  $\beta$ 7 subunits that form four stacked rings – two outer rings made out of  $\alpha$ -subunits and two inner rings made out of  $\beta$ -subunits. Among those subunits, the  $\beta$ 1,  $\beta$ 2 and  $\beta$ 5 units bear the proteolytic capacity to cleave peptide bonds. In addition, professional antigen-presenting cells constitutively express alternative  $\beta$ -subunits termed  $\beta$ 1i (LMP2),  $\beta$ 2i (MECL1) and  $\beta$ 5i (LMP7) that, when incorporated into the 20S proteasome, form the so-called immunoproteasome. Moreover, the immunoproteasome is also inducible by IFN- $\gamma$ -mediated signaling in non-professional APCs (21). Both “standard” and immunoproteasomes differ in their substrate preferences as well as peptide cleavage patterns, which overall lead to major changes in the immunopeptidome as shown by (22). For instance, the immunoproteasome displays a greater capacity to degrade misfolded proteins (23) and prefers to cleave more rapidly after hydrophobic and basic amino acid residues and less after acidic ones (24), which in particular might lead to preferentially suitable MHC-I peptide ligands (17, 25).

**Figure 1.3 | Classical MHC-I and -II antigen presentation pathways in a highly schematic view**



#### (a) MHC-I antigen presentation pathway.

Cytosolic proteins are degraded by the proteasome into peptide fragments and a fraction thereof is transported via the TAP complex into the endoplasmic reticulum (ER). Here, suitable peptides are loaded onto empty MHC-I complexes mediated by a multiprotein peptide-loading complex (PLC). Peptide-stabilized MHC-I are translocated through the Golgi to the plasma membrane (PM), where they are under CD8<sup>+</sup> T cell surveillance.

#### (b) MHC-II antigen presentation pathway.

Internalized exogenous proteins enter the endosomal-lysosomal vesicular system and are degraded within this compartments by a set of proteases. Nascent MHC-II molecules associate with an invariant chain (Ii) in the ER and are translocated to the late endosomes. Here, MHC-II associated Ii is cleaved, which leaves a peptide fragment (CLIP) bound to the MHC-II peptide-binding groove. Within endosome/lysosomal compartments exchange of CLIP by antigenic peptides is mediated and regulated by HLA-DM and HLA-DO. Peptide-exchanged MHC-II molecules traffic to the PM to present these peptides to CD4<sup>+</sup> T cells. Figure was adapted from (26) with permission.

**Peptide transport into the ER and association with MHC-I** | While the vast majority of cytosolic peptides are further destroyed by of different aminopeptidases and endopeptidases, only a small fraction (>0.1%) of short peptides (8–40 amino acids in length) are recognized and transported by the ATP-dependent transporter associated with antigen processing (TAP) into the endoplasmic reticulum (ER) (27, 28). TAP is heterodimeric complex composed of two subunits termed TAP1 and TAP2, which in turn associates with several other ER-located proteins to form the so-called MHC-I peptide-loading complex (PLC), that has been visualized by single-particle electron cryo-microscopy as a whole recently by (29). The PLC forms transiently within the ER lumen and orchestrates multiple functions including (i) peptide-translocation into the ER, (ii) editing and loading of these peptides onto receptive MHC-I molecules as well as (iii) proofreading (stability check) of peptide-MHC-I complexes. Prior to PLC formation, the nascent MHC-I heavy chain is initially stabilized by the chaperone BiP (Binding-immunoglobulin protein) and later calnexin, which is finally replaced by calreticulin upon association with  $\beta_2m$ . The heterodimeric peptide-receptive MHC-I complex is subsequently recruited to the PLC by calreticulin. The PLC is formed by a single TAP complex that associates with two pairs of tapasin, ERp57 and the calreticulin/MHC-I subcomplex. The via disulfide bridges covalently associated tapasin-ERp57 complex plays a central role for PLC stabilization as well as functions as peptide editor by catalyzing the exchange of low-affinity against high-affinity peptides of 8–10 amino acid length (30–32). Longer peptides that do not fulfill the MHC-I binding criteria are either N-terminally processed by the ER aminopeptidase 1 (ERAP1) and disulfide isomerase (PDI), or are rapidly transported back into the cytosol by the ER-associated degradation (ERAD) system for destruction. In case the peptide affinity is sufficiently high, the peptide-loaded MHC-I (pMHC-I) is released from the PLC and transported via the trans-Golgi network (TNG) to the cell surface (11).

#### 1.2.2.2 Classical MHC-II presentation pathway

**Internalization of exogenous proteins and lysosomal proteolysis** | Exogenous proteins are internalized by endocytosis either non-specifically via macropinocytosis, which is constitutively performed by DCs, or by various forms of receptor-mediated endocytosis triggered for instance by antigen-specific BCRs as well as Fc (“fragment crystallizable”) receptors for immunoglobulin G (Fc $\gamma$ R) expressed by B cells. After endocytosis exogenous proteins traffic through a vesicular pathway consisting of a progressively more acidic and proteolytically active compartments classically referred to as early endosomes (pH 6.5–6.8), late endosomes (pH 5.0–6.0) and lysosomes (pH 4.5) (33). Moreover, macrophages as well as conventional DCs can internalize larger particles (>3 $\mu$ m) including whole pathogens by phagocytosis resulting in so-called phagosomes. These phagosomes undergo fusion with lysosomes to form the proteolytically active phagolysosome. Within all these endocytic routes, a set of proteases called cathepsins degrade internalized proteins into peptide fragments under acidic conditions. These peptide fragments can subsequently encounter peptide-receptive MHC-II molecules throughout the endocytic pathway (as discussed below). The late endosome is typically considered as the main compartment for peptide-MHC-II formation. Following peptide binding, the pMHC-II molecules traffic to the plasma membrane ready for CD4<sup>+</sup> T cell surveillance (10).

**MHC class II assembly and transport to the late endosome** | Upon expression in the ER, MHC-II  $\alpha$ - and  $\beta$ -chains initially assemble as a complex with a membrane-associated chaperone protein of various isoforms termed invariant chain (Ii, CD74), which stabilizes and promotes the precursor MHC-II complex folding. Moreover, Ii marks the Ii-MHC-II complex to be translocated to the late endosomes via a cytoplasmic tail comprising two-leucine based sorting motives (34). Thus, Ii may direct Ii-MHC-II complexes to late endosomal compartments either directly from the TNG to the late endosome or firstly to the plasma membrane followed by clathrin-mediated endocytosis (10). Within the late

endosomal compartment often referred to as MHC class II compartment (MIIC), Ii is cleaved by cathepsin proteases that require an acidic environment. After cleavage a peptide fragment of ~20 residues remains within the MHC-binding groove, which has been termed accordingly the class II-associated Ii peptide (CLIP). CLIP must be released prior to loading of antigenic peptides derived from exogenous as well as endogenous sources. This process is catalyzed under mild acidic conditions (pH 5.5) by HLA-DM (35), which in addition has a similar peptide-editing function for MHC-II as tapasin for the MHC-I peptide loading process. HLA-DM mediates the replacement of bound low-affinity peptides leading to an accumulation of MHC-II complexes with high-affinity peptides (36, 37). The  $\alpha$ - and  $\beta$ -chains of HLA-DM are encoded by the MHC gene-cluster and the heterodimeric HLA-DM complex displays a very similar structural fold compared to classical MHC-II molecules, but lacks genetic polymorphism and an open or accessible peptide-binding groove. Moreover, another MHC class II-like protein, HLA-DO, is a known suppressor of HLA-DM activity in particular in naïve B cells and immature DCs, whereas HLA-DO is downmodulated upon DC-maturation as well as B cell activation, which has been suggested to be a mechanism that prevents presentation of self-antigens in steady state conditions (38).

### 1.2.3 Molecular clues required for T cell activation

The T cell receptor (TCR) is the defining receptor of a T cell, which confines the specificity of that particular T cell towards a certain peptide-loaded MHC complex. Upon interaction with an APC, T cells have to integrate generally three distinct signals provided by the cognate TCR/pMHC (signal 1) interaction, engagement of co-stimulatory (or co-inhibitory) receptors (signal 2) as well as activating or suppressing cytokine receptor signaling (signal 3). T cell activation that is characterized by the induction of T cell proliferation, differentiation and effector functions (i.e. cytokine production, migration, cytotoxicity of target cells) represents the net outcome of all three signals as summarized in **Fig. 1.4**. Whereas the cognate TCR/pMHC interaction (signal 1, antigen recognition) is the most crucial and decisive signal for the activation of any given T cell, the presence of signal 2 and 3 for T cell activation are more context and T cell differentiation-dependent. In particular upon initial encounter of an antigen-unexperienced naïve T cell with its cognate pMHC complex presented by a professional antigen-presenting cell – a phase referred to as T cell priming – that T cell becomes only fully activated in terms of cell proliferation and differentiation into mature effector/memory T cells, if all three signals are delivered (in more detail described in the following and in **Section 1.3**). But also beyond the priming phase, does the engagement of co-stimulatory or co-inhibitory receptors as well as of certain cytokines play a strong modulatory role for the activation of effector/memory T cells upon cognate antigen encounter. In the following a few molecular aspects of proximal T cell receptor signaling and co-receptor simulation leading to T cell activation will be introduced, which also have been reviewed in depth recently in (39–41).

#### **1.2.3.1 Structure of T cell receptor complex and early signaling events (signal 1)**

**TCR structure** | The heterodimeric  $\alpha\beta$  TCR is composed of membrane-spanning  $\alpha$ - and  $\beta$ -chains with a short C-terminal cytoplasmic tail that lacks inherent signaling capacity. The extracellular domains of the  $\alpha$ - and  $\beta$ -chain comprise an N-terminal variable (V) domain ( $V\alpha$  and  $V\beta$ ) followed by a constant ( $C\alpha$  and  $C\beta$ ) domain and membrane proximal short stalk segment that forms a disulfide bridge linking the  $\alpha$ - and  $\beta$ -chain.  $V\alpha$ ,  $V\beta$  and  $C\beta$  display a classical Ig-like fold, whereas  $C\alpha$  displays stronger deviations from the standard Ig-fold as described in (42). Moreover, the V-domains harbor the six (three per chain) hypervariable complementarity-determining regions (CDRs) that are formed through V(D)J-recombination during T cell development in the thymus. In particular the CDR3 regions (loops) display

the highest variability and mainly contacts the peptide residing in the MHC-binding groove, whereas the less variable CDR1 and CDR2 loops of the TCR mainly contact MHC residues. Thus, a given TCR typically recognizes the antigenic peptide as well as parts of the surrounding MHC binding groove as whole (1).

**TCR complex and early signaling events** | The TCR $\alpha\beta$  heterodimer associates non-covalently with multiple signal transduction molecules including CD3 $\gamma$ , CD3 $\delta$  and CD3 $\epsilon$  as well as CD3 $\zeta$  to a TCR complex of defined 1:1:1:1 stoichiometry comprising TCR $\alpha\beta$ :CD3 $\epsilon\gamma$ :CD3 $\epsilon\delta$  heterodimers and CD3 $\zeta\zeta$  homodimers as shown in (Fig. 1.4) and reviewed in (40, 43). The extracellular Ig-like domains of the heterodimeric membrane-spanning CD3 $\epsilon\gamma$  and  $\epsilon\delta$  subunits interact and flank the constant  $\alpha$ - and  $\beta$ -domains of the TCR and their intracellular cytoplasmic domains bears one immune-receptor-tyrosine-based-activation-motif (ITAM) each. The membrane-associated CD3 $\zeta\zeta$  homodimer lacks extracellular domains, while the cytoplasmic tail contains three tandem ITAMs resulting in ten ITAMs per single “octameric” TCR complex (43). Phosphorylation of the ITAM sequences by the tyrosine kinase LCK (Leukocyte-specific tyrosine kinase) links the TCR complex to multiple intracellular signal transduction pathways. LCK itself binds to the cytoplasmic domains of the CD4 and CD8 co-receptors and is recruited to the TCR complex by co-binding of CD8 or CD4 to pMHC-I or pMHC-II complexes, respectively.

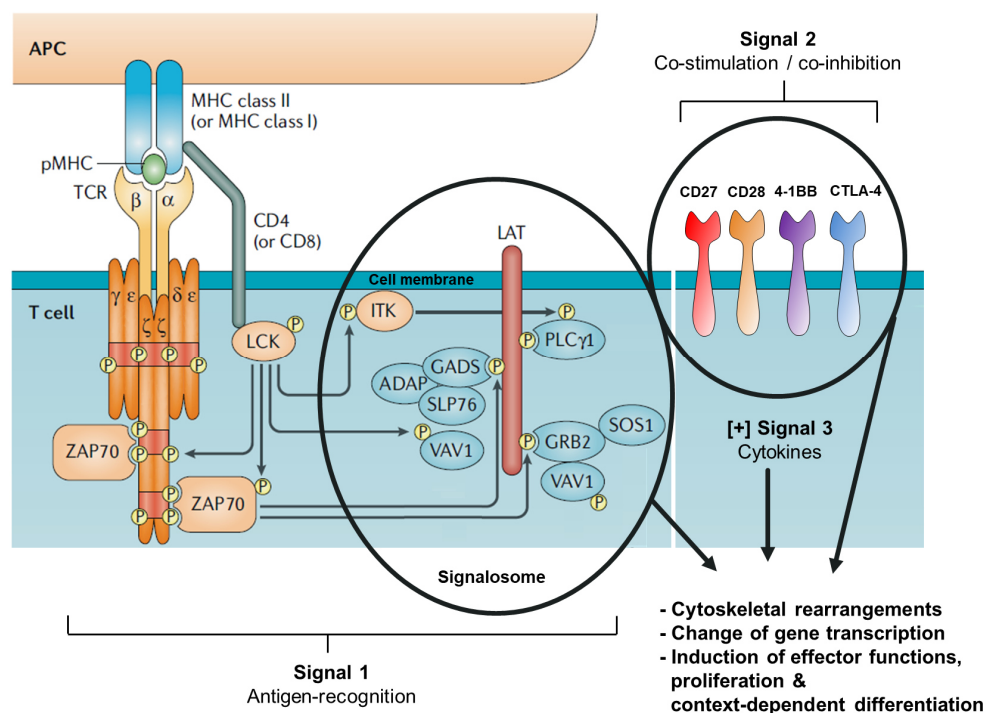


**Figure 1.4 | Overview of signals that drive T cell activation**

T cell receptor (TCR) complex-based signal transduction (signal 1) triggered through engagement of a cognate pMHC on the surface of an APC represents the most decisive event for a T cell. Signal 1 together with additional co-stimulatory and/or co-inhibitory receptor (signal 2) as well as cytokine receptor-derived signals (signal 3) converge into the decision of T cell activation associated with the induction of T cell proliferation, differentiation and effector functions. The figure provides a scheme of the TCR complex and selected intracellular effector molecules most notably kinases responsible for early signal propagation through phosphorylation (P) as partially explained in the main text and in depth by (39-43). Modified figure was adapted from (40) with permission.

## 1 | Introduction

Yet, the detailed molecular events that propagate the information of a cognate and stable TCR/pMHC interaction resulting in the initial phosphorylation of ITAMs by LCK remain even in 2020 highly debated (44), which has been described by several not mutually exclusive models as reviewed by (45). These models include the (i) conformational change of the TCR based on mechanical force, (ii) positioning and local concentration of ITAMs as well as (iii) the spatial reorganization of certain molecules within the T cell's plasma membrane upon TCR/pMHC interaction – most notably the steric exclusion of the membrane-associated phosphatase CD45.

Following initial ITAM phosphorylation of the TCR complex the ZAP70 tyrosine kinase (cytosol localized tyrosine-kinase zeta-activated protein of 70 kDa) is recruited via its SH2-domains to the TCR complex, where ZAP70 adopts an active conformation upon phosphorylation by LCK. As consequence, ZAP70 is able to phosphorylate the membrane-associated scaffolding adaptor termed LAT (Linker for Activation of T cells), which results in the generation of the so-called LAT signalosome by generating multiple docking sites for the recruitment of other adaptor proteins – most notably SLP76 (SH2-domain containing leukocyte protein of 76 kDa). Subsequent activation of LAT-associated signaling molecules most notably PLC- $\gamma$ 1 (phospholipase C- $\gamma$ 1) results in further signal propagation and amplification via three major signaling pathways: the Ca<sup>2+</sup>-calcineurin, MAPK (mitogen-activated protein kinase) and NF- $\kappa$ B (nuclear factor- $\kappa$ B) signaling pathway (in more detail illustrated in (1, 40)). These signaling events culminate in the activation and/or nuclear translocation of key transcription factors including NFAT (nuclear factor of activated T cells), NF- $\kappa$ B and AP-1 (activator protein 1) that act together to drive T cell proliferation, differentiation, migration as well as cytokine production (1, 40).

### 1.2.3.2 Role of co-stimulatory and co-inhibitory receptors during T cell activation (signal 2)

It is well known that antigen-naïve and -experienced T cells have different signaling requirements for full activation for reasons that are incompletely understood. For instance, an antigen-experienced cytotoxic CD8<sup>+</sup> T cell solely requires recognition of its cognate pMHC (signal 1) on a target APC to drive its effector function, while a naïve CD8<sup>+</sup> T cell is not activated solely upon encounter of its antigen but rather enter a hypo-responsive state termed T cell anergy (1). Thus, the parallel engagement of receptor-signaling that positively synergize with TCR signaling and avoid T cell anergy particularly of naïve T cells as well as further enhance T cell activation of antigen-experienced T cells are generally considered as co-stimulatory signals, and the responsible receptors as co-stimulatory receptors. On the contrary, a growing list of inhibitory acting receptors have been described that interfere with TCR signaling and thus dampen T cell responses as recently reviewed in (41, 46).

**Prototypic co-stimulatory receptors** | One of the most studied and prototypically co-stimulatory axis is the CD28/B7 interaction as reviewed in (47). The CD28 homodimer is expressed on the cell surface of ~ 80% of circulating human CD4<sup>+</sup> T cells as well as 50% of CD8<sup>+</sup> T cells and is the founding member of the immunoglobulin superfamily of co-stimulatory receptors. Upon engagement with its ligand B7-1 (CD80) or B7-2 (CD86) on APCs (i.e. mostly professional APCs), the short cytoplasmic tail of CD28 is phosphorylated by kinases of the Src family, which further downstream results in the recruitment and activation of PI3K (lipid kinase phosphatidylinositol 3-kinase). Activation of PI3K in turn leads the generation of the membrane-bound lipid PIP3 (phosphatidylinositol-3,4,5-trisphosphate) by phosphorylation of PIP2 (phosphatidylinositol-4,5-bisphosphate). PIP3 subsequently acts as recruiting signal for various downstream pleckstrin homology domain-containing kinases including the previously mentioned PLC- $\gamma$ 1 as well as PDK1 (phosphoinositide-dependent kinase 1) and its target AKT (protein kinase B). AKT acts as another signaling hub that culminates in the enhanced translocation of NF- $\kappa$ B as well as NFAT. Thus, CD28 stimulation results primarily in a quantitative support of T cell activation

resulting in an increased T cell survival and proliferation capacity, which is mediated most notably by an increased IL-2 expression. Beside the crucial requirement for naïve T cells priming, CD28 signaling also plays a vital role in the maintenance of antigen-experienced memory T cells (47). Moreover, other molecules belonging to the tumor necrosis factor receptor (TNFR) family such as OX40 (CD134) or 4-1BB (CD137) also provide co-stimulation upon engagement with their ligands OX40L and 4-1BBL, respectively. However, unlike CD28, which is constantly expressed on most resting T cells, OX40 and 4-1BB are upregulated after initial T cell activation (41, 46).

**Prototypic co-inhibitory receptors** | Besides co-stimulatory molecules also multiple inhibitory molecules have been described, which play an essential role in dampening an immune response and preventing autoimmune disorders. However, during cancer-progression T cell-inhibitory receptors, hereafter referred to as “checkpoints”, represent a major hurdle for an effective immune response against malignant cells. Thus, the blocking of inhibitory receptors is a central and successful approach in modern cancer immunotherapy (48), as introduced later in **Section 1.4**. The most prominent inhibitory molecules are CTLA-4/CD154 (cytotoxic T lymphocyte-associated protein 4) and PD-1 (programmed cell death protein-1). CTLA-4 is generally upregulated upon T cell activation as well as constantly expressed by so-called CD4<sup>+</sup> T regulatory cells and competes with higher affinity with the co-stimulatory receptor CD28 for binding to the same ligands B7-1 (CD80) and B7-2 (CD86). PD-1 in contrast is considered to be induced in T cells upon chronic antigen stimulation and reduced CD4<sup>+</sup> T cell-mediated help. PD-1 binds to its ligand PD-L1 (PD-ligand 1/B7-H1/CD274) as well as PD-L2 (B7-H2/CD273), which are expressed by activated T cells and are upregulated in peripheral tissues upon exposure to inflammatory cytokines such as IFN- $\gamma$ . Engagement of CTLA-4 as well as PD-1 results in the recruitment of tyrosine phosphatases such as SHP-2 (Src homology region 2 domain-containing tyrosine phosphatase-2), that switch off the TCR phosphorylation cascade and CD28-triggered PI3K/AKT pathways as reviewed in (48).

### **1.2.3.3 The role of inflammatory cytokines during T cell activation (signal 3)**

Signals provided by inflammatory cytokines that drive T cell differentiation and contribute to T cell survival and proliferation add up to the third layer (signal 3) of T cell activation as reviewed by (49). Particularly for naïve CD8<sup>+</sup> T cells it has been described that the presence of IL-12 and type I interferons (i.e. IFN- $\alpha$  and - $\beta$ ) is required to initiate full CD8<sup>+</sup> T cell differentiation into polyfunctional cytotoxic CD8<sup>+</sup> T cells (CTL) and the establishment of a long-lasting memory T cells pool upon antigen encounter. Both IL-12 and type I interferons are provided by mature DC upon engagement of PPRs such as TLRs or by CD40-dependent interaction with CD4<sup>+</sup> T helper cells (introduced in **Section 1.3.2**) (49), and, among other gene regulatory and chromatin remodeling functions, have been described to prolong the expression of the IL-2 receptor  $\alpha$ -chain (IL-2R  $\alpha$ -chain/CD25), which results in sustained cell division *in vivo* (50). Moreover, the cytokine environment at the time of antigen-encounter plays a pivotal role in determining the effector function of naïve CD4<sup>+</sup> T cell populations by differentially regulating key transcription factors involved their differentiation as further introduced in **Section 1.3.2**. In addition, a subset of multiple common  $\gamma$ -chain-dependent cytokines including IL-7, IL-15 and IL-21 provide supporting signals for the survival and persistence of antigen-experienced memory T cells (51).

### 1.2.3.4 The immunological synapse – The interface between T cell and APC

Upon productive and cognate TCR/pMHC interaction, T cells undergo rapid (< 10 min) rearrangements of the actin and microtubule cytoskeletal, vesicular system as well as membrane organization that form a highly polarized, structural, intercellular communication interface between the T cell and APC. This transiently stable interface or junction has been referred to as the immunological synapse (IS) – yet its detailed structural appearance as well as duration is highly depending on the intercellular context (professional APC vs. target APC), the T cell effector population (CD4<sup>+</sup> T cell vs. CD8<sup>+</sup> T cell) and their functional state (naïve vs. antigen-experienced T cell) as well as the experimental situation (*in vitro* vs. *in vivo*) (reviewed by (52–55)). The characteristic “bull’s-eye pattern” (symmetric) IS (shown in **Fig. 1.5a**) was initially described by Kupfer *et al.* for the interaction of a CD4<sup>+</sup> T cell with an antigen-presenting B cell, which comprises three concentric regions of differential molecular composition called supramolecular activation cluster (SMAC) (56). The central SMAC (cSMAC) contains a high concentration of TCR complexes as well as CD28 co-stimulatory receptors. The cSMAC in turn is surrounded by the cell adhesion molecules enriched peripheral SMAC (pSMAC), which most notably contains the integrin LFA-1 (lymphocyte function-associated antigen 1) and CD2. The pSMAC is encircled by the outermost CD45-enriched structure termed distal SMAC (dSMAC), which in addition comprises typically highly branched actin filaments that stabilizes the IS.

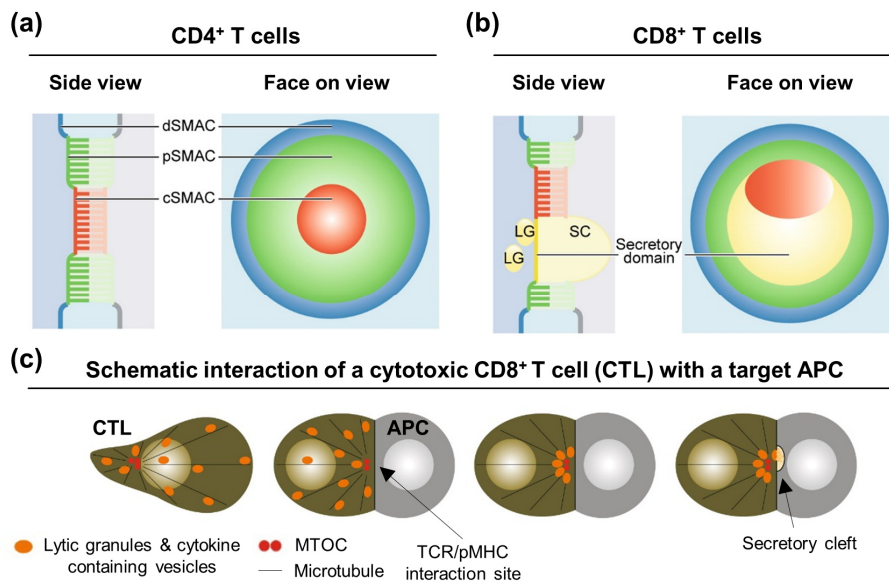


**Figure 1.5 | Scheme of a mature immunological T cell synapse and associated polarized effector molecule release**

Shown is a highly schematic organization of a mature immunological synapse (IS) formed by a CD4<sup>+</sup> T cell **(a)** or CD8<sup>+</sup> T cell **(b)** upon stable interaction with a cognate APC. The synapse is displayed either from the side view of a T cell interacting with an APC or from the face on view revealing the typical “bull’s eye” zone pattern. Distinct zones termed supramolecular activation clusters (SMAC) comprise a spatial organized set of surface receptors as well as cytosolic proteins. The central SMAC (cSMAC, red) is enriched for TCRs and co-signalling receptors (e.g. CD28; CTLA-4). The peripheral SMAC (pSMAC, green) comprise adhesion molecules (e.g. LFA-1; CD2) and the distal SMAC (dSMAC, blue) typically comprise a dense intracellular actin network as well as bulky molecules including CD45. **(b)** The IS formed by cytotoxic CD8<sup>+</sup> T cells (CTL) displays in addition a secretory domain (yellow) within the cSMAC that is devoid of TCRs but represents the site where lytic granules (LG) fuse with the T cell’s membrane and release their content into the secretory cleft (SC). **(c)** CTLs and also CD4<sup>+</sup> T cells (not shown) display massive cytoskeletal rearrangements upon target APC encounter leading to a polarized released of T cell subset-dependent effector molecules including granzymes, perforin and cytokines. In particular, a fast rearrangement of the microtubule-organizing center (MTOC) and its associated vesicular transport system from an initial perinuclear location in resting T cells towards the site of TCR/pMHC interaction in activated T cells has been observed. Modified figure was adapted from (64) with permission.

Initial structural description of the IS suggested that the cSMAC is the central signal-initiating and transducing structure. This, however, was revised more recently by findings that TCR signaling occurs rather in peripheral smaller TCR microclusters comprising multiple TCR complexes and associated signaling molecules including the LAT-associated signalosome (57). Thus, TCR microclusters are considered as “immature” IS signal-transducing substructures that are shortly sustained and then move inwards to form the cSMAC of a mature IS, which is facilitated by a bent contractile network of actin and myosin (58, 59). Thus, in a current view the cSMAC region is rather considered as signal regulatory hub, where on the one hand TCR complex signaling is terminated and TCR endocytosis occur and but on the other hand co-stimulatory (e.g. CD28) as well as co-inhibitory molecules (e.g. CTLA-4) accumulate as well. In addition, the accumulation of TCRs in the cSMAC as well as adhesion molecules in the pSMAC have been attributed to increase the cell adhesion between T cell and APC (52). *In vitro* co-culture experiments have shown, that a mature IS is formed within 5–30 minutes between antigen-experienced CD4<sup>+</sup> T cells and B cells as well as DCs after initial cell contact and can be stable maintained for several hours. Moreover, CD4<sup>+</sup> T cells rapidly polarizes their secretory machinery towards the IS, and in particular to that APC providing the strongest antigenic stimulus in case multiple APCs are present, which results in a polarized secretion of certain cytokines most notably IL-2 and IFN- $\gamma$  (60–62). In contrast, naïve CD4<sup>+</sup> T cells placed in a collagen matrix cell culture system interacted rather shortly and transiently with multiple antigen-presenting DC and did not form a stable synapse (63).

Mature synapses that are formed between antigen-experienced cytotoxic CD8<sup>+</sup> T cells and target APC can be further segregated into two functional domains, a TCR-enriched and a secretory domain (**Fig. 1.5b**). The secretory domain represents the structure, where cytotoxic granules containing perforin, granzymes as well as Fas ligand are secreted into a cleft between the T cell and consecrated target cell. This secretory cleft forms a small pocket between the cells and is sealed off from the external environment, ensuring that the concentration of lytic proteins remains high as they are released and preventing them from leaking out to the periphery (64, 65). Moreover, cytotoxic CD8<sup>+</sup> T cells have been attributed *in vitro* to form two distinct synapse modalities depending on the overall interaction with the APC and the antigen density termed lytic and stimulatory synapse. The lytic synapse that comprises the delivery of a lethal hit of cytotoxic granules towards the target cells forms rapidly and transiently within less than 6 minutes and seems to be fairly antigen-density independent *in vitro* (66, 67). For instance, pioneering work by Mark M. Davis and co-workers could show that as few as three pMHC-I per target cell where sufficient to induce their apoptosis by a CD8<sup>+</sup> T cell and that this process does not necessarily require the formation of a stable mature IS comprising the typical SMAC structures (67). In contrast, the stable and lasting formation of a stimulatory synapse occurs *in vitro* at higher antigen-densities, which displays sustained signaling and leads to the polarized secretion of cytokines towards the synapse even after annihilation and disintegration of the previously attached target cell (66, 68). This was partially contradicted by a recent study showing that cytotoxic CD8<sup>+</sup> T cells rather transiently and dynamically contact their target *in vivo* that is illustrated by sustained motility of the cytotoxic CD8<sup>+</sup> T cell on the target cell (69).

Nevertheless, independent of the modality of the IS (i.e. transient vs. stable) it has been shown for CD8<sup>+</sup> T cells as well as for CD4<sup>+</sup> T cells that TCR stimulation results in a rapid (< 2 min) polarized movement of the microtubule-organizing center (MTOC) towards the APC interaction site (60, 70), contributing to the formation of the IS and polarized release of effector molecules as schematically shown in (**Fig. 1.5c**) and described by (60–62, 66, 68), which in the herein presented study partially inspired the development of new assay platform for the detection of antigen-specific T cells.

### 1.3 The interplay of heterogeneous subsets of T cells and APCs

T cell-mediated immune responses typically begin in secondary lymphoid organs including lymph nodes, spleen and mucosa-associated lymphoid tissues when a naïve T cell encounters its cognate antigen (i.e. pMHC) presented by professional antigen-presenting cells (mostly dendritic cells) in the context of additional costimulatory signals as introduced in **Section 1.2**, resulting in antigen-dependent T cell proliferation and differentiation into effector T cells that then migrate to an effector site, which might be just the next lymph node in case of certain infections or distal organs. Here, short-lived effector T cells promote pathogen clearance as well as malignant cell eradication, as focused upon in **Section 1.4**, through production and release of effector cytokines and cytotoxic mediators. Moreover, a long-lived T cell pool defined as memory T cells persist that allow more rapid responses upon second antigen exposure (1).

In the following, further general principles required for the initiation of a T cell-mediated immune response and definitions of heterogeneous T cell subsets will be provided that in light of the presented study might allow for a better understanding.

#### 1.3.1 Dendritic cells – Unique and highly specialized professional antigen-presenting cells

Dendritic cells (DCs) are generally considered as most efficient professional antigen-presenting cells (pAPC) in particular because of their ability to activate (prime) naïve T cells recognizing pathogen or tumor antigens (described in **Section 1.4.2**). In the same breath DCs also prevent inappropriate T cell responses against self or environmental antigens typically defined as tolerance (71, 72). In the following four central DC aspects including their location, antigen-presentation machinery, maturation (activation) and functionally distinct cell subsets that uniquely steer T cell-mediated responses will shortly be introduced.

**DC location and antigen uptake** | In an immature state, non-activated, so-called migratory DCs are abundantly positioned at peripheral tissues in particular at potential “foreign” antigen encounter sites like beneath the skin or internal mucosal surfaces such as the respiratory and gastro-intestinal systems. Moreover, a fraction of DCs termed lymph node-resident DCs reside within the lymph nodes and continually enter from the blood circulation (around 1% of peripheral blood mononuclear cells are circulating DCs) (73, 74). Migratory as well as LN-resident immature DCs constantly take up antigens by various endocytic routes including phagocytosis, macropinocytosis as well as receptor-mediated endocytosis leading to MHC-II presentation, as previously introduced in **Section 1.2.2.2** and reviewed by (10). Moreover, a murine DC subset characterized by CD8 $\alpha$ , CD103 and XCR1 expression as well as basically all human DC subsets are able to cross-present exogenous antigens on MHC-I with different *in vitro* efficiencies (reviewed in (75)).

**DC maturation and migration** | The encounter of various environmental and endogenous danger signals that have the capacity to trigger pattern recognition receptors (PRR), most notably toll-like receptors (TLR), subsequently drive DC maturation (activation under inflammatory conditions). Mature DCs in turn have an increased expression of T cell co-stimulatory molecules including CD40, CD80 and CD86 as well as chemokine receptor CCR7, which allows mature DC unlike any other professional APC to migrate from peripheral tissues through the lymphatic system to a draining lymph node based on a constantly present CCL19 and CCL21 chemokine gradient (74). Within the lymph node mature DCs migrate to the T cell-rich zones and are capable to induce the clonal expansion of antigen-specific naïve T cells and also to drive their differentiation into effector T cells by context and DC subset depended

secretion of pro-inflammatory cytokines including IL-1 $\beta$ , IL-6, IL-12, IL-15, IL-23 and IFN- $\alpha$  (76). Moreover, mature DCs function as relay for CD4<sup>+</sup> T helper cells to promote the priming of naïve cytotoxic CD8<sup>+</sup> T cells (77) as introduced in the next section. Importantly, a fraction of DCs also undergo constitutive maturation in the absence of inflammatory signals, which has been referred to as “homoeostatic maturation”. These DCs also migrate to the lymph node but rather play an important role in mediating peripheral tolerance (72).

**Heterogenous pool of DC subsets** | DCs are a quite heterogeneous cell population comprising multiple specialized subtypes, which are currently defined by their developmental lineage (ontogeny) and who differ mostly in their localization, functional characteristics, morphology and transcriptional profile including the expression of surface markers, cytokines and transcription factors. Moreover, a certain functional homology of murine and human DC subsets exists – yet they display quite differential surface marker expression patterns as reviewed in detail by (73, 76). DCs are generally categorized by lineage into Langerhans cells (LC), conventional DCs (cDCs), plasmacytoid DCs (pDC) and DCs that differentiate from monocytes (Mo-DCs) due to tissue inflammation. cDCs are considered as most essential for mediating T cell responses against tumor diseases (as reviewed in (78)) due to their capacity to cross-present exogenous antigens on MHC-I and will be in brief focus here. Conventional DC are further divided (in both mice and humans) into two major subpopulations termed cDC1 and cDC2. Murine cDC1 have been typically characterized to have the highest intrinsic capacity to cross-present antigens to MHC-I and to activate naïve CD8<sup>+</sup> T cells as well as to promote CD4<sup>+</sup> T helper type 1 (Th1)-mediated responses through IL-12 secretion, whereas this feature is less restricted to the corresponding cDC1 lineage found in humans. Murine and human cDC1 uniquely express the chemokine receptor XCR1, which recruits cDC1 to XCL-producing activated T cells and thus supports close interaction of cDC1 and activated T cells (73, 75). Nevertheless, also human cDC2 who display a broader range of pattern recognition receptors compared to cDC1 have been shown to be potent drivers of CD4<sup>+</sup> Th1, Th2, Th17 cell as well as CD8<sup>+</sup> T cell responses. Thus, the exact division of labor between cDC1 and cDC2 in particular *in vivo* is less clear. Current research indicates a prominent role for cDC2 in priming and steering CD4<sup>+</sup> T cell helper responses (73, 77). Likewise the *in vivo* function of human monocyte-derived dendritic cells that expand upon tissue inflammation is less clear. Nevertheless, human monocytes that have been *ex vivo* differentiated into Mo-DCs upon *in vitro* culture with IL-4 and GM-CSF (granulocyte macrophage colony-stimulating factor) have been extensively investigated and partially combine features of cDC1 and cDC2 (76). Moreover, Mo-DCs that have been feed with antigen as well as matured by various stimuli including lipopolysaccharide (LPS) are frequently used to activate and expand *in vitro* antigen-specific naïve as well as memory CD4<sup>+</sup> and CD8<sup>+</sup> T cells and represent a corner stone of dendritic cell-based vaccines within the cancer immunotherapy field (79, 80).

### 1.3.2 CD4<sup>+</sup> T cells – Essential helpers and regulators of adaptive immune responses

CD4<sup>+</sup> T cells play a versatile and essential role in shaping adaptive and local innate immune responses through their secretion of defined sets of cytokines as well as by cell-cell contacts providing stimulatory or inhibitory signals for the interacting partner cell. Upon antigen-specific encounter of a professional antigen-presenting cell (pAPC), most importantly DCs and B cells, naïve CD4<sup>+</sup> T cells differentiate into specific effector subtypes depending on the cytokines present in the microenvironment as well as on the concentration of presented antigens, type of the pAPC and their expression of costimulatory molecules.

**Heterogenous CD4<sup>+</sup> T cell helper subsets** | Functionally distinct CD4<sup>+</sup> T cell differentiation profiles comprise the T helper 1 (Th1), Th2, Th17 and induced T regulatory (iTreg) subsets, which are induced by different cytokine signals that in turn drive the expression of certain fate-determining master transcription factors shown in **Table 1.1** and in depth reviewed by (81). In addition, several other subtypes have been described including Th9, regulatory type 1 (Tr1) and follicular helper T cells (Tfh), the latter being crucial for the development of germinal centers that is the primary site of B cell affinity maturation (82). Notably, the majority of CD4<sup>+</sup> T cells subsets display a certain plasticity and can be converted from one subset into another one depending on the overall cytokine context and differentiation stage (81). Beside naïve T cells that differentiate upon antigen-encounter, also a small fraction so-called natural regulatory T cells (nTreg) (< 4% in human peripheral blood) arise as an already distinct subpopulation during T cell development in the thymus, which similar to iTregs are characterized and maintained by the expression of the transcription factor FOXP3 (forkhead box P3) (83). The variety of CD4<sup>+</sup> T cell subsets orchestrate diverse effector functions mainly through secreting cytokines that activate and/or recruit other effector cells (**Table 1.1**). In addition also direct cytolytic activity of CD4<sup>+</sup> T helper cells have been observed in certain tumor contexts as shown by (84), that might contribute to tumor control (85) in particular if cytotoxic CD8<sup>+</sup> T cell-mediated responses are impaired as reviewed by (86).

**Table 1.1 | CD4<sup>+</sup> T cell subsets – Inducing extrinsic cytokines and secreted effector cytokines**

CD4 <sup>+</sup> T cell subset:	Th1	Th2	Th17	iTreg
Fate inducing cytokines:	IL-12, IFN- $\gamma$	IL-4, IL-2	TGF- $\beta$ , IL-1 $\beta$ , IL-6, IL-21, IL-23	TGF- $\beta$ , IL-2
Master transcription factor:	T-bet	GATA3	ROR $\gamma$ t	FOXP3
Secreted effector cytokines:	IFN- $\gamma$ , TNF- $\alpha$	IL-4, IL-5, IL-13 (IL-10)	IL-17a, IL-17f IL-21, IL-22	TGF- $\beta$ , IL-10 IL-35

Reference: (81)

Th1-differentiated CD4<sup>+</sup> T cells play a particular role in mediating immune responses against intracellular pathogens as well as tumor cells by secreting predominantly IFN- $\gamma$ , TNF- $\alpha$ , lymphotoxin- $\alpha$  and IL-2. Among multiple other functions, IFN- $\gamma$  and TNF- $\alpha$  (for more details see **Section 1.3.3**) activate macrophages and increase their microbicidal activity (87). Th2 cells on the contrary are strong mediators of immune responses against extracellular parasites, including notably helminths, by promoting humoral immune responses. A typically described effector mechanism of Th2 cells is the antibody class switching in activated B cells from IgM and IgD to IgG and IgE mediated by Th2 cell-secreted IL-4 and IL-5. IgE class switching in B cells steers responses of mast cells and basophils against IgE-bound target cells. Moreover, Th2 typically secrete IL-5 and IL-13, where IL-5 for instance recruits eosinophils to attack parasites. Th17 cells are predominantly characterized by their secretion of IL-17a and IL-17f, which in turn recruits and active neutrophils during immune responses against extracellular bacteria and fungi. nTreg as well as iTreg play a critical role in maintaining self-tolerance as well as in regulating/suppressing immune responses. Tregs pursue their mainly suppressive function through several mechanisms as reviewed by (88, 89). Tregs in particular secrete inhibitory cytokines including transforming growth factor- $\beta$  (TGF- $\beta$ ), IL-10 and IL-35, that directly block the effector functions of NK cells and other effector T cells including cytotoxic CD8<sup>+</sup> T cells, and furthermore drives DCs towards a tolerogenic / T cell non-activating DC phenotype, which contradicts the CD4<sup>+</sup> T cell helping function relevant for CD8<sup>+</sup> T cell activation as discussed further below. The latter is additionally mediated by the high expression of inhibitory-receptors like CTLA-4 and LAG-3 (lymphocyte activation gene 3 protein)

by Tregs. Last but not least, direct cytolysis of mature DCs by activated Tregs in an perforin- and granzyme-dependent manner represents another immunosuppressive mechanism (88, 89).

**CD4<sup>+</sup> T cells as essential helpers for inducing CD8<sup>+</sup> T cell responses** | Aside from the functions mentioned above, CD4<sup>+</sup> T helper cells (non-regulatory lineage) play a pivotal “helping” role in initiating a cytotoxic CD8<sup>+</sup> T cells (CTL) response by providing complementary stimulatory signals to a maturing DC in an antigen-specific manner, a phenomenon also called “DC licensing” (reviewed in (77)). The licensed DC passes on the stimulatory signals to an antigen-specific CD8<sup>+</sup> T cell interacting with the same DC to promote its activation as shown in (Fig. 1.6). Thus, a DC can be considered as a signaling relay that transmits activating signals from a CD4<sup>+</sup> T cells to CD8<sup>+</sup> T cells. When a CD4<sup>+</sup> T helper cell recognizes its cognate antigen on a DC, the CD4<sup>+</sup> T helper cell upregulates CD40L (CD154), which in turn triggers CD40 expression by pre-activated/maturing DC – most predominantly cDC1. CD40 signaling in turn provides additional maturation signals for the DC and leads to further upregulation of costimulatory molecules on the DC, most notably CD80 (B7-1), CD86 (B7-2) and CD70 (CD27L). Moreover, upon CD4<sup>+</sup> T cell interaction that particular DC also increases IL-12 and IL-15 secretion. The combined co-stimulatory signals provided by the engagement of CD27 and CD28 expressed by the interacting CD8<sup>+</sup> T cell as well as by IL-12, IL-15 and type I interferons (IFN- $\alpha$  and IFN- $\beta$ ) support their clonal expansion as well as differentiation into a cytotoxic CD8<sup>+</sup> T cells effector pool and establishment of a long-lived memory T cell pool. This helping role of CD4<sup>+</sup> T cells was shown to be particularly relevant for exogenous antigens that are cross-presented to CTL, which for instance holds true for responses against cancer cell antigens or vaccines based on cell fragments, larger proteins (cell lysate) or longer peptides (77). Taken together, every CD4<sup>+</sup> T cells subtype plays a particular role for the clearance of pathogens, maintaining tolerance against “self” and eradication of malignant cells – yet abnormal activation of Th1 and Th17 may lead to the induction of autoimmune diseases or in case of Th2 cells to allergy. Moreover, a strong increase of Treg within an established tumor contributes to immune suppression and favors tumor progression as introduced in more detail in **Section 1.4**.

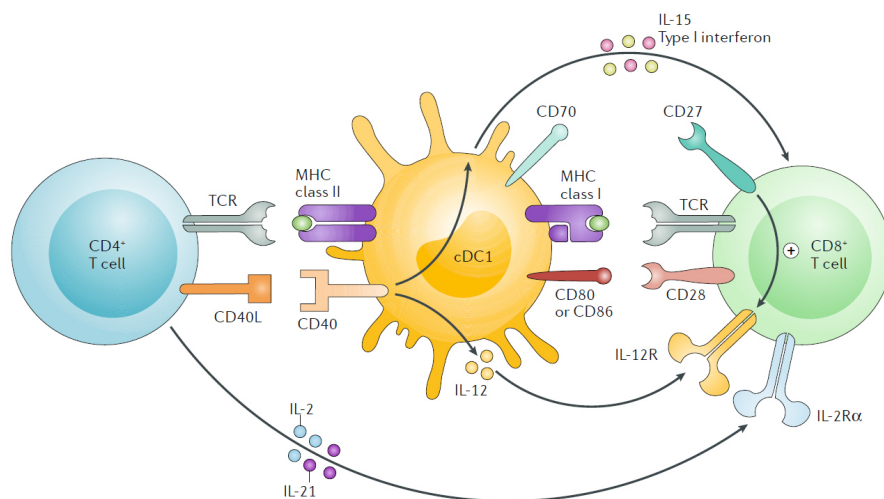


**Figure 1.6 | The helping feature of CD4<sup>+</sup> T cells for the priming of naïve CD8<sup>+</sup> T cells**

The antigen-specific interaction of cognate CD4<sup>+</sup> T helper cell (Th) with a matured cDC1 results in CD40L up-regulation of the Th cell. Subsequent CD40L-driven triggering of CD40 expressed by the matured DC results in further increased expression of cell surface co-stimulatory ligands including CD70, CD80, CD86 and secretion of cytokines including IL-12, IL-15 and IFN- $\alpha/\beta$ , which in turn support the activation and differentiation of a naïve CD8<sup>+</sup> T cells into cytotoxic effector T cells interacting in parallel with the same DC. CD70/CD27 signaling also upregulates IL-2, IL-2R $\alpha$  and IL-12R expression of the CD8<sup>+</sup> T cell. Moreover, secretion of IL-2 and IL-21 by the activated Th cell further supports the survival and differentiation of the interacting CD8<sup>+</sup> T cell. IL-12R: IL-12 receptor; IL-2R $\alpha$ : high-affinity IL-2 receptor  $\alpha$ -chain (CD25). Figure was adapted from (77) with permission.

### 1.3.3 CD8<sup>+</sup> T cells – Highly trained and precise cell killers

The successful priming of naïve CD8<sup>+</sup> T cell within secondary lymphoid organs is accompanied by profound changes in their migration capacity, overall gene expression profile and metabolism, which leads to the acquisition of effector functions (reviewed by (55, 90, 91)). Unlike CD4<sup>+</sup> T cells, antigen-experienced CD8<sup>+</sup> T cells are typically not subdivided into subsets that fulfill completely distinct functions and are usually considered as cytotoxic T cells (CTL). Nevertheless, the entire pool of CTL as well as the individual CD4<sup>+</sup> T cell subtypes display a heterogeneity with regard to their proliferation and effector function capacities as well as migration patterns and resulting tissue distributions, which is usually summarized as memory differentiation profile and will be discussed briefly in the next section and has been reviewed in depth by (91, 92).

**Overview of CTL effector functions |** A key effector function of CTL is the antigen-dependent and cell-to-cell contact-mediated cytolysis of most notably virus-infected and malignant cells that display the cognate peptide antigen on MHC-I, which are within this study also often considered as target APC. Thus, CTL can not only contribute to the clearance of infections but also to the eradication of cancer (2). Upon TCR-triggering, the CTL releases perforin and granzymes stored in cytotoxic granules in a polarized manner towards the target cell and thus spares adjacent bystander cells (reviewed by (64) and introduced in **Section 1.2.3.4**). Subsequently, perforin mediates the delivery of granzymes into the target cell leading to the induction of apoptosis. Moreover, activated CTL also translocate membrane-bound Fas ligand (FasL/CD178) to the cell surface, which upon binding to the Fas receptor (Fas/CD95) expressed by some target cells including cancer cells, can also induce apoptosis in a context dependent manner, which has been intensively shown in various *in vitro* experiments. Yet the physiological role of the CD95/CD95L pathway for cancer eradication *in vivo* is less clear, since tumors are often resistant to CD95-mediated apoptosis induction. However, CD95 is also strongly expressed by T cells upon activation suggesting a crucial role of the CD95/CD95L pathway to self-limit acute T cell responses (reviewed in (93)). In addition, CTLs that encounter their target cell may start the production and secretion of soluble cytokines including IFN- $\gamma$ , TNF- $\alpha$  and IL-2. In particular IFN- $\gamma$  and TNF- $\alpha$ , which are also expressed by activated Th1-differentiated CD4<sup>+</sup> T cells and NK cells, orchestrate multiple immunostimulatory effects. IFN- $\gamma$  mediated signaling, initially described to directly inhibit viral replication among multiple other effects, also induces the upregulation of (i) MHC-I and MHC-II, (ii) the associated antigen presentation machinery of MHC-I as well as (iii) the activation of macrophages (together with TNF- $\alpha$ ) and (iv) limits Treg, Th2 and Th17 differentiation and function (reviewed in (94)). Likewise TNF- $\alpha$  exerts quite versatile activities depending on binding to, and activation of, two distinct receptors termed TNF receptor 1 (TNFR1) and TNFR2 as reviewed in detail by (95). Initially, TNF- $\alpha$  was discovered to induce necrosis in the tumor microenvironment (96) – yet the picture is more complex since TNFR1 and TNFR2 signaling, depending on the cellular context, may either induce apoptosis or cell proliferation as well as drive the secretion of other inflammatory cytokines (95). Thus, TNF- $\alpha$  is typically considered to play a dual context-dependent role in cancer. During early cancer development TNF- $\alpha$  rather promotes tumor progression by contributing to a chronic inflammatory environment, whereas in late cancer stages it rather contributes to tumor elimination in particular by effecting the tumor vasculature and contradicting immune suppression (reviewed in (2, 97)).

### 1.3.3.1 Dynamics of a CD8<sup>+</sup> T cell response and CD8<sup>+</sup> T cell memory differentiation

**The dynamics of CD8<sup>+</sup> T cell responses** in particular against viral infections has been extensively studied in murine infection models as well as in cohorts of human volunteers receiving virus vaccination (98, 99). CD8<sup>+</sup> T cell responses are characterized by three distinct phases in both humans and mice: First naïve pathogen-specific T cells undergo massive clonal expansion upon successful priming and predominantly differentiate into short-lived effector T cells that further migrate from secondary lymphoid organs to the site of infection and mediate clearance of infection (expansion phase). As second step the majority (up to 95%) of the antigen-specific effector T cell pool is going into apoptosis shortly after viral clearance (contraction phase), whereas a small fraction of these initial primed pathogen-specific T cells persists as a heterogenic pool of long-term memory T cells that protect against subsequent pathogen encounter (memory phase). Memory T cells downregulate their effector program and rather acquire a stem cell-like ability to survive independently of constant antigen exposure and undergo slow homeostatic self-renewal driven by IL-7 and IL-15. Memory T cells can exert rapid effector functions in response to previously encountered antigens (reviewed in (98, 100)).

**Heterogeneous pool of memory T cells** | Currently the generation of the heterogenic pool of memory T cell subsets, which applies to CD8<sup>+</sup> as well as CD4<sup>+</sup> T cells, is mostly explained by the linear progressive differentiation model. This model suggests that the fate of an antigen-experienced T-cell predominantly depends on the immunomodulatory signals that the T cell successively receives throughout the priming phase and initial antigen encounter. The combinatory signal out of antigen presentation (signal 1), co-stimulation (signal 2) and local inflammatory micro-milieu (signal 3) pushes the antigen-primed naïve T cells (T<sub>N</sub>) towards progressive stages of differentiation starting from stem cell-like memory T cells (T<sub>SCM</sub>) to central memory T cells (T<sub>CM</sub>) to effector memory T cells (T<sub>EM</sub>), and finally into the accumulation of short-lived and terminally differentiated effector T cells (T<sub>Eff</sub>) (**Fig. 1.7**). Low-grade antigenic and inflammatory stimuli during infection would rather favor the maintenance of a less differentiated cells like T<sub>SCM</sub> and *vice versa* (91, 92, 100).

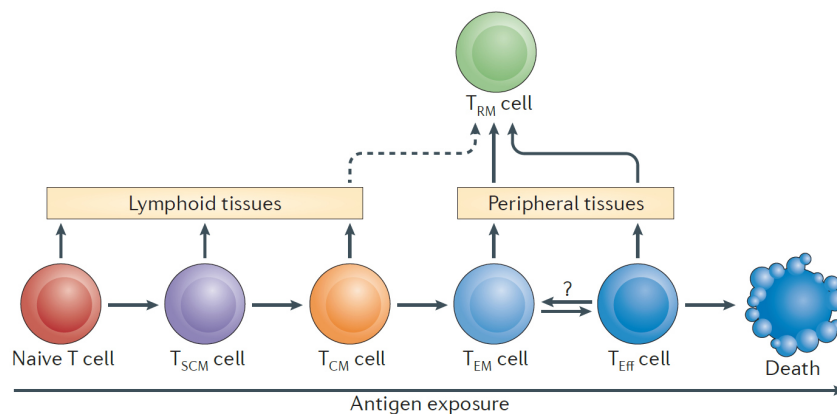


**Figure 1.7 | Linear progressive T cell differentiation model**

Upon priming of a naïve T cell by a professional antigen-presenting cell, the proliferating antigen-experienced T cell processes along a differentiation pathway depending on the overall antigen exposure and other co-stimulatory signals that finally culminates in the generation of terminally differentiated short-lived effector T cell pool (T<sub>Eff</sub>). Decreasing stimuli may keep the primed T cell within three major circulating memory subsets comprising stem cell-like memory T cells (T<sub>SCM</sub>), central memory T cells (T<sub>CM</sub>) and effector memory T cells (T<sub>EM</sub>). Naïve T cells, T<sub>SCM</sub> and T<sub>CM</sub> cells circulate and migrate to lymphoid tissues, whereas T<sub>EM</sub> and T<sub>Eff</sub> have the capacity to traffic and circulate between peripheral tissues. In contrast, tissue-resident memory T cells (T<sub>RM</sub>) do not circulate and reside within specific peripheral tissues to provide local immunity. The origin and development of T<sub>RM</sub> differentiated T cells is currently under investigation. Figure was adapted from (91) with permission.

## 1 | Introduction

Each individual memory subset displays a differential capacity to self-renew and to exert effector functions including cytotoxicity as well as the secretion of cytokines and can be distinguished by differential surface marker expression as reviewed by (100). Human naïve T cells ( $T_N$ ) are conventionally defined by the co-expression of the RA isoform of the transmembrane phosphatase CD45 (CD45RA) as well as the lymph node homing molecules L-selectin (CD62L) as well as CCR7 and the co-stimulatory receptors CD27 and CD28. Upon antigen encounter a rare fraction of cells appear as  $T_{SCM}$  cells within lymph nodes and other secondary lymphoid organs, which apparently have a naïve phenotype but in contrast to naïve T cells also upregulate the common IL-2 and IL-15 receptor  $\beta$ -chain (CD122) and CD95, as all antigen-experienced T cells in humans do (101).  $T_{SCM}$  cells display the highest proliferative and survival capacity and are considered to be multipotent since  $T_{SCM}$  can give rise to the whole spectrum of memory cells and terminal differentiated effector cells but mostly lack effector. Next in line are  $T_{CM}$  cells who lack the expression of CD45RA but instead express the alternative mRNA-spliced CD45RO isoform. Similar to  $T_N$  also antigen-experienced  $T_{CM}$  constantly circulate through secondary lymphoid organs for antigen scanning and maintain the expression of CD62L and CCR7. In contrast  $T_{EM}$  who lack the expression of CD62L and CCR7 ( $CD45RO^+$ ,  $CCR7^-$ ) rather patrol peripheral tissues and represent the major T cell population found in peripheral blood in middle-aged human adults. Among  $CD8^+$  T cells, the  $T_{EM}$ -differentiated population displays in general a higher relative proportion of cells that secrete IFN- $\gamma$  and/or TNF- $\alpha$  and a reduced fraction of cells that secrete IL-2 compared to  $T_{CM}$  cells (92, 100). In addition,  $T_{EM}$  can be further subdivided based on their expression of CD27 and CD28, where lack of CD27 and/or CD28 is associated with a reduced proliferative capacity (102, 103). Moreover, in humans and in particular among  $CD8^+$  T cells a terminally differentiated memory population can be found that re-expresses CD45RA but lacks CCR7 as well as CD45RO expression. This memory population designate as  $T_{EMRA}$  displays a high capacity for IFN- $\gamma$  production but only a low proliferative capacity and their frequency seem to increase with human age (92). Last but not least, a rather newly discovered memory subset designated as tissue-resident memory T cells ( $T_{RM}$ ) has been identified in mice and humans that may derive from  $T_{EM}$  cells and apparently play a pivotal role in mediating long-term local tissue-specific protection (reviewed by (104)). However, unlike  $T_{EM}$  and  $T_{CM}$ ,  $T_{RM}$  cells do not circulate but permanently reside in specific peripheral tissues including the lung, skin and intestine after the infection is already cleared. Regarding surface marker expression,  $T_{RM}$  cells resemble mostly  $T_{EM}$  cells but are prototypically defined by the constant expression of the early T cell activation marker CD69 as well a tissue-dependent (in humans) expression of CD103 (epithelial cell-binding  $\alpha E\beta 7$  integrin) (104).

### 1.3.3.2 $CD8^+$ T cell exhaustion as a consequence of chronic viral infections or cancer

In cases where the host's immune response fails to eradicate infections and malignant cells, the persistence of antigens and multiple other factors may drive antigen-specific  $CD8^+$  T cells into a heterogeneous differentiation state generally termed as T cell exhaustion ( $T_{EX}$ ), which is distinct from naïve, effector and memory  $CD8^+$  T cells as reviewed by (105, 106).

Although T cell exhaustion has been described for both  $CD4^+$  T cells and  $CD8^+$  T cells in murine models of chronic lymphocytic choriomeningitis virus (LCMV) infection (107, 108), exhausted  $CD8^+$  T cells are frequently observed in human chronic viral infections, including but not limited to human immunodeficiency virus (HIV), hepatitis C virus (HCV) and hepatitis B virus (HBV) (105). Moreover, it is well established that T cell exhaustion inhibits immune responses in human cancers including melanoma, chronic myeloid leukaemia, ovarian cancer and non-small cell lung carcinoma (105). On the contrary, induction of T cell exhaustion rather favors a better prognosis during multiple autoimmune diseases (109).

T<sub>EX</sub> cells typically display a progressive and hierarchical loss of effector functions. These include loss of cytokine production starting with IL-2 followed by TNF- $\alpha$  and finally IFN- $\gamma$ , where loss of IFN- $\gamma$  usually defines terminally and severely exhausted T cells. Moreover, a key hallmark of T<sub>EX</sub> cells is the increased and sustained expression of multiple inhibitory co-receptors including PD-1 (programmed cell death protein 1), LAG-3 (lymphocyte activation gene-3), TIM-3 (T cell immunoglobulin and mucin domain-containing-3), and TIGIT (T cell immunoreceptor with immunoglobulin and ITIM domains), which are only transiently expressed during acute infections by T<sub>Eff</sub> upon activation and only at low levels, if any, expressed by resting memory T cells. Thus, therapeutic targeting of T<sub>EX</sub> to reinvigorate their effector function by blocking inhibitory receptor signaling by antibodies (referred to as immune checkpoint blockers) are a key concept in cancer immunotherapy (110). In addition, T<sub>EX</sub> are unable to undergo IL-7- and IL-15-mediated homeostatic proliferation due to defects in various cytokine-receptor signaling pathways and rely on constant antigen encounter for proliferation as well as display almost unique transcriptional and epigenetic signatures and an altered metabolic fitness. The pathways that drive the development of T cell exhaustion remain poorly understood. However, persistence of high levels of antigen, sustained signals received by inhibitory receptors and the presence of inhibitory cytokines including IL-10 and TGF- $\beta$  derived from various sources including CD4<sup>+</sup> Tregs and activated CD8<sup>+</sup> T cells are considered as main drivers for T cell exhaustion (105, 106).

## **1.4 Tumor-specific T cells – Central agents for cancer immunotherapy**

### 1.4.1 From cancer immunosurveillance to cancer immunotherapy

**Cancer immunosurveillance** | The multistep transformation process of a normal healthy body cell into a cancerous cell that ultimately may give rise to the formation of a heterogeneous malignant tumor cell mass is fueled and accompanied by a series of genetic alterations caused by environmental and/or inherited factors (reviewed in (111)). By the same token, these genetic and associated cellular alternations represent the foundation to elicit innate as well as adaptive immune responses against malignant cells that may result in their direct elimination, which is also considered as “cancer immunosurveillance”. Here, the innate effector arm of the immune system such as NK cells and macrophages plays a pivotal role. However, a fundamental aspect of cancer immunosurveillance is that malignant cells may express a variety of collectively termed “tumor antigens” (as further introduced in **Section 1.4.2**) that distinguish them from non-transformed healthy cells and allow tumor-specific adaptive immune responses to occur (reviewed in (2, 112)). In the following we focus in particular on tumor-specific T cell mediated responses. Although naturally occurring antibodies against tumor antigens have been frequently found in the serum of cancer patients, the role of humoral responses in tumor immunity remains controversially discussed and poorly understood (reviewed in (113)).

**Cancer immunoediting** | Failure of the initial and fast clearance of malignant cells may result in a complex, long-lasting and dynamic interplay within the arising tumor microenvironment comprising immune cells, cancer cells and surrounding stroma cells (e.g. fibroblasts and endothelial cells in cases of solid tumors), which is currently described by a conceptual framework termed “cancer immunoediting” as initially proposed by Robert D. Schreiber and colleagues (reviewed in (2, 112)). The cancer immunoediting concept as shown by multiple murine tumor models places the net outcome of the immune response into three distinct phases termed elimination, equilibrium and escape. The elimination phase in its essence equals cancer immunosurveillance where innate and adaptive immunity may destroy developing tumors long before they become clinically apparent.

However, certain cancer cells may not be destroyed and enter the equilibrium phase. Here, in particular the T cell-mediated responses prevent and control further tumor growth over a long-lasting period. Consequently, the constant immune cell-mediated selection pressure may lead to a “shaping / editing” of the genetically unstable heterogeneous pool of cancer cells that lead to the emergence of cancer cells capable of entering the escape phase due to a variety of evasion mechanism, which finally leads to a clinically apparent tumor outgrowth. On the cancer cell level these evasion mechanisms may include most notably, the emergence of cancer cells that lost the expression of highly immunogenic antigens or essential components of the antigen processing and presentation machinery. In addition, cancer cells may promote a highly immunosuppressive tumor microenvironment that favors negative regulators of immune activation such as recruitment and induction of CD4<sup>+</sup> Treg cells and myeloid-derived suppressor cells (MDCS) and as well as the constant engagement of inhibitory receptors and their ligands (i.e. “immune checkpoints” such as PD-1 / PD-L1, CTLA-4) by effector T cells leading to their exhaustion (as discussed in the previous **Section 1.3.3.2**) (2, 112). In accordance, high amounts of infiltrating effector T cells including cytotoxic CD8<sup>+</sup> T cells and Th1-differentiated CD4<sup>+</sup> T cells into human tumors and a rather low abundance of regulatory immune cells have been consistently associated with improved disease outcome and *vice versa* (i.e. better overall survival, lower incidence of tumor recurrence and prolonged disease-free survival) (reviewed in (114)).

**Cancer immunotherapy** | Consequently, a variety of cancer immunotherapeutic interventions have been developed and are currently developed that ultimately may aim at (but are not limited to) (i) overcoming immune regulatory mechanism that block preexisting immunity, (ii) fostering novel endogenous tumor-specific T cell responses, or (iii) provide additional exogenous T cell support (115).

One of the earlier and quite successful therapeutic strategies as pioneered by the group of Steve A. Rosenberg comprise the *ex vivo* expansion and re-administration of autologous tumor-infiltrating lymphocytes (TIL) isolated from tumor specimen of metastatic melanoma patients. This so-called TIL-based adoptive T cell transfer (ACT) approach led to tumor regression in multiple cases and provided strong evidence that T cells are present in the tumor capable of recognizing cancer cells (reviewed in (116)). Other modalities of cancer immunotherapy for various solid tumors include most notably clinical approved immune checkpoint blocking (ICB) monoclonal antibodies targeting PD-1, PD-L1 or CTLA-4 (reviewed in (110)) and autologous T cells engineered to express a CD19-targeting chimeric antigen receptor (CAR) for several B cell-derived malignancies (reviewed in (117)). Moreover, ever since the discovery of selected tumor antigens it has been a major goal to manufacture therapeutic vaccines to boost endogenous T cell responses. However, many therapeutic cancer vaccine approaches used in the past lacked clinical efficacy due to the limited number of highly immunogenic and tumor-specific antigens as well as effective delivery systems (118). But with the advent of next-generation sequencing technologies (NGS) it is becoming more feasible to screen patient-derived tumor samples for the expression of unique mutation-derived antigens referred to as neoantigens, whose potential of serving as ideal targets for manufacturing of highly immunogenic, personalized and effective vaccines or TCR-engineered autologous T cells is currently highly investigated by multiple research groups (further discussed below) and reviewed recently in (119). In a final aspect also radiotherapy and conventional chemotherapy induce the release of tumor antigens and danger signals that ultimately may promote T cell priming and help to modulate immune suppression. Therefore, radiotherapy and chemotherapy may be also considered as indirect immunotherapy approaches that often display synergistic effects in combination with other immunotherapy modalities such as ICB (reviewed in (120)).

## 1.4.2 Tumor antigens – Cornerstones for multiple cancer immunotherapy approaches

**The ideal target antigen** | The identification and validation of a tumor antigen are the most critical aspects with respect to designing an effective and safe therapeutic cancer vaccine, or for the screening of cognate TCRs suitable for engineering an adoptive T cell transfer cell product. An ideal target antigen for cancer therapy should be expressed exclusively by all cancer cells and should be absent in normal tissues to ensure minimal side effects. In addition, the antigen may be present (i.e. “shared”) across a larger cancer patient cohort to ensure “off-the-shelf” treatment options. Moreover, the protein serving as antigen should ideally be essential for cancer cell survival such that the cancer may not simply escape through downregulation of the antigen. Finally the antigen should be highly immunogenic and thus allow the uprising of a potent, long-lasting, cytotoxic CD8<sup>+</sup> T cell-mediated immune response that was not previously affected by central tolerance mechanisms (118, 119, 121). However, few if any antigens known to date fulfill all these criteria as further highlighted below and summarized in **Table 1.2**. In general, tumor antigens may be classified into two major groups termed tumor-associated antigens (TAA) and tumor-specific antigens (TSA), which are based on their degree of “foreignness” as introduced in the following.

**Table 1.2 | Tumor antigen classifications**

	Tumor-associated antigens		Tumor-specific antigens		
<b>Sub-classification:</b>	Overexpressed proteins & differentiations antigens	Cancer / germline antigens	Oncoviral antigens	“Shared” mutated neoantigens	“Private” mutated neoantigens
<b>Tumor specificity:</b>	Moderate	Good	Exclusive		
<b>Central tolerance:</b>	High	Low	None		
<b>Prevalence across multiple patients:</b>	High		High	Low	None
<b>Examples:</b>	CEA, WT1, MART-1	NY-ESO-1, MAGE-A3	HPV E6, E7	KRAS, BRAF, IDH1, p53	“countless”

Table is based on (118, 119, 122).

### 1.4.2.1 Tumor-associated antigens

The group of tumor-associated antigens (TAA) comprise non-mutated self-proteins that are aberrantly expressed by cancer cells but otherwise are (i) generally expressed at very low levels by healthy cells, (ii) only expressed by certain restricted cell types, or (iii) predominantly expressed during embryonic development (122, 123).

One of the most prominent class of TAAs are the so-called cancer/germline antigens (also termed cancer/testis (CT) antigens), which are normally expressed during early embryonic development and show a restricted expression to testicular germ cells representing immune privileged sites (i.e. limited MHC expression) but mostly lack expression in somatic tissues. Prototype CT antigens are the NY-ESO-1 protein and the whole MAGE (e.g. MAGE-A1, MAGE-A3) protein family, which are both frequently expressed by melanoma and various other cancer types including breast, colorectal, prostate and lung-tissue derived cancer (reviewed in (124)). Another heavily investigated and exploited class of TAAs include differentiation antigens that are overexpressed by cancer cells but also show certain expression in the normal tissue of origin. These antigens include exemplarily the melanocyte

differentiation antigens, gp100, MART1 / Melan-A (melanoma antigen recognized by T cells) and tyrosinase (125). Another example is the carcinoembryonic antigen (CEA) that is expressed in embryonic tissue and normal epithelial cells at a low level but is often heavily overexpressed in colon- and other adenocarcinomas (123). Finally, several TAAs have been identified, which display only a minimal expression across adult tissues and but are overexpressed by certain cancer types. A good example is a transcription factor termed Wilms' tumor protein (WT1) that is overexpressed in most leukemia types but lacks considerable expression in normal tissues and also displays an overall strong immunogenicity as reviewed in (126).

As discussed above, most TAAs are typically expressed across various cancer types of different cellular origins and across multiple cancer patients, which made their predominant usage in the past for vaccine-based, antibody-based (i.e. only in case the antigen displays surface expression) and engineered adoptive T cell-based therapies quite appealing. However, due to their nature of being self-antigens with restricted expression, respective T cells with high-affinity TCRs are typically deleted from the immune repertoire due to central tolerance mechanism as for instance observed for MAGE and NY-ESO-1 (127), which in turn limits the capacity of these antigens to elicit potent anti-tumor immune responses *via* vaccines approaches. Yet, for instance adoptive transfer of genetically engineered T cells expressing a moderate-affine TCR specific for NY-ESO-1 led to durable tumor regression and was well tolerated in a small number of patients with metastatic melanoma or synovial cell sarcoma (128). On the contrary, a similar clinical trial using a TCR specific for MAGE-A3 revealed severe and fetal side-effects due to cross-reactivity with healthy brain tissue as described by (129, 130), highlighting the limited tumor specificity of certain TAAs.

### 1.4.2.2 Tumor-specific antigens with a focus on mutated neoantigens

The group of tumor-specific antigens (TSA) comprise a class of antigens that are exclusively expressed by cancer cells and secondly considered as truly "foreign" to the immune system. Thus, the quality of the available T cell repertoire against TSA should not be affected by tolerance mechanism.

**Oncoviral antigens** | A subclass of TSA are virus-derived antigens presented by certain virus-induced tumor entities including hepatocarcinoma, nasopharyngeal carcinoma and adult T cell leukemia. These oncoviral antigens are typically highly immunogenic and in certain cases also molecular drivers of oncogenesis. Prototypic antigen examples are the human papilloma virus (HPV) high-risk type 16 as well as HPV-18-derived oncoproteins E6 and E7 that are involved in the promotion of cervical cancer. These antigens are therefore highly attractive targets for therapeutic vaccine developments (reviewed in (131)), which, however, will not be further discussed here in this study.

**Mutation-driven neoantigens** | Another class of TSA are antigens, here for simplicity defined as neoantigens, that arise as a direct consequence of somatically acquired genetic changes in cancer cells, although formally any viral genome-derived (e.g. HPV) protein that is expressed in virus-associated cancer cells may be also considered as neoantigen. These genetic changes are most notably single-nucleotide variants and frameshift mutations caused by insertions and deletions and can potentially give rise to mutated, non-self peptides presented by MHC molecules. Neoantigens are of exquisite tumor specificity and can be highly immunogenic. In fact a multitude of recent studies as reviewed in (119, 132) substantiate the concept that neoantigen-specific T cells are important, if not the most important drivers of anti-tumor T cell responses in variety of cancer types including melanoma and non-small cell lung cancer (NSCLC). In this regard, several retrospective clinical studies demonstrated that response (i.e. survival benefit) to ICB therapy such as anti-PD-1 and anti-CTLA-4 often correlates with (i) a higher amount of identified mutations (tumor mutational burden), (ii) higher number of

predicted neoantigens as well as (iii) an increase in frequency of neoantigen-specific T cells (133–136). Consequently, additional clinically applicable strategies that further augment T cell response targeting tumor neoantigens are currently of high interest in the cancer immunotherapy field. These strategies show already promising results in clinical trials including most notably the manufacturing of neoantigen-based vaccines for melanoma patients as described by (137–139), and the adoptive T cell transfer of neoantigen-specific enriched TILs in cholangiocarcinoma (140), colorectal cancer (141) and breast cancer patients (142).

**Nature of neoantigens** | However, only a few examples of therapeutically exploitable neoantigens have been identified so far that are directly linked to the malignant cell transformation process (i.e. driver mutations, in this regard also referred to as “public” mutations) and that are potentially shared across patients and in some cases also across cancer types. In human cancer patients such T cell responses specific for “shared” neoantigens have been in particular reported for hotspot mutations in the well-known gene *TP53* encoding for the tumor-suppressor p53 (143), the tumor suppressor p16<sup>INK4a</sup>-insensitive cyclin-dependent kinase 4 (CDK4) (144), prominent mutations in the oncogenes *KRAS* (141) and *BRAF* (145), and in mutated isocitrate dehydrogenase-1 (*IDH1*) (146). In contrast, the vast majority of mutations occur as a byproduct of increasing genetic instability (i.e. passenger mutations) and are not shared at considerable frequency across patient populations and cancer types and are therefore considered as “private mutations” (147, 148). Consequently, screening and validation of neoantigens that might arise from the patient’s cancer mutagenome as well as subsequent translation into the manufacturing of therapeutic vaccines or adoptive T cell transfer products are highly demanding “personalized” therapeutic approaches. Although proven feasible as shown by the increasing number of neoantigen-based clinical studies, the associated labor-intensive workflow for the systematic identification of personalized neoantigens in cancer patients and subsequent monitoring of their T cell responses still requires constant innovations to make a neoantigen-based therapies broadly and routinely applicable (119, 132).

**Screening and validation of neoantigens** | Current neoantigen discovery workflows (**Fig. 1.8**) typically start with the identification of tumor-specific non-synonymous mutations (NSM) using whole exome sequencing (WES) data obtained from the individual patient’s normal/healthy- and tumor-derived DNA as also described in detail in (119, 132). Moreover, WES data is often combined with tumor-derived RNA sequencing data to identify NSMs that are actually expressed by the tumor. Yet, the vast majority of tumor-specific NSM (i.e. typically less than 1%) identified by NGS do not give rise to *bona fide* neoantigens, which are presented on the cell surface by MHC molecules or are not capable of triggering a T cell-driven immune responses (reviewed in (149)). Consequently, several partially interconnected and/or complementary downstream strategies have been exploited over the years to select and screen potential candidate neoantigens from the entire list of NSM for their subsequent immunogenicity evaluation and the final identification of the minimal epitope (i.e. exact peptide sequence that binds to MHC-I or MHC-II). These strategies include most notably the usage of computational algorithm for *in silico* prediction of peptide/MHC binding (e.g. NetMHCpan) and peptide processing (e.g. NetChop) that allow a certain prioritization and selection of neoantigen candidates. These predicted neoantigen candidates are subsequently screened for their immunogenicity using either functional T cell-assays (e.g. ELISpot) using synthetic peptides (150) or pMHC multimer-based T cell binding assays (135) (discussed in detail in **Section 1.5**). The *in silico* neoantigen prediction might further be supported or partially replaced by data gained from mass spectrometry-based analysis of tumor-specific peptides directly eluted from tumor-expressed MHC molecules (immunopeptidomics) (151).

## 1 | Introduction

Alternatively, all NSM are tested for immunogenicity in an “unfiltered” fashion using large long-peptide pools (i.e. 25–30 residues) (152) or so-called “tandem-minigenes” (153), which however is typically limited to tumors with low mutational burden and by the requirement of large numbers of autologous APCs and T cells to assess the immunogenicity of the generated neoantigen library and its subsequent deconvolution.

Thus, the preferred neoantigen screening strategy highly depends firstly on the number of identified NSM, secondly on the amount of available patient’s material including tumor material, TILs and/or peripheral blood and finally also on the laboratories’ know-how and equipment. Nevertheless, the final evaluation and monitoring of neoepitope-specific T cell populations and thus the validation of a panel of neoantigen candidates has mainly been achieved through *in vitro* assays measuring functional T cells responses (e.g. ELISpot) or by using pMHC multimer-based T cell binding assays. However, available standard approaches typically cannot handle the needed evaluation of larger numbers of potential neoepitopes in particular if the patient material is limited and the patient number increases (154). This issue will be partially addressed in this study. Therefore, state of the art methods to detect antigen-specific T cells and their responses will be discussed in the next chapter.

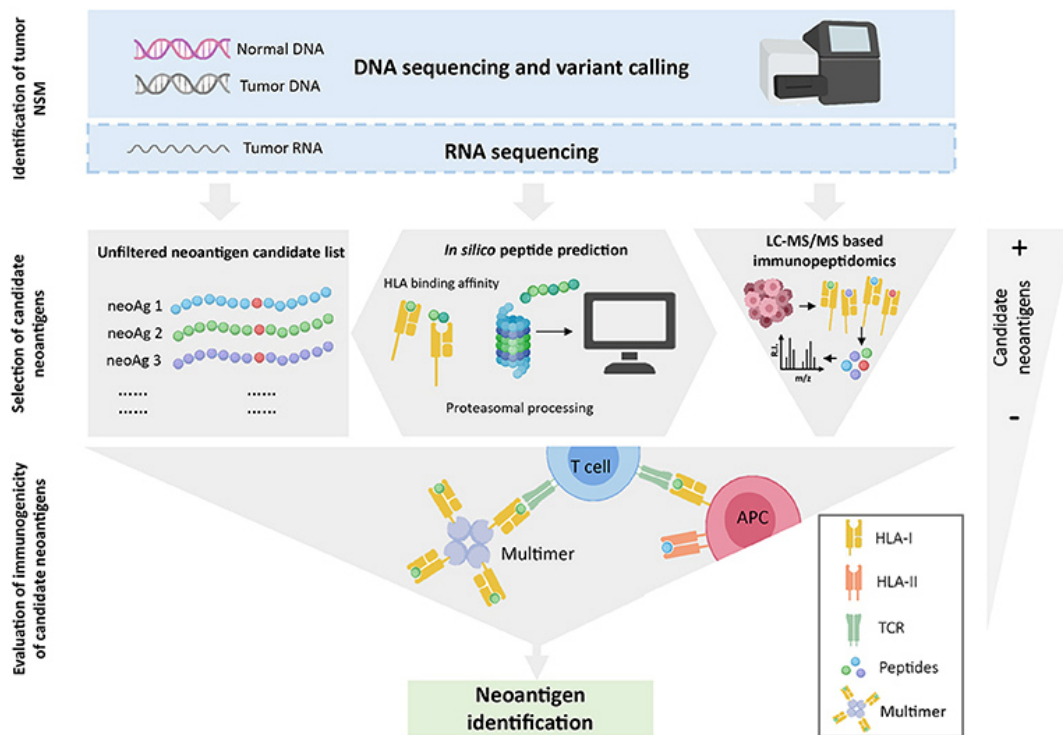


**Figure 1.8 | Overview of frequently applied cancer neoantigen discovery workflows**

As a starting point tumor-specific non-synonymous mutations (NSM) are typically identified by whole exome sequencing (WES) of normal/healthy- and tumor-derived DNA obtained from an individual cancer patient. Expression of NSMs may be further confirmed using complementary RNA sequencing data ideally obtained from the same tumor material. Upon identification of NSM representing putative neoantigens various strategies may be applied to finally screen their immunogenicity. Putative neoepitopes may be predicted and ranked *in silico* for their MHC binding capacity using various algorithms followed by screening of a filtered/selected candidate list. *In silico* prediction may be replaced or complemented by data obtained by mass spectrometry (MS)-based analysis of MHC-bound peptides eluted from tumor material (immunopeptidomics). Alternatively, an unfiltered list of NSM may be directly screened for their immunogenicity using large peptide or mini-gene libraries. Typical immunological screening assays to determine the immunogenicity and to validate putative neoantigens comprise the usage of pMHC multimers or T cell stimulation-based assays such as ELISpot. Figure was adapted from (132) with permission.

## 1.5 Methods to detect antigen-specific T cells – Invaluable tools to understand T cell biology and to make use of it for the clinical benefit.

Multiple *in vitro* assay platforms/methods that are thoughtfully engineered for the direct detection, enumeration and isolation of T cells in an antigen-specific manner have been proven invaluable over the last decades to gain deeper insights into the dynamics of T cell responses against pathogen-, tumor- and self-antigens as well as to being able to steer these T cell response against clinical relevant antigens as reviewed in (154–156) and partially depicted in **Fig. 1.9**. Each of these methods comes with a certain set of advantages as well as drawbacks especially with regard to the degree of *a priori* assumptions about the antigen (i.e. defined MHC alleles vs. MHC allele-independent), type of information gained by the assay (effector function vs. TCR-expression), the assay's sensitivity, required amounts of sample to be analyzed as well as the capacity to detect multiple T cell specificities at the same time referred to as antigen-specific multiplex T cell detection (summarized in **Table 1.3**). Other aspects of the assay design may comprise its practicability for routine laboratory usage including the overall workload, pricing, as well as the requirement of specialized laboratory equipment and highly trained personnel (155–157). In general, antigen-specific T cell populations may be characterized by their effector function in response to a certain antigen expressed as a pMHC molecule on the surface of an APC, which can be measured by the virtue of multiple conventional assays as introduced in **Section 1.5.1**.

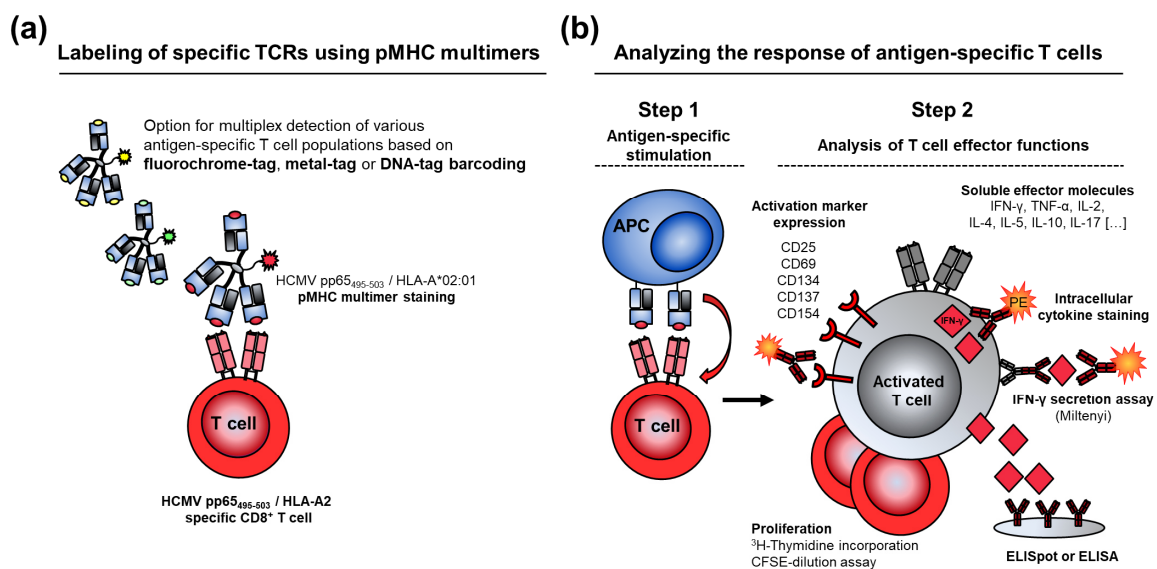


**Figure 1.9 | Overview of common approaches to detect T cells in an antigen-specific manner**

**(a) pMHC multimer-based labeling of an antigen-specific T cell pool.** Purposely designed soluble pMHC molecules that are multimerized and linked to a fluorochrome (i.e. more than two pMHC molecules are connected via a suitable scaffold such as fluorochrome-conjugated streptavidin) allow the direct flow cytometry-based visualization of antigen-specific T cells through binding to the cognate TCR. Usage of pMHC multimers requires prior knowledge about the minimal peptide epitope (e.g. human cytomegalovirus (HCMV) pp65 residue 495–503) and its MHC restriction element (e.g. HLA-A\*02:01) as well as the corresponding haplotype of the respective test sample to be analyzed for antigen-specific T cells. Recent technological advancements of pMHC multimer reagents allow reliable assessment of multiple antigen-specificities in parallel (multiplex detection) though barcoding of the pMHC multimers.

**(b) Analysis of activated T cells upon cognate antigen-specific APC interaction.** T cells are co-cultured with antigen-presenting cells (APC) presenting the cognate antigen of interest to elicit antigen-specific T cell activation (step 1). APCs may comprise cells or artificial surfaces that present the cognate pMHC. As a second step (step 2) multiple assays may be applied that analyse the effector function of the activated T cell pool including cytokine secretion (e.g. ELISpot), cytotoxicity (not shown) or proliferation. Moreover, various surface markers associated with T cell activation may be used for direct visualization of antigen-specific activated T cell populations. Depending on the APC design prior knowledge of the minimal epitope nor the MHC haplotype is not required. Typically T cell activation-based assays do not allow antigen-specific multiplex detection.

Alternatively, an antigen-specific T cell population may be directly visualized upon binding of an engineered soluble and multimerized version of a cognate pMHC complex to the TCR expressed by that particular T cell pool as introduced in more detail in **Section 1.5.2**.

**Frequencies of antigen-specific T cells — Finding the needle in the haystack** | Due to the nature of the entire T cell repertoire of being able to respond to a myriad of different antigens, the frequency of a particular T cell population specific for certain pMHC is very low and highly depends on the type of T cell (CD4<sup>+</sup> vs. CD8<sup>+</sup> T cell), its functional status (naïve vs. memory) and location (lymphatic system, peripheral blood or effector site e.g. within a tumor mass) as well as on the origin of the antigen (pathogen-, tumor-, environmental- or self-antigens) (155). Antigen-specific T cell frequencies within the memory T cell pool typically lie between 0.001% (1 out of 100,000 T cells) and 5% (1 out of 20) depending on the status of the immune reaction. For instance in the absence of an acute infection, the frequency of virus-antigen (e.g. human cytomegalovirus (HCMV) or Epstein-Barr virus (EBV)-specific memory CD8<sup>+</sup> T cells located in the peripheral blood is typically ~1% (1 out of 100 cells) among all CD8<sup>+</sup> T cells present, whereas CD4<sup>+</sup> T cells recognizing the same antigens often occur at 10-lower frequencies (158). T cells specific for tumor neoantigens can be found at frequencies between 0.02% (1 out of 5000 T cells) to 0.0007% (1 out of ~150,000 T cells) in peripheral blood in some cancer patients (159), which may be increased or *de novo* primed to a frequency of ~1% upon neoantigen-specific vaccination (137, 138). In contrast, T cells specific for certain self-antigen (including but not limited to gp100, fibrinogen and pre-proinsulin) were detected in the range of 1–10 per 1x10<sup>6</sup> T cells within the repertoire of naive T cells located in the blood of healthy humans (160), which is line with estimated frequencies of antigen-specific T cells within the naïve T cell population of 1 out of 10<sup>4</sup>–10<sup>7</sup> cells (161). Consequently, all assays suitable for the detection and enumeration of low-frequent antigen-specific T cells (or their antigen-specific response) within *ex vivo* sample material (i.e. peripheral blood or tumor biopsy) require a very high sensitivity associated with a very low background signal on the one hand, and must be able to process high cell sample numbers (ideally >10<sup>6</sup> cells) within a reasonable amount of time on the other hand. Most frequently applied standard flow cytometry-based assays fulfill these criteria including pMHC multimer staining, cytokine secretion assay and intracellular cytokine staining, which allow the detection of antigen-specific T cells with a typical technical (i.e. noise due to unspecific reagent binding) or natural background (i.e. unspecific cytokine expression) below 0.1% – 0.01% (155, 156). Moreover, several enrichment strategies have been developed over the last years that allow rapid processing of larger cell numbers (>10<sup>7</sup> cells), which include most notably direct *ex vivo* magnetic force-facilitated enrichment of antigen-specific T cells based on pMHC multimer binding or cytokine secretion (155, 162). In addition, preselection of phenotypically distinct T cell subpopulations within peripheral blood (i.e. T cell memory pool or T cells expressing certain exhaustion markers) prior to *in vitro* expansion based on defined antigens (e.g. peptide pulse) is another quite common used strategy particularly for the detection and mapping of T cell responses against tumor neoantigens as described by (159, 163, 164).

Apart from methods that allow direct antigen-specific detection of a T cell pool or its response, next-generation sequencing (NGS)-based methods for sequencing of TCRs (TCR-Seq) in particular on the single cell level (reviewed in (165)) provide a deeper insight into the TCR diversity / repertoire associated with certain diseases including cancer (166). However, TCR-Seq on its own may not provide information about the antigen-specific frequency of T cells unless for highly immunodominant T cell epitopes (e.g. for certain viral epitopes) often detected across the human population (167). Thus, TCR-Seq is instead rather combined with other assays including pMHC multimer staining or antigen-specific T cell stimulation-based assays and will not be covered in detail here (168–170).

**Table 1.3 | Overview of selected assays for the direct visualization of antigen-specific (Ag<sup>+</sup>) T cells or their antigen-specific response**

	Capabilities				Advantages (pro) and disadvantages (contra):	Ref.:
	Ag <sup>+</sup> T cell multiplex detection: <sup>(a)</sup>	Sensitivity: (frequency of Ag <sup>+</sup> T cells) <sup>(b)</sup>	Isolation of vital Ag <sup>+</sup> T cells:	Complete sample recovery:		
<b>“Conventional” <sup>(c)</sup> effector function-based assays requiring cognate Ag<sup>+</sup> T cell / APCs interactions:</b>						
ELISpot (i.e. typical 96-well PVDF membrane-based ELISpot with 250,000 – 400,000 PBMC per well)	No	~ 1:15,000 (0.01% – 0.005%)	No	Yes	<b>Pro:</b> Minimal epitope- and HLA-independent assessment of Ag <sup>+</sup> T cell responses (e.g. if long peptides are used), which holds true for all conventional functional assays listed. Highly automated read-out and analysis. <b>Contra:</b> Rather low dynamic range, long-lasting assay procedure and no Ag-specific multiplex detection capacity.	(171–173)
Intracellular cytokine staining (ICS) <sup>(e)</sup>	No	1:1000 – 1:10,000 (0.1% – 0.01%)	No	No	<b>Pro:</b> Detection of multiple cytokines and other phenotypic T cell markers possible (8 – 18 parameters in total). <b>Contra:</b> Often less sensitive compared to ELISpot and pMHC multimer-based analysis. Cells are permeabilized during assay procedure.	(174)
IFN- $\gamma$ -secretion assay (by Miltenyi) <sup>(e)</sup>	No	1:1000 – 1:10,000 (0.1% – 0.01%)	Yes	No	<b>Pro:</b> Only assay that allows enrichment and isolation of cytokine-secreting (i.e. responding) Ag <sup>+</sup> T cells. <b>Contra:</b> Assay procedure often results in strong background signals due to cytokine capture on non-responding bystander T cells (false positive).	(175, 176)
<b>“Unconventional” <sup>(d)</sup> functional multiplex-assays:</b>						
Cellular aAPC fluorochrome barcoding <sup>(e)</sup> (i.e. B cells labeled with three cell dyes)	Yes (7 specificities)	1:1000 (0.1%)	No	No	<b>Pro:</b> Allows multiplex detection of functional T cell responses. <b>Contra:</b> Low assay reliability due to Ag-independent APC cell membrane exchange during <i>in vitro</i> culture.	(177–179)
pMHC microarrays <sup>(f)</sup> (Rec. pMHC spotted on solid surfaces)	Yes (7 – 40 specificities)	Threshold >1000 Ag <sup>+</sup> T cells	No	Yes	<b>Pro:</b> As above. <b>Contra:</b> Low sensitive assay that typically requires >1000 Ag <sup>+</sup> T cells among bystander cells for their successful detection. Low assay reliability and reproducibility.	(180–183)
<b>Single-color pMHC multimer staining <sup>(c)</sup>:</b>						
Single fluorochrome (single-color) labeled pMHC multimers <sup>(e)</sup>	Yes (>4 specificities) <sup>(i)</sup>	1:10,000 (0.01%)	Yes	No	<b>Pro:</b> Allows direct <i>ex vivo</i> visualization and isolation of Ag <sup>+</sup> T cells with high sensitivity without the requirement of their prior activation. <b>Contra:</b> Requires demanding and expensive generation of individual pMHC multimers for each specificity. No information about the T cell function. Detection problems of T cells with low-affinity TCR.	(156, 162, 184)
<b>pMHC multimer barcoding-strategies for increased Ag<sup>+</sup> T cell multiplex detection capacities <sup>(d)</sup>:</b>						
Combinatorial fluorochrome encoded pMHC multimers <sup>(e)</sup>	Yes (27 – 36 specificities)	1:50,000 (0.002%)	Yes	No	<b>Pro:</b> Can be handled by typical flow-cytometers with 8 – 18 channels. Required reagents are broadly available. <b>Contra:</b> Demanding preparation and quality control of fluorochrome-barcode pMHC multimer libraries.	(185–187)
Combinatorial heavy metal-tags encoded pMHC multimers <sup>(g)</sup>	Yes (109 specificities)	1:100,000 (0.001%) <sup>(k)</sup>	No	No	<b>Pro:</b> Most comprehensive method to detect and phenotypically profile multiple antigen-specific T cell pools (>30 cell parameters & 120 specificities). <b>Contra:</b> Limited availability of CyTOF devices, high reagents costs, low sensitivity without prior cell enrichment.	(188)
Unique DNA barcodes encoded pMHC multimers <sup>(h)</sup>	Yes (1031 specificities)	1:20,000 (0.005%)	No	No	<b>Pro:</b> Highest (almost unlimited) Ag <sup>+</sup> T cell multiplex detection capacity among all assays. <b>Contra:</b> Demanding library preparation and specialized NGS procedure. Only indirect enumeration of Ag <sup>+</sup> T cells. Cell lysis during assay procedure.	(189)

**(a)** Reported order of complexity i.e. amount of different antigen specificities measured per sample. Individual platform may offer to handle higher complexities. **(b)** Reported sensitivity or typical sensitivity described as one Ag<sup>+</sup> T cell (positive event) detected out of a number of bystander cells. Most listed assays require typically at least 10-20 positive events above background **(c)** Assays frequently applied or **(d)** only applied by selected research groups. Read-out by **(e)** flow cytometry, **(f)** microscopy or similar **(g)** cytometry by time-of-flight (CyTOF) or **(h)** next-generation sequencing (NGS) analysis. **(i)** Various pMHC multimers conjugated individually to a different dye (e.g. PE, APC, PE/Cy7 or BV421) may be used within a single cell staining. **(k)** Based on magnetic enrichment of Ag<sup>+</sup> T cells by pMHC multimers prior to CyTOF analysis. **Ag<sup>+</sup> T cells:** Antigen-specific T cells. Here all cited studies referring to the detection of Ag<sup>+</sup> CD8<sup>+</sup> T cells. **aAPCs:** artificial antigen-presenting cells. **Rec.:** Recombinantly produced. **Ref.:** Selected references are cited.

### 1.5.1 Methods for analyzing the effector response of an antigen-specific T cell population

Various methods have been developed to analyze defined functional parameters of T cells upon cognate pMHC recognition. Thus, functional assays usually comprise two global steps including firstly the *in vitro* stimulation based on a co-culture of antigen-presenting cells (APC) with a T cell pool to be analyzed (e.g. derived from peripheral blood and/or tumor biopsy) and secondly measuring a defined parameter that is associated with T cell activation (i.e. cognate TCR triggering), which include cytokine release, cytotoxicity, expression of co-stimulatory or co-inhibitory molecules (hereinafter also defined as T cell activation markers) as well as T cell proliferation by different assays. The APC may be endogenously presenting the antigen (e.g. cancer patient-derived tumor cell line) or may be artificially generated by various ways including the usage of Mo-DCs or B cells pulsed with long or short antigenic peptides, entire antigens, tumor lysate or that have been genetically engineered to present the antigen of choice. Moreover, also peripheral blood mononuclear cells (PBMC) comprising T and B cells as well as monocytes may be directly loaded with antigenic peptides without prior separation to elicit functional T cell responses. A key advantage of most T cell stimulation-based methods is that *a priori* information about the MHC allele expression (MHC haplotype) as well as about the exact antigenic peptide sequence (minimal epitope) presented on pre-defined MHC alleles are not necessarily required in particular if longer antigenic peptide sequence (>25 amino acids) or entire antigens (i.e. whole proteins) are used. However, on the contrary these assays are usually a labor-intensive (i.e. >6 h hands on pipetting), complex (i.e. more than 30 steps) as well as long-lasting (i.e. 10–48 h overall assay duration) procedure. Another major limitation of all conventional stimulation-based assays is that different T cell antigen specificities cannot not be analyzed simultaneously in one sample (i.e. no multiplex capacity with regard to the antigen specificity), which consequently results in higher sample consumption if multiple putative antigens need to be screened and discriminated. Moreover, naïve T cells as well as anergic T cells may be partially excluded from the analysis by stimulation-based assays (173–175). In the following, we will focus on stimulation-based assays having cytokine secretion (e.g. ELISpot) or activation marker expression as read-out. These assays are frequently, and often in parallel and/or in combination, used with pMHC multimer staining (discussed in Section 1.5.2) for the initial detection of neoepitope-specific T cells (reviewed in (154)). Alternative assays interrogating the cytotoxic function of CD8<sup>+</sup> T cells (e.g. Chromium-51 release assay (190)) or measuring T cell proliferation (e.g. CFSE (carboxyfluorescein diacetate succinimidyl ester))-based dilution assay (191)) upon antigen-specific encounter of a cognate APCs will not be covered here.

#### **1.5.1.1 Conventional cytokine expression-based assays for antigen-specific T cell detection**

**The ELISpot** (Enzyme-linked immunospot assay) although now being over 35 years old (192), represents still one of the most frequently used and widely commercialized “gold-standard” assay in particular – but not limited to – for the direct *ex vivo* detection of T cell responses against tumor-antigens (154). Here, the co-culture of APCs and T cells occurs typically overnight in special 96-well plates bearing a PVDF (polyvinylidene difluoride) membrane at the well bottom that are pre-coated with a monoclonal antibody (mAb) specific for a certain effector cytokine (usually for IFN- $\gamma$ ). IFN- $\gamma$  secreted by activated T cells (e.g. memory CD8<sup>+</sup> T cells or Th1-differentiated CD4<sup>+</sup> T cells) is subsequently captured (i.e. immobilized) on the mAb-coated membrane. Upon removal of the cells, the immobilized IFN- $\gamma$  is finally visualized by means of secondary antibody coupled for instance to horseradish peroxidase combined with a substrate reagent that forms a colored insoluble precipitate. The precipitate in turn appears as a distinct spot at the sites of cytokine secretion, with each individual spot typically representing the “footprint” of a single cytokine-producing T cell. Finally, spots may be

counted by broadly available automated ELISpot readers. This allows for easy and rapid data analysis of larger number of samples, which makes the rather cost-effective ELISpot particularly attractive for the broad usage in clinical laboratories conducting larger clinical trials or routine diagnostic tests (173). Although generally considered as a highly sensitive method to detect antigen-specific T cells, ELISpot assays usually have a reliable detection limit of one antigen-specific T cell out of approximately 15,000 bystander cells. In the daily practice this correspond to the detection of approximately 25 antigen-dependent spots per  $2.5 \times 10^5$  cells seeded per ELISpot-96-well and a given typical background of 8–12 spots/ $2.5 \times 10^5$  cells. However, ELISpots typically suffer from a rather low dynamic range compared to flow cytometric based-assays with respect to an overall signal saturation occurring at approximately 1000 spots/well preventing reliable antigen-specific T cell enumeration above that threshold (171).

**Intercellular cytokine staining and cytokine secretion assay** | Alternatively, individual antigen-specific T cells may be detected through their expression of cytokines (e.g. IFN- $\gamma$ , TNF- $\alpha$ , IL-2) upon *in vitro* restimulation by two frequently applied conventional flow cytometry-based methods termed intracellular cytokine staining (ICS) (174) and cytokine secretion assay (175, 176), the latter has been developed as a commercial kit from Miltenyi Biotec. Both methods have a similar sensitivity compared to an ELISpot with a technical typical background between 0.5–0.01% depending on the sample type and reagent quality. However unlike the ELISpot, both methods allow for a more comprehensive profiling of the T cell response through optional flow-cytometric analysis of multiple additional phenotypic parameters typical up to 16 such as lineage (e.g. CD4, CD8), memory (e.g. CCR7, CD45RA) or exhaustion/activation marker expression (e.g. CD25, PD-1). For an ICS-based assay, the secretion of cytokines is typically blocked during the co-culture of T cells and APCs by the inhibitors of vesicular trafficking, brefeldin A and monensin, which subsequently enables detection of intracellular trapped cytokines by fluorochrome-labelled mAbs upon permeabilisation and fixation of the cell. The ICS method allows for detection of multiple cytokines in parallel that is only limited by the used flow cytometer, which may provide additional information about the T cell differentiation (e.g. Th1 vs. Th17 or polyfunctional vs. exhausted) (174). In contrast, the ELISpot or cytokine secretion assay is typically restricted to the analysis of one or at most two cytokines in parallel (173, 175). However, the ICS procedure does not allow the recovery and isolation of vital antigen-specific T cells unlike the cytokine secretion assay (Miltenyi Biotec). Here, secreted cytokines are captured directly at the cell surface by an engineered “cytokine catch reagent” composed of a cytokine-specific ‘catch’ antibody that is conjugated with a CD45-specific mAb allowing labeling of all leukocytes evenly. Subsequently, bound (i.e. cell surface-immobilized) cytokine is detected by second cytokine specific fluorochrome-conjugated mAb (typically phycoerythrin, PE) in combination with other surface marker usually CD3, CD4 and CD8 to detect antigen-specific stimulated T cells. Moreover, since the cytokine is captured at the cell surface, this opens the option to isolate vital low-frequent antigen-specific T cells either directly by flow-cytometric and/or through magnetic enrichment based on anti-PE mAb-conjugated magnetic beads (175, 176).

**ELISA and CD107a degranulation assay** | Last but not least, also a classical enzyme-linked immunosorbent assay (ELISA) for IFN- $\gamma$  may be used to detect an antigen-specific T cell response, which might be particularly useful if an entire antigenic peptide library is initially mapped for a cognate T cell response as described by (150). However, an ELISA typically has a lower sensitivity compared to the other methods such as ELISpot, ICS and pMHC multimer staining and does not allow for a direct enumeration of the antigen-specific T cell frequency (158). Apart from direct measurement of cytokine expression, also the flow-cytometric measurement of degranulation in general has been successfully used to detect antigen-specific activated CD8<sup>+</sup> T cells (CD107a-based degranulation assay).

Degranulation referring to the fusion of cytolytic granules with the outer cell membrane upon TCR triggering results in the transient cell surface exposure of lysosomal associated membrane glycoproteins (LAMPs) – most notably CD107a (LAMP-1) and CD107b (LAMP-2), which can be detected in a cumulative manner by respective fluorochrome-conjugated mAbs direct against CD107. However, the CD107a-degranulation assay has a rather high background of >0.5% and has been proven to be less reliable in detecting low-frequent cytotoxic CD8<sup>+</sup> T cell populations (193).

### 1.5.1.2 Analysis of activation marker expression by antigen-specific stimulated T cells

Upon T cell activation multiple surface markers are upregulated with different kinetics, which are mostly absent in resting T cells and therefore are considered as “activation markers”. These markers, that also exert important biological functions as partially discussed in **Section 1.2.3.2** include CD69, CD25, CD134 (OX40) CD137 (4-1BB), CD154 (CD40L) as well as PD-1 (CD279) which can be used for direct visualization of antigen-specific triggered T cells as reviewed in (155). However, although they are useful in combination for the comprehensive characterization of the total pool of specific T cells against a given antigen, they typically do not allow accurate detection of small antigen-specific T cell populations occurring at frequencies below 1%, due to their susceptibility to bystander activation (CD69, CD25) and partially constitutive expression on specialized T cell subsets (Treg, T<sub>RM</sub>). Yet detection of CD25/CD134 (after 16–44 h) (194) or CD154 (after 4–12 h) (195) expression of *in vitro/ex vivo* stimulated PBMC-derived CD4<sup>+</sup> T cells as well as CD137 expression for CD8<sup>+</sup> T cells (196) have proven equally efficient for the detection of antigen-specific T cell population compared to ICS particularly if the exact epitope and cytokine secretion profile of the T cell is less clear. More recently it also has been shown that flow-cytometric sorting for CD134, CD137 and/or PD-1 as well as CD39 expressing tumor-infiltrating lymphocytes enriches for the fraction of T cells that are specific for tumor-neoantigens and may be expanded *in vitro* in a second step as described by (164, 197–199).

### 1.5.1.3 Lack of simple and sensitive assays for antigen-specific multiplex detection of T cell responses

**aAPC barcoding approach** | Frequently used conventional assay for T cell epitope discovery that are based on detection of stimulated T cells via cytokines platforms (e.g. ELISpot, ICS, IFN- $\gamma$  secretion assay) or activation marker expression do not allow screening of multiple antigen specificities within a single reaction, which is an obstacle in case the sample material (i.e. T cells and suitable APCs derived from cancer patients) is highly limited. To address this limitation a small number of previous studies have used a cellular APC barcoding approach based on six different concentrations of up to three fluorescent cell labeling dyes (e.g. CFSE (carboxyfluorescein diacetate succinimidyl ester), CTV (CellTrace Violet™, Invitrogen), and CPD (cell proliferation dye eFluor 670, Invitrogen) allowing in principle the generation of up to 216 different fluorescently labeled APCs as illustrated in **Fig. 1.10a** and described by (177, 178).

Here, individual barcoded murine (177, 178) or human B cells (200) were pulsed with different antigenic peptides and subsequently barcoded and peptide-pulsed B cells were pooled, which then served as APC for the co-culture with CD4<sup>+</sup> T cells or CD8<sup>+</sup> T cells. Thus, multiple antigen-specific CD8<sup>+</sup> T cell responses could be analyzed in parallel either *in vivo* (177) or *in vitro* (200) by corresponding detection of cytolysis of the respective barcoded cognate APC population. In cases the response of CD4<sup>+</sup> T cells towards a peptide pool was interrogated, the cognate interaction was indirectly indicated through the antigen-specific CD4<sup>+</sup> T cell helper function leading either to CD69 and CD44 upregulation on cognate murine B cells or CD83 on human B cells, respectively (178, 200). However, this APC barcoding concept has not been further applied after the initial proof-of-concept publication, for instance for the identification of neoantigen-specific T cells. Reasons are most likely an overall lack of

sensitivity and the less robust read-out procedure in particular if only a few antigen-specific T cells are present in the test sample and probably because of the availability of efficient competitor assays such as barcoded pMHC multimers (**Section 1.5.2.2**).

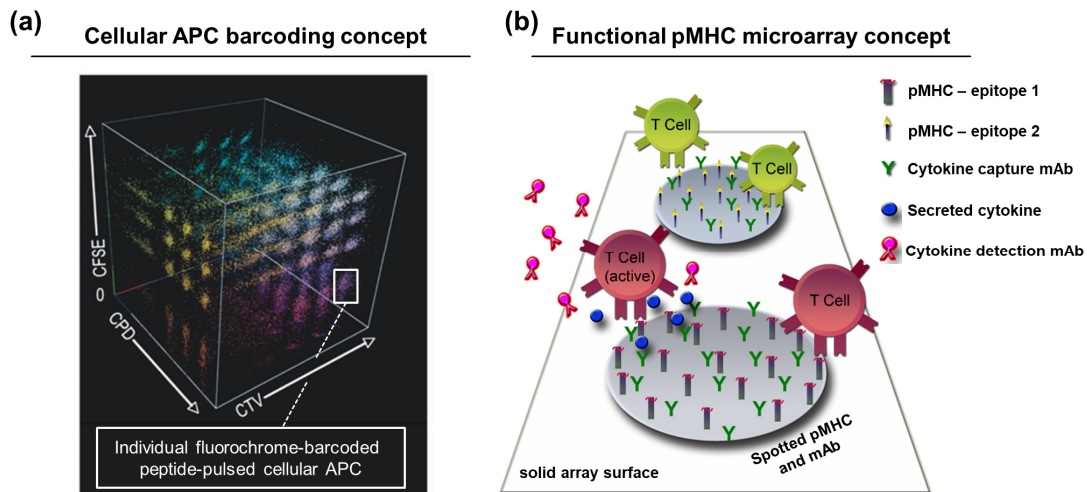


**Figure 1.10 | Cellular APCs barcoding and functional pMHC microarray concept – Two assay platforms for the detection of multiple functional T cell responses**

**(a) Cellular APCs barcoding concept.** Isolated murine splenocytes or human B cells are marked with a barcode based on multiple intensities of three different cell-labeling dyes e.g. carboxyfluorescein diacetate succinimidyl ester (CFSE), CellTrace violet (CTV), and cell proliferation dye eFluor 670 (CPD). Individual barcoded cells are pulsed with peptides of interest converting the individual cell pool into barcoded antigen-presenting cells (APCs). Pooled APCs may be co-cultured with a T cell containing sample. Presence of cognate cytotoxic CD8<sup>+</sup> T cells is indicated by the loss of the respective APC population, whereas presence of a cognate CD4<sup>+</sup> T cell population may be indicated by corresponding antigen-specific activation of cognate APC (i.e. B cells). The phenotype of the APC pool upon co-culture is analysed by flow cytometry. Modified figure was adapted from (177) with permission.

**(b) Functional pMHC microarray concept.** Multiple recombinantly produced pMHC molecules are immobilized individually at spatial defined areas (spots) on a solid surface (e.g. glass slide). In addition, the pMHC spots that may be considered as APCs are supplemented with cytokine capture monoclonal antibodies (mAbs). A T cell containing sample is cultured on the pMHC microarray leading to an antigen-specific accumulation of cognate T cells at the respective pMHC spots. This T cell accumulation may be visualized microscopically. In addition, cognate interaction of T cells with their cognate pMHC-spot may induce their activation resulting in cytokine release that are captured at the spot site. Captured cytokines may be detected by fluorescently labeled secondary cytokine-detection mAbs. Modified figure was adapted from (181) with permission.

**pMHC microarray approach |** Similar pitfalls also holds true for the concept of detecting antigen-responsive T cells using recombinantly produced pMHC molecules spotted as a microarray onto various surfaces including polyacrylamide gel coated microscope slides, polystyrene slides with hydrophobic barriers, LabTek II CC2 slides or hydrogel slides as described by (180–183). Here, each individual pMHC spot is considered as a cluster of artificial APCs that may also be supported by additional costimulatory molecules (e.g. anti-CD28, anti-CD2, anti-CD11a mAbs) (182) and/or cytokine capture antibodies (e.g. anti-IL-2, anti-INF- $\gamma$  mAbs) (180–182). Upon culture of a T cell containing sample on the pMHC functional microarray, individual antigen-specific T cells may recognize their cognate pMHC spot resulting in physical accumulation and subsequent activation of antigen-specific T cells at the cognate spot. Thus, “captured” antigen-specific T cells may be directly visualized through their localized pMHC-dependent adhesion at the pMHC spot (180, 182, 183) and/or through detection of activation marker expression (182) or the capture and detection of secreted effector cytokines in proximity to the pMHC molecules (180–182) (**Fig. 10b**). The pMHC microarray concept would ideally allow a convenient functional interrogation of several hundred T cell epitopes and up to 40 different T cell specificities were simultaneously analysis by (183).

However, compared to other flow cytometry-based assays pMHC microarrays suffer generally from poor sensitivity and have mostly a minimal requirement of 1000 antigen-specific T cells in a pool of up to  $1 \times 10^6$  bystander cells to allow a robust read-out (i.e. frequency of antigen-specific T cells must be  $>0.1\%$ ) (180–183). Moreover, poor assay reproducibility and data homogeneity prevent accurate quantification of T cell response and thus rather lead to poor acceptance in the research community.

Nevertheless, previous reported barcoding of APCs as well as the pMHC microarray represent two major and vital predecessor concepts that provided crucial inspirations to this current study.

### 1.5.2 pMHC multimers – Tools for direct visualization of antigen-specific T cell populations

The flow-cytometric detection of antigen-specific T cells labeled by recombinant-produced soluble pMHC molecules represent until today one of the most frequently applied and essential techniques to identify, monitor and enumerate T cell responses against well defined antigens. However, the binding affinity of a single TCR towards a monomeric pMHC complex is very low with dissociation constants ( $K_d$ ) in the range of 1–1000  $\mu\text{M}$  and has very fast dissociation kinetics (1–1500 seconds). Thus, the TCR-pMHC interaction is usually 1000–10,000-fold weaker compared to a typical antibody-antigen interaction, which makes monomeric pMHC staining reagents insufficient for the detection of antigen-specific T cells (201, 202). In the mid-90s the pioneering work of the laboratory of Mark M. Davis overcame this issue by taking advantage of engineered soluble multimeric pMHC molecules (pMHC multimer) to increase the relative binding avidity and to allow a remarkably sensitive and accurate detection of antigen specific T cell populations as shown initial by (203). Ever since, soluble pMHC multimer staining reagents have been proven vital to many areas ranging from basic to clinical immunological research, which motivated many researchers to contribute to pMHC multimer reagent and staining improvements and to broaden their application potential. Thus, pMHC multimers have been pushed constantly through an “evolutionary process” mainly focusing on (i) their design including their valency (i.e. the degree of multimerized pMHC molecules per given scaffold molecule), (ii) the production process as well as (iii) strategies that allow high-throughput detection of multiple T cell specificities within one labeling reaction (i.e. multiplex detection) as reviewed in-depth in (156, 162, 184) and further introduced in the next section. Most pMHC multimer technologies have been primarily developed and frequently applied for measuring  $\text{CD8}^+$  T cell responses, because soluble pMHC-I molecules have been proven easier to be produced and MHC-I binding peptides more accurately to predict compared to pMHC-II molecules (204). Yet, also pMHC-II staining reagents are coming of age and are more and more applied as well as commercialized as shortly introduced in **Section 1.5.2.3**.

A major advantage of pMHC multimer staining is that it may be applied independently of the functional status of the analyzed T cell population (i.e. naïve, memory or exhausted) and do not require additional preparation of APCs and secondly often display a superior sensitivity compared to most functional assays (e.g., ELISpot and ICS) and permit the isolation/sorting of vital antigen-specific T cells. Without the additional application of enrichment strategies, detection limits between 0.01–0.002% (1 out of 50,000 cells) have been observed for antigen-specific  $\text{CD8}^+$  T cells (156) that also generally highly depend on TCR binding affinity, pMHC multimer reagent quality and the usage of optimized staining protocols. The latter includes in particular the usage of (i) protein tyrosine kinase inhibitors (e.g., dasatinib) preventing pMHC multimer internalization and TCR downregulation, (ii) defining the optimal staining temperatures, and (iii) the usage of pMHC multimers with higher valency as shown by (205, 206). Moreover, magnetic enrichment strategies have been proposed for the detection of low-

frequent T cells populations that firstly enrich either for CD4<sup>+</sup> T cells or CD8<sup>+</sup> T cells and secondly for the target pMHC multimer binding T cell population allowing the visualization of e.g., naïve T cells with a frequency of 1 out of 1x10<sup>6</sup> and lower (160, 207). A limitation of the pMHC multimer technology is that the MHC allotype of the sample as well as the antigenic epitope has to be known or accurately predicted in detail, respectively, which always comes with a certain bias of the antigen selection and its application potential beyond model antigens, immunodominant viral antigens as well as mutation-driven cancer neoantigens needs to be demonstrated more vigorously. Moreover, the availability of pMHC multimer reagents is mostly restricted to the most frequent MHC alleles although the list is constantly expanding and most importantly analysis based on pMHC-I multimers are typically 10–100-times more costly compared to conventional ELISpots, which makes this technology often less attractive for broad and routine laboratory usage (208).

#### 1.5.2.1 Evolution of pMHC-I multimer design and production

**Conventional pMHC-I tetramers** | The recombinant soluble pMHC-I-multimer generation process as originally proposed by Altman *et al.* has been broadly continued in a similar fashion until today. Briefly,  $\beta_2$ -microglobulin ( $\beta_2m$ ) and the MHC class I heavy chain ectodomain (HC,  $\alpha 1$ - $\alpha 2$ - $\alpha 3$  domain) lacking the transmembrane and intracytoplasmic sequences but harboring a C-terminal site for enzymatic biotinylation (i.e. BirA biotin ligase acceptor peptide known as AviTag) are individually expressed in *Escherichia coli* (*E. coli*) bacteria and later purified from inclusion bodies through a laborious lysis/solubilization process. Next, the denatured HC-chain and  $\beta_2m$  are *in vitro* refolded over several days in the presence of a defined chemically synthesized peptide ligand prior to size-exclusion chromatography and enzymatic BirA ligase-mediated biotinylation as discussed in more detail in (209). Finally, properly folded and biotinylated soluble pMHC-I monomers are multimerized through complex formation with fluorochrome-conjugated streptavidin (SAv) comprising ideally four binding sites for biotin. pMHC-I multimers solely on the basis of a SAv backbone are conventionally referred to as “pMHC-I tetramers”, which still represent one of the most popular and broadly commercial available (e.g. MBL International) used pMHC-I multimer design. Notably, “pMHC-I tetramers” on the basis of SAv conjugated to protein-based fluorochromes such as phycoerythrin (PE) and allophycocyanin (APC) are in fact pMHC-I multimers (i.e. oligomers) comprising up to 12 pMHC-I monomers, because SAv-APC and SAv-PE comprise already inherent SAv multimers that are formed upon chemical crosslinking with the protein-based fluorochromes. Thus, SAv-PE or SAv-APC based pMHC-I multimers typically display a better staining performances compared to SAv linked to small-molecule fluorochromes (e.g. Cy5, Alexa Fluor 647) despite similar overall brightness (184).

**Other successful pMHC-I multimer formats** | Beside conventional pMHC-I tetramers several other pMHC-I multimer formats with better defined and/or higher valency have been developed. These comprise most notably the commercially available pMHC-I pentamers (by ProImmune), where five pMHC complexes face the same direction through the use of a five-stranded coiled-coil oligomerization domain placed C-terminal of the MHC-I heavy chain and pMHC-I dextramers (by Immudex), which consist of a long dextran fiber conjugated to multiple fluorochromes and pMHC / SAv complexes (184). With regard to their staining performance, pMHC-I as well as pMHC-II-based dextramers typically exceed the labeling and thus detection efficiency of antigen-specific T cells compared to “conventional” pMHC-I tetramers. In particular, if the underlying TCR affinity of the T cell population to be detected is low, which is often the case for self-antigens including non-mutated tumor-associated antigens (e.g. MART-1, NY-ESO-1) and autoimmune disease-associated antigens (e.g. preproinsulin) (210). In addition also pMHC-I multimers on the basis of commercially available SAv-conjugated

quantum dots (SAv-Qdots) (211) or purposely designed multimeric SAv comprising up to twelve biotin binding sites (dodecamer) (212) have been proposed.

**Less successful pMHC-I-Ig dimers** | On the other side of spectrum, the laboratory of Jonathan P. Schneck constructed and produced pMHC-I dimers (i.e. a valency of two pMHC-I) on the basis of the MHC-I heavy chain (i.e.  $\alpha 1 - \alpha 3$  domain of human HLA-A\*02:01 (213) or murine H-2K<sup>b</sup> (214)) fused to a murine IgG1 (mIgG1) full-length heavy chain (i.e. containing the variable domain of mIgG1 specific for the hapten 4-hydroxy-3-nitrophenylacetyl (NP)). These MHC class I-Ig fusion molecules were subsequently produced by stable transfection of the murine plasma cell line J558L, which expresses a murine  $\lambda$  (lambda) Ig light chain but lacked endogenous Ig heavy chain expression. This pMHC-I-Ig format has also been commercialized by the name “DimerX,I” (by BD Bioscience). An advantage of this approach over the *E. coli*-based production is that transfected mammalian J558L secrete already correctly folded MHC-I-Ig into the cell supernatant, which are loaded with undefined endogenous peptides and purified by simple affinity-chromatography without the need of labor-intensive *in vitro* refolding. A major drawback, however, is firstly the low valency (i.e. only maximal two pMHC-I), secondly the requirement of a largely insufficient passive peptide exchange of the endogenously loaded peptides of the pMHC-I-Ig molecules with a single synthetic peptide of interest in the presence of recombinant  $\beta_2m$ , and thirdly the requirement to use pMHC-I-mIgG1 molecules in combination with a fluochrome-conjugated anti-mouse IgG1 secondary antibody for the detection of antigen-specific T cells, which increases the staining background and restricts the usage of most surface marker mAbs for human T cells (215). Thus, although peptide-loaded (p) HLA-A2-Ig-molecules allowed the detection of virus-specific (i.e. HCMV, Influenza and human T lymphotropic virus type 1 (HTLV-1)) as well as tumor-associated antigen-specific T cells (i.e. MART-1) (213, 216), pHLA-A2-Ig consistently performed inferior compared to conventional pMHC-I tetramers as shown by (217) and did not gain any broad acceptance as direct staining tools for antigen-specific T cell. Yet, pMHC-I-Ig dimers have been successfully used by Schneck *et al.* and multiple other research groups for the generation of pMHC-I-coated microspheres (e.g. magnetic polystyrene Dynabeads, 4.5  $\mu m$  in size) that mimic APC function and thus are generally referred artificially APC (aAPC) to drive antigen-specific T cell activation and expansion (218, 219). In particular the concept of bead-based aAPC represents an important inspiration for this study and will be further introduced in **Section 1.7**.

**Different peptide-loading strategies** | Peptide-MHC-I complexes are highly unstable and quickly disassemble into their non-covalently associated single components (i.e. peptide,  $\beta_2m$ , MHC-I heavy chain), when they are not part of a complex with peptide (220). Thus, a crucial parameter for the successful generation of pMHC-I multimers is the method by which the recombinantly produced MHC molecule is loaded with a peptide of interest. Generally three peptide-loading strategies may be distinguished. Firstly, an antigenic peptide of choice may be directly genetically fused via a short amino-acid linker to the entire MHC complex. This approach has been demonstrated to be widely applicable for MHC-II molecules in case the antigenic peptide is fused to the MHC-II  $\beta$ -chain (221, 222) as well as for MHC-I in case the so-called “single-chain trimer” design is used (223), that will be detailedly introduced in **Section 1.6**. Secondly, the peptide may be included during the *in vitro* refolding process (i.e. a bacterial production system is used) as described above for the conventional pMHC-I tetramers or thirdly MHC molecules are loaded initially with “placeholder” peptide during their production process, which may be flexible exchanged by a peptide of interest prior to their usage as staining tools (224). Especially, the work of Ton Schumacher and colleagues demonstrated the feasibility of the latter approach by producing pMHC-I molecules loaded with thoughtfully designed so-called conditional MHC peptide ligands acting as “placeholder” that are cleaved upon exposure to

366 nm ultraviolet (UV) light followed by quick dissociation of the peptide fragments, but providing sufficient stability for a successful *in vitro* refolding of MHC complex a defined MHC-I allele. Following UV-light exposure the “placeholder” peptide is highly efficiently replaced by any suitable peptide of interest that is able to rescue the pMHC-I complex stability. Thus, a defined MHC allele refolded with UV-cleavable “placeholder” peptide may simply serve as stock for the generation of various pMHC-I multimer bearing different epitopes (i.e. a pMHC-I library), which overall dramatically simplifies the production process (217). Ever since, UV-light-based peptide-exchangeable MHC-I multimers in combination with fluoro-chrome barcoding (discussed below) have been frequently applied in multiple studies for the generation of larger pMHC-I libraries validating the presence of tumor neoepitope-specific T cell pools as shown by (134–136, 225). More recently, also other technique for efficient peptide-exchange have been proposed including the production of stabilized empty MHC-I molecules combined with a dipeptide acting as peptide-exchange catalysts (226) and the usage of conditional MHC-I ligands that allow temperature-induced peptide exchange (227).

#### **1.5.2.2 Evolution of multiplex detection of antigen-specific T cells by pMHC-I multimers**

A key advantage of the pMHC-I multimer staining over conventional functional assays is the capacity to detected multiple antigen specifies within a given sample through the usage of certain detectable barcodes attached the pMHC-I multimer, thus allowing comprehensive screens with large epitope panels. Over the years several pMHC-I multimer barcoding approaches have been proposed with increasing complexity based on the combinatorial encoding of attached fluorochromes (185, 187) or heavy metal-labels (188) as well as unique DNA barcode tags (189), which will be shortly introduced.

**pMHC-I multimer fluoro-chrome-barcoding** | In their seminal study, Hadrup *et al.* used a two-dimensional combinatorial encoding with eight fluorochromes (i.e. PE, APC and six different Qdots) assigned to a distinct pMHC multimer (i.e. each pMHC multimer specificity may be detected by the combination of two unique colors), which resulted in 25 reliable combinations out of ideally 28 possible combinations due to the lack of the sensitivity of three particular combinations. Thus, up to 25 different antigen-specific T cell population could be analyzed simultaneously in one sample, thereby reducing the amount of biological material required for analysis by approximately the same factor (185). In a parallel study Newell *et al.* proposed a similar approach using a multivalent code, where the number of different T cell specificities that can be detected equals  $2^N - 1$ , where N is the number of different fluorescent labels (i.e. pMHC multimer specificity is reflected by the combination of multiple colors). Thus, with six fluorochromes up to 63 antigen-specificities may be theoretically distinguished by using a multivalent code. Yet, a drawback of this approach is that the dilution of the pMHC multimer binding signal by the number of different fluorochromes used to stain the same cell, which significantly reduces the overall sensitivity (187). Consequently, particularly the two-dimensional fluoro-chrome-encoding has been successfully and is frequently applied for studies aiming at validating cancer patient-derived neoepitopes by detecting the respective antigen-specific T cell populations (134–136, 225).

**pMHC-I multimer heavy metal barcoding** | In another study, Newell *et al.* explored the usage of purified isotopes of heavy metals (i.e. certain lanthanide isotopes) as tags attached to a pMHC-I multimer library combined with mass spectrometry-based flow cytometry (mass cytometry) also called cytometry by time-of-flight (CyTOF). Here, the authors used a unique combination of three out of ten possible heavy metal tags attached to pMHC-I multimers to simultaneously measure 103 out of 120 possible antigen specificities (188). Moreover, in contrast to fluoro-chrome- and DNA-barcoding the mass cytometry-based approach allowed at the same time to roughly measure 30 additional parameters (i.e. surface marker expression) describing the memory, activation or exhaustion state of

the detected antigen-specific T cell pools. Thus, CyTOF-based analysis combined with heavy metal-tagged pMHC-I multimer library allows as a key advantage a more comprehensive and simultaneous detection of multiple antigen-specific T cell populations and the assessment of their corresponding phenotypes (188, 199). However, on the downside currently used mass cytometers display a relative slow collection speed that require by default to magnetically enrich for pMHC multimer binding cells prior to their analysis in order to increase the overall sensitivity of this method. Moreover, mass-cytometry does not allow recovery of the sample as the cells are disrupted during the measurement. Last but not least, the limited availability of mass cytometers as well as high reagent cost strongly limits a wide spread usage of this technology (228).

**pMHC-I multimer DNA-barcoding** | More recently, Bentzen and colleagues used unique DNA barcodes attached to pMHC-I multimers (i.e. every single antigen-specificity is defined by a DNA barcode) to generate an impressive library that could subsequently be applied to screen over 1000 antigen specificities in a single sample. The DNA barcoding technology may even allow for much more comprehensive screenings as the complexity of the tagging system is much wider, providing up to  $10^{10}$  unique tags. In their approach, all uniquely DNA-barcoded pMHC-I multimers (i.e. Dextramers, Immudex) were additionally conjugated to the same flurochrome (i.e. PE) to allow in a first step a bulk FACS sorting of any T cells that have bound pMHC-I multimers. Subsequently, DNA barcodes were amplified after cell lysis and subjected to high-throughput bulk sequencing, which ultimately revealed the number of reads for a specific DNA barcode matching the corresponding pMHC-I-multimer. Thus, in contrast to combinatorial encoding of pMHC-I-multimers by either using fluorochrome or metal tags, where the signal intensities are directly applied to visualize and enumerate certain antigen-specific T cell population, the DNA-barcoding approach rather provides an estimate for the number of antigen-specific T cells after retrospective analysis of sequence reads than the exact number. Thus, despite the key advantage to use DNA-barcoded pMHC multimers to possibly screen relevant T cell epitopes on an almost genome wide level, this method does not allow direct enumeration of antigen-specific T cell populations, their direct visualization, nor their isolation (189). Moreover, the comprehensive workflow including library preparation, FACS-sorting, high-quality sequencing procedure and complex data analysis may also limit a broad application of this approach.

### 1.5.2.3 Aspects of pMHC-II multimers regarding production, design and usage

In the last decades considerable progress has been made in the identification of pMHC-I restricted CD8<sup>+</sup> T cell responses towards non-mutated tumor-associated antigens and mutated tumor-neoantigens in particular through the development of more accurate and straightforward peptide epitope *in silico* prediction algorithms as well as efficient recombinant soluble pMHC-I production systems. In contrast, it has been proven to be much more challenging to reliably predict which peptides will form stable complexes with MHC-II molecules due to the less stringent binding properties of the MHC-II peptide-binding groove allowing peptide fragments to protrude from both ends of the groove and the limited overall understanding of the endosomal MHC-II peptide processing as reviewed in (229). In addition recombinant production of soluble peptide-loaded MHC-II complexes by various approaches have been consistently more laborious and often less efficient compared to the pMHC-I counterpart as reviewed in (184, 204). Consequently, recombinant pMHC-II multimers have been barely used so far in comprehensive clinical cancer neoantigen discovery and validation trails. Yet, the portfolio of commercially available pMHC-II multimer reagents (e.g. by ProImmune or Immudex) is consistently expanding. In addition, also pMHC-I multimer barcoding approaches may theoretically also be applied for the detection of antigen-specific CD4<sup>+</sup> T cells. For instance Uchtenhagen *et al.*

already used a fluorochrome-barcoding approach for the simultaneous detection of six antigen-specific CD4<sup>+</sup> T cells populations at once (230).

**pMHC-II multimer design** | A variety of methods have been successfully used to manufacture soluble pMHC-II multimers referring to the construct design, production system and peptide-loading strategy. The most frequently used construct scheme comprises the MHC-II  $\alpha$ - and  $\beta$ -chain extracellular domains, which have been C-terminally fused to coiled-coil acidic/basic 'leucine zipper' sequences (e.g. derived from transcription factor pair Fos/Jun) to promote and stabilize the assembly of heterodimers of MHC-II  $\alpha$ - and  $\beta$ -chain. In addition, the C-terminal end of the respective zipper sequences may be prolonged by flexible linker amino sequences (e.g. repeats of glycine and serine) followed by an AviTag sequence and Hexahistidine-tag (His<sub>6</sub>-tag) to allow affinity chromatography, site-specific enzymatic biotinylation and finally the generation of MHC-II multimer through complexation with streptavidin (184, 204). Alternatively, also the construction of defined pMHC-II dimers on the basis of Ig-Fc fusions (i.e. bivalent heterodimeric pMHC-II Fc-fusion molecule) have been proposed, that may subsequently be multimerized further using fluorochrome-conjugated protein A (231).

**pMHC-II multimer production and peptide-loading strategy** | Since the *in vitro* refolding efficiency of in *E. coli* inclusion bodies produce MHC II molecules is typically very low, mainly eukaryotic cell-based systems that allow secretion of mostly folded MHC-II molecules have been preferred. These systems include most typically the co-expression of MHC-II  $\alpha$ - and  $\beta$ -chains in insect cells such as transiently baculovirus-infected sf9 cells (222) or stably transfected *Drosophila melanogaster* Schneider 2 cells (232). An advantage of the insect cell system is their apparent secretion of mostly stable but 'empty' MHC-II molecules that may be directly purified from the culture medium and loaded with a defined peptide *in vitro* under acidic conditions and elevated temperatures (e.g. pH 5–6, 30–37°C for 24–72 h). However, a major issue with this approach is that the peptide loading efficiency may vary between 80% and 10% depending on the peptide's affinity towards the MHC-II molecule (184), which may result in poor staining or complete lack of antigen-specific T cells. This problem holds especially true for the detection of tumor-associated antigens or self-antigen-specific CD4<sup>+</sup> T cell populations as shown by (233, 234). Thus, several groups explored the use of antigenic peptides modified with either N-terminal (234, 235) or C-terminal (236) tag-sequences (e.g. histidine tag, dinitrophenyl tag) to allow for affinity chromatography of actually peptide-loaded MHC-II complexes. Alternatively, several studies took advantage of genetic fusion of the peptide of interest to N-terminus of the  $\beta$ -chain via a long and flexible linker (221, 222), which also permits the production in mammalian cells such as Chinese ovary hamster cells (CHO) (235). However, a concern of this approach is that depending on the peptide truncations and used linker length the covalently associated peptide may bind preferentially in non-natural registers within the MHC-II binding groove and hence may be differently recognized by different antigen-specific CD4<sup>+</sup> T cell pools (237).

## 1.6 Expression of covalent assembled pMHC-I – The single-chain trimer concept

Starting in the early 90s, many research groups envisioned to express the entire peptide- $\beta_2m$ -MHC I molecule as a covalently assembled complex derived from a single polypeptide chain to boost CD8<sup>+</sup> T cell mediated immune responses independently of the host's antigen-presentation machinery, which is often affected by various immune evasion mechanism during viral infection and cancer progression (2, 238). The pMHC-I construct design termed single-chain trimer (SCT), which was originally proposed by the pioneering work of Ted H. Hansen and colleagues in the early 2000s (223) became the most successful and frequently used format for covalent pMHC-I assembly until today. The "original" SCT format is expressed as a single polypeptide that comprises the antigenic peptide followed by a first flexible linker (i.e. GGGAS(G<sub>4</sub>S)<sub>2</sub>) that connects the C-terminus of the peptide to the N-terminus of  $\beta_2m$ , and another second flexible linker (i.e. (G<sub>4</sub>S)<sub>4</sub>) that connects the C-terminus of  $\beta_2m$  with the N-terminus of the MHC-I heavy chain (**Fig. 1.11a**) (223). In their initial report Yu *et al.* demonstrated that SCTs on the basis of the full-length murine H2-K<sup>b</sup> (K<sup>b</sup>) heavy chain (i.e. including transmembrane domain) presenting the ovalbumin (OVA)-derived peptide<sub>257–264</sub> [SIINFEKL] are efficiently cell surface-expressed and recognized by an anti-OVA/K<sup>b</sup> TCR-like antibody (clone 25D-1.16) as well as by cognate OVA/K<sup>b</sup>-specific CD8<sup>+</sup> T cells derived from OT-1 TCR-transgenic mice. Moreover, the SCT format was shown to be highly refractory to peptide exchange by high-affinity competitor peptides compared to native K<sup>b</sup> loaded with endogenous peptides (223). Within the same year, a very similar SCT construct design (with slightly different linker lengths) was independently described by Greten *et al.* for the HLA-A\*02:01 allele, but who genetically fused the extracellular part of the SCT polypeptide to the variable domain of murine IgG1 (as already described for pMHC-I-dimers by Schneck *et al.* in **Section 1.5.2.2**) to produce soluble SCT-Ig molecules that could be used for the antigen-specific staining of cognate T cells (239). Ever since, the SCT format appears to be widely generalizable among MHC class I molecules since efficient SCT expression has also been reported for various other murine alleles including H2-K<sup>k</sup>, H2-D<sup>b</sup> and H2-D<sup>d</sup> as well as the human HLA-B\*27:05, HLA-A\*02:01 molecules, the non-classical MHC-I allele HLA-E (reviewed in (240)) and more recently HLA-A\*24:02 (241).

**Evolution of SCT design** | Most importantly, crystal structure analysis has confirmed that SCTs adopt the same structural conformation as native pMHC-I and are equivalently recognized by cognate TCRs (242). However, the binding groove of pMHC-I displays a "closed" configuration typically accommodating peptides of defined length (i.e. 8–10 residues). In particular the highly conserved MHC-I heavy chain tyrosine residue 84 (Y84) contributes to the formation of the F pocket, where it creates a "wall" that helps to position the C-terminal end of the antigenic peptide. Thus, with respect to the C-terminal peptide extension (i.e. first linker) used to construct the SCT, the Y84 residue forces the peptide extension to turn 90° and to project away from the plane of the binding groove as described in (242) and shown in **Fig. 1.11b**. Consequently, Hansen *et al.* reasoned to construct SCTs with a mutated residue Y84 to alanine (Y84A) to "open" the MHC binding groove at the C-terminal end to allow a better accommodation of the peptide linker extension. These SCT<sup>Y84A</sup> constructs displayed a very similar surface half-life compared to wild type (WT) SCTs (SCT<sup>WT</sup>). However, SCT<sup>Y84A</sup> were approximately 5-fold more refractory to peptide displacement and were also slightly better recognized by cognate CTL (243). In a subsequent study Hansen *et al.* additionally anchored the antigenic peptide within the binding groove by introducing an artificial disulfide bond termed "disulfide trap" into the SCT design. Based on structural data analysis, the disulfide bond was engineered between the second glycine residue of the C-terminal peptide extension (i.e. linker) mutated to cysteine (C) and MHC-heavy chain Y84 mutated to C (Y84C). These disulfide-trapped SCT (dt-SCT<sup>Y84C</sup>) displayed an improved thermal stability and were completely refractory to peptide-exchange. Moreover, the dt-SCT<sup>Y84C</sup> design

allowed the recombinant expression of pMHC-I complexes comprising very low-affinity peptides that typically failed to form without additional disulfide trap (242, 244, 245).

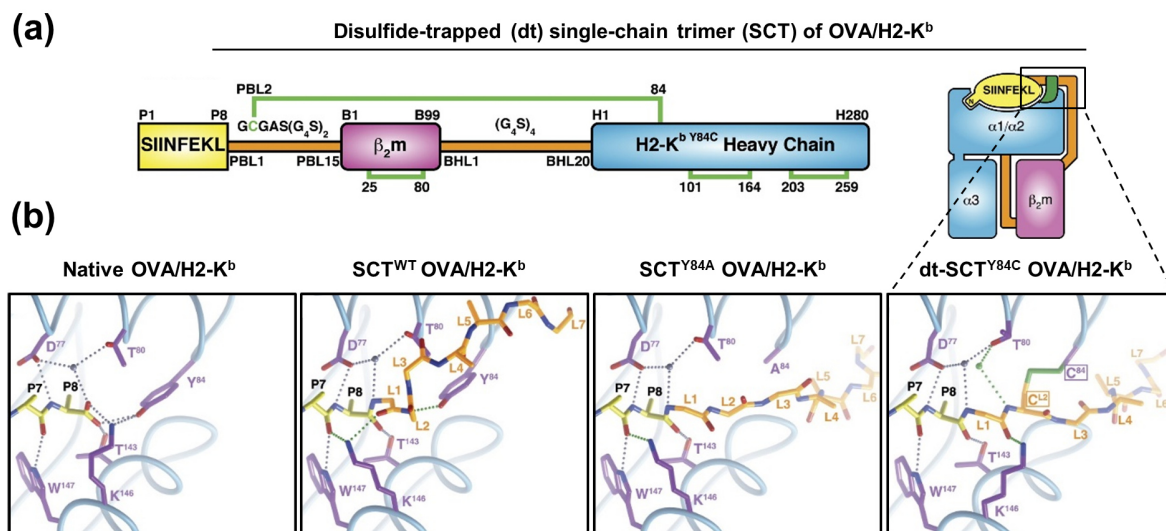


**Figure 1.11 | Disulfide-trapped single-chain trimer design and peptide anchoring in the MHC-I F pocket**

(a) **Schematic representation of the disulfide-trapped (dt) single-chain trimer (SCT) design.** The dt-SCT polypeptide for covalently-linked ovalbumin (OVA) peptide<sub>257-264</sub> [SIINFEKL] ligand (yellow box),  $\beta_2$ -microglobulin ( $\beta_2$ m, magenta) and murine MHC-I allele H2-K<sup>b</sup> heavy chain (HC, blue) is shown. The peptide- $\beta_2$ m (PBL) and  $\beta_2$ m-HC (BHL) linkers are shown in orange and comprise multiple glycine (G) and serine (S) residues. Amino acid residue numbering for the peptide ligand,  $\beta_2$ m and HC are indicated. Disulfide bonds bridging the respective cysteine (C) residues are illustrated by green brackets. The artificially introduced disulfide bridge between PBL residue 2 (PBL2) and HC residue tyrosine (Y) 84 mutated to C (Y84C) anchors the antigenic peptide at the F pocket and has been termed disulfide trap as shown in (b), on the very right site.

(b) **Structure analysis of the F pocket main chain anchoring across three SCT generations vs. native pMHC-I.** Crystal structural data illustration of HC residues (purple) involved in the C-terminal hydrogen bonding (dotted lines) of the OVA peptide main chain (i.e. the last two residues p7 and p8, yellow) in the F pocket of K<sup>b</sup>. HC residue Y84 of native OVA peptide loaded K<sup>b</sup> molecule sequesters the peptide C-terminal end inside the binding groove (left panel). In wild-type (WT) SCT residue Y84 forces the PBL (orange) to turn in a 90° degree (second left panel). Mutation Y84 to alanine (A) in SCT<sup>Y84A</sup> opens the binding groove and leads to a relaxation of the PBL. A PBL with a cysteine at position 2 (C<sup>2</sup>) and HC Y84C (C<sup>84</sup>) mutation leads to an additional peptide anchoring via a disulfide bridge (shown in green, right panel). Modified figure was adapted from (242) with permission.

**Application of SCTs as vaccine and cellular APCs |** The extended cell-surface half-life and the expression in an antigen-presentation machinery independent manner as shown by efficient SCT expression in TAP- as well as  $\beta_2$ m-deficient cells (246, 247), made cell membrane-associated SCT-encoding vectors an attractive vaccine approach to promote antigen-specific immunity against cancer or pathogens. To this end, several *in vivo* studies based on SCTs encoding DNA vaccines incorporating tumor antigens (e.g. oncoviral tumor antigens) have been conducted with moderate success (reviewed in (248)). Alternatively, SCT-expressing cells (e.g. autologous Mo-DCs, B cells or “universal” MHC-I negative cells) may also serve as potent cellular artificial APCs (aAPCs) for the *ex vivo* expansion of tumor-antigen specific CD8<sup>+</sup> T cells followed by adoptive cell transfer into cancer patients (248).

**Application of SCTs as pMHC-multimer staining tools |** Nevertheless, with regard to this study the application of SCTs for generation of reagents and assay platforms for the detection of antigen-specific T cells is most appealing, because the dt-SCT design may allow the generation of pMHC-I multimers presenting rather low affinity peptides, which often limits successful *in vitro* refolding of conventionally produced soluble pMHC-I complexes (209). Hansen *et al.* demonstrated the production of soluble

biotinylated SCTs that may be multimerized on the basis of streptavidin and could be equally applied as staining tools compared to conventionally produced pMHC-I (i.e. soluble peptide of interest is added during the *in vitro* refolding) (243, 245). In particular, pMHC-I multimers on the basis of dt-SCTs are attractive because they are hardly affected by peptide dissociation and thus may display longer shelf-lives. Yet, when produced *in E. coli* also soluble dt-SCTs require a labor-intensive *in vitro* refolding process (240), which may be circumvented by taking advantage of fusing the SCT to an IgG followed by the usage of mammalian expression system permitting native expression of SCTs as proposed by (239). However, as discussed above pMHC-I-IgG-dimers performed inferior as staining tools compared to pMHC-I-multimers and also in this case generation of stable producer cell lines were required for each new antigen to obtain sufficient amount of soluble SCT-Ig (239). Taken together, this made the mentioned production approach not attractive yet for the high-throughput generation of soluble pMHC-I libraries suitable for neoantigen discovery.

### **1.7 Artificial antigen-presenting cells – Flexible systems for cognate T cell activation**

With no doubt DCs are by far the most capable professional antigen-presenting cells to activate and drive the *in vitro* and *in vivo* expansion of naïve and memory T cells, making them invaluable tools for therapeutic applications such as cellular vaccines or the *ex vivo* expansion of antigen-specific T cells followed by adoptive T cell transfer (ACT) into patients in need (71). Yet, despite the successful and frequent usage of peripheral blood-derive Mo-DCs, there are often logistical issues typically regarding the functionality and quantity as well as laborious procedures to generate these cells from tumor-bearing patients, which are suffering from low blood cell counts and poor health status. Thus, various platforms have been engineered that mimic DC function referred to as artificial antigen-presenting cells (aAPCs) cells that typically comprise the expression or synthetic coupling of T cell activating proteins (e.g. cognate pMHC and co-stimulatory molecules) on the surface of cell lines (e.g., K562), biocompatible particles (e.g., microspheres/beads or liposomes) and complex 3D scaffolds (e.g. mesoporous silica rods). Ideally, aAPC represent “off-the-shelf” platforms that can be flexibly modulated with regard to the presented antigen or combination of co-stimulatory molecules allowing optimal triggering of T cell activation and expansion (reviewed in (249, 250)). Yet, one has to keep in mind, that these engineered platforms mimicking only the most rudimentary interactions that occur during T cell activation that is typically the delivery of “signal 1” by means of immobilized cognate pMHC for antigen-specific or agonistic anti-CD3 mAb (e.g. clone OKT3) for polyclonal T cell expansion in addition to “signal 2” provided by B7.1 (CD80), B7.2 (CD86) molecules or respective agonistic anti-CD28 mAbs. The missing “signal 3” is usually provided by soluble recombinant cytokines.

With regard to this study, the successful application of magnetic polystyrene beads of large diameters (>4.5  $\mu\text{m}$ ) (e.g. anti-mouse IgG Dynabeads) loaded with pMHC-I-Ig-dimers and anti-CD28 mAb for the *ex vivo* activation and expansion of tumor-associated antigen specific T cells (e.g. MART-1) have been of key interest. Since magnetic polystyrene beads allow easy manufacturing of various aAPCs as well as simple removal from cell suspension by application of a magnet as proposed by (216).

## 1.8 Aim of the study

**Rationale and global project objectives** | Targeting the individual cancer patient's mutagenome by manufacturing personalized tumor neoantigen-specific vaccines or performing adoptive transfer of neoantigen-specific T cell products are highly promising and currently developed immunotherapeutic approaches (119). However, the often limiting amounts of patient-derived cell material represents a bottle-neck for currently used processes aiming at the identification and validation of putative neoantigens derived from a single cancer patient, which includes as a major obstacle the monitoring of multiple respective neoantigen-specific T cell responses. This issue has been partially addressed by the development of barcoded pMHC multimer reagents or the interrogation of long-peptide pools or tandem minigenes combined with functional T cell assays (154). However, all these technological approaches, although being elegant and comprehensive, are not well suited for a broad and routine laboratory usage due to highly demanding and not cost-effective procedures as well as the partial requirement of highly specialized staff and equipment. Thus, to overcome limitations of these precursor technologies, the primary aim of this study was to develop a novel easy-to-use assay platform for the detection of multiple antigen-specific T cell responses within a single experimental multiplex reaction in a robust, sensitive as well as ideally cost- and time-effective manner. In addition, this multiplex assay platform should ideally permit recovery of the analyzed patient-derived T cell sample to allow for subsequent isolation, expansion and further comprehensive analysis of selected antigen-specific T cell populations. In a parallel and interlinked study aspect, we also sought for improved methods allowing for highly efficient and convenient recombinant production of soluble pMHC molecules that shall be the basis for the novel multiplex assay platform. In a final aspect of this study, we aimed for the validation of putative neoantigens derived from a cohort of cancer patients through the detection of respective neoantigen-specific T cell populations using our novel developed assay platform in comparison to available state-of-the-art assays such as pMHC multimer staining or ELISpot.

**Part 1 – A novel simplified and efficient approach for soluble pMHC production** | Prior to this presented study, the laboratory of PD Dr. Frank Momburg already cloned vector constructs of soluble pMHC-I molecules following the disulfide-trapped single-chain trimer (dt-SCT) design that were fused to the Fc portion of murine IgG2a (dt-SCT-Fc) (see results **Section 3.1** for construct scheme). These dt-SCT-Fc constructs were efficiently expressed and secreted by stable transfected human embryonic kidney 293 cells (HEK 293), which allowed simply purification of already correctly folded dt-SCT-Fc from cell supernatants by affinity chromatography. Yet, this approach still required the generation of stable cell lines. Thus, to further simplify and accelerate dt-SCT-Fc production, we wanted to take advantage of various published or commercially available, highly efficient protein production systems based on transient gene expression (TGE) in mammalian cells, which may offer convenient parallelized mass production of correctly folded and read-to-use soluble dt-SCT-Fc molecules. In addition, we wanted to explore novel dt-SCT-Fc designs suitable for bead-based aAPC assembly as well as for the generation of pMHC-I multimer reagents. And last but not least, we aimed for the implementation of novel pMHC-II-Fc molecules, which could be efficiently produced in transiently transfected mammalian cells.

**Part 2 – The rise of a novel multiplex assay** | We envisioned to develop an assay based on fluorescently color-coded (i.e. "barcoded") magnetic microbeads such as commercially available MagPlex<sup>®</sup> microspheres provided by Luminex (hereafter termed "Luminex beads") that, when conjugated with recombinant pMHC molecules, could potentially serve as artificial antigen-presenting cells (aAPCs) for the stimulation of cognate T cell populations resulting in the release of effector molecules.

## 1 | Introduction

Further, we hypothesized that conjugation of antibodies specific for effector molecules to the barcoded aAPCs could be used to leave a molecular “footprint” on aAPCs that have been in antigen-specific contact with the respective T cell (see for more details see **Section 4.1**). Thus, the presence of an antigen-specific T cell pool is indirectly detected by the T cell’s “footprint” left on the manufactured aAPCs, which in turn can be simply separated by magnetic force from the T cell sample for analysis. This novel assay approach might be highly attractive, since it would theoretically allow multiplex detection of functional T cell responses towards desired antigens, while leaving the T cell containing sample in culture for additional applications such as expansion, isolation or more comprehensive analysis of the already validated antigen-specific T cell populations.

Hence, the goals of the **first part** of this study were:

- i. Establishment of pMHC-I production using mammalian transient gene expression systems.
- ii. Validation of recombinant produced pMHC-I molecules with respect to their specific binding to cognate antigen-specific CD8<sup>+</sup> T cells.
- iii. Usage and testing of dt-SCT-Fc-based pMHC-I-conjugated beads serving as artificial antigen-presenting cells for the induction of antigen-specific T cell activation as well as proliferation.
- iv. Implementation of defined antigen-specific T cell lines serving as easily accessible model system for the development and validation of novel pMHC constructs and assay procedures.
- v. Development and testing of various novel pMHC-I SCT-Fc construct designs that allow the generation of higher-order pMHC multimers and are well suited for bead-based aAPC generation.
- vi. Production and validation of suitable pMHC-II-Fc molecules for the detection and stimulation of cognate antigen-specific CD4<sup>+</sup> T cells.

The goals of the **second part** of this study were:

- i. Development of a novel bead-based aAPC-barcoded multiplex assay platform for the detection of multiple antigen-specific T cell responses using recombinant soluble pMHC-I and pMHC-II molecules as well as fluorescently color-coded microbeads as a core concept.
- ii. Further optimization of an initial assay prototype and proof of an equally, if not better, detection of previously well-defined antigen-specific T cell populations in comparison to conventional state-of-the-art assays platforms.
- iii. Incorporation of the newly developed multiplex assay into a clinical study aiming for the identification and subsequent validation of an individual cancer patient-derived list of putative neoantigens.

## 2| Material and methods

### 2.1 Maintenance cell culture

#### 2.1.1 T2 cell line culture

##### Cell lines:

Name	Origin	Source / Cat. No. / [Reference]
<b>T2</b>	Human lymphoblastoid	ATCC / CRL-1992
<b>T2.DM.DR3</b>	Human lymphoblastoid	German Cancer Research Center (DKFZ) [(251)]

##### Cell culture media, consumables and equipment:

Name / Ingredients	Supplier	Cat. No.
<b>RPMI Medium 1640 (1x)</b> (Roswell Park Memorial Institute) <ul style="list-style-type: none"><li>▪ <i>Phenol red, without L-glutamine</i></li></ul>	Thermo Scientific	31870-025
[+] 10% (v/v) Heat-inactivated fetal bovine serum (FBS)	Biochrom	S 0615
[+] 2 mM GlutaMAX™ (L-alanyl-L-glutamine dipeptide)	Thermo Scientific	35050-038
[+] 100 Units/mL penicillin and 0.1 mg/mL streptomycin (Pen-Strep)	Sigma-Aldrich	P4333-100 ml
<b>Tissue culture flask</b> <ul style="list-style-type: none"><li>▪ <i>75 cm<sup>2</sup> vented screw lid, cell culture-treated</i></li></ul>	TPP	90076
<b>Trypan Blue Solution, 0.4%</b>	Thermo Scientific	15250-061
<b>Brand® counting chamber</b> (improved Neubauer chamber)	Sigma-Aldrich	BR717805-1EA
<b>Heracell™ 240i CO<sub>2</sub></b> Incubator with stainless steel chamber	Thermo Scientific	-

- Suppliers' specifications | [+] Medium supplements additionally added | Cat. No.: Suppliers' catalogue numbers

##### T2 cell line culture conditions:

The cell lines **T2** and **T2.DM.DR3** were routinely cultured in RPMI supplemented with 10% FBS, 2 mM GlutaMAX™ and Pen-Strep at 37°C in a humidified 5% CO<sub>2</sub> atmosphere. T2 is a TAP (transporter associated with antigen processing)-deficient lymphoblastoid suspension cell line that exclusively expresses HLA-A\*02:01 on the cell surface and lacks other HLA-allele surface expression (252). The T2.DM.DR3 cell line has been generated and previously described by Verreck *at al.* (251) and is derived from the T2 cell line. T2.DM.DR3 stably expresses the HLA-DRB1\*03:01/DRA\*01:01 (HLA-DR3) allele and HLA-DM in addition to HLA-A\*02:01. Homogeneous HLA-DR expression was confirmed for T2.DM.DR3 cells by anti-HLA-DR mAb (clone L243) surface staining using the general flow cytometry analysis procedure described in **Section 2.7.1 (data not shown)**.

## 2 | Material and methods

### 2.1.2 Mammalian cell lines for recombinant protein production

Suspension-adapted cell lines for protein production:

Name	Origin	Source / Cat. No.
<b>FreeStyle™ CHO-S cells</b>	Chinese hamster ovary (CHO)	Thermo Scientific / R80007
<b>ExpiCHO-S™ cells</b>	Chinese hamster ovary (CHO)	Thermo Scientific / A29127
<b>FreeStyle™ 293-F cells</b>	Human embryonic kidney (HEK)	Thermo Scientific / R79007
<b>Expi293F™ Cells</b>	Human embryonic kidney (HEK)	Thermo Scientific / A14528

Cell culture media, consumables and equipment:

Name / Ingredients	Supplier	Cat. No.
<b>PowerCHO-2 CD</b> (chemically defined) <ul style="list-style-type: none"> <li>▪ <i>HEPES, 1x Pluronic® F-68 without L-glutamine, HT, phenol red</i></li> </ul>	Lonza	BE12-771Q
[+] 8 mM GlutaMAX™ (L-alanyl-L-glutamine dipeptide)	Thermo Scientific	35050-038
[+] 1x HT Media Supplement Hybridmax™ (2 vials / 1L) <ul style="list-style-type: none"> <li>▪ <i>13.6 mg/L hypoxanthine, 3.9 mg/L thymidine</i></li> </ul>	Sigma-Aldrich	H0137-10VL
[+] 0.5x Antibiotic Antimycotic solution (Anti-Anti) <ul style="list-style-type: none"> <li>▪ <i>50 units/mL penicillin; 0.05 mg/mL streptomycin; 0.1 µg/mL amphotericin B</i></li> </ul>	Sigma-Aldrich	A5955-100 ml
<b>ExpiCHO™ Expression Medium</b> <ul style="list-style-type: none"> <li>▪ <i>GlutaMAX™, 1x Pluronic® F-68</i></li> </ul>	Thermo Scientific	A29100-01
<b>FreeStyle™ 293 Expression Medium</b> <ul style="list-style-type: none"> <li>▪ <i>GlutaMAX™, serum free,</i></li> </ul>	Thermo Scientific	12338-018
<b>Expi293™ Expression Medium</b> <ul style="list-style-type: none"> <li>▪ <i>GlutaMAX™, serum free</i></li> </ul>	Thermo Scientific	A1435101
<b>Corning® Erlenmeyer cell culture flask 125 mL</b> <ul style="list-style-type: none"> <li>▪ <i>125 mL Erlenmeyer flask with vent cap, polycarbonate</i></li> </ul>	Sigma-Aldrich	CLS431143-50EA
<b>Corning® Erlenmeyer cell culture flask 250 mL</b> <ul style="list-style-type: none"> <li>▪ <i>250 mL Erlenmeyer flask with vent cap, polycarbonate</i></li> </ul>	Sigma-Aldrich	CLS431144-50EA
<b>Corning® Erlenmeyer cell culture flask 500 mL</b> <ul style="list-style-type: none"> <li>▪ <i>500 mL Erlenmeyer flask with vent cap, polycarbonate</i></li> </ul>	Sigma-Aldrich	CLS431145 -25EA
<b>Laboratory round-bottom glass bottle 500 mL</b>	Duran	218014418
<b>Heracell™ 240i CO<sub>2</sub> Incubator</b> with stainless steel chamber	Thermo Scientific	-
[+] MaxQ™ 2000 Benchtop <b>Orbital Shaker</b> CO <sub>2</sub> resistant <ul style="list-style-type: none"> <li>▪ <i>19 mm shaking diameter</i></li> </ul>	Thermo Scientific	SHKE2000CO2

▪ Suppliers' specifications | [+] Medium supplements additionally added | Cat. No.: Suppliers' catalogue numbers

Maintenance culture conditions:

**Freestyle™ CHO-S** cells (CHO-S) were cultured routinely in 500 mL round-bottom glass bottles filled with 100 mL PowerCHO-2CD medium supplemented with 8 mM GlutaMAX™, 0.5x Anti-Anti and 1x HT at 37°C, 130 rpm with a 19 mm shaking diameter in a humidified 8% CO<sub>2</sub> atmosphere. CHO-S were cultured until a density of 4x10<sup>6</sup> cells/mL was reached and were subsequently either 1:10 diluted for subculture or directly processed for transfection as described in **Section 2.3.1**.

**ExpiCHO-S™ cells (CHO-X), 293-F cells and Expi293F™ cells (293-X)** were routinely cultured depending on the experimental needs in polycarbonate Erlenmeyer cell culture flask of various size filled with ExpiCHO expression medium, 293 expression medium or Expi293 expression medium, respectively, at 37°C, 130 rpm (19 mm shaking diameter) in a humidified 8% CO<sub>2</sub> atmosphere. CHO-X were cultured until a density of 4–6x10<sup>6</sup> cells/mL was reached and were subsequently either 1:10 diluted for subculture or directly processed for transfection (**Section 2.3.2**). 293-F cells were cultured until a density of 2x10<sup>6</sup> cells/mL was reached and were subsequently either 1:10 diluted for subculture or directly processed for transfection (**Section 2.3.3**). 293-X cells were cultured until a density of 3–5x10<sup>6</sup> cells/mL was reached and were subsequently either 1:10 diluted for subculture or directly processed for transfection (**Section 2.3.4**).

### 2.1.3 T cell line culture

#### Human CD8<sup>+</sup> T cell lines:

Short-Name	Specificity (peptide/MHC-allele)	Source / Reference
<b>Survivin/A2 T cell line</b>	Survivin <sub>96–104</sub> /HLA-A*02:01	DKFZ/BHC Joint Immunotherapy Laboratory / (253)
<b>CMV/A2 T cell lines:</b> #104 #315 #416 #8667 #5561	HCMV pp65 <sub>495–503</sub> / HLA-A*02:01	All virus-specific T cell lines were generated within this study according to <b>Section 2.8</b> and were derived from healthy blood donors.
<b>EBV/A2 T cell lines:</b> #0144	EBV BMLF-1 <sub>259–267</sub> / HLA-A*02:01	
<b>FLU/A2 T cell lines:</b> #3628	Flu A MP-1 <sub>58–66</sub> / HLA-A*02:01	

#### Human CD4<sup>+</sup> T cell lines:

Clone name [Short-Name]	Specificity (peptide/MHC-allele)	Source / Reference
<b>RP15.1.1</b> [MTB/DR3 CD4 <sup>+</sup> T cells]	MTB Hsp65 <sub>1–13</sub> / HLA-DRB1*03:01/DRA*01:01 (HLA-DR3)	Fritz Koning & Yvonne Kooy Leiden University Medical Center / (254, 255)

#### Cell culture media, reagents and consumables:

Name / Ingredients	Supplier	Cat. No.
<b>AIM V™ Medium</b> ▪ with L-glutamine, gentamicin, streptomycin sulfate, phenol red [+] 10% (v/v) Human serum type AB [+] 20 – 50 units/mL human interleukin-2 (IL-2) [+] 2.5 – 10 ng/mL human interleukin-15 (IL-15)	Thermo Scientific PAN Biotech Miltenyi Biotec Miltenyi Biotec	12055091 P30-2501 130-097-748 130-095-764
<b>Benzonase® Nuclease (DNase)</b>	Sigma-Aldrich	E1014-25KU
<b>Phaseolus Vulgaris Leucoagglutinin (PHA-L)</b>	Sigma-Aldrich	EDTA
<b>24-well cell culture plate flat-bottom</b>	TPP	92024
<b>Tissue culture flask, 75cm<sup>2</sup>, vented closure, cell culture treated</b>	TPP	90076

▪ Suppliers' specifications | [+] Medium supplements additionally added | Cat. No.: Suppliers' catalogue numbers

### 2.1.3.1 Survivin/HLA-A2-specific CD8<sup>+</sup> T cell line maintenance culture

The human **Survivin<sub>96-104</sub>/HLA-A2-specific** CD8<sup>+</sup> T cell line (Sur/A2 T cells), which specifically recognizes the human Survivin<sub>96-104</sub> [LMLGEFLKL] peptide presented on the MHC-I allele HLA-A\*02:01 was previously described by Leisegang *et al.* (253). For this study, Sur/A2 T cells were kindly provided and have routinely been expanded by the DKFZ-Bayer HealthCare (BHC) Joint Immunotherapy laboratory, Heidelberg. Briefly, Sur/A2 T cells have been expanded over a period of 4-weeks using irradiated (33 Gy) HLA-A2-matched PBMC feeder cells as well as irradiated (180 Gy) Epstein-Barr virus (EBV)-transformed B-lymphoblastoid cells (B-LCL) and an initial addition of 10 ng/mL anti-human CD3 (clone OKT3) mAb on day 1. Cells were cultured in AIM-V supplemented with 10% human serum type AB, interleukin (IL)-2 [50 units/mL] and IL-15 [2.5 ng/mL]. 50% of the medium was changed on a weekly basis within the 4-week expansion phase. After the expansion phase, the Sur/A2 T cell culture was used for experiments and further maintained at 37°C and 8% CO<sub>2</sub> by weekly addition of 20 units/mL IL-2 and 2.5 ng/mL IL-15 without changing the medium itself.

### 2.1.3.2 Virus-specific CD8<sup>+</sup> T cell line maintenance culture

Within this study several virus epitope-specific and HLA-A\*02:01-restricted human CD8<sup>+</sup> T cell lines have been generated according to **Section 2.8**. After an antigen-specific expansion phase for approximately 4 weeks including an enrichment step for antigen-specific T cells, the established and pure virus-specific CD8<sup>+</sup> T cell lines were routinely cultured in 24-well cell culture plates using AIM-V supplemented with 10% human serum type AB, IL-2 [20 units/mL] and IL-15 [5 ng/mL] at 37°C and 5% CO<sub>2</sub>. 50% of the medium was exchanged on a weekly basis.

### 2.1.3.3 MTB/HLA-DR3-specific CD4<sup>+</sup> T cell line expansion and maintenance culture

The human **MTB Hsp65<sub>1-13</sub>/HLA-DR3-specific** CD4<sup>+</sup> T cell line clone RP15.1.1 (MTB/DR3 T cells), which specifically recognizes the Mycobacterium tuberculosis (MTB) heat shock protein of 65-kDa (Hsp65) derived peptide MTB Hsp65<sub>1-13</sub> [MAKTIAYDEEARR] presented on the MHC-II allele HLA-DRB1\*03:01/DRA\*01:01 (HLA-DR3) (254, 255) was a generous gift from Yvonne Kooy and Fritz Koning (Leiden University Medical Center, Netherlands). Cryostocks of the MTB/DR3 T cell line were quickly thawed at 37°C using pre-warmed complete medium (AIM-V + 10% human AB serum) supplemented with 1 unit/mL DNase to prevent cell clumping caused by dying cells. For initial cell expansion, freshly thawed MTB/DR3 T cells were seeded at 0.3x10<sup>6</sup> cells/mL onto 1x10<sup>6</sup> cells/mL irradiated PBMC feeder cells (33 Gy) derived from two different healthy donors and were cultured in 24-well cell culture plates using 1mL/well AIM-V supplemented with 10% human serum type AB, IL-2 [20 units/mL], IL-15 [10 ng/mL] and PHA-L [1 µg/mL]. After 3 days, 0.5 volume of fresh medium without PHA-L was added. Thereafter, medium was replaced every 3–4 days and MTB/DR3 T cells were used for experiments starting from day 14 of the initial PHA-L-based cell expansion.

### 2.1.4 Culture and preparation of human peripheral blood mononuclear cells (PBMC)

Human blood samples:

Name:	Source
Human buffy coats obtained from blood donations of healthy volunteers	Blut Bank Heidelberg / Mannheim Deutsches Rotes Kreuz

### Cell culture media, reagents and consumables for PBMC generation and culture:

Name / Ingredients	Supplier	Cat. No.
<b>RPMI Medium 1640 (1x)</b> <ul style="list-style-type: none"><li>▪ <i>Phenol red, without L-glutamine</i></li></ul>	Thermo Scientific	31870-025
[+] 2 mM GlutaMAX™ (L-alanyl-L-glutamine dipeptide)	Thermo Scientific	35050-038
[+] 20 units/mL human interleukin-2 (IL-2)	Miltenyi Biotec	130-097-748
[+] 10 µg/mL Gentamicin	Sigma-Aldrich	G1272-100ML
[+] 1 unit/mL Benzonase® Nuclease (DNase)	Sigma-Aldrich	E1014-25KU
<b>Biocoll Separating Solution</b> <ul style="list-style-type: none"><li>▪ <i>1.077 g/mL, isotonic solution</i></li></ul>	Biochrom	L 6115
<b>DPBS (1x)</b> (Dulbecco's Phosphate Buffered Saline) <ul style="list-style-type: none"><li>▪ <i>pH 7.2, no MgCl<sub>2</sub> and CaCl<sub>2</sub></i></li></ul>	Sigma-Aldrich	D8537-500ML
<b>RPMI Medium 1640 (1x)</b> <ul style="list-style-type: none"><li>▪ <i>without L-glutamine, phenol red</i></li></ul>	Thermo Scientific	11835-063
<b>Tissue culture flask, 75cm<sup>2</sup> vented closure, cell culture treated</b>	TPP	90076
<b>BD Falcon™ Conical 50 mL.flat-top screw cap tube, polypropylene</b>	BD Bioscience	352070

▪ Suppliers' specifications | [+] Medium supplements additionally added | Cat. No.: Suppliers' catalogue numbers

### PBMC preparation procedure:

**Human peripheral blood mononuclear cells (PBMCs)** were isolated from blood sample preparations using standard gradient centrifugation. Blood samples from healthy donors were collected according to the principles of the Declaration of Helsinki and were obtained from Deutsches Rotes Kreuz (DRK) Blutspendedienst Baden-Württemberg-Hessen gGmbH, Mannheim. Briefly, the content of a blood bag was ~1:1 diluted using DPBS stored at RT. 15 mL Biocoll separating solution (pre-warmed to RT) were transferred to a 50 mL tube and 30 mL diluted blood was carefully layered on top without mixing. Next, the filled tube was centrifuged at 1800 rpm, 30 min at RT with the centrifuge's brake turned off. After the centrifugation, the mononuclear cells containing interphase (buffy coat) between blood plasma (top) and separating solution (bottom) was collected and transferred into a new tube. To wash the cells, the tube was filled with RPMI (without supplements and phenol red) and centrifuged at 800 rpm, 10 min at RT with the centrifuge brake turned on. This washing step was repeated for 2 times using 5 min centrifugation instead. Finally, the washed PBMC pellet was resuspended in a culture medium depending on the subsequent experimental needs as discussed below.

### PBMC culture conditions:

For short-term culture of up to 5 days and usage as feeder cells for T cell line expansion as well as for the FACS compensation set-up, PBMC were cultured at a concentration of  $\sim 3 \times 10^6$  cells/mL in RPMI supplemented with GlutaMAX™ [2 mM], gentamicin [10 µg/mL], IL-2 [20 units/mL] and DNase [1 unit/mL] at 37°C in a humidified 5% CO<sub>2</sub> atmosphere. In case the PBMC sample was intended for additional analytical experiments or kept for longer than 5 days in culture, 2% human serum type AB and IL-15 [2.5 ng/mL] was added. In case a long-term CD8<sup>+</sup> T cell culture was intended, AIM-V medium supplemented with 10% human serum type AB, IL-2 [20 units/mL], IL-15 [5 ng/mL] was used and 50% of the medium was changed on a weekly basis.

## 2.2 Molecular biology related work

**Initial remarks** | All constructs used in this study were designed and kindly provided by PD Dr. Frank Momburg (DKFZ). Cloning strategies were developed by PD Dr. Frank Momburg and carried out by Nadja Bulbuc (DKFZ). Individual protein sequences are shown in the **Appendix section**. Fully assembled expression vectors were confirmed by DNA sequencing prior subsequent protein production. The cloning process will be described schematically for the used constructs in the following.

### 2.2.1 Cloning of various disulfide-trapped pMHC-I single-chain trimer Fc-fusion constructs

The core-concept of peptide-MHC-I complexes (pMHC-I) assembled and expressed as a covalently-linked peptide- $\beta_2$ -microglobulin-MHC-I-ectodomain single-chain trimeric complex (pMHC-I [SCT]) have been previously described by (223, 243, 245) and previously introduced in **Section 1.6 / Fig. 1.11**. Moreover, we adopted an engineered intramolecular disulfide-bridge designated as “disulfide trap” (dt) between the C-terminal peptide ligand extension (2<sup>nd</sup> residue of the linker between peptide’s C-terminus and the  $\beta_2$ m’s N-terminus) and a cysteine (C) replacing a highly conserved tyrosine (Y) at position 84 within the MHC-I heavy chain (242, 244, 245). In this study, constructs were predominantly used that encode for a pMHC-I [SCT] fused to a mIgG2a-Fc followed by a C-terminal Strep-tag II sequence, which were recently described by us on the basis of the allele HLA-E\*01:03 (256). Briefly, disulfide-trapped (dt) peptide-HLA-A\*02:01-mIgG2a-Fc fusion constructs (dt-pHLA-A2-Fc / **Results Section 3.1 / Figure 3.1**) were assembled in pBluescript KS II(+) (Stratagene) using oligonucleotides or PCR products coding for (listed in 5’–3’):

- 1) The modified influenza virus hemagglutinin H1N1 leader sequence (MAKANLLVLLCALAAADA),
- 2) a 9–11 amino acid long peptide epitope sequence of choice (**Table 3.1 & 4.5**),
- 3) the glycine-serine linker #1 containing a **cysteine** residue at position 2 (GCGSGGGGAPGSGGGS),
- 4) the human  $\beta_2$ -microglobulin sequence (GenBank: BC064910, Ile<sub>21</sub>–Met<sub>119</sub>),
- 5) glycine-serine linker #2 (RSASGGGGSGGGGSGGGGSASGGG),
- 6) the ectodomain of HLA-A\*02:01 (GenBank: BC019236, Gly<sub>25</sub>–Pro<sub>307</sub>), with a Tyr to Cys mutation at position 84 [Y84C] to form a disulfide-bridge with Cys<sub>2</sub> in linker #1 (disulfide trap) as described by (242, 245),
- 7) linker #3 TSQLTS,
- 8) the hinge-CH2-CH3-Fc portion of mouse IgG2a (NCBI GenBank: BC031470; Glu<sub>215</sub>–Lys<sub>447</sub>, containing mutations Cys<sub>224</sub>/Ser [C224S] and Asn<sub>297</sub>/Gln [N297Q],
- 9) a C-terminal **Strep-tag II** (IBA Lifesciences) with adaptor sequences (DPGWSHPQFEKSR).

The finally assembled cDNA sequence was cloned between the *NheI* and *XbaI* sites of the expression vector pcDNA3.1(+) (Invitrogen), that provided for an in-frame stop codon.

#### 2.2.1.1 Cloning of a heterodimeric pMHC-I-Fc construct with a single AviTag (pMHC-I-pCC-Fc)

Heterodimeric pMHC-I-pCC-Fc constructs [ID: 9237.1 and 10347.7] harboring a single AviTag (Avidity) sequence for enzymatic site-specific biotinylation (**Results Section 3.3 / Fig. 3.8**) were assembled as a bicistronic cassette in pBluescript KS II(+) (Stratagene) using oligonucleotides or PCR products coding for (listed in 5’–3’):

- 1–6) Element as described in **Section 2.2.1** comprising the whole dt-pHLA-A2 sequence,
- 7) linker #3 (ASGNSGGGGSKQLKKKQLQALKKKNAQLKWKLQALKKKLAQ) containing the basic parallel coiled-coil heterodimerization domain (**pCC-basic**) as described by (257),

**8)** the hinge-CH2-CH3-Fc portion of mouse IgG2a (GenBank: BC031470; Glu<sub>215</sub>–Lys<sub>447</sub>, containing mutations Cys<sub>224</sub>/Ser [C224S] and Asn<sub>297</sub>/Gln [N297Q]),

**9)** a C-terminal AviTag (258) followed by a **hexa histidine-tag** (His<sub>6</sub>-tag) sequence (DPGLNDIFEAQKIEWHEHHHHH),

**10)** the *Thosea asigna* virus-derived 2A-like (T2A) sequence (GSGEGRGSLTCGDVEENPGP) as described by (259, 260),

**11)** in frame elements **1–6** as described in **Section 2.2.1**,

**12)** linker #3 (ASGNSGGGGSKQLEKELQALEKENAQLWELQALEKELAQ) containing the complementary acidic parallel coiled-coil heterodimerization domain (**pCC-acidic**),

**13)** followed by the Hinge-CH2-CH3-Fc of mouse IgG2a [C224S / N297Q]

**14)** a C-terminal **tandem-Strep-tag II** (DPGWSHPQFEKSSGGGGSGGGGGSSWSHPQFEKV) with flexible glycine-serine spacer and flanking amino acids coding for restriction sites.

The finally assembled cDNA sequence was cloned between the *NheI* and *XbaI* sites of expression vector pcDNA3.1(+) (Invitrogen), that provided for an in-frame stop codon.

### **2.2.1.2 Cloning of homodimeric pMHC-I-Fc construct with an optionally cleavable Fc (pMHC-I-\*Fc)**

In a modified version of the in **Section 2.2.1** introduced dt-pMHC-I-mIgG2a-Fc [Hinge-CH2-CH3] construct design, solely the linker #3 was replaced by an extended linker version (linker #3\*) containing in N- to C-terminal order an octa histidine-tag (**His<sub>8</sub>-tag**), an AviTag (biotinylated at the lysine residue indicated in **bold**) and a **tandem thrombin cleavage site** (flanked by amino acids coding for restriction sites) (TSQLASTGQLHHHHHHHHQLGLNDIFEAQKIEWHEL**VPRSLVPR**STS). This modified linker #3\* was C-terminal fused to hinge-CH2-CH3-Fc portion of mouse IgG2a followed by a C-terminal Strep-Tag II sequence. The resulting constructs based on the HLA-A\*02:01 allele ectodomain are shown in **Results Section 3.4 / Fig. 3.10 and Supplementary Table S1**. These constructs allow the initial production of homodimeric dt-pMHC-I-\*mIgG2a-Fc molecules with the option to enzymatically cleave the Fc portion (cleavable Fc / \*Fc) and purify monomeric pMHC-I (Fc-cleaved pMHC-I / pMHC-I\*) molecules as described in more detail in (**Section 2.5.2.2 – 2.5.2.3 and Results Section 3.4**).

### **2.2.1.3 Cloning of a Fc-free monomeric pMHC-I construct**

For cloning of Fc-free monomeric pMHC-I constructs based on a dt-SCT (**Supplementary Fig. S5 and Supplementary Table S2**), the in **Section 2.2.1** introduced dt-pHLA-A2-mIgG2a-Fc [Hinge-CH2-CH3] construct was modified by replacing the linker #3 by an extended linker containing in N- to C-terminal order a hexa histidine-tag (**His<sub>6</sub>-tag**), a triple **FLAG-tag** followed by an C-terminal AviTag (**HHHHHHGIQDYKDDDDKADYKDDDDKALDYKDDDDKALEVLFQGPALHPMAGGLNDIFEAQKIEWHEVD**), which was not genetically fused to a mIgG2a-Fc as described before.

### **2.2.1.4 Cloning of pMHC-I-Fc with HLA-I $\alpha$ 2-domain Q115E mutation and pMHC-I-CH1-Fc constructs** dt-pMHC-I-Fc construct with $\alpha$ 2-domain Gln<sub>115</sub> to Glu mutation [Q115E]:

For selected experiments (**Results Section 4.3.4 / Fig. 4.18**), modified dt-pMHC-I-Fc constructs [9670.1 & 9672.1] comprising the HLA-A\*02:01 ectodomain (dt-pHLA-A2-Fc) were cloned as described in **Section 2.2.1**, which contained an additional Gln to Glu [Q115E] point mutation at position 115 within the  $\alpha$ 2-domain of the HLA-A\*02:01 allele as previously described by (261).

## 2 | Material and methods

### pMHC-I-CH1-Fc constructs:

In addition to the dt-pMHC-I-mIgG2a-Fc [Hinge-CH2-CH3] constructs as described in **Section 2.2.1**, a modified version was cloned that comprised the dt-pHLA-A2 **elements 1–6 / Section 2.2.1** fused to the CH1-Hinge-CH2-CH3 portion of mouse IgG2a (GeneBank: BC031470; residues Thr<sub>114</sub>–Lys<sub>447</sub>), containing mutations Cys<sub>224</sub>/Ser [C224S] resulting in constructs 8414.1 and 8415.2.

### 2.2.2 Cloning of a heterodimeric monovalent pMHC-II-pCC-Fc construct

Heterodimeric peptide-conjugated MHC-II-pCC-Fc constructs on the basis of the MHC-II allele ectodomain derived from the HLA-DRB1\*03:01  $\beta$ -chain ( $\beta$ 1- $\beta$ 2) and the monomorphic  $\alpha$ -chain ( $\alpha$ 1- $\alpha$ 2) DRA\*01:01 (pHLA-DR3-pCC-Fc) (**Results Section 3.6.1 / Fig. 3.14 and Supplementary Table S3**) were either assembled as a two-vector system as described in detail below or as single-vector system comprising the elements 1–7 fused to 1'–4' via a T2A sequence.

#### **2.2.2.1 Cloning of a pMHC-II-pCC-Fc construct as a two-vectors system**

For pMHC-II-pCC-Fc expression using two separated vectors encoding the following oligonucleotides or PCR products were assembled in pBluescript KS II(+) as listed in 5'–3':

#### Peptide-HLA-DRB1\*03:01 $\beta$ -chain constructs:

- 1) The human serum albumin (HSA) leader sequence (Met<sub>1</sub>–Ser<sub>18</sub>) (MKWVTFISLLFLFSSAYS),
- 2) a 13–20 amino acid long peptide epitope sequence of choice,
- 3) glycine-serine linker #1 (GSGGGGSGGGGSGGGGSG),
- 4) the HLA-DRB1\*03:01 (DR  $\beta$ -chain) ectodomain sequence (GenBank: NM\_001243965, residues Gly<sub>30</sub>–Lys<sub>238</sub>)
- 5) linker #2 (NSGGGGSKQLKKKLQALKKKNAQLKWKLQALKKKLAQ) containing the **basic parallel coiled-coil heterodimerization domain** (pCC-basic),
- 6) the Hinge-CH2-CH3-Fc portion of mouse IgG2a (GenBank: BC031470; Glu<sub>215</sub>–Lys<sub>447</sub>, containing mutations Cys<sub>224</sub>/Ser [C224S] and Asn<sub>297</sub>/Gln [N297Q]),
- 7) a C-terminal hexa histidine-tag (**His<sub>6</sub>-tag**) sequence (DPGHHHHHSS) (flanked by amino acids coding for restriction sites).

#### DRA\*01:01 $\alpha$ -chain construct:

- 1\*) the HLA-DRA\*0101  $\alpha$ -chain ectodomain sequence including ER leader (GenBank: BC071659, residues Met<sub>1</sub>-Glu<sub>216</sub>),
- 2\*) linker #3 (NSGGGGSKQLEKELQALEKENAQLWELQALEKELAQ) containing the complementary **acidic parallel coiled-coil heterodimerization domain** (pCC-acidic).
- 3\*) the hinge-CH2-CH3-Fc portion of mouse IgG2a [C224S / N297Q],
- 4\*) a C-terminal tandem-Strep-tag II or AviTag sequence.

The finally assembled cDNA sequence was cloned between the *Bsp120I* and *NotII* sites of expression vector pcDNA3.1(-) (Invitrogen), that provided for an in-frame stop codon.

#### **2.2.2.2 Cloning of a peptide-exchangeable (px) MHC-II-pCC-Fc construct**

To generate a pMHC-II-pCC-Fc construct that allows the optional replacement of a covalently associated placeholder peptide-ligand by addition of suitable chemically synthesized soluble peptide

of choice (**Section 2.10 and Results Section 3.6.3 / Fig. 3.16**), two major deviations from the elements in **Section 2.2.2.1** described construct were made:

**2)** the CLIP<sub>103–117</sub> (class II-linked invariant chain peptide) (PVSKMRMATPLLMQA) peptide was selected as universal placeholder peptide,

**3)** glycine-serine linker #1 contains the canonical human **thrombin cleavage site** (GSGGSLVPRGSGGSGS) for the enzymatic removal of the peptide-place holder.

### **2.2.2.3 Cloning of a pMHC-II-pCC-Fc constructs as an one-vector system**

For pMHC-II-pCC-Fc expression using a single vector the following oligonucleotides or PCR products were assembled in pBluescript KS II(+) as listed in 5'-3':

**1–6) Elements as described in 2.2.2.1** comprising the pHLA-DRB1\*03:01-pCC-basicFc sequence

**7)** a C-terminal AviTag followed by a His<sub>6</sub>-tag sequence

**8)** the *Thosea asigna* virus-derived 2A-like (T2A) sequence (GSGEGRGSLTCDVEENPGP) as described by (259, 260),

**9) Elements 1\*–4\* as described in 2.2.2.1** comprising the HLA-DRA\*01:01-pCC-acidic-Fc sequence

**10)** a C-terminal tandem-Strep-Tag II.

The finally assembled cDNA sequence was cloned between the *Bsp120I* and *NotI* sites of expression vector pcDNA3.1(-) (Invitrogen), that provided for an in-frame stop codon.

### 2.2.3 Cloning of a heterodimeric HLA-DM-pCC-Fc construct

To facilitate a peptide-exchange of peptide-exchangeable HLA-DR3-pCC-Fc constructs, also HLA-DM was additionally cloned and expressed (**Results Section 3.6.1 / Fig. 3.17**). The heterodimeric HLA-DM-pCC-Fc construct follows the design principle of the pMHC-II-pCC-Fc constructs described before, using oligonucleotides or PCR products assembled in pBluescript KS II(+) as listed in 5'-3' below. The finally assembled cDNA sequence was cloned between the *Bsp120I* and *NotI* sites of expression vector pcDNA3.1(-) (Invitrogen), that provided for an in-frame stop codon.

#### HLA-DMB-pCC-basic-Fc construct:

**1)** The HLA-DM  $\beta$ -chain (HLA-DMB) ectodomain sequence including ER leader (GenBank: NM\_002118.5, residues Met<sub>1</sub>-Lys<sub>218</sub>),

**2)** a linker sequence (NSGGGSKQLKKKLQALKKKNAQLKWKLQALKKKLAQ) containing a **basic parallel coiled-coil heterodimerization domain** (pCC-basic),

**3)** the Hinge-CH2-CH3-Fc portion of human IgG1 (NCBI GenBank: AJ294730.1, residues Glu<sub>216</sub> – Lys<sub>447</sub>), containing mutations Cys<sub>220</sub>/Ser [C220S] and Asn<sub>297</sub>/Gln [N297Q],

**4)** a C-terminal His<sub>6</sub>-tag sequence.

#### HLA-DMA-pCC-acidic-Fc construct:

**1)** The HLA-DM  $\alpha$ -chain (HLA-DMA) ectodomain sequence including ER leader (GenBank: NM\_006120.4, residues Met<sub>1</sub>–Leu<sub>232</sub>),

**2)** a linker (NSGGGSKQLEKELQALEKENAQLQEWELQALEKELAQ) containing an **acidic parallel coiled-coil heterodimerization domain** (pCC-acidic).

**3)** the Hinge-CH2-CH3-Fc portion of human IgG1 [C220S / N297Q],

**4)** a C-terminal tandem-Strep-Tag II.

### 2.2.4 Cloning of an ER-retained enzyme biotin ligase (BirA<sub>KDEL</sub>)

For the metabolic biotinylation of secreted AviTag-fused proteins (*in vivo* biotinylation) in mammalian cells as previously described by (262, 263) and performed in this study as described in **Section 2.3.5**, the bacterial *birA* gene (NCBI GenBank: M15820.1) was amplified directly from genomic DNA extracted from *E. coli* DH5 $\alpha$  strain by a PCR using a forward primer coding for the C-terminal end of the human Ig kappa antibody leader sequence (**MDFQVQIFSFLLISASVIMSRGVHS**) and 5' end (minus Met<sub>1</sub>) of the *birA* gene and a reverse primer with the 3' end of *birA* and a C-terminal extension coding for the endoplasmic reticulum (ER) retention signal sequence Lys-Asp-Glu-Leu (264) and an in-frame stop codon (KDEL\*). The PCR product was gel purified and the finally assembled cDNA sequence was cloned between the *XhoI* and *NotI* sites of expression vector pcDNA3.1(-) (Invitrogen) resulting in the construct 8521.1.

### 2.2.5 Recombinant DNA plasmid amplification and purification for protein production

Bacteria, culture reagents and consumables for bacteria transformation and plasmid purification:

Name / Ingredients	Recipe	Supplier	Cat. No.
<b>Escherichia coli strain XL1-Blue competent cells</b>		Agilent	200249
<b>LB medium, pH 7.0</b>	1000 mL ddH <sub>2</sub> O [+] 10 g Peptone from casein, tryptic digest [+] 5 g Yeast Extract Ultrapure [+] 5 g NaCl Adjusted to pH 7.0 with NaOH; autoclaved	Sigma Aldrich Gerbu Carl Roth	70172-500G 1133.0500 9265.1
<b>LB AMP medium</b>	LB medium [+] 0.1 mg/mL ampicillin	Sigma Aldrich	A5354-10ML
<b>LB AMP agar plates</b>	1000 mL LB medium, pH 7.0 [+] 15 g Agar-Agar autoclaved [+] 1 mL ampicillin (100 mg/mL stock) purred into petri dishes	Roth Sigma Aldrich Greiner bio-one	5210.3 A5354-10ML 633180
<b>Nuclease-free water</b>		Thermo Scientific	AM9938
<b>Inoculation spreader</b>		Sarstedt	86.1569.005
<b>QIAGEN Plasmid Maxi Kit</b>		QIAGEN	12163

- Suppliers' specifications | [+] Medium supplements additionally added | Cat. No.: Suppliers' catalogue numbers

### Plasmid amplification and purification procedure:

For plasmid amplification chemocompetent bacteria were transformed by standard heat-shock procedure. Briefly, 1  $\mu$ g plasmid DNA was added to thawed bacterial stocks (10  $\mu$ L bacteria + 40  $\mu$ L H<sub>2</sub>O) and subsequently incubated for 20 min on ice. Next, a 90 sec heat-shock at 42°C was performed followed by a 5 min incubation step on ice. Transformed bacteria were plated onto LB AMP agar plates and incubated at 37°C overnight. Next, 100 mL LB AMP medium-based liquid bacterial cultures were prepared using scraped bacteria from the agar plate. Liquid cultures were incubated overnight at 180 rpm at 37°C. Finally, plasmids were purified using the QIAGEN Plasmid Maxi preparation kit according to the manufacturer's protocol. Plasmid concentration was measured at 260nm (A<sub>260</sub>) and 280nm (A<sub>280</sub>) absorbance. Only plasmid preparations with A<sub>260</sub>/A<sub>280</sub> ratios between 1.87 and 1.92 were used for subsequent mammalian cell-based protein productions (**Section 2.3**).

## 2.3 Recombinant mammalian cell-based transient gene expression (TGE) systems

Equipment used for suspension mammalian cell culture-based TGEs:

Name / Ingredients	Supplier	Cat. No.
<b>Heracell™ 240i CO<sub>2</sub> Incubator</b> with stainless-steel chamber [+] <b>MaxQ™ 2000 Benchtop Orbital Shaker</b> CO <sub>2</sub> resistant ▪ 19 mm shaking diameter	Thermo Scientific Thermo Scientific	- SHKE2000CO2
<b>INFORS HT Minitron, CO<sub>2</sub> incubator</b> ▪ Integrated orbital shaker with 50 mm shaking diameter [+] plate heat exchanger, 1.5KW	INFORS HT Wutke	72945 -
<b>MTS 2/4 digital microtiter plate shaker</b> ▪ 3 mm shaking diameter	IKA	0003208000

- Suppliers' specifications | [+] Medium supplements additionally added | Cat. No.: Suppliers' catalogue numbers

### 2.3.1 CHO-S/ProCHO-4/PEI system for protein production

Components of the CHO-S/ProCHO-4/PEI transient gene expression system:

Name / Ingredients	Supplier	Cat. No.
<b>FreeStyle™ CHO-S cells</b>	Thermo Scientific	R80007
<b>ProCHO-4 serum-free medium</b> ▪ HEPES, 1x Pluronic® F-68 without L-glutamine, HT, phenol red  [+] 4 mM GlutaMAX™ (L-alanyl-L-glutamine dipeptide) [+] 1x HT Media Supplement Hybridmax™ (2 vials / 1L) ▪ 13.6 mg/L hypoxanthine, 3.9 mg/L thymidine [+] 0.5x Antibiotic Antimycotic solution (Anti-Anti) ▪ 50 units/mL penicillin; 0.05 mg/mL streptomycin; 0.1 µg/mL amphotericin B	Lonza  Thermo Scientific Sigma-Aldrich  Sigma-Aldrich	BE12-029Q  35050-038 H0137-10VL  A5955-100 ml
<b>25 kDa-Linear Polyethyleneimine (PEI)</b>  PEI was dissolved according to (265): Briefly, 100 mg PEI in 100 mL ddH <sub>2</sub> O [1 mg/mL] was stirred at pH 2.0 for 3 hours until PEI was completely dissolved, followed by pH 7.0 neutralization and 0.22 µm sterile filtration. 5 mL PEI aliquots were stored at -80°C and thawed directly before its usage for transfection.	Polysciences	23966-2
<b>Valproic acid sodium salt (VPA)</b> 500 mM VPA in ddH <sub>2</sub> O stock solution was always prepared freshly and 0.22 µm sterile filtrated prior usage.	Sigma-Aldrich	P4543-25G
<b>Laboratory round-bottom glass bottle 500 mL</b>	Duran	218014418
<b>24-deep well blocks</b> ▪ 24-well blocks with 10 mL square wells and round bottoms	Qiagen	19583
<b>Breath-easy sealing membrane</b> ▪ gas permeable sealing membrane for microtiter plates	Sigma-Aldrich	Z380059-1PAK

- Suppliers' specifications | [+] Medium supplements additionally added | Cat. No.: Suppliers' catalogue numbers

Additional tested CHO-media for protein production (relates to **Results Section 3.1.2 / Fig. 3.2**):

Name / Ingredients	Supplier	Cat. No.
<b>ProCHO-5 serum-free medium</b> <ul style="list-style-type: none"> <li>▪ <i>HEPES, 1x Pluronic® F-68 without L-glutamine, HT, phenol red</i></li> </ul>	Lonza	BE12-766Q
[+] 4 mM GlutaMAX™ (L-alanyl-L-glutamine dipeptide)	Thermo Scientific	35050-038
[+] 1x HT Media Supplement Hybridmax™ (2 vials / 1L)	Sigma-Aldrich	H0137-10VL
[+] 0.5x Antibiotic Antimycotic solution (Anti-Anti)	Sigma-Aldrich	A5955-100 ml
<b>FreeStyle™ CHO Expression Medium</b> <ul style="list-style-type: none"> <li>▪ <i>without L-glutamine, HT, phenol red</i></li> </ul>	Thermo Scientific	10651-014
[+] 4 mM GlutaMAX™ (L-alanyl-L-glutamine dipeptide)	Thermo Scientific	35050-038
[+] 1x HT Media Supplement Hybridmax™ (2 vials / 1L)	Sigma-Aldrich	H0137-10VL
[+] 0.5x Antibiotic Antimycotic solution (Anti-Anti)	Sigma-Aldrich	A5955-100 ml
<b>EX-CELL® CD CHO Serum-Free Medium</b> <ul style="list-style-type: none"> <li>▪ <i>with HT, without L-glutamine, phenol red</i></li> </ul>	Sigma-Aldrich	14361C-500ML
[+] 4 mM GlutaMAX™ (L-alanyl-L-glutamine dipeptide)	Thermo Scientific	35050-038
[+] 0.5x Antibiotic Antimycotic solution (Anti-Anti)	Sigma-Aldrich	A5955-100 ml

▪ Suppliers' specifications | [+] Medium supplements additionally added | Cat. No.: Suppliers' catalogue numbers

**2.3.1.1 PEI-based transfection procedure for large-scale 100 mL CHO-S TGE batches**

Transient gene expression (TGE) for protein production on the basis of the CHO-S/ProCHO4/PEI system was performed and optimized as described previously by (266–269). FreeStyle™ CHO-S were routinely cultivated in complete PowerCHO-2 CD medium as described in **Section 2.1.2**. One day prior to transfection (day -1), when CHO-S cells reached a density of  $4 \times 10^6$  cells/mL, CHO-S were splitted to a final density of  $2 \times 10^6$  cells/mL using fresh complete PowerCHO-2 CD (8 mM GlutaMAX). On the transfection day (day 0), cells were centrifuged and resuspended in complete ProCHO-4 (4 mM GlutaMAX) (267) at a cell density of  $3 \times 10^6$  cells/mL. For a default large-scale protein production always 100 mL cell suspension were seeded in 500 mL autoclaved round-bottom glass bottles. Transfections were performed by sequential addition of 25 kDa-linear PEI [ $2.5 \mu\text{g}/1 \times 10^6$  cells] and plasmid DNA [maximal  $0.625 \mu\text{g}/1 \times 10^6$  cells] directly to the cell suspension (266). The transfected cultures were maintained for 6 h at 37°C, 130 rpm with a 19 mm shaking diameter in a humidified 8% CO<sub>2</sub> atmosphere. 6 h after transfection, dissolved valproic acid (VPA) was added to the transfected culture to a final concentration of 1 mM (268). Subsequently, the culture was maintained for 6 days under hypothermic conditions at 32°C (269), 5% CO<sub>2</sub> and 100 rpm (50 mm shaking diameter) prior harvest.

**2.3.1.2 Procedure for small-scale protein-production using 2 mL CHO-S batches**

Unless otherwise mentioned in the experimental figure, the same transfection procedure as described above was used for small-scale protein productions using 2 mL CHO-S cell suspensions seeded into 24-deep well plates. 24-deep well-based CHO-S cultures were maintained at 450 rpm (3 mm shaking diameter).

### 2.3.2 ExpiCHO TGE system for protein production

Components of the ExpiCHO system:

Name / Ingredients	Supplier	Cat. No.
<b>ExpiCHO-S™ cells</b>	Thermo Scientific	A29127
<b>ExpiCHO™ Expression Medium</b> ▪ Contains GlutaMAX™	Thermo Scientific	A29100-01
<b>ExpiFectamine™ CHO Transfection Kit</b>	Thermo Scientific	A29129
<b>OptiPRO™ SFM (Serum free medium)</b>	Thermo Scientific	12309-050
<b>100x Antibiotic Antimycotic solution (Anti-Anti)</b>	Sigma-Aldrich	A5955-100 ml
<b>Corning® Erlenmeyer cell culture flask 125 mL</b> ▪ 125 mL Erlenmeyer flask with vent cap, polycarbonate	Sigma-Aldrich	CLS431143-50EA
<b>Corning® Erlenmeyer cell culture flask 250 mL</b> ▪ 250 mL Erlenmeyer flask with vent cap, polycarbonate	Sigma-Aldrich	CLS431144-50EA
<b>Corning® Erlenmeyer cell culture flask 500 mL</b> ▪ 500 mL Erlenmeyer flask with vent cap, polycarbonate	Sigma-Aldrich	CLS431145 -25EA

▪ Suppliers' specifications | [+] Medium supplements additionally added | Cat. No.: Suppliers' catalogue numbers

Transfection procedure for high-yield protein-production using the ExpiCHO system:

Transfection of ExpiCHO-S cells for transient gene expression-based protein production was largely performed according to the manufacturer's protocol. ExpiCHO-S cells were routinely cultivated in ExpiCHO expression medium filled polycarbonate vented Erlenmeyer flasks, which were 5-times bigger in size than the actual culture volume (**Section 2.1.2**). One day prior to transfection (day -1), when ExpiCHO-S cells reached a density of  $6 \times 10^6$  cells/mL, ExpiCHO-S cells were diluted to a final density of  $3 \times 10^6$  cells/mL using fresh ExpiCHO medium. On the transfection day (day 0), cells were diluted to a final density of  $6 \times 10^5$  cells/mL using fresh ExpiCHO medium. Next, 0.8 µg total plasmid DNA were combined with 3 µL ExpiFectamine CHO reagent in 40 µL OptiPro SFM medium per mL of TGE culture volume to be transfected. The ExpiFectamine CHO/plasmid DNA complexes formation was incubated for less than 5 min at RT and added dropwise to the culture. In the next step, transfected ExpiCHO-S were cultured overnight (~18 h) at 37°C, 100 rpm (50 mm shaking diameter), 8% CO<sub>2</sub>. One day after transfection (day 1), 6 µL ExpiCHO Enhancer, 160 µL ExpiCHO Feed and 5 µL Anti-Anti per mL TGE volume was added and the culture was transferred to hypothermic conditions at 32°C, 5% CO<sub>2</sub> and 100 rpm (50 mm shaking diameter). On day 5 post transfection, additional 160 µL ExpiCHO Feed per mL of TGE culture volume was added. The cultured was finally harvested 9–12 days after initial transfection.

### 2.3.3 293-F TGE system for protein production

Components of the 293-F transient expression system:

Name / Ingredients	Supplier	Cat. No.
<b>FreeStyle™ 293-F cells</b>	Thermo Scientific	R79007
<b>FreeStyle™ 293 Expression Medium</b> ▪ Contains GlutaMAX, serum free,	Thermo Scientific	12338-018
<b>OptiPRO™ SFM</b>	Thermo Scientific	12309-050
<b>293-Free™ Transfection Reagent</b>	Merck	72181-3
<b>100x Antibiotic Antimycotic solution (Anti-Anti)</b>	Sigma-Aldrich	A5955-100 ml
<b>Valproic acid sodium salt (VPA)</b> 500 mM VPA in ddH <sub>2</sub> O stock solution was always prepared freshly and 0.22 µm sterile filtrated prior usage.	Sigma-Aldrich	P4543-25G

Transfection procedure for protein-production using the 293-F system:

FreeStyle™ 293-F cells were routinely cultivated in FreeStyle™ 293 expression medium at 37°C, 8% CO<sub>2</sub> and 130 rpm (19 mm shaking diameter) using polycarbonate vented Erlenmeyer flasks as described in **Section 2.1.2**. One day prior to transfection (day -1), when 293-F cells reached a density of 2x10<sup>6</sup> cells/mL, 293-F cells were diluted to a final density of 1x10<sup>6</sup> cells/mL using fresh 293-F medium. On the next day (day 0), cells were again diluted to a final density of 1x10<sup>6</sup> cells/mL using fresh 293-F. For transfection the 293-free transfection reagent (Merck / Novagen) was used according to the manufacture's protocol. Briefly, 0.5 µg total plasmid DNA were combined with 1 µL 293-free reagent in 40 µL OptiPro SFM medium per mL of culture volume to be transfected and incubated for 15 min at RT. The 293-free/plasmid DNA complexes were added dropwise to the TGE culture, which was in the following cultured overnight (~18 h) at 37°C, 100 rpm (50 mm shaking diameter), 8% CO<sub>2</sub>. On the next day, freshly dissolved valproic acid (VPA) was added to the transfected culture to a final concentration of 4 mM as previously described by (267) as well as anti-anti solution (final 0.5x). Subsequently, the culture was maintained for 6 days at 37°C, 100 rpm, 8% CO<sub>2</sub> prior to the harvest of the cell supernatant.

2.3.4 Expi293F TGE system for protein productionComponents of the Expi293F transient expression system:

Name / Ingredients	Supplier	Cat. No.
Expi293F™ cells	Thermo Scientific	A14527
Expi293™ Expression Medium ▪ GlutaMAX, serum free	Thermo Scientific	A1435101
ExpiFectamine™ 293 Transfection Kit	Thermo Scientific	A14524
Opti-MEM I Reduced Serum Media	Thermo Scientific	31985062
100x Antibiotic Antimycotic solution (Anti-Anti)	Sigma-Aldrich	A5955-100 ml

Transfection procedure for protein production using the Expi293F system

Transfection of Expi293F cells for transient-gene expression-based protein production was largely performed according to the manufacture's protocol. Expi293F cells were routinely cultivated in Expi293 expression medium filled polycarbonate vented Erlenmeyer flasks, which were 5-times bigger in size than the actual culture volume (**Section 2.1.2**). On the day prior to transfection (day -1), when Expi293F cells reached a density of 3–5x10<sup>6</sup> cells/mL, Expi293F cells were diluted to a final density of 2.5x10<sup>6</sup> cells/mL using fresh Expi293 medium. On the transfection day (day 0), cells were diluted to a final density of 3x10<sup>6</sup> cells/mL using fresh Expi293 medium. Next, 1.0 µg total plasmid DNA were combined with 3 µL ExpiFectamine 293 reagent in 120 µL Opti-MEM medium per mL of TGE culture volume to be transfected. The ExpiFectamine 293/plasmid DNA complexes formation was incubated for 15 min at RT and added dropwise to the culture. Transfected Expi293F were cultured overnight (~18 h) at 37°C, 100 rpm (50 mm shaking diameter), 8% CO<sub>2</sub>. One day post transfection (day 1), 6 µL ExpiFectamine 293 transfection enhancer 1, 60 µL ExpiFectamine 293 transfection enhancer 2 and 5 µL Anti-Anti per mL TGE culture volume was added. Subsequently, the culture was maintained for 5-6 days at 37°C, 100 rpm, 8% CO<sub>2</sub> prior to the harvest of the cell supernatant.

### 2.3.5 *In vivo* biotinylation of AviTag-fusion proteins during mammalian cell-based TGE

Additional reagents used for *in vivo* biotinylation:

Name / Ingredients	Supplier	Cat. No.
<b>D-biotin</b> 4 mg/mL D-biotin stock solution was always prepared freshly. To completely dissolve D-biotin in ddH <sub>2</sub> O, ~20 µL NaOH was added to 1 mL D-biotin solution followed by 0.22 µm sterile filtration.	Sigma-Aldrich	B4639-1G

For metabolic *in vivo* biotinylation as in more detail introduced in **Results Section 3.3**, an AviTag-fused protein-of-interest encoding vector was co-transfected with the IgL-BirA<sub>KDEL</sub> construct [8521.1] at a 1:1 ratio according to the transfection procedures described in **Section 2.3.1 – 2.3.4** comprising the CHO-S/PEI/ProCHO4, ExpiCHO-S, Freestyle 293-F and Expi293F TGE systems. Independent of the used TGE system, the used cell culture medium was supplemented with 4 µg/mL D-biotin prior to transfection.

## 2.4 Transient gene expression (TGE) validation and IgG titer quantification

### 2.4.1 Validation of protein expression by intracellular FACS staining

Reagents and consumables used for intracellular staining of transfected protein producer cells:

Name / Ingredients	Supplier	Cat. No.
<b>"FACS-buffer"</b> DPBS (1x), pH7.2, without MgCl <sub>2</sub> and CaCl <sub>2</sub> [+] 2% (v/v) heat-inactivated fetal bovine serum (FBS)	Sigma-Aldrich Biochrom	D8537-500ML S 0615
<b>BD Cytofix/ Cytoperm™ Fixation/Permeabilization Solution Kit</b> <ul style="list-style-type: none"> <li>▪ BD Perm/ Wash Buffer (10x)</li> <li>▪ BD Cytofix/ Cytoperm™ fixation/permeabilization solution</li> </ul>	BD Bioscience	554714
<b>Zombie Aqua Fixable Viability Kit</b>	BioLegend	423102
<b>DPBS (1x) (Dulbecco's Phosphate Buffered Saline)</b> <ul style="list-style-type: none"> <li>▪ pH 7.2, no MgCl<sub>2</sub> and CaCl<sub>2</sub></li> </ul>	Sigma-Aldrich	D8537-500ML
<b>Nunc™ 96-well polypropylene V-bottom plate</b>	Thermo Scientific	249944

- Suppliers' specifications | [+] Medium supplements additionally added | Cat. No.: Suppliers' catalogue numbers

Antibodies used for intracellular FACS staining of transfected protein producer cells:

Specificity [Clone]:	Conjugated dye	Isotype	Supplier	Cat. No.	µL /test
<b>Anti-human HLA-A2 [BB7.2]</b>	APC	Mouse IgG2b	BioLegend	343308	1
<b>Anti-human HLA-DR [L243]</b>	APC	Mouse IgG2a	BioLegend	307610	1
<b>Anti-human HLA-DM [MaP.DM1]</b>	PE	Mouse IgG1	BioLegend	358004	2.5
<b>Anti-mouse IgG2a [RMG2a-62]</b>	APC	Rat IgG	BioLegend	407110	1
<b>Anti-BirA [6C4c7] (1 mg/mL)</b>	-	Mouse IgG1	Arigo Biolab.	ARG10834	0.5
<b>[+] Goat-anti-Mouse Ig (GαM-Ig)</b>	APC	Polyclonal	BD Bioscience	550826	1.0

Intracellular FACS staining of transfected protein producer cells:

Three days post-transfection, aliquots of approximately  $2.5 \times 10^5$  transfected cells were collected to confirm the expression and protein structure of novel cloned and designed vectors. Cells were seeded into 96-well V-bottoms plates and washed once using 200  $\mu$ L/well DPBS. To exclude dead cells, cells were stained with Zombie Aqua™ (1:300 diluted in DPBS, 100  $\mu$ L/well) for 10 min at RT in the dark and washed once using 200  $\mu$ L/well FACS-buffer (DPBS + 2% FBS). Next, cells were permeabilized and fixated using the BD Cytofix/Cytoperm solution kit according to the manufacturer's protocol. Briefly, 100  $\mu$ L/well of BD Cytofix / Cytoperm solution was added to the cell pellet, mixed and incubated for 15 min on ice. Next, cells were washed once using 200  $\mu$ L/well 1x BD Perm/Wash buffer. Antibodies for intracellular staining were diluted in 1x BD Perm/Wash buffer solution and 100  $\mu$ L/well was added to the cells, followed by a 30 min incubation on ice in the dark. Stained cells were washed twice with 1x BD Perm/Wash buffer and finally resuspended in FACS buffer. Flow cytometric measurement was performed on a BD FACS Canto II and analyzed using the FlowJo™ software. Untransfected cells were used as negative control, which have been cultured under the same conditions as transfected cells. For the detection of *BirA*-expression an unconjugated mouse- $\alpha$ -BirA monoclonal antibody (mAb) was used, which was subsequently detected by G $\alpha$ M-Ig-APC secondary staining for 30 min at 4°C. Also the latter staining were performed in 1x BD Perm/Wash Buffer. All centrifugation / washing steps were performed at 1550 rpm, 4°C for 3 min.

2.4.2 Mouse/human IgG titer quantification of cell supernatants by ELISAELISA buffer, reagents and consumables:

Name / Ingredients	Supplier	Cat. No
<b>PBS-T (washing buffer):</b> DPBS (1x), pH7.2, no MgCl <sub>2</sub> and CaCl <sub>2</sub> [+] 0.05% (v/v) Tween-20	Sigma-Aldrich Sigma-Aldrich	D8537-500ML P1379-100ML
<b>PBS-T + 2.5% BSA (blocking buffer):</b> DPBS (1x), pH7.2, no MgCl <sub>2</sub> and CaCl <sub>2</sub> [+] 0.05% (v/v) Tween-20 [+] 2.5% (w/v) Bovine Serum Albumin (BSA)	Sigma-Aldrich Sigma-Aldrich PAA	D8537-500ML P1379-100ML K45-001
<b>PBS-T + 0.5% BSA (sample buffer):</b> DPBS (1x), pH7.2, no MgCl <sub>2</sub> and CaCl <sub>2</sub> [+] 0.05% (v/v) Tween-20 [+] 0.5% (w/v) bovine serum albumin (BSA)	Sigma-Aldrich Sigma-Aldrich PAA	D8537-500ML P1379-100ML K45-001
<b>Carbonate-Bicarbonate Buffer (coating buffer)</b> ▪ 0.05 M carbonate-bicarbonate buffer, pH 9.6	Sigma-Aldrich	C3041-50CAP
<b>TMB Substrate Set (HRP substrate solution)</b>	BioLegend	421101
<b>1 M H<sub>2</sub>SO<sub>4</sub></b>	Carl Roth	9316.1
<b>Nunc-Immuno™ 96-well MaxiSorp™ plate</b>	Sigma-Aldrich	M9410-1CS
<b>Greiner multiwell plate sealers</b>	Sigma-Aldrich	A5596-100EA

- Suppliers' specifications | [+] Medium supplements additionally added | Cat. No.: Suppliers' catalogue numbers

#### Antibodies used mouse/human IgG-titer quantification ELISA:

Specificity :	Conjugated enzyme	Isotype	Supplier	Cat. No	Usage
Anti-Human IgG-Fc	-	Polyclonal Goat serum	Sigma-Aldrich	I2136-1ML	5 µg/mL
	Peroxidase			A0170-1ML	1:10000
Anti-mouse IgG-Fc	-			M2650-1ML	5 µg/mL
	Peroxidase			A0168-1ML	1:10000

#### Mouse/human IgG-titer quantification ELISA:

6 days after CHO-S/293-F/Expi293F or 10 days after ExpiCHO-S transfection (**Section 2.3**), respectively, the cell supernatant was collected and cleared from cells by two successive centrifugation steps: **(1.)** 10 min at 1500 rpm, 4°C and **(2.)** at 4000 rpm for 30 min, 4°C. In some cases ExpiCHO-S supernatants were additionally sterile filtered using a 0.22 µm PES filter (TPP 99950). To validate successful secretion and production of a vector of interest (usually encoding for pMHC-I-Fc or pMHC-II-pCC-Fc) prior affinity-chromatography, anti-mouse-IgG-Fc or anti-human-IgG-Fc sandwich ELISA were performed depending on the Fc-fusion protein's design.

**Coating:** Unconjugated anti-human IgG-Fc or anti-mouse IgG-Fc capture antibodies (polyclonal goat serum) was diluted to a final concentration of 5 µg/mL in coating buffer (pH 9.6). 100 µL/well diluted capture antibody was transferred to a 96-well MaxiSorb ELISA plate. The plate was sealed and incubated at 37°C for 45 min. After the incubation, the plate was washed three times using 200 µL/well PBS-T washing buffer. **Blocking:** Unspecific protein interactions were blocked by adding 100 µL/well of PBS-T + 2.5% BSA blocking solution followed by an incubation at 37°C for 45 min and one timing washing.

**Sample and standard:** Affinity-chromatography purified disulfide-trapped single-chain trimer-based pMHC-I-mIgG2a-Fc [8195.1] or pMHC-I-hlgG1-Fc [8755.1] constructs with known concentrations were used for standard-curve-based IgG-Fc quantification of fresh TGE-derived supernatants. Initially mouse reference serum (Bethyl RS10-101) and human reference serum (Bethyl RS10-110) were used as standards, which however had the tendency to underestimating the actual pMHC-Fc titer. Samples (cleared TGE supernatants, diluted 1:100–1:900) and standard (in the range of 900 ng/mL – 1 ng/mL) were diluted in PBST + 0.5% BSA sample buffer and 100 µL/well were transferred in duplicates to the coated and blocked MaxiSorb ELISA plate. Samples and standard were incubated for 45 min at RT.

**Detection:** The plate was washed three times as described before, followed by the addition of 100 µL/well of anti-human IgG-Fc-peroxidase or anti-mouse IgG-Fc-peroxidase detection antibodies diluted in sample buffer and incubation at RT for 45 min. After washing, TMB peroxidase substrate was added (100 µL/well) and incubated for 5 min – 15 min until the standard became clearly visible. Finally, the reaction was stopped by addition of TMB stop solution (1M H<sub>2</sub>SO<sub>4</sub>) and absorbance was measured at 450 nm and 540 nm using a microplate reader.

## 2.5 Affinity chromatography-based protein purification

Equipment used for low-pressure liquid chromatography (LPLC)-based protein purifications:

Name / Ingredients	Supplier	Cat. No
<b>Low-pressure liquid chromatography columns</b> <ul style="list-style-type: none"> <li>Luer Lock inlet and outlet fittings, non-jacketed, polyethylene bed supports,</li> </ul> <p><i>Inner diameter (I.D) x length:</i>            1.5 cm x 10 cm columns            0.7 cm x 10 cm columns</p>	Sigma-Aldrich Sigma-Aldrich	C4169-5EA C3669-10EA
<b>REGLO digital MS-4/6-100 peristaltic pump</b> <ul style="list-style-type: none"> <li>4 channels, 6 rolls, 0.002 – 43 mL/min</li> </ul>	Ismatec	ISM 833
<b>Saint-Gobain Tygon™ LMT-55 Tubing</b> <ul style="list-style-type: none"> <li>3.17 mm inner diameter, wall: 0.86 mm, length 38.1 mm</li> <li>Material: Tygon R3607</li> <li>Three stop configuration, black and white</li> </ul>	Fisher Scientific	11749744
<b>Cassettes with occlusion lever (Pressure lever)</b> <ul style="list-style-type: none"> <li>Material: POM-C</li> </ul>	Ismatec	IS 0649

▪ Suppliers' specifications | Cat. No.: Suppliers' catalogue numbers

Equipment used for magnetic sepharose-based for small-scale protein and other batch purifications:

Name / Ingredients	Supplier	Cat. No
<b>MagRack 6</b> <ul style="list-style-type: none"> <li>6x 1.5 mL tubes magnetic separation rag</li> </ul>	GE HealthCare	28-9489-64
<b>MagRack Maxi</b> <ul style="list-style-type: none"> <li>Magnetic separation rag for 15 mL and 50 mL tubes</li> </ul>	GE HealthCare	28-9464-41
<b>Magentic 96-well separator</b> <ul style="list-style-type: none"> <li>Magnetic plate suitable for 96-well plates</li> </ul>	Thermo Scientific	A14179
<b>IKA tube roller 6, digital</b> <ul style="list-style-type: none"> <li>Smooth rocking (24.5 mm) and rolling action (5–80 rpm)</li> </ul>	IKA	0004011000

▪ Suppliers' specifications | Cat. No.: Suppliers' catalogue numbers

General used buffers for washing, column equilibration steps and protein dialysis:

Name / Ingredients	Recipe	Supplier	Cat. No
<b>10x PBS, pH 7.4:</b> 80 mM NaH <sub>2</sub> PO <sub>4</sub> 15 mM KH <sub>2</sub> PO <sub>4</sub> 27 mM KCl 1.45 M NaCl	1000 ml ddH <sub>2</sub> O (final) [+ ] 11.0 g NaH <sub>2</sub> PO <sub>4</sub> · H <sub>2</sub> O (MW 137.99 g/mol) [+ ] 2.0 g KH <sub>2</sub> PO <sub>4</sub> (MW 136.09 g/mol) [+ ] 2.0 g KCl (MW 74.56 g/mol) [+ ] 84.7 g NaCl (MW 58.44 g/mol)  - Set to pH 7.4 using HCl - 0.22 µm sterile filtration	Carl Roth Carl Roth Carl Roth Carl Roth  Merck TPP	T878.2 3904.1 6781.1 9265.1  109060 99500

Other consumables used for all protein purifications:

Name / Ingredients	Supplier	Cat. No
Slide-A-Lyzer™ Dialysis Cassettes, 20 kDa MWCO, 3 mL	Thermo Scientific	66003
Slide-A-Lyzer™ Dialysis Cassettes, 10 kDa MWCO, 0.5 mL	Thermo Scientific	66383
Pur-A-Lyzer Mini Dialysis Kit, 6–8 kDa MWCO, 10 – 250 µL	Sigma-Aldrich	PURN60030
Millex-GV, 0.22 µm PVDF, 4 mm syringe-driven filter unit	Merck	SLGV004SL
Millex-GV, 0.22 µm PVDF, 13 mm syringe-driven filter unit	Merck	SLGV13SL
Millex-GV, 0.22 µm PES, 30 mm syringe-driven filter unit	Merck	SLGP033RB
TPP Vacuum filtration “rapid”-Filtermax, 0.22 µm PES	TPP	99950
Amicon® Ultra Centrifugal Filters (10K), cellulose, 0.5 mL	Merck	UFC5010BK
50 ml / Luer Lock Solo Syringe	Terumo	SS+50L1
2 ml / Luer Lock Solo Syringe Omnifix	Braun	4617029V

- Suppliers' specifications | [+] Medium supplements additionally added | Cat. No.: Suppliers' catalogue numbers

Cell supernatant harvest and clearance for affinity chromatography-based protein purification:

6 days after CHO-S/293-F/Expi293-F or 10 days after ExpiCHO-S transfection, respectively, the cell supernatant was cleared from cells by two successive centrifugation steps: **(1.)** 10 min at 1500 rpm, 4°C and **(2.)** at 4000 rpm for 30 min, 4°C. All supernatants were stored at 4°C under sterile conditions and successful protein expression and IgG-tier was determined prior to affinity chromatography-based protein purification according to **Section 2.4.2**.

### 2.5.1 Strep-tag II / Strep-Tactin-based protein affinity chromatography

Resin and buffers used for Strep-Tag II / Strep-Tactin-based purifications:

Name / Ingredients	Supplier	Cat. No
<b>Strep-Tactin® Superflow® high capacity resin</b> ▪ 50% suspension	IBA Lifesciences	2-1208-010
<b>10x Buffer R; Strep-Tactin® regeneration buffer with HABA</b> 1 M TRIS-Cl, pH 8.0 1.5 M NaCl 10 mM EDTA 10 mM HABA (hydroxy-azophenyl-benzoic acid)	IBA Lifesciences	2-1002-100
<b>10x Buffer W; Strep-Tactin® wash Buffer</b> 1 M TRIS-Cl, pH 8.0 and pH 10.5 1.5 M NaCl 10 mM EDTA	IBA Lifesciences	2-1003-100
<b>BioLock – Biotin blocking/masking solution</b> ▪ Avidin containing solution	IBA Lifesciences	2-0205-050
<b>Strep-Tactin elution buffer:</b> 1x PBS, pH 7.4 (self-prepared) [+] 5 mM desthiobiotin	IBA Lifesciences	2-1000-002

- Suppliers' specifications | [+] Medium supplements additionally added | Cat. No.: Suppliers' catalogue numbers

Strep-tag II / Strep-Tactin resin column-based purification:

Cleared TGE cell culture supernatants of Strep-tag II or Twin-Strep-tag-fused proteins were purified using the Strep-Tactin-based purification system according to the manufacturer's protocol and previously described by (270) with minor modifications. Briefly, a LPLC column with an inner diameter (I.D.) of 0.7 cm or 1.5 cm was filled with a column-bed volume (CV) of 0.5 mL or 1.5 mL Strep-Tactin Superflow high capacity resin, respectively, depending on the anticipated protein yield and TGE culture volume. If the expected protein yield determined by ELISA (**Section 2.4.2**) exceeded 2 mg or the overall TGE culture volume exceeded 250 mL, a CV of 2 mL Strep-Tactin resin and a 1.5 cm I.D. LPLC column was selected. Cleared supernatants were supplemented with 0.1 volume of 10x PBS pH 7.4 prior purification. In case the ExpiCHO system or 293-F protein-production system was used, the respective supernatants were additionally supplemented with 0.3 mL BioLock solution / mL TGE culture volume to mask biotin present in the medium, which would otherwise bind irreversible to Strep-Tactin (270). Strep-Tactin resin filled columns were equilibrated two times with 5 CV 1x PBS pH 7.4 followed by loading of cleared and biotin-masked TGE supernatants at a flowrate of 1.5–2.5 mL/min at RT using a peristaltic pump. Next, the column was washed by gravity flow using two times 5 CV 1x PBS pH 7.4. Elution of purified proteins was performed at a flowrate of 1.5 mL/min using 5 CV PBS pH 7.4 supplemented with 5 mM desthiobiotin. 0.25–0.5 mL elution fractions were separately collected and protein concentration was measured at 280 nm absorbance. The highest protein fractions were pooled and dialyzed in PBS 7.4 to remove the excess of desthiobiotin. Finally, all purified and dialyzed proteins were analyzed by SDS-PAGE according to **Section 2.5.4**. Strep-Tactin resin-filled columns were recycled afterwards according to the manufacturer's protocol using buffer R and buffer W and were only reused for productions of the same protein.

2.5.2 His-tag-based protein purification and Fc-cleavage of pMHC-I\*Fc molecules**2.5.2.1 His-tag / Ni-NTA Sepharose-based batch affinity chromatography**

Reagents used for Polyhistidine-tag / Ni-NTA-based batch affinity chromatography:

<b>Name / Ingredients</b>	<b>Supplier</b>	<b>Cat. No</b>
<b>Ni-NTA (Nitrilotriacetic acid) Superflow resin</b> ▪ 50% suspension	Qiagen	30410
<b><u>10x His-tag/Ni-NTA sample binding buffer</u></b> 10x PBS, pH 7.4 (self-prepared) [+] 100 mM imidazole  <b><u>1x His-tag/Ni-NTA purification wash buffer</u></b> 1x PBS, pH 7.4 (self-prepared) [+] 20 mM imidazole  <b><u>1x His-tag/Ni-NTA purification elution buffer</u></b> 1x PBS, pH 7.4 (self-prepared) [+] 300 mM imidazole	Sigma-Aldrich	56750-500G
<b>Protein assay dye reagent (concentrate)</b> ▪ Bradford reagent The protein assay dye reagent was 1:5 diluted with ddH <sub>2</sub> O prior usage.	Bio-Rad	35000006

▪ Suppliers' specifications | [+] Medium supplements additionally added | Cat. No.: Suppliers' catalogue numbers

### His-tag / Ni-NTA batch-based batch affinity chromatography:

*In vivo* biotinylated His<sub>6</sub>-tagged pMHC-I-pCC-Fc and pMHC-II-pCC-Fc constructs discussed in **Results Section 3.3** and **3.6**, respectively, were purified using standard Ni-NTA-sepharose-based affinity chromatography.

As an initial step, Ni-NTA resin was collected in a 1.5 cm I.D. LPLC column and washed twice with 1x PBS pH 7.4 (column completely filled). Next, cleared TGE cell culture supernatants were supplemented with 0.1 volume of 10x His-tag/Ni-NTA sample binding buffer (final 10 mM imidazole). 50 mL supplemented TGE culture volume was transferred to a 50 mL tube and 0.5 mL washed Ni-NTA resin was added. Filled 50 mL tubes were rotated for 1 h at RT (“batch”-based protein binding). Next, protein-bound Ni-NTA resin was collected in a 1.5 cm I.D. LPLC column letting the supernatant flow through the column. Next, the column was washed with 10–20 mL of His-tag/Ni-NTA wash buffer (20 mM imidazole) at gravity flow. Elution of purified proteins was performed at a flowrate of 1.5 mL/min using a peristaltic pump and 2.5 mL His-tag/Ni-NTA elution buffer (300 mM imidazole). 0.25–0.5 mL elution fractions were separately collected. To assess fractions with high protein-concentration, 10 µL elution fraction were combined with 40 µL Bradford reagent in a transparent 96-well flat bottom plate. The highest protein fractions were pooled and dialyzed in PBS 7.4. The final protein concentration was measured at 280 nm absorbance. Ni-NTA resin was afterwards recycled according to the manufacture’s protocol and reused only for productions of the same protein.

### **2.5.2.2 His-tag / His Mag Sepharose Excel-based batch affinity chromatography**

#### Reagents used for His-tag / His Mag Sepharose Excel-based batch affinity chromatography:

<b>Name / Ingredients</b>	<b>Supplier</b>	<b>Cat. No</b>
<b>His Mag Sepharose Excel (HMSE) [10% Slurry]</b> <ul style="list-style-type: none"><li>▪ <i>Magnetic resin charged with nickel ions specifically designed for purification of histidine-tagged proteins secreted into eukaryotic cell culture supernatants.</i></li></ul>	GE HealthCare	17-3712-22
<b><u>HMSE equilibration buffer</u></b> 25 mM NaH <sub>2</sub> PO <sub>4</sub> 500 mM NaCl pH 7.4	Sigma-Aldrich Carl Roth	71507-1KG 9265.1
<b><u>HMSE wash buffer</u></b> 25 mM NaH <sub>2</sub> PO <sub>4</sub> 500 mM NaCl 20 mM imidazole pH 7.4	Sigma-Aldrich Carl Roth Sigma-Aldrich	56750-500G 9265.1 56750-500G
<b><u>HMSE elution buffer</u></b> 25 mM NaH <sub>2</sub> PO <sub>4</sub> 500 mM NaCl 500 mM imidazole pH 7.4	Sigma-Aldrich Carl Roth Sigma-Aldrich	56750-500G 9265.1 56750-500G

- Suppliers’ specifications | Cat. No.: Suppliers’ catalogue numbers

His-tag / His Mag Sepharose Excel-based affinity chromatography:

*In vivo* biotinylated His<sub>8</sub>-tagged pMHC-I-\*Fc fusion proteins bearing a thrombin-mediated cleavable Fc portion (\*Fc) as discussed in **Results Section 3.4** as well as monomeric biotinylated His-tagged pMHC-I constructs lacking a fusion to a Fc portion (**Supplementary Fig. S5**) were purified using His Mag Sepharose Excel resin-based affinity chromatography.

Cleared TGE cell culture supernatants of His-tag-fused proteins as well as prior thrombin-digested supernatants (**Section 2.5.2.3**) were purified using the His Mag Sepharose Excel purification resin according to the manufacturer's protocol. Briefly, per purification 200  $\mu$ L of His Mag Sepharose Excel beads were once washed with 1 mL equilibration buffer using a magnetic rag suitable for 1.5 mL tubes. Equilibrated beads were resuspended in 200  $\mu$ L equilibration buffer and combined with 2.5–25 mL cleared TGE cell supernatant in 15 mL or 50 mL tubes. Filled tubes were subsequently placed on a rolling device set to 65 rpm and incubated overnight at RT. On the next day, the beads were immobilized using a magnet and the cell supernatant was removed. As a next step, the beads were transferred to a 1.5 mL tube using equilibration buffer. Subsequently, the tubes were placed into a magnet and the beads were washed three times using 500  $\mu$ L wash buffer (20 mM imidazole). Finally the bound proteins were eluted using 200  $\mu$ L elution buffer (500 mM imidazole), which was incubated for 1 minute prior to the transfer of the eluted proteins to new tube. The bead-free 200  $\mu$ L elution fraction was directly dialyzed in PBS 7.4 for 2 h at RT using a suitable Pur-A-Lyzer mini dialysis tube (Sigma-Aldrich). The final protein concentration of the dialyzed elution fraction was measured at 280 nm absorbance and subsequently analyzed by SDS-PAGE (**Section 2.5.4**).

**2.5.2.3 Thrombin-mediated enzymatic cleavage of pMHC-I-\*Fc constructs**

Reagents enzymatic cleavage of pMHC-\*Fc constructs by thrombin:

Name / Ingredients	Supplier	Cat. No
<b>Thrombin, restriction grade (Factor IIa / FIIa)</b> <ul style="list-style-type: none"> <li>▪ Recommended usage of <math>4.8 \times 10^{-5}</math> thrombin units/pmol substrate</li> </ul>	Merck	69671-3
<b>10x DPBS, pH 7.2</b> <ul style="list-style-type: none"> <li>▪ <i>Without MgCl<sub>2</sub> and CaCl<sub>2</sub>, suitable for cell culture</i></li> </ul>	Sigma-Aldrich	D1408

▪ Suppliers' specifications | Cat. No.: Suppliers' catalogue numbers

Enzymatic cleavage of pMHC-I-\*Fc constructs by thrombin:

For enzymatic thrombin-mediated Fc cleavage of pMHC-I-\*Fc constructs (in more detail described in **Results Section 3.4** and **Section 2.2.1.3**) cleared TGE cell supernatants were supplemented with 0.1 volume of 10x DPBS stock solution followed by the addition of an approximate 2–5x excess of the manufacturer's recommended  $4.8 \times 10^{-5}$  thrombin units/pmol substrate. Supplemented supernatants were incubated overnight at 37°C prior to His Mag Sepharose Excel resin-based purification (**Section 2.5.2.2**) of Fc-cleaved (\*) monomeric pMHC-I\* molecules. Notably, a single pMHC-I-\*Fc molecule (160 kDa) contains in total four thrombin-recognition sites, thus  $\sim 160 \mu$ g pMHC-I-\*Fc represents 4000 pmol substrate. Consequently, 10–20 mL supernatant containing typically 250–500  $\mu$ g pMHC-I-\*Fc (according to quantitative anti-mIgG-Fc-based ELISA data (**Section 2.4.2**)) was routinely supplemented with 1 unit thrombin.

### 2.5.3 Protein A resin-based affinity chromatography

Resin, buffers and reagents used for Protein-A based protein affinity chromatography:

Name / Ingredients	Supplier	Cat. No
<b>ProSep-vA High Capacity Protein-A resin</b>	Merck	113115827
<b>Protein A wash buffer 1:</b> 1x PBS, pH 7.4 (self-prepared)		
<b>Protein A Wash buffer 2:</b> 1x PBS, pH 7.4 (self-prepared) [+] 100 mM NaCl (extra, final 250 mM NaCl) [+] 0.1% (v/v) Tween-20	Carl Roth Sigma-Aldrich	9265.1 P1379-100ML
<b>Protein A elution buffer:</b> 100 mM glycine in ddH <sub>2</sub> O, pH 3.0	Sigma-Aldrich	G8898-1KG
<b>Protein A neutralization buffer:</b> 1 M TRIS-HCl, pH 7.4	Sigma-Aldrich	T1503-500G

### Protein-A resin filled column affinity chromatography

Almost all pMHC-I-Fc or pMHC-II-Fc proteins used in this study have been purified via Strep-tag II- or His<sub>6</sub>-tag- based affinity chromatography, exceptions are the used pHLA-A2-Fc constructs 7409.4 and 8195.1 in **Results Section 3.2.1 / Fig. 3.4** and **Supplementary Figure S2**, which have been purified by protein-A based affinity chromatography as described below. Briefly, a LPLC column with an inner diameter of 1.5 cm was filled with a CV of 1.0 mL ProSep-vA High Capacity Protein A and washed twice with 10 CV 1x PBS pH 7.4 (wash buffer 1). Cleared TGE cell culture supernatants was loaded at a flowrate of 1.5 mL/min at 4°C using a peristaltic pump. Afterwards the column was washed by gravity flow at RT using: **(1.)** 5 CV wash buffer 1, **(2.)** 5 CV wash buffer 2 and **(3.)** 5 CV wash buffer 1. Elution of purified proteins was performed at a flowrate of 1.5 mL/min using 5 CV protein A elution buffer (0.1 M glycine, pH 3.0). 500 µL elution fractions were separately collected into tubes already filled with 250 µL neutralization buffer (1 M TRIS-HCl, pH 7.4). Protein concentration of elution fractions was measured at 280 nm absorbance and the highest protein fractions were pooled and dialyzed in PBS 7.4. Finally, dialyzed proteins were analyzed by SDS-PAGE according to **Section 2.5.4** prior to functional testing.

### 2.5.4 SDS-PAGE analysis

Name / Ingredients	Supplier	Cat. No
<b>RunBlue™ TEO-Tricine SDS-Precast Gels</b> ▪ 10%, 10x10 cm, 12 well ▪ 10%, 10x10 cm, 17 well	Expedeon	NXG01012 NXG01027
<b>RunBlue™ SDS Running Buffer 20x</b>	Expedeon	NXB50500
<b>RunBlue™ LDS Sample Buffer – TEO-Tricine 4x</b> [+] 40 mM dithiothreitol (DTT) for reducing conditions	Expedeon Sigma-Aldrich	NXB31010 D0632-1G
<b>RunBlue™ prestained dual colour marker</b>	Expedeon	NXA05160
<b>InstantBlue™ Coomassie protein staining solution</b>	Expedeon	NXB50500
<b>XCell SurLock™ Mini-Cell Electrophoresis System</b>	Thermo Scientific	EI0001

## 2 | Material and methods

### SDS-PAGE analysis procedure:

All shown SDS-PAGE analysis were performed using the RunBlue™ Teo-Tricine precast gel system (Expedeon) according to the manufacture's protocol. For reducing conditions protein samples were combined with LDS sample buffer and a final concentration of 10 mM DTT and were heated at 70°C for 10 min prior to loading onto the SDS-PAGE. Electrophoresis was performed at RT at 140V for 90 minutes. SDS-PAGE gels were stained at RT using the InstantBlue™ Coomassie staining solution for 3–4 h at constant orbital shaking. After the incubation, the staining solution was removed and replaced by ddH<sub>2</sub>O followed by an overnight incubation for destaining. Usually, 2.5 µg of dialyzed protein sample was loaded per lane.

## 2.6 pMHC multimer generation and quality control

### 2.6.1 Streptavidin-based multimerization of biotinylated soluble pMHC molecules

In vivo biotinylated constructs used for pMHC multimer generation:

Structure	Allele	Antigen	Peptide Seq.	Construct ID:
dt-pMHC-I (SCT)-pCC-mIgG2a-Fc-biotin	HLA-A*02:01	HCMV pp65 495–503	NLVPMVATV	10347.7
	HLA-A*02:01	Survivin 96–104	LMLGEFLKL	9237.1

dt-SCT-pCC-mIgG2a-Fc-biotin: Disulfide-trapped (dt) pMHC-I (single-chain trimer) fused to a parallel coiled-coil (pCC) heterodimerization domain followed by the hinge-CH2-CH3 domains of mIgG2a (Fc) and a C-terminal Strep-tag II as well as His<sub>6</sub>-tag and AviTag for site-specific biotinylation (biotin).

Structure	Allele	Antigen	Peptide Seq.	Construct ID:
pMHC-II-pCC-mIgG2a-Fc-biotin	HLA-DRB1*03:01 / DRA*01:01	MTB Hsp65 1–13	MAKTIAYDEEARR	9260.3
px-EK-MHC-II-pCC-mIgG2a-Fc-biotin	HLA-DRB1*03:01 / DRA*01:01	CLIP 103–117	PVSKMRMATPLLMQA	9261.3

px-EK: Placeholder peptide followed by C-terminal linker bearing an enterokinase cleavage site

Structure	Allele	Antigen	Peptide Seq.	Construct ID:
dt-pMHC-I (SCT)-biotin-*mIgG2a-Fc	HLA-A*02:01	HCMV pp65 495–503	NLVPMVATV	11097.1
	HLA-A*02:01	Survivin 96–104	LMLGEFLKL	11290.1
	HLA-A*02:01	Flu A MP 58–66	GILGFVFTL	11291.1
	HLA-A*02:01	EBV BMLF-1 259–267	GLCTLVAML	11292.1

Disulfide-trapped (dt) pMHC-I (single-chain trimer) fused to the hinge-CH2-CH3 domains of mIgG2a (Fc) via a linker bearing in N- to C-terminal order a His<sub>6</sub>-tag, AviTag (biotin) and tandem-thrombin recognition site allowing for enzymatic cleavage of the Fc portion (\*).

Structure	Allele	Antigen	Peptide Seq.	Construct ID:
dt-pMHC-I (SCT)-biotin	HLA-A*02:01	HCMV pp65 495-503	NLVPMVATV	10473.1
	HLA-A*02:01	Survivin 96-104	LMLGEFLKL	10469.1
	HLA-A*02:01	Flu A MP 58-66	GILGFVFTL	10471.1

Fc-free monomeric disulfide-trapped (dt) pMHC-I (single-chain trimer) followed by a C-terminal linker comprising in N- to C-terminal order a His<sub>6</sub>-tag, triple FLAG-tag and AviTag (biotin).

### Additional reagents used for pMHC multimer generation:

Name / Ingredients	Supplier	Cat. No.
<b>Streptavidin-Alexa Fluor® 647 (A647) conjugate</b> ▪ Reconstituted in PBS at 0.5 mg/mL	Thermo Scientific	S21374
<b>Streptavidin-APC conjugate</b> ▪ 0.2 mg/mL (relates to streptavidin only)	BioLegend	405207
<b>Streptavidin-PE conjugate</b> ▪ 0.2 mg/mL (relates to streptavidin only)	BioLegend	405204
<b>Streptavidin</b> (unconjugated)	BioLegend	405150
<b>DPBS (1x), pH 7.2, no MgCl<sub>2</sub> and CaCl<sub>2</sub></b> [+] 1% (w/v) BSA [+] 0.1% (w/v) NaN <sub>3</sub>	Sigma-Aldrich PAA Sigma-Aldrich	D8537-500ML K45-001 71289-50G
<b>Eppendorf® Protein LoBind tubes</b>	Eppendorf	0030108116

▪ Suppliers' specifications | [+] Medium supplements additionally added | Cat. No.: Suppliers' catalogue numbers

### Streptavidin-based multimerization of biotinylated soluble pMHC molecules:

*In vivo* biotinylated and subsequently His-tag-based purified monomeric pMHC-I molecules as well as pMHC-I-pCC-Fc as well as pMHC-II-pCC-Fc heterodimers were multimerized by incubation with streptavidin at a final molecular ratio of 4–5 times more biotinylated proteins than streptavidin as described previously by (209). In most cases, 100 pmol corresponding to 5.5 µg monomeric pMHC-I (55 kDa), ~ 15–20 µg of pMHC-II-pCC-Fc (140 kDa) and pMHC-I-pCC-Fc (170 kDa), respectively, were diluted to 0.1 mg/mL in DPBS. Subsequently, streptavidin was added stepwise in 15 min intervals to the diluted pMHC molecules placed at 4°C to ensure complete saturation of all streptavidin binding sites. Streptavidin-A647 or unconjugated streptavidin has been used for pMHC multimerization followed by NativePAGE analysis (**Section 2.6.2**). Streptavidin-APC and streptavidin-PE was used for multimerization, if pMHC multimers were subsequently used in T cell binding assays (**Section 2.7.3**). pMHC multimers on the basis of streptavidin-APC or streptavidin-PE were finally supplemented with 1% BSA (w/v) and 0.1% (w/v) NaN<sub>3</sub> and stored at 4°C.

### 2.6.2 NativePAGE-based analysis of pMHC multimer formation

Name / Ingredients	Supplier	Cat. No.
<b>NativePAGE™ 3–12% Bis-Tris Protein Gels</b> ▪ 1.0 mm, 10 well, resolving range 15 – 10,000 kDa	Thermo Scientific	BN1001BOX
<b>NativePAGE™ Running Buffer Kit 20x</b> ▪ Running Buffer and Cathode Additive (contains G-250)	Thermo Scientific	BN2001
<b>NativePAGE™ Sample Buffer 4x</b>	Thermo Scientific	BN2003
<b>NativeMark™ Unstained Protein Standard</b>	Thermo Scientific	LC0725
<b>NativePAGE™ 5% G-250 Sample Additive</b>	Thermo Scientific	BN2004
<b>XCell SurLock™ Mini-Cell Electrophoresis System</b>	Thermo Scientific	EI0001
<b>Fixation solution</b> ddH <sub>2</sub> O (50%) [+] 40% (v/v) methanol [+] 10% (v/v) acetic acid	Sigma-Aldrich Sigma-Aldrich	322415-1L 33209-2.5L-M
<b>Destain solution</b> ddH <sub>2</sub> O (90%) [+] 10% (v/v) acetic acid	Sigma-Aldrich	33209-2.5L-M

▪ Suppliers' specifications | [+] Medium supplements additionally added | Cat. No.: Suppliers' catalogue numbers

NativePAGE analysis procedure:

All shown NativePAGE analysis were performed using the NativePAGE™ precast gel system (Thermo Scientific) according to the manufacture's protocol. Briefly, 7.5 µg protein of interest were combined with NativePAGE sample buffer in a total volume of 25 µL and were additionally supplemented with 2 µL 5% G-250 sample additive. Diluted samples were directly loaded onto a 3–12% NativePAGE gel, which had been fixed inside the electrophoresis system. Afterwards 1x running buffer and 1x cathode buffer were filled into the outer and inner chamber, respectively. In all cases the dark blue cathode buffer option (inner chamber buffer) was used (i.e. 0.05 volume NativePAGE cathode additive in 1x Running Buffer), which directly stains the gel during the electrophoresis procedure with Coomassie G-250. Electrophoresis was performed at 150V at RT for 115 min. Afterwards the gel was placed in 100 mL fixation solution and microwaved at 1000 watts for 45 seconds, followed by an incubation at 15 min at RT under agitation. The fixation solution was replaced by destain solution and the gel was again microwaved and left overnight to achieve a desired background signal.

**2.7 Flow cytometric analysis of T cell specificity, phenotype and activation**

**Initial remarks** | All flow cytometric measurements were performed on a BD FACS Canto II system with a three laser set-up allowing up to eight suitable colors to be measured at once. All antibodies and staining reagents used have been tested and titrated to an optimal concentration before using them in functional assays. All acquired FACS data were processed using the FlowJo™ software version 10. If necessary, gates were set with the help of fluorescence-minus-one (FMO) controls as described by (271).

General used reagents and consumables used for FACS-staining:

Name / Ingredients	Supplier	Cat. No.
<b>"FACS buffer"</b> DPBS (1x), pH7.2, without MgCl <sub>2</sub> and CaCl <sub>2</sub> [+] 2% (v/v) heat-inactivated fetal bovine serum (FBS)	Sigma-Aldrich Biochrom	D8537-500ML S 0615
<b>Zombie Aqua™ Fixable Viability Kit</b>	BioLegend	423102
<b>Human TruStain FcX™ (Fc receptor blocking solution)</b>	BioLegend	422302
<b>DPBS (1x) (Dulbecco's Phosphate Buffered Saline)</b> ▪ pH7.2, without MgCl <sub>2</sub> and CaCl <sub>2</sub>	Sigma-Aldrich	D8537-500ML
<b>Fixation solution</b> DPBS (1x); pH7.2, without MgCl <sub>2</sub> and CaCl <sub>2</sub> [+] 2.5% (v/v) paraformaldehyde (PFA) [+] 1% FBS	Sigma-Aldrich Thermo Scientific Biochrom	D8537-500ML 28908 S 0615
<b>Nunc™ 96-well polypropylene V-bottom plate</b> ▪ Capacity of 0.45 mL volume per well	Thermo Scientific	249944

- Suppliers' specifications | [+] Medium supplements additionally added | Cat. No.: Suppliers' catalogue numbers

## 2.7.1 Surface staining for T cell lineage, activation, memory and exhaustion markers

### Used antibody staining panels for T cell lineage, activation, memory and exhaustion markers

Specificity [Clone]:	Conjugated dye	Isotype	Supplier	Cat. No.	µL /test
<b>Lineage marker panel [LM-1]</b>					
Anti-human CD3 [UCHT1]	FITC	Mouse IgG1	BioLegend	300440	2.0
Anti-human CD8a [SK1]	Pacific Blue	Mouse IgG1	BioLegend	344718	1.0
Anti-human CD14 [M5E2]	BV 510	Mouse IgG2a	BioLegend	301842	1.0
Anti-human CD19 [HIB19]	BV 510	Mouse IgG1	BioLegend	302242	1.0
<b>[+] Memory marker panel [A]</b>					
Anti-human CD27 [M-T271]	PE	Mouse IgG1	BioLegend	356406	2.0
Anti-human CD28 [CD28.2]	PE/Cy7	Mouse IgG1	BioLegend	302926	2.0
Anti-human CD45RA [HI100]	APC/Cy7	Mouse IgG2b	BioLegend	304128	2.0
Anti-human CCR7 [G043H7]	PerCP/Cy5.5	Mouse IgG2a	BioLegend	353220	2.0
<b>[+] Exhaustion marker [B]</b>					
<i>Individual stained</i>					
Anti-human TIM-3 [F38-2E2]	APC	Mouse IgG1	BioLegend	345012	2.0
Anti-human LAG-3 [11C3C65]	PE	Mouse IgG1	BioLegend	369306	2.0
Anti-human TIGIT [MB5A43]	PE	Mouse IgG1	eBioscience	12-9500-42	2.0
Anti-human PD-1 [EH12.2.H7]	PE	Mouse IgG1	BioLegend	329906	2.0
<b>[+] Activation marker panel [C]</b>					
Anti-human CD25 [BC96]	A647	Mouse IgG1	BioLegend	302618	1.0
Anti-human 4-1BB [4B4-1]	PE/Cy7	Mouse IgG1	BioLegend	309818	1.0
<b>[+] Isotype control panel for [A]</b>					
Mouse IgG1 Isotype [MOPC-21]	PE	Mouse IgG1	BioLegend	400114	1.0
Mouse IgG1 Isotype [MOPC-21]	PE/Cy7	Mouse IgG1	BioLegend	400126	1.0
Mouse IgG2a Isoty. [MOPC-173]	PerCP/Cy5.5	Mouse IgG2a	BioLegend	400250	1.0
Mouse IgG2b Isoty. [MPC-11]	APC/Cy7	Mouse IgG2b	BioLegend	402210	1.0
<b>[+] Isotype control panel for [B]</b>					
Mouse IgG1 Isotype [MOPC-21]	PE	Mouse IgG1	BioLegend	400114	1.0
Mouse IgG1 Isotype [MOPC-21]	APC	Mouse IgG1	BioLegend	400122	1.0
<b>[+] Isotype control panel for [C]</b>					
Mouse IgG1 Isotype [MOPC-21]	PE	Mouse IgG1	BioLegend	400114	1.0
Mouse IgG1 Isotype [MOPC-21]	A647	Mouse IgG1	BioLegend	400136	1.0
<b>Lineage marker panel [LM-2]</b>					
Anti-human CD3 [UCHT1]	FITC	Mouse IgG1	BioLegend	300440	2.0
Anti-human CD8a [SK1]	Pacific Blue	Mouse IgG1	BioLegend	344718	1.0
Anti-human CD14 [M5E2]	PerCP/Cy5.5	Mouse IgG2a	BioLegend	325622	1.0
Anti-human CD19 [HIB19]	PE/Cy7	Mouse IgG1	BioLegend	302216	1.0
Anti-human CD4 [RPA-T4]	APC/Cy7	Mouse IgG1	BioLegend	300518	1.0
<b>[+] Exhaustion / activation</b>					
Anti-human PD-1 [EH12.2.H7]	PE	Mouse IgG1	BioLegend	329906	2.0
Anti-human CD25 [BC96]	A647	Mouse IgG1	BioLegend	302618	1.0

A647: Alexa Fluor 674 | APC: Allophycocyanin | BV: Brilliant Violet | PE: Phycoerythrin

Protocol for surface staining of T cell lineage, activation, memory and exhaustion markers:

**Initial remarks** | Staining panel [A] and [B] in combination with the lineage marker panel [LM] and corresponding isotype control antibody panels were used to assess the memory or exhaustion phenotype of resting CD8<sup>+</sup> T cell lines. Panel [C] was used to assess the activation state of at least 18 hours stimulated CD8<sup>+</sup> T cell lines as described in **Section 2.9.2**. In addition, the mentioned staining protocol below applies for all used cell surface stainings unless deviations are explicitly mentioned.

For all mentioned experiments unless otherwise mentioned in the figure legend, at least 25,000 cells/well were transferred to a 96-well V-bottom plate and washed once using 200 µL/well DPBS. For life/dead cell discrimination, cells were stained with Zombie Aqua™ (1:300 diluted in DPBS, 100 µL/well) for 10 min at RT in the dark. In case, PBMC cultures were stained, 100 µL/well FACS buffer (DPBS + 2% FBS) supplemented with 1 µL TruStain FcX™ solution were added after the 10 min and the plate was incubation on ice for 5 additional minutes to block Fc receptors. Otherwise, cells were washed once using 200 µL/well FACS buffer. Antibodies were diluted in FACS buffer (staining solution) and subsequently cells were stained at the cell surface using 50 µL/well staining solution on ice for 15 min in the dark. Finally, stained cells were washed twice and were left in fixation solution at 4°C in the dark until FACS-measurement. All centrifugation / washing steps were performed at 1550 rpm, 4°C for 3 min.

2.7.2 Intracellular staining for cytokines (ICS) and CD107a degranulation assay

Additional reagents and buffers used for ICS and CD107a degranulation assay:

Name / Ingredients	Supplier	Cat. No.
<b>BD Cytofix/ Cytoperm™ Fixation/Permeabilization Solution Kit</b> <ul style="list-style-type: none"> <li>▪ BD Perm/ Wash Buffer (10x)</li> <li>▪ BD Cytofix/ Cytoperm™ fixation/permeabilization solution</li> </ul>	BD Bioscience	554714
<b>Monensin Solution “BD GolgiStop™”</b>	BD Bioscience	554724
<b>Brefeldin A Solution “BD GolgiPlug™”</b>	BD Bioscience	555029
<b>Phorbol-12-myristate-13-acetate (PMA)</b> <i>1 mg/mL in DMSO</i>	Sigma Aldrich	P8139-1MG
<b>Ionomycin calcium salt</b> <i>1 mg/mL in ethanol</i>	Sigma Aldrich	I0634-1MG
<b>96-well U-bottom cell culture plate, PS (Greiner CELLSTAR)</b>	Sigma Aldrich	M0812-100EA

▪ Suppliers' specifications | [+] Supplements additionally added | Cat. No.: Suppliers' catalogue numbers | PS: Polystyrene

Used antibody staining panels for intracellular cytokine staining and CD107a degranulation assay (1)

Specificity [Clone]:	Conjugated dye	Isotype	Supplier	Cat. No	µL /test
<b><u>Lineage Marker Panel – [LM2]</u></b>					
Anti-human CD3 [HIT3]	APC/Cy7	Mouse IgG2a	BioLegend	300318	1.0
Anti-human CD8a [RPA-T8]	V450	Mouse IgG1	BD Bioscience	560347	1.0
Anti-human CD4 [SK3]	A488	Mouse IgG1	BioLegend	344618	1.0
Anti-human CD14 [M5E2]	BV 510	Mouse IgG2a	BioLegend	301842	1.0
Anti-human CD19 [HIB19]	BV 510	Mouse IgG1	BioLegend	302242	1.0
<b><u>[+] ICS Panel [A]</u></b>					
Anti-human IFN-γ [4S.B3]	PE	Mouse IgG1	BioLegend	502509	2.0
Anti-human IL-2 [MQ1-17H12]	PE/Cy7	Rat IgG2a	Ebioscience	25-7029-42	2.0
Anti-human TNF-α [MAb11]	A647	Mouse IgG1	BioLegend	502916	2.0
<b><u>[+] ICS Panel [B]</u></b>					
Anti-human IFN-γ [4S.B3]	PE	Mouse IgG1	BioLegend	502509	2.0
Anti-human IL-2 [MQ1-17H12]	PE/Cy7	Rat IgG2a	Ebioscience	25-7029-42	2.0
Anti-human IL-4 [MP4-25D2]	APC	Rat IgG1	BioLegend	500834	2.0
<b><u>[+] anti-CD107a + ICS Panel [C]</u></b>					
Anti-human CD107a [H4A3]*	A647	Mouse IgG1	BioLegend	328612	0.25
Anti-human IFN-γ [4S.B3]	PE	Mouse IgG1	BioLegend	502509	2.0
Anti-human TNF-α [MAb11]	PE/Cy7	Mouse IgG1	BioLegend	502930	1.0

**Note** \*: anti-human CD107a mAb was already added during the stimulation and prior to the ICS staining as described below.

A647: Alexa Fluor 674 | APC: Allophycocyanin | BV: Brilliant Violet | PE: Phycoerythrin

Used antibody staining panels for intracellular cytokine assay (2)

Specificity [Clone]:	Conjugated dye	Isotype	Supplier	Cat. No	µL /test
<b><u>Lineage Marker Panel – [LM3]</u></b>					
Anti-human CD3 [HIT3]	APC/Cy7	Mouse IgG2a	BioLegend	300318	1.0
Anti-human CD8a [RPA-T8]	APC	Mouse IgG1	BioLegend	301049	1.0
Anti-human CD19 [HIB19]	PE/Cy7	Mouse IgG1	BioLegend	302216	1.0
<b><u>[+] ICS Panel [D]</u></b>					
Anti-human IFN-γ [4S.B3]	PE	Mouse IgG1	BioLegend	502509	2.0

A647: Alexa Fluor 674 | APC: Allophycocyanin | BV: Brilliant Violet | PE: Phycoerythrin

Intracellular cytokine staining (ICS) and CD107a degranulation assay procedure:

Intracellular cytokine staining and CD107a degranulation assay were performed as described previously (174, 193). Depending on the specific experimental layout as described in the figure legends as well as in general in **Section 2.9.2**, approximately  $5 \times 10^4$  cells of an antigen-specific CD8<sup>+</sup> or CD4<sup>+</sup> T cell line or  $2 \times 10^6$  PBMC were seeded per condition/well in a volume of 200 µL RPMI supplemented with 10% FBS into a 96-well U-bottom plate. T cells were stimulated for 4–5 hours at 37°C using various artificial antigen-presenting cells (aAPCs), 10 µM peptide pulse or PMA (10 ng/mL) and Ionomycin (1 µg/mL) in the presence of BD GolgiStop™ (1:1000) and BD GolgiPlug™ (1:1500) to ensure intracellular cytokine accumulation upon stimulation. To measure T cell degranulation parallel to cytokine expression, anti-human CD107a mAb was added at 0.25 µg/mL during the T cell stimulation (193). After the T cell stimulation, cells were transferred to a 96-well V-bottom plate and washed once with 200 µL/well DPBS. For life/dead cell discrimination, cells were stained with Zombie Aqua™ (1:300 diluted

## 2 | Material and methods

in DPBS, 100 µL/well) for 10 min at RT in the dark. In case PBMC cultures were stimulated, 100 µL/well FACS buffer (DPBS + 2% FBS) supplemented with 1 µL/well TruStain FcX™ solution were added after the 10 min and the plate was incubation on ice for additional 5 min to block Fc receptors. Otherwise, cells were washed once using 200 µL/well FACS buffer. Subsequently, cells were stained at the cell surface for 15 min on ice as described in **Section 2.7.1**. Next, cells were permeabilized and fixated using the BD Cytofix/Cytoperm solution kit according to the manufacturer's protocol. Briefly, 100 µL/well of BD Cytofix/Cytoperm solution was added and incubated for no longer than 7 min on ice. Afterwards, 100 µL/well 1x BD Perm/Wash buffer was directly added to quench the fixation. Next, cells were washed once with 1x BD Perm/Wash buffer. Antibodies for intracellular cytokine staining were diluted in BD Perm/Wash buffer solution and 100 µL/well was added to the cells, followed by a 30 min incubation on ice in the dark. Stained cells were washed twice with 1x BD Perm/Wash buffer and finally resuspended in FACS buffer and left at 4°C in the dark prior to flow cytometric measurement.

### 2.7.3 pMHC multimer and pMHC-Fc staining

Used antibody staining panels and staining reagents for pMHC multimer staining:

Specificity [Clone]:	Conjugated dye	Isotype	Supplier	Cat. No.	µL /test
<b>Lineage Marker Panel [LM1]</b>					
Anti-human CD3 [UCHT1]	FITC	Mouse IgG1	BioLegend	300440	2.0
Anti-human CD14 [M5E2]	BV 510	Mouse IgG2a	BioLegend	301842	1.0
Anti-human CD19 [HIB19]	BV 510	Mouse IgG1	BioLegend	302242	1.0
<i>Anti-human CD8a [SK1] or</i>	Pacific Blue	Mouse IgG1	BioLegend	344718	1.0
<i>Anti-human CD4 [SK3]</i>	Pacific Blue	Mouse IgG1	BioLegend	344620	2.0
<b>Anti-mouse-IgG2a</b>					
Anti-mouse-IgG2a [RMG2a-62]	Biotin	Rat IgG1	BioLegend	407104	0.025
[+] Streptavidin	APC	-	BioLegend	405237	0.062
Anti-mouse-IgG2a [RMG2a-62]	APC	Rat IgG1	BioLegend	407110	0.062
<b>Anti-mouse IgG (GαM-Ig-APC)</b>					
Anti-mouse IgG-Fc	APC	Goat-Poly.	BD Bioscience	550826	0.5
<b>Strep-Tactin®</b> fluorochrome-conjugated	APC	-	IBA Lifescience	6-5010-001	0.25

APC: Allophycocyanin | BV: Brilliant Violet | PE: Phycoerythrin | Goat-Poly.: Goat-anti-mouse IgG-Fc polyclonal serum

Used commercial pMHC-I multimers (Pro5 / Pentamers):

Allele	Antigen	Peptide sequence	Label	Supplier	Cat. No.	µL /test
HLA-A*02:01	Flu A MP 58–66	GILGFVFTL	none	ProImmune	F007-0A-E	0.5
HLA-A*02:01	Survivin 96–104	LMLGEFLKL	none	ProImmune	F391-0A-E	1.0
HLA-A*02:01	EBV BMLF-1 259–267	GLCTLVAML	none	ProImmune	F001-0A-E	0.5
HLA-A*02:01	HCMV pp65 495–503	NLVPMTATV	none	ProImmune	F008-0A-E	0.5
Flurotag (Reagent to detect unlabeled Pro5 Pentamers)			APC	ProImmune	K4B-E	2.0

| APC: Allophycocyanin

Used commercial pMHC-II tetramers (all supplied from ProImmune) :

Allele	Antigen	Epitope sequence	Label	Cat. No.	µL/test
HLA-DRB1*03:01 / DRA*01:01	MTB Hsp65 1–13	MAKTIAYDEEARR	APC	Custom	1.0
	HCMV pp65 510–522	YQEFFWDANDIYR	APC	Custom	1.0
	CLIP 103–117	PVSKMRMATPLLQA	APC	MTN02B-1A-E	1.0

APC: Allophycocyanin

Additional used buffers and reagents pMHC multimer and pMHC-Fc staining:

Name / Ingredients	Supplier	Cat. No.
<b>pMHC staining buffer 1 (buffer 1)</b> DPBS (1x), pH7.2, without MgCl <sub>2</sub> and CaCl <sub>2</sub> [+] 2% (v/v) heat-inactivated fetal bovine serum (FBS) [+] 50 nM dasatinib	Sigma-Aldrich Biochrom BioVision	D8537-500ML S 0615 1586-100
<b>pMHC staining buffer 2 (buffer 2)</b> DPBS (1x), pH7.2, without MgCl <sub>2</sub> and CaCl <sub>2</sub> [+] 0.1% (w/v) bovine serum albumin (BSA) [+] 50 nM dasatinib [+] 0.1% (w/v) NaN <sub>3</sub>	Sigma-Aldrich PAA BioVision Sigma-Aldrich	D8537-500ML K45-001 1586-100 71289-50G
<b>pMHC-I-Fc-STag [+] Strep-Tactin-APC staining buffer</b> 1x Buffer IS for Streptamer [+] 50 nM dasatinib	IBA Lifesciences BioVision	6-5602-050 1586-100
<b>Fixation Solution</b> DPBS (1x); without MgCl <sub>2</sub> and CaCl <sub>2</sub> [+] 2.5% (v/v) paraformaldehyde (PFA) [+] 1% FBS	Sigma-Aldrich Thermo Scientific Biochrom	D8537-500ML 28908 S 0615

▪ Suppliers' specifications | [+] Medium supplements additionally added | Cat. No.: Suppliers' catalogue numbers

### 2.7.3.1 pMHC-I multimer and pMHC-I-Fc staining for the detection of antigen-specific CD8<sup>+</sup> T cells

Depending on the specific experimental layout as also indicated in the figure legends, approximately  $5 \times 10^4$  cells of an antigen-specific CD8<sup>+</sup> T cell line or  $2 \times 10^6$  PBMC of HLA-A2 haplotype were transferred into a 96-well V-bottom plate. Next, cells were stained with Zombie Aqua™ dye (1:300) (RT, 10 min) in the presence of 50 nM dasatinib to improve the subsequent pMHC multimer staining as described previously by (206). Subsequently, cells were stained in 50 µL pMHC staining buffer 1 (buffer 1) for 20 min at RT with commercial pMHC-I pentamer (ProImmune) or in-house produced pMHC-I-Fc dimers as well as pMHC-I monomer-based as well as pMHC-I-pCC-Fc-based multimers (**Section 2.6.1**). Staining concentrations between 1–50 µg/mL were used depending on the experimental needs as indicated in the figure legends. Cells were washed once using 200 µL/well buffer 1.

**Follow-up commercial pMHC multimer staining:** If commercial pMHC-I pentamer (ProImmune) or pMHC-I multimer stainings were performed, cells were labeled in the next step with lineage marker antibody panel 1 [LM1] diluted in buffer 1 for 20 min on ice. During this step also the FluroTag was added for the detection of unlabeled pMHC-I pentamers. Cells were washed two times using buffer 1 and were finally resuspended in and left in fixation solution until FACS measurement.

**Follow-up pMHC-Fc staining and detection via GαM-Ig-APC:** In case pMHC-Fc binding was sequentially detected by goat-anti-mouse-IgG-Fc-APC (GαM-Ig-APC) (**Results Section 3.2.1 / Fig. 3.4**), GαM-Ig-APC staining was performed for 20 min on ice prior to lineage marker staining (described above) followed by three times washing with buffer 1. Subsequently, cells were stained for lineage markers and fixed.

**Follow-up pMHC-Fc detection via biotinylated anti-mouse-IgG2a mAb + Streptavidin-APC:**

For the detection of pMHC-Fc binding via biotinylated anti-mouse-IgG2a and subsequent streptavidin-APC staining, cells were stained in buffer 1 with biotinylated anti-mouse-IgG2a parallel to the lineage marker panel 1 [LM1] (all mouse IgG1) for 20 min, on ice. Next, cells were washed twice with 200  $\mu$ L/well buffer 1, followed by Streptavidin-APC staining for 15 min, on ice. Cells were washed again twice and left in fixation solution.

**pMHC-I-Fc-STag detection by sequential addition of Strep-Tactin-APC and pMHC-I-streptamer staining:**

In some cases, binding of pMHC-I-Fc-STag constructs was detected by sequential staining with Strep-Tactin-APC parallel to the lineage marker staining 1 [LM1]. In that case, all stainings but the ZombieAqua staining were performed in 1x IS-buffer supplemented with 50 nM dasatinib. Alternatively, pMHC-I-Fc-STag constructs were multimerized with Strep-Tactin-APC to form so-called Streptamers (272). pMHC-I-Fc-STag precomplexation was done at a molar ratio of 75 pMHC-Fc-STag (15 pmol / 2.5  $\mu$ g) to 1 Strep-Tactin-APC (0.2 pmol /  $\sim$  40 ng) in 50  $\mu$ L 1x IS-buffer supplemented 50 nM dasatinib for 30 min on ice. Titration of Strep-Tactin-APC during the precomplexation has shown, that a molar increase of Strep-Tactin-APC leads to an unspecific staining signal / higher background (**Supplementary Figure S2d**). This might be caused by the formation of larger protein-aggregates due to the presence of two Strep-tag II per pMHC-I-Fc-STag construct (one on each Fc chain). Streptamer-based staining was performed for 20 min at RT followed by lineage marker staining panel 1 [LM1] as described above using 1x IS-buffer supplemented with 50 nM dasatinib instead of buffer 1.

**2.7.3.2 pMHC-II tetramer staining for the detection of antigen-specific CD4<sup>+</sup> T cells**

Approximately  $5 \times 10^4$  MTB Hsp65<sub>1-13</sub>/HLA-DR3 specific CD4<sup>+</sup> T cells (clone RP15.1.1) per condition were transferred into a 96-well V-bottom plate and stained with Zombie Aqua<sup>TM</sup> viability dye (1:300 in PBS) (RT, 10 min) in the presence of 50 nM dasatinib (206). Next, cells were stained for 2 h at 37°C in 50  $\mu$ L pMHC staining buffer 2 (buffer 2) using 20  $\mu$ g/mL commercial pMHC-II tetramers (ProImmune) and pMHC-II-pCC-Fc multimers (**Section 2.6.1**). Cells were washed once using 200  $\mu$ L/well buffer 2 and were subsequently stained with the lineage marker antibody panel 1 (using Pacific Blue-conjugated anti-human CD4 mAb instead of anti-human CD8 mAb) diluted in buffer 2 for 15 min on ice. Cells were washed two times using buffer 2 and were finally resuspended and left in fixation solution until FACS measurement.

**2.8 Generation of virus antigen-specific HLA-A2-restricted CD8<sup>+</sup> T cell lines**

Used peptides for expansion of virus-specific HLA-A2-restricted CD8<sup>+</sup> T cells:

Name	Sequence	Protein	Position	Preferred binding to:	Ref.
HCMV pp65 <sub>495-503</sub>	NLVPMVATV	HCMV pp65	495-503	HLA-A*02:01	(273)
Flu A MP <sub>58-66</sub>	GILGFVFTL	Flu A MP-1	58-66	HLA-A*02:01	(274)
EBV BMLF-1 <sub>259-267</sub>	GLCTLVAML	EBV BMLF-1	259-267	HLA-A*02:01	(275)

All peptides were synthesized at the DKFZ peptide synthesis core facility unit. Ref.: Reference of peptide discovery / HLA-binding properties

Corresponding used pHLA-A2-Fc-STag constructs for antigen-specific T cell isolation (**Section 2.8.2**):

Structure	Allele	Antigen	Sequence	Construct:
dt-SCT-mIgG2a-Fc-STag	HLA-A*02:01	HCMV pp65 495-503	NLVPMVATV	8558.1
dt-SCT-mIgG2a-Fc-STag	HLA-A*02:01	Flu A MP 58-66	GILGFVFTL	8557.1
dt-SCT-mIgG2a-Fc-STag	HLA-A*02:01	EBV BMLF-1 259-267	GLCTLVAML	8804.1

Additional used cell culture media, reagents and consumables:

Name / Ingredients	Supplier	Cat. No.
<b>AIM V™ Medium</b>	Thermo Scientific	12055091
<ul style="list-style-type: none"> <li>▪ with L-glutamine, gentamicin, streptomycin sulfate, phenol red</li> </ul>	PAN Biotech	P30-2501
[+] 10% (v/v) human serum type AB	Miltenyi Biotec	130-097-748
[+] 20 – 50 units/mL human interleukin-2 (IL-2)	Miltenyi Biotec	130-095-764
[+] 2.5 – 10 ng/mL human interleukin-15 (IL-15)		
<b>Anti-human HLA-A2-APC</b>	BioLegend	343308
<ul style="list-style-type: none"> <li>▪ Clone BB7.2, APC-conjugation, mouse IgG2b isotype</li> </ul>		
<b>Red blood cell (RBC) Lysis Buffer (10x)</b>	BioLegend	420301
<b>96-well U-bottom cell culture plate, PS (Greiner CELLSTAR)</b>	Sigma-Aldrich	M0812-100EA
<b>24-well cell culture plate flat-bottom</b>	TPP	92024

▪ Suppliers' specifications | [+] Medium supplements additionally added | Cat. No.: Suppliers' catalogue numbers

Additional used reagents and consumables for antigen-specific T cell isolation (Section 2.8.2):

Name / Ingredients	Supplier	Cat. No.
<b>Strep-Tactin® Magnetic Nanobeads for MHC-I Streptamers</b>	IBA Lifesciences	6-5500-005
<b>IS Buffer (10x) for Streptamers</b>	IBA Lifesciences	6-502-050
<ul style="list-style-type: none"> <li>▪ Washing buffer for Strep-Tactin magnetic nanobeads</li> </ul>		
<b>D-biotin solution (100 mM) for Streptamers</b>	IBA Lifesciences	6-0219-001
<b>MACS (magnetic activated cell sorting) columns and magnets</b>		
OctoMACS™ Separator	Miltenyi Biotec	130-042-109
QuadroMACS™ Separator	Miltenyi Biotec	130-090-976
MS columns	Miltenyi Biotec	130-042-201
LS columns	Miltenyi Biotec	130-042-401

▪ Suppliers' specifications | Cat. No.: Suppliers' catalogue numbers

2.8.1 Peptide pulse-based antigen-specific expansion of CD8<sup>+</sup> T cells

**HLA-A\*02:01 expression analysis:** For the purpose of virus-specific HLA-A2-restricted CD8<sup>+</sup> T cell line generation, a panel of healthy blood donors were screened for HLA-A2 expression by flow cytometry prior to PBMC preparation. For this a small blood sample was directly depleted from erythrocytes using red blood cell (RBC) lysis buffer (BioLegend) according to the manufacture's protocol. RBC-lysed blood was subsequently stained for 15 min with anti-HLA-A2 mAb (clone BB7.2) as described in **Section 2.7**. Subsequently, PBMC were isolated from blood of donors with HLA-A2 genotype (HLA-A2<sup>+</sup>) as described in (**Section 2.1.4**). **pMHC multimer staining:** Freshly HLA-A2<sup>+</sup> PBMC were left overnight (37°C, 5% CO<sub>2</sub>) and were subsequently analyzed for the presence of virus-epitope specific HLA-A2 restricted CD8<sup>+</sup> T cell population by commercial pMHC-I pentamer staining as described in **Section 2.7.3**. **Peptide pulse:** After the identification of either human cytomegalovirus (HCMV) pp65<sub>495–503</sub>/HLA-A2, Influenza A (Flu) MP<sub>58–66</sub>/HLA-A2 or Epstein-Barr virus (EBV) BMLF-1<sub>259–267</sub> /HLA-A2 specific CD8<sup>+</sup> T cell populations, these populations were expanded using a corresponding 100 nM peptide pulse. Briefly, 1x10<sup>6</sup> PBMC/well were seeded in a 96-well U-bottom plate and cultured in AIM-V supplemented with 10% human serum type AB, 50 units/mL IL-2, 5 ng/mL IL-15 and 100 nM peptide. Every 3–5 days, 50% of the medium was replaced with fresh medium but without peptide supplementation. In some cases antigen-specific T cells expansion was monitored by pMHC multimer staining on day 5 and day 13 after the initial peptide pulse (**Results Section 3.2.2 / Fig. 3.5**). 15–16 days post peptide pulse, expanded antigen-specific CD8<sup>+</sup> T cells were isolated using pMHC-I-Fc-coated nanobeads as described in **Section 2.8.2**. Finally, 3x10<sup>5</sup> isolated antigen-specific T cells per 24-well were subsequently co-cultured with 1x10<sup>6</sup> HLA-A2-matched PBMC feeder cells, that have been beforehand 100 nM peptide pulsed and

## 2 | Material and methods

irradiated (33 Gy). Purity and successful 2<sup>nd</sup> antigen-specific T cell expansion was analyzed by pMHC-multimer staining 7–14 days after the antigen-specific isolation (also see **Results Section 3.2.2**).

### 2.8.2 MACS-based isolation of antigen-specific CD8<sup>+</sup> T cell populations

For antigen-specific T cell isolation, Strep-Tactin-conjugated magnetic nanobeads (IBA Lifesciences) were used and cell isolation was performed according to manufacturer's protocol. However, in-house produced dt-pMHC-I-mIgG2a-Fc-Strep-tag II fusion proteins were used instead of commercially available soluble pMHC-I-Strep-tag II monomers (IBA Lifesciences). Briefly, 50 µL Strep-Tactin-conjugated nanobeads (IBA Lifesciences) were combined with 10 µg purified dt-pMHC-I-mIgG2a-Fc-Strep-tag II construct in 100 µL 1x IS buffer (IBA Lifesciences) and incubated for 45 min at 4°C. Afterwards, pMHC-I-coupled nanobeads were washed using a MACS MS-column placed into a magnet according to the manufacturer's protocol. Washed beads were incubated with 1x10<sup>7</sup> cells derived from **Section 2.8.1** for 45 min on ice and finally antigen-specific T cells were isolated using a MACS LS-column. Eluted antigen-specific T cells were incubated for 10 min in 1x IS-buffer supplemented with 1 mM D-biotin to disassemble dt-pMHC-I-mIgG2a-Fc-Strep-tag II-coated nanobeads. Finally, 3x10<sup>5</sup> isolated T cells/well of a 24-well plate were directly seeded on 1x10<sup>6</sup> HLA-A2<sup>+</sup>, 100 nM peptide-pulsed and irradiated (33 Gy) PBMC feeders and were cultured in 1 mL/well AIM-V supplemented with 10% human serum type AB, 20 units/mL IL-2, 5 ng/mL IL-15.

## 2.9 Conventional assays for measuring functional T cell responses

### 2.9.1 Assembly of various bead- and cell-based artificial antigen presenting cells (aAPCs)

Reagents, equipment and consumables generally used for bead-based aAPC assembly:

Name / Ingredients	Supplier	Cat. No
<b>DynaMag™-2 Magnet</b>	Thermo Scientific	12321D
<b>Protein LoBind Tube 1.5 mL</b>	Eppendorf	0030 108.116
<b>Magnetic 96-well Separator (magnet for 96-well F-bottom plates)</b>	Thermo Scientific	A14179
<b>96-well non-binding, black, F-bottom/Chimney Well</b>	Greiner bio-one	655900
<b>Bead buffer</b> DPBS (1x), pH 7.2, without MgCl <sub>2</sub> and CaCl <sub>2</sub> [+] 0.5% (w/v) BSA [+] 0.1% (w/v) NaN <sub>3</sub> 0.22 µm sterile filtration	Sigma-Aldrich PAA Sigma-Aldrich Merck	D8537-500ML K45-001 71289-50G SLGP033RB
<b>Mouse serum</b>	Sigma-Aldrich	M5905

Commercial cell culture-grade antibodies used for aAPC generation:

Specificity [Clone]:	Dye / Conjugation	Isotype	Supplier	Cat. No
<b>Anti-human CD3 [OKT3]</b>	-	Mouse IgG2a	BioLegend	317326
<i>Co-stimulatory mAbs:</i>				
<b>Anti-human CD2 [RPA-2.10]</b>	-	Mouse IgG1	BioLegend	300212
<b>Anti-human CD28 [CD28.2]</b>	-	Mouse IgG1	BioLegend	302923
<b>Anti-human CD28 [15E8]</b>	-	Mouse IgG1	Miltenyi Biotec	130-093-375
<b>Anti-human 4-1BB [4B4-1]</b>	-	Mouse IgG1	BioLegend	309811

Produced soluble pMHC molecules for aAPC generation:

Structure	Allele	Antigen	Peptide Seq.	Construct:
dt-pMHC-I (SCT)-mIgG2a-Fc	HLA-A*02:01	HCMV pp65 495–503	NLVPMVATV	7409.4
	HLA-A*02:01	Survivin 96–104	LMLGEFLKL	8195.1
dt-pMHC-I (SCT)-mIgG2a-Fc-S-Tag	HLA-A*02:01	Survivin 96–104	LMLGEFLKL	8556.1
	HLA-A*02:01	Flu A MP 58–66	GILGFVFTL	8557.1
	HLA-A*02:01	HCMV pp65 495–503	NLVPMVATV	8558.1
	HLA-A*02:01	EBV BMLF-1 259–267	GLCTLVAML	8804.1
	HLA-A*02:01	NY-ESO-1 157–165	SLLMWITQV	8807.1
	HLA-A*02:01#	Survivin 96–104	LMLGEFLKL	9670.1
	HLA-A*02:01#	HCMV pp65 495–503	NLVPMVATV	9672.1
	dt-pMHC-I (SCT)-CH1-mIgG2a-Fc*	HLA-A*02:01	Survivin 96–104	LMLGEFLKL
HLA-A*02:01		HCMV pp65 495–503	NLVPMVATV	8414.1

dt: disulfide trap; SCT: single-chain trimer | Note #: HLA-A\*02:01 harbors an additional Q115E point mutation within the  $\alpha$ 2-domain (261) | Note \*: dt-pMHC-I is fused to the CH1-Hinge-CH2-CH3 domain of mIgG2a (CH1-mIgG2a-Fc).

Structure	Allele	Antigen	Peptide Seq.	Construct:
dt-pMHC-I (SCT)-pCC-mIgG2a-Fc-biotin	HLA-A*02:01	HCMV pp65 495–503	NLVPMVATV	10347.7
	HLA-A*02:01	Survivin 96–104	LMLGEFLKL	9237.1

pCC-mIgG2a-Fc-biotin: parallel coiled-coil (pCC) heterodimerization domain followed by the hinge domain and CH2 and CH3 of mIgG2a (Fc) and a C-terminal Strep-Tag II/His<sub>6</sub>Tag and AviTag for site-specific biotinylation (biotin). Tested construct were *in vivo* biotinylated.

Structure	Allele	Antigen	Peptide Seq.	Construct:
pMHC-II-pCC-mIgG2a-Fc	HLA-DRB1*03:01 / DRA*01:01	MTB Hsp65 1–13	MAKTIAYDEEARR	9260.3
	HLA-DRB1*03:01 / DRA*01:01	HCMV pp65 510–522	YQEFFWDANDIYR	10320.1
px-FII-MHC-II-pCC-mIgG2a-Fc	HLA-DRB1*03:01 / DRA*01:01	CLIP 103–117	PVSKMRMATPLLMQA	9221.1 [+] 8746.1
px-EK-MHC-II-pCC-mIgG2a-Fc	HLA-DRB1*03:01 / DRA*01:01	CLIP 103–117	PVSKMRMATPLLMQA	9261.3

px-FII: peptide-ligand followed by C-terminal linker bearing a thrombin cleavage site. px-EK: peptide-ligand followed by C-terminal linker bearing a enterokinase cleavage site.

Structure	Allele	Antigen	Peptide Seq.	Construct :
dt-pMHC-I (SCT)-biotin-*mIgG2a-Fc	HLA-A*02:01	HCMV pp65 495–503	NLVPMVATV	11097.1
	HLA-A*02:01	Survivin 96–104	LMLGEFLKL	11290.1
	HLA-A*02:01	Flu A MP 58–66	GILGFVFTL	11291.1
	HLA-A*02:01	EBV BMLF-1 259–267	GLCTLVAML	11292.1

Disulfide-trapped (dt) pMHC-I (single-chain trimer) fused to the hinge-CH2-CH3 domains of mIgG2a (Fc) via a linker bearing in N- to C-terminal order a His<sub>6</sub>-tag, AviTag (Biotin) and tandem-thrombin recognition site allowing for enzymatic cleavage of the Fc portion (\*).

### 2.9.1.1 DynaBead Goat-anti-mouse IgG-based aAPC assembly

Additional used reagents for Dynabead™ Goat-anti-mouse IgG-based aAPC assembly:

Name / Ingredients	Supplier	Cat. No.
<b>Dynabeads™ Goat anti-Mouse IgG (GαM-IgG-Dynabeads)</b> <ul style="list-style-type: none"> <li>▪ 4.5 μm in size</li> </ul>	Thermo Scientific	11033

▪ Suppliers' specifications | Cat. No.: Suppliers' catalogue number

Dynabead™ Goat-anti-mouse IgG-based aAPC assembly:

Depending on the specific experimental and technical needs,  $2.5 \times 10^5$ – $1 \times 10^6$  magnetic GαM-IgG-Dynabeads™ were transferred to 1.5 mL Eppendorf LoBind tubes and washed once using 1 mL bead buffer (DPBS + 0.5% BSA + 0.1% NaN<sub>3</sub>) and a DynaMag™-2 magnet. Washed beads were usually resuspended in the following in 200 μL bead buffer supplemented various pMHC-mIgG2a-Fc constructs and additional co-stimulatory mAbs at a final concentration of 20–50 μg/mL (also indicated in the respective figure legends). Beads were incubated at 1100 rpm shaking for at least 1 h at RT or left at 4°C overnight. Thereafter, 2 μL mouse serum was directly added to the beads to block remaining free binding sides followed by an incubation at RT for 15 min at 1100 rpm. pMHC-Fc-loaded beads, considered as artificial antigen-presenting cell (aAPC), were washed once using bead buffer and once with the specific culture medium used in subsequent experiments (usually complete RPMI + 10% FBS) and finally resuspended in that cell culture medium.

### 2.9.1.2 MACS® anti-mouse IgG microbead-based aAPC assembly

Additional used reagents for anti-mIgG MACS microbeads aAPC assembly:

Name / Ingredients	Supplier	Cat. No.
<b>Anti-Mouse IgG MicroBeads</b> <ul style="list-style-type: none"> <li>▪ 50 nm in size</li> </ul>	Miltenyi Biotec	130-048-402

▪ Suppliers' specifications | Cat. No.: Suppliers' catalogue number

anti-mIgG MACS MircoBeads aAPC assembly:

10 μL anti-mIgG MACS MircoBeads, 5 μg pMHC-Fc and 90 μL bead-buffer were combined in a 1.5 mL Eppendorf LoBind tube and incubated overnight at 4°C and 1100 rpm shaking. Next, 2 μL mouse serum was added to the beads and incubated at RT for 15 min at 1100 rpm. Subsequently, beads were centrifuged at 13,000 rpm for 10 min. Supernatant was carefully removed and replaced by 1 mL bead buffer followed by centrifugation. Next, beads were washed once with culture medium and finally resuspended in the medium used for subsequent experiments (usually complete RPMI + 10% FBS).

### 2.9.1.3 xMAP MagPlex microspheres (Luminex bead)-based aAPC assembly

Additional used reagents and antibodies for Luminex bead-based aAPC assembly:

Name / Ingredients	Supplier	Cat. No.
<b>xMAP MagPlex® Microspheres (Luminex beads)</b> <ul style="list-style-type: none"> <li>▪ 6.5 μm in size, bear surface carboxyl groups</li> </ul>	Luminex Corp.	MC10012 <i>till</i> MC100100 for bead region 12 <i>till</i> 100 (bead color code)

Specificity [Clone]:	Conj.	Isotype	Supplier	Cat. No.
Rat anti-mouse IgG2a [RMG2a-62]	-	Rat monoclonal IgG	BioLegend	407102
Goat anti-mouse IgG (Poly4053)	-	Goat polyclonal	BioLegend	405301

Name / Ingredients	Supplier	Cat. No
<b>Activation buffer</b> 0.1 M NaH <sub>2</sub> PO <sub>4</sub> in ddH <sub>2</sub> O, pH 6.2 [+] 5 mg/mL EDC* [+] 5 mg/mL Sulfo-NHS*	Sigma-Aldrich Thermo Scientific Sigma-Aldrich	S3139-500G 22980 56485-1G
<b>Coupling buffer:</b> DPBS, pH 7.2, without MgCl <sub>2</sub> and CaCl <sub>2</sub>	Sigma-Aldrich	D8537-500ML
<b>Quenching buffer</b> DPBS, pH 7.2, without MgCl <sub>2</sub> and CaCl <sub>2</sub> [+] 50 mM TRIS (pH adjusted) [+] 0.05% (v/v) Tween-20	Sigma-Aldrich Carl Roth Sigma-Aldrich	D8537-500ML 4855.2 P9416-100ML
<b>Wash buffer</b> DPBS, pH 7.2, without MgCl <sub>2</sub> and CaCl <sub>2</sub> [+] 0.05% (v/v) Tween-20	Sigma-Aldrich Sigma-Aldrich	D8537-500ML P9416-100ML
<b>Storage buffer</b> DPBS, pH 7.2, without MgCl <sub>2</sub> and CaCl <sub>2</sub> [+] 0.5% (w/v) bovine serum albumin (BSA) [+] 0.05% (v/v) Tween-20 [+] 0.05% (w/v) NaN <sub>3</sub>	Sigma-Aldrich PAA Sigma-Aldrich Sigma-Aldrich	D8537-500ML K45-001 P9416-100ML 71289-50G

- Suppliers' specifications | [+] Medium supplements additionally added | Cat. No.: Suppliers' catalogue number
- \* EDC / Sulfo-NHS solutions were always freshly prepared

#### Luminex bead carbodiimide coupling procedure for proteins of interest:

Depending on the specific experimental and technical needs, Luminex beads were covalently coupled with pMHC-Fc constructs or were coupled alternatively with goat anti-mouse pan-IgG (Luminex-GαM-IgG beads) or rat anti-mouse IgG2a mAbs (Luminex-RαM-IgG2a beads). Anti-mouse IgG antibody-conjugated Luminex beads were subsequently non-covalently loaded with various soluble pMHC-mIgG2a-Fc constructs (as described in **Section 2.9.1.1**). Luminex beads coupling with proteins of interest was performed according to the manufacturer's protocol using carbodiimide coupling chemistry. Briefly, up to 2.5x10<sup>6</sup> magnetic Luminex beads were transferred to 1.5 mL Eppendorf LoBind tubes and washed twice using 1 mL activation buffer (0.1 M NaH<sub>2</sub>PO<sub>4</sub>, pH 6.2) and a DynaMag<sup>TM</sup>-2 magnet. Washed beads were finally resuspended in 400 μL activation buffer. Next, 50 μL activation buffer supplemented freshly with EDC and sulfo-NHS (50 mg/mL), respectively, were added to the washed beads to form a sulfo-NHS-ester intermediate at the bead surface (bead activation). Beads were incubated at 1100 rpm shaking at RT for 20 min. Subsequently, beads were washed twice with coupling buffer (DPBS, pH 7.2). Proteins of interest were diluted at 50 μg/mL in DPBS and beads were subsequently resuspended in 200 μL of that protein solution followed by an incubation for at least 2 h at RT, 1100 rpm. Thereafter, 200 μL quenching buffer (DPBS + 50 mM TRIS + 0.05% Tween-20, pH 7.2) was added and incubated for additional 15 min. Afterwards, beads were washed twice with wash buffer (DPBS + 0.05% Tween-20) and left in storage buffer (DPBS + 0.5% BSA + 0.05% Tween-20 + 0.05% NaN<sub>3</sub>) at 1x10<sup>4</sup> beads/μL and 4°C until usage in subsequent experiments.

### 2.9.1.4 Peptide pulse of T2 and T2.DR3.DM cells to generate cellular aAPCs

List of used peptides for cell-based aAPC generation and T cell stimulation:

Name	Sequence	Protein	Position	Preferred binding to:	Ref.
HCMV pp65 <sub>495-503</sub>	NLVPMVATV	HCMV pp65	495-503	HLA-A*02:01	(273)
Flu A MP <sub>58-66</sub>	GILGFVFTL	Flu A MP-1	58-66	HLA-A*02:01	(274)
EBV BMLF-1 <sub>259-267</sub>	GLCTLVAML	EBV BMLF-1	259-267	HLA-A*02:01	(275)
Survivin <sub>96-104</sub>	LMLGEFLKL	Survivin	96-104	HLA-A*02:01	(276)
NY-ESO-1 <sub>157-165</sub>	SLLMWITQV*	NY-ESO-1	157-165	HLA-A*02:01	(277)
MTB Hsp65 <sub>1-13</sub>	MAKTIAYDEEARR	MTB Hsp65	1-13	HLA-DRB1*03:01 / DRA*01:01	(254, 255)
HCMV pp65 <sub>510-522</sub>	YQEFFWDANDIYR	HCMV pp65	510-522	HLA-DRB1*03:01 / DRA*01:01	(278)

All peptides were synthesized at the DKFZ peptide-synthesis unit. | Ref.: Reference of peptide discovery / HLA binding properties

#### Peptide pulse of T2 and T2.DR3.DM cells:

Per peptide to be loaded onto T2 or T2.DR3.DM cells (peptide pulse), typically  $1 \times 10^6$  cells were harvested depending on the experimental needs and washed once with complete RPMI + 10% FBS. Next, cells were resuspended in 1 mL complete medium supplemented with a peptide of choice in the range of 100 nM – 10  $\mu$ M depending on the experimental needs (usually 10  $\mu$ M). Cells were transferred to a 24-well culture plate and cultured overnight (at least 12 h) at 37°C, 5% CO<sub>2</sub>. Finally, cells were washed three times with 1 mL DPBS and resuspended in the assay medium used for subsequent T cell stimulations (usually RPMI + 10% FCS).

### 2.9.2 Stimulation for 4 h or 18 h of T cell lines and PBMC using aAPCs or direct peptide pulse

Depending on the specific experimental and technical needs as also indicated in the figure legends,  $5 \times 10^4$  cells/test of an antigen-specific T cell line or  $2 \times 10^6$  PBMC/test derived from a healthy donor were seeded into a well of 96-well U-bottom plate in a total volume of 200  $\mu$ L complete RPMI + 10% FBS. In case cells were stimulated for 4–5 h followed by an intracellular staining for cytokines (ICS) and/or CD107a degranulation assay, the culture medium was additionally supplemented with monensin, brefeldin A and anti-CD107a mAb as previously described in **Section 2.7.2**. If cells were left for 18 h with stimulating agents, the corresponding T cell activation was analyzed by the expression of T cell activation markers as described in **Section 2.7.1** (Lineage marker mAb panel 1 [LM-1] + activator marker panel [C]). For antigen-specific T cell stimulation, bead- as well as cell-based artificial antigen-presenting cells (aAPCs / targets) were added usually in a 1:1 or 1:2 effector-to-target (E/T) ratio to the respective T cell line (effectors) or PBMC cultures containing a defined antigen-specific T cell population. In indicated cases (**Results Section 3.2.1 / Fig 3.4a** and **Section 4.2.5 / Fig. 4.13b**), the minimal T cell epitope bearing peptide was directly added at to the PBMC culture at a final concentration of 10  $\mu$ M (peptide pulse). For antigen-independent T cell stimulation either PMA (10 ng/mL) combined with ionomycin (1  $\mu$ g/mL) were used or anti-human CD3 mAb (clone OKT3) coated beads.

### 2.9.3 Assessment of T cell-mediated antigen-specific killing by chromium-51 release assay

Chromium-51 (<sup>51</sup>Cr) release assays were performed as described previously by (190). In a first step T2 cells serving as target cells were pulsed with 100 nM cognate or control peptide as described in **Section 2.9.1.4**. As a second step, peptide pulsed T2 cells were labeled with 100  $\mu$ Ci Cr<sup>51</sup> for 1 h at 37°C and subsequently were washed using DPBS. Next, T2 cells were incubated together with defined T cell lines (effectors) at different effector-to-target ratios in 96-well U-bottom culture plates and a total volume of 200  $\mu$ L complete RPMI. Controls were included to determine spontaneous (no effector cells) and total release of <sup>51</sup>Cr (supernatant plus labeled T2 cells). After 4 h of co-incubation at 37°C, 100  $\mu$ L supernatants were carefully harvested and transferred to a 96-well LumaPlate™ (PerkinElma / 6006633). The plate was left to dry for 24 h at RT until measurement in a Topcount NXT microplate scintillation and luminescence counter (Packard Instrument). Raw data was generated using the TopCount NXT v2.13 software and was further processed using Microsoft Excel 2016. Specific target cell lysis in % was calculated using the formula: (Sample release counts - spontaneous release counts)/(total release counts - spontaneous release counts) x 100.

### 2.9.4 Measurement of antigen-specific T cell proliferation upon pMHC-based stimulation

Reagents and medium used for T cell line proliferations assays:

Name / Ingredients	Supplier	Cat. No.
<b>Nunc-Immuno™ 96-well MaxiSorp™ plate</b>	Sigma-Aldrich	M9410-1CS
<b>96-well U-bottom cell culture plate</b>	TPP	92097
<b>Human T Cell Activation/Expansion Kit</b> <ul style="list-style-type: none"> <li>▪ Anti-Biotin MACSiBead™ particles, cell culture grade</li> <li>▪ Biotinylated anti-CD2 mAb</li> <li>▪ Biotinylated anti-CD3 mAb</li> <li>▪ Biotinylated anti-CD28 mAb</li> </ul>	Miltenyi Biotec	130-091-441
<b>Proliferation Assay Medium</b> AIM V™ medium, with L-glutamine, gentamicin, streptomycin [+] 1 mM sodium pyruvat [+] 10% (v/v) human serum type AB [+] 20 units/mL human interleukin-2 (IL-2) [+] 5 ng/mL human interleukin-15 (IL-15) [+] 5 ng/mL human interleukin-7 (IL-7)	Thermo Scientific Thermo Scientific PAN Biotech Miltenyi Biotec Miltenyi Biotec Miltenyi Biotec	12055091 11360-070 P30-2501 130-097-748 130-095-765 130-095-363
<b>Precision Count Beads™</b> (Counting beads)	BioLegend	424902
<b>CellTrace™ Violet (CTV)</b>	Thermo Scientific	C34557

- Suppliers' specifications | [+] Medium supplements additionally added | Cat. No.: Suppliers' catalogue numbers

CHO-produced soluble pHLA-A2-Fc-STag and biotinylated pHLA-A2-pCC-Fc constructs:

Structure	Allele	Antigen	Peptide Seq.	Construct:
dt-pMHC-I (SCT)-mIgG2a-Fc-STag	HLA-A*02:01	HCMV pp65 495–503	NLVPMVATV	8558.1
	HLA-A*02:01	Survivin 96–104	LMLGEFLKL	8556.1
dt-pMHC-I (SCT) pCC-mIgG2a-Fc-biotin	HLA-A*02:01	HCMV pp65 495–503	NLVPMVATV	10347.7
	HLA-A*02:01	Survivin 96–104	LMLGEFLKL	9237.1

pCC-mIgG2a-Fc-biotin: parallel coiled-coil (pCC) heterodimerization domain followed by the hinge-CH2-CH3 domains of mIgG2a (Fc) and a C-terminal Strep-Tag II/His<sub>6</sub>Tag and AviTag for site-specific biotinylation (biotin).

293-F-produced soluble biotinylated pHLA-A2-\*Fc constructs:

Structure	Allele	Antigen	Peptide Seq.	Construct:
dt-pMHC-I (SCT)-biotin-*mIgG2a-Fc	HLA-A*02:01	HCMV pp65 495–503	NLVPMVATV	11097.1
	HLA-A*02:01	Survivin 96–104	LMLGEFLKL	11290.1

Disulfide-trapped (dt) pMHC-I (single-chain trimer) fused to the hinge-CH2-CH3 domains of mIgG2a (Fc) via a linker bearing in N- to C-terminal order a His<sub>6</sub>-tag, AviTag (biotin) and tandem-thrombin recognition site allowing for enzymatic cleavage of the Fc portion (\*).

Commercial cell culture-grade antibodies used for T cell line proliferations assays:

Specificity [Clone]:	Conjugation	Isotype	Supplier	Cat. No.
Anti-human CD3 [OKT3]	-	Mouse IgG2a	BioLegend	317326
Anti-human CD2 [RPA-2.10]	-	Mouse IgG1	BioLegend	300212
Anti-human CD28 [15E8]	-	Mouse IgG1	Miltenyi Biotec	130-093-375
Mouse IgG2a isotype ctrl. [MOPC-173]	-	Mouse IgG2a	BioLegend	400224
Mouse IgG2a isotype ctrl. [MOPC-173]	Biotin	Mouse IgG2a	BioLegend	400204

**2.9.4.1 Plate immobilized pMHC-I-Fc-based induction of T cell proliferation**

In a first step, 96-well MaxiSorp™ plates were placed under a cell culture hood and were sterilized by UV-light exposure for 30 min. The sterile plate was then coated at 0.5 µg/mL (total for all proteins) with pMHC-I-Fc (cognate or control) or alternatively αCD3 mAb (clone OKT3 or mouse IgG2a Isotype control) together with αCD28 mAb (clone 15E8) and αCD2 mAb (clone RPA-2.10) at an equimolar ratio for 1 h at 37°C. All proteins were diluted in DPBS, pH 7.2. After the incubation, the supernatant was removed by pipetting and the plate was knocked on a pile of paper towels. Afterwards, the plate was washed twice with 200 µL DPBS. The washed and coated plate was filled with 100 µL/well proliferation assay medium and incubated at 37°C for 15 min prior to the addition of T cells. Finally, 5x10<sup>4</sup> cells/well in triplicates in 100 µL assay medium of a CellTrace™ violet (CTV)-labeled antigen-specific T cell line were transferred to the plate and incubated at 37°C, 5% CO<sub>2</sub> for 6 days prior the assay read-out was carried out (**Section 2.9.4.3**).

**2.9.4.2 MACSiBead immobilized biotinylated pMHC-I-based induction of T cell proliferation**

1x10<sup>6</sup> anti-biotin MACSiBeads™ were transferred to a 1.5 mL protein LoBind tube and combined with 200 µL bead buffer (DPBS + 0.5% BSA + 0.1% NaN<sub>3</sub>) as well as a total concentration of 15 – 20 µg/mL biotinylated proteins. Beads were loaded with a mix of biotinylated **(1.)** 2 µg pMHC-I-Fc (cognate or control), **(2.)** 1 µg αCD2 mAb (Miltenyi) and **(3.)** 1 µg αCD28 mAb (Miltenyi) mAb derived from Miltenyi's human T cell expansion kit. Alternatively for **(1.)**, 1 µg of biotinylated αCD3 mAb (Miltenyi) or 1 µg of mIgG2a isotype control mAb (Biolegend) were used instead. Biotinylated pMHC-I-pCC-Fc as well as Fc-cleaved (\*) monomeric pMHC-I\* was used in double amounts to slightly correct for the fact, that biotinylated pMHC-I-pCC-Fc or pMHC-I\* carries only one biotin/pMHC whereas non-site-specific biotinylated antibodies carry 4–10 biotin molecules/mAb. The bead/protein mix was then incubated at RT and 1100 rpm shaking for 1 h and washed once using 1 mL bead buffer and a DynaMag™-2 magnet. In addition, beads were washed once with proliferation assay medium. Finally, 5x10<sup>4</sup> / well CellTrace™ violet-labeled T cells (**Section 2.9.4.3**) were seeded in triplicates together 5x10<sup>4</sup> loaded beads in a total volume of 200 µL proliferation assay medium into 96-well U-bottom plates and were co-cultured for 6 days at 37°C, 5% CO<sub>2</sub> prior to analysis.

### 2.9.4.3 Read-out of antigen-specific T cell proliferation after a 6-day stimulation

Prior to the induction of proliferation of T cells based either on plate- or bead-immobilized pMHC (**Section 2.9.4.1 and 2.9.4.2**), the respective T cell line or PBMCs were labeled with 1  $\mu$ M CellTrace™ Violet (CTV) according to the manufacture's protocol. Similar to carboxyfluorescein diacetate succinimidyl ester (CFSE), also CTV stably labels molecules within cells, resulting in a sequential halving of fluorescence upon cell division (191). Upon 6 days of culture, all cells were collected and stained for lineage and activation marker expression as described in **Section 2.7.1** using staining panel LM1 + C. After the final FACS-staining wash step, cells were resuspended in 90  $\mu$ L FACS-buffer (DPBS + 2% FBS) and supplemented with 10  $\mu$ L counting beads prior to FACS analysis.

## 2.10 Exogenous peptide-exchange of biosynthetic peptide-loaded px-MHC-II-pCC-Fc

Reagents and consumables used for peptide-exchange of bead-immobilized px-MHC-II-pCC-Fc:

Name / Ingredients	Supplier	Cat. No.
Dynabeads™ Goat anti-Mouse IgG (G $\alpha$ M-IgG-DynaBeads)	Thermo Scientific	11033
96-well non-binding, black, F-bottom, chimney well	Greiner bio-one	655900
Magnetic 96-well Separator (Magnet for 96-well F-bottom plates)	Thermo Scientific	A14179
Thrombin, Restriction Grade (Factor IIa / FIIa) <ul style="list-style-type: none"> <li>▪ Cleavage control protein included</li> <li>▪ 10x Thrombin cleavage buffer included : 200 mM TRIS-HCl, pH 8.4, 1.5 M NaCl and 25 mM CaCl<sub>2</sub></li> </ul>	Merck	69671-3

Used CHO-produced soluble px-MHC-II-pCC-mIgG2a-Fc and HLA-DM-pCC-hIgG1-Fc constructs:

Structure	Allele	Antigen	Peptide Seq.	Construct:
px-FIIa-HLA-DR3 -pCC-mIgG2a-Fc	HLA-DRB1*03:01 / DRA*01:01	CLIP 103–117	PVSKMRMATPLLMQA	9221.1 [+] 8746.1
HLA-DM -pCC-hIgG1-Fc	HLA-DMB*01:01 / DMA*01:01	-	-	8635.1 [+] 8743.1

**px-FII:** Place-holder peptide-ligand (CLIP) followed by C-terminal linker bearing a thrombin cleavage site.

Peptides used for peptide-exchange of px-FIIa-HLA-DR3-pCC-mIgG2a-Fc:

Name	Sequence	Protein	Position	Preferred binding to:	Ref.
MTB Hsp65 <sub>1–13</sub>	MAKTIAYDEEARR	MTB Hsp65	1–13	HLA-DRB1*03:01 / DRA*01:01	(254, 255)
DM function mimicking peptide	LRLKLPK	Modified sequence derived from the N- terminus of CLIP		-	(279)

All peptides were synthesized at the DKFZ peptide synthesis unit | Ref.: Reference of peptide sequence and its properties

## 2 | Material and methods

### Buffers used for peptide-exchange of bead-immobilized px-FIIa-HLA-DR3-pCC-mIgG2a-Fc (1):

Name / Ingredients	Recipe	Supplier	Cat. No.
<b>Citrate buffer, pH 5.5</b>  25 mM Citrate 25 mM NaCl	(Solution A) 100 ml ddH <sub>2</sub> O [+] 0.53 g Citric acid monohydrate (MW 210.14 g/mol)	Sigma-Aldrich	C1909-1KG
	(Solution B) 100 ml ddH <sub>2</sub> O [+] 0.74 g Sodium citrate tribasic dihydrate (MW 294.10 g/mol)	Sigma-Aldrich	C8532-500G
	Combine ~ 23 mL of A with ~77 mL of B to obtain a 25 mM citrate solution of pH 5.5  Add 0.146 g NaCl (MW 58.44 g/mol) <i>0.22 µm sterile filtration</i>	Carl Roth	9265.1
<b>DPBS (1x)</b> , pH 7.2, without MgCl <sub>2</sub> and CaCl <sub>2</sub>		Sigma-Aldrich	D8537-500ML

### Buffers used for peptide-exchanged of bead-immobilized px-FIIa-HLA-DR3-pCC-mIgG2a-Fc (2):

Name / Ingredients	Supplier	Cat. No.
<b>Peptide-exchange (PX1) buffer 1:</b> 25 mM Citrate, 25 mM NaCl <sub>2</sub> , pH 5.5 [+] 3% (w/v) BSA [6x] [+] 0.1% (v/v) Tween-20 [6x] [+] 0.3% (w/v) NaN <sub>3</sub> [6x] <i>pH adjustment with citric acid (solution A)</i> <i>0.22 µm sterile filtration</i>	PAA Sigma-Aldrich Sigma-Aldrich	K45-001 P9416-100ML 71289-50G
<b>Peptide-exchange (PX) buffer 2:</b> 1x DPBS, pH 7.2 [+] 3% (w/v) BSA [6x] [+] 0.1% (v/v) Tween-20 [6x] [+] 0.3% (w/v) NaN <sub>3</sub> [6x] <i>0.22 µm sterile filtration</i>	Sigma-Aldrich PAA Sigma-Aldrich Sigma-Aldrich	D8537-500ML K45-001 P9416-100ML 71289-50G
<b>Mouse-Ig blocking buffer:</b> 1x DPBS, pH 7.2 [+] 2% mouse serum	Sigma-Aldrich Sigma-Aldrich	D8537-500ML M5905
<b>Peptide-exchange beads wash buffer (PXW):</b> 1x DPBS, pH 7.2 [+] 0.5% (w/v) BSA [+] 2 mM EDTA [+] 0.05% (v/v) Tween-20 [+] 0.05% (w/v) NaN <sub>3</sub> <i>0.22 µm sterile filtration</i>	Sigma-Aldrich PAA Sigma-Aldrich Sigma-Aldrich Sigma-Aldrich	D8537-500ML K45-001 03690-100ML P9416-100ML 71289-50G

#### Peptide-exchange of bead-immobilized px-FIIa-HLA-DR3-pCC-mIgG2a-Fc and read-out:

Peptide-exchange of bead-immobilized peptide-exchangeable (px) px-FIIa-HLA-DR3-pCC-mIgG2a-Fc construct was performed at pH 5.5 (citrate buffer) or at pH 7.2 (DPBS) in the presence as well as absence of HLA-DM-Fc and thrombin as described in the **Results Section 3.6.3 / Fig. 3.16**. Per condition  $2.5 \times 10^5$  G $\alpha$ M-IgG-Dynabeads in 25  $\mu$ L PX-buffer 1 (pH 5.5) or PX-buffer 2 (pH 7.2) were transferred to a 96-well non-binding F-bottom plate. Reagents were either diluted in citrate buffer (pH 5.5) or DPBS (pH 7.2). Next, 25  $\mu$ L was sequentially added of **(1.)** 24  $\mu$ M MTB Hsp65<sub>1-13</sub> peptide (becomes finally 4  $\mu$ M), **(2.)** 0.05 units (final) thrombin, **(3.)** 600 nM HLA-DM-hIgG1-Fc (final 100 nM) or 6  $\mu$ M HLA-DM-mimicking peptide (final 1  $\mu$ M) and last but not least **(4.)** 300 nM px-FIIa-HLA-DR3-pCC-mIgG2a-Fc (final 50 nM, corresponding to 1  $\mu$ g protein and a coating concentration of  $\sim 7$   $\mu$ g/mL). The final reaction volume of 150  $\mu$ L was always substituted using the respective buffer in case reagents 1–4 were omitted. As a next step, the plate was incubated at RT, 1100 rpm shaking for 18 h. After the initial incubation, 150  $\mu$ L mouse-Ig blocking buffer (DPBS, pH 7.2 + 2% mouse serum) was added to the peptide-exchange/aAPC reaction mix independent of the previously used buffer followed by an incubation for 30 min at RT, 900 rpm. Next, peptide-exchanged and bead-immobilized pMHC-II-pCC-Fc were washed once with 200  $\mu$ L PXW washing buffer using a 96-well magnet. Beads were additionally washed twice with complete RPMI + 10% FBS prior to co-culture with MTB Hsp65<sub>1-13</sub>/HLA-DR3-specific CD4<sup>+</sup> T cells (clone RP15.1.1) for 5 h followed by an intracellular cytokine staining as described in **Section 2.7.2** (staining panel LM2 + C).

#### Digestion of thrombin cleavage control protein and analysis for off-target activity:

0.001 ( $1 \times 10^{-3}$ ) units of thrombin (Merck / 69671-3) is sufficient to digest 1  $\mu$ g (20 pmol) of cleavage control protein (48 kDa) at RT within 16 h in a buffer comprising 20 mM TRIS-HCl, pH 8.4, 150 mM NaCl and 2.5 mM CaCl<sub>2</sub> as defined by Merck / Novagen. To analyze the performance of thrombin at pH 5.5, 1  $\mu$ g of the 48 kDa cleavage control protein (provided as kit together with thrombin) was combined with a range of  $1$ – $50 \times 10^{-3}$  units of thrombin in a total volume of 20  $\mu$ L citrate buffer. In addition, 1  $\mu$ g control protein was digested using the recommended amount of  $1 \times 10^{-3}$  unit of thrombin and provided 1x cleavage buffer (TRIS-HCl, pH 8.4). Successful digestion was monitored by the presence of 35 and 13 kDa fragment from the 48 kDa cleavage control protein on a 10% SDS-PAGE followed by Coomassie staining as described in **Section 2.5.4**. As shown in **Results Section 3.6.3 / Fig. 3.16**, at pH 5.5 and the absence of CaCl<sub>2</sub> rather 50 times more thrombin ( $2.5 \times 10^{-3}$  units/pmol substrate) is needed compared to a digestion performed in the recommended buffer ( $0.05 \times 10^{-3}$  units/pmol substrate). To analyze a possible off-target cleavage of the px-FIIa-HLA-DR3-pCC-mIgG2a-Fc ( $\sim 120$  kDa) or HLA-DM-pCC-hIgG1-Fc ( $\sim 120$  kDa) constructs by thrombin, 2  $\mu$ g (i.e. 15 pmol) of the aforementioned proteins were combined with the required amounts of  $37.5 \times 10^{-3}$  units thrombin (2.5 units/pmol substrate) in 20  $\mu$ L citrate-buffer pH 5.5. After an incubation at RT for 18 h, product formation was monitored by SDS-PAGE analysis as mentioned above.

## 2.11 T-Plex Assay related workflows and protocols

**Initial remarks** | Within this study, we developed a novel multiplex platform called T-Plex Assay for the functional detection of antigen-specific T cells. The underlying core-concept as also described in **Results Section 4.1 / Fig. 4.1** are so-called T-Plex beads, which are essentially bead-based color-coded artificial antigen-presenting cells (aAPC) with T cell effector cytokine capture capacity, in particular interferon- $\gamma$  (IFN- $\gamma$ ). More generalized protocols and workflows related to the T-Plex Assay development and execution will be described in the following. Specific experimental details are additionally mentioned in the respective figures and their legends.

### 2.11.1 Generation of T-Plex beads – Color-coded aAPCs with cytokine capture capacity

Reagents, buffers and equipment generally used to handle magnetic beads as well as to covalently conjugate Luminex beads via carbodiimide crosslinker chemistry with proteins of interest have been described in **Sections 2.9.1 and 2.9.1.3**. In the following specific reagents and in particular antibody panels used for T-Plex bead generation are listed.

Beads used for T-Plex bead generation:

Name / Ingredients	Supplier	Cat. No.
<b>xMAP® MagPlex® Microspheres (Luminex beads)</b> <ul style="list-style-type: none"> <li>▪ 6.5 <math>\mu\text{m}</math> in size</li> <li>▪ Carboxylated</li> </ul>	Luminex Corp.	MC10012 <i>till</i> MC100100 for bead region 12 till 100 (bead color code)

Antibodies and reagents used for T-Plex bead generation and cytokine binding read-out (1):

Specificity [Clone]:	Dye / Conj.	Isotype	Supplier	Cat. No.	$\mu\text{L}$ /test
<b>Used for pMHC-Fc immobilization:</b>					
Goat anti-mouse IgG (Poly4053)	-	Goat polyclonal IgG	BioLegend	405301	-
Rat anti-mouse IgG2a [RMG2a-62]	-	Rat monoclonal IgG	BioLegend	407102	-
<b>Used for biotinylated pMHC:</b>					
Streptavidin	-	-	BioLegend	280302	-
<b>Used for IFN-<math>\gamma</math> capture:</b>					
Anti-human IFN- $\gamma$ [NIB42]	-	Mouse IgG1	BioLegend	502404	-
Anti-human IFN- $\gamma$ [MD-1]	-	Mouse IgG1	BioLegend	507513	-
<b>Used for IFN-<math>\gamma</math> detection:</b>					
Anti-human IFN- $\gamma$ [4S.B3]	PE	Mouse IgG1	BioLegend	502509	2.5
Anti-human IFN- $\gamma$ [4S.B3]	Biotin	Mouse IgG1	BioLegend	502504	1
[+] Streptavidin	PE	-	BioLegend	405204	0.25
<b>Used for cytokine capture (Multiple)</b>					
Anti-human IFN- $\gamma$ [MD-1]	-	Mouse IgG1	BioLegend	507513	-
Anti-human TNF- $\alpha$ [MAb1]	-	Mouse IgG1	BioLegend	502802	-
Anti-human IL-2 [MQ1-17H12]	-	Rat IgG2a	BioLegend	500302	-
Anti-human IL-4 [8D4-8]	-	Mouse IgG1	BioLegend	500702	-
<b>Used for cytokine detection (Multiple)</b>					
Anti-human IFN- $\gamma$ [4S.B3]	BV421	Mouse IgG1	BioLegend	502531	0.5
Anti-human TNF- $\alpha$ [MAb11]	PE/Cy7	Mouse IgG1	BioLegend	502930	0.5
Anti-human IL-4 [MP4-25D2]	PE	Rat IgG1	BioLegend	500810	0.5
Anti-human IL-2 [Poly5176]	Biotin	Goat polyclonal IgG	BioLegend	517605	0.25
[+] Streptavidin	A488	-	BioLegend	405235	0.25

A488: Alexa Fluor A488 | BV: Brilliant Violet | PE: Phycoerythrin | Final staining concentrations of detection mAbs were 0.25–2  $\mu\text{g}/\text{mL}$

### Antibodies and reagents used for T-Plex bead generation and cytokine binding read-out (2):

Specificity [Clone]:	Dye / Conj.	Isotype	Supplier	Cat. No.	µL /test
<b>Used for cytokine detection (All biotin)</b>					
Anti-human IFN $\gamma$ [4S.B3]	Biotin	Mouse IgG1	BioLegend	502504	0.25
Anti-human TNF $\alpha$ [MAB11]	Biotin	Mouse IgG1	BioLegend	502904	0.25
Anti-human IL4 [MP4-25D2]	Biotin	Rat IgG1	BioLegend	500804	0.25
Anti-human IL2 [Poly5176]	Biotin	Goat polyclonal IgG	BioLegend	517605	0.25
[+] Streptavidin	PE	-	BioLegend	405204	0.25
<b>Used for co-stimulation on T-Plex bead:</b>					
Anti-human CD2 [RPA-2.10]	-	Mouse IgG1	BioLegend	300212	
Anti-human CD28 [15E8]	-	Mouse IgG1	Miltenyi Biotec	130-093-375	

PE: Phycoerythrin

#### 2.11.1.1 Assembly of 1<sup>st</sup> generation T-Plex beads

In the pilot and early T-Plex Assay development phase (**Results Section 4.1**), 1<sup>st</sup> generation T-Plex beads (**Results Section 4.1 / Fig. 4.1d**) were generated on the basis of purchased goat-anti-mouse IgG serum-conjugated magnetic Dynabeads ( $\alpha$ M-IgG-Dynabeads, Thermo Scientific / Cat. No. 11033) or color-coded magnetic Luminex beads, previously conjugated with goat-anti-mouse IgG serum ( $\alpha$ M-IgG-Luminex beads) as described in **Section 2.9.1.3**. Depending on the experimental needs, usually  $1 \times 10^5$   $\alpha$ M-IgG-Dynabeads or  $\alpha$ M-IgG-Luminex beads and 200  $\mu$ L bead buffer (DPBS + 0.5% BSA + 0.1% NaN<sub>3</sub>) were transferred to 1.5 mL Eppendorf LoBind tubes. Next, 2  $\mu$ g purified anti-IFN- $\gamma$  capture mAb (clone NIB42) and 3  $\mu$ g purified dt-pMHC-I-Fc dimer were added followed by an incubation at 1100 rpm shaking at RT for 1 h or overnight at 4°C. After the incubation, dt-pMHC-I-Fc and anti-IFN- $\gamma$  capture mAb loaded  $\alpha$ M-IgG-beads (now called 1<sup>st</sup> generation T-Plex beads) were washed once with 1 mL bead buffer (DPBS + 0.5% BSA + 0.1% NaN<sub>3</sub>) and once with 1 mL assay medium (complete RPMI + 10% FCS) using a DynaMag<sup>TM</sup>-2 magnet. Depending on the experimental layout, washed color-coded Luminex beads-based T-Plex beads were subsequently pooled in assay medium (complete RPMI + 10% FCS) and used directly for the T-Plex assay.

#### 2.11.1.2 Assembly of 2<sup>nd</sup> generation T-Plex beads and their optimization

In a later project phase starting from **Results Section 4.2** the architecture of the T-Plex beads was improved by covalently conjugating Luminex beads with monoclonal rat anti-mouse IgG2a [clone RMG2a-62] mAb and anti-IFN- $\gamma$  capture mAb (initially clone NIB42, later clone MD-1) initially in a 3 to 2 ratio and later in a 1:1 ratio according to **Section 2.9.1.3**. In a second step, these so called 2<sup>nd</sup> generation T-Plex beads of a defined region/color were loaded with saturating amounts of defined pMHC-mIgG2a-Fc by directly using crude supernatants from CHO-S transient transfections or alternatively but not necessarily purified pMHC-mIgG2a-Fc constructs. Depending on the experimental needs, usually  $1 \times 10^5$  2<sup>nd</sup> generation T-Plex beads of a defined color were combined with 100  $\mu$ L bead buffer and 200  $\mu$ L crude supernatant from CHO-S-based transient gene expressions containing 10 – 30  $\mu$ g/mL pMHC-mIgG2a-Fc (according to mIgG titer quantification ELISA, **Section 2.4.2**), which was incubated at 1100 rpm at RT for 1h or overnight at 4°C. In the next step, pMHC-Fc loaded T-Plex beads were washed according to the procedure described in **Section 2.11.1.1**. Moreover, several modifications of pMHC-Fc-loaded 2<sup>nd</sup> generation T-Plex beads ( $\alpha$ -mIgG2a mAb /  $\alpha$ -IFN- $\gamma$  mAb) were tested to optimize the T-Plex Assay performance as indicated in the figure legends, including the ratio between anti-mIgG2a mAb and anti-IFN $\gamma$  mAb and the additional conjugation of co-stimulatory acting mAbs (**Results Section 4.3**). All these modifications follow the conjugation protocol described in

**Section 2.9.1.3**, with the exception that usually a non-binding 96-well plate and corresponding 96-well magnet was used during the protein coupling procedure.

### 2.11.1.3 Additional T-Plex beads assembly variations

To test the impact of T-Plex bead assembly on T-Plex Assay performance apart from the already mentioned 1<sup>st</sup> and 2<sup>nd</sup> generation T-Plex bead concepts, pMHC-I molecules were also immobilized on Luminex beads either via a “streptavidin/biotin bridge” or directly via carbodiimide crosslinker chemistry. As also described in **Results Section 4.3.5 / Fig. 4.19**, Luminex beads were covalently conjugated with unlabeled streptavidin and anti-IFN- $\gamma$  capture mAb (clone MD-1) in a 1:1 ratio in terms of  $\mu\text{g}$  according to **Section 2.9.1.3**. As a next step,  $1 \times 10^5$  T-Plex beads conjugated with streptavidin / anti-IFN- $\gamma$  capture mAb were combined with 200  $\mu\text{L}$  bead buffer and 5  $\mu\text{g}$  biotinylated pMHC-I-pCC-Fc (**Fig. 4.19**) or monomeric Fc-cleaved pMHC-I\* construct (**Fig. 4.24 & Supplementary Fig. S11**) followed by an incubation at 1100 rpm shaking at RT for 1 h and the wash procedure described in **Section 2.11.1.1**. Alternatively, Luminex beads were directly conjugated with pMHC-I-Fc-STag constructs and anti-IFN- $\gamma$  capture mAb at a 1:1 or 1:3 ratio. Subsequently, beads were used for T-Plex Assays. As conjugation quality control the IFN- $\gamma$  capture capacity was analyzed by incubating the respective T-Plex beads with 4 ng/mL recombinant IFN- $\gamma$  (BioLegend / Cat. No. 570209) in 200  $\mu\text{L}$  bead buffer for 2 h at 37°C followed by anti-IFN- $\gamma$  staining as described in **Section 2.11.2.3**. pMHC-Fc immobilization was analyzed by staining T-Plex beads for 15 min at RT with anti-HLA-A2-APC (clone BB7.2) mAb.

### 2.11.1.4 Assembly of T-Plex<sup>2</sup> beads for the detection of multiple cytokines (pilot experiment)

To enable the detection of multiple cytokines on a T-Plex beads, Luminex beads were conjugated with anti-IFN- $\gamma$ , anti-TNF- $\alpha$  and anti-IL-4 capture mAbs (each 1/5 [20%] of the total Luminex bead protein binding capacity) and monoclonal  $\alpha$ -mIgG2a mAb (2/5 [40%]) according to **2.9.1.3**. These so called T-Plex<sup>2</sup> beads were subsequently loaded with pMHC-Fc constructs as described in **2.11.1.2**.

## 2.11.2 T-Plex Assay – Co-culture of T-Plex beads and T cells and subsequent bead read-out

Equipment, reagents and consumables generally used for T-Plex Assays:

Name / Ingredients	Supplier	Cat. No.
DynaMag™-2 Magnet	Thermo Scientific	12321D
Protein LoBind Tube 1.5 ml (Eppendorf LoBind tubes)	Eppendorf	0030 108.116
Magnetic 96-well Separator (Magnet for 96-well F-bottom plates)	Thermo Scientific	A14179
96-well non-binding, black, F-bottom, chimney well	Greiner bio-one	655900
Phorbol-12-myristate-13-acetate (PMA)	Sigma Aldrich	P8139-1MG
Ionomycin calcium salt	Sigma Aldrich	I0634-1MG
Mouse serum	Sigma-Aldrich	M5905
<b>T-Plex Assay medium:</b> RPMI Medium 1640, <i>without L-glutamine</i> [+] 10% (v/v) Heat-inactivated fetal bovine serum (FBS) [+] 10 mM HEPES [+] 2 mM GlutaMAX™ (L-alanyl-L-glutamine dipeptide) [+] 100 Units/mL penicillin and 0.1 mg/mL streptomycin (Pen-Strep)	Thermo Scientific Biochrom Thermo Scientific Thermo Scientific Sigma-Aldrich	31870-025 S 0615 15630056 35050-038 P4333-100 ml
<b>T-Plex bead staining buffer:</b> 1x DPBS, <i>pH 7.2</i> [+] 0.5% (w/v) bovine serum albumin (BSA) [+] 2 mM EDTA [+] 0.05% (v/v) Tween-20 [+] 0.05% (w/v) NaN <sub>3</sub> [+] 0.22 $\mu\text{m}$ sterile filtration	Sigma-Aldrich PAA Sigma-Aldrich Sigma-Aldrich Sigma-Aldrich	D8537-500ML K45-001 03690-100ML P9416-100ML 71289-50G

### 2.11.2.1 T-Plex Assay based on a 96-well magnet and 3D/wave shaking system

Additional used equipment and consumables:

Name / Ingredients	Supplier	Cat. No.
<b>96 Magnet Plate (Plate with 96 individual magnets)</b>	IBA Lifesciences	7-2004-000
<b>6-well cell culture plate</b>	TPP	92006
<b>Heidolph Polymax 1040 3D Shaker</b> <ul style="list-style-type: none"> <li>▪ 5° tilt angle, wave motion (3D motion)</li> </ul>	Heidolph	543-42205-00

T-Plex Assays based on a 96-well magnet and 3D/wave shaking system (pilot experiment):

The first successful and multiplex-capable T-Plex Assay was facilitated by a 96-well magnet (IBA Lifesciences), which displayed 96 individual magnetic spots (**Results Section 4.1.2**). As first step, a 6-well cell culture plate was placed above that magnet and filled with 2 mL assay medium (complete RPMI + 10% FBS + 10 mM HEPES). Next,  $1 \times 10^4$  –  $2.5 \times 10^5$  pMHC-I-Fc-loaded 1<sup>st</sup> generation T-Plex beads as described in **Section 2.11.1.1** in 50 µL assay medium were individually spotted/immobilized on the magnetic reaction fields provided by the underlying magnet (**Fig. 4.3**). After bead spotting,  $2 \times 10^2$  –  $2.5 \times 10^5$  human Survivin<sub>96-104</sub>/HLA-A\*02:01 (Sur/A2)-specific CD8<sup>+</sup> T cells were added in 2 mL assay medium. Next, the whole plate including the magnet was placed on a 3D/wave orbital shaking platform placed in a cell culture incubator and was incubated at 37°C, 8% CO<sub>2</sub>, 25 rpm for 4 h. After the incubation, the 4 mL culture supernatant was carefully removed, while the magnet was still placed below the 6-well plate. Afterwards the 96-well magnet was removed and the 6-wells were rinsed with 1 mL T-Plex bead staining buffer (T-Plex buffer). The T-Plex beads were subsequently transferred to a 1.5 mL Eppendorf protein LoBind tube and stained according to **Section 2.11.2.3**. To demonstrate an equal IFN-γ-binding capacity of all used T-Plex beads as an assay control, selected T-Plex bead and T cell co-cultures were additionally supplemented with PMA (10 ng/mL) and ionomycin (1 µg/mL) resulting in a maximal IFN-γ release and capture.

### 2.11.2.2 T-Plex Assay based on a “one-tube-reaction” using a tube rolling system

Additional used equipment and consumables:

Name / Ingredients	Supplier	Cat. No.
<i>Tested tubes having an overall outer cylindrical-shape:</i> <b>Nunc® CryoTubes, 1.8 mL, round bottom, free standing (skirted)</b> <b>Screw cap micro tubes 0.5 mL, free standing (skirted), sterile</b> <b>Screw cap micro tubes 1.5 mL, free standing (skirted), PCR clean</b> <b>Screw cap micro tubes 2.0 mL, free standing (skirted), sterile</b>	Sigma-Aldrich Sarstedt Sarstedt Sarstedt	V7884-450EA 72.730.006 72.703.406 72.694.006
<i>Tube rolling systems:</i> <b>Rotating Mixer With Integral Rolls RM 5W-40</b> <ul style="list-style-type: none"> <li>▪ Smooth rocking and 40 rpm fixed speed, tilt angle: 3°</li> </ul> <b>IKA tube roller 6, digital</b> <ul style="list-style-type: none"> <li>▪ Smooth rocking (24.5 mm) and rolling action (5–80 rpm)</li> </ul>	Schubert Medizinprodukte  IKA	08178501  0004011000

### T-Plex Assays based on co-culture of T-Plex beads and T cells within a rotating tube:

As an initial step prior to performing the T-Plex Assay in closed screw-cap tubes without gas exchange, the used assay medium (complete RPMI + 10% FBS + 10 mM HEPES) was CO<sub>2</sub> saturated/equilibrated by transferring it to a T25 cell-culture flask (TPP / Cat. No. 90026) followed by an incubation at 37°C, 5% CO<sub>2</sub> for at least 2 h (usually overnight). Unless otherwise mentioned in the figure legend, 1x10<sup>4</sup> T-Plex beads/T cell specificity (pMHC) of assembled T-Plex beads were transferred to a screw-cap tube. Indicated amounts of a T cell containing test-sample was added including various established T cell lines as well as isolated T cells from pre-characterized healthy-donor derived PBMC. Alternatively, PBMC were depleted for CD14<sup>+</sup> cells as described in **Section 2.11.3** prior the co-culture with T-Plex beads. Within the initial T-Plex Assay development phase (**Results Section 4.1**), 1.8 mL cryotubes were used for the T-Plex Assay, which were completely filled with ~ 1.9 mL CO<sub>2</sub>-saturated assay medium. However, quite early on this was changed to 0.5 mL screw-cap tubes filled with a total amount of ~ 600 µL assay medium (**Results Section 4.2**), which became the used standard assay procedure. Filled tubes were then vortexed and placed horizontally between the gap of two rolling tubes of a rocking/rolling device placed inside a cell incubator leading to a rotation of the assay tube along the longitudinal X axis. Initially, tubes were rotated at 40 rpm for 4 h at 37°C, which was later on (**Results Section 4.3**) increased to 60 rpm and 4.5 – 5 h at 37°C. Moreover, to improve the assay sensitivity as discussed in **Results Section 4.3.1 / Fig. 4.14**, tubes filled with test sample and T-Plex beads were centrifuged prior to starting the rolling at 37°C. In case the test sample was brought back into culture after T-Plex co-culture, beads and cells were transferred to a sterile 1.5 mL Eppendorf protein LoBind tube and T-Plex beads were immobilized using DynaMag<sup>TM</sup>-2 magnet. The cell containing supernatant was carefully transferred to a new tube and beads were rinsed once with 1 mL assay medium, which was then collected in the same tube. The cell containing supernatant was subsequently centrifuged and the cells were resuspended in T cell culture medium (AIM-V + 10% human serum type AB, 5 ng/mL IL-15, 20 units/mL IL-2) and finally cultured at 37°C, 5% CO<sub>2</sub>. Remaining T-Plex beads were stained according to **Section 2.11.2.3**.

#### **2.11.2.3 T-Plex bead anti-cytokine staining**

Depending on the sample number, the T-Plex bead staining was either performed in 1.5 mL Eppendorf protein LoBind tubes together with a DynaMag<sup>TM</sup>-2 magnet or alternatively beads were transferred to 96-well non-binding F-bottom plate and beads were immobilized using a strong 96-well magnet suitable plate-based bead washing. Notably, for Luminex/T-Plex bead washing the “magnetic 96-well separator” purchased from Thermo Scientific (“designed for Luminex beads”) was used instead of the aforementioned “96 Magnet Plate” from IBA Lifesciences. The latter 96-well magnet leads to a significant bead lost after magnet/plate inversion for removal of the supernatant. After the initial co-culture of T-Plex beads and T cells, the T-Plex beads were depending on the vessel either washed once with 1 mL T-Plex buffer (1.5 mL tubes) or twice with 200 µL T-Plex buffer (96-well plate). As a next step, 1<sup>st</sup> gen. T-Plex beads were resuspended in 200 µL buffer supplemented with 2% mouse serum and incubated for 15 min at RT, 1100 rpm to block remaining mouse IgG binding sites. This step was skipped for 2<sup>nd</sup> gen. T-Plex beads since no detection mAbs of mouse IgG2a isotype were used. Next, T-Plex beads were stained with anti-IFN-γ-biotin mAb (clone 4S.B3) diluted 1:200 (1 µg/mL) in buffer for 45 min at RT and 1100 rpm (200 µL staining volume). Afterwards, T-Plex beads were washed as described above and subsequently stained with streptavidin-PE diluted 1:800 in 200 µL buffer for 15 min, RT, 1100 rpm. Beads were washed again and finally resuspended in 50 µL buffer prior to flow cytometric measurement. Notably, streptavidin-PE was always centrifuged for 10 min at 13,000 rpm, 4°C and 0.22 µm filtrated prior usage to avoid staining artifacts due to protein aggregates.

### 2.11.3 T cell isolation or CD14<sup>+</sup> cells depletion from PBMC by MACS

Equipment, reagents and consumables used for sample preparations for T-Plex Assays:

Name / Ingredients	Supplier	Cat. No.
<b>Pan T Cell Isolation Kit, human</b> ▪ Isolation of untouched T cells	Miltenyi Biotec	130-096-535
<b>CD8<sup>+</sup> T Cell Isolation Kit, human</b> ▪ Isolation of untouched CD8 <sup>+</sup> T cells	Miltenyi Biotec	130-096-495
<b>Anti-human CD14 antibody - biotinylated (clone HCD14)</b> [+] Anti-Biotin Microbeads	BioLegend Miltenyi Biotec	355624 130-090-485
<b>Anti-human CD19 antibody - biotinylated (Clone HIB19)</b> [+] Anti-biotin Microbeads	BioLegend Miltenyi Biotec	302204 130-090-485
<b>Human TruStain FcX™ (Fc receptor blocking solution)</b>	BioLegend	422302
<b>MACS buffer:</b> 1x DPBS, pH 7.2 [+] 5% (w/v) BSA [+] 2 mM EDTA [+] 0.22 µm sterile filtration	Sigma-Aldrich PAA Sigma-Aldrich	D8537-500ML K45-001 03690-100ML
<b>MACS columns and magnets</b> QuadroMACS™ Separator LS columns	Miltenyi Biotec Miltenyi Biotec	130-090-976 130-042-401
<b>Falcon® 40 µm cell strainer, sterile</b>	NeoLab	352340

Antibody panel used for sample preparation validation:

Specificity [Clone]:	Conjugated dye	Isotype	Supplier	Cat. No.	µL /test
<b>Lineage Marker Panel (LM-4)</b>					
Anti-human CD3 [UCHT1]	FITC	Mouse IgG1	BioLegend	300440	2.0
Anti-human CD4 [RPA-T4]	PE	Mouse IgG1	BioLegend	300508	1.0
Anti-human CD8a [SK1]	Pacific blue	Mouse IgG1	BioLegend	344718	1.0
Anti-human CD14 [HCD14]	PerCP/Cy5.5	Mouse IgG2a	BioLegend	355622	1.0
Anti-human CD19 [HIB19]	APC	Mouse IgG1	BioLegend	302212	1.0
[+] <i>Zombie Aqua Viability Kit</i>	(BV 510)*	-	BioLegend	423102	0.3

Note \*: (BV 510) refers to the used detection channel of the BD FACS Canto II.

T cell isolation or CD14<sup>+</sup> cells depletion from PBMC:

Depending on the experimental layout, ~1–5x10<sup>7</sup> cells of freshly cultured and pre-characterized PBMC were once passed through a 40 µm cell strainer, centrifuged and washed once with MACS buffer prior to MACS-based cell isolation or depletion. Next, pan T cells or CD8<sup>+</sup> T cells were isolated using respective MACS isolation kits according to the manufacture's protocol. For CD14<sup>+</sup> or CD19<sup>+</sup> cell depletion instead (**Results Section 4.2.4 / Fig. 4.12**), ~1x10<sup>7</sup> PBMC were resuspended in 40 µL MACS buffer and 10 µL biotinylated anti-human CD14 and/or CD19 mAb (BioLegend). The mix was incubated for 5 min at 4°C. Next, 500 µL MACS buffer was added and the cells were centrifuged followed by removal of the supernatant. The cell pellet was resuspended in 80 µL MACS buffer and 20 µL anti-biotin MACS microbeads were added followed by an incubation for 10 min at 4°C. Next, 400 µL MACS buffer was added and the whole cell mix was subjected to an equilibrated MACS LS-column placed into a MACS magnet and the flow-through was collect. The LS-column was washed with 3 mL MACS buffer and all flow-throughs were combined. The CD14/CD19 depleted cell flow-through was used subsequently used for the T-Plex Assay. After MACS-based cell isolation or depletion, the cells were washed twice with T-Plex Assay medium to remove any EDTA contamination, which might interfere

## 2 | Material and methods

with subsequent T cell stimulations. Cells were finally resuspended in assay medium, which was optionally supplemented with TruStain FcX™ solution (1:100) as indicated in the figure legends.

### Confirmation of T cell isolation or CD14<sup>+</sup> cells depletion from healthy donor PBMC:

To confirm proper T cell isolation as well as CD14<sup>+</sup> cell depletion, a small aliquot from the intended T-Plex Assay test sample corresponding to  $\sim 5 \times 10^4$  –  $1 \times 10^5$  cells were analyzed by lineage marker surface staining (i.e. mAb panel described in above [LM-4]) using the procedure described in **Section 2.7.1**.

### **2.11.3.1 Analysis of phagocytosis of Luminex beads by CD14<sup>+</sup> monocytes and partial block by CD47**

#### Additional reagents used for coating Luminex beads with CD47-hlgG1-Fc:

Name / Ingredients	Supplier	Cat. No.
Human CD47-ecodomain-hlgG1-Fc fusion protein	R&D Systems	4670-CD-050
Human IgG1 isotype control	Thermo Scientific	02-7102

#### Conjugation of Luminex beads with CD47-hlgG1-Fc or human IgG1 isotype control:

Luminex beads were covalently conjugated either with CD47-hlgG1-Fc (R&D Systems) or human IgG isotype control according to **Section 2.9.1.3**. Briefly,  $2.5 \times 10^5$  Luminex beads per condition were activated by incubation with sulfo-NHS and EDC for 20 min, at RT, 1100 rpm. As a next step, activated and washed Luminex beads were incubated with 1  $\mu$ g CD47-hlgG1-Fc or human IgG isotype control mAb diluted in 100  $\mu$ L DPBS at RT, 1100 rpm for 2 h followed by quenching of the coupling reaction using TRIS-containing buffer. Alternately, Luminex beads were covalently conjugated with rat-anti-mouse IgG2a (clone RMG2a-62), anti-human IFN- $\gamma$  mAb (clone MD-1) and CD47-hlgG1-Fc at a 55:35:10 ratio. These T-Plex bead precursor were subsequently loaded with pMHC-I-Fc as described **Section 2.11.1.2** and termed T-Plex bead (+10% CD47-Fc) as shown in **Results Section 4.2.4.2 / Fig. 4.12c**.

#### Co-culture of PBMC with CD47-Fc coated Luminex beads and follow-up analysis:

$4 \times 10^4$  CD47-Fc or IgG1-isotype coated Luminex beads as well as standard T-Plex beads or CD47-Fc modified T-Plex beads (10% of the Luminex beads' total protein binding capacity was conjugated to CD47-Fc) were combined with  $1 \times 10^6$  whole PBMC in a 600  $\mu$ L T-Plex Assay medium filled screw-cap tube (0.5 mL). The tube was incubated for 4 h at 37°C under constant rolling at 40 rpm. Next, the whole reaction mix was transferred to a 96-V bottom plate. Cells were washed once with DPBS, followed by a staining for 10 min at RT with Zombie Aqua™ (1:300) in 100  $\mu$ L DPBS. Afterwards, 100  $\mu$ L FACS buffer (DPBS + 10% FBS) supplemented with 1  $\mu$ L/well TruStain-FcX™ agent and 2  $\mu$ L/well mlgG2a-isotype control mAb (clone MOPC-173, BioLegend / Cat. No. 400202) was added and incubated for 5 min prior centrifugation. The sample was subsequently stained for 15 min on ice with anti-CD14 mAb conjugated to PerCP/Cy5.5 (clone HCD14, BioLegend / Cat. No. 325622), washed and analyzed by flow cytometry.

## 2.12 T-Plex Assay-based immunogenicity analysis of *in silico* predicted putative neoepitopes using cancer patient-derived peripheral blood

### 2.12.1 Patient material, mutation calling, *in silico* HLA typing and neoepitope prediction

Patient ID:	Cancer type:	Enrolled by:
Patient 1	Neuroendocrine tumor of the thymus	HIPO-DKFZ
Patient 2	Malignant solitary fibrous sarcoma	HIPO-DKFZ
Patient 3	Prostate carcinoma	NCT
Patient 4	Pancreatic adenocarcinoma	HIPO-DKFZ

HIPO-DKFZ: Heidelberg Center for Personalized Oncology (HIPO) at the German Cancer Research Center (DKFZ)

NCT: National Center for Tumor Diseases, Heidelberg

Four NCT cancer patients suffering from various tumor diseases as listed above have been selected for a T-Plex Assay-based immunogenicity validation of putative cancer neoepitopes (**Results Section 4.5**). Pseudonymized whole exome sequencing (WES), RNASeq, single nucleotide variations (SNV) as well as transcriptome data from patients 1, 2 and 4 were kindly provided by the MASTER (Molecularly Aided Stratification for Tumor Eradication) program of the Heidelberg Center for Personalized Oncology (HIPO) at the German Cancer Research Center (HIPO-DKFZ) to the Department of Medical Oncology, (NCT, Heidelberg) and the Clinical Cooperation Unit “Applied Tumor Immunity” (D120, DKFZ, Heidelberg), both headed by Prof. Dr. Dirk Jäger. For patient 3, WES data have been generated externally at GATC Biotech AG (Konstanz, Germany). *In silico* HLA-typing and HLA neoepitope binding predictions for long peptide design was coordinated by Dr. Inka Zörnig and carried out by Dr. Zeynep Koşaloğlu and Dr. Zhiqin Huang using an in-house analysis pipeline as described previously by Koşaloğlu *et al.* (280) and further unpublished developments thereof. Patients’ blood samples were obtained by the Department of Medical Oncology (NCT), Heidelberg University Hospital (MASTER program, ethic’s votes S022-2013; 205 / 2007).

### 2.12.2 Peptide vaccination and ELISpot follow-up analysis

Several patient-specific long peptides comprising selected putative neoepitopes were synthesized at the DKFZ Peptide Synthesis Core Facility headed by Prof. Dr. Stefan Eichmüller. For long peptide design, the SNV was positioned in the middle of the respective long peptide sequence, which in turn was flanked N- and C-terminally by 14 amino acid residues of the naturally occurring gene sequence (**Results Part Section 4.5 / Table 4.4**). As an individual treatment approach in addition to the standard treatments in the Department of Medical Oncology of the NCT, patients 1–4 were vaccinated with the neoepitope bearing long peptides (i.e. 60 µg per peptide and vaccination) combined with the adjuvant Montanide ISA-51 in approximately monthly intervals. At various time points (i.e. before, 1–5 months and 12 months after the vaccination) blood samples from the respective patients were taken for subsequent ELISpot analysis as described previously (280). ELISpot analysis was coordinated by Dr. Inka Zörnig and carried out by Iris Kaiser (Department of Medical Oncology, NCT, Heidelberg).

### 2.12.3 T-Plex Assay- and pMHC-I multimer-based analysis of cancer patient-derived peripheral blood

#### **2.12.3.1 Production of putative neoepitope- or corresponding wt-peptide presenting pHLA-A2-\*Fc**

Based on the long peptide sequence (**Results Section 4.5 / Table 4.4**) several putative mutation-spanning HLA-A2-restricted minimal epitopes were selected using the *in silico* HLA-binding prediction algorithms NetMHC 4.0 (281) as well as NetMHCpan 4.0 (282) interrogating 9 to 11-mer peptides

(**Table 4.5**). HLA-A2-restricted neo-epitopes with a HLA-A2 binding rank score of <2 for the mutant peptide variant obtained by at least one of the used algorithms were chosen to be cloned into the Fc-cleavable pHLA-A2-\*Fc vector backbone described in **Section 2.2.1.2** and listed in detail in **Results Section 4.5 / Table 4.5**. All constructs were produced as described in **Sections 2.3.3** and **2.5.2**.

#### **2.12.3.2 T-Plex Assay and pMHC-I multimer-based analysis of patient-derived peripheral blood**

Frozen cryostocks of PBMC preparations of patients 1–4 were kindly provided by the Department of Medical Oncology (NCT, Heidelberg). Thawed PBMC cryostocks were cultured overnight in AIM-V supplemented with 10% human AB serum and IL-2 [20 units/mL], IL-15 [5 ng/mL] and DNase [1 unit/mL] (**Section 2.1.4**). Streptavidin/anti-IFN- $\gamma$  mAb-conjugated precursor T-Plex beads (**Section 2.11.1.3**) were loaded with biotinylated Fc-cleaved pHLA-A2\* molecules. The T-Plex Assay was conducted using “untouched” isolated CD8<sup>+</sup> T cells as described in **Sections 2.11.2** and **2.11.3**. Corresponding pHLA-A2\*-based multimers were generated according to **Section 2.6** and used for staining of patient-derived CD8<sup>+</sup> T cells as described in **Section 2.7.3.1**.

## 3| Results Part 1

### Paving the way for a new multiplex assay to detect antigen-specific T cells

**Initial remarks** | Within the early conceptual phase of the present study, we defined a set of parameters for the development of a novel multiplex assay for the detection of antigen-specific T cells. First, the novel multiplex assay shall be constructed based on recombinant peptide-MHC class I and class II (pMHC-I / -II) complexes, which should be expressed robustly and efficiently in terms of production workload. Secondly, spectral color-coded Luminex' xMAP® MagPlex® microspheres (Luminex beads) or similar in combination with pMHC-I / pMHC-II shall be the core concept for the novel multiplex assay, that should feature a simple workflow, high-sensitivity and straightforward data-analysis in particular.

The establishment and subsequent validation of recombinantly produced pMHC-I as well as pMHC-II constructs will be the focus of the first results section. The second part will describe the iterative development a novel assay for the detection of antigen-specific T cells including the validation and optimization of that particular assay. Nevertheless, findings and results described in both parts have been made mostly in parallel.

#### 3.1 Establishment of pMHC-I-Fc mammalian-cell-based productions and validation

##### 3.1.1 Successful production of pMHC-I-Fc proteins and antigen-specific binding to a T cell line

To produce multiple recombinant peptide-MHC class I complexes (pMHC-I) in a time-, workload- and cost-efficient manner, we took advantage of the designated pMHC-I single-chain trimer (SCT) format (223, 245) fused to an murine IgG-Fc as similarly described by Greten *et al.* (215, 239). The core design of pMHC-I-Fc dimers used in this study is presented essentially in **Fig. 3.1a**. According to the SCT-format pMHC-I-Fc dimers are expressed as a single polypeptide chain comprising the covalently linked T cell peptide ligand, human  $\beta_2$ -microglobulin ( $\beta_2m$ ) and the HLA-class I allele A\*02:01 (HLA-A2) ectodomain fused to the constant heavy chain domains (CH) 2 and 3 of murine immunoglobulin isotype IgG2a (abbreviated with “Fc” unless otherwise noticed). Moreover, we adopted an engineered intramolecular disulfide-bridge designated as “disulfide trap” (dt) between the C-terminal peptide ligand extension (2<sup>nd</sup> residue of the linker between peptide's C-terminus and the  $\beta_2m$ 's N-terminus) and a cysteine (C) replacing a highly conserved tyrosine (Y) at position 84 within the MHC-I heavy chain. This disulfide-trap provides for further stabilization of the whole pMHC-I complex since peptide ligand dissociation and subsequent pMHC destabilization is prevented. Moreover, even the incorporation of low-affinity peptide-ligands have been tested to be completely refractory to exogenous peptide-exchange (242, 244, 245). Notably, unless otherwise mentioned all used pHLA-A2-Fc constructs within this study bear the disulfide-trap.

Our initial aim was to gain the ability to produce correctly folded “ready-to-use” soluble pMHC either in large- as well as parallelized small-scale in a flexible and feasible manner. We therefore envisioned that efficient and transient expression of pMHC-Fc constructs in mammalian cell lines like human embryonic kidney 293 (HEK 293) or Chinese hamster ovary cells (CHO) displays a fast and much more convenient alternative production route compared the recombinant expression in *E. coli* bacteria. Unlike, pMHC-I expression in *E. coli*, pMHC-I-Fc production in mammalian cells would not require laborious inclusion body preparation from bacteria and tedious protein refolding efforts (240).

Consequently, we implemented a highly efficient and inexpensive transient gene expression system (TGE) based on Chinese hamster ovary cells growing in suspension (CHO-S), serum-free ProCHO-4 medium and transfection agent polyethyleneimine (PEI) as described previously (266–269). Using this production system, we successfully expressed initially over 20 different pHLA-A2-Fc constructs harboring published and validated peptide-ligands (**Fig. 3.1, 3.2 and Table 3.1**). Moreover, we aimed for affinity-chromatography of mammalian supernatants under more physiological conditions (pH 7.4) using the Strep-Tactin® system (IBA Lifesciences) (270). Thus, we cloned the Strep-tag II (STag) sequence at the C-terminal end of the pHLA-A2-Fc construct (pHLA-A2-Fc-STag) (**Fig. 3.1a**). Subsequent Strep-Tactin-based purifications of CHO-S supernatants containing pHLA-A2-Fc-STag constructs displayed an overall very high purity with no visible by-products, aggregates or other obvious impurities as shown by SDS-PAGE analysis. The SDS-PAGE indicated a single expected band at ~150–155 kDa under non-reducing conditions, which fits well with the calculated molecular weight of a pHLA-A2-mIgG2a-STag homodimer of 154 kDa as well as an expected 75–80 kDa band under reducing conditions representing the pHLA-A2-mIgG2a-STag monomer having a calculated molecular weight of 77 kDa (**Fig. 3.1b**). In addition, pHLA-A2-Fc expression and correct protein folding was confirmed by intracellular staining of transfected CHO-S with anti-HLA-A2 monoclonal antibody ( $\alpha$ -HLA-A2 mAb, clone BB7.2) (283) as shown in **Fig. 3.1c** for the Survivin<sub>96–104</sub> [LMLGEFLKL] /HLA-A2-Fc-STag construct [8556.1]. Moreover, intracellular  $\alpha$ -HLA-A2 mAb as well as  $\alpha$ -mIgG2a mAb (clone RMG2a-62) staining suggested an overall transfection efficiency between 30–60% across different (various peptides) pHLA-A2-Fc-STag constructs (**Fig. 3.1c and data not shown**) resulting in production yields of 3–20  $\mu$ g/mL of pHLA-A2-Fc-STag / CHO-S culture volume (**Table 3.1**).

For antigen-specific binding validation of pHLA-A2-Fc-STag constructs to their cognate T cell receptors as discussed below and shown in **Fig. 3.1d**, we initially took advantage of a pre-characterized Survivin<sub>96–104</sub> / HLA-A\*02:01-restricted, allogenic (HLA-A2<sup>neg</sup>) CD8<sup>+</sup> T cell line (Sur/A2 CD8<sup>+</sup> T cells) kindly provided by the DKFZ/BHC Joint Immunotherapy Lab and previously described by Leisegang *et al.* (253). The Sur/A2 CD8<sup>+</sup> T cell line displays an exquisite purity/specificity of >99% as shown by cognate staining with a commercial pHLA-A2 pentamer (ProImmune) which in particular became apparent when the Src/Bcr-Abl kinase inhibitor dasatinib, previously described as pMHC multimer staining enhancer (206) was present during the staining process (**Supplementary Fig. S1a**). Thus, unless otherwise mentioned we also incorporated dasatinib in all pMHC-based direct binding assays. Moreover, the Sur/A2 CD8<sup>+</sup> T cell line displays a terminally differentiated effector memory phenotype (100, 103) (CD45RA<sup>neg</sup> / CCR7<sup>neg</sup>) with a complete lack of CD28 and only partial CD27 expression (**Supplementary Fig. S1b**). In addition, the Sur/A2 CD8<sup>+</sup> T cell line strongly co-expresses TIM-3 and LAG-3 but lacks expression of TIGIT and PD-1 (**Supplementary Fig. S1c**), which might be considered as an early sign of T cell dysfunction / exhaustion (106). However, this issue will be not considered in this study, since Sur/A2 T cells do express effector cytokines upon stimulation and do kill cognate target cells efficiently (**Fig. 3.3 and data not shown**). As shown in **Fig. 3.1d**, Sur/A2 CD8<sup>+</sup> T cells were specifically bound by the purified Survivin<sub>96–104</sub> /HLA-A2-Fc-STag construct [8556.1] either pre-complexed with Strep-Tactin-APC to form so called *Streptamers* (272) (*middle panel*) or sequentially detected by  $\alpha$ -mIgG2a-Fc secondary mAb staining (*right panel*), which was in accordance with the commercial pHLA-A2 pentamer staining (*left panel*). Control pentamer and corresponding HCMV pp65<sub>495–503</sub> [NLVPMVATV]/HLA-A2-Fc-STag [8558.1] displayed no binding signal as expected.

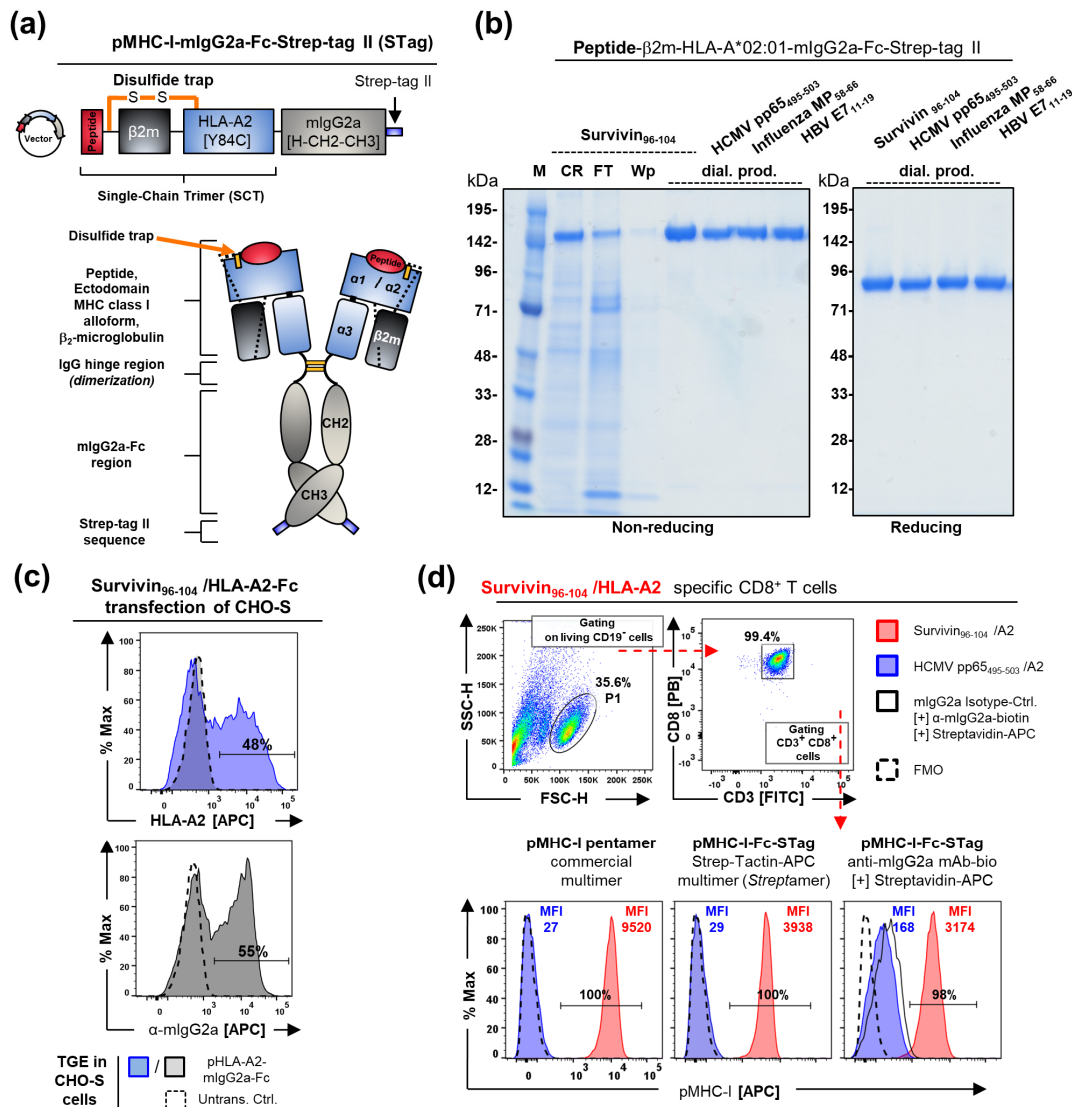


**Figure 3.1 | Successful mammalian cell-based production and antigen-specific binding of pMHC-I-Fc molecules**

**(a)** Disulfide-trapped (dt) peptide-MHC-Class I (pMHC-I) immunoglobulin Fc (Fc) dimers consist of a single polypeptide chain comprising a covalently linked T cell epitope peptide ligand (9–10 amino acids), human  $\beta_2$ -microglobulin ( $\beta_2m$ ), MHC-I ectodomain (in this case exemplary shown for the HLA-A\*02:01 allele) and constant heavy chain (CH) domains 2 and 3 of murine immunoglobulin isotype IgG2a. Dotted lines indicate flexible glycine-serine linkers. The intramolecular disulfide trap between the C-terminal peptide extension and a cysteine (C) residue replacing MHC-I tyrosine (Y) 84 residue provides further for stabilization of the pMHC complex. The C-terminal Strep-tag II (STag) sequence allows affinity-purification under neutral conditions.

**(b)** dt-pHLA-A2-Fc-STag affinity chromatography. CHO-S supernatant from a 6-day transient dt-pHLA-A2-Fc-STag expression was purified using Strep-Tactin high-capacity resin filled columns at pH 7.4. Shown is a 10% SDS-PAGE under non-reducing and reducing conditions after Coomassie staining. M: marker; CR: crude / CHO-S supernatant; FT: Flow-through; Wp: pooled buffers used for washing; dial. prod; dialysed product 2.5  $\mu$ g/lane.

**(c)** Validation of dt-pHLA-A2-Fc expression and structural conformation. Survivin<sub>96-104</sub>/HLA-A2-Fc-STag (8556.1) expressing CHO-S cells were intracellularly stained either with  $\alpha$ -HLA-A2 mAb (clone BB7.2) (blue) or with  $\alpha$ -mIgG2a mAb (clone RMG2a-62) (grey) 3 days after transfection.

**(d)** Antigen-specific binding of dt-pHLA-A2-Fc-STag proteins. Survivin<sub>96-104</sub>/A2 specific CD8<sup>+</sup> T cell line was stained in the presence of Dasatinib [50 nM] with cognate [red] and control [blue] pMHC-I multimers at 25  $\mu$ g/mL followed by lineage marker staining. (Left panel) Commercial pMHC-I pentamer (ProlImmune); (Middle panel) dt-pHLA-A2-Fc-STag in complex with Strep-Tactin-APC; (Right panel) dt-pHLA-A2-Fc-STag and sequential staining with  $\alpha$ -mIgG2a-Biotin (RMG2a-62) and Streptavidin-APC. T cells were labeled with ZombieAqua (BioLegend) prior pMHC-based staining to exclude dead cells. MFI: Median fluorescent intensity; FMO: fluorescence-minus-one background ctrl. Shown pHLA-A2-Fc-STag constructs [peptide sequence / construct ID]: Survivin<sub>96-104</sub> [LMLGEFLKL / 8556.1], HCMV pp65<sub>495-503</sub> [NLVPMVATV / 8558.1], Influenza-A MP-1<sub>58-66</sub> [GILGFVFTL / 8557.1] and HPV E7<sub>11-19</sub> [YMLDLQPEV / 8559.1].

**Table 3.1| dt-pHLA-A2-Fc-STag production efficiency across different published peptide ligands using the CHO-S/PEI/ProCHO-4 TGE system**

pHLA-A2-Fc-STag construct ID <sup>(a)</sup> :	Antigen	Peptide Sequence <sup>(a)</sup> :	TGE system <sup>(b)</sup>	Purification system	Production efficiency [µg yield/mL culture vol.]:	NetMHC 4.0 <sup>(c)</sup>			SignalP -5.0 <sup>(d)</sup>
						Affinity [nM] to HLA-A2	%Rank to bind HLA-A2	Bind level	Cleavage probability:
8556.1	Survivin 96–104 / T97M	LMLGEFLKL	CHO-S / PEI / ProCHO-4	StrepTactin-High Capacity filled column	18.0	25.41	0.40	SB	0.73
8557.1	Flu A MP 58–66	GILGFVFTL			3.3	15.71	0.20	SB	0.72
8558.1	HCMV pp65 495–503	NLVPMVATV			14.3	25.85	0.40	SB	0.85
8559.1	HPV-16 E7 11–19 / T19V	YMLDLQPEV			18.55	3.95	0.01	SB	0.87
8803.1	MART-1 26–35 / A27L	ELAGIGILTV			21.60	253.92	1.90	WB	0.69
8804.1	EBV BMLF-1 259–267	GLCTLVAML			3.0	138.63	1.30	WB	0.73
8805.7	MUC-1 927–935	STAPPVHNV			9.0	650.57	3.50	-	0.67
8806.1	TP53 264–272	LLGRNSFEV			12.0	24.20	0.40	SB	0.57
8807.1	NY-ESO-1 157–165 / C165V	SLLMWITQV			24.0	6.13	0.05	SB	0.77
8808.1	NY-BR-1 960–968	SLSKILDTV			14.70	27.70	0.40	SB	0.68
8809.1	CEA 605–613	YLSGANLNL			18.0	12.58	0.15	SB	0.75
8810.2	HIV p17 gag 77–85	SLYNTVATL			11.25	53.76	0.70	WB	0.77
8811.2	HER-2/neu 369–377	KIFGSLAFL			22.0	14.35	0.20	SB	0.86
8812.1	KRAS 5–14	KLVVVGAGGV			2.3	506.61	3.0	-	0.84
8814.3	KRAS 5–14 / G12V	KLVVVGAVGV			7.63	300.18	2.0	WB	0.82
8815.1	KRAS 5–14 / G12D	KLVVVGADGV			8.0	498.01	3.0	-	0.84
8826.3	KRAS 5–14 / G13D	KLVVVGAGDV			3.75	506.91	3.0	-	0.85
8816.2	BRAF 597–605/ S605V	LATVKSRWV			N.P.	20640.77	28.0	-	0.44
8817.2	BRAF 597–605/ V600E / S605V	LATEKSRWV			N.P.	13028.59	19.0	-	0.52
8818.1	c-Met 630–638	YVDPVITSI			18.05	25.64	0.40	SB	0.85
8819.1	hTERT 540–548	ILAKFLHWL	0.6	9.05	0.10	SB	0.47		
8820.3	HPV-16 E7 11–19	YMLDLQPET	16.80	21.23	0.30	SB	0.88		

(a) Indicated published peptides (<https://www.iedb.org>) were cloned in the disulfide-trapped (dt) single-chain trimer-based peptide-HLA-A\*02:01-mIgG2a-Fc-Strep-tag II (pHLA-Fc-STag) construct backbone as introduced in Fig. 3.1. (b) dt-pHLA-Fc-STag constructs were produced and purified using the indicated eukaryotic transient gene expression system (TGE) as described in the material and methods section. Production efficiency has been calculated based on the obtained yield of purified protein [µg] of a given construct divided by the TGE culture volume [mL] used for the corresponding purification. N.P.: pHLA-A2-Fc constructs were repeatedly not producible. (c) HLA-A\*02:01 (HLA-A2) peptide binding predictions for the shown peptide sequence were performed by the NetMHC 4.0 algorithm (281). Peptides with %rank <0.5 were classified as putative strong binders (SB), %rank <2 as weak binders (WB) and %rank >2 as potential non binders (-) according to both NetMHC 4.0 default prediction thresholds. (d) Shown is the signal peptidase I cleavage probability between the C-terminal residue (A<sub>10</sub>) of the used signal peptide sequence and the first N-terminal residue (X<sub>1</sub>) of the peptide sequences (X<sub>1</sub>-X<sub>9/10</sub>) indicated in table followed by a short C-terminal flanking sequence of linker #1 (MAKANLLVLLCALAAADA-X<sub>1</sub>-X<sub>9/10</sub>-GCGSGGGG) according to the SignalP 5.0 algorithm (284).

However, although the specificity was equal between our pHLA-A2-Fc-STag dimers and pHLA-A2 pentamers, the commercial pentamers displayed an overall superior staining performance (increased MFI) compared to a consecutive pHLA-A2-Fc-STag and anti-mIgG2a-APC mAb staining presumably due to the in general higher off-rate of dimeric pMHC-I-Fc compared to pMHC-I multimers (162, 217). Moreover, for *Streptamer* complex assembly using our pHLA-A2-Fc-STag constructs, we had to use an approximated molar ratio of 75:1 pHLA-A2-Fc-STag to Strep-Tactin-APC (IBA Lifesciences) instead of the previously published approximated molar ratios of 4:1 (272, 285), which might reduce overall signal intensities due to binding of a pHLA-A2-Fc-STag molecule to the TCR with no fluorochrome attached. At lower ratios than 75:1 (pHLA-A2-Fc-STag / StrepTactin) we observed strong aggregate formation resulting in an overall unspecific staining performance (**Supplementary Fig. 2d**). Notably, molar ratios

were calculated based on the molecular weight of a single Strep-Tactin-APC molecule and pHLA-A2-Fc-STag (both ~155 kDa). However, this indicated ratio is only a rough approximation, since Strep-Tactin-APC is provided as an undefined polymer (IBA Lifesciences).

Prior to the establishment of the Strep-Tactin-based purification, pHLA-A2-Fc constructs lacking a C-terminal Strep-tag II were alternatively purified by protein-A-based affinity-chromatography (**Supplementary Fig. S2a–c**). However, protein-A-based purified pHLA-A2-Fc constructs displayed an increased unspecific staining background to Sur/A2-specific CD8<sup>+</sup> T cells compared to the usage of corresponding crude CHO-S supernatants containing pHLA-A2-Fc at equal concentrations. This increased unspecific staining-background was not observed when pHLA-A2-Fc-STag constructs were purified via Strep-Tactin-based affinity chromatography. Although not investigated in more detail, this initial finding suggested that protein-A-based purifications of pMHC-I-Fc dimers including a glycine/HCl pH 3.0-based elution step might be partially denaturing pMHC-I-Fc proteins leading to aggregation (**Supplementary Fig. S2a–c**).

### 3.1.2 Validation of optimal CHO-S/ProCHO-4/PEI TGE parameters for small-scale productions

An exquisite benefit of the pHLA-A2-Fc-STag construct design combined with mammalian cell-based production is a long lasting shelf-life at 4°C. Sterile filtered pHLA-A2-Fc containing CHO-S cell supernatants stored at 4°C have been used experimentally for up to one year without any signs of loss of functionality. In accordance, also Strep-Tactin-based purified pHLA-A2-Fc-STag constructs displayed no prominent signs of degradation after 6 or even 18 months storage at 4°C (**Fig. 3.2a**). The aforementioned Strep-Tactin-based purified pHLA-A2-Fc-STag constructs were routinely produced and transiently expressed in 100 mL CHO-S cell cultures using serum-free ProCHO-4 medium and PEI (25 kDa linear polyethyleneimine) as transfection agent (CHO-S/ProCHO-4/PEI TGE system). This production system has been largely optimized and characterized by the laboratory of Florian Wurm (École polytechnique fédérale de Lausanne, Switzerland) (266–269).

In order to gain optimal production yields of pMHC-I-Fc-STag dimers in parallelized small-scale (2 mL) productions based on 24-deep well plates, we verified some key parameters of the production system CHO-S/ProCHO-4/PEI TGE system as shown in **Fig. 3.2b–d**. Addition of 1 mM valproic acid (VPA) has been shown previously to increase production yields of up to 30%, when CHO-S are cultured under hypothermic conditions (i.e. 32°C) (268). In accordance, we observed an approximate 17% increased titer of the representative Survivin/HLA-A2-Fc-STag [8556.1] compared to untreated cultures, which was quantified by an anti-mouse IgG-Fc sandwich ELISA (**Fig. 3.2b**). Moreover, 0.625 µg DNA and 2.5 µg PEI per 1x10<sup>6</sup> cells to be transfected were suggested to be optimal for CHO-S transfected at 2–4x10<sup>6</sup> cells/mL (266). These previous published results could be confirmed by our own PEI/DNA titrations (**Fig. 3.2c**). In addition, we tested several commercially available serum-free chemical defined (CD) CHO media shown in **Fig. 3.2d**. Among the tested media, we did not observed any obvious differences in term of Survivin/HLA-A2-Fc-STag titers after 6 days of culture. The used chemically defined CHO media, however, did not support PEI-based transfections. As a next step, we performed parallel transient gene expressions of over 20 different available pHLA-A2-Fc-STag constructs harboring published and previously validated peptide ligands (**Table 3.1**) within one 24-deep well plate (**Fig. 3.2e**). The average titer as was 27 (± 12) µg/mL among all tested pHLA-A2-Fc constructs and the majority of constructs (16 of 21) displayed a titer >20 µg/mL according to anti-mIgG-Fc sandwich ELISA. Moreover, the overall production efficiency among the selected peptide ligands was largely independent of the predicted binding affinity (**Table 3.1**).

### 3| Results Part 1 – Production and validation of soluble pMHC-Fc proteins

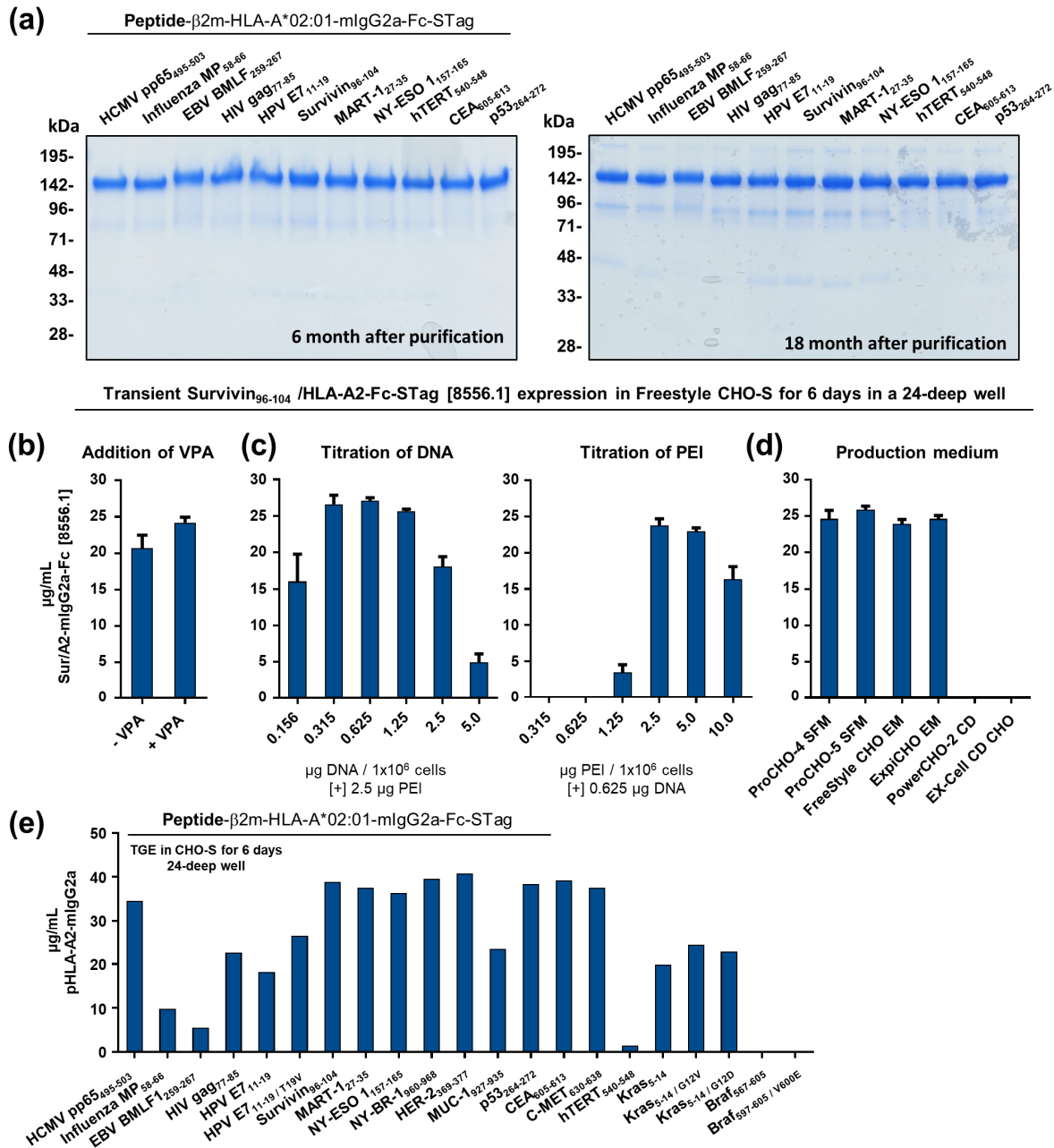


**Figure 3.2 | Long stability of dt-pHLA-A2-Fc-STag proteins and 24-deep well-based small-scale production**

**(a)** Follow-up assessment of purified dt-pHLA-A2-Fc-STag proteins. Shown dt-pHLA-A2-Fc-STag proteins were purified by Strep-Tactin-based affinity chromatography and were stored at 4°C for over 18 months thereafter. 10% SDS-PAGE under non-reducing conditions of various dt-pHLA-A2-Fc-STag batches after 6 months (left panel) and 18 months storage (right panel). **(b–d)** Verification of key parameters of the CHO-S/PEI/ProCHO-4 TGE protein production system. Freestyle CHO-S cells were transfected at  $3 \times 10^6$  cells/ml with Survivin<sub>96–104</sub>/HLA-A2-Fc-STag [8556.1] construct in a total volume of 2 mL ProCHO-4 SFM by default. Cells were cultured in a 24-deep well block cultured at 450 rpm 37°C, 8% CO<sub>2</sub> for 6 h followed by culture at 32°C and 5% CO<sub>2</sub> for 6 additional days. To assess production efficiency, supernatants were collected and analysed by quantitative  $\alpha$ -mouse IgG-Fc sandwich ELISA. **(b)** Transfected CHO-S cell cultures were supplemented with 1 mM valproic acid (VPA) (default) or left untreated. **(c) (Left panel)** CHO-S were transfected using 2.5  $\mu$ g PEI /  $1 \times 10^6$  cells (default) and various amount of DNA. **(Right panel)** CHO-S were transfected using 0.625  $\mu$ g DNA /  $1 \times 10^6$  cells (default) and various amounts of PEI. **(d)** CHO-S cells were transfected using default transfection conditions but various other commercially available CHO media. SFM: serum-free medium; EM: expression medium; CD: chemically defined medium. **(e) Production of 21 different dt-pHLA-A2-Fc-STag constructs within one 24-deep well block.** Shown is the result of a quantitative  $\alpha$ -mouse IgG sandwich ELISA of CHO-S supernatants (2 mL batches) after 6 days of transient gene expression (TGE).

Surprising exceptions however were pHLA-A2-Fc-STag constructs harboring the well-known HLA-A2 restricted peptides Influenza-A (Flu) MP-1<sub>58-66</sub> [GILGFVFTL], EBV BMLF-1<sub>259-267</sub> [GLCTLVAML] and hTERT<sub>540-548</sub> [ILAKFLHWL] peptides, which were consistently weakly expressed throughout the study compared to the large majority of tested constructs. Nevertheless, both Flu MP-1<sub>58-66</sub>/A2-Fc and EBV BMLF-1<sub>259-267</sub>/A2-Fc constructs were completely functional as shown by subsequent experiments (**Fig. 3.4c and 3.6**). In this regard, Strønen *et al.* also experimentally confirmed a very high stability (i.e. half-life >25 h at 37°C) of a non-covalently associated Flu MP-1<sub>58-66</sub>/HLA-A2 complex in a pMHC-stability assay (286). Thus, we still lack an explanation why the Flu MP-1<sub>58-66</sub> and EBV BMLF-1<sub>259-267</sub> bearing pHLA-A2-Fc constructs are consistently less efficiently produced. In case of the hTERT<sub>540-548</sub> [ILAKFLHWL]/HLA-A2-Fc construct, we hypothesized that the peptide ligand may be partially cleaved by the signal peptidase after its third amino acid residue (i.e. alanine) resulting in an unproductive expression. In fact, SignalP 5.0 algorithm-based predictions (284) indicated a low signal peptidase cleavage probability (i.e. 47% / **Table 3.1**) for a cut between the last residue of the used modified influenza virus HA1 leader sequence (HA-leader sequence shown in *italic*) and the first residue of the hTERT<sub>540-548</sub> peptide (i.e. *MAKANLLVLLCALAAADA*<sup>↓</sup>*ILAKFLHWL*). Moreover, the algorithm indicated a second cleavage site between residue 3 and 4 of the aforementioned peptide (i.e. *MAKANLLVLLCALAAADAILA*<sup>↓</sup>*KFLHWL*). To overcome this issue, we are currently testing alternative leader sequences that provide more favorable cleavage probabilities, which however is beyond the scope of this study. Furthermore, pHLA-A2-Fc constructs accommodating the previously reported HLA-A\*02:01 binding peptides wild-type-BRaf<sub>597-605</sub> [LATVKSRRWS] and mutated-BRaf<sub>597-605</sub> / V600E [LATEKSRRWS] (287) were repeatedly not expressed. Notably, in our constructs we mutated serine (S) at position 605 to valine (V) resulting in wild-type-BRaf<sub>597-605</sub> [LATVKSRRVV] and mutated-BRaf<sub>597-605</sub> / V600E [LATEKSRRVV], respectively, which should even improve the overall binding to HLA-A\*02:01 (17). Still, the alanine (A) residue at position 2 remains a poor anchor residue for HLA-A\*02:01 leading to very low predicted binding affinities above 10000 nM even for the valine-substituted peptides (NetMHC 4.0 algorithm, (281)). Moreover, it has been previously shown that TAP-deficient CHO cells only express disulfide-trapped HLA-A\*02:01 single-chain trimers at the cell surface accommodating a suitable HLA-A2-restricted peptide like the HIV-1 gag<sub>77-85</sub> [SLYNTVATL] peptide but not an irrelevant HLA-B\*27:05-restricted Flu NP<sub>383-391</sub> [SRYWAIRTR] peptide lacking suitable anchor residues (247). In accordance, we also observed that a HLA-A2-Fc single-chain dimeric constructs only comprising the β<sub>2</sub>m-HLA-A2-Fc fusion but lacking an attached peptide was not expressed by our CHO-S production system (**data not shown**).

### 3.1.3 Cognate stimulation of Sur/A2 CD8<sup>+</sup> T cells by bead-immobilized pHLA-A2-Fc (aAPCs)

After confirmation that the Survivin<sub>96-104</sub>/HLA-A2-mIgG2a-Fc construct (Sur/A2-Fc [8556.1]) binds specifically to the cognate Sur/A2 CD8<sup>+</sup> T cell line, we were interested if bead-immobilized Sur/A2-Fc would drive antigen-specific stimulation of that T cell line leading to effector cytokine secretion (**Fig. 3.3a**). Thus, we non-covalently conjugated Sur/A2-Fc or control with a selection of magnetic anti-mouse-IgG-Fc associated beads including MACS<sup>®</sup> MicroBeads (50 nm in size, Miltenyi), Dynabeads<sup>®</sup> (4.5 μm, Invitrogen) and spectral color-coded MagPlex<sup>®</sup> microspheres (Luminex-beads, 6.5 μm). Moreover, we covalently conjugated Sur/A2-Fc directly to carboxylated Luminex beads via EDC/sulfo-NHS catalyzed crosslinking (see **Material & methods section 2.9.1.3**). In addition, HLA-A\*02:01-expressing T2 cells were pulsed (10 μM) with Survivin<sub>96-104</sub> or control peptide. Peptide-pulsed T2 cells served as cellular artificial antigen-presenting cells (aAPC), whereas beads conjugated with pMHC-I-Fc were considered as bead-based aAPCs. Co-culture for 4 h of Sur/A2 CD8<sup>+</sup> T cells with the above-mentioned set of aAPCs induced a moderated to strong antigen-specific expression of effector

### 3 | Results Part 1 – Production and validation of soluble pMHC-Fc proteins

cytokines including TNF- $\alpha$ , IFN- $\gamma$  and IL-2 depending on the used aAPC shown in **Fig. 3.3b**. Sur/A2-Fc conjugated Dynabeads as well as Luminex-beads (independent of the conjugation) lead in up to 90% of the cells to an IFN- $\gamma$  and/or TNF- $\alpha$  expression but only in 30 – 50% of the cells to an additional IL-2 expression.

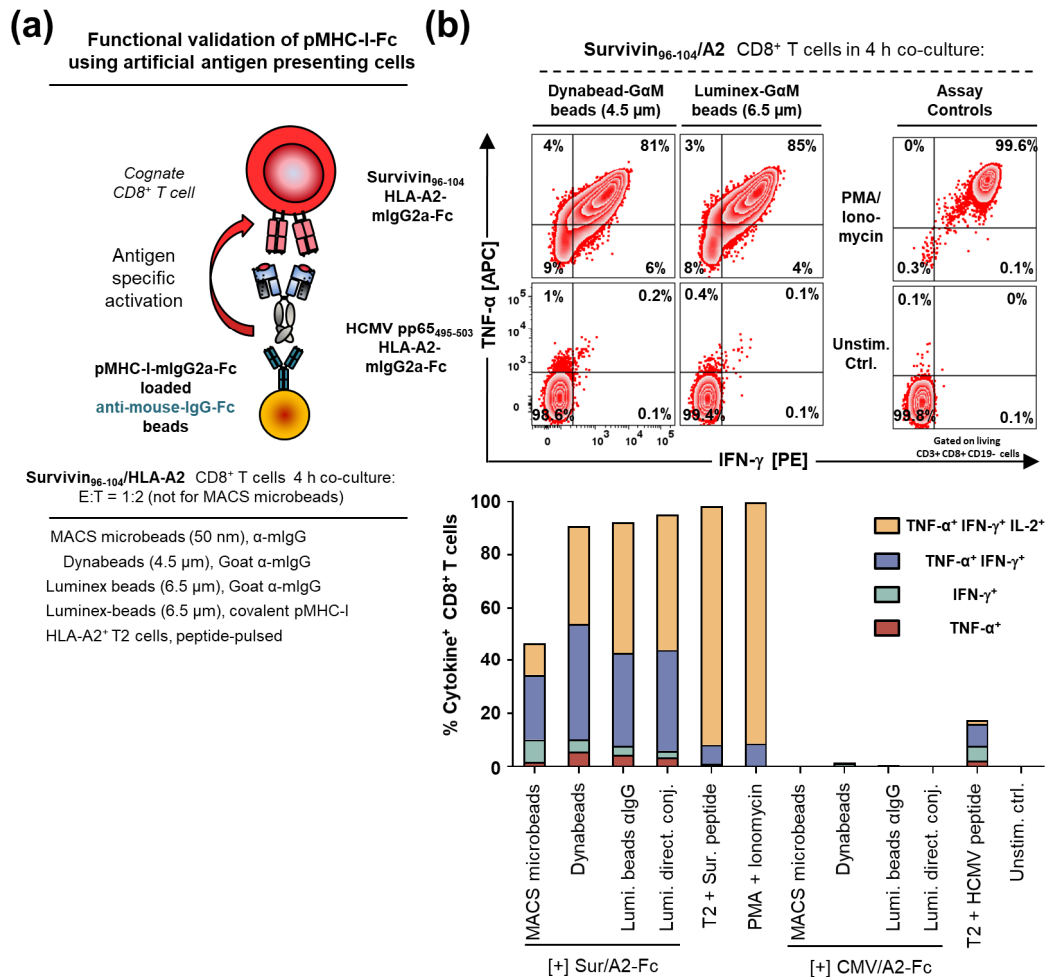


**Figure 3.3 | Antigen-specific stimulation of Sur/A2 CD8<sup>+</sup> T cells by bead-immobilized cognate pHLA-A2-Fc**

**(a) Construction of artificial antigen-presenting cells (aAPC)** by coupling of dt-pMHC-I-Fc onto magnetic  $\alpha$ -mouse IgG-Fc beads. Co-culture of aAPCs with cognate CD8<sup>+</sup> T cells results into antigen-specific stimulation.

**(b) Assessment of the specificity and stimulatory capacity of bead- and cell-based aAPCs.** Result of a 4 h co-culture of Sur/A2 T cells (effectors (E)) and aAPCs (targets (T)) (E:T = 1:2) in the presence of brefeldin-A and monensin to ensure intracellular cytokine accumulation.  $\alpha$ -mouse IgG-Fc magnetic MACS microbeads-; Dynabeads or Luminex beads loaded with saturating amounts of cognate Survivin<sub>96-104</sub>/HLA-A2-Fc [8556.1] (Sur/A2-Fc) or control HCMV pp65<sub>495-503</sub>/HLA-A2-Fc [8558.1] (HCMV/A2-Fc) were used as bead-based aAPCs. Additionally, Luminex beads were covalently conjugated with pMHC-I-Fc. HLA-A2 expressing T2 cells were pulsed overnight with 10  $\mu$ M Survivin<sub>96-104</sub> peptide (Sur. peptide) or HCMV pp65<sub>495-503</sub> peptide (HCMV peptide) as control. Stimulation of the Sur/A2 CD8<sup>+</sup> T cell line is shown by induction of cytokine expression analyzed by intracellular staining for TNF- $\alpha$ , IFN- $\gamma$  and IL-2 after lineage marker staining.

GαM-IgG: Goat-anti-mouse IgG polyclonal antibody

In contrast, peptide-pulsed T2 cell-based aAPC stimulated Sur/A2 CD8<sup>+</sup> T cells almost completely (>95%) and induced in over 90% of the cells a polyfunctional expression of all three measured effector cytokines indicating an overall inferior stimulation capacity of the used bead-based aAPCs compared to T2 cell-based aAPCs. However, T2 cells pulsed with control peptide also stimulated over 10% of the Sur/A2 CD8<sup>+</sup> T cells in a peptide-independent fashion, which might be explained by the fact that Sur/A2-specific T cell line has been generated from an allogeneic HLA-A2<sup>neg</sup> donor (253) and thus might be under optimal conditions slightly alloreactive. Interestingly, cognate Sur/A2-Fc-conjugated MACS

microbeads only stimulated ~50% of the Sur/A2 T cells (**Fig. 3.3b**). In accordance Perica *et al.* also observed that the T cell activation threshold for Dynabead-based aAPC (4.5  $\mu\text{m}$ ) was significantly lower compared to MACS microbead<sup>®</sup> aAPCs (50 nm) unless an external magnetic field was applied while T cell are in co-culture with nano-aAPCs (288). Notably, the addition of soluble Sur/A2-Fc at a final concentration of up to 10  $\mu\text{g}/\mu\text{L}$  was not sufficient to induce stimulation of the Sur/A2 T cells (**data not shown**). Nevertheless, in particular pHLA-A2-Fc conjugated to color-coded Luminex beads led to an antigen-specific stimulation of the Sur/A2 CD8<sup>+</sup> T cell line that was at least regarding IFN- $\gamma$  and TNF- $\alpha$  cytokine expression quite comparable to cellular aAPCs, which paved the path for the future multiplex assay development described in the 2<sup>nd</sup> results part starting from **Section 4.1**.

## **3.2 Generation of multiple virus-specific T cell lines using pMHC-I-Fc-based magnetic enrichment**

### 3.2.1 Detection and stimulation of virus-specific CD8<sup>+</sup> T cell populations within healthy donor-derived PBMC using pMHC-I-Fc

In order to validate the functionality and specificity of our pHLA-A2-Fc constructs beyond the available Sur/A2 CD8<sup>+</sup> T cell line, we screened throughout the study several healthy blood donor-derived peripheral blood mononuclear cells (PBMC) for HLA-A2 allele expression (HLA-A2<sup>+</sup>), which was assessed by staining with the HLA-A2-specific antibody BB7.2 (**data not shown**). In the next step, HLA-A2<sup>+</sup> PBMC were analyzed by commercially available pHLA-A2 pentamers or our in-house produced pHLA-A2-Fc constructs accommodating peptide epitopes from common viral recall antigens including HCMV pp65<sub>495-503</sub>, EBV BMLF-1<sub>259-267</sub> and Flu-A MP-1<sub>58-66</sub>. pHLA-A2 presenting the Survivin<sub>96-104</sub> peptide served as a negative staining control in this setting, since Survivin, a well-characterized inhibitor of apoptosis has been rather considered as tumor-associated antigen leading to immune responses rather in cancer patient than healthy persons (289).

Both HLA-A2<sup>+</sup> healthy donors #6691 and #6556 displayed a HCMV pp65<sub>495-503</sub>/HLA-A2 specific CD8<sup>+</sup> T cell population (HCMV/A2 CD8<sup>+</sup> T cells), which was clearly revealed by the cognate commercial pHLA-A2 pentamer as well as by our corresponding HCMV pp65<sub>495-503</sub>/HLA-A2-Fc construct [7409.4] staining. The latter was subsequently detected by an anti-mouse-Fc antibody (**Fig. 3.4a**, left panels). Although the commercial pHLA-A2 pentamer had an expected, slightly superior staining performance compared to the pHLA-A2-Fc-based staining, both reagents indicated the same frequency of HCMV/A2-specific CD8<sup>+</sup> T cells in both donors. Besides the direct pHLA-A2-based binding analysis mentioned above, we also compared the stimulation capacity of HCMV pp65<sub>495-503</sub>/HLA-A2-Fc-loaded Dynabeads (aAPCs) to a corresponding HCMV pp65<sub>495-503</sub> peptide pulse [10  $\mu\text{M}$ ]. In accordance with the previous pHLA-A2 binding data, similar frequencies of antigen-specific stimulated IFN- $\gamma$ <sup>+</sup> CD8<sup>+</sup> T cell were detected by cognate peptide pulse and subsequent intracellular cytokine staining (**Fig. 3.4a**, right panels). Also HCMV/A2-Fc-loaded Dynabeads stimulated the corresponding HCMV/A2 specific CD8<sup>+</sup> T cell population in an antigen-specific fashion, however to a smaller extent in terms of frequency and also quality (reduced MFI) compared to the 10  $\mu\text{M}$  peptide pulse, which converts every cell in the culture into an APC. We reasoned that the reduced frequency of stimulated T cells by cognate bead-based aAPCs might be due to an unfavorable accessibility between cognate CD8<sup>+</sup> T cells and Dynabead-based aAPCs and that the reduced stimulation quality might be caused by the lack of co-stimulation.

### 3 | Results Part 1 – Production and validation of soluble pMHC-Fc proteins

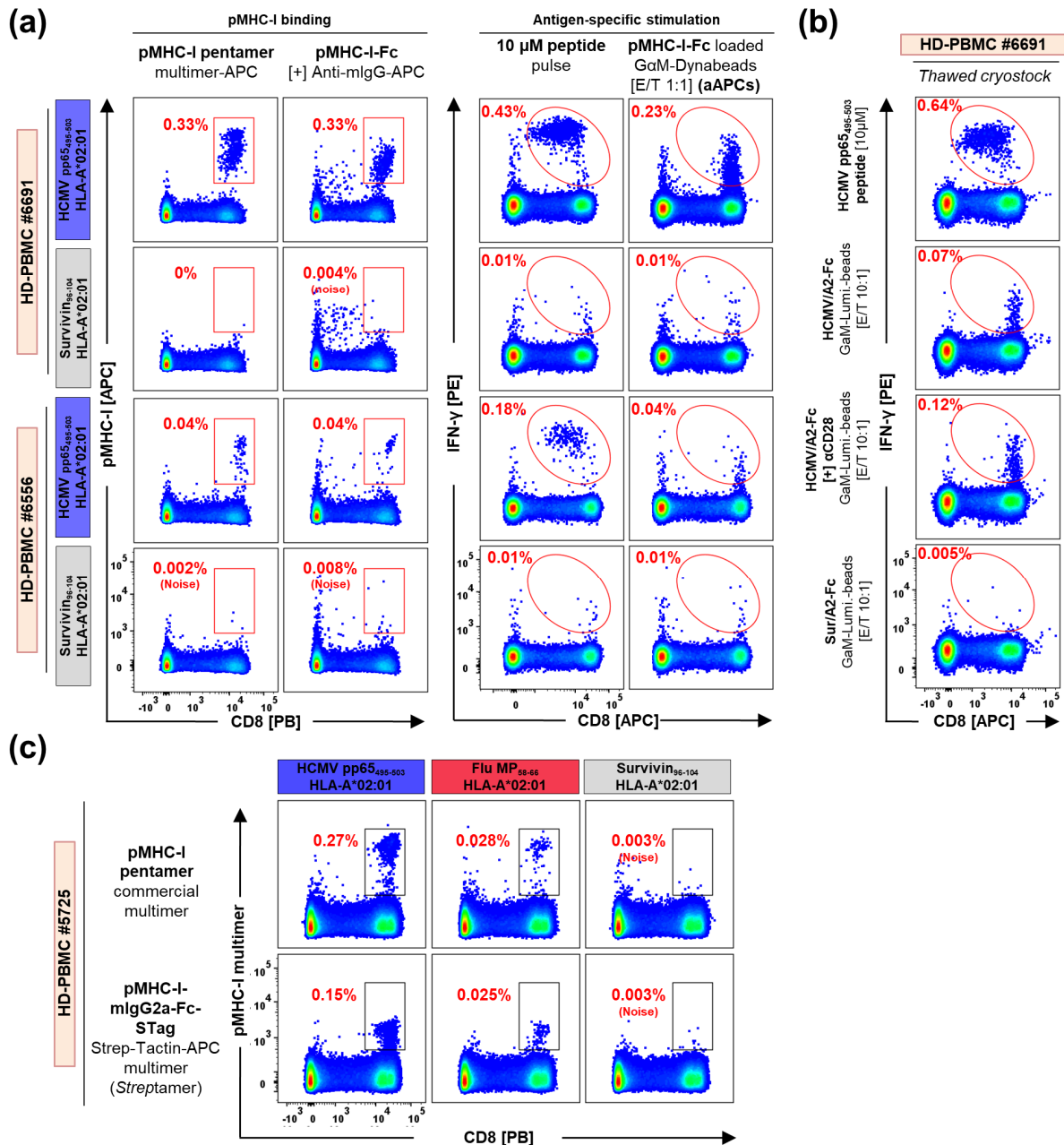


**Figure 3.4 | Detection and stimulation of virus-specific CD8<sup>+</sup> T cells within healthy donor PBMC using pMHC-I-Fc**

**(a) pMHC-I-Fc-based staining and aAPC-based stimulation of healthy donor #6691 and #6556.** (Left panel) pMHC-I binding analysis.  $1 \times 10^6$  cells per condition of HLA-A2<sup>+</sup> healthy donor (HD) PBMC were individually stained with commercial pMHC-I pentamers or pMHC-I-Fc detected by Goat- $\alpha$ -mouse-IgG-APC (GaM) followed by lineage marker staining. The frequency of pMHC-I multimer<sup>+</sup> cells within the CD3<sup>+</sup> T cell population is shown. (Right panel) *In vitro* restimulation of cognate T cell pools.  $1 \times 10^6$  PBMC per condition were stimulated for 4 h using a 10  $\mu$ M peptide pulse (HCMV pp65<sub>495-503</sub> or control) or  $1 \times 10^6$  pMHC-I-Fc loaded GaM-Dynabeads (aAPCs) (E:T = 1:1) in the presence of brefeldin A and monensin to block cytokine secretion. Cells were lineage marker stained followed by an intracellular IFN- $\gamma$  staining (ICS). The frequency of IFN- $\gamma$ <sup>+</sup> cells within the CD3<sup>+</sup> T cell population is shown.

**(b) Stimulation of donor #6691 using cognate aAPCs additional supplemented with  $\alpha$ CD28 mAb.**  $1 \times 10^6$  cells of HD-PBMC #6556 (thawed cryostock) were brought in co-culture for 4 h with  $1 \times 10^6$  GaM-Luminex beads loaded with HCMV pp65<sub>495-503</sub>/HLA-A2-Fc alone or in addition with  $\alpha$ CD28 mAb (clone CD28.2) followed by ICS.

**(c) pMHC-I-Fc-STag based Streptamer staining vs. pMHC-I pentamer staining of HD-PBMC #5725.**  $1 \times 10^6$  cells of HLA-A2<sup>+</sup> HD-PBMC #5725 were either stained with commercial pMHC-I pentamers or pMHC-I-Fc-STag constructs previously incubated with Strep-Tactin-APC to generate *Streptamers* (IBA Lifescience). All pMHC-I stainings were performed at 25  $\mu$ g/mL in the presence of 50 nM dasatinib followed by lineage marker staining. Construct Survivin<sub>96-104</sub>/HLA-A2-Fc [8195.1] (Sur/A2-Fc) and HCMV pp65<sub>495-503</sub> /HLA-A2-Fc [7409.4] (HCMV/A2-Fc) were used in (a) and Sur/A2-Fc-STag [8556.1]; HCMV/A2-Fc-STag [8558.1]; Flu MP-1<sub>58-66</sub>/A2-Fc-STag [8557.1] were used in (b & c).

Consequently, we repeated the stimulation of donor #6691 with beads that were simultaneously loaded with cognate HCMV/A2-Fc and anti-CD28 mAb (clone CD28.2). However, also bead-based aAPCs with combined conjugation of anti-CD28 mAb and HCMV/A2-Fc revealed no improved stimulation quality compared to aAPCs lacking the anti-CD28 mAb (**Fig. 3.4b**) and thus might rather indicate an inherent property of the used bead-based aAPC.

As an alternative to the sequential pMHC-I-Fc and anti-mouse-antibody staining shown in **Fig. 3.4a**, we also tested *Streptamers* based on our pHLA-A2-Fc-STag construct for the detection of virus-specific T cells with PBMC of healthy donor #5725 (**Fig. 3.4c**). Both HCMV pp65<sub>495-503</sub>/HLA-A2-Fc-STag [8558.1] and Flu-A MP-1<sub>58-66</sub>/HLA-A2-Fc-STag [8557.1] based *Streptamers* indicated a cognate antigen-specific CD8<sup>+</sup> T cell population of HLA-A2<sup>+</sup> donor #5725. However, in a corresponding staining the commercial pHLA-A2 pentamers demonstrated a superior performance resulting in a higher sensitivity.

### 3.2.2 Generation, validation and characterization of virus-specific HLA-A2-restricted CD8<sup>+</sup> T cell lines derived from healthy donors

As a next step, we aim at generating multiple pure virus-specific HLA-A2-restricted CD8<sup>+</sup> T cell lines, which would serve as an invaluable tool for the subsequent multiplex assay development and for quality control of newly produced pHLA-A2-Fc batches. For this several HLA-A\*02:01 (HLA-A2<sup>+</sup>) positive healthy donors were initially screened using commercially available pHLA-A2 pentamers for viral recall antigens including HCMV pp65<sub>495-503</sub>, EBV BMLF-1<sub>259-267</sub> and Flu MP-1<sub>58-66</sub>. Upon identification of a preexisting virus-specific CD8<sup>+</sup> T cell population, we induced an antigen-specific proliferation of that particular population by a low-dose (0.1 μM) peptide pulse directly added to unseparated PBMC. Subsequently, the antigen-specific T cell expansion was monitored over a period of two weeks as exemplary shown for the HCMV<sub>495-503</sub>/HLA-A2 specific CD8<sup>+</sup> T cell line generated from healthy donor #8867 (**Fig. 3.5a**). After 13–15 days of the first round of antigen-specific proliferation resulting in a 75–130 fold increase of the desired T cell population, we isolated the antigen-specific T cell population based on Strep-Tactin-coated nanobeads (IBA Lifesciences) loaded with our pHLA-A2-Fc-STag molecules and a subsequent MACS step. Upon magnetic antigen-specific enrichment, we usually observed an 80–90% purity of antigen-specific T cells. These freshly isolated T cells were again restimulated for 1–2 weeks using peptide pulsed, HLA-A2-matched and irradiated PBMC-feeder cells resulting in an overall T cell line purity of 95% after the second expansion (**Fig. 3.5a and Fig. 3.6**).

The HCMV<sub>495-503</sub>/HLA-A2 specific CD8<sup>+</sup> T cell line #8867 (HCMV/A2 CD8<sup>+</sup> T cell line #8867) displayed an expected effector memory phenotype (CD45RA<sup>neg</sup>, CCR7<sup>neg</sup>) with 50% of the cells still expressing CD27 and CD28 (**Fig. 3.5b**). Moreover, 35 days after the start of the T cell expansion, the subpopulations of HCMV/A2 CD8<sup>+</sup> T cell line #8867 still expressed the exhaustion/activation-related markers TIGIT, TIM-3, PD-1 and LAG-3 (**Fig. 3.5c**). Nevertheless, the majority (>85%) of the cells were antigen-specifically stimulated upon co-culture with cognate Luminex-beads conjugated with HCMV/HLA-A2-Fc-STag [8558.1] leading to degranulation and TNF-α and IFN-γ expression (**Fig. 3.5d**). In addition, multiple generated HCMV/A2-specific T cell lines were able to kill cognate peptide pulsed HLA-A2-expressing target cells as shown by chromium (<sup>51</sup>Cr)-release assay (**Fig. 3.5e**). Thus, our implemented T cell line generation workflow let to multiple highly pure and functional virus-specific T cell line including the HLA-A2-restricted epitopes HCMV pp65<sub>495-503</sub>, EBV BMLF-1<sub>259-267</sub> and Flu MP-1<sub>58-66</sub> (**Fig. 3.6**), which could be easily cultured over a period of 4 months as well as cryopreserved without obvious reduction in functionality.

### 3| Results Part 1 – Production and validation of soluble pMHC-Fc proteins

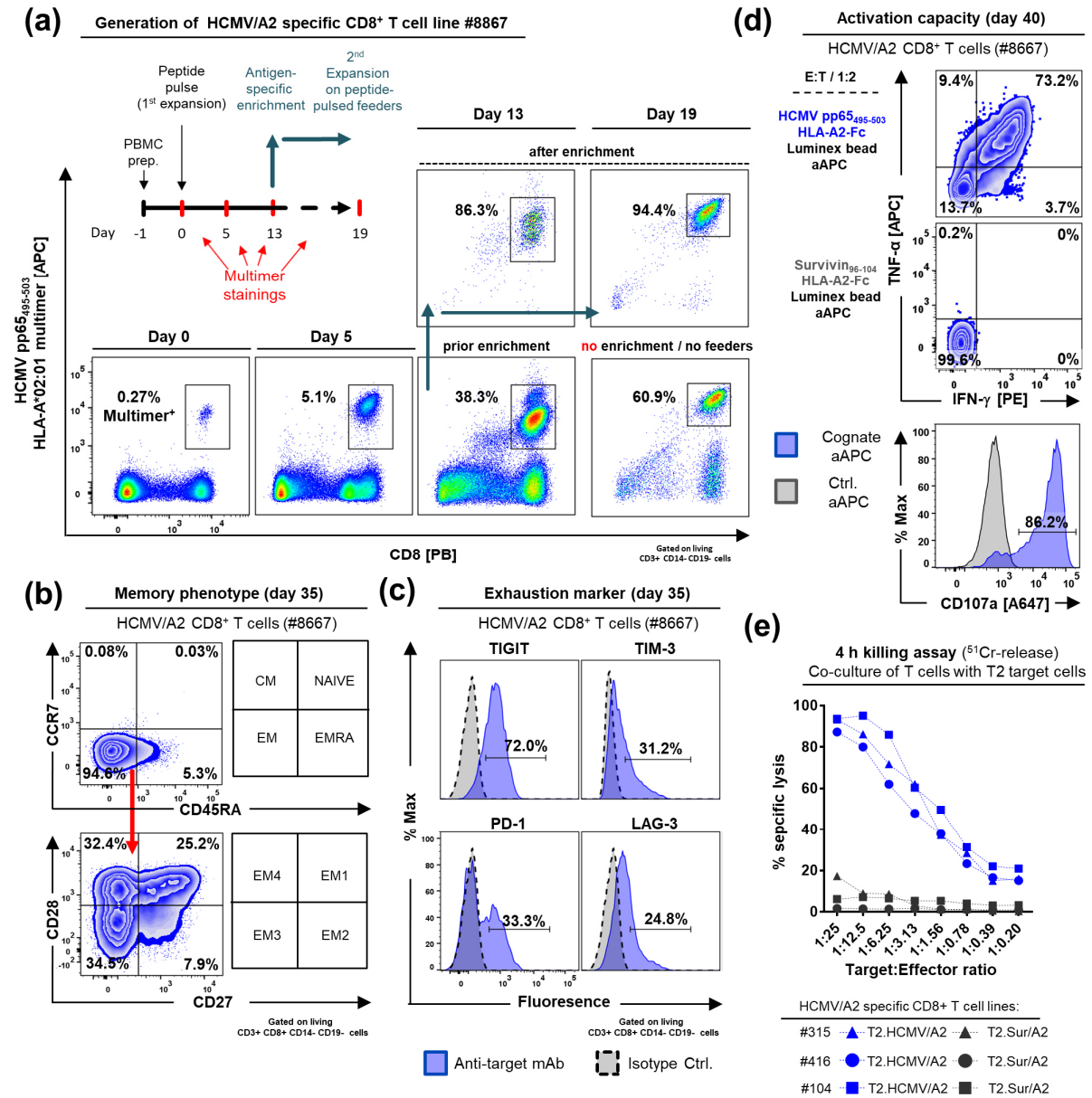


**Figure 3.5 | Generation, validation and characterization of HCMV pp65<sub>495-503</sub>/HLA-A2-specific CD8<sup>+</sup> T cell lines**

**(a) Generation of a HCMV/A2-specific T cell line using antigen-specific expansion and pMHC-I-Fc-based enrichment.** A HCMV pp65<sub>495-503</sub>/HLA-A2-specific CD8<sup>+</sup> T cell population of PBMC derived from an HLA-A2<sup>+</sup> healthy donor (HD) #8867 was initially detected by commercial HCMV pp65<sub>495-503</sub> (HCMV) /A2 pentamer staining (day 0). Subsequently, a 100 nM HCMV pp65<sub>495-503</sub> peptide pulsed was used to induce antigen-specific T cell expansion. On day 13, magnetic Strep-Tactin-coated nanobeads (IBA Lifesciences) loaded with HCMV/A2-Fc-STag [8558.1] were used to isolate cognate T cells. Isolated T cells were plated on irradiated HCMV-peptide pulsed HLA-A2<sup>+</sup> feeder cells for a 2<sup>nd</sup> expansion step. The frequency of HCMV/A2 multimer<sup>+</sup> cells within the CD3<sup>+</sup> T cell population is shown at various time points. This workflow became our default workflow to generate multiple virus-specific CD8<sup>+</sup> T cell lines.

**(b–c) Memory phenotype and exhaustion marker expression of HCMV/A2 CD8<sup>+</sup> T cell line (TC) #8667 on day 35.**

**(d) Antigen-specific 4 h stimulation of HCMV/A2 CD8<sup>+</sup> T cell line #8667** using Luminex bead-based aAPCs loaded with HCMV/A2-Fc-STag [8558.1] (cognate) or Sur/A2-Fc-STag [8556.1] (Ctrl.) followed by ICS. T cell activation is shown by induction of cytokine expression (TNF- $\alpha$ /IFN- $\gamma$ ) and degranulation ( $\alpha$ CD107a mAb accumulation).

**(e) Similar antigen-specific killing-capacity of multiple generated CMV/A2 specific CD8<sup>+</sup> T cell lines.** T2 cells were pulsed with 10  $\mu$ M HCMV pp65<sub>495-503</sub> peptide (T2.HCMV/A2) or Survivin<sub>96-104</sub> peptide (T2.Sur/A2) and subsequently labeled with radioactive <sup>51</sup>Cr. After 4 h co-culture of HCMV/A2-specific T cell lines derived from HD-#315, #416, #104 (effector cells) with T2 cells (targets) at various E:T ratios, <sup>51</sup>Cr release was measured. % specific target cell lysis is shown. EM: effector memory; CM: central memory

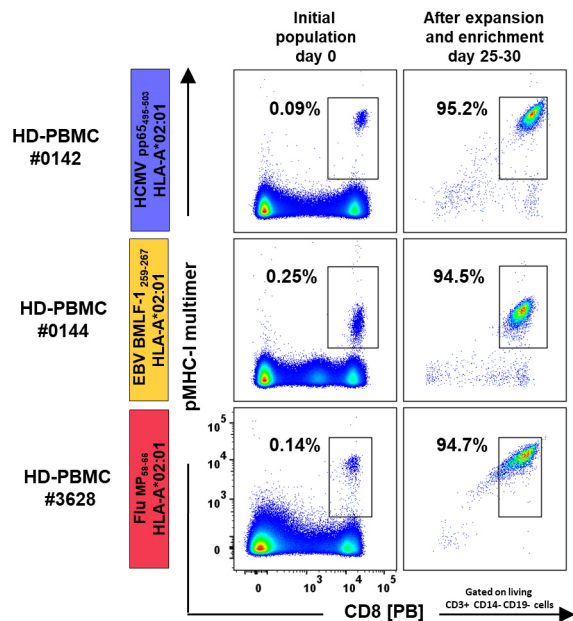


**Figure 3.6 | Generation of three virus-specific HLA-A2 restricted CD8<sup>+</sup> T cell lines**

Screening for virus-specific CD8<sup>+</sup> T cell populations of three HLA-A2<sup>+</sup> healthy donors (HD) and subsequent establishment of pure T cell lines using peptide pulsed antigen-specific expansion and pHLA-A2-Fc-based enrichment. The frequency of indicated virus-epitope /HLA-A2 pentamer<sup>+</sup> (Proimmune) cells within the CD3<sup>+</sup> T cell population is shown prior to (day 0) and after successful T cell line generation (day 25–30).

### 3.2.3 pHLA-A2-Fc-conjugated microbeads partially do not meet the T cell activation threshold

Throughout the study, we observed that microbeads including Dynabeads (4.5 μm) and Luminex-beads (6.5 μm) conjugated with our pHLA-A2-Fc constructs usually did not let to a 100% activation upon co-culture with cognate T cell lines, which yet remains an elusive phenomenon as shown in the following. Similar as already seen for the Sur/A2 T cell line (**Fig. 3.3b**) also the HCMV/A2 CD8<sup>+</sup> T cell line #416 was only activated by ~80% (cytokine<sup>+</sup> CD8<sup>+</sup> T cells) upon co-culture for 4 h with α-mouse-IgG Luminex-beads previously loaded with cognate HCMV/HLA-A2-Fc-STag [8558.1] (**Fig. 3.7a**). A follow-up corresponding control HCMV/HLA-A2 pentamer staining however confirmed a >99% purity for HCMV/A2-specific CD8<sup>+</sup> T cells displaying overall high levels of CD28 expression (**Fig. 3.7b**).

Thus, we reasoned that the aAPC-based stimulation-refractory population might be a kinetic artifact or due lack of T cell/bead contacts or co-stimulation. Consequently, we repeated the stimulation for 18 h of the HCMV/A2 CD8<sup>+</sup> T cell line #416 using α-mouse-IgG Luminex beads previously loaded with cognate HCMV/HLA-A2-Fc-STag or anti-CD3 mAb (clone OKT-3) in combination with a panel of co-stimulatory acting mAbs (**Fig. 3.7c**). Interestingly, again ~ 20% of HCMV/A2 T cell line #416 was not activated upon 18 h co-culture with HCMV/A2-Fc-loaded beads, which was in accordance with the previous 4 h stimulation shown in **Fig. 3.7a**. Co-association of α-CD28 mAb (clone CD28.2 [shown] or clone 15E8 [not shown]) with HCMV/A2-Fc on α-mouse-IgG Luminex beads let to an increased frequency of stimulated cells by approximately 10%. In contrast, anti-CD3-loaded beads applied at the same bead-number stimulated over >99% of the cells independent of presence of α-CD28 mAb, which rules out a bias due to insufficient bead/T cell accessibility during the stimulation. The combination of anti-CD28 mAb and anti-CD3 mAb on the bead however increased the fraction of 4-1BB<sup>+</sup> T cells. Moreover, HLA-A2 expressing T2 cells previously peptide-pulsed with the HCMV pp65<sub>495–503</sub> peptide, but not the Survivin<sub>96–104</sub> control peptide stimulated over 99% of the HCMV/A2 CD8<sup>+</sup> T cell line #416 (**Fig. 3.7c**). The latter indicated that the HCMV/A2 CD8<sup>+</sup> T cell line #416 still had capacity to completely respond to its cognate pMHC when presented on a cellular membrane but is partially refractory to bead-immobilized HCMV/HLA-A2-Fc. In sharp contrast, the HCMV/A2 CD8<sup>+</sup> T cell line #5561 shown in **Fig. 3.7d** displayed a refractory population of 1%. Moreover, the type of pHLA-A2-Fc immobilization on the Luminex-beads either via covalent crosslinking or via bead-associated anti-mouse-Fc-mAb did

### 3 | Results Part 1 – Production and validation of soluble pMHC-Fc proteins

not affected the stimulation capacity (**Fig. 3.7d**). We concluded that the manifestation of the bead-based aAPC stimulation-refractory sub-population is to some extent depending on the generated T cell line and displays an inherent feature of the used imperfect bead-based aAPCs.

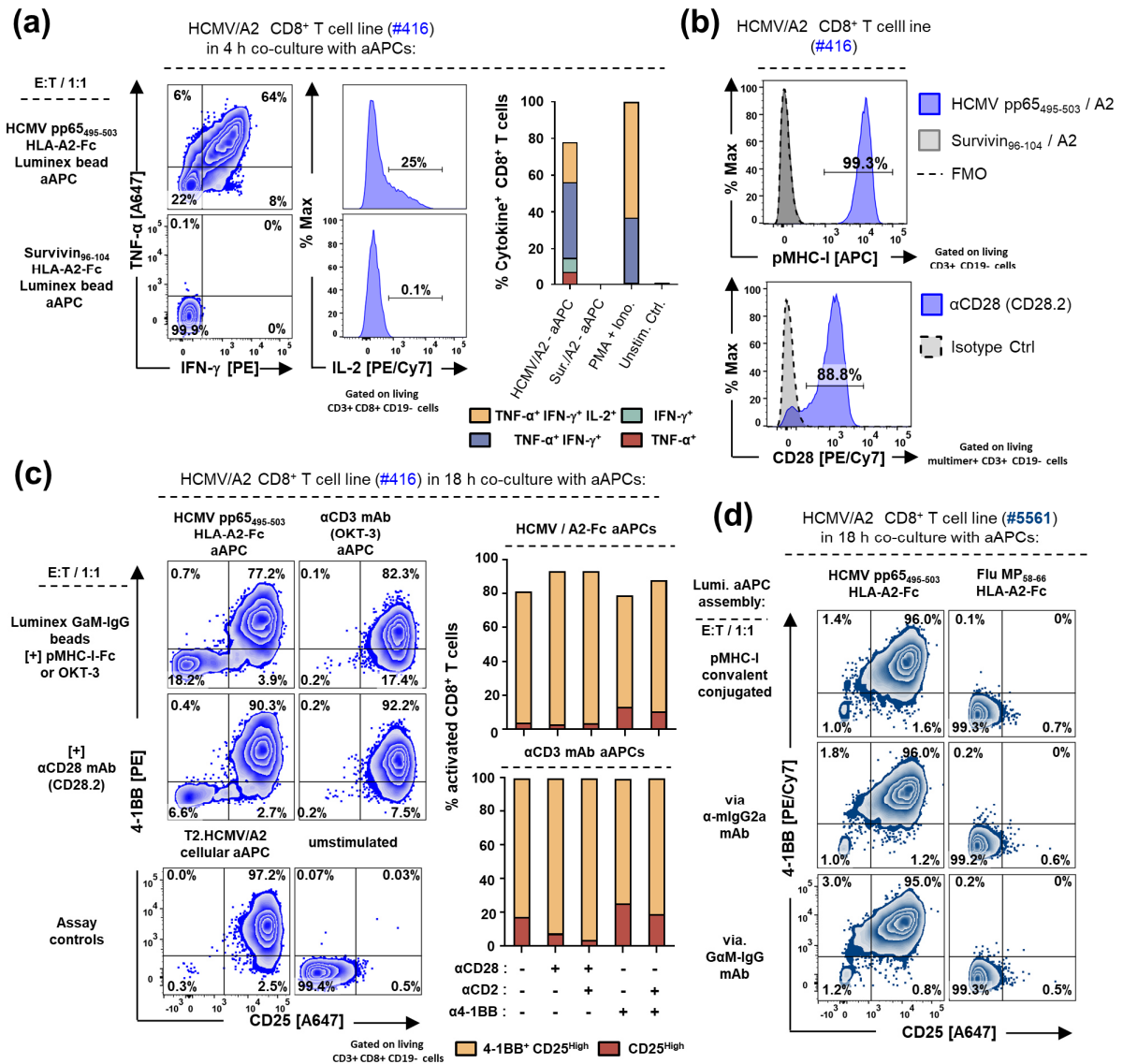


**Figure 3.7 | Stimulation of HCMV pp65<sub>495-503</sub> / A2 specific CD8<sup>+</sup> T cell line #416 and #5561 with various kinds of aAPCs**

**(a) Short-term aAPC-based antigen-specific stimulation of HCMV pp65<sub>495-503</sub>/A2 specific CD8<sup>+</sup> T cell line (TC) #416:** HCMV/A2 TC#416 was co-cultured for 4 h at a E:T of 1:1 with GaM-IgG-Luminex beads pre-loaded with HCMV pp65<sub>495-503</sub>/HLA-A2-Fc [8558.1] (HCMV/A2-Fc) or Survivin<sub>96-104</sub>/HLA-A2-Fc [8556.1] (Sur/A2-Fc) followed by ICS. T cell activation is shown by the induction of cytokine expression (TNF-α/IFN-γ/IL-2).

**(b) Purity and CD28 expression of HCMV/A2 TC#416.** HCMV/A2 TC#416 was labeled with the commercial HCMV/A2 pentamer (Prolimmune) or control in the presence of dasatinib [50 nM] followed by lineage marker and αCD28 staining. The frequency of HCMV/A2 multimer<sup>+</sup> cells (**Upper panel**) within the CD3<sup>+</sup> T cell population and their CD28 expression is shown (**Lower panel**).

**(c) Long-term aAPC-based antigen-specific stimulation of HCMV/A2 TC#416 for 18 h.** HCMV/A2 TC#416 was co-cultured with various bead-based aAPC compositions or cellular aAPC at an E:T of 1:1. GaM-IgG-Luminex beads were loaded with: **(1)** HCMV/A2-Fc or αCD3 mAb (OKT-3), **(2)** [+]<sup>+</sup> αCD28 mAb (CD28.2) or α4-1BB mAb (4B4-1) at a 3 to 2 ratio, **(3)** [-]<sup>-</sup> αCD28 mAb + αCD2 mAb (RPA-2.10) at a 12 to 7 to 1 ratio. T2 cells were pulsed overnight with 10 μM HCMV pp65<sub>495-503</sub> peptide (T2.HCMV/A2) or Survivin<sub>96-104</sub> peptide (T2.Sur/A2). Activation of the HCMV/A2 TC#416 is shown by a CD25<sup>high</sup> +/- 4-1BB<sup>+</sup> expressing cell subset. No stimulation of HCMV/A2 TC#416 was observed upon co-culture with T2.Sur/A2 (not shown).

**(d) aAPC-based antigen-specific stimulation of CMV/A2 TC#5561 for 18 h.** HCMV/A2 TC#5561 was co-cultured with various bead-based aAPC compositions: **(1)** GaM-IgG Luminex beads or, **(2)** α-mIgG2a Luminex beads loaded with HCMV/A2-Fc or Sur/A2-Fc or, **(3)** Luminex beads were covalently conjugated with HCMV/A2-Fc or Sur/A2-Fc. Activation of HCMV/A2 TC#5561 is by CD25<sup>+</sup> 4-1BB<sup>+</sup> expressing cell subset. E:T: effector to target ratio; GaM-IgG: Goat-anti-mouse IgG-Fc polyclonal antibody; ICS: Intracellular cytokine staining.

### 3.3 Production and validation of *in vivo* biotinylated heterodimeric pMHC-I-pCC-Fc

To overcome the well-known inferior staining performance of dimeric Fc- or whole IgG-Based pMHC-I compared to multimeric/tetrameric pMHC-I molecules (290), we decided to modify our pMHC-I-Fc backbone to allow site-directed biotinylation via an attached biotin acceptor peptide sequence (258) [GLNDIFEAQKIEWHE] referred to as AviTag<sup>TM</sup> (Avidity) followed by streptavidin-based multimerization. Moreover, to minimize the overall production workload caused by this additional step, we aimed for site-specific biotinylation during protein-of-interest expression often referred to as “*in vivo* biotinylation” (262) by co-transfecting CHO-S cells with an AviTag<sup>TM</sup>-fused pMHC-I-Fc construct as well as *E. coli*-derived biotin-protein ligase BirA. Previous studies have already shown the feasibility of this production approach for the *in vivo* biotinylation of soluble pMHC-II molecules in insect cells (291) as well as pMHC-I in bacteria (292). In addition, it has been reported that an endoplasmic reticulum (ER) retained BirA leads to higher biotinylation efficiencies in mammalian cells (263, 293).

Thus, we cloned the *birA* gene in frame with a C-terminal extension encoding for the ER retaining signal sequence KDEL (264) as well as a N-terminal human immunoglobulin light chain leader sequence (IgkL) resulting in construct 8521.1. IgkL-BirA<sub>KDEL</sub> construct 8521.1 expression of transfected CHO-S was validated by intracellular staining for BirA by  $\alpha$ -BirA mAb (clone 6C4c7, novus) (**Fig. 3.8c**). In parallel, we designed a heterodimeric pMHC-I-Fc construct containing a single AviTag<sup>TM</sup> based on an amphiphilic basic/acidic parallel coiled-coil heterodimerization domain (pCC) (257) depicted and explained in **Fig. 3.8a**. We reasoned that a single biotinylated AviTag<sup>TM</sup> attached to the heterodimeric pMHC-I-pCC-Fc construct would be crucial to form multimers upon addition of streptavidin in a controlled manner. In contrast, homodimeric constructs harboring two C-terminal biotinylated AviTag<sup>TM</sup> sequences might bear the risk of uncontrolled oligomer formation resulting in potential high staining backgrounds.

The engineered HCMV pp65<sub>495-503</sub>/HLA-A2-pCC-Fc [10347.7] and Survivin<sub>96-104</sub>/HLA-A2-pCC-Fc [9237.1] constructs were subsequently co-expressed with IgkL-BirA<sub>KDEL</sub> using the CHO-S/PEI/ProCHO-4 system supplemented with biotin and finally purified by Ni-NTA-based affinity chromatography. SDS-PAGE analysis revealed an expected pHLA-A2-pCC-Fc product at ~165 kDa under non-reducing conditions (**Fig. 3.8b**). Notably, an additional band at >200 kDa was exclusively observed in non-reducing conditions by SDS-PAGE as well as by NativePAGE suggesting that pMHC-I-pCC-Fc constructs have a tendency to form multimers most likely via ionic interactions due to the introduced pCC already in the absence of streptavidin. This higher molecular weight band was not seen for corresponding pHLA-A2-Fc-STag constructs lacking the additional heterodimerization domain (**Fig. 3.1b and 3.8d**). To confirm successful biotinylation and formation of streptavidin-associated multimeric pMHC-I-complexes, streptavidin (SAv) was added to purified biotinylated pHLA-A2-pCC-Fc (MHC) constructs at a 1:4 (SAv / MHC) molar ratio. Consecutive NativePAGE analysis as shown in **Fig. 3.8b** indicated a very efficient *in vivo* biotinylation of the Sur/HLA-A2-pCC-Fc [9237.1] construct as shown by an almost complete “gel-shift” upon addition of streptavidin. However, the formation of a range of pMHC-I multimer valencies mostly between 2 to 4 was observed (regarding the total amount of associated heterodimeric pMHC-I-pCC-Fc constructs) rather than the desired formation of a pMHC multimer with a single defined valency upon streptavidin addition. No gel-shift was observed as expected for the corresponding Sur/HLA-A2-Fc construct [8556.1] lacking the AviTag-sequence (**Fig. 3.8d**). As a next step, we compared the staining performance of streptavidin-APC multimerized HCMV/A2-pCC-Fc [10347.7] and Sur/A2-pCC-Fc [9237.1] in comparison to commercially available corresponding pMHC-I pentamers (ProImmune). Optimal titrated multimeric pHLA-A2-pCC-Fc constructs displayed an overall similar

### 3 | Results Part 1 – Production and validation of soluble pMHC-Fc proteins

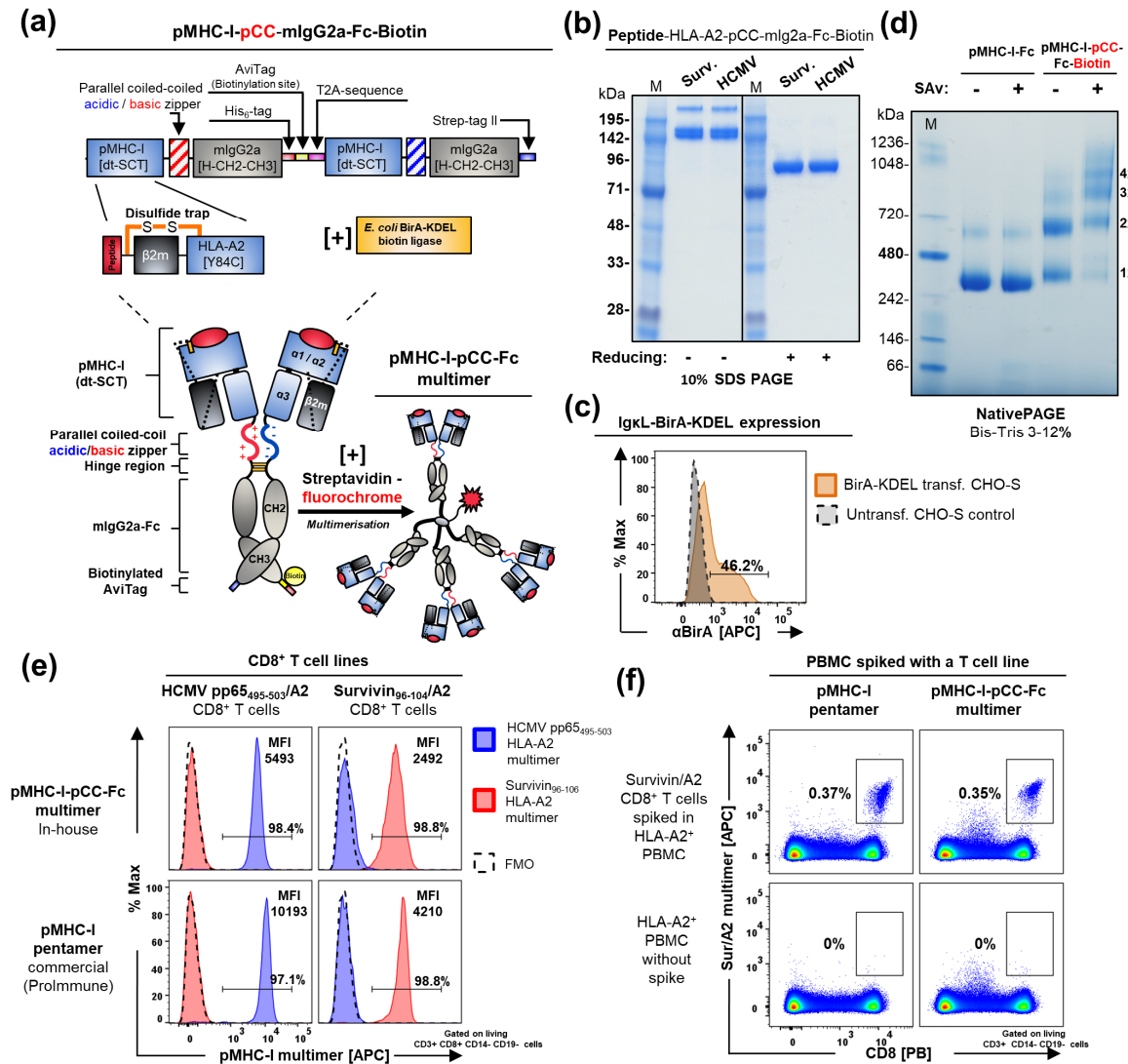


**Figure 3.8 | Production and validation of pMHC-I multimers based on a biotinylated heterodimeric Fc**

**(a) pMHC-I-heterodimeric biotin-tagged Fc construct (pMHC-I-pCC-Fc)** consists of two separated polypeptide chains co-expressed in a single vector via a T2A sequence. The first polypeptide chain comprised the pMHC-I complex as single-chain-timer (disulfide-trapped peptide ligand, β<sub>2</sub>m, HLA-class I allele ectodomain) fused to a parallel coiled-coil (pCC) basic zipper followed by the hinge domain and CH2 and CH3 of mIgG2a (Fc) and a C-terminal His<sub>6</sub>-tag and AviTag™ (Avidity) for site-specific biotinylation. The second chain comprised the same pMHC-I complex fused a complementary acidic pCC-Fc and C-terminal Strep-tag II. The pMHC-I-pCC-Fc construct is site-specific *in vivo* biotinylated by co-expression with BirA. The BirA-ligase is fused to the C-terminal ER-retention signal KDEL and a N-terminal leader sequence (IgkL-BirA<sub>KDEL</sub>). Biotinylated pMHC-I-pCC-Fc is multimerized by addition of streptavidin.

**(b) Biotinylated pMHC-I-pCC-Fc affinity chromatography.** CHO-S supernatants from a 6-day transient pHLA-A2-pCC-Fc [9237.1] and [10347.7] expression was purified using Ni-NTA resin-filled columns at pH 7.4. 10% SDS-PAGE under non-reducing and reducing conditions is shown.

**(c) Validation of IgkL-BirA<sub>KDEL</sub> expression.** IgkL-BirA<sub>KDEL</sub> expressing CHO-S cells (orange) and untransfected control cells (grey) were intracellularly stained with α-BirA mAb (Clone 6C4c7) and GαM-IgG-APC mAb 3 days after transfection.

**(d) Validation of biotinylation and multimer formation.** pMHC-I-Fc [8556.1] and pMHC-I-pCC-Fc-Biotin [9237.1] were incubated with streptavidin (SAV) at a 4:1 molar ratio and subsequently analyzed by NativePAGE (Invitrogen).

**(e) Antigen-specific binding of pMHC-I-pCC-Fc multimers to T cell lines.** Survivin<sub>96-104</sub>/A2 and HCMV pp65<sub>495-503</sub>-specific CD8<sup>+</sup> T cell lines were stained in the presence of dasatinib [50 nM] with cognate and control pMHC-I multimers at 1 μg/mL followed by lineage marker staining. (**Upper panel**) pMHC-I-pCC-Fc multimer; (**Lower panel**) Commercial pMHC-I pentamer (Prolimmune). The frequency of multimer<sup>+</sup> cells within the CD8<sup>+</sup>/CD3<sup>+</sup> T cell population is shown.

**(f) Specific detection of antigen-specific T cells within PBMC.** 2x10<sup>6</sup> HLA-A2<sup>+</sup> PBMC were spiked with 10,000 Sur/A2 T cells and subsequently analyzed by cognate pMHC-I-pCC-Fc multimer or pMHC-I pentamer as described above. The frequency of multimer<sup>+</sup> cells within the CD3<sup>+</sup> T cell population is shown. FMO: Fluorescence-minus-one background control. GαM-IgG: Goat-anti-Mouse IgG polyclonal antibody; MFI: Median fluorescent intensity.

staining performance compared to pHLA-A2 pentamers and reliably detected the cognate Sur/A2 CD8<sup>+</sup> T cell line and HCMV/A2 CD8<sup>+</sup> T cell line #5561 (**Fig. 3.8e**) as well as Sur/A2 CD8<sup>+</sup> T cells spiked into PBMC of an HLA-A2<sup>+</sup> healthy donor (**Fig. 3.8f**). However, the pHLA-A2 pentamer overall demonstrated a superior brightness (MFI) when used at equal concentrations compared to multimeric pHLA-A2-pCC-Fc (**Fig. 3.8e–f and 3.9**). Notably, when used at higher concentrations than 1 µg/mL multimeric pHLA-A2-pCC-Fc consistently (across batches) bound to a certain extent unspecifically to irrelevant T cells, which was not observed for corresponding pHLA-A2 pentamers (**Fig. 3.9**). In conclusion, the elaborated pMHC-I-pCC-Fc design with a single AviTag<sup>TM</sup> was overall successfully produced and *in vivo* biotinylated by the CHO-S/PEI/ProCHO-4 system when co-transfected with IgκL-BirA<sub>KDEL</sub>. Moreover, streptavidin-APC multimerized pMHC-I-pCC-Fc reliably detected cognate antigen-specific T cells but displayed a higher tendency to bind unspecifically at higher staining concentrations most likely caused by the required pCC heterodimerization domains. Thus, we developed a homodimeric pMHC-I-Fc construct backbone omitting the pCC-domain, which can be subsequently cleaved into biotinylated monomeric pMHC-I as shown next section.

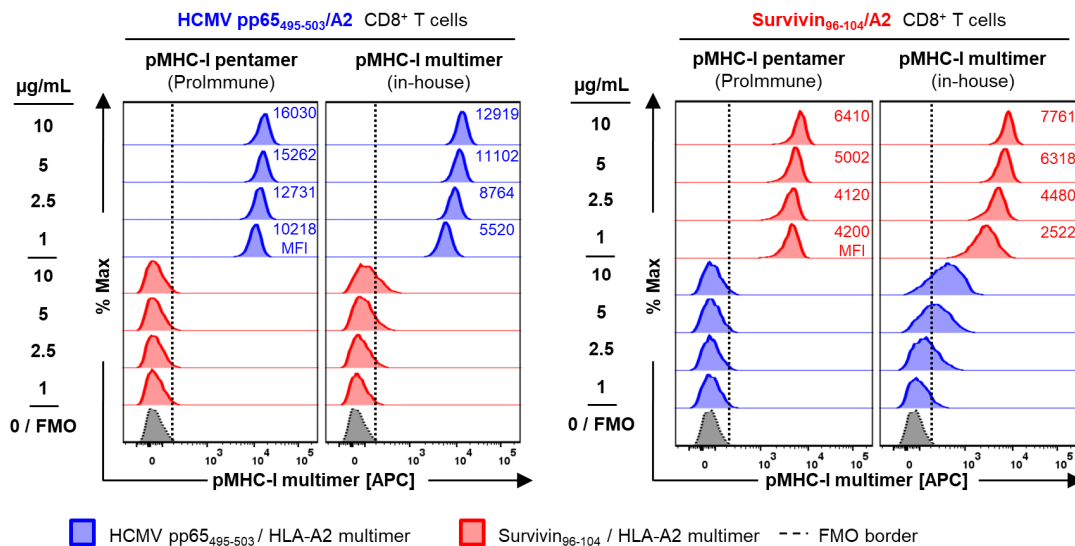


**Figure 3.9 | Unspecific binding of pMHC-I-pCC-Fc-based multimers at higher staining concentrations**

The HCMV pp65<sub>495-503</sub>/HLA-A2 CD8<sup>+</sup> T cell line #5561 (**right panel**) and the Survivin<sub>96-104</sub>/HLA-A2 specific CD8<sup>+</sup> T cell line (**left panel**) were stained in the presence of dasatinib [50 nM] with cognate and control pMHC-I-pCC-Fc-based multimer (in-house) as well as corresponding pMHC-I pentamers (ProImmune) at indicated concentrations followed by lineage marker staining. pMHC-I multimer signal of the CD8<sup>+</sup>/CD3<sup>+</sup> T cell population is shown. MFI: Median fluorescent intensity.

### 3.4 Production and validation of pMHC-I multimers based on *in vivo* biotinylated homodimeric dt-SCT fused to a cleavable Fc (\*Fc)

#### 3.4.1 Equal staining performance of pMHC-I multimers formed by monomeric dt-SCT produced as homodimer fused to a cleavable Fc compared to commercial pMHC-I pentamers

Previous results mentioned above have shown that heterodimeric pMHC-I-pCC-Fc constructs bearing a C-terminal AviTag could be successfully biotinylated in a site-specific manner and were overall well producible. However pMHC-I-pCC-Fc-based multimers lead to higher unspecific staining backgrounds (**Fig. 3.9**). Moreover, exchange of the immunogenic peptide at the DNA level within the T2A sequence-based heterodimeric pMHC-I-pCC-Fc construct (**Fig. 3.8a**) requires a higher cloning workload than for a molecular peptide exchange of the homodimeric pMHC-Fc constructs introduced in **Fig. 3.1a**.

Subsequently, we reasoned to design a novel optimized dt-SCT-Fc-based pMHC-I construct that bears the option for site-specific biotinylation as well as removal of the Fc portion post expression in order to gain monomeric biotinylated pMHC-I molecules that allow generation of pMHC-I multimers. Moreover, we kept the Fc-portion fused to the dt-SCT to still enable immobilization of pMHC-I-Fc molecules on anti-Fc mAb-conjugated beads using crude TGE cell supernatants and thus omitting the need of prior pMHC-I-Fc purification steps as discussed later in the second results part **Section 4.2 and 4.3.5**. The subsequently elaborated homodimeric pMHC-I (dt-SCT)-His<sub>8</sub>/AviTag\*mlgG2a-Fc construct shown in (**Fig. 3.10a**) distinguishes particularly through the placement of novel functional linker sequence between the C-terminus of the dt-SCT and N-terminus of the mlgG2a-Fc [Hinge-CH2-CH3] compared to the previous dt-SCT-Fc-STag construct (**Fig. 3.1a**). This novel linker sequence comprises a His<sub>8</sub>-tag for affinity chromatography followed by an AviTag sequence for site-specific biotinylation and two consecutive Fc-proximal thrombin cleavage-sites (\*) [LVPR<sup>↓</sup>SLVPR<sup>↓</sup>ST] allowing optional enzymatic cleavage of the mlgG2a-Fc domain from the dt-SCT domain post expression upon *in vitro* addition of thrombin.

The respective pHLA-A2-\*Fc constructs bearing the immunogenic peptide HCMV pp65<sub>495–503</sub> [Construct ID: 11097.1], Survivin<sub>96–104</sub> [11290.1], Flu MP<sub>58–66</sub> [11291.1] or EBV BMLF<sub>259–267</sub> [11292.1] were successfully cloned and subsequently transiently co-expressed with IgkL-BirA<sub>KDEL</sub> [8521.1] for site-specific *in vivo* biotinylation during protein expression. Moreover, we tested four different mammalian transient gene expression (TGE) systems in order to identify the most efficient TGE system for pHLA-A2-\*Fc production, which we will focus on in the next **Section 3.4.2** and **Fig. 3.11**, respectively. Furthermore, we reasoned to switch from column-based Ni-NTA-purification (used in **Section 3.3**) to His Mag Sepharose Excel (GE HealthCare)-based purifications, which allows convenient purification of multiple (i.e. >30) pHLA-A2-\*Fc mammalian TGEs using magnets designed for 96-well plates or various tubes. Notably, among the tested TGE systems particularly the FreeStyle 293-F cell-based TGE has been proven to be more efficient compared to the previously used CHO-S TGE system (**Fig. 3.11**). Thus, we focused for further intensive validation of pHLA-A2-\*Fc vector backbone using 293-F TGE system-based protein productions.

We reasoned that digestion of 293-F TGE supernatants of *in vivo* biotinylated pHLA-A2-\*Fc using an excess of thrombin units would allow direct purification of Fc-free monomeric pHLA-A2\* molecules. As shown by SDS-PAGE analysis, an expected ~160 kDa band representing the pHLA-A2-\*Fc homodimer is cleaved into ~55 kDa bands comprising the two cleaved pHLA-A2 monomers (pHLA-A2\*) and the remaining cleaved Fc portion (\*Fc) upon overnight incubation of the respective TGE 293-F supernatant with an excess of thrombin (**Fig. 3.10b**). Notably, the used FreeStyle 293-F cell medium apparently allowed for optimal thrombin cleavage since the manufacturer's (Novagen) recommended usage of 4.8x10<sup>-5</sup> thrombin units/pmol substrate (no excess of thrombin units) already led to a complete digestion of pHLA-A2-\*Fc molecules secreted into the 293-F supernatant (**Supplementary Fig. S3a**). Nevertheless, TGE supernatants were routinely incubated with a 5-fold excess of thrombin units to secure complete cleavage of pHLA-A2-\*Fc, which was calculated based on pHLA-A2-\*Fc-titers of the respective supernatants obtained by quantitative anti-IgG ELISA data. Thrombin-digested monomeric pHLA-A2\* molecules were subsequently successfully purified using His-tag-based affinity chromatography (i.e. magnetic His Mag Sepharose Excel). To confirm efficient *in vivo* biotinylation, streptavidin (SAv) was added at an equimolar ratio to the purified pHLA-A2\* followed by SDS-PAGE analysis, which resulted in an observed complete gel shift shown in **Fig. 3.10b**. Notably, upon addition of the non-covalently assembled tetrameric SAv (i.e. 4 x 13 kDa) to biotinylated pHLA-A2\* molecules (55 kDa) an expected ~ 107 kDa band (pHLA-A2\* + tetrameric SAv) becomes visible as well as an

additional ~80 kDa band, which may represent a dimer of two SA<sub>v</sub> chains (2x 13 kDa) bound by a biotinylated pHLA-A2\* molecule. Furthermore, the formation of multimers of higher valency based on monomeric pHLA-A2\* was additionally confirmed by NativePAGE analysis (**Supplementary Fig. S3b**). As an alternative to the cleavage of the Fc portion prior to purification of monomeric pHLA-A2\* molecules, also homodimeric pHLA-A2-\*Fc molecules were successfully His-tag-based purified and were efficiently cleaved by thrombin after the purification (**Supplementary Fig. S4a–b**).

As a next step, we evaluated the staining performance of pMHC-I multimers assembled on the basis of streptavidin-APC (SA<sub>v</sub>-APC) and purified monomeric pHLA-A2\* (pMHC-I\* multimers) in comparison to commercial corresponding pHLA-A2 pentamers (ProImmune). Subsequent staining of the HCMV/A2-specific CD8<sup>+</sup> T cell line #5561 with in-house produced pHLA-A2\* multimers indicated an overall equal brightness (MFI) as well as specificity of pMHC-I\* multimers and pMHC-I pentamers in general when used at the same concentration (**Fig. 3.10c**). Notably, no unspecific signal of control Survivin<sub>96-104</sub>/HLA-A2\* [11290.1] multimers was observed even at the highest analysed staining concentration of 10 µg/mL (**Fig. 3.10c**), which represented a strong improvement compared to the previously used pMHC-I-pCC-Fc construct design (**Fig. 3.9**). Interestingly, also in-house produced pMHC-I multimers using biotinylated homodimeric HCMV/A2-\*Fc [11097.1] molecules bound the HCMV/A2 CD8<sup>+</sup> T cell line #5561 in an antigen-specific manner and no unspecific binding of corresponding control Survivin/HLA-A2\*-Fc multimers was observed. Thus, the risk seems to be neglectable that (i) the staining background increases, (ii) uncontrolled MHC-multimer polymers or (iii) even aggregates are formed, if homodimeric constructs harboring two C-terminal biotinylated AviTag sequences are used for streptavidin-based MHC-multimer generation (**Supplementary Fig. S4c**).

As a final validation step, staining of two HLA-A2<sup>+</sup> healthy donors by virus epitope-specific pHLA-A2 multimers and corresponding commercial pHLA-A2 pentamers was performed (**Fig. 3.10d**). As hoped, in-house produced pHLA-A2\* multimers as well as pHLA-A2 pentamers detected very similar frequencies of cognate virus-specific T cell populations. However, the overall staining intensities (MFI) of the in-house produced pHLA-A2\* multimers were slightly lower compared to the corresponding pHLA-A2 pentamers.

In conclusion, the novel pHLA-A2-\*Fc vector combined with the already previously established *in vivo* biotinylation approach has been proven robust and reliable for large-scale as well as small-scale pHLA-A2 multimer generation.

### 3 | Results Part 1 – Production and validation of soluble pMHC-Fc proteins

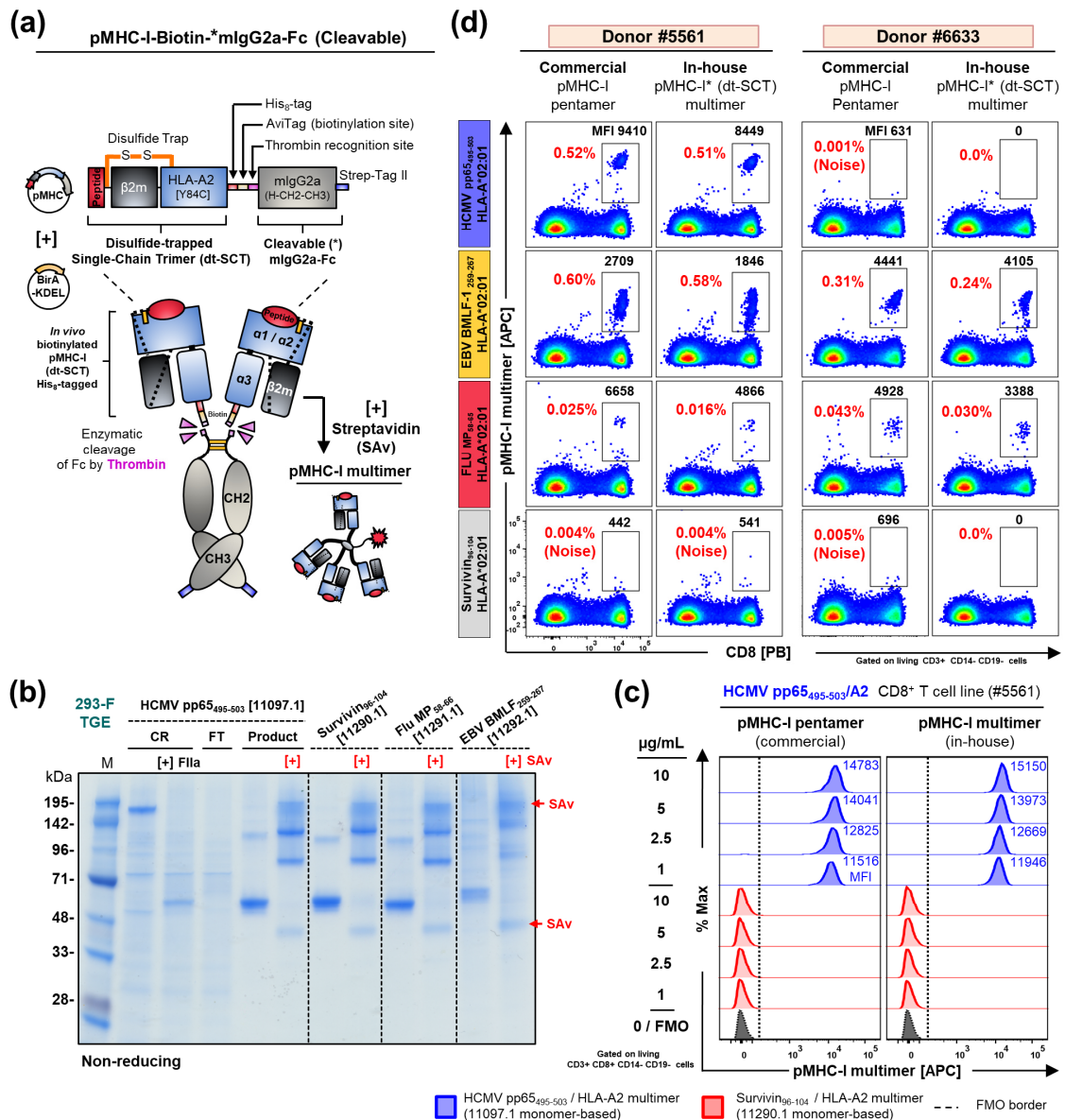


**Figure 3.10 | Successful production and validation of *in vivo* biotinylated monomeric pMHC-I fused to a cleavable Fc**

**(a) pMHC-I homodimeric construct with cleavable Fc region (pMHC-I-\*Fc)** consist of a single polypeptide chain, which comprises the pMHC-I complex as a disulfide-trapped single-chain-trimer (dt-SCT) fused to a His<sub>6</sub>-tag and AviTag for site specific biotinylation followed by two consecutive thrombin-cleavage sites (FIIa-CS). The FIIa-CS is C-terminal fused to the hinge (H) domain and CH2 and CH3 of mIgG2a (Fc) followed by a Strep-tag II. Optional co-expression with IgκL-BirA<sub>KDEL</sub> [8521.1] allows for site-specific *in vivo* biotinylation of the pMHC-I-\*Fc construct. The Fc can be optionally cleavage off by addition of thrombin (FIIa) to generate Fc-free monomeric pMHC-I (pMHC-I\*). Biotinylated pMHC-I\* can be multimerized by the addition of streptavidin (SAv).

**(b) Affinity chromatography of biotinylated representative monomeric pHLA-A2\*Fc constructs.** 293-F supernatants of 6 days transient gene expressions (TGE) of construct HCMV/HLA-A2\*Fc [11097.1], Survivin/HLA-A2\*Fc [11290.1], Flu/HLA-A2\*Fc [11291.1] and EBV/HLA-A2\*Fc [11292.1] were digested with an excess of FIIa units followed by His Mag Sepharose Excel (GE Healthcare)-based purification. Biotinylation of monomeric pHLA-A2\* were confirmed upon equimolar addition (SAv) prior to SDS-PAGE analysis leading to a gel shift. Shown is a 10% SDS-PAGE under non-reducing conditions after Coomassie staining. Arrows indicate unconjugated SAv. M: marker; CR: crude; FT: Flow-through.

**(c) Antigen-specific staining of a cognate T cell line by pMHC-I\*-based multimers.** The HCMV pp65<sub>495-503</sub>/HLA-A2 CD8<sup>+</sup> T cell line #5561 was stained in the presence of dasatinib [50 nM] with indicated pHLA-A2\*-based multimers (own) as well as corresponding commercial pHLA-A2 pentamers (ProImmune) at indicated concentrations. pMHC-I multimer signal of the CD8<sup>+</sup> / CD3<sup>+</sup> T cell population is shown.

**(d) Reliable detection of virus-specific T cell populations within PBMC by in-house pMHC-I\*-based multimers.** PBMC of cryopreserved HLA-A2<sup>+</sup> healthy donors #5561 and #6633 were analyzed by indicated pHLA-A2\*-based multimers (own) and pHLA-A2 pentamers (ProImmune) both used at 10 µg/mL. The frequency and MFI of multimer<sup>+</sup> cells within the CD3<sup>+</sup> T cell population is shown. FMO: Fluorescence-minus-one background control; MFI: Median fluorescence intensity.

### 3.4.2 Comparison of four HEK- and CHO-based TGE systems for the production of dt-pMHC-I-\*Fc molecules

In order to identify the most efficient TGE system for our pHLA-A2-\*Fc constructs introduced in the previous **Section 3.4.1**, we co-expressed HCMV pp65<sub>495-503</sub>/A2-\*Fc [11097.1], Survivin<sub>96-104</sub>/A2-\*Fc [11290.1], Flu MP<sub>58-66</sub>/A2-\*Fc [11291.1] or EBV BMLF<sub>259-267</sub>/A2-\*Fc [11292.1] together with IgκL-BirA<sub>KDEL</sub> [8521.1] in four different mammalian transient gene expression (TGE) systems. These systems include: (i) the previously used CHO-S/PEI/ProCHO-4 system (CHO-S TGE system), (ii) FreeStyle 293-F cells transfected by the 293-Free transfection reagent (Novagen) and cultured in FreeStyle 293-Expression Medium (Thermo Scientific) (293-F TGE system) as well as the kit-based TGE (iii) ExpiCHO-S system as well as (vi) Expi293-F system (both Thermo Scientific). All pHLA-A2-\*Fc constructs were successfully expressed by all four TGE systems as initially indicated by quantitative anti-mIgG ELISA (**data not shown**). Further, an expected ~55 kDa band was observed by SDS-PAGE analysis representing the two cleaved pHLA-A2 monomers (pHLA-A2\*) and the remaining cleaved Fc portion (\*Fc) upon overnight incubation of all TGE supernatants with an excess of thrombin units (FIIa) indicating that all used culture media support thrombin activity (**Fig. 3.11a**). In the next step, non-saturating amounts of TGE supernatants were subjected to His Mag Sepharose Excel (GE HealthCare)-based purification. In all but the used CHO-S TGE system a >90% pure ~55 kDa product band appeared, whereas CHO-S TGE system-derived elution fractions typically contained several high molecular weight by-products (**Fig. 3.11a**). To confirm successful *in vivo* biotinylation, streptavidin (SAv) was added at an equimolar ratio to purified monomeric pHLA-A2\* molecules followed by SDS-PAGE analysis. As a result, we observed an incomplete gel-shift (<50%) in case of both CHO cell-based TGE systems but a complete gel-shift (>95%) if the 293-F or Expi293-F TGE system were used instead. These result indicated that under the conditions used both CHO-S and in particular the ExpiCHO-S TGE systems only bear a moderate to low *in vivo* biotinylation efficiency, whereas both 293-F and Expi293-F systems lead to a consistent complete biotinylation (**Fig. 3.11a**). Moreover, this higher biotinylation efficiency of the 293-based TGE systems may be the cause for the observed slightly higher staining brightness when corresponding purified pHLA-A2\* molecules were used for pHLA-A2 multimer generation compared to CHO-based pHLA-A2\* multimer (**Fig. 3.11d**). In terms of production efficiencies the CHO-S system lead to an average final yield of purified pHLA-A2\* of 11 µg/mL culture volume, followed by the 293-F system with 25 µg/mL and both ExpiCHO-S and Expi293-F system with 44 µg/mL among all tested pHLA-A2-\*Fc constructs (**Fig. 3.11b and Supplementary Table S1**). Interestingly, all four TGE system share quite similar costs for reagents required for the theoretical expression of 100 µg monomeric dt-SCT-based pHLA-A2\* (**Fig. 3.11c**) and are therefore quite similar in terms of cost efficiency. Nevertheless, because of the higher *in vivo* biotinylation efficiency as well as overall slightly higher product purity after His Mag Sepharose Excel (GE HealthCare)-based purification, both 293-F as well as Expi293-F are more favorable for the production of the pHLA-A2-\*Fc constructs than the previous used CHO-S system.

Notably, we also successfully produced various monomeric dt-SCT-based pHLA-A2 constructs lacking the Fc domain (**Supplementary Fig. S5a-b**). Using the 293-F TGE system combined with His Mag Sepharose Excel-based purification, we achieved production efficiencies of 11–23 µg yield /mL culture volume across the tested constructs (**Supplementary Table S4**). Most importantly, in-house produced pHLA-A2 multimers performed equally independently if they were generated based on *in vivo* biotinylated pHLA-A2 molecules lacking the Fc-fusion already during the expression or on pHLA-A2-\*Fc homodimers that were subsequently purified as monomeric pHLA-A2\* upon thrombin-mediated Fc cleavage (**Supplementary Fig. S5c**).

### 3| Results Part 1 – Production and validation of soluble pMHC-Fc proteins

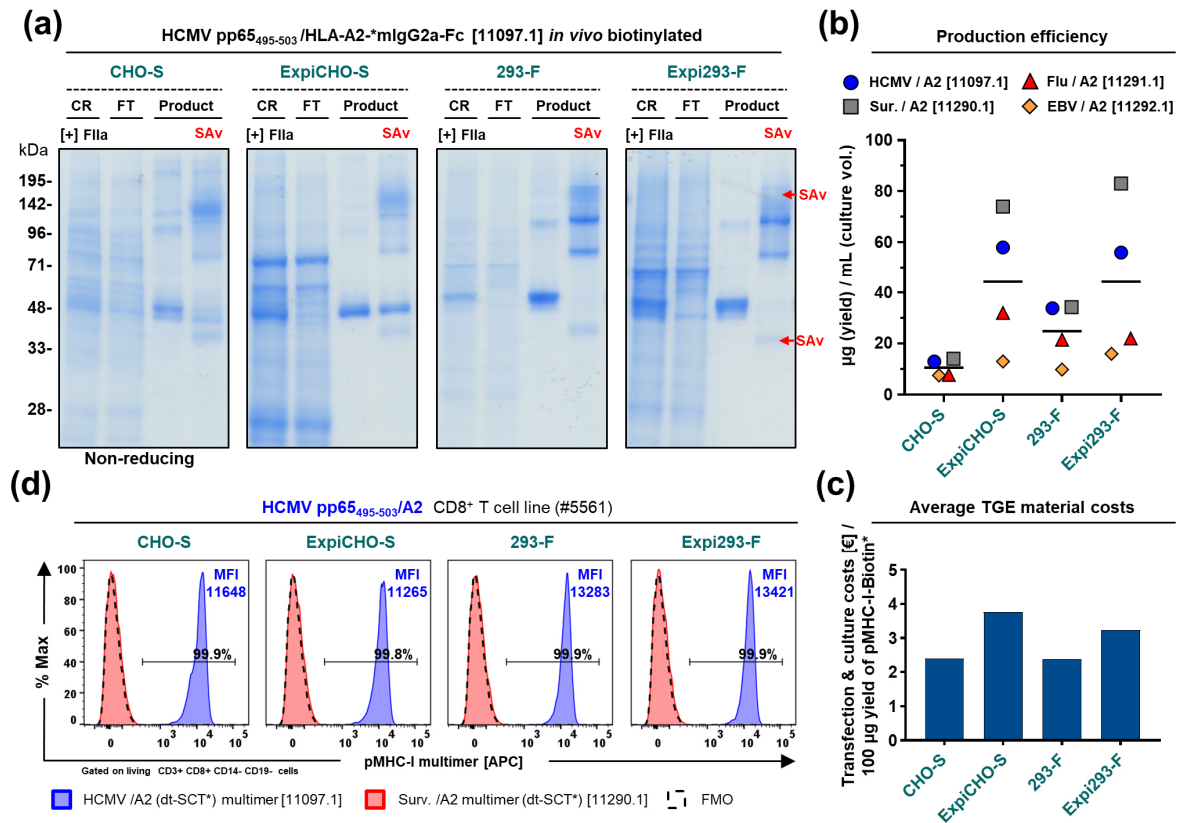


**Figure 3.11 | Comparison of different transient expression systems (TGE) for the production of *in vivo* biotinylated pMHC-I\*Fc molecules**

Homodimeric HCMV/HLA-A2-\*Fc [11097.1], Survivin/HLA-A2-\*Fc [11290.1], Flu/HLA-A2-\*Fc [11291.1] and EBV/HLA-A2-\*Fc [11292.1] constructs were transiently co-expressed with IgκL-Bir<sub>A</sub>K<sub>DEL</sub> [8521.1] by four eukaryotic protein production systems comprising: (i) PEI-based transfected FreeStyle CHO-S cells (CHO-S) cultured in ProCHO-4 medium (Lonza) in the presence of VPA under hypothermic conditions, (ii) FreeStyle 293-F cells (293-F) cultured in FreeStyle 293-Expression Medium (Thermo Scientific) transfected with 293-Free transfection reagent (Novagen) and (iii) the ExpiCHO-S as well as (iv) the Expi293-F (both Thermo Scientific) complete TGE systems. All culture media were additionally supplemented with 4 µg/mL D-biotin prior to cell transfection. CHO-S, 293-F, Expi293-F supernatants were harvested after 6 days culture and supernatants of ExpiCHO-S after 9 days upon transfection, respectively. mIgG titers of each TGE were assessed by α-mIgG sandwich ELISA prior to affinity chromatography (data not shown).

**(a) Affinity chromatography of biotinylated monomeric pMHC-I\* produced by various TGE systems.** TGE supernatants (CR) were digested with an excess of thrombin (Fila) overnight at 37°C followed by His Mag Sepharose Excel (GE Healthcare)-based purification. The used volume of supernatant was limited to ~50–150 µg protein of interest to avoid complete resin binding saturation. The degree of biotinylation was confirmed by equimolar addition of streptavidin (SAV) prior to SDS-PAGE analysis. SDS-PAGE of the 293-F-based production of 11097.1 is an excerpt from **Fig. 3.10b**.

**(b) Production efficiency of various pHLA-A2-\*Fc constructs based on the used TGE systems.** Values were calculated using the yield of final purified protein divided by the used supernatant volume (culture vol.). Additional culture volume dilutions caused by the addition of medium supplements during the culturing of the ExpiCHO and Expi293 TGE system were considered for the calculation of the final production efficiency. Horizontal bars indicate the mean production efficiency across all four produced and cleaved pHLA-A2-\*Fc constructs.

**(c) Average TGE material cost per 100 µg yield of biotinylated pMHC-I\*.** Shown values were calculated based on the mean production efficiencies displayed in (b) as well as material costs for all TGE-related reagents for each TGE system including plasmid DNA, cell culture media and transfection reagents based on respective reagent pricing valid on January 14<sup>th</sup> 2020 (including German sales taxes).

**(d) Overall similar performance of pMHC-I multimers based on monomeric pMHC-I\* derived from different TGE systems.** pMHC-I multimers were generated on the basis of SAV-APC as well as digested and purified monomeric HCMV/HLA-A2\* [11097.1] or Survivin/HLA-A2\* [11290.1] derived from transient CHO-S, ExpiCHO-S, 293-F and Expi293-F expressions. HCMV/HLA-A2 specific CD8<sup>+</sup> T cell line #5561 was stained with pMHC-I multimer [2.5 µg/mL] in the presence of 50 nM dasatinib. pMHC-I multimer signal of the CD8<sup>+</sup> / CD3<sup>+</sup> T cell population is shown. FMO: Fluorescence-minus-one background control; FT: Flow-through; MFI: Median fluorescent intensity.

### 3.5 Usage of immobilized pMHC-I-Fc to drive antigen-specific T cell proliferation

An overall low frequency of neoantigen-specific T cells combined with the low availability of patient material often requires an expansion step of the desired T cell population prior to their experimental discovery and their clinical utilization (132). For this purpose, the entire T cell pool is often expanded in a polyclonal and antigen-independent manner for instance by usage of  $\alpha$ CD3,  $\alpha$ CD28 and  $\alpha$ CD2 mAb-coated microbeads (286). Alternatively, T cells might be antigen-specifically expanded by taking advantage of minimal- (294) or long-peptide (152) pulses in the presence of cellular APCs or aAPCs might be genetically modified to express the antigen-of-choice using tandem-minigenes or stabilized mRNAs (85, 153). Since the latter approaches are quite labor-intensive and costly, we were interested if our pMHC-I-Fc proteins could also directly be used for the antigen-specific expansion of a desired T cell population in parallel to their usage as tool to detect and monitor antigen-specific T cells.

Thus, HCMV pp65<sub>495-503</sub>/HLA-A2-Fc-STag [8558.1] (HCMV/A2-Fc) or irrelevant control pMHC-I-Fc [8556.1] were immobilized together with co-stimulatory acting  $\alpha$ CD28 mAb (clone 15E8) and  $\alpha$ CD2 mAb (clone RPA-2.10) on a flat-bottom plate with a high-protein binding capacity (MaxiSorp™, Nunc) (**Fig. 3.12a**). Alternatively, polyclonal activating  $\alpha$ CD3 mAb (clone OKT3) or isotype control mAb were coated together with the aforementioned co-stimulatory mAbs. Next, cells from CellTrace™ Violet-labeled (CTV) HCMV pp65<sub>495-503</sub>/HLA-A2 CD8<sup>+</sup> T cell line #5561 were cultured for 6 days on the coated wells in the presence of IL-2, IL-7 and IL-15 prior to analysis of the absolute fold-expansion (assessed by counting-reference beads), relative proliferation (CTV-staining) and overall activation (CD25 expression). As shown in **Fig. 3.12a**, HCMV/A2-Fc as well as  $\alpha$ CD3 mAb coated-wells drove an approximate 10-fold expansion (*upper panel*) of the HCMV/A2 T cell line #5561 after 6-days of culture to a similarly extent, whereas immobilized control pMHC-I-Fc or as mIgG2a-isotype control in addition to co-stimulatory mAbs did not affect the T cell culture as expected. Moreover, 98% of the cells had proliferated and displayed an activated (CD25<sup>+</sup>) phenotype (**Fig. 3.12a**, *lower panels*). We concluded that plate-immobilized pMHC-I-Fc had a strong capacity to drive antigen-specific T cell proliferation, which is in a similar range as polyclonal activation based on a  $\alpha$ CD3 mAb.

As an alternative to pMHC-I-Fc plate-based immobilization, we also tested a selection of different microbeads coated with pMHC-I-Fc and co-stimulatory mAbs to drive antigen-specific proliferation. Although, successful antigen-specific T cell expansion has been previously described on the basis of pMHC-I-coated M450 (4.5  $\mu$ m) (218) as well as M270 (2.8  $\mu$ m) Dynabeads (Invitrogen) (295), we failed to induce efficient T cell expansion based on the aforementioned beads conjugated with our pMHC-I-Fc constructs. In contrast, we rather observed a steady-state of proliferating and dying cells caused most likely by activation-induced cell death (AICD) (**data not shown**). Therefore, we took advantage of the  $\alpha$ -biotin mAb-conjugated MACSiBeads derived from Miltenyi's "Human T Cell Activation/Expansion Kit", which have been exclusively developed for T cell expansion rather than isolation. MACSiBeads were conjugated with our biotinylated HCMV/A2-pCC-Fc-Biotin [10347.7] or Sur/A2-pCC-Fc-Biotin [9237.1] constructs together with provided biotinylated  $\alpha$ CD28 mAb and  $\alpha$ CD2 mAb but replacing the provided biotinylated  $\alpha$ CD3 mAb (all from Miltenyi) (**Fig. 3.12b**). Upon 6-days co-culture at a 1:1 bead-to-cell ratio, we observed an antigen-specific 9-fold absolute expansion of the HCMV/A2 CD8<sup>+</sup> T cell line #5561 when cultured with HCMV/A2-Fc coated MACSiBeads compared to a 4-fold expansion with polyclonal activating  $\alpha$ CD3-coated MACSiBeads. Although not experimentally shown, this might indicate that the  $\alpha$ CD3-coated MACSiBeads partially induced AICD, thereby spoiling the net expansion of the T cell line. This is supported by the comparable relative activation (CD25 expression) and proliferation of the HCMV/A2 CD8<sup>+</sup> T cell line #5561 upon co-culture with HCMV/A2-Fc or  $\alpha$ CD3-

### 3 | Results Part 1 – Production and validation of soluble pMHC-Fc proteins

coated-MACSiBeads ruling out an overall reduced activation-capacity of  $\alpha$ CD3-coated-MACSiBeads (Fig. 3.12b).

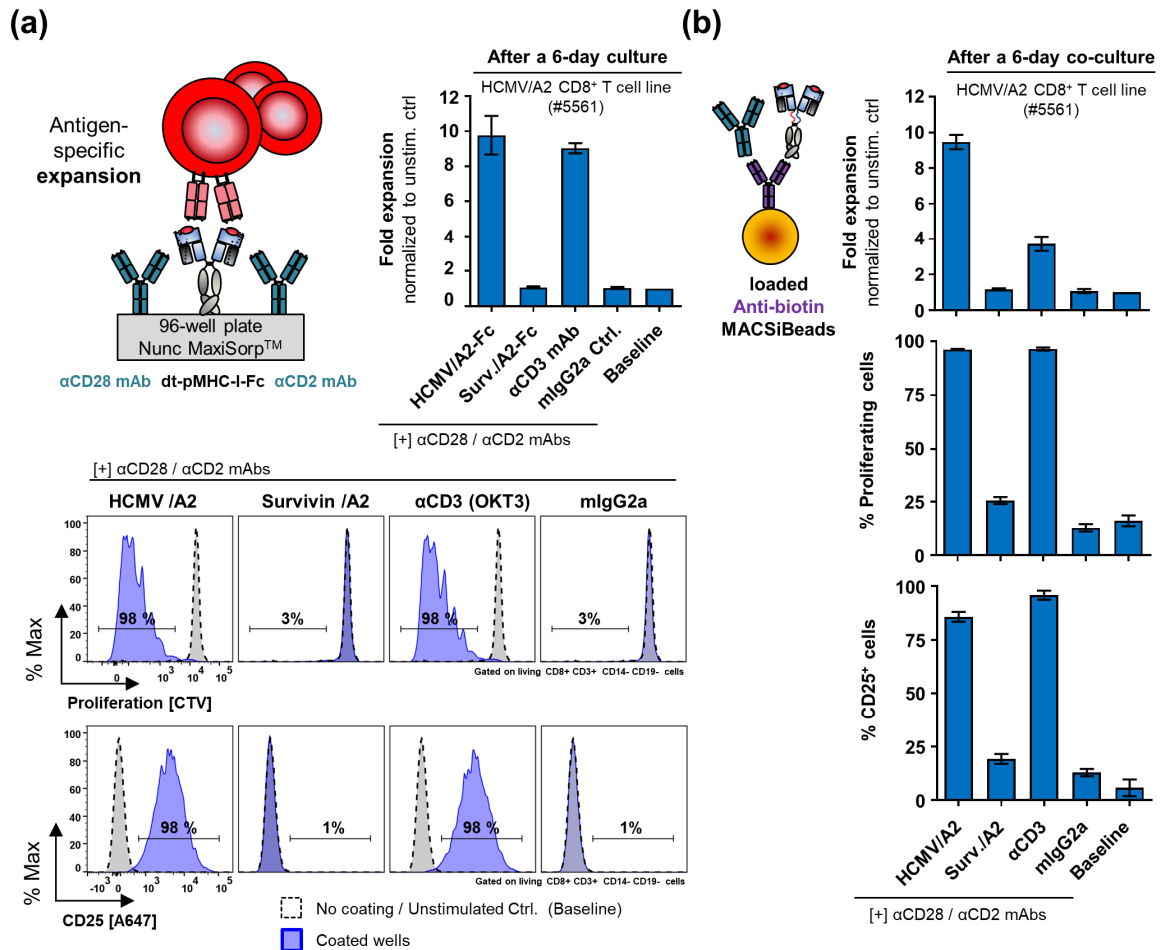


**Figure 3.12 | Induction of antigen-specific proliferation based on plate- and bead-immobilized pMHC-I-Fc**

**(a) Culture of HCMV pp65<sub>495-503</sub>/HLA-A2 CD8<sup>+</sup> T cell line #5561 (HCMV/A2 TC#5561) on plate-bound pHLA-A2-Fc.**

96-well MaxiSorp™ flat-bottom plates (Nunc) were coated at 0.5  $\mu$ g/mL with HCMV pp65<sub>495-503</sub>/HLA-A2-Fc [8558.1] (HCMV/A2-Fc), Survivin<sub>96-104</sub>/HLA-A2-Fc [8556.1] (Sur/A2-Fc),  $\alpha$ CD3 mAb (clone OKT3) or mlgG2a control together with  $\alpha$ CD28 mAb (clone 15E8) and  $\alpha$ CD2 mAb (clone RPA-2.10) at an equimolar ratio.  $5 \times 10^4$  cells/well of CellTrace Violet-labeled (CTV) HCMV/A2 TC#5561 were seeded in triplicates into coated wells and cultured for 6 days prior to analysis. (Upper panel) Calculated absolute fold-expansion of HCMV/A2 TC#5561 normalized to unstimulated control (baseline) is shown. Absolute cell counts were determined based on counting beads (BioLegend). (Lower panel) Percent of proliferating (CTV<sup>dim</sup>) and CD25 expressing CD8<sup>+</sup> CD3<sup>+</sup> T cells is shown. Error bars indicate standard deviations.

**(b) Co-culture of HCMV/A2 TC#5561 with MACSiBead-based aAPCs.** Artificial antigen-presenting cells (aAPC) were assembled based on anti-biotin MACSiBeads (Miltenyi) loaded with biotinylated HCMV/A2-pCC-Fc [10347.7], Sur/A2-pCC-Fc [9237.1], or biotinylated  $\alpha$ CD3 mAb (Miltenyi) or mlgG2a isotype control (BioLegend) together with biotinylated  $\alpha$ CD28 mAb (Miltenyi) and  $\alpha$ CD2 mAb (Miltenyi).  $5 \times 10^4$  cells/well CTV-labeled HCMV/A2 TC#5561 were seeded in triplicates together  $5 \times 10^4$  aAPC into 96-well U-bottom plates and co-cultured for 6 days prior to analysis. Shown is the absolute fold-expansion, percent proliferating cells as well as percent CD25<sup>+</sup> cells of the CD8<sup>+</sup> CD3<sup>+</sup> T cell population.

As a next step, we aimed for the direct *ex vivo* expansion of HCMV/A2-specific CD8<sup>+</sup> T cells present in HLA-A2<sup>+</sup> healthy donor #0988, which was previously confirmed by a corresponding pMHC-I multimer staining (data not shown). Subsequently, healthy donor #0988-derived isolated CD8<sup>+</sup> T cells were co-cultured with MACSiBeads conjugated with Fc-cleaved monomeric biotinylated HCMV/HLA-A2\* [11097.1] or Survivin/A2\* [11290.1] molecules and biotinylated  $\alpha$ CD28 mAb and  $\alpha$ CD2 mAb. During a 7-day co-culture, only cognate HCMV/A2-conjugated aAPCs induced an antigen-specific proliferation of the HCMV/A2-specific CD8<sup>+</sup> T cell population as indicated by (i) an increased frequency of the respective population, (ii) its CTV-signal reduction as well as (iii) by a measured absolute 10-fold

cell expansion of this population (**Fig. 3.13**). In conclusion, immobilization of biotinylated pMHC-Fc as well as monomeric pMHC-I constructs in combination with co-stimulatory mAbs on MACSiBeads drove antigen-specific T cell expansion.

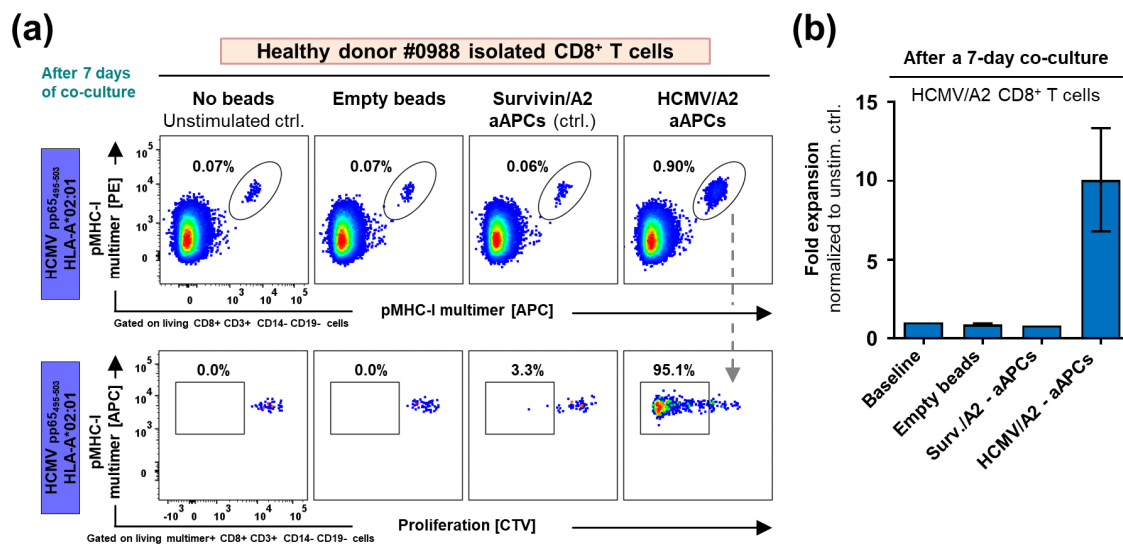


**Figure 3.13 | Direct *ex vivo* expansion of healthy donor-derived HCMV/A2-specific CD8<sup>+</sup> T cells by cognate aAPCs**

**(a)** Co-culture of *ex vivo* healthy donor #0988 derived CD8<sup>+</sup> T cells with MACSiBead-based aAPCs for 7 days. Artificial antigen-presenting cells (aAPC) were assembled based on anti-biotin MACSiBeads (Miltenyi) loaded with monomeric biotinylated (Fc-free) HCMV/A2\* [11097.1] or Survivin/A2\* [11290.1] together with biotinylated  $\alpha$ CD28 mAb and  $\alpha$ CD2 mAb (both Miltenyi) or left empty. Isolated untouched healthy donor #0988-derived CD8<sup>+</sup> T cells were CellTrace Violet-labeled (CTV) and subsequently co-cultured for 7 days in triplicates in a 1:1 ratio with aAPCs seeded into 96-well U-bottom plates. (**Upper panel**) Co-staining of a representative 7 day co-culture with in-house produced HCMV/A2-multimers generated with streptavidin-APC or streptavidin-PE as well as monomeric biotinylated HCMV/A2\* [11097.1]. Frequencies of double pMHC-I multimer<sup>+</sup> cells within the CD8<sup>+</sup> T cell population are shown. (**Lower panel**) Representative FACS-plot showing the percent of proliferating (CTV<sup>dim</sup>) multimer<sup>+</sup> CD8<sup>+</sup> T cells. **(b)** Corresponding absolute fold-expansion of HCMV/A2-specific CD8<sup>+</sup> T cells after 7 days of aAPC co-culture. Absolute cell count was determined based on counting beads (BioLegend) and normalized to the unstimulated control (baseline). Error bars indicate standard deviations.

### 3.6 Establishment of soluble pMHC-II-pCC-Fc production and their validation

#### 3.6.1 Antigen-specific stimulation of bead-immobilized pHLA-DR3-pCC-Fc molecules

A major technical challenge in the immune monitoring field remains the assessment of antigen-specific CD4<sup>+</sup> T cell responses, since production of soluble peptide-loaded MHC-II (pMHC-II) complexes has been notoriously difficult and antigen-specific CD4<sup>+</sup> T cell populations generally occur at lower frequencies compared to the CD8<sup>+</sup> T cell compartment (156, 184, 204). To address and partially overcome this issue, we also wanted to gain the ability to detect antigen-specific CD4<sup>+</sup> T cell responses based on own soluble pMHC-II-Fc constructs. For the heterodimeric soluble pMHC-II-pCC-Fc construct design depicted and explained in **Fig. 3.14a**, we took again advantage of the amphiphilic basic/acidic parallel coiled-coil heterodimerization domain (pCC) (257) fused to a mIgG2a-Fc (pCC-Fc) followed by a single AviTag<sup>TM</sup>, His<sub>6</sub>-tag and optional Strep-tag II sequence. Moreover, we cloned the pMHC-II-pCC-Fc either as a single-vector or a two-vector construct (**Section 2.2.2**). The single vector comprises the entire pMHC-II-pCC-Fc via T2A-sequence-based fusion of peptide-ligand associated MHC-II  $\beta$ -chain-pCC-Fc and MHC-II  $\alpha$ -chain-pCC-Fc. The two-vector construct requires co-transfection encoding individually either for the pMHC-II  $\beta$ -chain-pCC-Fc or MHC-II  $\alpha$ -chain-pCC-Fc. Similar two-vector peptide tethered MHC-II constructs without Fc-fusion have been described previously (221).

Due to the availability of the cognate antigen-specific CD4<sup>+</sup> T cell clone RP15.1.1, we designed a corresponding pMHC-II-pCC-Fc construct [9260.3] presenting the Mycobacterium tuberculosis (MTB) heat shock protein 65 kDa (Hsp65) antigen derived epitope MTB Hsp65<sub>1-13</sub> in a HLA-DRB1\*03:01/HLA-DRA\*01:01 (HLA-DR3) context (254, 255). The resulting MTB/DR3-pCC-Fc construct was successfully expressed and correctly folded as shown by intracellular staining of transfected CHO-S by the conformation depend anti-pan-HLA-DR mAb L243 (296) (**Fig. 3.14b**). SDS-PAGE analysis of the final products upon Strep-Tactin-based affinity chromatography revealed an apparent molecular weight of ~ 120 kDa for the non-reduced heterodimer and ~ 73 / 66 kDa for the reduced monomers. This was overall in accordance with the theoretical molecular weight of ~59 kDa for the pCC-Fc-fused pHLA-DR β-chain and 56 kDa for the corresponding α-chain leading to heterodimer of ~115 kDa in size (**Fig. 3.14c**). The slightly slower migration on the SDS-PAGE might be consequence of the introduced highly charged pCC-domains and tag-sequences. Moreover, additional bands appear at >200 kDa similar to the already discussed pMHC-I-pCC-Fc, which suggest that also the pMHC-II-pCC-Fc have a tendency to form non-covalently associated multimers. Next, we confirmed the stimulation-capacity of the purified MTB/DR3-pCC-Fc construct used for assembly of bead-based artificial antigen-presenting cells (aAPCs) (**Fig. 3.14d**). To this end MTB/DR3-pCC-Fc or control pMHC-II-pCC-Fc (HCMV pp65<sub>510-522</sub>/HLA-DR3, (278) , [10320.1]) were immobilized on goat-anti-mouse-IgG (GαM-IgG) Dynabeads (4.5 μm) and brought in co-culture at a 2:1 ratio with the MTB/DR3-specific CD4<sup>+</sup> T cell clone RP15.1.1. In addition, T2 cells stable expressing HLA-DR3 (T2.DR3.DM) (251) were pulsed with corresponding MTB Hsp65<sub>1-13</sub> peptide or HCMV pp65<sub>510-522</sub> control peptide and served as cellular aAPCs. Upon co-culture MTB-peptide-loaded T2.DR3.DM as well as MTB/HLA-DR3-pCC-Fc-loaded Dynabeads stimulated the RP15.1.1 clone to a similar extent in antigen-specific manner resulting in IFN-γ as well as TNF-α expression. However, peptide-pulsed T2.DR3.DM aAPCs led to an overall superior stimulation quality manifested by a higher MFI of the TNF-α and IFN-γ expression and higher frequency of IFN-γ-expressing cells (**Fig. 3.14d**). Nevertheless, the established recombinant pMHC-II-pCC-Fc constructs proved to be reliably expressed by CHO-S cells and was successfully validated functionally for a selected T cell specificity.

#### 3.6.2 Antigen-specific binding of *in vivo* biotinylated pHLA-DR3-pCC-Fc-based multimers

As next step, our peptide tethered MTB Hsp65<sub>1-13</sub>/HLA-DR3-pCC-Fc (MTB/DR3-pCC-Fc) [9260.3] as well as CLIP<sub>103-117</sub>/HLA-DR3-pCC-Fc (CLIP/DR3-pCC-Fc) [9261.3] constructs were co-expressed with IgκL-BirA<sub>KDEL</sub> [8521.1] for site-specific *in vivo* biotinylation during the transient expression in CHO-S (**Fig. 3.15a**). After subsequent Ni-NTA-based affinity chromatography (data not shown), we could again confirm a very high biotinylation efficiency shown by complete “gel-shift” upon addition of streptavidin (SAv) at a 1:4 (SAv / MHC) molar ratio. However, similar to the already described heterodimeric pMHC-I-pCC-Fc constructs (**Fig. 3.8c**), we also observed the formation of heterogeneous pMHC-II multimers with valencies mostly between 2 to 4 of associated pMHC-II-pCC-Fc molecules (**Fig. 3.15b**). Next, we compared the staining performance of our monomeric MTB/DR3-pCC-Fc [9260.3] and CLIP/DR3-pCC-Fc [9261.3] in comparison to corresponding commercial *in vitro* peptide-loaded pMHC-II monomers (ProImmune) upon multimerization by addition of streptavidin-APC. As show in **Fig. 3.15c**, commercial as well as our in-house preduced pMHC-II multimers bound specifically to the cognate MTB/DR3-specific CD4<sup>+</sup> T cell clone RP15.1.1. However, our pMHC-II multimer outperformed the commercial pMHC-II multimer in terms of brightness (MFI) when used at the same concentration (20 μg/mL). Although a direct explanation at this point remains elusive, it has been shown that peptide loading *in vitro* of empty MHC-II monomers prior to multimerization may be incomplete and inefficient and thus account for the reduced staining performances (184, 204, 234). In conclusion, our multimerized MHC-

II-pCC-Fc constructs with tethered-peptide bound antigen-specifically and apparently with a high avidity to cognate antigen-specific T cells resulting in an overall high staining performance.

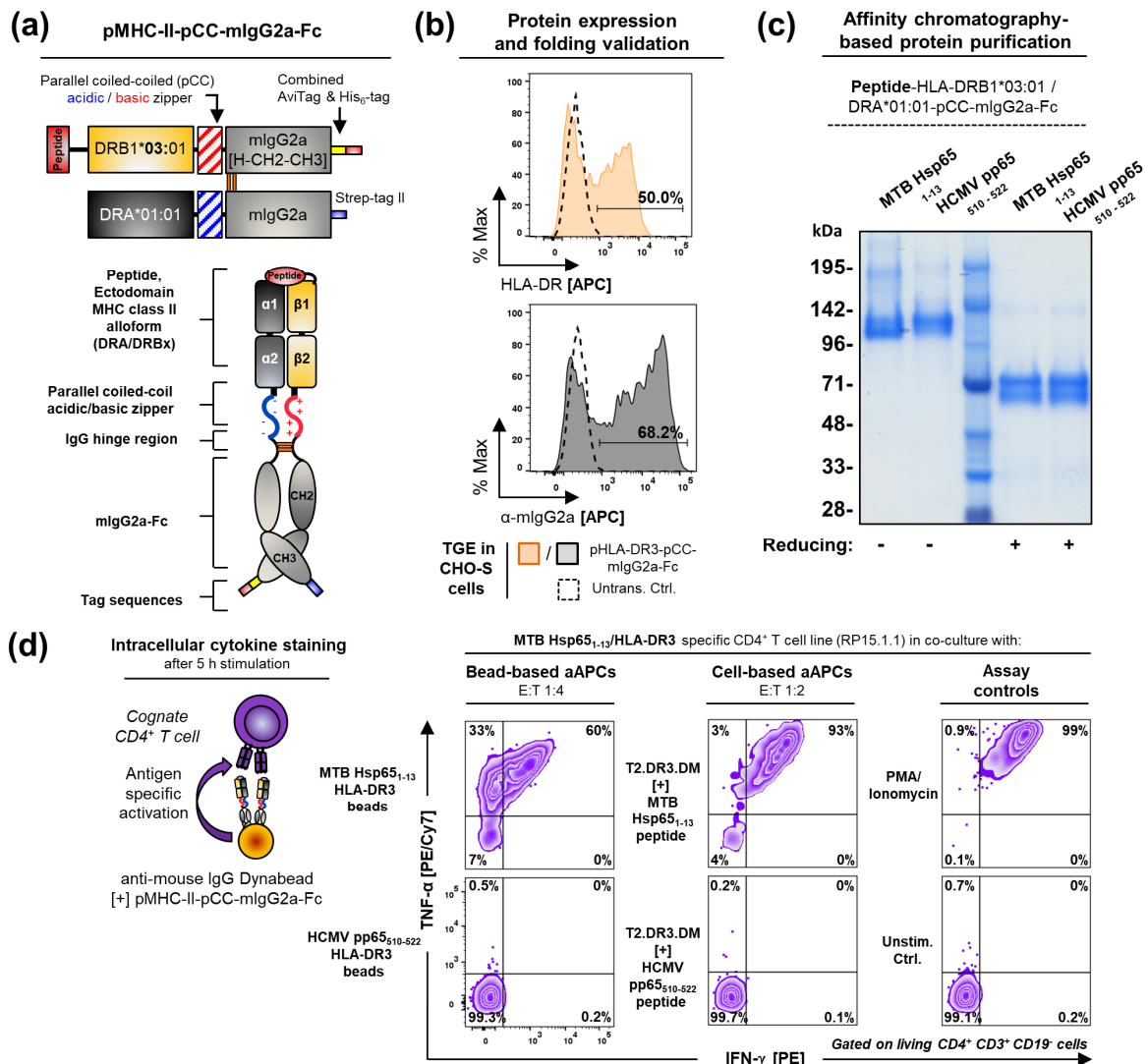


**Figure 3.14 | Successful production and antigen-specific stimulation of bead-immobilized pMHC-II-pCC-Fc molecules**

**(a) Peptide-MHC class II (pMHC-II) monomer pCC-mIgG2a-Fc fusion constructs** consist of two separate polypeptide chains. The MHC-II  $\beta$ -chain is N-terminally fused with an antigenic peptide via a flexible glycine-serine linker. The C-terminus of the  $\beta$ -chain ectodomain ( $\beta$ 1- $\beta$ 2) is fused to a parallel coiled-coil (pCC) basic zipper followed by the hinge (H) domain and CH2 and CH3 of mIgG2a (Fc) and a C-terminal His<sub>6</sub>-tag and AviTag for site-specific biotinylation. The ectodomain of the  $\alpha$ -chain ( $\alpha$ 1- $\alpha$ 2) is C-terminally fused to a complementary acidic pCC-Fc and a C-terminal Strep-tag II.

**(b) Validation of pHLA-DR3-pCC-Fc expression and structural conformation.** MTB Hsp65<sub>1-13</sub>/HLA-DRB1\*03:01/DRA\*01 (MTB/DR3)-pCC-Fc [9260.3] expressing CHO-S cells were intracellularly stained either with  $\alpha$ -pan-HLA-DR mAb (clone L243) [orange] or with  $\alpha$ -mIgG2a-Fc mAb (clone RMG2a-62) [grey] 3 days after transfection.

**(c) pHLA-DR3-pCC-Fc affinity chromatography.** CHO-S supernatant of 6 days transient pHLA-DR3-pCC-Fc expression was purified at pH 7.4 using Strep-Tactin resin filled columns. 10% SDS-PAGE under non-reducing and reducing conditions.

**(d) Validation of MTB/DR3-pCC-Fc specificity and bead-bound stimulatory capacity using a cognate CD4<sup>+</sup> T cell clone.** Result of a 5 h co-culture of the MTB/DR3-specific CD4<sup>+</sup> T cell clone RP15.1.1 with bead- or cell-based aAPCs. GaM IgG-Dynabeads (M450) previously loaded with MTB/DR3-Fc [9260.3] or HCMV pp65<sub>510-522</sub>/HLA-DR3 (CMV/DR3-Fc) [10320.1] were used as bead-based aAPCs. HLA-DR3 and HLA-DM expressing T2 cells (T2.DR3.DM) were pulsed overnight with 10  $\mu$ M MTB Hsp65<sub>1-13</sub> peptide or HCMV pp65<sub>510-522</sub> (control) and used as cellular aAPCs. Stimulation of the MTB/DR3 CD4<sup>+</sup> T cell clone is shown by induction of TNF- $\alpha$  and IFN- $\gamma$  expression analyzed by intracellular staining after lineage marker staining. aAPC: artificial antigen-presenting cells

### 3 | Results Part 1 – Production and validation of soluble pMHC-Fc proteins

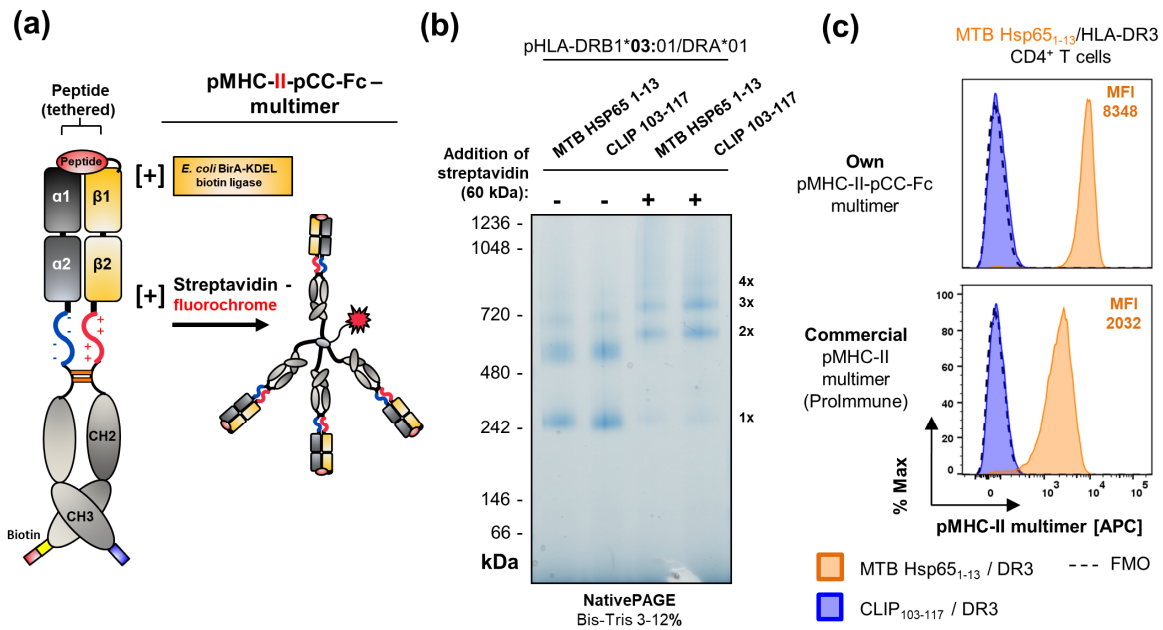


**Figure 3.15 | Antigen-specific and superior binding of tethered-peptide associated MHC-II-pCC-Fc multimers**

(a) **Generation of pMHC-II-Fc multimers.** Monovalent heterodimeric tethered peptide-MHC-II-pCC-Fc constructs as described in Fig. 3.14 were co-transfected with BirA<sub>KDEL</sub> [8521.1] for site-specific *in vivo* biotinylation. Biotinylated monovalent pMHC-II-pCC-Fc were incubated with streptavidin (in b) or streptavidin-APC (in c) in a 4:1 ratio to generate pMHC-II-pCC-Fc multimers.

(b) **Validation of *in vivo* biotinylation and multimer formation** of biotinylated MTB/DR3-pCC-Fc [9260.3] and CLIP<sub>103-117</sub>/DR3-pCC-Fc- [9261.3] upon streptavidin addition analyzed by NativePAGE.

(c) **Antigen-specific binding of pMHC-II multimers to cognate CD4<sup>+</sup> T cell clone.** MTB/DR3 specific CD4<sup>+</sup> T cell clone RP15.1.1 was stained with in-house produced cognate and control pMHC-II-pCC-Fc multimers (upper panel) or commercial pMHC-II multimers (ProImmune) (lower panel) at 20 µg/mL for 2 h at 37°C in the presence of 50 nM dasatinib.

#### 3.6.3 Implementation of HLA-DM-mediated peptide-exchange of soluble px/HLA-DR3-pCC-Fc

As an alternative to the production of peptide-HLA-DR-pCC-Fc constructs in which a known peptide of interest is covalently linked to the N-terminus of HLA-DR β-chain during protein expression (previously shown in Fig. 3.14a), we aimed at implementing a “precursor” HLA-DR construct receptive to an exogenous peptide exchange after initial protein production and purification. This peptide-exchangeable (px) px/MHC-II is of interest since it would allow systematic screening for novel putative peptide ligands for instance by high-throughput binding assays based on peptide-spotted (297, 298) or peptide-printed microchips (299). The seminal studies by Kozono *et al.* as well as Day *et al.* previously reported peptide-exchangeable murine and human MHC-II constructs, respectively by attaching a placeholder peptide to the MHC-II β-chain via a flexible linker bearing a thrombin cleavage-site [LVPRGS]. Subsequent peptide-exchange was achieved upon thrombin-based linker cleavage and addition of a molar excess of a peptide-of-interest under acidic conditions (pH 5.0–5.5) (221, 235). Moreover, Day *et al.* showed that additional presence of HLA-DM accelerates this process and increased the dissociation of the class II-linked invariant chain peptide (CLIP)<sub>103–117</sub> [PVSKMRMATPLLMQA] and the association of a target peptide (235).

**CLIP/HLA-DR3 and HLA-DM production |** In the line with previous publications, we designed a construct comprising the CLIP<sub>103–117</sub> placed-holder peptide attached to the truncated β-chain (lacking the transmembrane domain) of HLA-DRB1\*03:01 (HLA-DR3) via a flexible linker sequence comprising a thrombin cleavage site [GSGSLVPRGSGGSGS]. The resulting peptide-exchangeable β-chain was fused in turn to the parallel coiled-coil (pCC) basic zipper followed by the hinge domain and CH2 and

CH3 of mIgG2a (Fc) and a C-terminal His<sub>6</sub>-tag (**Fig. 3.16a**). Co-expression in CHO-S cells of the CLIP-linked HLA-DR3  $\beta$ -chain [9221.1] and the corresponding  $\alpha$ -chain construct [8746.1] resulted in successful production and purification of the peptide-exchangeable CLIP/HLA-DR3-pCC-mIgG2a-Fc proteins (**Fig. 3.16d**). In addition, we expressed a human IgG1-Fc-fused soluble version of HLA-DM lacking the respective transmembrane domains by again taking advantage of the parallel coiled-coil (pCC) basic zipper (**Fig. 3.17a**). Similar to the pxHLA-DR3-pCC-mIgG2a-Fc construct design, also fusions of a truncated HLA-DM  $\alpha$ -chain [8743.1] and HLA-DM  $\beta$ -chain [8635.1] to the respective acidic/basic pCC-hIgG1-Fc resulted in successful expression of a soluble HLA-DM-pCC-hIgG1-Fc fusion-protein upon co-transfection in CHO-S cells. Successful expression was validated by intracellular staining with  $\alpha$ -HLA-DM mAb (clone MaP.DM1) (**Fig. 3.17b**) as well as shown by SDS-PAGE analysis after Strep-Tactin-based affinity chromatography (**Fig. 3.17c**).

**Peptide-exchange of CLIP/HLA-DR3-pCC-Fc** | Prior to functional analysis of the CLIP/DR3-Fc construct, we tested the thrombin (Factor IIa, Merck) activity at pH 5.5 (citrate buffer) compared to the recommended pH 8.4 (TRIS buffer). At pH 5.5 and the absence of CaCl<sub>2</sub>, roughly 50-times more thrombin (2.5x10<sup>-3</sup> units/pmol substrate) were required to achieve complete digestion of a cleavage-site bearing control substrate after 18 h incubation at RT (**Fig. 3.16c**). Moreover, no off-target cleavage of the CLIP/DR3-pCC-mIgG2a-Fc or HLA-DM-pCC-hIgG1-Fc constructs by thrombin was observed (**Fig. 16d**). Notably, cleavage of the linker between CLIP and the N-terminus of the HLA-DR  $\beta$ -chain is expected to result in a ~2.4 kDa CLIP-peptide-linker fragment upon dissociation. However, we failed to observe a corresponding shift in the molecular weight upon thrombin-based digestion of the CLIP/DR3-pCC-Fc construct possible due to a lack of resolution or lack of dissociation without presence of HLA-DM as discussed below (**Fig. 3.16d**). To replace the linked CLIP-peptide of the CLIP/DR3-mIgG2a-Fc by the MTB Hsp65<sub>1-13</sub> target peptide, the latter was added at an 80-fold molar excess in the presence as well as absence of thrombin and soluble HLA-DM. Moreover, we added magnetic goat- $\alpha$ -mouse IgG (G $\alpha$ M-IgG) Dynabeads to the reaction to immobilize the HLA-DR3-mIgG2a-Fc, which allows for simple separation of unbound peptide, thrombin as well as HLA-DM-hIgG1-Fc after an 18 h incubation at pH 5.5 at RT (**Fig. 3.16a**). Moreover, immobilization of CLIP/HLA-DR3-Fc on Dynabeads serving as bead-based artificial antigen-presenting cells (aAPCs) enabled a straightforward read-out of the MTB Hsp65<sub>1-13</sub> target-peptide exchange upon co-culture with the cognate RP15.1.1 CD4<sup>+</sup> T cell line (**Fig. 3.16b**). Surprisingly, addition of thrombin and excess amounts of target peptide alone to CLIP/HLA-DR at pH 5.5 did not let to an efficient peptide exchange reaction as indicated by a poor cognate T cell activation (6%) compared the T cell activation (85%) achieved by a co-culture with beads previously loaded with covalently linked MTB/HLA-DR3-Fc [9261.3]. Only if the soluble HLA-DM was present during the peptide exchange at pH 5.5 (independently of the additional presence of thrombin), a complete antigen-specific T cell activation (84%) was observed that was comparable to aAPC-based on MTB Hsp65<sub>1-13</sub> peptide covalently-linked HLA-DR3-Fc. In contrast, Day *et al.* observed CLIP peptide dissociation and target peptide association already upon addition of thrombin without HLA-DM to the analyzed CLIP-loaded HLA-allele DR4 (235). Interestingly, a suboptimal peptide-exchange performed at pH 7.2 of our CLIP/HLA-DR3 construct showed a synergistic effect of soluble HLA-DM and thrombin leading to 58% T cell activation and indicating an overall functional thrombin-cleavage site. Apart from recombinantly produced soluble HLA-DM-Fc, we also tested the activity of the previously by Chou *et al.* described HLA-DM function mimicking peptide [LRLKLPK] (279), which would theoretically replace costly HLA-DM-Fc productions by an inexpensive peptide. However, in contrast to Chou *et al.* we observed no activity of the DM function-mimicking peptide added either at a 10-fold (**Fig. 3.16b**) or 500-fold molar excess (**data not shown**) during the peptide exchange reaction.

### 3| Results Part 1 – Production and validation of soluble pMHC-Fc proteins

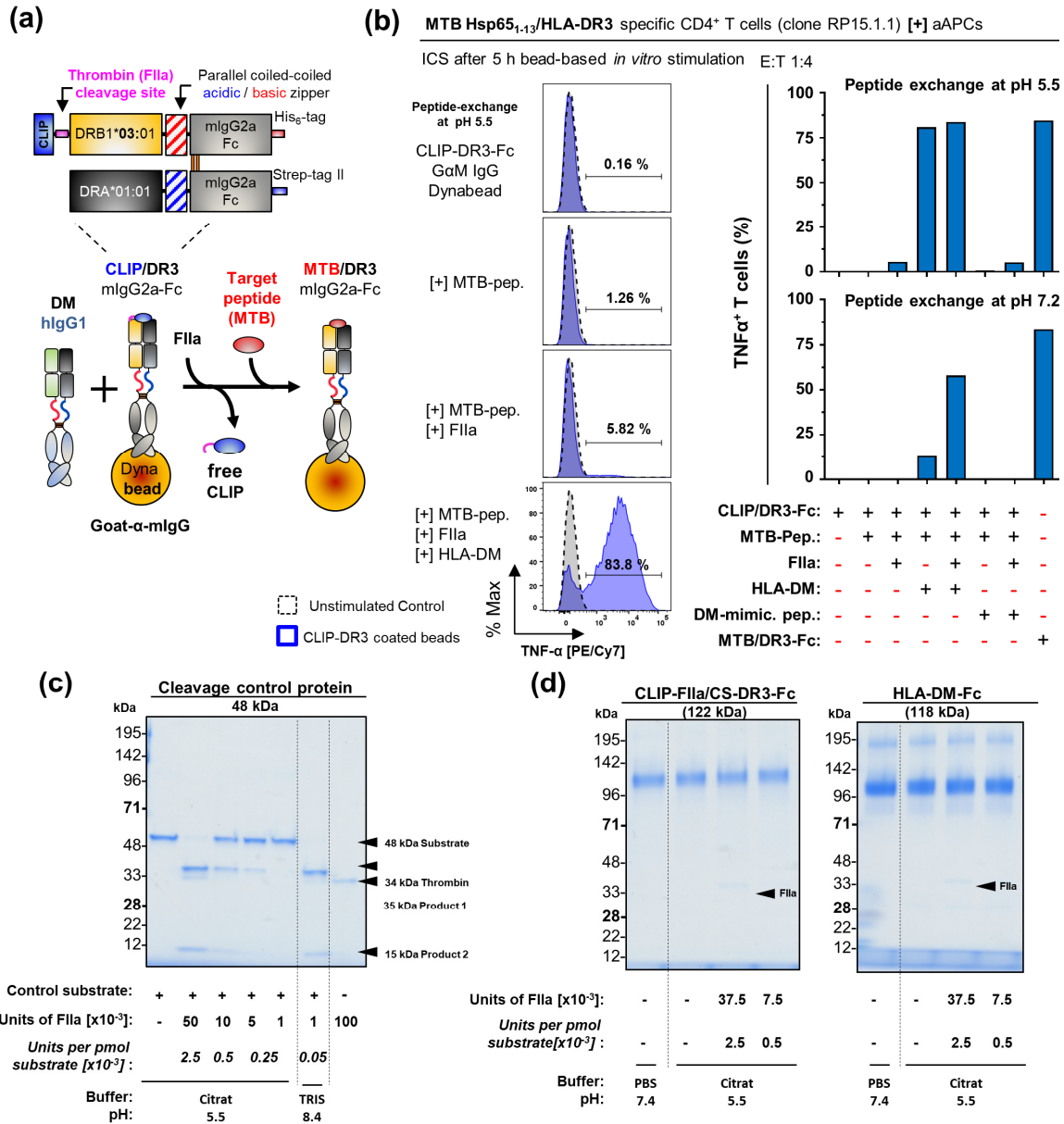


**Figure 3.16 | Validation of a HLA-DM-dependent peptide-exchangeable HLA-DR3-pCC-Fc construct**

**(a)** The peptide-exchangeable (px) px/HLA-DR3-pCC-mIgG2a-Fc construct comprise the structure as described in Fig. 3.14a, but has an additional cleavage-site for thrombin (FIIa) within the linker between the CLIP<sub>103-117</sub> place holder peptide ligand and the DR3 β-chain (CLIP/DR3-pCC-mIgG2a-Fc). For peptide exchange, CLIP/DR3-mIgG2a-Fc constructs were immobilized on magnetic GαM-IgG Dynabeads to form aAPCs. Target peptide is added at 80x molar excess in the presence of a 2x molar excess of soluble HLA-DM-hlgG1-Fc (DM) (described in Fig. 3.17) and FIIa. The peptide exchange reaction was incubated for RT for 20 h at pH 5.5. Magnetic aAPCs were then washed to remove unbound peptides, FIIa and DM.

**(b)** Co-culture of aAPCs and MTB/DR3 CD4<sup>+</sup> T cell clone RP15.1.1 for 5 h followed by ICS. GαM-IgG-Dynabeads were loaded with CLIP/DR3-mIgG2a-Fc (aAPCs) in the presence or absence of individual components required for peptide-exchange as indicated at pH 5.5 or pH 7.2. After the 5 h co-culture of aAPCs with MTB/DR3 CD4<sup>+</sup> T cells, successful peptide exchange was indicated by the induction of TNF-α expression of the cognate T cell clone. DM-mimicking peptide (LRLKLPK) was added at a 10x molar excess. As positive control MTB/DR3-mIgG2a-Fc [9260.3] was used.

**(c)** Digestion of thrombin cleavage site bearing control protein using various amounts of thrombin at pH 5.5 and 8.4.

**(d)** Analysis for off-target digestion of HLA-DR3-Fc and HLA-DM-Fc. Test control digestion of CLIP/DR3 and DM using indicated amounts thrombin. No off-target effect of thrombin can be seen. **(c-d)** 10% SDS PAGE, non-reducing.

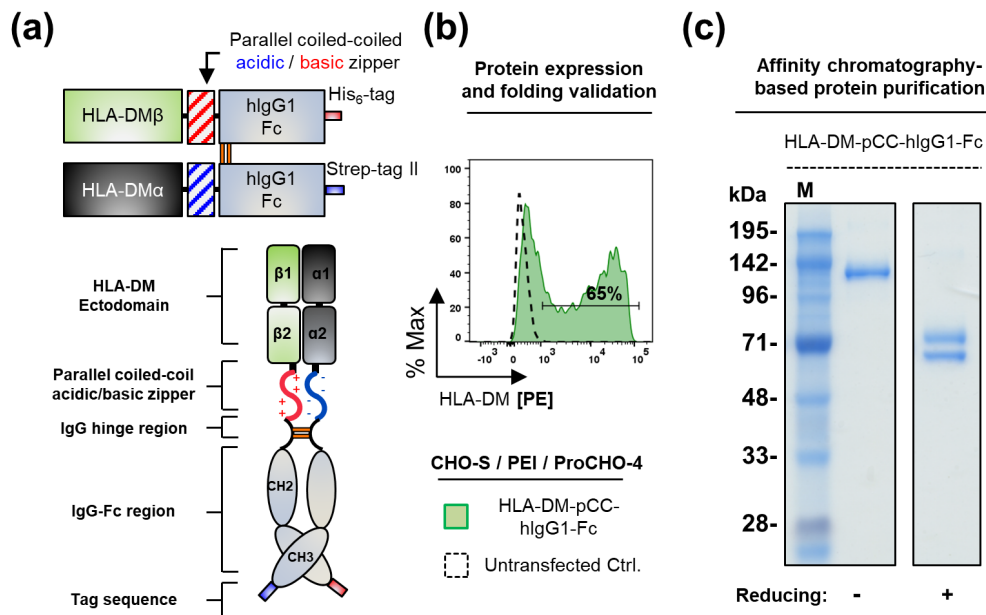


**Figure 3.17 | Production and validation of a soluble HLA-DM-pCC-Fc construct**

**(a) HLA-DM immunoglobulin Fc fusion constructs** consist of two separate polypeptide chains similar to the pMHC-II-pCC-Fc construct shown in Fig. 3.14. The C-terminus of the HLA-DM  $\beta$ -chain ectodomain ( $\beta$ 1- $\beta$ 2) is fused to a parallel coiled-coil (pCC) basic zipper followed by the hinge domain and CH2 and CH3 of hlgG1 (Fc) and a C-terminal His<sub>6</sub>-Tag. The ectodomain of the HLA-DM  $\alpha$ -chain ( $\alpha$ 1- $\alpha$ 2) is C-terminally fused to a complementary acidic pCC-Fc and a Strep-tag II.

**(b) Validation of HLA-DM-pCC-hlgG1-Fc expression and structural conformation.** HLA-DM-pCC-Fc [8635.1 (+) 8743.1] expression in CHO-S cells was confirmed by intracellular staining with  $\alpha$ -HLA-DM mAb (clone MaP.DM1) 3 days after transfection.

**(c) Result of a HLA-DM-pCC-hlgG1-Fc Strep-Tactin-based affinity chromatography.** 10% SDS-PAGE under non-reducing and reducing conditions after Coomassie staining. M: Marker.

In summary, our CLIP/HLA-DR3-Fc construct was receptive to an exogenous peptide exchange, which was almost exclusively HLA-DM mediated. Moreover, HLA-DR3 constructs remained completely functional upon peptide exchange as shown by stimulation of a cognate DR3 restricted CD4<sup>+</sup> T cell line.



## 4| Results Part 2

### Development of a novel easy-to-use multiplex assay to detect antigen-specific T cells *in vitro*

**Initial remarks** | Multiplex immunoassays based on fluorescence-encoded microspheres (beads) have emerged as a key tool to deconvolute complex immune responses within the tumor microenvironment by measuring simultaneously multiple immune cell effector cytokines (300, 301) or to assess the humoral immune response against tumor-associated antigens (302, 303). In particular, the Luminex® xMAP (multi-analyte profiling) technology comprising color-coded MagPlex® microspheres (hereinafter termed Luminex beads) allows the measurement of up to 100 analytes using the proprietary bench top flow cytometer Luminex® analyzer 100/200™ or of up to 500 analytes using the Luminex® FLEXMAP 3D® bead system. Moreover, Luminex beads are distributed as carboxylated microbeads allowing covalent immobilization of any proteins of interest bearing free amino groups based on carbodiimide-coupling chemistry, which in turn permits individual and flexible immunoassay development (304, 305).

Thus, we envisaged that Luminex beads in combination with our already established pMHC-I-Fc as well as pMHC-II-Fc production pipeline could be a novel concept for a robust and easy-to-use multiplex assay platform that allows simultaneous detection of antigen-specific T cells. However, unlike a fluorochrome-combinatorial pMHC-I-multimer staining using various fluorochrome-streptavidin (SAv) conjugates and multiple SAv-conjugated quantum dots (QD) (185), pMHC-I-conjugated color-coded magnetic Luminex-beads cannot be used directly for antigen-specific T cell staining due their almost cellular size (6.5  $\mu\text{m}$ ) (own observations, **data not shown**). Nevertheless, pMHC-conjugated Luminex beads can function as artificial antigen-presenting cells (aAPCs) bearing the capacity to stimulate cognate T cells resulting in effector cytokine secretion as previously demonstrated in **Section 3.1.3**. Thus, we ultimately aimed at engineering an assay platform that shares a similar sensitivity for the detection of low frequency antigen-specific T cell populations as compared to highly sensitive and often used gold-standard assays including the ELISpot assay and pMHC multimer staining. ELISpots usually have a reliable detection limit of 1 antigen-specific T cell out of  $\sim 10,000$  PBMC corresponding practically to  $\sim 25$  spots observed per  $2.5 \times 10^5$  PBMC seeded per ELISpot-well and a typical background of 4–6 spots/ $10^5$  PBMC (171). Although, routinely and reliably used in clinical immune monitoring units, an ELISpot assay bears a labor-intensive workload and does not allow multiplex detection of multiple T cell antigen-specificities consequently high amounts of patient material is needed for this kind of analysis. In contrast, non-fluorochrome-combinatorial pMHC multimer stainings have a typical detection limit of one antigen-specific T cell out of  $\sim 50,000$  PBMC corresponding practically to 0.01% pMHC multimer<sup>+</sup> cells among the CD8<sup>+</sup> T cell population with a minimal required amount of 10 events considers as multimer<sup>+</sup> (156). Moreover, recent technological advances have shown that combinatorial encoding of pMHC multimer fluorescence (185, 187), metal (188), or DNA barcode tags (189) allow parallel analysis of multiple T cell specificities (**Section 1.5.2.2**). However, these platforms are yet not suitable for routine laboratory practice a due to the reagents of high pricing, requirement of highly trained and specialized staff and complex data analysis. Consequently, we aimed for developing a novel assay platform that overcomes limitations of both ELISpot and pMHC multimer staining platforms.

## 4.1 Pilot - Development of a novel multiplex assay to detect antigen-specific T cells

### 4.1.1 Linking T cell specificities to defined Luminex beads – The T-Plex Assay (TPA) concept

**The invention of T-Plex beads** | We hypothesized that conjugating a defined Luminex bead species (i.e. beads with the same spectral color-code) with a defined pMHC molecule of choice as well as an anti-effector cytokine monoclonal antibody (e.g. anti-IFN- $\gamma$  mAb) would allow the detection of antigen-specific T cells (**Fig. 4.1a**). Thus, a certain T cell specificity of interest will be represented by the pMHC complex that is linked to a defined bead color (ID) (**Fig. 4.1c**). We reasoned that commercially available MagPlex<sup>®</sup> microspheres (Luminex beads) conjugated with pMHC molecules, optional co-stimulatory acting molecules and an IFN- $\gamma$ -capture antibody, hereafter called T-Plex beads, would have the capacity to activate cognate T cells in an antigen-specific manner, which in turn would drive IFN- $\gamma$  secretion of that activated T cell. The secreted IFN- $\gamma$  is proximally captured on the same bead and is detected by a fluorochrome-labeled secondary IFN- $\gamma$  detection mAb. T-Plex beads are finally analyzed based on their intrinsic color (bead classifier) and their IFN- $\gamma$  load using a suitable flow cytometric instrument, hereafter referred to as T-Plex Assay principle / concept (**Fig. 4.1b**). Unfortunately, the Luminex<sup>®</sup> analyzer 100/200<sup>™</sup> flow-based bead reader only records median fluorescence intensities (MFI) of homogeneously loaded Luminex bead populations and thus not allow data analysis based on “gating” of individual subpopulations, which we assumed would be strongly required for our assay approach. Thus, we decided to develop our T-Plex Assay platform for the commonly used BD FACS Canto II system equipped with a 488 nm blue, 633 nm red and additional 405 nm violet laser. When measured by a BD FACS Canto II system, we initially observed that a panel of Luminex bead colors (ID) were still reliably separated and the corresponding bead coordinate system became visible when the APC channel was plotted against the APC/Cy7 channel (**Fig. 4.1c**).

**The obvious IFN- $\gamma$  cross-bleeding problem** | To experimentally validate our T-Plex bead concept, we initially loaded goat-anti-mouse IgG (G $\alpha$ M-IgG) covalent-conjugated magnetic Luminex beads with anti-human IFN- $\gamma$  monoclonal antibody ( $\alpha$ -IFN- $\gamma$  mAb, clone NIB42) and purified disulfide-trapped peptide-loaded-HLA-A2-mIgG2a-Fc constructs (pHLA-A2-Fc, as described in **Fig. 3.1a**) in a 3 to 2 ratio, hereafter termed 1<sup>st</sup> generation T-Plex beads (**Fig. 4.1d**). Subsequently, the Survivin<sub>96-104</sub>/HLA-A2-specific CD8<sup>+</sup> T cell line (Sur/A2 T cells) was co-cultured under static conditions for 4 h at 37°C within a 96-U-bottom well either with cognate pMHC-I-loaded T-Plex beads (ID 019) (**Fig. 4.2, upper panel**), irrelevant pMHC-I-loaded T-Plex beads (ID 012) (*middle panel*) or both T-Plex beads pools together (ID 012 + 019, *lower panel*). After the co-culture, the T cell and bead mix was blocked with mouse serum and subsequently stained with  $\alpha$ -IFN- $\gamma$  detection mAb conjugated to PE (clone 4S.B3).

As a result, cognate T-Plex beads displayed an expected load with IFN- $\gamma$ , whereas spatially separated T-Plex beads harboring an irrelevant pMHC-I did not activate the T cell line and showed no IFN- $\gamma$  load. However, a co-culture within a 96-well of the Sur/A2 T cell line with a mixture of T-Plex beads conjugated either with cognate or irrelevant pMHC-I within one 96-well resulted in a detectable IFN- $\gamma$  “cross-bleeding” onto all beads irrespective of the pMHC due to the close proximity of “cognate” and “irrelevant” T-Plex beads (**Fig. 4.2**). The initial results suggested that a T-Plex Assay performed under static conditions either based on Luminex beads (**Fig. 4.2**) or non-color coded Dynabeads (**Supplementary Fig. S6**) is in general feasible for the detection of a single T cell specificity, but does not allow simultaneous detection of multiple T cell specificities due to IFN- $\gamma$  cross-bleeding.

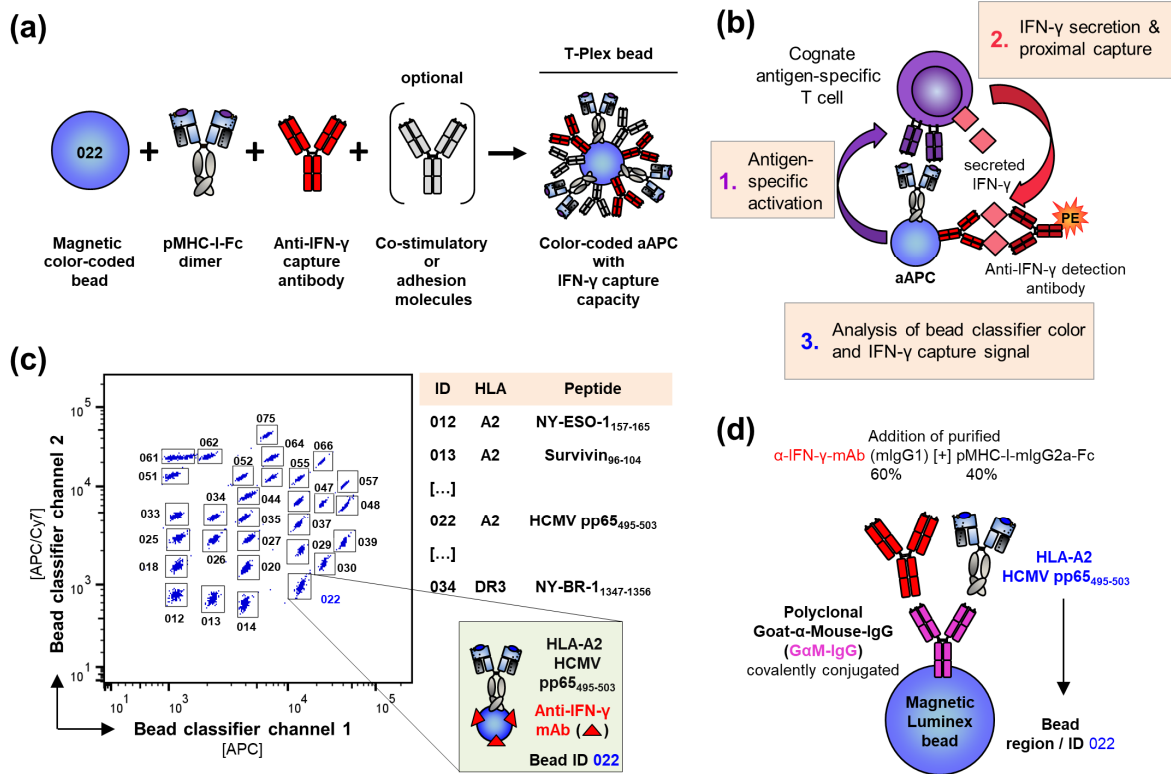


**Figure 4.1 | Linking T cell specificities to defined bead colors – The T-Plex Assay core concept**

**(a) T-Plex bead core concept.** T-Plex beads are bead-based color-coded artificial antigen-presenting cells (aAPC) with T cell effector cytokine capture capacity, in particular interferon- $\gamma$  (IFN- $\gamma$ ). T-Plex beads are assembled by coupling defined pMHC-I or -II and other optional co-stimulatory molecules together with an effector cytokine-capture antibody to a color-coded bead, preferentially to Luminex xMAP MagPlex<sup>®</sup> microspheres (Luminex beads).

**(b) Working principle of the T-Plex Assay:** pMHC and  $\alpha$ -IFN- $\gamma$  capture mAb coupled color-coded beads (T-Plex beads) activate cognate T cells in an antigen-specific manner, which drives IFN- $\gamma$  secretion of that activated T cells. The secreted IFN- $\gamma$  is proximally captured on the same bead and can be detected by a fluorochrome-labeled  $\alpha$ -IFN- $\gamma$  detection antibody. T-Plex beads can be subsequently analyzed in a suitable flow cytometric instrument based on their intrinsic color (bead classifier) and their IFN- $\gamma$  load.

**(c) Luminex bead coordinate system.** Shown are 30 different Luminex bead species and their region (ID) measured by a BD FACS Canto II. Each bead species can be theoretically linked to defined T cell epitopes through conjugation with respective pMHC-I-Fc or pMHC-II-Fc molecules.

**(d) 1<sup>st</sup> generation T-Plex bead.** In the pilot and early T-Plex Assay development phase, T-Plex beads were generated as shown. Polyclonal goat-anti-mouse IgG (G $\alpha$ M-IgG) serum-conjugated magnetic color-coded Luminex beads were loaded with mouse- $\alpha$ -human IFN- $\gamma$  mAb ( $\alpha$ -IFN- $\gamma$  mAb, mIgG1) and purified disulfide-trapped (dt) pMHC-I-mIgG2a-Fc (**Fig. 3.1**) in a 3 to 2 ratio. dt-pMHC-I-Fc dimer: Disulfide-trapped peptide-loaded MHC-class I-mIgG2a-Fc dimers.

#### 4 | Results Part 2 – Development of the T-Plex Assay

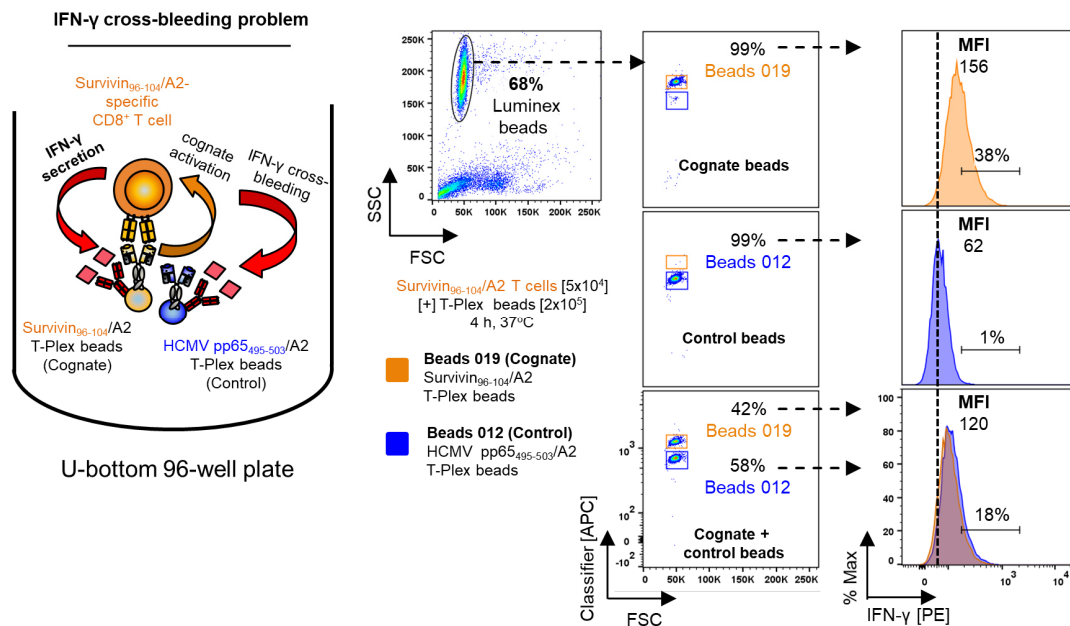


**Figure 4.2 | Observed IFN-γ “cross-bleeding” onto control T-Plex beads using static assay conditions**

Two color-coded magnetic GαM-IgG-Luminex bead species were separately conjugated with different dt-pMHC-I-Fc dimers and an α-IFN-γ capture mAb (red) in a 2 to 3 ratio (T-Plex beads). T-Plex-beads with label intensity (internal color) 019 (orange) were conjugated with Survivin<sub>96-104</sub>/HLA-A2-Fc (cognate pMHC-I) [8195.1] and 012-beads (blue) were loaded with HCMV pp65<sub>495-503</sub>/HLA-A2-Fc (irrelevant pMHC-I) [7409.4], respectively. Cognate and control T-Plex beads were co-cultured separately and in combination (multiplex) with Survivin<sub>96-104</sub>/A2 specific CD8<sup>+</sup> T cells under static conditions in a 96-well U-bottom (200 μL assay volume) for 4 h, 37°C, 8% CO<sub>2</sub> (E:T = 1:4) and subsequently analyzed for their IFN-γ-load. Shown is fraction and MFI of individual IFN-γ-loaded cognate or control T-Plex beads. MFI: Median fluorescence intensity. GαM-IgG: Goat-anti-mouse IgG. E:T: Effector (T cells) to target (T-Plex bead) ratio.

**Bringing in movement to the T-Plex Assay |** To overcome this aforementioned cross-bleeding problem and to gain a T-Plex Assay with multiplex capacity, we reasoned that the T-Plex beads needs to be spatially separated and immobilized while the T cells are kept in motion to ensure access of the T cells to all beads. As an alternative, we speculated that it might sufficient to just co-culture T-Plex beads and T cells under constant movement without prior immobilization of beads or T cells. We hypothesized that under agitation an antigen-specific T cell would still preferentially stably interact and bind to a cognate T-Plex bead, while irrelevant T-Plex beads would be constantly spatially separated from that particular T cell. Consequently, a T-Plex bead in proximity to the cognate T cell would be loaded with a higher IFN-γ payload upon T cell activation compared to bystander T-Plex beads until the whole assay volume saturates with secreted IFN-γ. To realize these concepts, we envisioned that color-coded magnetic fully assembled (pMHC-loaded) T-Plex beads can be immobilized using a 96-well magnet placed below a 6-well or lid of 96-well plate. Here, color-coded T-Plex beads representing different antigen-specificities are spotted onto individual magnetic reaction fields and finally a sample containing T cells is added into the whole reaction chamber. Finally, the whole reaction is incubated at 37°C under constant agitation using a 3D orbital shaking system (Fig. 4.3a). Alternatively, we assumed that T-Plex beads and test-sample can be simply combined in a single round tube like a frequently used cryovial. The assay tube is placed horizontally between the gap of two rolling tubes of a rolling device, which leads to rotation of the assay tube along the longitudinal x-axis (Fig. 4.3b). After agitation for 4 h at 37°C, beads and sample are separated from each other using magnet force. T cells are easily washed of the T-Plex-beads and can be brought back into culture for additional experiments. Finally, T-Plex beads are collected and stained with an IFN-γ-detection mAb to assess their individual IFN-γ-payload reflecting the presence of antigen-specific T cells in the sample.

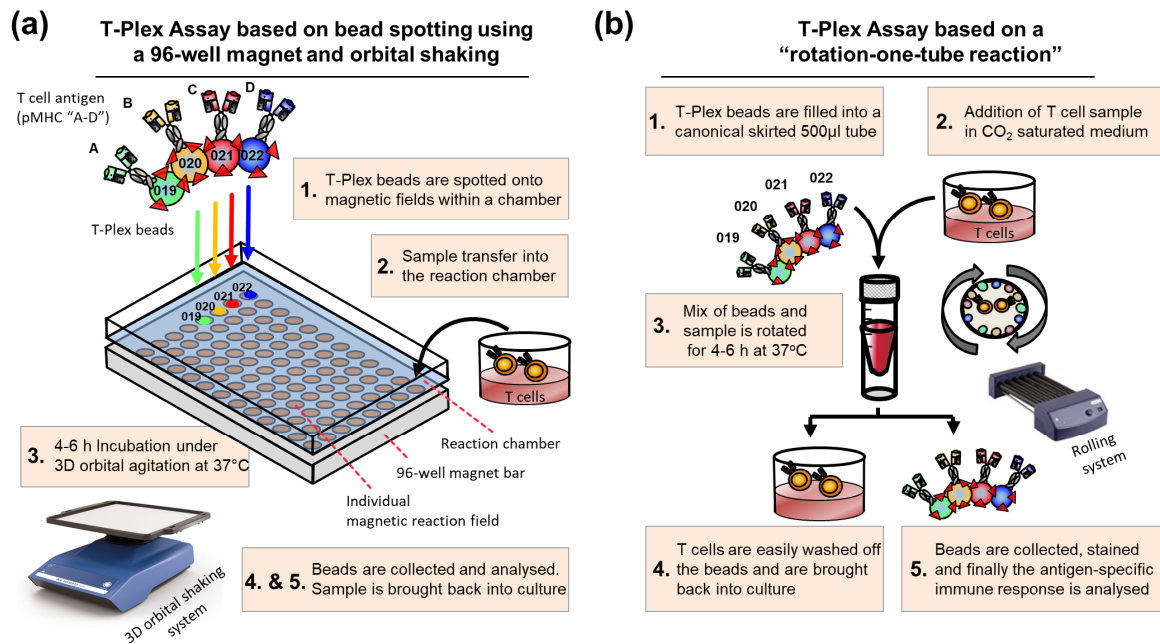


**Figure 4.3 | Agitation during T cell stimulation by T-Plex beads as key to overcome IFN- $\gamma$  cross-bleeding**

**(a) T-Plex Assay workflow based on bead spotting followed by 3D/wave orbital shaking.** To enable a multiplex T-Plex Assay and avoid IFN- $\gamma$  cross-bleeding, color-coded T-Plex beads loaded with different pMHC-Fc are spotted onto individual magnetic reaction fields generated by means of a 96-well magnet placed below a suitable reaction chamber (6-well plate or lid of plate). T cells are added to the medium-flooded chamber and the whole reaction is incubated for 4–6 h at 37°C under gentle and constant 3D orbital agitation. After the incubation, T-Plex beads can be magnetically separated from T cells. T cells are easily washed off the beads and can be brought back into culture for additional experiments. The 96-well magnet is removed and all bead spots are pooled. Finally, the IFN- $\gamma$  payload of individual T-Plex species is analyzed.

**(b) T-Plex "rotation-one-tube-reaction" principle:** Color-coded T-Plex beads loaded with different pMHC-Fc molecules are filled into a skirted conical tube combined with CO<sub>2</sub>-saturated assay medium and the T cell sample to be analyzed. The assay tube is closed and rotated for 4–6 h at 37°C along its longitudinal x-axis. After the incubation, magnetic T-Plex beads are collected by means of a magnet suitable for plates or tubes and T cells are washed off. Subsequently, T-Plex beads are analyzed for their IFN- $\gamma$  load.

#### 4.1.2 Proof-of-concept for a T-Plex Assay facilitated by spatially separated immobilized beads

The first successful and multiplex-capable T-Plex Assay was experimental validated by spatial separation and immobilization of T-Plex bead pools representing different T cell antigen-specificities by means of a 96-well magnet (IBA Lifesciences), which displayed 96 individual magnetic spots (**Fig. 4.3a & Fig. 4.4a**). The experimental workflow also described in the material and methods **Section 2.11.2.1** started with a 6-well cell culture plate placed above the 96-well magnet. Next, 2 mL assay medium was filled in the respective 6-wells and pMHC-I-Fc loaded 1<sup>st</sup> generation T-Plex beads were individually spotted/immobilized on the magnetic reaction fields provided by the underlying magnet as illustrated in **Fig. 4.4a & c**. After bead spotting, the Survivin<sub>96-104</sub>/HLA-A2 (Sur/A2)-specific CD8<sup>+</sup> T cell line was added in 2 mL assay medium serving as test sample. The whole plate including the attached magnet was placed on a 3D/wave orbital shaking platform previously transferred to a cell culture incubator and was incubated at 37°C, 8% CO<sub>2</sub>, 25 rpm for 4 h. After the incubation, the 4 mL culture cell supernatant was carefully removed, while the magnet was still placed below the 6-well plate. Afterwards the 96-well magnet was detached and finally the T-Plex beads were pooled, stained and analyzed for their IFN- $\gamma$  load. As shown in **Fig. 4.4a**, cognate pMHC-I-loaded T-Plex beads (ID 019, orange) displayed a clearly distinct IFN- $\gamma$  load compared to irrelevant pMHC-I-loaded T-Plex beads (ID 012, blue) after the incubation with the Sur/A2 T cell line. Thus, although the T cell sample had access to both immobilized T-Plex bead species within a given 6-well, the cognate T-Plex beads are almost

exclusively loaded with IFN- $\gamma$ , whereas the irrelevant pMHC-I-loaded T-Plex beads displayed only little bystander IFN- $\gamma$  load when compared to T cell “untouched” T-Plex beads. This initial finding demonstrated for the first time the true multiplex-capacity of the T-Plex Assay principle. Moreover, as little as 10,000 T-Plex beads per magnetic spot were sufficient to get a clear difference between pMHC-dependent IFN- $\gamma$  load and background signal **Fig. 4.4b**. In the follow up experiment, we immobilized 10,000 beads/magnet spot of six different 1<sup>st</sup> generation T-Plex beads pools pre-loaded with different pMHC-I-Fc constructs as shown in **Fig. 4.4c**. Subsequently, 10-fold diluting amounts [ $2 \times 10^2$ – $2 \times 10^5$  cells] of the Sur/A2 CD8<sup>+</sup> T cell line was added as test sample, which accordingly resulted in approximately 10-fold reductions of IFN- $\gamma$ -loaded (IFN- $\gamma^+$ ) cognate T-Plex beads upon incubation at 37°C for 4 h under 3D orbital agitation. The lower detection limit in this pilot experiment was ~2000 Sur/A2 T cells, which resulted in 1% IFN- $\gamma^+$  T-Plex beads among the cognate T-Plex bead pool (100 cognate IFN- $\gamma^+$  T-Plex beads out of 10,000 spotted cognate T-Plex beads). Notably, the shown closely linked FACS plots represent data analysis from the same T-Plex Assay reaction / T-Plex bead mix (multiplex detection) and the respective baseline was set on control T-Plex beads loaded with an irrelevant pMHC-I. Moreover, strong antigen-independent stimulation of the Sur/A2 T cell line by PMA and Ionomycin led to a homogeneous IFN- $\gamma$ -loading of all control beads compared to T-Plex beads left without T cells indicating an overall homogeneous IFN- $\gamma$ -binding capacity of all used and assembled T-Plex beads independent of the coated pMHC-I-Fc (**Fig. 4.4c**).

Interestingly, when lower amounts of cognate T cells were added as test-sample, we observed rather the appearance of an IFN- $\gamma^+$  T-Plex bead “subpopulation” than a global shift in fluorescence (MFI). This implies firstly, that it is possible that a given T cell pool interact with a single cognate T-Plex bead resulting in a striking IFN- $\gamma^+$  load even under agitation. Secondly, there seems to be a certain linear relationship between the total amounts antigen-specific T cells to be analyzed and corresponding appearance of an IFN- $\gamma^+$  T-Plex population. Thirdly, the BD FACS Canto II, unlike the Luminex<sup>®</sup> analyzer 100/200<sup>™</sup> bead reader allows data analysis based on “gating” of individual sub populations, which is required to detect lower T cell frequencies by the T-Plex Assay.

In conclusion, spatially distributed immobilization of T-Plex bead pools by means of a 96-well magnet allows multiplex-capable detection of antigen-specific T cell responses. However, the usage of a 96-well magnet-based assay format introduces some logistical challenges, since only up to six specificities per 6-well could be measured due to the limited availability of magnetic spots. Alternatively, the whole area could be used to spot up to 96-antigen-specificities represented by the respective T-Plex bead pools but this would also decrease the probability that a given T cell interacts with their cognate T-Plex bead pool. Moreover, the pioneering work of the laboratory of Mark M. Davis at the beginning of the 2000s have already demonstrated that soluble pMHC-complexes can be directly spotted onto polyacrylamide gel-coated microscope slides resulting in pMHC microarrays eliciting functional T cell responses (180, 181) (also described in **Section 1.5.1.3**), requiring however also a spatially defined readout of T cells activation. Therefore, we reasoned that spatially defined immobilization of already color-coded aAPCs on a magnet plate would be redundant for our assay concept. Thus, we sought to omit the 96-well magnet and to simply combine T-Plex beads and a T cell containing sample in a single rotating tube that would still allow for a proper read out of multiple antigen specificities based on the inherent bead color-coding. This approach will be discussed in the next section.

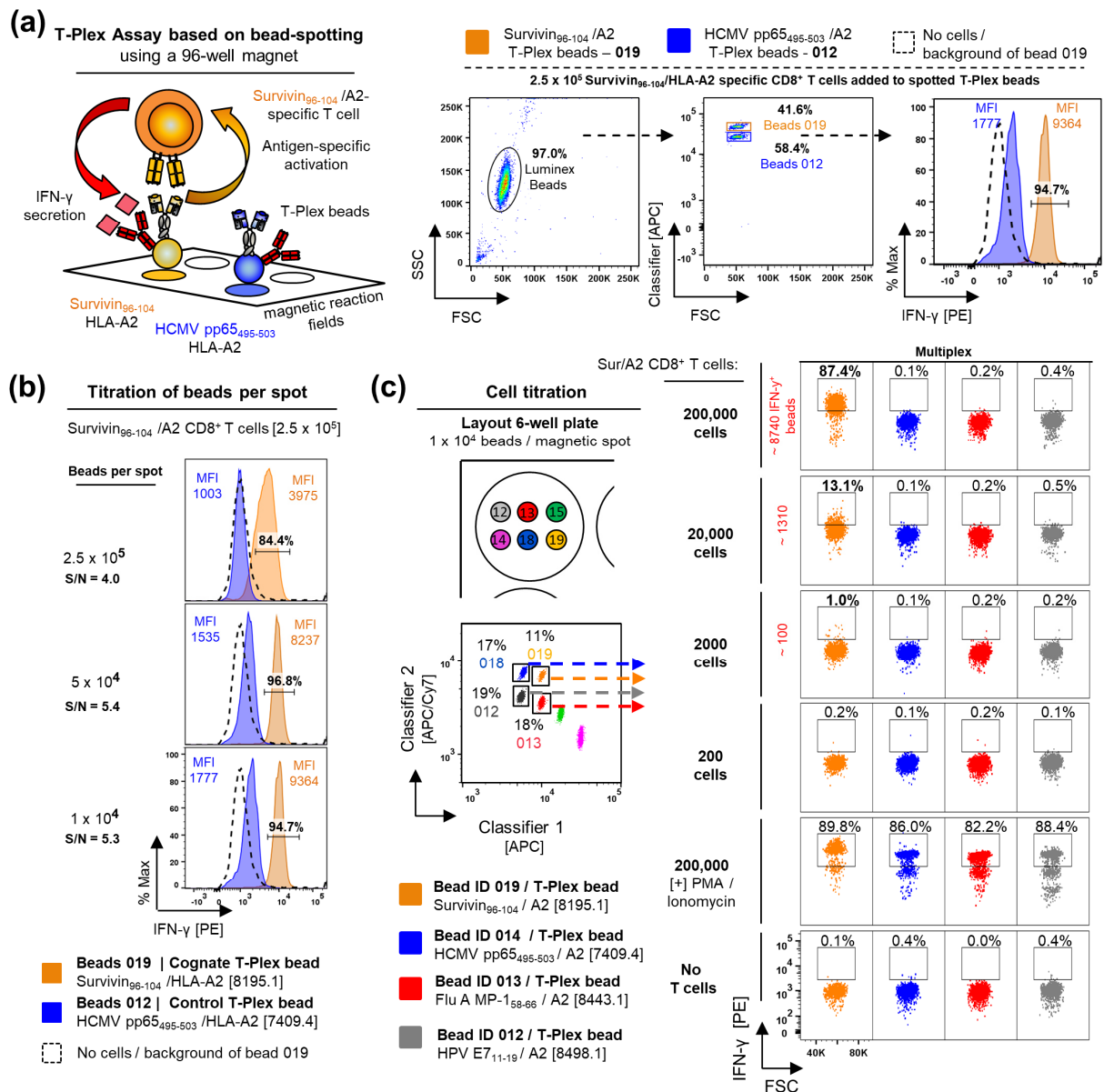


**Figure 4.4 | T-Plex Assay-based detection of an antigen-specific T cell response facilitated by a 96-well magnet**

**(a) T-Plex Assay layout and respective data.** Two color-coded magnetic GαM-IgG Luminex-bead species were separately conjugated with different purified dt-pMHC-I-Fc dimers and an α-IFN-γ capture mAb (clone NIB42) in a 3 to 2 ratio (1<sup>st</sup> generation T-Plex beads). T-Plex beads with bead ID-019 (019 beads, orange) were conjugated with Survivin<sub>96-104</sub>/HLA-A2-Fc (cognate, [8195.1]) and 012 beads (blue) were loaded with HCMV pp65<sub>495-503</sub>/HLA-A2-Fc (control, [7409.4]).  $\sim 1 \times 10^4$  beads per T-Plex bead ID were spotted onto an individual magnetic reaction field (spot) generated by a 96-well magnet placed below a 6-well plate. After bead spotting,  $2.5 \times 10^5$  human Survivin<sub>96-104</sub>/HLA-A2 (Sur/A2)-specific CD8<sup>+</sup> T cells were added in a total volume of 4 mL complete medium (filled histograms) or no T cells were added (dotted histogram). The assay plate was placed on a 3D/wave-orbital shaker platform and incubated under agitation for 4 h at 37°C, 8% CO<sub>2</sub>. Beads were subsequently (i) pooled, (ii) washed and (iii) incubated with a biotinylated α-IFN-γ detection mAb for 1 h followed by a (iv) wash step and (v) incubation with streptavidin-PE for 15 min before analysis on a BD FACS Canto II. Gating of Luminex beads is shown as well as the fraction and MFI value of the IFN-γ payload.

**(b) Titration of T-Plex beads per magnetic spot.** Same experimental set-up as above, but various amounts of beads per magnetic spot were used. Signal-to-noise ratio (S/N) based on MFI values of control and cognate T-Plex bead are shown.

**(c) Titration of Sur/A2 CD8<sup>+</sup> T cells.** Same experimental set-up as above, but additional pMHC-I-Fc-loaded T-Plex beads as described in the figure were spotted and various amounts of Sur/A2 CD8<sup>+</sup> T cells were added. Bead ID 14 and 15 displayed a similar signal as the other control beads (**data not shown**). To assess the maximal and homogeneous IFN-γ-binding capacity of all used T-Plex beads, T cells were stimulated using PMA and Ionomycin. MFI: Median fluorescence

### 4.1.3 Proof-of-concept for a T-Plex Assay within one constantly rotating cryotube

As introduced in **Fig. 4.3b**, we hypothesized that pMHC-I-Fc-loaded T-Plex beads and a given T cell containing test sample might be simply combined in a single cylindrical tube followed by rotation along its longitudinal x-axis in order to measure an antigen-specific T cell response by corresponding T-Plex beads. For experimental validation, four separated T-Plex bead species were individually assembled by loading  $\alpha$ M-IgG-Luminex beads with cognate or control pMHC-I-Fc and  $\alpha$ -IFN- $\gamma$  capture mAb in a 3 to 2 ratio. As a next step, the four T-Plex bead species were combined to a single bead pool and 10,000 T-Plex beads per antigen-specificity were added to a cell culture cryotube. Subsequently, 10-fold diluting amounts [ $2 \times 10^2$  –  $2 \times 10^5$  cells] of the Sur/A2 CD8<sup>+</sup> T cell line was added as test sample in a final volume of 2 mL assay medium. Notably, the assay medium (RPMI supplemented with 10% FBS, 2 mM GlutaMAX™, 10 mM HEPES and antibiotics) was kept for at least 2 h in a CO<sub>2</sub>-incubator before experimental usage. Finally, the closed tube was incubated for 4 h at 37°C on a roller system with a fixed speed of 40 rpm prior to analysis of the IFN- $\gamma$  payload per T-Plex bead. As shown in **Fig. 4.5** also constant rolling of a pool of T-Plex beads and Sur/A2 CD8<sup>+</sup> T cells within one tube resulted in antigen-dependent and cell number-dependent IFN- $\gamma$  loading of the cognate Survivin<sub>96-104</sub>/HLA-A2-Fc but not irrelevant pHLA-A2-Fc-conjugated T-Plex bead pools. Surprisingly, the overall assay performance in terms of sensitivity was similar compared to the previously discussed magnet-based T-Plex Assay approach indicating agitation of both T-Plex beads and T cells in a given volume does not necessarily lead to a reduced assay sensitivity. For both assay settings (96-well magnet or “one-tube”-based T-Plex Assay) 2000 antigen-specific T cells was the initial lower detection limit. Conclusively, by taking advantage of a frequently available laboratory rolling system we could achieve for the first time the detection of an antigen-specific T cell response by means of T-Plex beads previously co-cultured with T cells in a single tube.

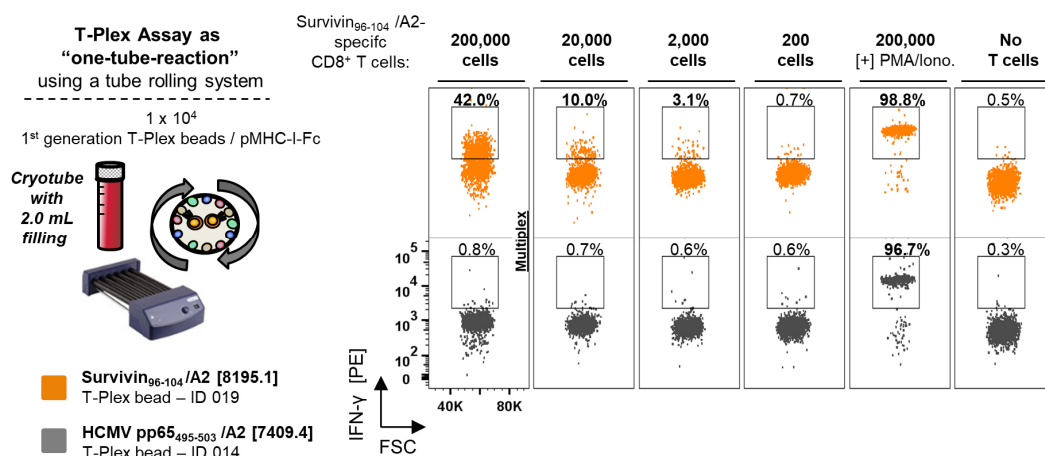


**Figure 4.5 | Detection of an antigen-specific human T cell line by a one-tube-rolling multiplex T-Plex Assay**

Four different color regions (Bead ID: 012, 013, 014, 019) of  $\alpha$ M-IgG-Luminex beads were separately loaded with pMHC-I-Fc dimers and  $\alpha$ -IFN- $\gamma$  capture mAb (clone NIB42) in a 3 to 2 ratio (1<sup>st</sup> generation T-Plex beads). T-Plex beads with bead ID-019 (019-beads, orange) were conjugated with Survivin<sub>96-104</sub>/HLA-A2-Fc (cognate, [8195.1]) and 012-beads (grey) were loaded with HCMV pp65<sub>495-503</sub>/HLA-A2-Fc (control, [7409.4]). T-Plex beads with ID 012 and 013 were loaded with other irrelevant pMHC-I-Fc and behaved similarly to control T-Plex bead 014 (**data not shown**). 10,000 T-Plex beads per antigen were combined with the indicated amounts of pure Survivin<sub>96-104</sub>/HLA-A2 (Sur/A2)-specific CD8<sup>+</sup> T cells in one cylindrical 2 mL cryotube filled with 2 mL CO<sub>2</sub>-saturated medium. The closed tube was incubated for 4 h at 37°C on a roller system set to ~40 rpm. Beads were subsequently collected, washed and stained with an anti-IFN- $\gamma$  detection mAb prior to flow cytometric analysis. Detection of the Sur/A2 T cell line was indicated by appearance of an IFN- $\gamma$ <sup>+</sup> subpopulation of cognate T-Plex beads that were above control beads. To assess the maximal and homogeneous IFN- $\gamma$ -binding capacity of all used T-Plex beads, T cells were stimulated using PMA and Ionomycin (Iono.). Pairs of upper and lower FACS plot represent data analysis from the same T-Plex Assay / combined bead pool.

#### 4.1.4 The “pilot” T-Plex Assay does detect antigen-specific T cell responses with poor sensitivity among healthy donor-derived isolated CD8<sup>+</sup> T cells but not among unseparated PBMC.

After defining the general working principle of the T-Plex Assay based on a rotating cylindrical tube, we were keen to detect frequently occurring virus-specific CD8<sup>+</sup> T cell populations within HLA-A2<sup>+</sup> healthy donor PBMC. For this several HLA-A\*02:01 (HLA-A2<sup>+</sup>) positive healthy donors were initially screened using commercially available pHLA-A2 pentamers (ProlImmune) for viral recall antigens including HCMV pp65<sub>495-503</sub> and Flu MP-1<sub>58-66</sub>. In addition, a Survivin<sub>96-104</sub>/A2 pentamer served as negative control. Upon identification of a preexisting virus-specific CD8<sup>+</sup> T cell population by pHLA-A2 pentamers, we selected that particular donor for analysis by a corresponding T-Plex Assay (**Fig. 4.6**). As shown in **Fig. 4.6a**, HLA-A2<sup>+</sup> healthy donor #901215 displayed a prominent HCMV pp65<sub>495-503</sub>/HLA-A2 multimer<sup>+</sup> population corresponding to 1.1% among all CD8<sup>+</sup> T cells (~ 861 cells out of 1x10<sup>6</sup> complete PBMC) as well as a Flu-A MP-1<sub>58-66</sub> /HLA-A2 multimer<sup>+</sup> population (0.22% of CD8<sup>+</sup> T cells). Subsequently, we analyzed the 1x10<sup>6</sup> (data not shown) and 10x10<sup>6</sup> complete PBMC derived from donor #901215 using the corresponding pMHC-I-Fc-loaded T-Plex beads reflecting the same antigen specificities.

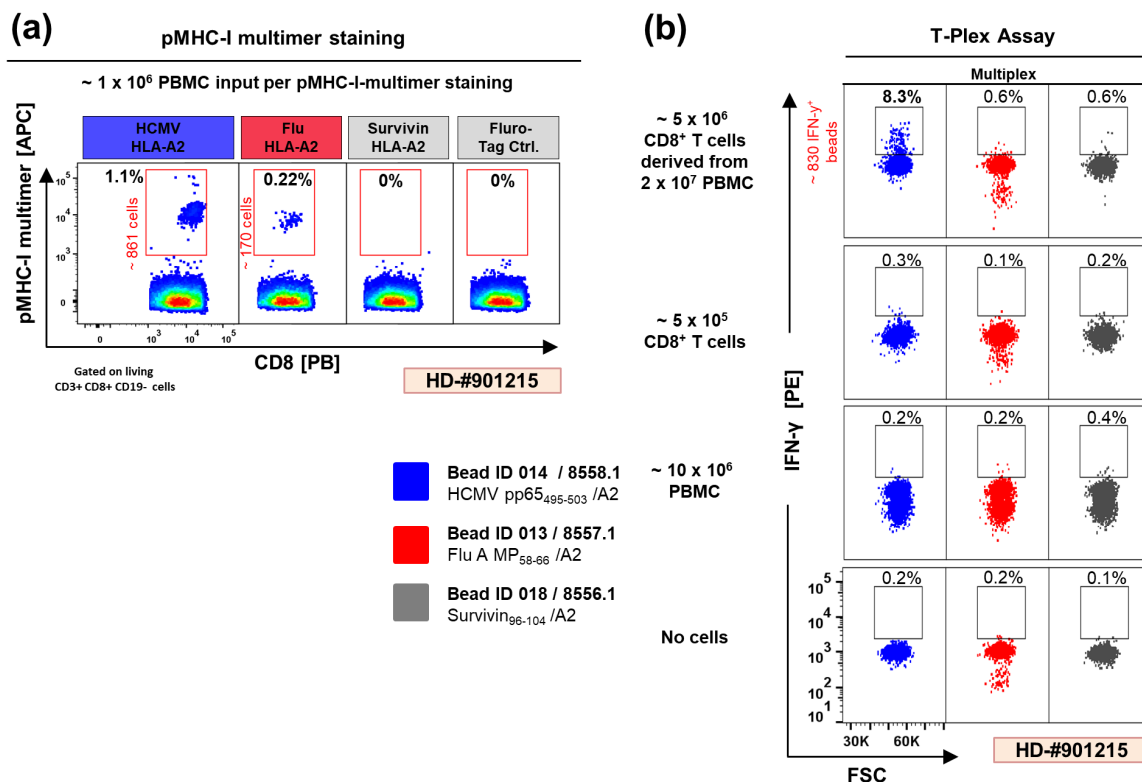


**Figure 4.6 | T-Plex Assay-based detection of HCMV pp65<sub>495-503</sub>/A2-specific T cells derived from isolated CD8<sup>+</sup> T cells but not from unseparated PBMC**

**(a) pMHC-I multimer staining of HLA-A2<sup>+</sup> healthy donor (HD)-#901215:** 1x10<sup>6</sup> PBMC from HD-#901215 were individually stained (no multiplex) with commercial pMHC-I multimers (Pentamer, ProlImmune). The frequency of pMHC-I multimer<sup>+</sup> cells within CD8<sup>+</sup> T cells and extrapolated total amounts of cells within 1x10<sup>6</sup> PBMC is shown. HD-#901215 displayed a prominent HCMV pp65<sub>495-503</sub>/HLA-A2 (HCMV/A2) and a minor Flu MP<sub>58-66</sub> (Flu/A2)-specific CD8<sup>+</sup> T cell population.

**(b) Corresponding T-Plex Assay of HD-#901215:** T-Plex bead-pools (4x multiplex / 10,000 beads per T cell epitope / bead ID 012-[8559.1] HPV E7<sub>11-19</sub>/A2 T-Plex beads are not shown) were incubated (4 h) either with indicated amounts of isolated untouched CD8<sup>+</sup> T cells derived from PBMC HD-#901215 or complete PBMC. Cylindrical 2 mL cryotubes filled with 2 mL CO<sub>2</sub>-saturated cell medium and a roller system at ~ 40 rpm were used. Presence of HCMV/A2-specific CD8<sup>+</sup> T cells was indicated by the appearance of an IFN-γ<sup>+</sup> subpopulation of cognate T-Plex beads that were above control beads.

The T-Plex Assay was performed as already described in **Fig. 4.5** using cryotubes filled with a total volume of 2 mL containing the indicated test sample and 10,000 beads/antigen-specificity of 1<sup>st</sup> generation T-Plex beads. However, we failed to detect any IFN- $\gamma$ -loaded T-Plex beads and thus any antigen-specific T cell response, when unseparated PBMC were used as test sample (**Fig 4.6b, lower panel**). Moreover, the overall number of beads to be analyzed was partially reduced, indicating a partial bead loss at the end of the T-Plex Assay procedure. We reasoned that this phenomenon might be caused due to phagocytosis of the T-Plex beads by macrophages (306) or a general absorbance by other immune cells for instance via Fc-receptors (307) as later again elucidated in **Section 4.2.4**. Therefore, we MACS-isolated untouched CD8<sup>+</sup> T cells from donor #901215 and repeated the T-Plex analysis as shown in **Fig 4.6b, upper panels**. The T-Plex Assay was performed using  $\sim 5 \times 10^6$  CD8<sup>+</sup> T cells (derived from  $2 \times 10^7$  PBMC) containing approximately 17,000 HCMV/A2-specific CD8<sup>+</sup> T cells as well as 3400 Flu/A2-specific CD8<sup>+</sup> T cells. As a result,  $\sim 8.3\%$  (830 out of 10,000) of the HCMV/HLA-A2-Fc-conjugated T-Plex beads were IFN- $\gamma$ -loaded in an antigen-specific manner, which was in line with previous results showing that the presence of 20,000 Sur/A2 T cells resulted in  $\sim 1000$  out of 10,000 cognate IFN- $\gamma$ <sup>+</sup> T-Plex beads. However, IFN- $\gamma$ <sup>+</sup> Flu/A2-Fc-loaded T-Plex beads reflecting the presence of  $\sim 3400$  Flu/A2-specific CD8<sup>+</sup> T cells was not detected and thus indicating an overall lack of sensitivity compared to the corresponding pMHC-I multimer staining. In accordance, usage of one tenth of the CD8<sup>+</sup> T cells ( $5 \times 10^5$ ) for T-Plex Assay-based analysis, which approximately contained  $\sim 1700$  HCMV/A2-specific CD8<sup>+</sup> T cells resulted in no detectable IFN- $\gamma$ <sup>+</sup> T-Plex bead population. Summarizing, the T-Plex Assay using the conditions described above did allow the detection of an antigen-specific T cell response among healthy donor-derived isolated CD8<sup>+</sup> T cells but not among unseparated PBMC. Moreover, there was strong need to improve the sensitivity of the T-Plex Assay.

## 4.2 T-Plex Assay optimization phase 1 – Moving to 2<sup>nd</sup> generation T-Plex beads

### 4.2.1 Optimized T-Plex bead architecture leads to a higher assay sensitivity

#### 4.2.1.1 Validation of the 2<sup>nd</sup> gen. T-Plex beads using the Survivin<sub>96-104</sub>/A2-specific CD8<sup>+</sup> T cell line

In the proof-of-principle experiments described in the previous **Section 4.1**, T-Plex beads were assembled based on carboxylated magnetic Luminex beads, which have been covalently conjugated with a polyclonal goat-anti-mouse IgG-Fc serum (G $\alpha$ M-IgG). In the next step, purified pHLA-A2-mIgG2a-Fc and human IFN- $\gamma$ -capture mAb (clone NIB42, isotype mouse IgG1) were added to G $\alpha$ M-IgG-Luminex-beads in a 2:3 ratio resulting in the first generation of T-Plex beads (1<sup>st</sup> gen. T-Plex beads, **Fig. 4.7a, upper panel**). However, this approach displayed several major drawbacks. First, it is absolutely required that pMHC-I-mIgG2a-Fc molecules in combination with the IFN- $\gamma$ -capture mAb are transferred at exactly the same ratio onto their associated G $\alpha$ M-IgG-Luminex-beads across an intended panel of antigen-specificities, since otherwise the resulting panel of T-Plex beads would have different IFN- $\gamma$ -binding capacities. Thus, it was required to have highly pure pHLA-A2-Fc constructs and correct protein concentrations. Since both, the human IFN- $\gamma$  capture (clone NIB42) and detection mAb (clone 4S.B3), are derived from a mouse hybridoma of IgG1 isotype, it was required to block free mouse-IgG-binding sites of the T-Plex beads using mouse serum after the co-culture with T cells. Omitting this blocking step otherwise resulted in high unspecific signals after staining with the IFN- $\gamma$ -detection mAb (**data not shown**).

To overcome these drawbacks, we covalently conjugated a monoclonal rat anti-mIgG2a antibody ( $\alpha$ -mIgG2a, clone RMG2a-62, BioLegend) and the IFN- $\gamma$ -capture mAb (clone NIB42, mIgG1) directly in

a 2:3 ratio to carboxylated magnetic Luminex beads, hereafter called “precursor” 2<sup>nd</sup> generation T-Plex beads (Fig. 4.7a, lower panel). In a second step, these precursor T-Plex beads of a single defined region/color are simply loaded alone with a pMHC-I-mIgG2a-Fc fusion constructs of choice and thus become fully assembled T-Plex beads. As a key advantage “precursor” 2<sup>nd</sup> generation T-Plex beads can directly be assembled by the usage of “crude” CHO-S cell supernatants containing pMHC-I-mIgG2a-Fc molecules instead of using affinity-chromatography purified pMHC-I-Fc proteins. In addition, it becomes easier to standardize the production of “precursor” T-Plex bead pools (multiple bead regions) sharing the same IFN- $\gamma$ -binding and pMHC-Fc binding capacity.

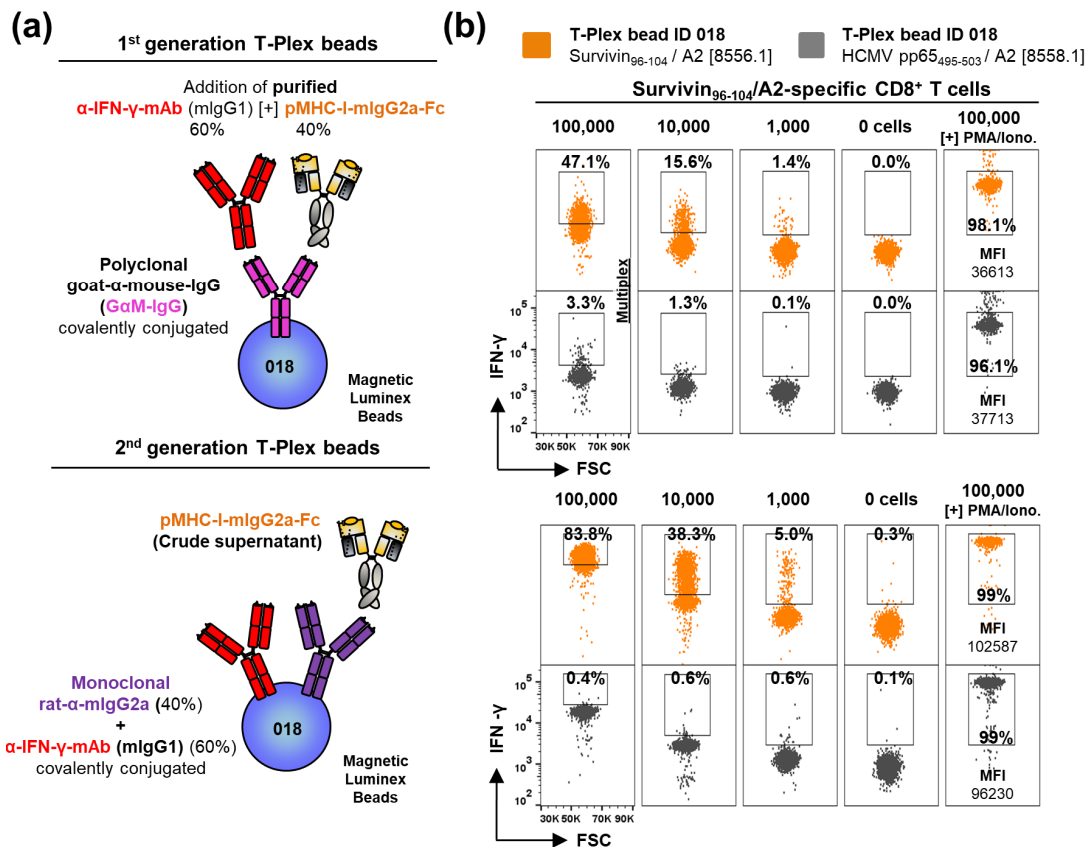


**Figure 4.7 | Optimized 2<sup>nd</sup> generation T-Plex architecture leads to an improved assay sensitivity**

**(a) (Upper panel) Architecture of 1<sup>st</sup> generation T-Plex beads.** Commercial magnetic carboxylated Luminex beads are covalently conjugated with a polyclonal goat-anti-mouse IgG (G $\alpha$ M-IgG) serum. In a second step, T-Plex beads of a defined region/color are generated by loading a  $\alpha$ -IFN- $\gamma$  capture mAb (mIgG1) together with a purified pMHC-I-mIgG2a-Fc in a 3 to 2 ratio. **(Lower panel) Architecture of 2<sup>nd</sup> generation T-Plex beads.** Luminex beads are covalently conjugated to an  $\alpha$ -IFN- $\gamma$  capture mAb (mIgG1 isotype) and a monoclonal rat- $\alpha$ -mIgG2a mAb in a 3 to 2 ratio. In a second step, T-Plex bead precursors of a defined region/color are loaded with saturating amounts of defined pMHC-I-mIgG2a-Fc constructs by directly using crude supernatants from CHO-S transient transfections.

**(b) Comparison of performance of 1<sup>st</sup> and 2<sup>nd</sup> generation T-Plex beads.** Bead ID: 012, 013, 014, 018 of 1<sup>st</sup> generation T-Plex beads were loaded with purified  $\alpha$ -IFN- $\gamma$  mAb and pMHC-I-mIgG2a-Fc dimers (upper panel) or corresponding CHO-supernatants in case of 2<sup>nd</sup> generation T-Plex beads (lower panel). 10,000 beads per T-Plex bead species (4x multiplex) were combined with the indicated amounts of pure Survivin<sub>96-104</sub>/HLA-A2 (Sur/A2)-specific CD8<sup>+</sup> T cells in one skirted cone-shaped 500  $\mu$ L tube filled with  $\sim$ 500  $\mu$ L CO<sub>2</sub>-saturated cell medium. The T-Plex Assays were performed at 37°C, 4 h, 40 rpm. T-Plex-beads ID 18 (orange) were conjugated with Survivin<sub>96-104</sub>/HLA-A2-Fc [8556.1] and 014-beads (grey / control) were loaded with HCMV pp65<sub>495-503</sub>/HLA-A2-Fc [8558.1]. T-Plex beads 012 and 013 were loaded with other irrelevant pMHC-I-Fc and behaved similar to control T-Plex bead 014 (data not shown). Fraction of IFN- $\gamma$ <sup>+</sup> beads that were above control T-Plex beads are shown. Maximal and homogeneous IFN- $\gamma$ -binding capacity of used T-Plex bead pools was assessed by additional PMA / ionomycin-based T cell stimulation. A pair of upper and lower FACS plots represent data analysis from the same reaction / bead mix (multiplex detection). MFI: Median fluorescence intensity.

Surprisingly, 2<sup>nd</sup> generation T-Plex beads also had an improved sensitivity for the detection of low frequency antigen-specific T cell responses resulting in overall 2–5-fold higher frequencies of IFN- $\gamma$ -loaded cognate T-Plex beads compared to 1<sup>st</sup> generation T-Plex beads (**Fig. 4.7b**). Moreover, 2<sup>nd</sup> generation T-Plex beads had an overall higher IFN- $\gamma$ -binding capacity shown by higher MFI values upon co-culture with maximally stimulated T cells (PMA and ionomycin). Notably, the T-Plex Assay experiments shown in **Fig. 4.7b** were performed in skirted cone-shaped 500  $\mu$ L tubes (Sarstedt) filled with  $\sim$ 500  $\mu$ L CO<sub>2</sub>-saturated cell medium instead of the previously used cryotubes filled with 2000  $\mu$ L medium, which also improved the assay performance and will be discussed in more detail in **Section 4.3.2 / Fig. 4.15**.

##### 4.2.1.2 Validation of 2<sup>nd</sup> gen. T-Plex beads using isolated CD8<sup>+</sup> T cells from healthy-donor PBMC

In the following, we were interested if the 2<sup>nd</sup> generation T-Plex bead concept would also improve the detection of low-frequency antigen-specific T cell populations within healthy donor PBMC. Thus, two suitable HLA-A2<sup>+</sup> healthy blood donors termed A-07-06-17 and B-07-06-17 were pre-characterized using a panel of pHLA A2-multimers presenting the peptides HCMV pp65<sub>495–503</sub>, Flu MP-1<sub>58–66</sub>, Survivin<sub>96–104</sub> and NY-ESO-1<sub>157–165</sub>. Among the tested specificities, donor A only displayed a small Flu MP-1<sub>58–66</sub>/HLA-A2-specific T cell population (0.2%) among all CD8<sup>+</sup> T cells, whereas donor B had only a prominent HCMV pp65<sub>495–503</sub>/HLA-A2-specific CD8<sup>+</sup> T cell population (0.9%) (**Fig. 4.8a, left panels for each donor**). Next, isolated “untouched” CD8<sup>+</sup> T cells derived from donor A and B were analyzed by a T-Plex Assay, which reflected the same T cell specificities (**Fig. 4.8b, upper panels**). In detail, for donor A roughly 2.5x10<sup>6</sup> total CD8<sup>+</sup> T cells were used as T-Plex Assay input, which according to the pMHC-I multimer staining would correspond to  $\sim$  5,000 Flu/A2-specific T cells (0.2%). For donor B, 1.3x10<sup>6</sup> isolated CD8<sup>+</sup> T cells harboring a fraction of  $\sim$  11,250 HCMV/A2-specific T cell cells (0.9%) were used as T-Plex Assay input. In both cases, the T-Plex Assay successfully detected the cognate T cell population revealing 4.5% / 450 IFN- $\gamma$ <sup>+</sup> cognate Flu/A2-T-Plex beads for donor A and 11% / 1100 IFN- $\gamma$ <sup>+</sup> cognate HCMV/A2-T-Plex beads for donor B that were above background. Thus, 2<sup>nd</sup> generation T-Plex beads successfully detected reliably  $\sim$  5,000 Flu/A2-specific T cells within 2.5x10<sup>6</sup> bystander cells. Notably, the frequency of IFN- $\gamma$ <sup>+</sup> T-Plex beads gained upon co-culture with CD8<sup>+</sup> T cells derived from donor A and B were somewhat lower compared to the cell titration based on the Survivin/A2 T cell line shown in **Fig. 4.7b**. In contrast previously used 1<sup>st</sup> generation T-Plex beads failed to detect  $\sim$  3800 Flu/A2-specific T cells (**Fig. 4.6**) indicating an improved sensitivity of 2<sup>nd</sup> generation T-Plex beads.

Since only the T-Plex beads are finally analyzed but not the actual test sample itself, we were intrigued by the idea, that the T-Plex Assay concept would in theory allow complete sample recovery. Thus, after co-culture of T-Plex beads and CD8<sup>+</sup> T cells from donor A and B, the cells were taken directly back into culture without further ado. 10 days later  $\sim$  1/10 of the samples was monitored by pMHC-I multimer analysis. Interestingly, the pMHC-I multimer staining indicated that in case of donor A the Flu/A2-specific CD8<sup>+</sup> T cell population had apparently expanded (**Fig. 4.8a, middle panels for each donor**). However, since a control culture without prior T-Plex analysis was not included it remains elusive if the proliferation of the Flu/A2-specific CD8<sup>+</sup> T cells was only due to the culture conditions itself comprising IL-2, IL-15, 10% human-serum in AIM-V or due to the prior conducted T-Plex Assay. In contrast, CD8<sup>+</sup> T cells of donor B displayed no change in frequency of the HCMV/A2-specific CD8<sup>+</sup> T cell population. Conclusively, execution of the T-Plex Assay did not result in a subsequent loss of the population of interest in both analyzed donors. Moreover, on day 16, we conducted a second T-Plex Assay using the same cultured sample that have been directly cultured after the first T-Plex Assay. Surprisingly, over 50% of the cognate T-Plex assay beads became IFN- $\gamma$ <sup>+</sup>, which is roughly 5–10-fold more compared to the first T-Plex Assay run (**Fig 4.8b, lower panels**). However, a subsequent pMHC-I multimer staining

one day after the 2<sup>nd</sup> T-Plex showed no striking changes in the population frequency (**Fig. 4.8a, right panels**). In addition, the total amount of cells used as input for the second T-Plex Assay was almost unchanged. Thus, a direct molecular explanation for the dramatic increase of cognate IFN- $\gamma$ <sup>+</sup> obtained in a second T-Plex Assay, that was also observed in subsequent experiments (**Fig. 4.13d**) remains elusive and beyond the scope of this study. However, it is well described that T cells upon cognate antigen recognition display an increased T cell receptor avidity by several mechanism and thus have an increased sensitivity towards their cognate antigen (308–310).

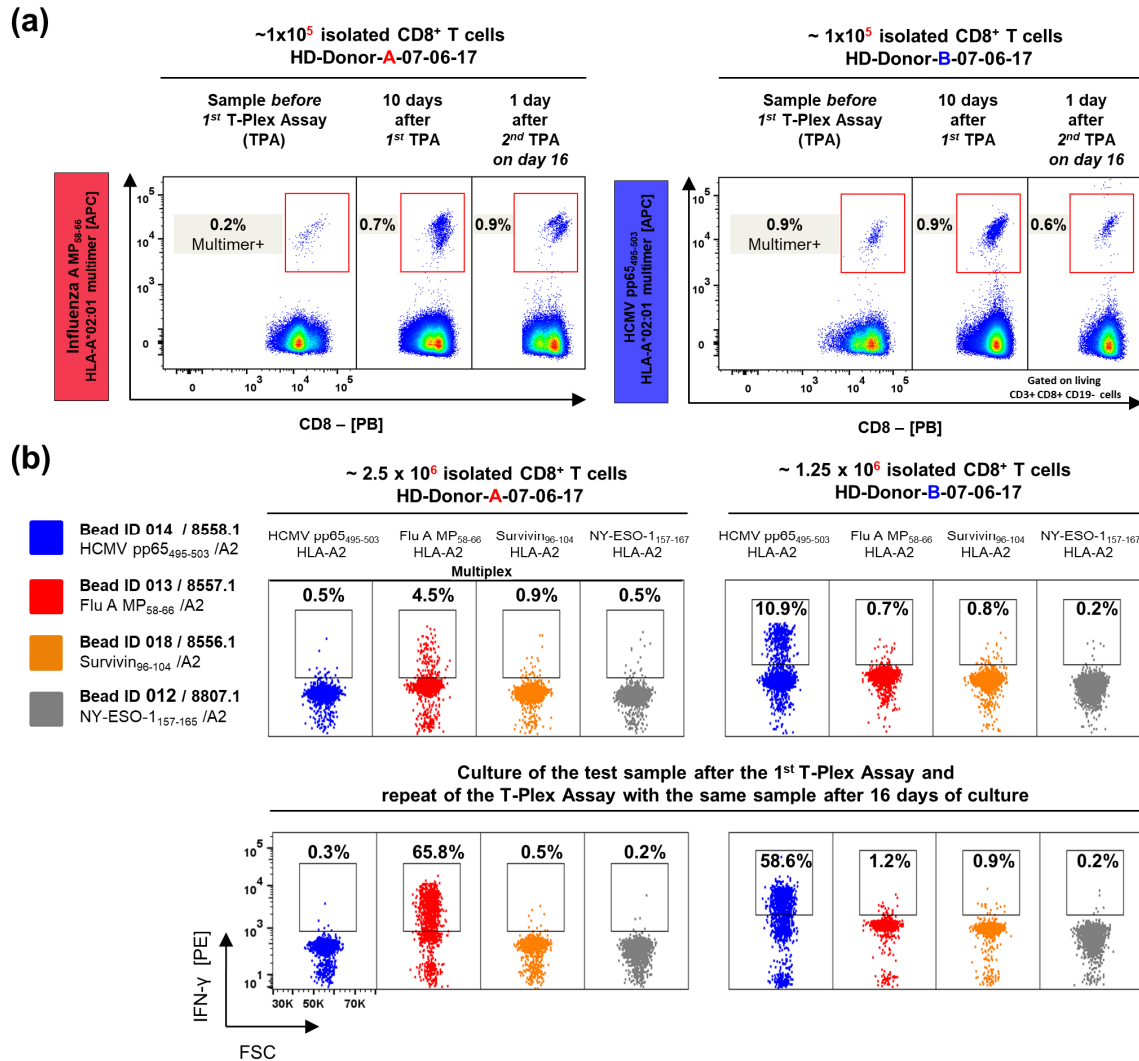


**Figure 4.8 | 2<sup>nd</sup> generation T-Plex beads allows detection of minor T cell populations and complete cell recovery**

Two HLA-A2<sup>+</sup> healthy donor (A & B) were pre-characterized by a panel of commercial pHLA-A2 multimers (pentamer, ProImmune) including HCMV pp65<sub>495-503</sub> / Flu A MP-1<sub>58-66</sub> / Survivin<sub>96-104</sub> / NY-ESO-1<sub>157-165</sub> specificities and which revealed only a prominent Flu/A2-specific CD8<sup>+</sup> population in case of donor A and a HCMV/A2-specific CD8<sup>+</sup> T cell population (donor B). Untouched CD8<sup>+</sup> T cells from these donors were isolated and ~ 1/10 of that sample was analyzed again by pMHC-I multimer staining (**a, right panels**) and the remaining sample was analyzed in parallel by a T-Plex Assay based on 2<sup>nd</sup> generation T-Plex beads (**b, upper panels**). After conduction of the first T-Plex Assay, beads were collected and analyzed and the T cell test sample was taken back into culture. After 10 days, the initial test sample was again analyzed by pMHC-I multimer staining (1/10 of the sample) (**a, middle panels**). On day 16 the remaining sample was again analyzed by a 2<sup>nd</sup> T-Plex Assay run (**b, lower panels**). The test sample was again taken back in culture after the 2<sup>nd</sup> T-Plex run. One day later after a second T-Plex Assay has been conducted ~ 1/10 sample was analyzed by pMHC-I multimer staining (**a, right panels**). (**b**) T-Plex Assays were performed in 500  $\mu$ L tubes rotating at 37°C for 4 h at 40 rpm. Used 2<sup>nd</sup> generation T-Plex beads with IDs and pMHC-I-Fc loaded constructs are indicated in the figure. The presence of the antigen-specific T cells was indicated by the appearance of an IFN- $\gamma$ <sup>+</sup> subpopulation of cognate T-Plex beads that were above control beads. Rows of linked T-Plex data represent analysis from the same reaction / bead mix (multiplex detection).

Therefore, it seems reasonable that the cognate T cells in donor A and B previously activated by the first T-Plex Assay might have had a lower activation threshold towards cognate T-Plex beads. In line, also CD8 co-receptor expression increases after antigen-encounter, which additionally increases the sensitivity of T cells (311, 312). In accordance, we also often observed an increase in CD8 co-receptor expression after antigen-encounter for instance during T cell line generation (**Fig. 3.5**), which might explain the different sensitivities of the T-Plex Assay for detecting either a CD8<sup>+</sup> T cell line or the corresponding antigen-specificity within “freshly” isolated CD8<sup>+</sup> derived from a healthy donor.

Taken together, the optimized 2<sup>nd</sup> generation T-Plex bead precursor architecture overall allows more straightforward assembly of T-Plex beads by addition of pMHC-Fc containing cell supernatants and most importantly also improves the T-Plex Assay’s sensitivity to a great extent. Moreover, complete sample recovery is possible after conducting a T-Plex Assay, which is a unique feature of the T-Plex Assay concept in contrast to a pMHC multimer staining unless the target population is directly FACS sorted.

#### 4.2.2 Parallel detection of multiple T cell lines by 2<sup>nd</sup> generation T-Plex beads

In order to further demonstrate and assess the multiplex capacity of the T-Plex Assay concept, we aimed at detecting multiple T cell specificities within a single assay reaction. To this end, we took advantage of previously established and verified virus epitope-specific and HLA-A2-restricted CD8<sup>+</sup> T cell lines (**Section 3.2.2**) in addition to the available Survivin<sub>96-104</sub>/A2-specific T cell line. Thus, 1000 cells of the EBV BMLF-1<sub>259-267</sub>/A2-specific CD8<sup>+</sup> T cell line #0144 alone or in combination with the same amount of the HCMV pp65<sub>495-503</sub>/A2-specific CD8<sup>+</sup> T cell line #416 and Survivin<sub>96-104</sub>/A2-specific T cell line were brought in co-culture with a pool of T-Plex beads reflecting the same antigen specificities as well as one control epitope **Fig. 4.9**. 10,000 beads/epitope of color-coded pHLA-A2-Fc-loaded 2<sup>nd</sup> generation T-Plex beads were combined with the individual T cell mixtures in skirted cone-shaped 500 µL tubes and rotated for 4 h at 37°C and 40 rpm, hereinafter referred to as standard T-Plex Assay. As a result, cognate T-Plex beads contained a distinct subpopulation of IFN-γ<sup>+</sup> loaded beads, only when the cognate T cell lines were present during the assay reaction. Importantly, the presence of all three T cell lines within one T-Plex reaction was clearly detected by the corresponding T-Plex bead species demonstrating capacity to detect multiple T cell specificities within one assay.

Notably, the activation of 1000–3000 T cells by cognate T-Plex bead led to a consistent and homogeneous “bystander” IFN-γ loading of T-Plex beads present when directly compared to “T cell untouched” T-Plex beads. Therefore, it is always required to set a threshold for “cognate” IFN-γ<sup>+</sup> T-Plex beads within each T-Plex Assay experiment (tube) based on the “bystander” IFN-γ-load of a control T-Plex pool (grey) either without or with an irrelevant pMHC-I-Fc conjugation. Moreover, the repetitive measurement of 1000 EBV/A2-specific CD8<sup>+</sup> T cells by the T-Plex Assay (different tubes) consistently resulted in very similar frequencies of cognate IFN-γ<sup>+</sup> T-Plex corresponding to an average amount of ~ 600 IFN-γ<sup>+</sup> beads and a standard deviation of only 51 beads. In accordance, also the presence of 1000 Sur/A2- or HCMV/A2-specific CD8<sup>+</sup> T cells resulted in 440–1000 cognate IFN-γ-loaded T-Plex beads suggesting an apparent linear relationship for that particular absolute T cell count and corresponding fraction of IFN-γ<sup>+</sup> cognate T-Plex beads (**Fig. 4.9**). In conclusion, T-Plex beads allow a reliable parallel detection of multiple T cell responses within a single T-Plex reaction.

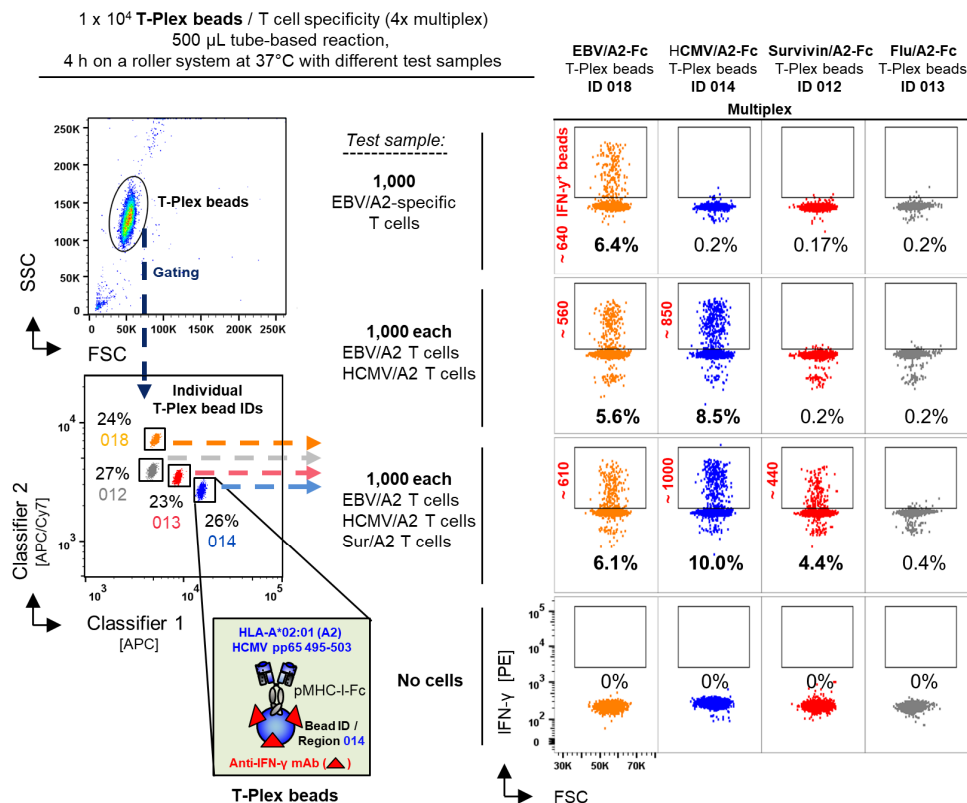


**Figure 4.9 | T-Plex Assay-based antigen-specific multiplex detection of a defined set of CD8<sup>+</sup> T cell lines**

Four different color regions (bead ID: 012, 013, 014, 018) of 2<sup>nd</sup> generation T-Plex beads were loaded with a defined set of pHLA-A2-Fc molecules (construct IDs: 8556.1 / 8557.1 / 8558.1 / 8804.1). 10,000 beads per T-Plex bead ID / T cell epitope were combined with the indicated amounts of antigen-specific T cell lines in one cone-shaped 500  $\mu$ L tube filled with ~500  $\mu$ L CO<sub>2</sub>-saturated cell medium. The T-Plex Assay was performed at 37°C, 4 h, 40 rpm. The presence of a T cell line was indicated by the appearance of an IFN- $\gamma$ <sup>+</sup> subpopulation of cognate T-Plex beads that was above control beads. EBV BMLF-1<sub>259-267</sub>/HLA-A2-specific CD8<sup>+</sup> T cell line #0144 (EBV/A2 T cells), HCMV pp65<sub>495-503</sub>/HLA-A2-specific CD8<sup>+</sup> T cell line #416 (HCMV/A2 T cells) and Survivin<sub>96-104</sub>/HLA-A2-specific CD8<sup>+</sup> T cell line (Sur/A2 T cells) were used. Rows of linked T-Plex data represent analysis from the same reaction / bead mix (multiplex detection).

#### 4.2.3 Assessment of the sensitivity and dynamic range of 2<sup>nd</sup> generation T-Plex beads compared to pMHC-I multimer staining

In subsequent experiments, we wanted to address the following questions: Firstly, do bystander T cells have a strong impact on the detection capacity of the T-Plex Assay? Secondly, what is the overall sensitivity and dynamic range of 2<sup>nd</sup> generation T-Plex beads and associated assay procedure?

Thus, 1000 cells of the HCMV pp65<sub>495-503</sub>/A2-specific T cell line #416 were spiked into 250,000 Survivin<sub>96-104</sub>/A2-specific T cells serving as bystander T cells. The spiked test sample and 1000 HCMV/A2 T cells alone were subjected side-by-side to a standard T-Plex Assay comprising HCMV/A2-Fc-loaded 2<sup>nd</sup> generation T-Plex beads and three irrelevant pMHC-I-Fc loaded T-Plex bead pools (Fig. 4.10). Surprisingly, the presence or absence of 250,000 bystander T cells resulted only in minor changes ( $\pm$  2%) in the frequency of IFN- $\gamma$ <sup>+</sup> cognate HCMV/A2-T-Plex beads, which was also observed as an intra-experimental variation in the previous described experiment (Fig. 4.9). This initial finding, which was later again confirmed in Fig. 4.12, suggested that bystander T cells are neglectable for the T-Plex Assay's performance.

#### 4 | Results Part 2 – Development of the T-Plex Assay

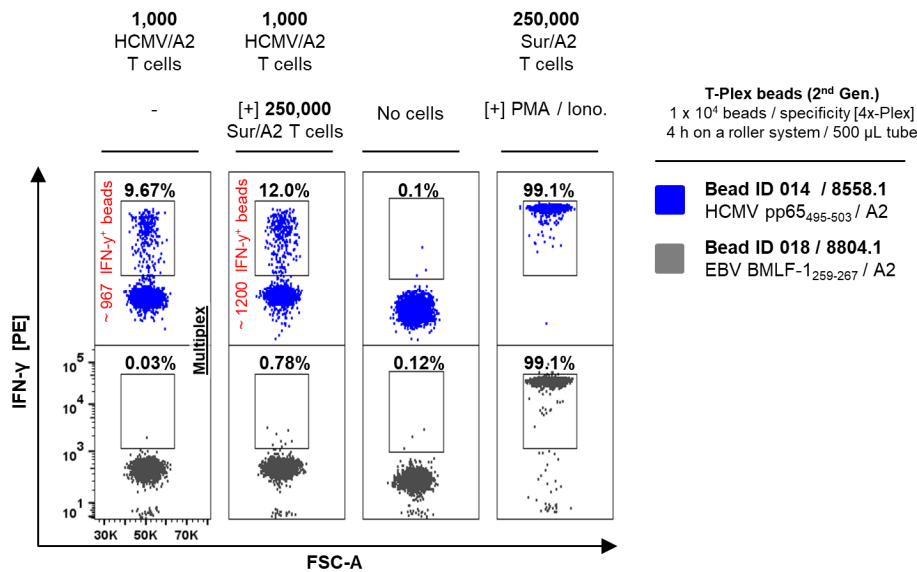


**Figure 4.10 | Bystander T cells do not decrease the sensitivity of the T-Plex Assay**

pMHC-I-Fc-loaded 2<sup>nd</sup> generation T-Plex beads (10,000 beads per T-Plex bead ID and T cell epitope) were combined either with 1,000 cells of the HCMV pp65<sub>495-503</sub>/A2-specific CD8<sup>+</sup> T cell line #416 (HCMV/A2 T cells) or 1,000 CMV/A2 T cells spiked into 250,000 bystander Survivin<sub>96-104</sub>/A2-specific CD8<sup>+</sup> T cells (Sur/A2 T cells). The T-Plex Assay was performed in a 500 μL tube rotating at 37°C for 4 h at 40 rpm. The presence of the T cell line was indicated by the appearance of an IFN-γ<sup>+</sup> subpopulation of cognate T-Plex beads. Functionality of the Sur/A2 T cells and all used T-Plex beads was verified by PMA / ionomycin (Iono.) stimulation. In this experiment four different color regions (bead ID: 012, 013, 014, 018) of 2<sup>nd</sup> generation T-Plex beads were loaded with a defined set of pHLA-A2-Fc molecules (construct IDs 8557.1 / 8558.1 / 8804.1 / 8807.1). Shown is only the IFN-γ signal of the cognate HCMV/A2-T-Plex beads ID 014 (*blue*) and one representative corresponding control-bead signal ID 018 (*grey*). Linked pairs of upper and lower FACS-plots represent data analysis from the same multiplex reaction / bead mix.

Next, HCMV pp65<sub>495-503</sub>/A2-specific T cells were spiked in a dilutive manner into Survivin<sub>96-104</sub>/A2-specific T cells to define the T-Plex Assay's sensitivity in comparison to a corresponding pMHC-I multimer staining. The spiked T cell sample was analyzed side-by-side either by pMHC-I multimer-based staining (**Fig. 4.11a**) or T-Plex Assay (**Fig. 4.11b**). As shown in **Fig. 4.11a**, a very low frequency of 0.06% (~200 cells out of 2.5x10<sup>5</sup> cells) and even 0.005% (~20 out of 2.5x10<sup>5</sup> cells) could be reliably detected by commercial HCMV pp65<sub>495-503</sub>/A2 multimer (pentamer, ProImmune) staining, which is in accordance with the published detection limit of a pMHC-I multimer staining without any experimental enrichment strategies (156). Moreover, in line with previous publications (313, 314), we also observed a perfect linearity between the HCMV/A2 T cell dilution and fraction of pMHC-I multimer binding cells (multimer<sup>+</sup>) (**Fig. 4.11c, left panel**). In contrast, 200 antigen-specific T cells out of 2.5x10<sup>5</sup> bystander cells (0.06%) represent the lower detection limit of the T-Plex Assay (**Fig. 4.11b**). Thus, the pMHC-I multimer staining was approximately 10x more sensitive compared to the T-Plex Assay. In terms of dynamic range, the presence of more than 10,000 cognate T cells led to a severe IFN-γ bystander capture onto control T-Plex beads resulting in a less distinct separation between cognate and control T-Plex beads, which dampens the sensitivity for the parallel detection of other antigen-specific T cells present at lower frequencies. In that sense, the T-Plex Assay performs similar to an ELISpot assay, which also lacks dynamic range at high frequency T cell responses resulting in complete signal saturation. For a standard 96-well plate-based ELISpot this signal saturation however is already reached at 900–1000 spot-forming cells/well resulting in a lack of distinction of single spot-forming cells (315). The T-Plex Assay in contrast displayed a linear relationship between 200 and 10000 cognate T cells under the conditions used (10,000 T-Plex beads/T cell epitope, 500 μL tubes, 40 rpm, 4 h at 37°C) (**Fig. 4.11c, right panel**). However, the T-Plex Assay may be prone to underestimate the cognate

response at T cell numbers higher than 1000 cells resulting in strikingly less IFN- $\gamma$  T-Plex beads compared to the actual cell input. Consequently, there is still need to optimize the assay procedure further and to increase firstly the sensitivity and secondly the dynamic range of the T-Plex Assay.

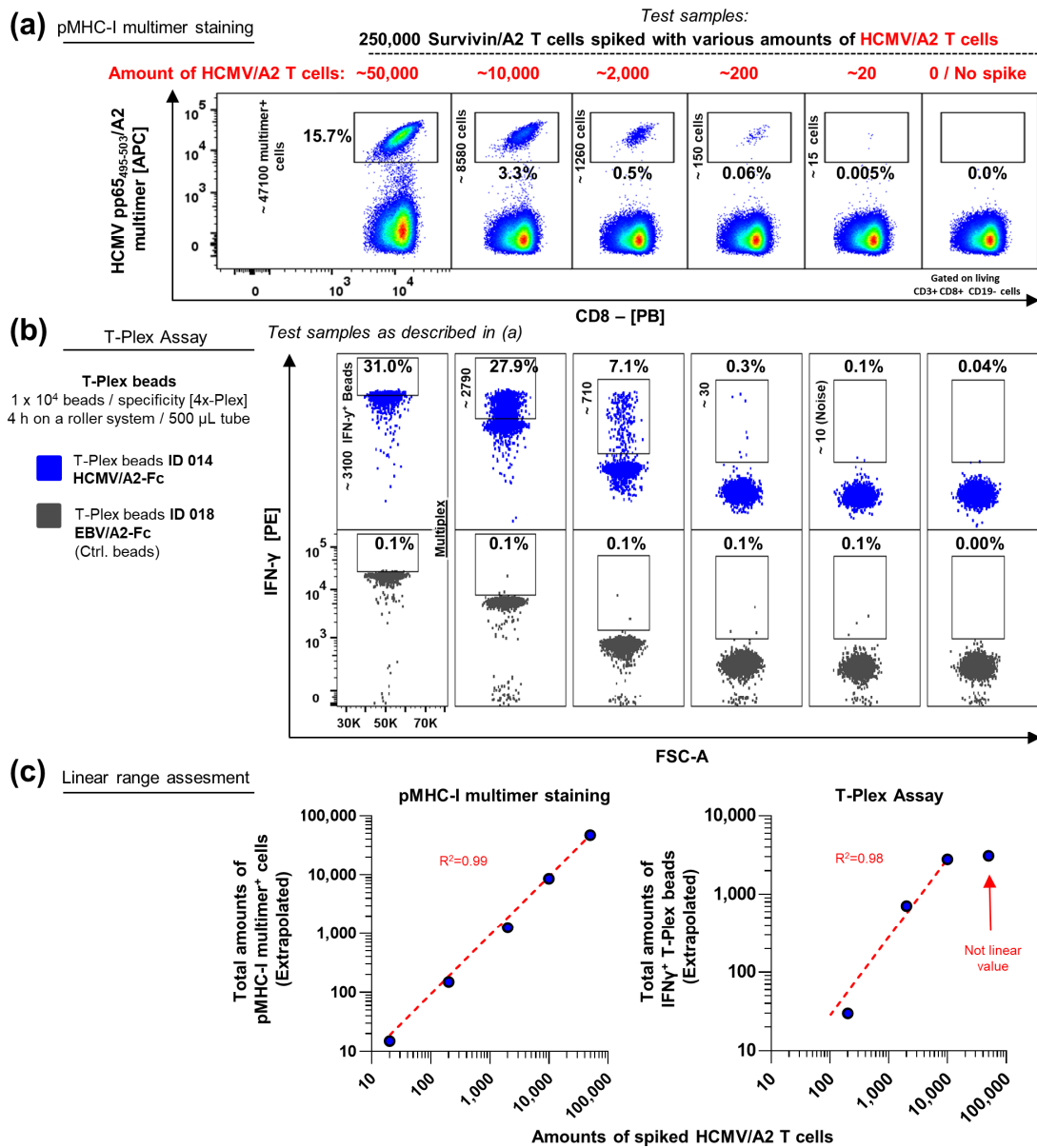


**Figure 4.11 | pMHC-I multimer staining in comparison to T-Plex Assay of T cell line spiked samples**

A defined amount (~40 – 100,000) of the HCMV pp65<sub>495–503</sub>/A2-specific CD8<sup>+</sup> T cell line #416 (HCMV/A2 T cells) was spiked into a pool of 500,000 Survivin<sub>96–104</sub>/A2-specific T cells. The spiked test sample was split in half and either analyzed by commercial pMHC-I multimer staining (a) or T-Plex Assay (b).

**(a) pMHC-I multimer staining:** The spiked sample was stained with a commercial HCMV/A2-multimer (pentamer, ProImmune) in the presence of 50 nM dasatinib. The frequency of pMHC-I multimer<sup>+</sup> cells within the CD8<sup>+</sup> / CD3<sup>+</sup> T cell population is shown. In addition extrapolated total amounts of pMHC-I multimer<sup>+</sup> cells are shown.

**(b) Corresponding T-Plex Assay:** Four different 2<sup>nd</sup> generation T-Plex bead species (10,000 beads / T cell epitope, bead ID: 012, 013, 014, 018) either loaded with cognate HCMV/A2-Fc [8558.1] or irrelevant pMHC-I-Fc [8557.1 / 8804.1 / 8807.1] were combined with the spiked T cell sample followed by T-Plex Assay analysis. T-Plex Assays were performed in a 500  $\mu$ L tubes rotating at 37°C for 4 h at 40 rpm. Shown is the IFN- $\gamma$  signal of the cognate HCMV/A2 T-Plex beads (blue) and one representative corresponding control bead signal (grey). Extrapolated total amounts of IFN- $\gamma$  T-Plex beads are shown. Linked pairs of upper and lower FACS-plots represent data analysis from the same reaction / bead mix

**(c) Linear range comparison.** Amounts of spiked HCMV/A2 T cells derived from counting chamber-based calculations is plotted in a bilogarithmic fashion against extrapolated total amounts of pMHC-I multimer<sup>+</sup> cells (left panel) or extrapolated total amounts of IFN- $\gamma$  T-Plex beads (right panel). Linear regression is shown through linear points only (red dotted line).

#### 4.2.4 The T-Plex Assay is impaired by CD14<sup>+</sup> cells but not by other bystander cells present in PBMC

##### **4.2.4.1 T-Plex Assay performance based on the cellular composition of the test sample**

In previous experiments (**Fig. 4.6**), we observed that T-Plex beads failed to detect an antigen-specific T cell population within “complete” unseparated PBMC, which had been confirmed by pMHC-I multimer staining. However, if isolated CD8<sup>+</sup> T cells were used as test sample instead, the antigen-specific T cell population was detectable by cognate T-Plex beads. Therefore, we wanted to elucidate which cell types within PBMC might impact the T-Plex Assay performance. PBMC of HLA-A2<sup>+</sup> healthy blood donor #3838, who harbored according to pMHC-I multimer staining a pronounced EBV BMLF-1<sub>259-267</sub>/A2-specific CD8<sup>+</sup> T cell population (~2% of all CD8<sup>+</sup> T cells) (**Fig. 4.12a**), was subsequently analyzed by a corresponding T-Plex Assay (10,000 T-Plex beads/T cell epitope, 500 µL tubes, 40 rpm, 4 h at 37°C) using different cell compositions. For this experiment either pan-T cells or CD8<sup>+</sup> T cells were negatively (“untouched”) isolated or alternatively CD14<sup>+</sup> cells were depleted from PBMC using respective MACS-isolation kits (Miltenyi). Successful cell isolation / depletion was confirmed by flow cytometry analysis (**Supplementary Fig. S7**). As shown in **Fig. 4.12b**, the T-Plex Assay displayed no signal for EBV/A2-specific CD8<sup>+</sup> T cells when unseparated PBMC were used as sample, nor if the PBMC were previously incubated with human IgG1 (TruStain FcX<sup>TM</sup>, Biolegend) to block Fc-receptors. Depletion of CD19<sup>+</sup> B cells also did not allow T-Plex Assay-based detection of the EBV/A2-specific CD8<sup>+</sup> T cells (**data not shown**). However, the T-Plex Assay revealed the EBV/A2-specific CD8<sup>+</sup> T cell population, if either pan-T cells, CD8<sup>+</sup> T cells or PBMC depleted from CD14<sup>+</sup> monocytes were used (**Fig. 4.12b**). In all conditions shown in **Fig. 4.12b**, the used amounts of cells within a T-Plex Assay was always derived from the same total quantity of complete PBMC (6.5x10<sup>6</sup> cells) regardless if pan-T cells, PBMCs without CD14<sup>+</sup> cells or only CD8<sup>+</sup> T cells were used. Based on the obtained pMHC-I multimer data, we extrapolated that approximately 14,000 EBV/A2-specific CD8<sup>+</sup> T cells were present in the cell mixture subjected to T-Plex Assay in all conditions shown. In accordance, all corresponding T-Plex Assays performed with a depletion of CD14<sup>+</sup> cells displayed almost equal amounts of ~9.9% ± 0.7 (990 ± 70 beads) cognate IFN-γ loaded (IFN-γ<sup>+</sup>) T-Plex beads. This result was in line with previous results (**Fig. 4.10**) showing that the outcome of the T-Plex Assay as reflected by the percentage of cognate IFN-γ<sup>+</sup> T-Plex beads is hardly influenced by irrelevant bystander T cells. Moreover, also in the previous experiment shown in **Fig. 4.8**, the presence of 10,000 HCMV/A2-specific T cells within healthy donor CD8<sup>+</sup> T cells resulted in the appearance of ~ 1000 cognate IFN-γ<sup>+</sup> T-Plex again demonstrating on overall robustness of the T-Plex Assay across different experiments.

##### **4.2.4.2 Playing with food – Phagocytosis of T-Plex beads by CD14<sup>+</sup> monocytes**

The depletion of CD14<sup>+</sup> cells from the PBMC pool clearly proved our hypothesis that CD14<sup>+</sup> monocytes / macrophages interfere with the T-Plex Assay due to phagocytosis or absorbance of the T-Plex beads. Thus, we were interested in strategies to inhibit phagocytosis of the T-Plex beads, which would omit additional preparation steps of PBMC comprising CD14<sup>+</sup> cell depletion or T cell isolation prior to a T-Plex Assay run. The ubiquitously expressed transmembrane cell surface glycoprotein CD47 functions as ligand to the receptor signal regulatory protein alpha (SIRPα), which in turn is mostly expressed on monocytes, granulocytes and subsets of dendritic cells. Binding of CD47 to SIRPα results in an inhibitory signal that ultimately counteracts phagocytosis leading to the proposed functions of CD47 as “marker of self” and “don’t eat me signal” (316).

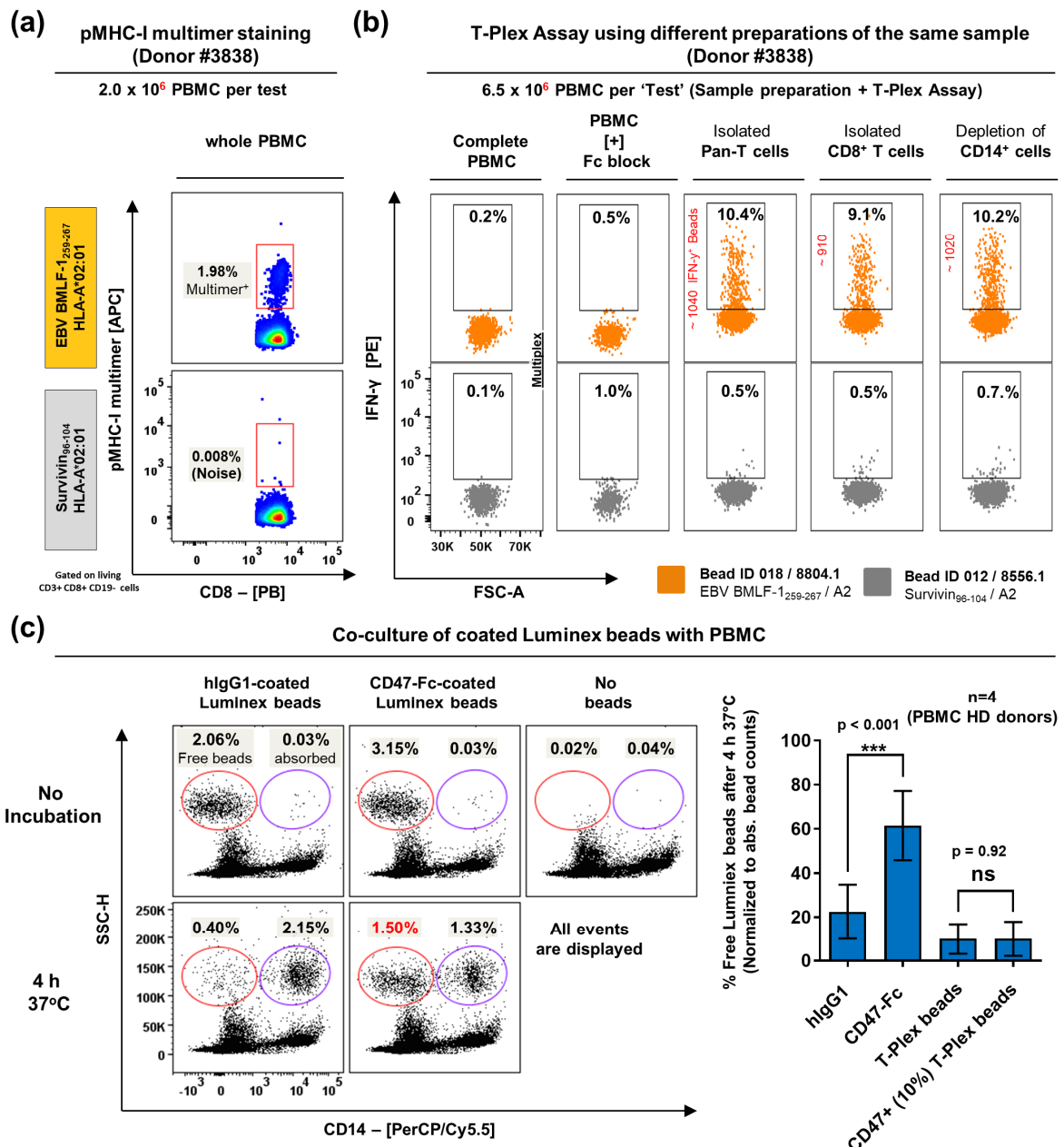


**Figure 4.12 | T-Plex Assay performance is impaired by CD14<sup>+</sup> monocytes present in PBMC**

**(a) pMHC-I multimer staining of healthy donor (HD) #3838:** 2x10<sup>6</sup> PBMC were individually stained with commercial pMHC-I multimers (pentamer, ProImmune) as indicated in the figure (no multiplex). The frequency of pMHC-I multimer<sup>+</sup> cells within the CD8<sup>+</sup> T cell population is shown.

**(b) T-Plex Assay performance based on sample type.** Corresponding T-Plex bead-based analysis of the same donor #3838. 2<sup>nd</sup> generation pMHC-I-Fc-loaded T-Plex bead pools (4x multiplex / 10,000 beads per T cell specificity) were incubated (4 h) either with (i) 6.5x10<sup>6</sup> unseparated PBMC; (ii) with PBMC previously incubated with hlgG1 (Fc-block); (iii) with MACS-isolated “untouched” pan-T cells or (vi) CD8<sup>+</sup> T cells derived from 6.5x10<sup>6</sup> PBMC; (v) or with 6.5x10<sup>6</sup> PBMC depleted from CD14<sup>+</sup> cells. The presence of antigen-specific T cells was indicated by the appearance of an IFN-γ<sup>+</sup> subpopulation of cognate T-Plex beads that was above control T-Plex beads. Pairs of upper and lower plots are from the same T-Plex Assay.

**(c) Partial block of phagocytosis by CD47-Fc coated Luminox beads:** Luminox beads were covalently conjugated either with CD47-hlgG1-Fc (R&D) or hlgG1-isotype control. 4x10<sup>4</sup> CD47- or IgG1-coated Luminox beads as well as standard T-Plex beads or CD47-Fc modified T-Plex beads (10% of the Luminox beads’ total protein binding capacity was conjugated to CD47-Fc) were incubated with 1x10<sup>6</sup> unseparated PBMC for 4 h at 37°C under constant rolling. The sample mix was subsequently stained with α-CD14 mAb and analyzed by FACS. The FACS plots display the fraction “free beads” defined as SSC<sup>high</sup>/CD14<sup>neg</sup> and “adsorbed / engulfed beads” defined as SSC<sup>high</sup>/CD14<sup>+</sup> within all events. Bar diagram shows the normalized percent of free beads based on the total count of beads (free & adsorbed beads) for a given condition. Error is shown as standard deviation; n = 4 different PBMC from healthy donors; ns: non significant; Student’s t-test

Thus, we envision that coating of T-Plex beads with a soluble CD47-IgG1-Fc fusion protein (CD47-Fc) might provide a sufficient "don't eat me signal" that will prevent bead engulfment during the assay procedure. This concept has already been successfully exploited in the past for particles / beads of various sizes ranging from 100 nm to 6  $\mu\text{m}$  (306, 317, 318) as well as of artificial antigen-presenting cells explicitly comprising pMHC-I-Ig fusion proteins and  $\alpha\text{CD28}$ -mAb-coated Dynabeads (2.8  $\mu\text{m}$ ) (295). Subsequently, we covalently conjugated recombinant soluble human CD47-hIgG1-Fc fusion protein (CD47-Fc, R&D) or human IgG1 isotype control to Luminex-beads. In the next step, CD47-coated or control-Luminex beads were incubated for 4 h at 37°C with PBMC from various healthy-donors followed by FACS analysis (**Fig. 4.12c**). As expected, after the incubation  $77 \pm 12\%$  previously "free" IgG1-control Luminex beads (no incubation) became absorbed / engulfed by CD14<sup>+</sup> cells. This process was significantly reduced by approximately 40% when the bead surface was completely coated with CD47-Fc instead. Unfortunately, if only 10% of the maximal protein binding capacity of the Luminex beads represented CD47-Fc, no blocking of the phagocytic activity was observed (**Fig. 4.12c**) and thus also did not facilitate T-Plex reactions in the presence of CD14<sup>+</sup> cells (**data not shown**). Our data are somewhat in contrast to the publication by Bruns *et al.*, where the authors demonstrated that additional coating of artificial antigen-presenting Dynabeads (2.8  $\mu\text{m}$ ) with recombinant CD47 does efficiently block phagocytosis of the particles by approximately 60% at very low surface densities (less than 1% of the bead protein-binding capacity) (295). However, in their experiments they used a 1:1 bead-to-monocyte ratio, whereas in our experiments roughly 10–20 times more monocytes were present compared to beads (**Fig. 4.12c**). Moreover, even completely CD47-coated beads (10  $\mu\text{m}$ ) used by Tsai *et al.* blocked the phagocytic activity of human monocytes by no more than 50% nor did small molecule-based (i.e. blebbistatin) inhibition of phagocytosis (318). In conclusion, our results strongly suggest that CD47-Fc coating of particles is not efficient enough to completely protect a small amount of beads over a 4–5 h duration from phagocytosis. Apparently, the decision to phagocytose an IgG-coated particle by a monocyte / macrophage represents a delicate balance of a variety of pro-phagocytic cell signaling events mediated by scavenger receptors and Fc-receptors as well as the balance of inhibitory signaling driven by the SIRP $\alpha$  / CD47 axis, which does not act in our favor (319). Thus, depletion of CD14<sup>+</sup> cells remains a prerequisite for the T-Plex Assay.

#### 4.2.5 Sensitivity issue of the T-Plex Assay in comparison to pMHC multimer staining and ICS

Previous T cell line-dilution experiments demonstrated that roughly 200 antigen-specific T cells are required to obtain a signal on cognate T-Plex beads (2<sup>nd</sup> generation) that is above background (**Fig. 4.11**). To further evaluate the detection limit determined by the T cell line, we firstly wanted to validate this T-Plex Assay detection threshold using freshly healthy donors derived CD8<sup>+</sup> T cells and secondly to compare the performance with pMHC-I multimer staining and peptide-based 4 h *in vitro* restimulation followed by IFN- $\gamma$  intracellular cytokine staining (ICS) (**Fig. 4.13**).

pMHC-I multimer staining of HLA-A2<sup>+</sup> healthy donor #3838 revealed a prominent EBV BMLF-1<sub>259–267</sub>/A2 (EBV/A2)-specific CD8<sup>+</sup> T cell population as already presented previously in **Fig. 4.12**. In addition, a respective pMHC-I multimer also indicated a minor Flu MP-1<sub>58–66</sub>/A2 (Flu/A2)-specific CD8<sup>+</sup> T cell population comprising 0.065% among all CD8<sup>+</sup> T cells, which in turn corresponded to approximately 60 cells out of  $1 \times 10^6$  PBMC (**Fig. 4.13a**, upper panels & **Table 4.1**). For this initial pMHC-I multimer analysis,  $2 \times 10^6$  PBMC were used per individual pMHC-I multimer staining. The same amount of cells was subjected to individual, corresponding peptide-based *in vitro* restimulations for 4 h followed by ICS shown in **Fig. 4.13b**, which revealed almost the same percentage of Flu MP-1<sub>58–66</sub> as well as EBV BMLF-1<sub>259–267</sub> peptide-based activated IFN- $\gamma$ <sup>+</sup> CD8<sup>+</sup> T cells as previously detected by the pMHC-I-multimer

staining. This demonstrated that both EBV/A2- and Flu/A2-specific CD8<sup>+</sup> T cell populations are fully functional and respond to an antigen-specific stimulation. In the next step, isolated CD8<sup>+</sup> T cells derived from 6.5x10<sup>6</sup> PBMC (donor #3838) containing roughly 14,000 EBV/A2- as well as 400 Flu/A2-specific CD8<sup>+</sup> T cells were subject to a multiplex T-Plex reaction (Fig. 4.13c).

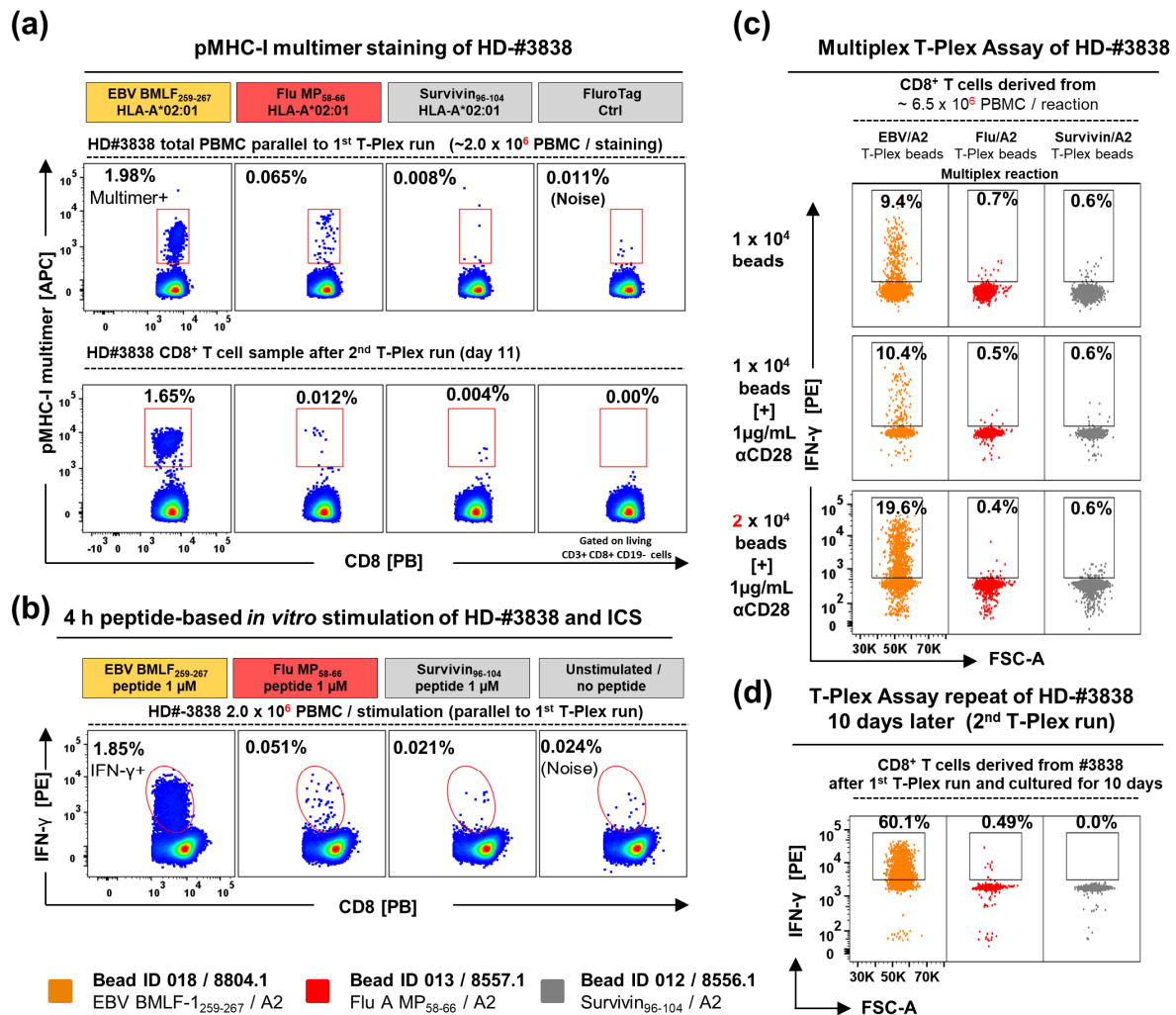


**Figure 4.13 | Sensitivity of the T-Plex Assay in comparison to pMHC-I multimer staining and ICS**

**(a) pMHC-I multimer staining of healthy donor (HD) #3838:** (Upper panel) 2x10<sup>6</sup> unseparated PBMC were individually stained with commercial pMHC-I multimers (pentamer, ProImmune, no multiplex) parallel to T-Plex analysis. The frequency of pMHC multimer<sup>+</sup> cells within the CD8<sup>+</sup> T cell population is shown. See also Table 4.1, which shows in addition the extrapolation of antigen-specific T cells subjected to corresponding T-Plex Assays. (Lower panel) pMHC-I multimer re-analysis of isolated HD-#3838 CD8<sup>+</sup> T cells one day after 2<sup>nd</sup> T-Plex run.

**(b) Corresponding 4 h peptide-based restimulation assay followed by ICS:** 2x10<sup>6</sup> PBMC were individually stimulated using a 1 μM peptide pulse (no multiplex) in the presence of brefeldin A and monensin to block cytokine secretion. Cells were surface stained followed by an IFN-γ intracellular cytokine staining (ICS). The frequency of IFN-γ<sup>+</sup> cells within the CD8<sup>+</sup> T cell population is shown.

**(c) Corresponding T-Plex Assay of HD-#3838:** 2<sup>nd</sup> generation T-Plex bead pools (4x multiplex / 10,000 beads per T cell epitope) were incubated with CD8<sup>+</sup> T cells derived from 6.5x10<sup>6</sup> PBMC HD-#3838 in a 500 μl tube rotating at 37°C for 4 h at 40 rpm. In parallel, T-Plex reactions were additionally supplemented with α-CD28-mAb (clone 15E8) or the T-Plex Assay was conducted in the presence of αCD28 mAb and twice as much T-Plex beads. The presence of antigen-specific T cells was indicated by the appearance of an IFN-γ<sup>+</sup> subpopulation of cognate T-Plex beads. T-Plex beads with IDs and pMHC-I-Fc-loaded constructs are indicated in the figure except for the Bead ID 014 / 8558.1 loaded with HCMV/A2-Fc (2<sup>nd</sup> negative control not shown). Rows of T-Plex data represent analysis from the same reaction / bead mix (multiplex detection).

**(d) Consecutive 2<sup>nd</sup> T-Plex Assay run of HD-#3838 10 days later.** After conduction of the first T-Plex Assay, T-Plex beads were collected and analyzed and in parallel the T cell test sample [1<sup>st</sup> condition shown in (c)] was brought back into culture. After 10 days, the sample comprising isolated CD8<sup>+</sup> T cells was again analyzed by the same panel of T-Plex beads.

**Table 4.1 | Quantitative analysis of the pMHC-I multimer staining of HD-PBMC #3838 and extrapolated cell quantities used for a corresponding T-Plex analysis (linked to Fig. 4.13)**

Result of pMHC-I multimer staining			T-Plex Assay input
Population:	% Parent:	Count events:	Cell input:
P1 [Complete PBMC]	92 %	1,096,904	~ 6,500,000
Living CD3 <sup>+</sup> CD19 <sup>-</sup> CD14 <sup>-</sup>	45 %	395725	~ 2,900,000
CD3 <sup>+</sup> CD8 <sup>+</sup>	24 %	85307	~ 700,000
CD8 <sup>+</sup> CD3 <sup>+</sup> EBV/A2 multimer <sup>+</sup>	1.98 %	1693	~ 14000
CD8 <sup>+</sup> CD3 <sup>+</sup> Flu/A2 multimer <sup>+</sup>	0.065 %	60	~ 400

Unfortunately, only the prominent EBV/A2-specific T cell population was detected by the T-Plex Assay, whereas the ~400 Flu/A2-specific CD8<sup>+</sup> T cells remained undetected. Also the addition of soluble  $\alpha$ CD28 mAb (1  $\mu$ g/mL), which has been shown to lower the T cell activation threshold and enhances cytokine production (320), did not improve the detection sensitivity of T-Plex Assay, nor did a 2-fold increase of used T-Plex beads during the reaction (**Fig. 4.13c**). Taken together, ~ 120 antigen-specific T cells among  $2 \times 10^6$  bystander cells corresponding to 0.065% among CD8<sup>+</sup> T cells were reliably detected either by direct respective pMHC-I multimer binding or upon peptide-based stimulation and ICS follow-up resulting in similar frequencies of IFN- $\gamma$ <sup>+</sup> CD8<sup>+</sup> cells. In contrast, the corresponding T-Plex Assay failed to detect even three-times more (~400 cells) antigen-specific T cells indicating a strong need to improve the sensitivity of the so far implemented T-Plex Assay.

In addition, CD8<sup>+</sup> T cells were brought back into culture after the co-culture with T-Plex beads. Subsequently, a repeat of the T-Plex Assay using the sample size after 10 days of culture revealed a higher fraction of IFN- $\gamma$ <sup>+</sup> EBV/A2-Fc-conjugated T-Plex beads compared to the initial T-Plex Assay and also the minor Flu/A2-specific T cell population was detected (**Fig. 4.13d**). These results were in line with previous observations suggesting that culture using IL-15 and previous antigen-specific activation of T cells might lower the detection threshold for a 2<sup>nd</sup> T-Plex Assay (**Fig. 4.8**). Moreover, a consecutive pMHC-I multimer staining of the isolated CD8<sup>+</sup> T cells on day after the 2<sup>nd</sup> T-Plex Assay (**Fig. 4.13a, lower panels**) showed only minor changes in frequencies of the T cell populations compared to the initial pMHC-I multimer staining performed parallel to the 1<sup>st</sup> T-Plex Assay (**Fig. 4.13a, upper panels**). This finding indicated that the 1<sup>st</sup> T-Plex run and subsequent culture hardly influenced the cell number of the respective T cell populations, which will be further elucidated in **Section 4.4.2**.

### 4.3 T-Plex Assay optimization phase 2 – Advancing to an optimized assay protocol

In order to improve the T-Plex Assay's sensitivity we analyzed the impact of various parameters including the (i) T-Plex bead composition itself, (ii) duration of the T-Plex Assay reaction, (iii) tube rolling speed as well as (iv) initial proximity of the test sample and T-Plex beads prior to rolling (**Fig. 4.14**). In addition, the impact of (v) the used assay tube shape and size, (vi) presence of co-stimulatory mAbs on the T-Plex bead, (vii) the amount of used T-Plex beads per test and (viii) additional supplementation with bystander beads with IFN- $\gamma$ -capture capacity (IFN- $\gamma$  scavenger beads) was assessed in (**Fig. 4.15**). Finally, the outcome on T-Plex Assay performance based on (ix) pMHC-I-Fc construct as well as (x) T-Plex bead assembly variations was addressed in **Fig. 4.18** and **Fig. 4.19**, respectively. In all experiments described in the following 1,000 cells derived of a HCMV pp65<sub>495-503</sub>/HLA-A2-specific CD8<sup>+</sup> T cells have been used as test sample. Assay protocol modifications that overall lead to an increased fraction of IFN- $\gamma$ <sup>+</sup> T-Plex upon co-culture with cognate T-cells are considered as improvement of the T-Plex Assay performance since this would correspond to an increased assay sensitivity due to a specific signal enhancement.

#### 4.3.1 Increased tube rotation speed, reaction duration, initial proximity of T-Plex beads and sample as well as another IFN- $\gamma$ capture mAb clone improves the T-Plex Assay

**Impact of pMHC to  $\alpha$ -IFN- $\gamma$  mAb coating ratio on T-Plex beads** | Capture of IFN- $\gamma$  secreted from an activated T cell on a proximal binding T-Plex bead is a key feature of the T-Plex Assay. Consequently, we reasoned that the choice and inherent properties of the IFN- $\gamma$  mAb used for IFN- $\gamma$  capture might have a strong influence on the T-Plex Assay's performance and compared the usage of the two commercially available anti-human IFN- $\gamma$  monoclonal antibodies termed NIB42 and MD-1, which are recommended for ELISA-based IFN- $\gamma$  detection (BioLegend). Surprisingly, when conjugated at the same ratio on T-Plex beads (40% pMHC-I-Fc / 60%  $\alpha$ -IFN- $\gamma$  mAb), the MD-1 mAb outperformed the NIB42 mAb regarding the overall brightness and clustering of cognate IFN- $\gamma$ -loaded T-Plex beads as well as the total fraction of beads that actually become IFN- $\gamma$ <sup>+</sup> (**Fig. 4.14a**). These early results indicated that the presumably higher affinity of the MD-1 clone does directly improve the T-Plex Assay's performance and sensitivity. Interestingly, the pMHC-I-Fc /  $\alpha$ -IFN- $\gamma$  mAb ratio on the surface of the Luminex bead, however, is of lesser influence on the result of the T-Plex Assay within a wide range in particular when the NIB42 mAb was used. Nevertheless, in case of the MD-1 antibody, coating of only 20–50% rather than the previously used 60% of the maximal binding capacity of a Luminex bead, while leaving the remainder for pMHC complexes, seemed more favorable than coating higher amounts of the capture antibody (**Fig. 4.14a**). A variety of literature suggest that already a very small number pMHC molecules on the surface of an antigen-presenting cell (in the range of 10–400 complexes) are sufficient to trigger the activation of a cognate T cell (321), which is vastly exceeded by a theoretical binding capacity of over  $1 \times 10^6$  molecules per Luminex bead (304). Therefore, we think that larger quantities of pMHC per Luminex bead rather enhance the overall binding avidity towards a cognate T cell and thus increases the interaction time of a T-Plex bead and its cognate T cell, which in turn would favor the proximal loading of IFN- $\gamma$  onto the same bead.

**Kinetics of the T-Plex Assay reaction** | In the next step, we analyzed the kinetics of the T-Plex reaction showing that the amount of cognate IFN- $\gamma$ -loaded beads gradually increased after 2 h incubation, which was in line with literature showing that the secretion of IFN- $\gamma$  by activated CD8<sup>+</sup> T cell has a lag phase of roughly 90 minutes (322). Moreover, Betts *et al.* observed a maximal IFN- $\gamma$  secretion and degranulation (CD107a<sup>+</sup>) response of stimulated antigen-specific CD8<sup>+</sup> T cells after 4 hours stimulation (193). In accordance with these data, we also observed that the increase of cognate IFN- $\gamma$ <sup>+</sup> T-Plex beads appeared to saturate after 4–6 hours (**Fig. 4.14b**). On the contrary, also bystander loading of IFN- $\gamma$  to control T-Plex beads did increase after 4 hours (**Supplementary Fig. S8**). Consequently, it seemed that stopping the T-Plex reaction after 4–5 h was optimal.

**Impact of rolling speed on T-Plex Assay performance** | In all previous experiments, we conducted the T-Plex Assay on a rolling system with a fixed speed of 40 rotations per minute (rpm). After purchasing a device that allowed flexible adjustment of the rolling speed, we were interested how the rolling speed might influence the T-Plex Assay performance. Surprisingly, an increase of the rpm to 60 during the T-Plex reaction first of all also increased the amount of IFN- $\gamma$ -loaded T-Plex beads (**Fig. 4.14c, upper panel**) and secondly did also increase the total amount of T cells that were actually activated as shown by a parallel performed CD107a-degranulation assay (**Fig. 4.14c, lower panel**). In contrast, reduced rpm decreased the amount of activated T cells by cognate T-Plex beads and the amount of IFN- $\gamma$ -loaded T-Plex beads. From this result, we concluded that a higher rolling velocity and thus higher mechanical forces do not impair the physical interaction of T-Plex beads and T cells, but rather increases the chance that beads and T cells encounter each other and thus increase the overall T-Plex assay performance.

Under static conditions (96-well, U-bottom plate), 61% of the 1,000 HCMV/A2 T cells (TC#416) were activated as shown by degranulation (CD107a<sup>+</sup>) in the presence of 10-times more cognate T-Plex beads, which can be considered as maximal aAPC-based activation capacity of the #416 HCMV/A2 T cell line. Also in previous experiments where the HCMV/A2 T cell line #416 has been used in co-cultures with HCMV/A2-Fc loaded G $\alpha$ M-IgG-Luminex beads, the corresponding stimulation resulted in 72% IFN- $\gamma$  expressing T cells (**Fig. 3.7**). In contrast, only 37.2% of the T cells were activated (CD107a<sup>+</sup>) under rotation at 60 rpm in the presence of cognate T-Plex beads indicating that ~20% of cells that still could have potentially been activated by a T-Plex bead presumably missed the interaction with a cognate T-Plex under rotation. Ironically, twice as many extrapolated cognate IFN- $\gamma$ -loaded T-Plex were detected as compared with cells number that had actually degranulated under 60 rpm rotation (**Fig. 4.14c**).

**Impact of initial T-Plex bead and T cell proximity prior to rolling** | From the last experiment, we additionally concluded that enhancing the probability that a T cell interacts with their cognate T-Plex bead is key to an overall improvement of the assay. However, simply incubating T cells with beads under static conditions is not an option as shown in **Fig. 4.14c**, since this leads to indistinguishable “bystander” loading on a T-Plex bead species independent of their linked T cell epitope. But we reasoned that co-centrifugation of a given T cell sample with the T-Plex beads would form a dense pellet within the assay tube prior to starting the rolling procedure, which in turn might improve the T-Plex Assay’s sensitivity. In fact, centrifugation prior to rolling did increase the amount of cognate IFN- $\gamma$  loaded T-Plex beads by roughly 1.5-fold consistently. Moreover, this increase was independent of how the pellet of cells and beads was treated after the centrifugation and before the rolling of the tube started (**Fig. 4.14d**). Thus, co-centrifugation of sample and beads prior to rolling as well as rolling at higher rpm appears to be key to dramatically increase the T-Plex Assay’s sensitivity.

#### 4.3.2 Increased tube filling volume and additional conjugation of co-stimulatory mAbs decrease the T-Plex Assay performance

**Impact of tube shape, size and filling level on T-Plex Assay performance** | An alternative to steer the interaction of T cells and cognate T-Plex beads might be the shape and filling volume of the used assay tube. Thus, we tested 0.5 mL, 1.5 mL and 2.0 mL tubes (all from Sarstedt). The 0.5 mL and 1.5 mL tube had a cone-shaped reservoir, whereas the 2.0 mL tube was cylindrical as shown in **Fig. 4.15a, left panel**. However, we observed no striking differences in performance between the aforementioned tubes when filled with 500  $\mu$ L medium during the co-culture of T-Plex bead and 1,000 HCMV/A2 T cells #416 (**Fig. 4.15a, left panel**). In a separate experiment, we also tested 2 mL cryotubes (Nalgene) either filled with 0.5 mL, 1.5 mL or 2.0 mL assay medium, respectively. Interestingly, 500  $\mu$ L filling volume resulted in the highest fraction of IFN- $\gamma$ <sup>+</sup> T-Plex beads, which had already been used by default. In contrast, 8-fold less cognate T-Plex beads became IFN- $\gamma$ <sup>+</sup> if a filling volume of 2 mL was used instead (**Fig. 4.15a, right panel**). This was in accordance with previous results, where co-culture of T-Plex beads with 1000–2000 cognate T cells of a T cell line in 2 mL volume led to 1–3% IFN- $\gamma$ <sup>+</sup> T-Plex beads (**Fig. 4.6 & 4.7**), whereas a filling with 500  $\mu$ L lead to 5–12% IFN- $\gamma$ <sup>+</sup> T-Plex beads (**Fig. 4.7**). Conclusively, an increased tube filling appeared to rather decrease the chance of an interaction between T cells and T-Plex beads and thus decreases the overall sensitivity.

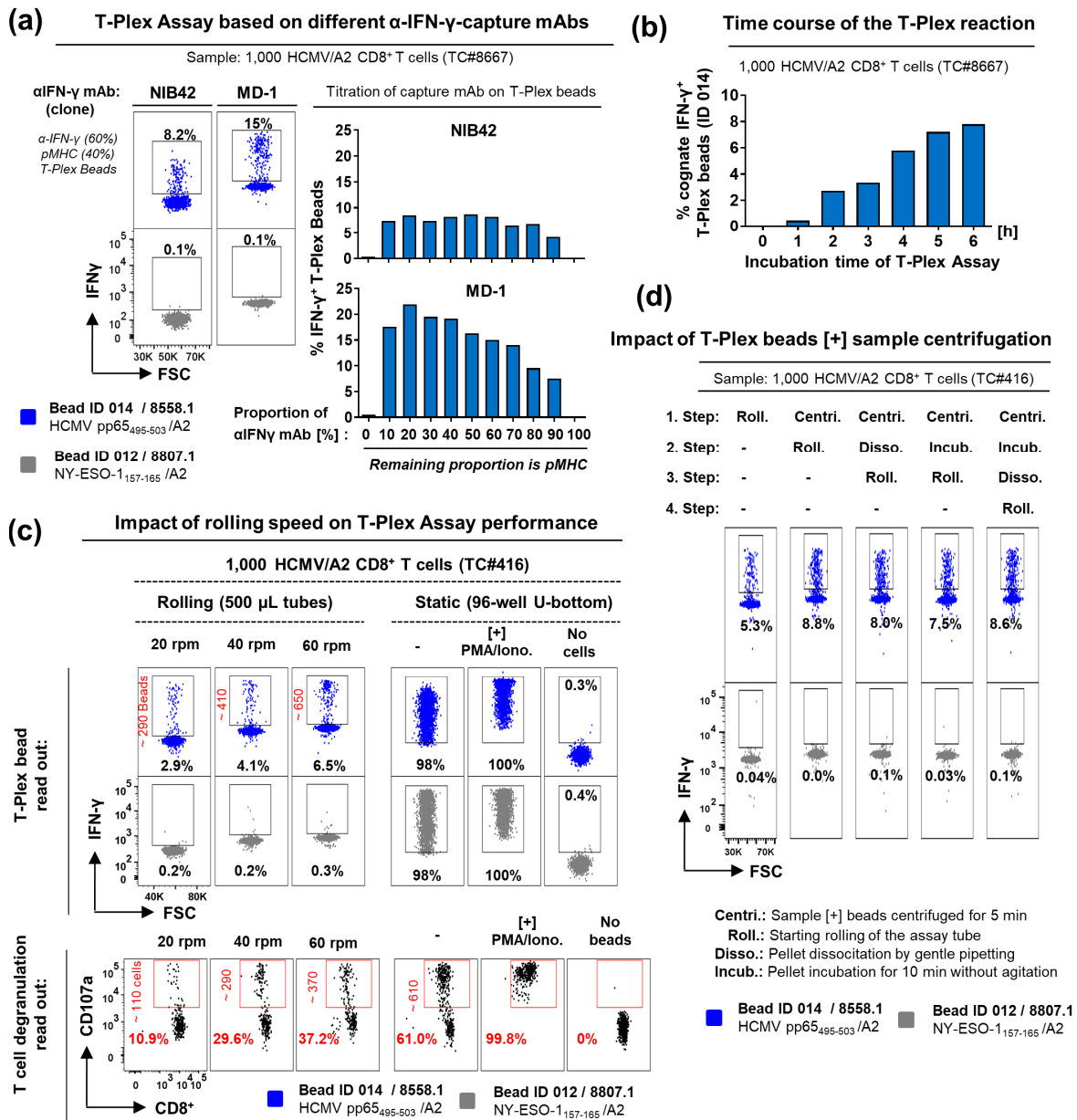


**Figure 4.14 | Systemic optimization of the T-Plex Assay and identification of crucial assay parameters – Part 1**

In all experiments shown, ~1,000 cells of a HCMV pp65<sub>495-503</sub>/HLA-A2 (CMV/A2) specific CD8<sup>+</sup> T cell line were used as test sample for T-Plex Assay reactions. In **(a & b)** the T cell line (TC) was generated from healthy donor #8667 and in **(c & d)** from #416. Unless otherwise indicated 2<sup>nd</sup> generation T-Plex beads were assembled using covalently conjugated  $\alpha$ -IFN- $\gamma$  capture mAb clone MD-1 (MD-1) and rat  $\alpha$ -mIgG2a (RMG2a-62) at a 3 to 2 ratio (60% MD-1 / 40% RMG2a-62). Subsequently, defined bead regions (ID) were loaded with pMHC-I-mIgG2a-Fc constructs. Assembled T-Plex beads (4x multiplex / 10,000 beads per T cell epitope) and test sample were rotated in 500  $\mu$ L tubes at 40 rpm, 37°C for 4 h. Next, T-Plex beads were stained with  $\alpha$ -IFN- $\gamma$  detection mAb (clone 4S.B3) and analyzed.

**(a) Titration of  $\alpha$ -mIgG2a/pMHC-I-Fc to  $\alpha$ -IFN- $\gamma$  mAb ratio on T-Plex beads:** Shown is a representative T-Plex Assay result as FACS blot for standard 60:40  $\alpha$ -IFN- $\gamma$ /pMHC-I-Fc T-Plex beads either on the basis of the  $\alpha$ -IFN $\gamma$  clone NIB42 or clone MD-1 (both BioLegend). Shown is the IFN- $\gamma$  signal of the cognate HCMV/A2 T-Plex beads (*blue*) and one-out-of-three corresponding control bead signals (*grey*). The bar diagram displays the performance of T-Plex beads depending on the ratio of  $\alpha$ -IFN- $\gamma$  to  $\alpha$ -mIgG2a/pMHC-I-Fc on the T-Plex beads. **(b) Kinetics of the T-Plex Assay:** The T-Plex Assay was conducted as mentioned above and the reaction was stopped and analyzed after the indicated incubation times.

**(c) T-Plex Assay performance based on rolling speed:** T-Plex Assays were conducted at various rpm or in static conditions using a 96-well of U-bottom plate. Degranulation of CD8<sup>+</sup> T cells was analyzed in parallel by intracellular accumulation of  $\alpha$ -CD107a mAb in the presence of monensin (**Section 2.7.2**).

**(d) Centrifugation of test sample and T-Plex beads prior to rolling:** Test sample and T-Plex beads were filled in a conically skirted 500  $\mu$ L tube combined with CO<sub>2</sub>-saturated assay medium and vortexed. The next steps were performed as indicated prior to rolling at 40 rpm for 4 h.

**Performance of T-Plex beads additionally supplemented with co-stimulatory mAbs** | We observed previously that an increased ratio of pMHC-I to IFN- $\gamma$ -capture mAb on T-Plex beads rather led to an higher fraction of IFN- $\gamma$ <sup>+</sup> T-Plex beads upon co-culture with cognate T cells (**Fig. 4.14a**). These results suggested that a T-Plex bead with a higher pMHC load has apparently an increased binding avidity towards cognate T cells, which might favor a stable interaction in particular under agitation. Thus, we hypothesized that direct conjugation of antibodies against co-stimulatory receptor CD28 as well as adhesion-molecule CD2 (LFA-2) on the T-Plex beads might additionally improve the T-Plex Assay by either lowering the T cell activation threshold or by supporting the binding of the T-Plex bead to cognate T cells. Both CD2 and CD28 are highly expressed on memory T cells and their engagement by respective co-stimulatory acting antibodies as well as their natural ligands CD58 and CD80/CD86, respectively have been shown to lower the T cell activation threshold and enhances cytokine production (41, 320, 323). Thus, we covalently conjugated at different ratios, an  $\alpha$ -CD28 mAb (15E8) and  $\alpha$ -CD2 mAb (RPA-2.10) in addition to the rat  $\alpha$ -mIgG2a (RMG2a-62) and  $\alpha$ -IFN- $\gamma$  capture mAb to the Luminex-beads as indicated in **Fig. 4.15b**. In a second step, pMHC-I-mIgG2a-Fc constructs were loaded to generate fully assembled T-Plex beads, which have been subsequently co-cultured with 1,000 HCMV/A2-specific T cells. Unfortunately, in all cases the additional conjugation of co-stimulatory mAbs on T-Plex beads reduced the overall assay performance leading to reduced fractions of cognate IFN- $\gamma$ <sup>+</sup> T-Plex beads compared to standard 2<sup>nd</sup> generation T-Plex beads. Moreover, particularly the addition of the  $\alpha$ -CD2 mAb (RPA-2.10) increased the fraction of control T-Plex beads (i.e. irrelevant pMHC-I) becoming IFN- $\gamma$ <sup>+</sup> and thus increased the overall assay background (**Fig. 4.15b**). We concluded that the additional covalent attachment of co-stimulatory mAbs to T-Plex beads rather decreases the overall assay performance and should be avoided. However, this does not rule out that a supplementation of soluble co-stimulatory mAbs during the co-culture of T-Plex beads and T cells might still improve the assay outcome in particular if the T cells have a higher activation threshold, which has been observed especially for tumor infiltrating lymphocytes (106, 324).

**Titration of T-Plex beads and addition of IFN- $\gamma$  scavenger beads** | The amount of T-Plex beads used per T cell epitope, might be another crucial parameter that impact the T cell assay performance. In almost all previously conducted experiments, we used by default 10,000 T-Plex beads (2<sup>nd</sup> generation) per T cell epitope. In **Fig. 4.15c**, we titrated the amounts T-Plex beads that were brought in co-culture with 1,000 HCMV/A2-specific T cells. Interestingly, within the range of 10,000 – 40,000 T-Plex beads used per epitope also the total amounts of cognate IFN- $\gamma$ <sup>+</sup> T-Plex beads increased by the same factor resulting in similar relative fractions of IFN- $\gamma$ <sup>+</sup> T-Plex beads. This result suggested that a given number of T cells encounters multiple rather than a single cognate T-Plex bead interaction. In particular, an excess of cognate beads leads to more T-Plex beads become IFN- $\gamma$ <sup>+</sup> as actual T cells were present during the reaction. Secondly, since overall more cognate T-Plex were becoming IFN- $\gamma$ <sup>+</sup> after increasing the overall number of T-Plex beads, this would partially imply an enhanced assay sensitivity. However, in a previous experiment shown in **Fig. 4.13**, a two-fold increase of T-Plex beads did not improved the detection of a small T cell population. Moreover, the usage of more beads per analysis would also increases the cost per T-Plex-based analysis. On the contrary, usage of 10,000 T-Plex beads/T cell epitope have been proven robust enough to allow to some extent the enumeration of antigen-specific T cell population as a linear correlation in the range of 200 – 10,000 antigen-specific T cells and corresponding cognate IFN- $\gamma$ <sup>+</sup> T-Plex bead could be observed (**Fig. 4.11**).

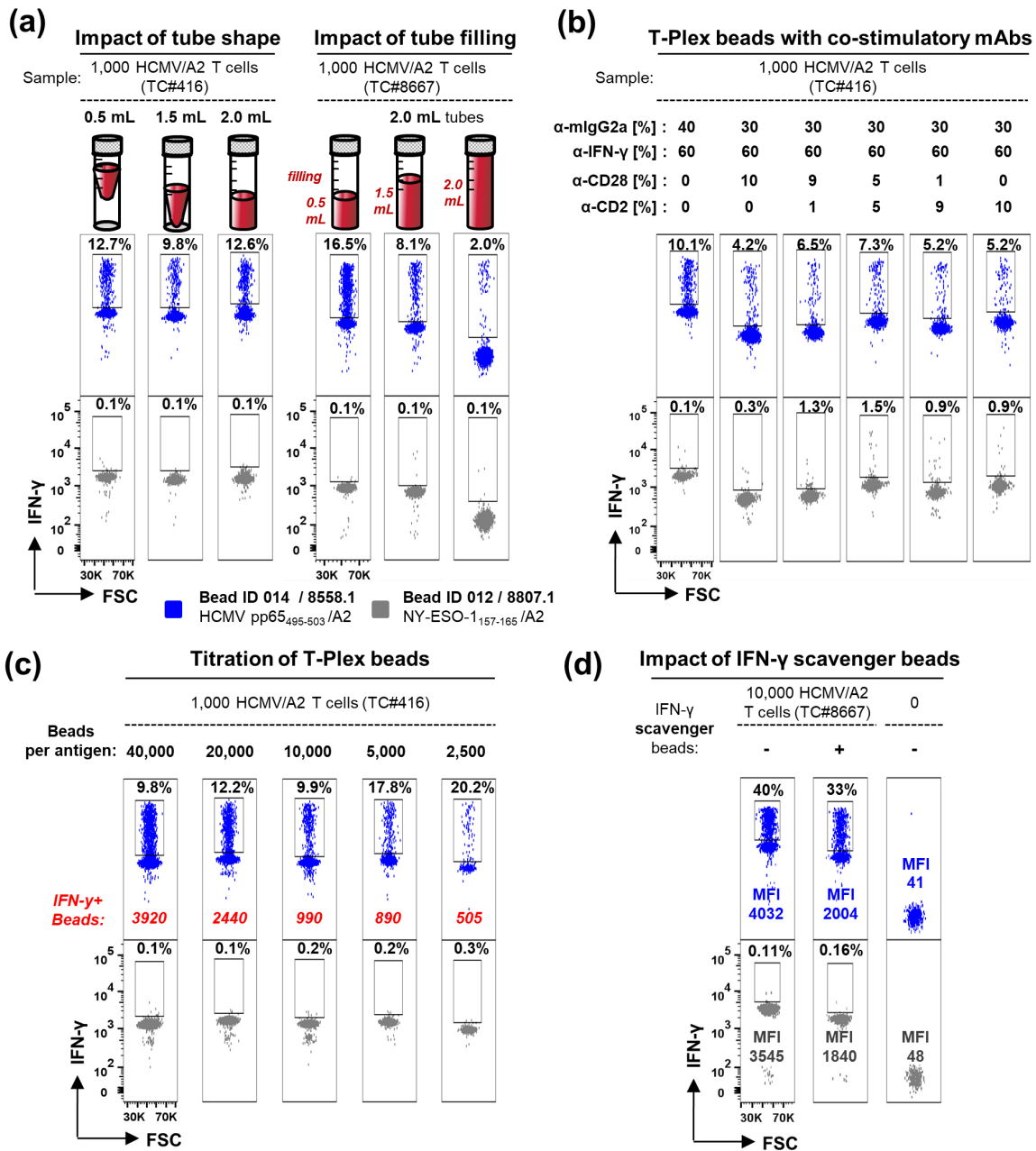


**Figure 4.15 | Optimization of the T-Plex Assay and identification of crucial assay parameters – Part 2**

In experiments **(a, c and d)**, 2<sup>nd</sup> generation T-Plex beads were assembled using covalently conjugated α-IFN-γ capture mAb (clone MD-1) and rat α-mIgG2a (RMG2a-62) at a 3 to 2 ratio (60% MD-1 / 40% RMG2a-62). Subsequently, defined bead regions (ID) were loaded with pMHC-I-mIgG2a-Fc constructs. Unless otherwise mentioned assembled T-Plex beads (4x multiplex / 10,000 beads per epitope) and test samples were rotated in 500 μL tubes at 60 rpm, 37°C for 4 h 30 min. Next, T-Plex beads were stained with α-IFN-γ detection mAb and analyzed. In **(a–c)** ~1,000 cells and in **(d)** ~10,000 of a HCMV pp65<sub>495–503</sub>/HLA-A2 (HCMV/A2)-specific CD8<sup>+</sup> T cell line (TC) were used as test sample for the T-Plex Assay reactions either derived from healthy donor #8667 or #416. **(a–d)** Shown is the IFN-γ signal of the cognate HCMV/A2 T-Plex beads (*blue*) and one-out-of-three corresponding control T-Plex bead signals (*grey*).

**(a) Impact of tube shape, size and filling level on T-Plex Assay performance.** The T-Plex Assay was performed as described above using different kinds of tube sizes/shapes and filling levels (*red*) as indicated in the figure.

**(b) Performance of T-Plex beads additionally supplemented with co-stimulatory mAbs.** Here, T-Plex beads were assembled using covalently conjugation of the indicated ratios of rat α-mIgG2a (RMG2a-62), IFN-γ capture mAb (MD-1) and α-CD28 mAb (15E8) as well as α-CD2 mAb (RPA-2.10). In a second step, pMHC-I-mIgG2a-Fc was loaded to generate fully assembled T-Plex beads. **(c) Titration of T-Plex beads.** The T-Plex Assay was performed using the indicated amounts of 60:40 α-IFN-γ/pMHC-I-Fc T-Plex beads and 1,000 CMV/A2 T cells as test sample. Extrapolated total amounts of IFN-γ<sup>+</sup> T-Plex beads are shown as red numbers. **(d) Impact of IFN-γ scavenger beads.** The T-Plex assay was performed in the absence or presence of 2x10<sup>5</sup> IFN-γ scavenger beads, which are goat-α-mouse IgG Dynabeads solely loaded with α-IFN-γ mAb (MD-1). The T-Plex assay was performed using 10,000 HCMV/A2 T cells, which represent the T-Plex Assay's outer dynamic range. Median fluorescence intensity (MFI) of the total bead population is shown.

In order to improve the dynamic range antigen-specific T cell populations of higher frequencies, we speculated that addition of beads that displayed a high IFN- $\gamma$ -capture capacity yet lack a T cell stimulation capacity (IFN- $\gamma$  scavenger beads) might reduce the overall bystander (antigen-independent) IFN- $\gamma$  loading onto all T-Plex beads present during the co-culture. Thus, we added in a pilot experiment  $2 \times 10^5$  solely IFN- $\gamma$ -capture mAb conjugated Dynabeads to a 2<sup>nd</sup> generation T-Plex bead pool, which were co-cultured with 10,000 HCMV/A2 T cells (**Fig. 4.15d**). As expected, the presence of IFN- $\gamma$  scavenger beads reduced the overall IFN- $\gamma$  bystander loading reflected by decreased MFI values of control T-Plex beads. Moreover, the presence of IFN- $\gamma$  scavenger beads increased the “MFI-spreading” of cognate IFN- $\gamma^+$  T-Plex beads implying an increased dynamic range at higher cell numbers compared to the absence of IFN- $\gamma$  scavenger beads. However, in this experiment we also observed a slightly reduced overall fraction of cognate IFN- $\gamma^+$  T-Plex (**Fig. 4.15d**). However, we have not yet further elucidated the benefit of IFN- $\gamma$  scavenger beads. In a related experiment, we address the question if the fraction of T-Plex beads that become IFN- $\gamma^+$  upon cognate T cell interaction is influenced by the number of bystander T-Plex beads loaded with irrelevant pMHC molecules. Thus, HCMV/A2-specific T cells were combined with cognate HCMV/A2-loaded T-Plex beads in the presence of 3 (in total 4x multiplex) or 29 (in total 30x multiplex) irrelevant bystander T-Plex bead species (10,000 beads per bead species / ID) for a T-Plex Assay. Importantly, the resulting fraction of cognate IFN- $\gamma^+$  T-Plex bead was the same independent if in total four or thirty different T-Plex bead species (IDs) were combined in a single T-Plex bead pool (**Supplementary Fig. S9**). Solely, the usage of more irrelevant T-Plex beads led to a more distributed bystander (antigen-independent) IFN- $\gamma$  loading onto all T-Plex beads present during the co-culture, which was similar to the observed effect when IFN- $\gamma$  scavenger beads are used.

#### 4.3.3 Integration of optimal T-Plex Assay parameters leads to a very high sensitivity that is comparable to pMHC-I multimer stainings.

In previous performance assessments the T-Plex Assay failed to detect HCMV pp65<sub>495–503</sub>/A2-specific T cells present below an absolute number of 200 cells, whereas a corresponding pMHC-I multimer staining was able to detect reliably only 20 HCMV/A2-specific T cells out of  $2.5 \times 10^5$  cells bystander CD8<sup>+</sup> T cells (**Fig. 4.11b**). Thus, we were highly interested if an optimized T-Plex Assay would allow the detection of lower frequencies of antigen-specific T cells. In a representative experiment shown in **Fig. 4.16**, the impact of these newly identified crucial assay parameters were compared side-by-side using the same test sample. In particular the combined usage of a (i) 0.5 mL tubes, (ii) co-centrifugation of T-Plex beads and sample prior rolling at (iii) an increased rolling speed of 60 rpm dramatically increased the detection capacity of the T-Plex Assay, which was now able to consistently detect only 100 HCMV/A2-specific T cells, whereas previously used assay conditions failed to do so. Subsequently, we assessed the detection limit as well as dynamic range of the optimized T-Plex Assay. Therefore, a serial-dilution in the range of 10,000 down to approximately 2–3 cells of HCMV/A2-specific T cells was subjected to the optimized T-Plex Assay. Surprisingly even 2–3 cells of HCMV/A2-specific T cell line were consistently detected by the T-Plex Assay (**Fig. 4.17a**), whereas in agreement with earlier results the lower detection limit of a corresponding pMHC-I multimer staining was  $\sim 0.01\%$  referring to 10–20 total HCMV/A2-specific T cells (**Fig. 4.17c & 4.11a**). Moreover, technical replica of the T-Plex Assay performed on the same day representing separated tubes filled with the same sample and pool of T-Plex beads led to almost identical results displaying a typical intra-experimental variation of 5–10%, which held especially true in case 5–5000 antigen-specific T cells are present. In the same range of antigen-specific T cells present, two T-Plex Assays performed on two consecutive days displayed also a low inter-experimental variation of 5–20% (**Fig. 4.17b**), which further demonstrated a very high

reproducibility of the T-Plex Assay procedure. Moreover, when using the optimized parameters the T-Plex Assay displayed a linear relationship between ~2–3 and 625 HCMV/A2-specific T cells. In contrast, more than 5,000 HCMV/A2-specific T cells resulted in a complete IFN- $\gamma$ <sup>+</sup> saturation of all cognate T-Plex beads, whose IFN- $\gamma$ <sup>+</sup>-binding signal was, however, still clearly distinct from control T-Plex beads. Yet, at 10,000 HCMV/A2-specific T cells also the background on control T-Plex beads strongly increased (Fig. 4.17a). In accordance with previous results, the corresponding pMHC-I multimer staining displayed a linearity for all cell dilutions analyzed (Fig. 4.17c). In conclusion, the usage of the combined optimized T-Plex Assay procedure did strikingly improve the overall assay sensitivity, which was in case of the detection of HCMV/A2-specific CD8<sup>+</sup> T cells even higher than a corresponding pMHC-I multimer staining.

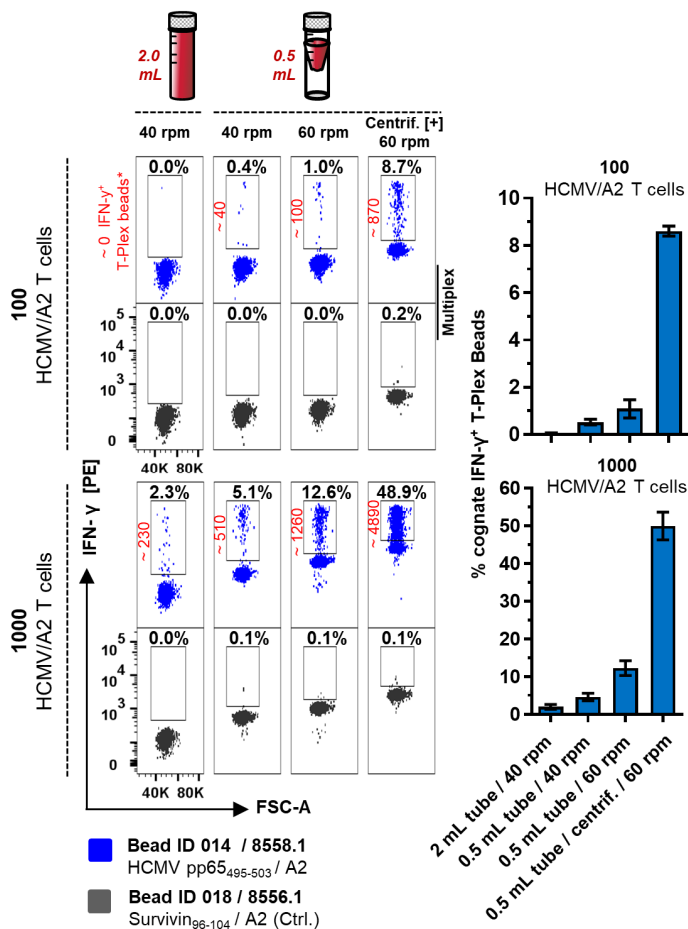


**Figure 4.16 | Combination of optimal assay parameters improved dramatically the T-Plex Assay's sensitivity**

2<sup>nd</sup> generation T-Plex beads were generated using covalently conjugated  $\alpha$ -IFN $\gamma$  capture mAb (clone MD-1) and rat  $\alpha$ -mIgG2a-Fc mAb (RMG2a-62) at a 1 to 1 ratio and loaded with indicated pMHC-I-mIgG2a-Fc constructs. Assembled T-Plex beads (10,000 beads per T cell epitope, 4x multiplex) were combined either with 100 or 1,000 cells of the HCMV pp65<sub>495-503</sub>/A2-specific CD8<sup>+</sup> T cell line #5561 (HCMV/A2 T cells). The T-Plex Assay was either conducted using completely filled 2 mL or 0.5 mL tubes that have been either rotated on a rolling device set to 40 rpm or 60 rpm for 5 h at 37°C. In another condition, filled 0.5 mL tubes were centrifuged (centrif.) at 2500 rpm prior to rolling at 60 rpm. All conditions were performed in triplicates. Shown is the representative IFN- $\gamma$  signal of the cognate HCMV/A2 T-Plex beads (blue) and one-out-of-three corresponding control (ctrl.) bead signals (grey). Pairs of upper and lower FACS-plots represent data analysis from the same reaction. Extrapolated total amounts of IFN- $\gamma$ <sup>+</sup> T-Plex beads are shown in red numbers. Error bars represent the standard deviation.

#### 4 | Results Part 2 – Development of the T-Plex Assay

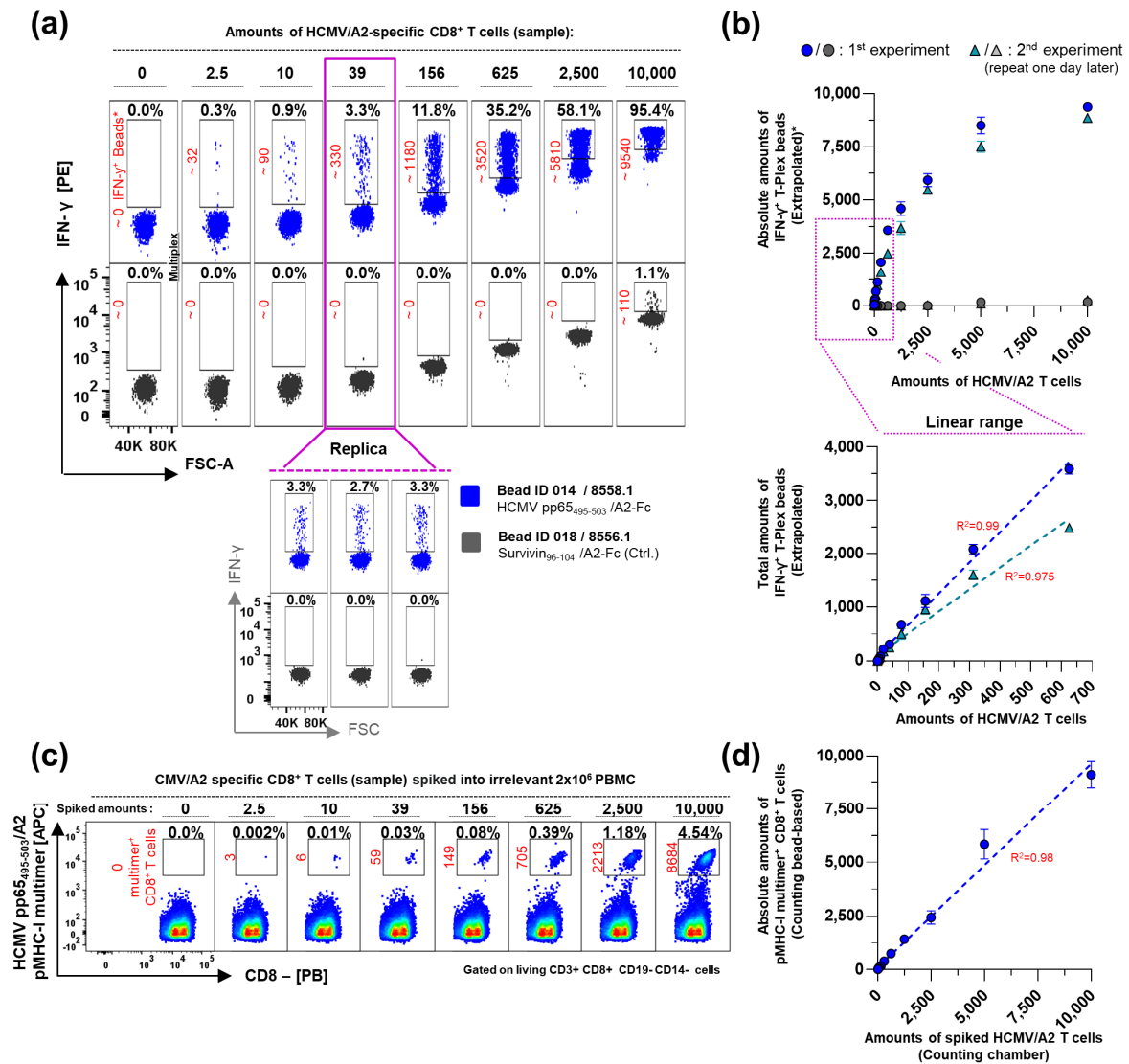


**Figure 4.17 | Optimized T-Plex Assay outperforms the sensitivity for the detection of HCMV/A2-specific T cells compared to a corresponding pMHC-I multimer staining but has a limited quantitative dynamic range**

**(a) Assessment of diluting amounts of antigen-specific T cells by the optimized T-Plex Assay.**

Four different 2<sup>nd</sup> generation T-Plex bead pools (10,000 beads / T cell epitope, bead ID: 012, 013, 014, 018) were either loaded with cognate HCMV/A2-Fc [8558.1] or irrelevant pHLA-A2-Fc [8557.1 / 8804.1 / 8556.1]. Assembled T-Plex beads were combined in 0.5 mL tubes with a two-fold serial dilution of HCMV pp65<sub>495-503</sub>/A2-specific CD8<sup>+</sup> T cell line #5561 (HCMV/A2 T cells) ranging from 10,000 to ~2.5 cells. Combined cell sample and T-Plex beads were centrifuged for 5 min at 2500 rpm prior to rolling at 60 rpm for 5 h at 37°C. All conditions were performed in triplicates. Shown is one representative IFN-γ signal of the cognate HCMV/A2 T-Plex beads (blue) and one-out-of-three corresponding control bead signals (grey) as well as a selective triplicate of one cell dilution. Pairs of upper and lower FACS-plots represent data analysis from the same reaction. Extrapolated total amounts of IFN-γ<sup>+</sup> T-Plex beads are shown in red numbers.

**(b) Corresponding T-Plex Assay linear range assessment and inter-experimental reproducibility.** Amounts of total HCMV/A2 T cells derived from counting chamber-based calculations is plotted against extrapolated total amounts IFN-γ<sup>+</sup> T-Plex beads. Linear regression is shown through linear points only. Two experiments are shown that have been conducted on two consecutive days.

**(c) Analysis of diluting amounts of antigen-specific T cells spiked into PBMC by pMHC-I multimer staining.**

A two-fold serial dilution of HCMV/A2 T cells ranging from 10,000 to 2.5 cells was spiked into 2x10<sup>6</sup> PBMC derived from an irrelevant HLA-A2<sup>neg</sup> healthy donor. Spiked samples were stained in the presence of 50 nM dasatinib with in-house produced HCMV/A2-multimers generated with streptavidin-APC and monomeric Fc cleaved biotinylated HCMV/HLA-A2\* [11097.1]. Analysis was performed in duplicates. Representative pMHC-I multimer stainings and frequencies of pMHC-I multimer<sup>+</sup> cells within the CD8<sup>+</sup> T cell population are shown. Red numbers indicate absolute multimer<sup>+</sup> CD8<sup>+</sup> T cells per sample calculated using reference counting beads (BioLegend).

**(d) Corresponding linear regression of the pMHC-I multimer data.** Amounts of spiked HCMV/A2 T cells derived from counting chamber-based calculations is plotted against the total amounts of detected pMHC-I multimer<sup>+</sup> cells calculated using counting beads. Standard deviations are shown as error bars.

#### 4.3.4 pHLA-A2-Fc variations harboring the mutation Q115E in the HLA-A2 $\alpha$ 2-domain or a mIgG2a-Fc with additional CH1-domain did not influenced the T-Plex Assay's performance

The T-Plex Assay requires a stable interaction of T-Plex bead with its cognate T cell triggering their activation. Thus, it seemed reasonable to evaluate the activation potential and usability in T-Plex Assays of different modified pMHC-I-Fc constructs summarized in **Fig. 4.18a**. Wooldridge *et al.* reported that a glutamine (Q) to glutamic acid (E) point mutation at position 115 [Q115E] within the  $\alpha$ 2-domain of the HLA-A2 allele enhanced the binding to co-receptor CD8 without affecting the TCR's specificity, which in turn rather drove greater cytokine production upon TCR:pHLA-A2-[Q115E] encounter rather than increasing the staining performance of pHLA-A2-[Q115E] multimers (261). Thus, we introduced the Q115E mutation into the HCMV pp65<sub>495-503</sub> as well as Survivin<sub>96-104</sub> presenting disulfide-trapped single-chain trimer-based (dt-SCT) HLA-A2-mIgG2a-Fc constructs [9670.1 & 9672.1]. Successfully produced Q115E-mutated Sur/HLA-A2-Fc construct bound specifically to the cognate Sur/A2 T cells line resulting in slightly higher MFI values and higher fraction of detected cells compared to the wild-type Sur/HLA-A2-Fc [Q115] construct (**Fig. 4.18b**). However, when functionalized as aAPC on  $\alpha$ -mIgG2a-Luminex beads, the Q115E-mutated pHLA-A2-Fc constructs did not increase the quality of IFN- $\gamma$  expression in cognate T cell lines (**Fig. 4.18c**), which is in contrast to the previous published results (261).

In addition, we cloned and successful produced dt-SCT-based Sur/A2 [8414.1] as well as HCMV/A2 [8415.2] constructs fused to a mIgG2a-Fc bearing an additional CH1 domain N-terminal of the hinge domain (CH1-Fc). We speculated that the additional CH1-domain might increase the mobility of the pMHC-I complex, which in turn may influence the overall TCR-binding and T cell stimulation capacity. However, also the pHLA-A2-CH1-Fc fusion protein did not displayed a superior stimulation capacity when compared to pHLA-A2-Fc constructs lacking the additional CH1 domain (**Fig. 4.18c**). Nevertheless, we tested all constructs side-by-side in a corresponding T-Plex Assays based on 2<sup>nd</sup> generation T-Plex beads, that have been co-cultured either with 1,000 cells of the HCMV/A2 T cell line #416 or Sur/A2 T cell line (**Fig. 4.18d**). In line with the previous results, neither the Q115E-mutated nor the pHLA-A2-CH1-Fc constructs significantly affected the T-Plex Assay performance in comparison to the wild-type pHLA-A2-Fc constructs.

#### 4| Results Part 2 – Development of the T-Plex Assay

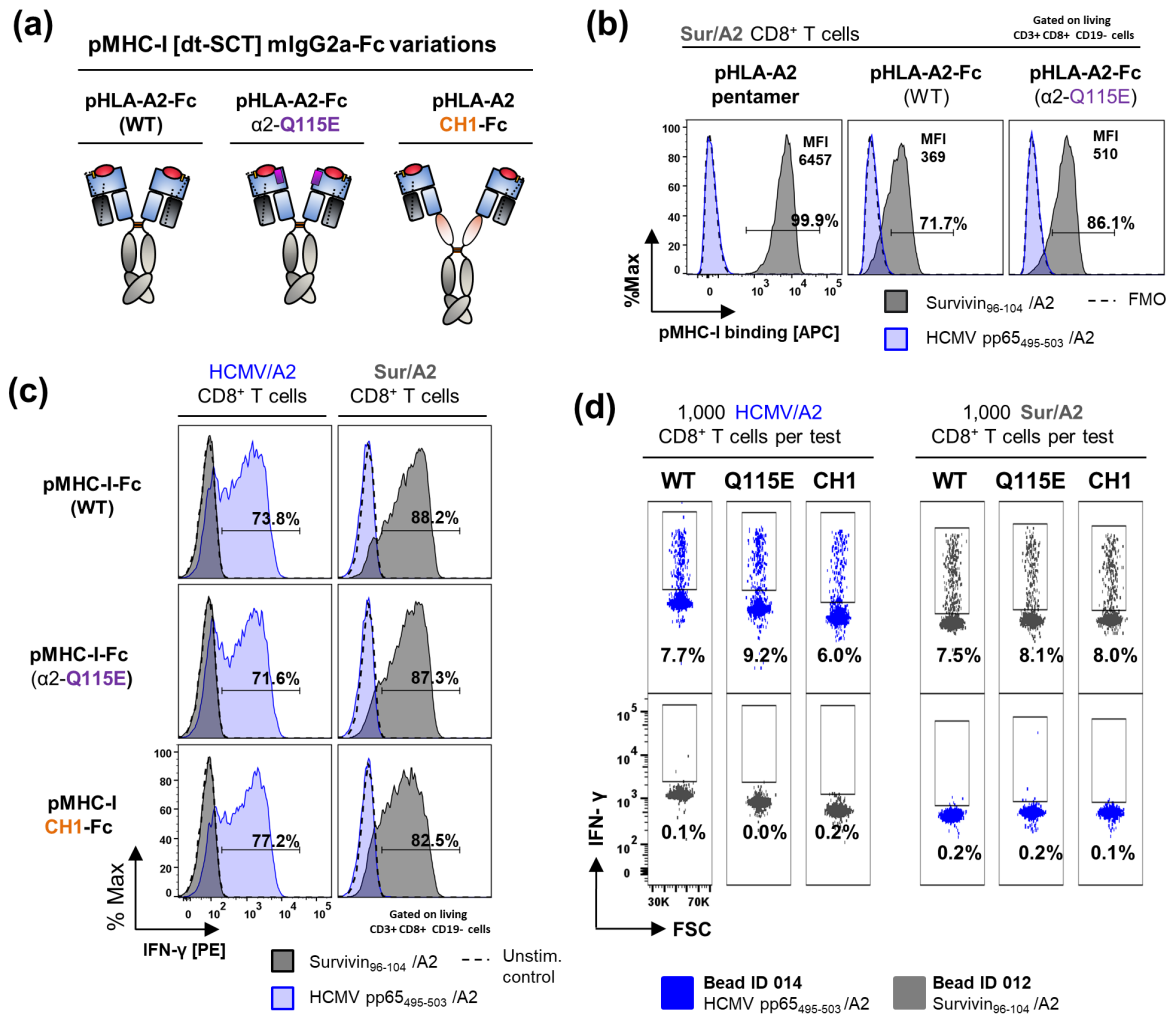


**Figure 4.18 | pHLA-A2-Fc variations harboring the α2-domain Q115E mutation or a CH1-mlgG2a-Fc marginally affected T cell binding and stimulation capacity as well as T-Plex Assay performance**

**(a) Variations of disulfide-trapped (dt) peptide-MHC-class I (pMHC-I) immunoglobulin-Fc (Fc) dimers.** Two additionally modified construct versions were cloned and produced, apart from the dt-pMHC-I-mlgG2a-Fc (CH2-CH3) constructs (here considered as “wild-type / WT”) [8556.1 & 8558.1] comprising the structure of a single-chain trimer as described in Fig. 3.1. The first modified version harbors an additional Q115E point mutation within the α2-domain of HLA-A2 [9670.1 & 9672.1]. The second modified version is a dt-pMHC-I fused to mlgG2a comprising the CH1-Hinge-CH2-CH3 domain (CH1-Fc) [8414.1 & 8415.2].

**(b) Antigen-specific binding of dt-pMHC-I-Fc (WT) and α2-Q115E in comparison to commercial pMHC-multimers.** The Survivin<sub>96-104</sub>/HLA-A2 (Sur/A2)-specific CD8<sup>+</sup> T cell line was stained in the presence of dasatinib [50 nM] with Sur/A2 [grey] or HCMV pp65<sub>495-503</sub>/HLA-A2 (HCMV/A2) [blue] pMHC-I-Fc or pMHC-I-multimer at 25 μg/mL followed by lineage marker staining. (Left panel) Commercial pMHC-I pentamer (ProImmune); (middle and right panel) purified dt-pHLA-A2-Fc-STag (WT) and purified dt-pHLA-A2-Fc-STag (Q115E) sequentially stained with Strep-Tactin-APC. The frequency of pMHC-I-multimer<sup>+</sup> / pMHC-I-Fc<sup>+</sup> cells within the CD3<sup>+</sup>/CD8<sup>+</sup> T cell population is shown.

**(c) Stimulation capacity of bead-immobilized dt-pMHC-I-Fc variants.** Supernatants derived from CHO-transfections of dt-pMHC-I-Fc variants were immobilized on α-mlgG2a mAb (RMG2a-62) conjugated Luminex beads. pMHC-I-loaded beads and Sur/A2 T cells or HCMV/A2-specific CD8<sup>+</sup> T cell line (#416) were co-cultured at a 1:1 ratio in the presence of brefeldin A and monensin for 4 h. Cognate stimulation of the T cell lines is shown by the induction of IFN-γ expression.

**(d) Impact of dt-pMHC-I-Fc variants on T-Plex Assay performance.** 2<sup>nd</sup> generation T-Plex beads (60% αIFN-γ / 40% α-mlgG2a) were loaded with the indicated dt-pMHC-I-Fc variations followed by a T-Plex Assay using 1000 HCMV/A2 T cells or Sur/A2 T cells as sample. The T-Plex Assay was performed in 500 μL tubes at 60 rpm and 37°C for 4 h 30 min.

#### 4.3.5 pMHC-I-Fc immobilization on T-Plex beads via anti-IgG-Fc/IgG-Fc or biotin/streptavidin interactions leads to equal T-Plex Assay outcomes and similar T-Plex bead properties.

As a final optimization step, we were interested, if further modifications of the T-Plex bead “architecture” improve or dampens the overall T-Plex Assay performance compared to 2<sup>nd</sup> generation T-Plex bead concept. As discussed previously, the 2<sup>nd</sup> generation T-Plex bead concept comprises the combined covalent conjugation of an IFN- $\gamma$ -capture mAb together with an  $\alpha$ -mIgG2a-Fc mAb to carboxylated Luminex beads followed by the non-covalent association with soluble pMHC-mIgG2a-Fc constructs to gain fully assembled T-Plex beads (**Fig. 4.19a–c, upper panels**). Derived from that concept two additional T-Plex bead architectures were conceived. Firstly, we simply replaced the  $\alpha$ -mIgG2a-Fc mAb by streptavidin (**Fig. 4.19a–c, middle panels**) allowing immobilization of the *in vivo* biotinylated constructs such as the HCMV pp65<sub>495–503</sub>/HLA-A2-pCC-Fc [10347.7] and Survivin<sub>96–104</sub>/HLA-A2-pCC-Fc [9237.1] previously introduced in **Section 3.3** and HCMV/A2-\*Fc [11097.1] and Sur/A2-\*Fc [11290.1] bearing a cleavable Fc [\*Fc] (**Section 3.4**). A key advantage of this approach is the almost irreversible conjugation of biotinylated pMHC complexes to the T-Plex beads, which allows for long-term storage of fully assembled (i.e. pMHC-linked) “ready-to-use” T-Plex beads. Moreover, precursor T-Plex beads based on streptavidin and IFN- $\gamma$ -capture mAb can be flexible and universally associated with any commercially available or self-produced biotinylated pMHC complex. In contrast,  $\alpha$ -mIgG2a-Fc mAb-based T-Plex needs to be either freshly associated with pMHC-Fc prior usage or kept in an excess of pMHC-Fc molecules to avoid the effects of pMHC-Fc dissociation during storage. As an alternative architecture, T-Plex beads were generated by direct covalent conjugation of pMHC-Fc and IFN- $\gamma$  capture mAb to carboxylated Luminex beads (**Fig. 4.19a–c, lower panels**).

Surprisingly, Luminex beads that were firstly covalently conjugated either with a 1:1 ratio of  $\alpha$ -mIgG2a-Fc ( $\alpha$ -Fc) mAb [RMG2a-62] / IFN- $\gamma$  capture mAb [MD-1] or streptavidin [SAv] / IFN- $\gamma$  capture mAb [MD-1] and then loaded with pHLA-A2-Fc or biotinylated pHLA-A2-pCC-Fc displayed very similar pMHC-Fc binding and maximal IFN- $\gamma$  capture capacities (**Fig. 4.19b**). However, staining for HLA-A2 (clone BB7.2, IgG2b isotype) of pMHC-Fc-loaded  $\alpha$ -Fc-based T-Plex beads revealed roughly 4-fold higher MFI values compared to pMHC-pCC-Fc-loaded SAv-based T-Plex beads indicating a slightly higher pMHC-binding capacity of the  $\alpha$ -Fc-based precursor T-Plex beads. Nevertheless, a T-Plex Assay for the detection of 1,000 HCMV/A2-specific CD8<sup>+</sup> T cells (HD #5561) using either  $\alpha$ -Fc- or SAv-based T-Plex beads performed almost equally well supporting the alternative SAv-based T-Plex bead concept (**Fig. 4.19c**). Notably, T-Plex Assays shown in **Fig. 4.19c** were performed in triplicates. For each condition shown, 1,000 T cells and T-Plex beads (10,000 beads / epitope) were centrifuged prior to rolling in a 500  $\mu$ L tube at 60 rpm for 4 h 30 min (37°C). The optimized assay conditions elaborated in **Section 4.3.1** let to a fraction of 35.9% ( $\pm$  8%) cognate IFN- $\gamma$ <sup>+</sup>  $\alpha$ -Fc-based T-Plex beads and 34.2% ( $\pm$  2%) SAv-based T-Plex beads (Student’s T-test  $p$ = 0.73 with  $n$ =3). In sharp contrast, all T-Plex Assays failed to detect 1,000 HCMV/A2 T cells, which were based on Luminex beads that have been covalently conjugated at 1:1 or 1:3 ratios pMHC-Fc and IFN- $\gamma$ -capture mAb (**Fig. 4.19, lower panels**). In order to distinguish bystander from antigen-specific IFN- $\gamma$  loaded T-Plex beads it is essential, that control and cognate T-Plex beads have all the same IFN- $\gamma$  binding capacity. This is easily achieved, if multiple Luminex beads of different color but with homogenous protein-binding capacity are covalently conjugated as “production batch” with a shared master mix comprising the IFN- $\gamma$  capture mAb and streptavidin or alternatively an  $\alpha$ -mIgG2a-Fc mAb.

#### 4 | Results Part 2 – Development of the T-Plex Assay

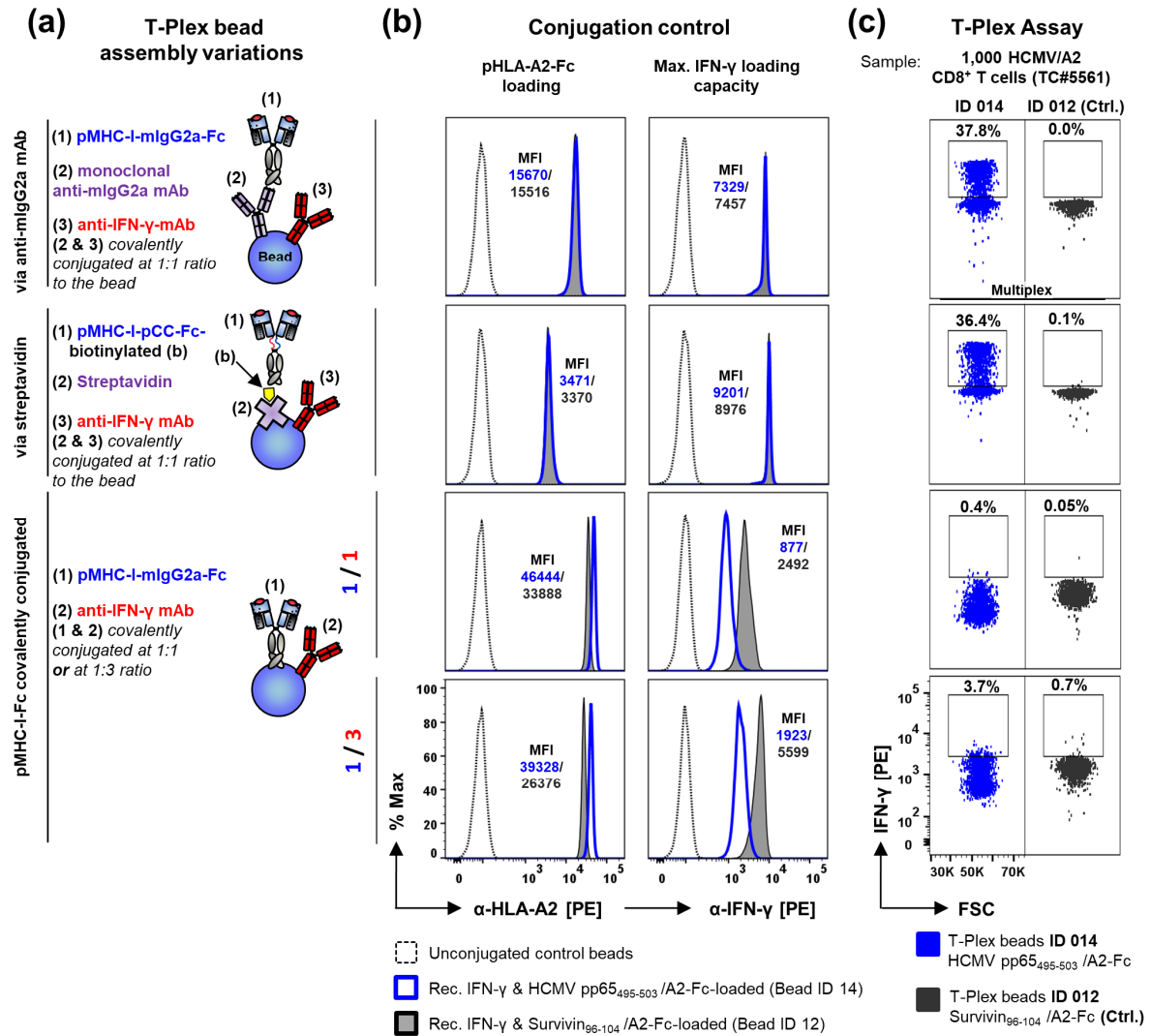


**Figure 4.19 | T-Plex bead assembly variations and impact on T-Plex Assay performance**

**(a) Scheme of T-Plex bead assembly variations. (Upper panel)** The 2<sup>nd</sup> generation T-Plex beads concept was used as previously described with the modification that color-coded Luminex beads (Bead) were covalently conjugated with IFN- $\gamma$  capture mAb (MD-1) and rat  $\alpha$ -mIgG2a (RMG2a-62) in a 1 to 1 ratio. Subsequently defined bead regions (ID) were loaded with soluble pHLA-A2-mIgG2a-Fc [8556.1 or 8558.1] derived from supernatants of construct expressing CHO-S cells. **(Middle panel)** Luminex-beads were covalently conjugated with streptavidin and IFN- $\gamma$  capture mAb in a 1:1 ratio and subsequently loaded with purified biotinylated pHLA-A2-pCC-Fc [9237.1 or 10337.7]. **(Bottom panel)** Luminex beads were directly covalently conjugated with purified pHLA-A2-mIgG2a-Fc [8556.1 or 8558.1] constructs and IFN- $\gamma$  mAb either in a 1 to 1 or 1 to 3 ratio.

**(b) Corresponding conjugation quality control.** pHLA-A2 conjugation was analyzed by staining pHLA-A2-associated T-Plex beads with  $\alpha$ -HLA-A2 mAb (clone BB7.2, IgG2b isotype). Maximal IFN- $\gamma$ -capture capacity was analyzed by incubating fully assembled T-Plex beads with 4 ng/mL recombinant IFN- $\gamma$  (BioLegend) for 2 h at 37°C followed by an IFN- $\gamma$ -PE detection mAb staining (clone 4S.B3 / BioLegend). Shown is the fluorescence signal of the HCMV pp65<sub>495-503</sub>/HLA-A2 (HCMV/A2) (blue) or Survivin<sub>96-104</sub>/HLA-A2 (grey) conjugated T-Plex beads and unloaded beads (dotted line).

**(c) Corresponding T-Plex Assay performance.** T-Plex Assay was performed using the T-Plex bead assembly variations indicated in (a). 1,000 HCMV/A2-specific T cells (TC#5561) were combined with T-Plex beads (4x multiplex / 10,000 beads per T cell epitope) in a 500  $\mu$ L tube and centrifuged prior to rolling at 60 rpm for 4 h, 30 min at 37°C. Shown is the IFN- $\gamma$  signal of the cognate HCMV/A2 T-Plex beads (blue) and one-out-of-three corresponding control bead signals (grey). Rows of T-Plex Assay FACS plots represent data analysis from the same reaction / bead mix (multiplex detection).

Although we tried multiple times, unfortunately we failed to generate T-Plex beads with equal IFN- $\gamma$ -capture capacity based on covalent conjugation of individual pMHC-I-Fc and IFN- $\gamma$ -capture mAb possible due to even slight concentration variations or impurities of our pMHC-I-Fc purifications. Consequently, no antigen-specific IFN- $\gamma$ <sup>+</sup> cognate T-Plex population could be well defined that was above the background of control beads, since the control beads had an overall higher IFN- $\gamma$ -capture capacity (**Fig. 4.19**, lower panels).

In summary, the T-Plex bead architectures either on the basis of IFN- $\gamma$ -capture mAb/ $\alpha$ -mIgG2a-Fc mAb or IFN- $\gamma$ -capture mAb/streptavidin followed by loading of pMHC-Fc or biotinylated pMHC molecules, respectively, are interchangeable concepts leading to an overall similar T-Plex Assay performance. However, we failed to assemble functional T-Plex beads based on direct conjugation of IFN- $\gamma$ -capture mAb and pMHC-Fc that allowed the detection of antigen-specific T cells.

#### **4.4 Successful detection of minor T cell populations in healthy donors by the T-Plex Assay**

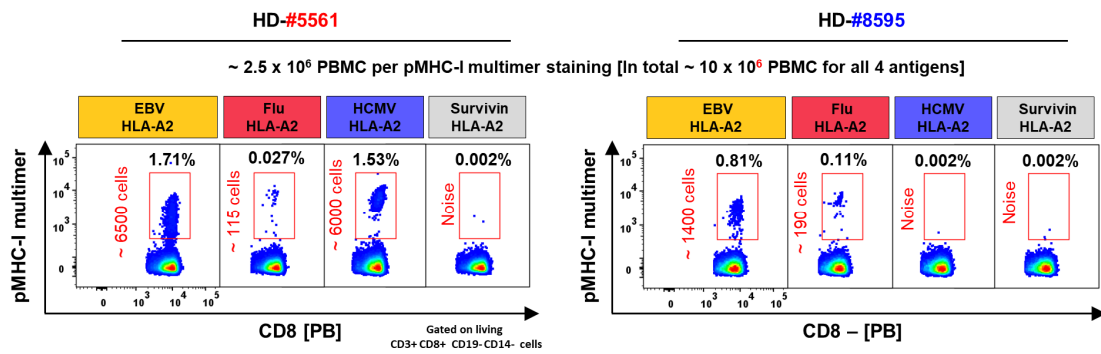
##### **4.4.1 Comparable sensitivities of an optimized T-Plex Assay and commercial pMHC-I multimer for the detection of low-frequent virus-specific CD8<sup>+</sup> T cell populations**

The optimization phase of the T-Plex Assay revealed that in particular a centrifugation step of the T cells together with the T-Plex beads prior to the co-culture at increased rolling speeds remarkably improves the T-Plex Assay performance. The optimized assay protocol led in average to a 10–20x increased fraction of IFN- $\gamma$ <sup>+</sup> T-Plex beads compared to previously used conditions suggesting an overall improved assay sensitivity (**Fig. 4.16**). Thus, we once more aimed for detection of T cell populations present at low frequencies within healthy donor derived PBMC. In previous experiments using suboptimal T-Plex Assay conditions, we failed to detect ~390 Flu/A2-specific CD8<sup>+</sup> T cells within ~5x10<sup>5</sup> bystander CD8<sup>+</sup> T cells isolated from 6.5x10<sup>6</sup> PBMC of healthy donor #3838 (**Fig. 4.13 & Table 4.1**). Since the sample material of donor #3838 was no longer available to test the optimized T-Plex Assay conditions, we screened several HLA-A2<sup>+</sup> healthy donors by commercial pMHC-I multimer staining and identified donor #5561 and #8595 to have similar frequencies of Flu/A2-specific CD8<sup>+</sup> T cells (0.03–0.1% / ~60 cells out of 1x10<sup>6</sup> PBMC) (**Fig. 4.20 & Table 4.2**). In addition, donor #5561 displayed a pronounced EBV/A2- as well as HCMV/A2-specific CD8<sup>+</sup> T cell population, whereas donor #8595 displayed solely an additional EBV/A2-specific CD8<sup>+</sup> T cell population among the analysed T cell specificities (**Fig. 4.20a**).

In the next step, isolated CD8<sup>+</sup> T cells from donors #5561 and #8595 were analysed by a multiplex T-Plex reaction under optimized conditions including co-centrifugation of beads and sample prior to rolling and increasing the rolling speed to 60 instead of 40 rpm (**Fig. 4.20b**). As hoped, even the minor Flu/A2-specific CD8<sup>+</sup> T cell population and all other T cell specificities were detected by the T-Plex beads in accordance with the corresponding pMHC-I multimer staining. Importantly, the rare Flu/A2-specific CD8<sup>+</sup> T cell population present in both donors was detected, even when the same amount of sample was used (2.5x10<sup>6</sup> PBMC / pMHC-I multimer or CD8<sup>+</sup> T cells derived from 2.5x10<sup>6</sup> PBMC / T-Plex Assay) either for the T-Plex Assay as or the respective pMHC-I multimer staining. The latter result finally indicated comparable sensitivities of T-Plex beads as well as pMHC-I multimers for the detection antigen-specific T cell populations of low frequency.

#### 4 | Results Part 2 – Development of the T-Plex Assay

##### (a) pMHC-I multimer staining



##### (b) T-Plex Assay

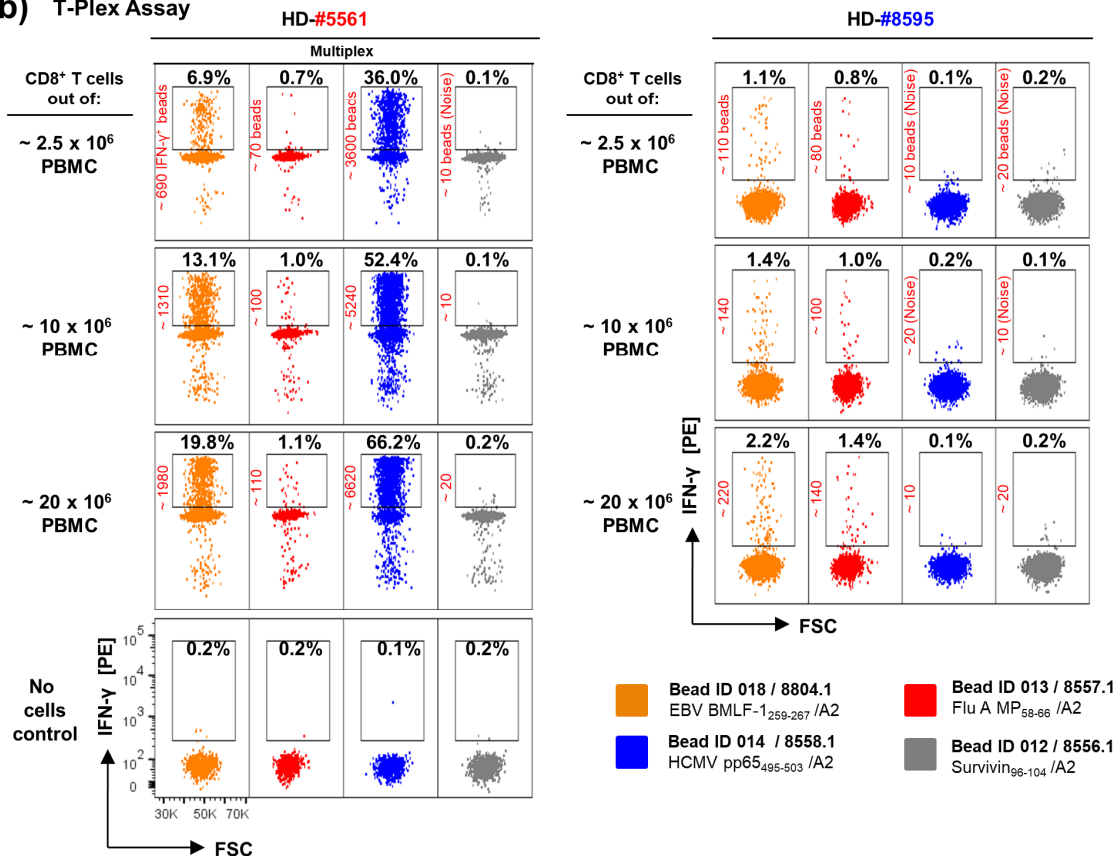


**Figure 4.20 | Reliable detection of small T cell populations using the optimized T-Plex Assay**

(a) pMHC multimer staining of healthy donor (HD) #5561 & #8595: 2.5x10<sup>6</sup> PBMC were individually stained with commercial pMHC-I multimers (pentamer, ProImmune) (no multiplex) in the presence of dasatinib [50 nM]. The frequencies of pMHC-I multimer<sup>+</sup> cells within the CD8<sup>+</sup> T cell population are shown in black. Extrapolated total amounts of respective antigen-specific CD8<sup>+</sup> T cells within 2.5x10<sup>6</sup> PBMC are shown in red numbers.

(b) Corresponding T-Plex Assay-based analysis of the same donors: 2<sup>nd</sup> generation (60%  $\alpha$ -IFN- $\gamma$  [MD-1] / 40%  $\alpha$ -mIgG2a) T-Plex beads were loaded with respective pMHC-I-Fc constructs as indicated in the figure. Loaded T-Plex bead pools (4x multiplex / 10,000 beads per T cell epitope) were incubated with isolated CD8<sup>+</sup> T cells derived from either 2.5x10<sup>6</sup>, 10x10<sup>6</sup> or 20x10<sup>6</sup> PBMC. Prior to rolling at 60 rpm for 5 h at 37°C, the in a 500  $\mu$ L tube combined test sample and T-Plex beads were centrifuged for 5 min at 2500 rpm. The presence of antigen-specific T cells was indicated by the appearance of an IFN- $\gamma$ <sup>+</sup> subpopulation of cognate T-Plex beads that is above T-Plex control beads (grey). Extrapolated total amounts of IFN- $\gamma$ <sup>+</sup> T-Plex beads are shown in red numbers and relative percent in black numbers. Linked FACS plots of the individual T-Plex Assays represent data analysis from the same reaction / T-Plex bead pool mix (multiplex detection).

**Table 4.2 | Quantitative analysis of the pMHC-I multimer staining of HD-#5561 and HD-#8595 shown in Fig. 4.20 and extrapolated absolute cell quantities used for corresponding optimized T-Plex analysis**

Population:	Healthy donor #5561		Healthy donor #8595	
	% Parent:	Cell count	% Parent:	Cell count
Result of pMHC-I multimer staining		Extrapolated		Extrapolated
P1 [Lymphocytes (+) monocytes]	92%	~ 2.5 x 10 <sup>6</sup>	79%	~ 2.5 x 10 <sup>6</sup>
Single, living CD3 <sup>+</sup> CD19 <sup>-</sup> CD14 <sup>-</sup>	55%	~ 1.4 x 10 <sup>6</sup>	43%	~ 1.1 x 10 <sup>6</sup>
CD3 <sup>+</sup> CD8 <sup>+</sup>	28%	~ 4 x 10 <sup>5</sup>	16%	~ 1.7 x 10 <sup>5</sup>
CD8 <sup>+</sup> CD3 <sup>+</sup> EBV/A2 multimer <sup>+</sup>	<b>1.71%</b>	~ <b>6500</b>	<b>0.81%</b>	~ <b>1400</b>
CD8 <sup>+</sup> CD3 <sup>+</sup> Flu/A2 multimer <sup>+</sup>	<b>0.03%</b>	~ <b>115</b>	<b>0.11%</b>	~ <b>190</b>
CD8 <sup>+</sup> CD3 <sup>+</sup> HCMV/A2 multimer <sup>+</sup>	<b>1.53%</b>	~ <b>6000</b>	-	-

However, an issue that still needs to be resolved is the apparent discrepancy of the extrapolated absolute amounts of antigen-specific T cells within the T-Plex reaction and the amounts of cognate IFN- $\gamma$  loaded T-Plex beads, which appears to be dependent on the antigen itself. In case of HCMV pp65<sub>495-503</sub>/HLA-A2-specific CD8<sup>+</sup> T cells, similar amounts of antigen-specific T cells in the reaction mix and amounts of loaded IFN- $\gamma$  loaded T-Plex beads could be observed, whereas we detected almost 10x less corresponding IFN- $\gamma$ <sup>+</sup> T-Plex beads, when EBV/A2-specific T cells were analyzed. One explanation could be the exceptionally high affinity of the HCMV pp65<sub>495-503</sub>/HLA-A2-specific T cell receptor that is partially even shared between HLA-A2<sup>+</sup> individuals (325) and may act in favor of the T-Plex Assay.

#### 4.4.2 Antigen-specific detection by the T-Plex Assay does not alter the cognate T cell pool

Previous experiments shown in **Fig. 4.8 & Fig. 4.13** revealed that usage of a T-Plex Assay barely changed the frequency of a given detected antigen-specific T cell population when the entire sample is directly cultured after the T-Plex Assay run. In other words, this result suggested that the T cell phenotype after initial analysis by a T-Plex Assay is hardly altered. To confirm these initial findings, we set out to analyze the phenotype of the antigen-specific T cell populations that had been detected upon co-culture with cognate T-Plex beads and subsequently cultured after a completed T-Plex Assay run. As shown in **Fig. 4.21a**, HLA-A2<sup>+</sup> healthy donor #3637 displayed an EBV/A2-specific CD8<sup>+</sup> T cell population (0.16% among CD8<sup>+</sup> T cells) as well as a Flu/A2-specific CD8<sup>+</sup> T cell population (0.25%), which was revealed by commercial pMHC-I multimer staining. Subsequently, PBMC of donor #3637 were labeled with a proliferation tracking dye (CellTrace™ Violet / CTV) and isolated CD8<sup>+</sup> T cells were subject to a corresponding T-Plex Assay. In line with the pMHC-I multimer results, also the T-Plex Assay successfully detected the EBV/A2- and Flu/A2-specific CD8<sup>+</sup> T cell population when performed under optimized conditions and using the same amount of sample (**Fig. 4.21b**). Here, the T-Plex Assay indicated similar absolute numbers of T-Plex beads that had been loaded in an antigen-dependent manner with IFN- $\gamma$  and the absolute extrapolated amounts of cognate antigen-specific T cells present in the test sample (**Fig. 4.21b & Table 4.3**). HD-#3637-derived CTV-labeled CD8<sup>+</sup> T cells were brought back into culture after the initial T-Plex Assay run. In parallel, corresponding CD8<sup>+</sup> T cells served as control culture, that were not previously analyzed by a T-Plex Assay. After 6 days, both CD8<sup>+</sup> T cell cultures previously subjected either to a T-Plex Assay, or left untouched, were analyzed for proliferation, activation marker expression and change in EBV/A2- and Flu/A2-specific CD8<sup>+</sup> T cell population frequencies (**Fig. 4.21c**). As expected and in line with previous results, we did not observe a notable change of antigen-specific T cell frequencies subsequent to the T-Plex Assay analysis. Moreover, neither the EBV/A2- nor the Flu/A2-specific CD8<sup>+</sup> T cell population previously detected by T-Plex Assay had proliferated or

#### 4| Results Part 2 – Development of the T-Plex Assay

expressed activation markers compared to the control culture (**Fig. 4.21c**). These data strongly suggest that antigen-specific T cell detection by a T-Plex Assay does not result in a significantly altered phenotype of the analyzed T cell sample.

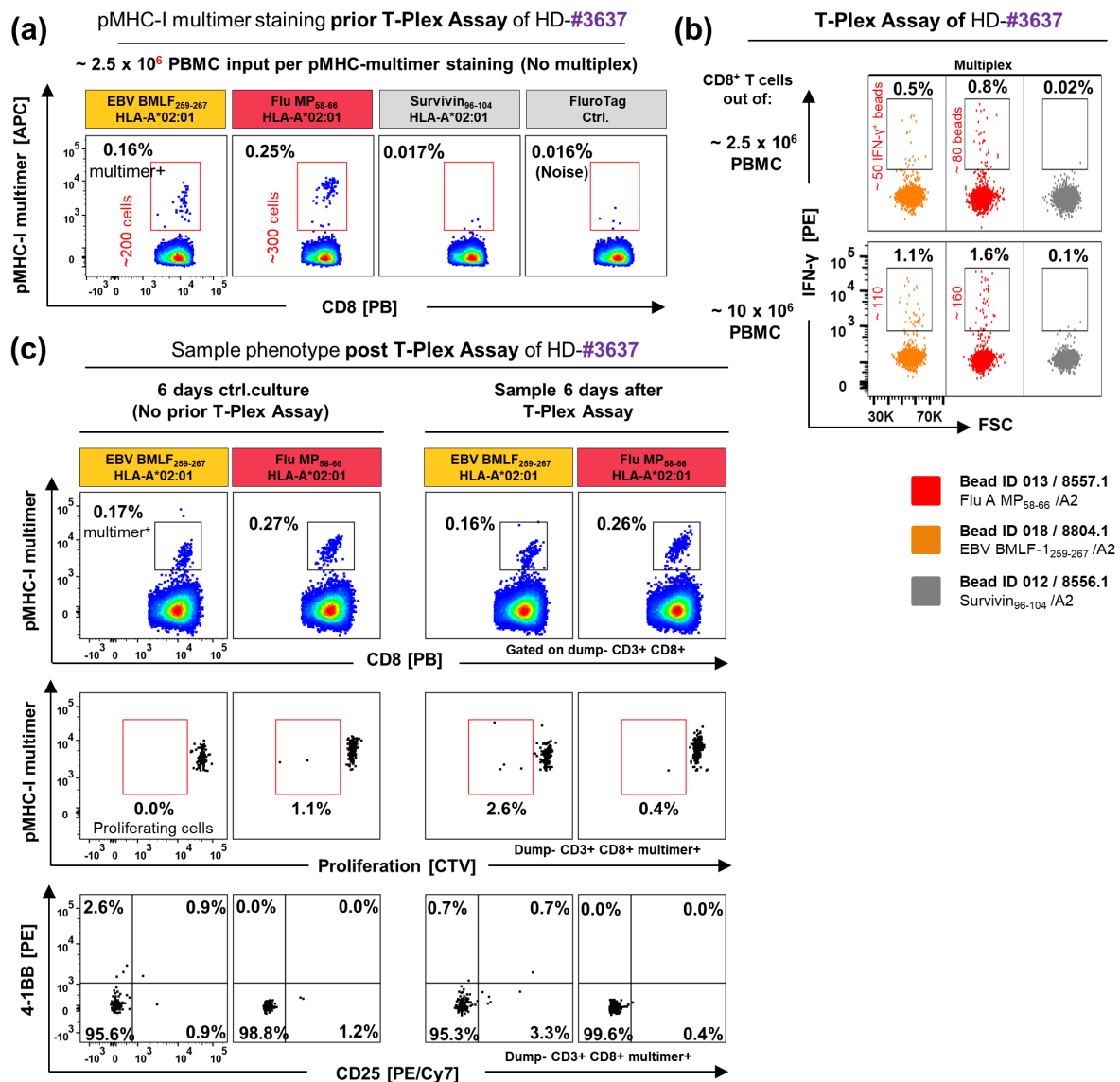


**Figure 4.21 | Antigen-specific T cell detection by the T-Plex Assay does not alter the original sample's phenotype**

**(a) pMHC-I multimer staining of healthy donor (HD) #3637.** HLA-A2<sup>+</sup> healthy donor (HD) #3637 was initially analyzed by pMHC-I multimer staining (ProImmune) (no multiplex). The frequencies of pMHC-I multimer<sup>+</sup> cells within the CD8<sup>+</sup> T cell population are shown in black. Extrapolated total amounts of respective antigen-specific CD8<sup>+</sup> T cells within 2.5x10<sup>6</sup> PBMC are shown in red numbers.

**(b) Corresponding T-Plex Assay-based analysis of the same donor:** To analyze if a T-Plex run induces antigen-specific proliferation, PBMC of HD#3637 were labeled with CellTrace violet-labeled (CTV / Invitrogen) prior to isolation of untouched CD8<sup>+</sup> T cells. 2<sup>nd</sup> generation pMHC-I-Fc-loaded T-Plex bead pools (4x multiplex / 10,000 beads per T cell epitope) were incubated with isolated CD8<sup>+</sup> T cells derived from either 2.5x10<sup>6</sup>, 10x10<sup>6</sup> total PBMC in 500 μL tubes. Prior to rolling at 60 rpm for 5 h, 37°C, the combined test sample and T-Plex beads were centrifuged for 5 min at 2500 rpm. After 5 h T-Plex beads were magnetically separated from T cells and analyzed. T cell sample was brought back into culture.

**(c) Sample phenotype after a T-Plex Assay run in comparison to an untouched control culture.** After a 6 days culture CTV-labeled HD#3637 CD8<sup>+</sup> T cells either previously subjected to a T-Plex Assay or left untouched (no T-Plex Assay) were stained with pMHC-I multimers prior to lineage and activation marker staining. **(Upper panel)** Frequencies of pMHC-I multimer<sup>+</sup> cells within the CD8<sup>+</sup> T cell population are shown. **(Middle and bottom panel)** Percent of proliferation (CTV<sup>dim</sup>) and activation marker (CD25<sup>+</sup> / 4-1BB<sup>+</sup>) expression of pMHC-I multimer<sup>+</sup> CD8<sup>+</sup> T cells are shown.

**Table 4.3 | Quantitative analysis of the pMHC-I multimer staining of HD-#3637 PBMC shown in Fig. 4.21 and extrapolated absolute cell quantities used for a corresponding T-Plex analysis**

Healthy donor #3637		
Population:	% Parent:	Cell count
Result of pMHC-I multimer staining		Extrapolated
P1 [Lymphocytes (+) monocytes]	90%	~ 2.5 x 10 <sup>6</sup>
Single, living CD3 <sup>+</sup> CD19 <sup>-</sup> CD14 <sup>-</sup>	53%	~ 1.3 x 10 <sup>6</sup>
CD3 <sup>+</sup> CD8 <sup>+</sup>	9%	~ 1.2 x 10 <sup>5</sup>
CD8 <sup>+</sup> CD3 <sup>+</sup> EBV/A2 multimer <sup>+</sup>	0.16%	~ 200
CD8 <sup>+</sup> CD3 <sup>+</sup> Flu/A2 multimer <sup>+</sup>	0.25%	~ 300

#### **4.5 *In silico* predicted HLA-A2-restricted neopeptides of four cancer patients were not immunogenic as shown by T-Plex Assay- and pMHC-I multimer-based analysis**

There is a key interest of validating the immunogenicity of mutation-derived cancer neoantigens by detecting corresponding neoantigen-specific T cell pools either for monitoring the success of therapeutic vaccinations (137–139) or to directly exploit these T cells for adoptive T cell transfer therapies (140–142), as previously introduced in **Section 1.4.2.2**. In order to prove the capability of the T-Plex Assay to detect cancer neoantigen-specific T cells, we wanted to apply the T-Plex Assay to a clinical setting, where tumor material of individual cancer patients has been analyzed beforehand by whole exome sequencing (WES) and if applicable RNA-sequencing followed by mutagenome and allele haplotype assessment and T cell neoepitope *in silico* prediction (**Material and Methods Section 2.12**). To this end, we received PBMC cryostocks from four cancer patients (Patient 1–4) (**Table 4.4**), who have been treated with standard therapies as well as with personalized neoantigen-targeting long peptides as cancer vaccines that have been selected based on WES and if available RNA-sequencing data (**Fig. 4.22**). All four patients displayed overall a low mutational burden according to (326). In the following, individual T cell responses were monitored by conventional ELISpot analysis. The selected long peptides comprised the single nucleotide variation-based mutation that was flanked N- and C-terminally by 14 residues of the naturally occurring gene sequence (**Table 4.4**). At the indicated time points, peripheral blood was taken from each individual patient and an ELISpot analysis was performed based on restimulation with the long peptides. In case of patients 2–4, the ELISpot data clearly indicated T cell responses towards the respective long peptides suggesting an overall successful immunization. In case of patient 1, the performed ELISpot data was inconclusive (**Fig. 4.22 & Table 4.4**).

All four patients expressed the HLA-A\*02:01 allele as confirmed by WES data as well as by positive staining of patient-derived PBMC with the HLA-A2-specific BB7.2 mAb (**data not shown**). Subsequently, we used the long peptide sequence as template to predict putative mutation-spanning HLA-A2-restricted minimal epitopes using the NetMHC 4.0 algorithm (281) as well as NetMHCpan 4.0 (282) algorithm interrogating 9 to 11-mer peptides (**Table 4.5**). HLA-A2-restricted neopeptides with an HLA-A2 binding rank score of <2 for the mutant peptide variant obtained by at least one of the used algorithms were selected. Next, peptide-loaded HLA-A2 molecules following the dt-SCT construct design fused to a cleavable Fc (pHLA-A2\*-Fc, previously described in **Fig. 3.10**) presenting all selected mutated peptide (neopeptide) as well as corresponding wildtype peptide (wt-peptides) candidates were cloned (**Table 4.5**) and subsequently produced as described in **Section 3.4**.

**Table 4.4 | Cancer patient characteristics, used long peptides for vaccination and ELISpot results**

Patient ID:	Cancer type	No. of mutations of a resected metastasis		RNASeq data integrated for peptide selection
		SNVs	Indels	
Patient 1	Neuroendocrine tumor of the thymus	68	2	Yes
Patient 2	Malignant solitary fibrous sarcoma	29	2	Yes
Patient 3	Prostate carcinoma	104	15	N/A
Patient 4	Pancreatic adenocarcinoma	105	9	Yes

N/A: data not available; SNV: single nucleotide variations

Patient ID:	Gene symbol:	Mutation:	Long peptides ID:	Long peptide sequence (Mutated AA and residues of predicted minimal peptides are highlighted):	ELISpot analysis		
					Before vaccination	1 - 5 months post vaccination	>12 months post vaccination
1	HTT	E2170V	HD-Pep-295	ISGGQKSALFEAARVVTLARVSGTVQQLP	-	- / +	N/A
2	SHPK	T323M	HD-Pep-365	MYNEILMLGAKLHPMLKLEELTNKKGMP	-	+	N/A
3	C7orf41	T81M	HD-Pep-647	LQLAQDYISSCGKMLHEVLEKVFKSFRP	++	(+)	N/A
4	GUF1	E411D	HD-Pep-375	GAGWRLGFLGLLHMDVFNQRLEQEYNASV	N/A	++	++
	CNNM1	R636W	HD-Pep-378	EPFKSLYLSEKILLWLLKHPNVIQELKFD	N/A	++	++
	BBS4	D13V	HD-Pep-379	MLGKIHLLEGDLVKAIEVYKKAVEFSP	N/A	++	++

“-”: ELISpot was considered negative, i.e. restimulation with the indicated long-peptide resulted in less spots than twice the background. “+/-”: ELISpot was inconclusive, i.e. very high standard deviation of background and peptide restimulation. “(+) / + / ++”: ELISpot was considered positive, i.e. long-peptide restimulation lead to spots that were exactly “(+)”, higher than twice “+”, or 50-fold higher “++” than the background. N/A: data not available

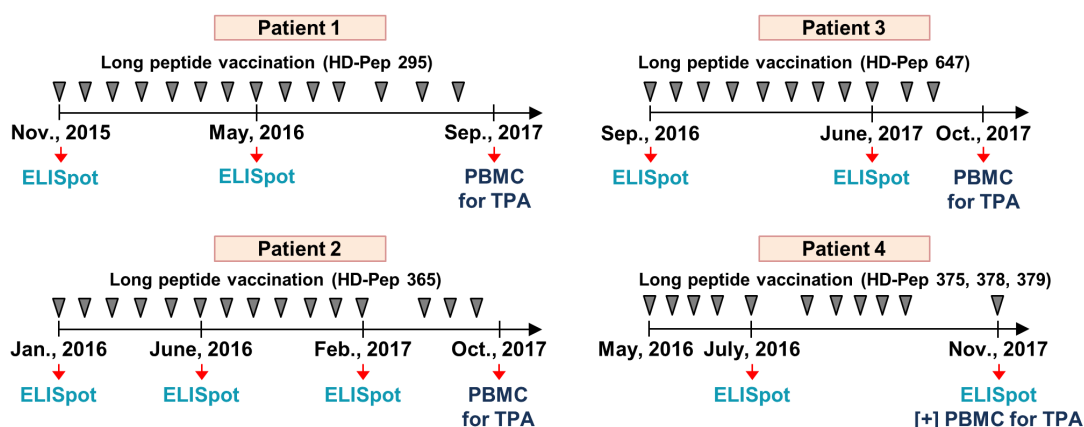


**Figure 4.22 | Long peptide vaccination schedule and time points of blood taken from each individual patient**

Cancer patients 1–4 received personalized long-peptides (HD-Pep) combined with Montanide ISA-51 serving as adjuvant in roughly monthly intervals for a time span of more than one year. Grey arrows indicate individual vaccination time points and time points of peripheral blood taken followed by ELISpot analysis and/or T-Plex Assay (TPA) are shown with red arrows.

Successful production and purification of 293-F-derived *in vivo* biotinylated, monomeric Fc-cleaved (\*) pHLA-A2\* molecules for all selected wt- and neopeptides was confirmed by SDS-PAGE analysis showing an expected 55 kDa band that represents the main product (**Fig. 4.23a, upper panel**). Moreover, in every case this 55 kDa band shifts upon addition of streptavidin (SAv) towards a higher molecular weight (**Fig. 4.23a, lower panel**) indicating an overall very efficient biotinylation of these constructs. Notably, elution fractions of purified pHLA-A2\* [11477.1] as well as pHLA-A2\* [11478.1] productions presenting the GFLGLLHMEV (wt) and GFLGLLHMDV (neo) peptide, respectively, displayed multiple byproducts as well as only a minimal proportion of the expected 55 kDa product. This could be a consequence of the less optimal phenylalanine (F) anchor residue at position 2 or the overall rather less optimal predicted binding property for HLA-A\*02:01. Similar also the HMEVFNQRL (wt) peptide was predicted to bind only poorly to HLA-A\*02:01, which may also explain the rather low abundance of a 55 kDa product of the corresponding pHLA-A2\* [11479.1] construct.

As next step, we sought to evaluate the antigenicity of the predicted HLA-A2-restricted peptide epitopes using corresponding pHLA-A2-loaded T-Plex beads and patient-derived peripheral blood taken several months post initial long-peptide vaccination (**Fig. 4.22**). Streptavidin / IFN- $\gamma$ -capture mAb [MD-1] covalently conjugated T-Plex beads were loaded with the individual patient-specific set of biotinylated pHLA-A2\* molecules presenting wild-type as well as neo-peptide. Successful pHLA-A2\* conjugation to defined T-Plex bead species was confirmed for every putative epitope by anti-HLA-A2 BB7.2 mAb-staining as shown in **Fig. 4.23b**. Notably, also GFLGLLHMEV (wt) and GFLGLLHMDV (neo) pHLA-A2\* [11477.1] and [11478.1] molecules were detected on respective T-Plex bead species although the HLA-A2 signal intensity of these beads were strikingly lower compared to T-Plex beads loaded with other pHLA-A2\* constructs. In addition, the homogenous IFN- $\gamma$  capture capacity of the entire used T-Plex bead batch was confirmed by incubating an aliquot of the entire T-Plex bead batch with saturating amounts of recombinant IFN- $\gamma$  followed by an IFN- $\gamma$  detection mAb staining (**Fig. 4.23d**). After all pHLA-A2-loaded T-Plex beads passed the initial quality control, patient-derived peripheral blood cryostocks were defrozen and were left overnight in culture prior to further analysis. Unfortunately, the overall viable cell recovery after thawing was only approximately 10% of the original frozen cell number as assessed by counting chamber-based analysis and flow cytometric analysis of a small cell sample (**Supplementary Fig. S10**). The cell material either contained a rather low fraction of T cells (33%, in case of patient 1) or an overall low fraction of CD8<sup>+</sup> T cells (5.6%, in case of patient 4), which allowed for the isolation of only 100,000 to 250,000 viable CD8<sup>+</sup> T cells per patient in total. To increase the chance of detecting also lower frequencies of antigen-specific CD8<sup>+</sup> T cells, the entire pool of isolated CD8<sup>+</sup> T cells was combined with T-Plex beads conjugated with the patient-specific set of predicted HLA-A2-restricted neopeptides as well as corresponding wt-peptides. In addition for every T-Plex Assay performed, at least one T-Plex bead species was integrated that lacked any pHLA-A2 loading, which served as internal negative control and was used to set the baseline for bystander (i.e. antigen-independent) IFN- $\gamma$ -loading. Moreover, T-Plex Assays were performed using the previously identified optimal assay parameters including co-centrifugation of fully assembled T-Plex beads and patient-derived CD8<sup>+</sup> T cells transferred to 0.5 mL tubes followed by rotation at 60 rpm on a rolling device for 5 h at 37°C. After the T-Plex Assay was conducted, beads and patient-derived CD8<sup>+</sup> T cells were magnetically separated from each other and the patient sample was brought back into culture.

Unfortunately, as shown in **Fig. 4.23c**, individual T-Plex bead species reflecting the predicted HLA-A2-restricted neopeptides as well as wt-control peptides displayed no IFN- $\gamma$ <sup>+</sup> bead population that was above background upon co-cultured with the isolated CD8<sup>+</sup> T cells. These data strongly indicated that the predicted HLA-A2 neo-epitopes were not immunogenic in all four patient cases and that the

#### 4| Results Part 2 – Development of the T-Plex Assay

previous immunization of the patients with the respective long peptides did not elicit a detectable neoepitope-responsive, HLA-A2-restricted CD8<sup>+</sup> T cell population.

**Table 4.5 | Produced neoepitope and corresponding wt-peptide-loaded HLA-A2 molecules**

Patient ID:	Long peptide ID:	Gene / HUGO Symbol:	pHLA-A2-Fc* construct ID (a):	Peptide sequence (Variable AA highlighted) (b):		NetMHC 4.0			NetMHCpan 4.0	
						Affinity [nM] to HLA-A2	%Rank to bind HLA-A2	Bind level	%Rank to bind HLA-A2	Bind level
1	295	HTT	11475.1	ALFEAAREV	wt	15.04	0.20	SB	0.03	SB
			11660.2	ALFEAARVV	neo	54.68	0.70	WB	0.16	SB
			11473.1	ALFEAAREVTL	wt	499.96	3.0	-	0.25	SB
			11474.1	ALFEAARVTL	neo	255.38	1.90	WB	0.26	SB
2	365	SHPK	11467.1	MLGAKLHPT	wt	76.10	0.90	WB	2.52	-
			11468.1	MLGAKLHPM	neo	27.74	0.40	SB	1.37	WB
			11488.1	LMLGAKLHPT	wt	243.52	1.80	WB	8.07	-
			11466.1	LMLGAKLHPM	neo	61.41	0.80	WB	5.41	-
			11487.1	MLGAKLHPTL	wt	69.01	0.80	WB	1.77	WB
			11465.1	MLGAKLHPML	neo	69.19	0.80	WB	2.48	-
3	647	C7orf41	11484.1	TLHEVLEKV	wt	39.50	0.50	SB	0.04	SB
			11483.1	MLHEVLEKV	neo	10.87	0.12	SB	0.02	SB
			11481.1	KTLEVLEKV	wt	116.21	1.20	WB	0.49	SB
			11482.1	KMLEVLEKV	neo	15.07	0.20	SB	0.36	SB
4	375	GUF1	11480.1	FLGLLHMEV	wt	12.14	0.15	SB	0.22	SB
			11486.1	FLGLLHMDV	neo	56.06	0.70	WB	0.85	WB
			11479.1	HMEVFNQRL	wt	4413.99	9.0	-	2.44	-
			11485.1	HMDVFNQRL	neo	572.73	3.0	-	0.47	SB
			11477.1	GFLGLLHMEV	wt	52.69	0.70	WB	3.46	-
			11478.1	GFLGLLHMDV	neo	236.24	1.80	WB	7.94	-
	378	CNNM1	11471.1	YLSEKILLRL	wt	13.59	0.17	SB	0.15	SB
			11472.1	YLSEKILLWL	neo	9.21	0.10	SB	0.20	SB
			11464.1	YLSEKILLRLL	wt	94.87	1.00	WB	0.91	WB
			11470.1	YLSEKILLWLL	neo	13.19	0.17	SB	0.78	WB
			11463.1	ILLRLLKHPNV	wt	189.58	1.60	WB	6.24	-
			11469.1	ILLWLLKHPNV	neo	57.70	0.70	WB	5.41	-
379	GUF1	11461.1	HLLEGDLVKA	wt	1169.64	4.50	-	1.06	WB	
		11462.1	HLLEGDLVKA	neo	348.33	2.50	-	0.29	SB	

(a) Shown candidate peptides were cloned in the peptide-HLA-A2 homodimeric construct with cleavable Fc region (pHLA-A2-\*Fc) previously introduced in Fig. 3.10. (b) HLA-A\*02:01 (HLA-A2) peptide binding predictions were performed by the NetMHC 4.0 algorithm (281) as well as NetMHCpan 4.0 algorithm (282) for both mutated (neo) and corresponding wildtype (wt) peptide epitopes using the in Table 4.4 indicated long peptide sequence. With few exceptions candidate peptides were selected based on a %rank <2 predicted by at least one used algorithm. Peptides with %rank <0.5 were classified as putative strong binders (SB), %rank <2 as week binders (WB) and %rank >2 as potential non binders (-) according to both NetMHC 4.0 and NetMHCpan 4.0 default prediction thresholds.

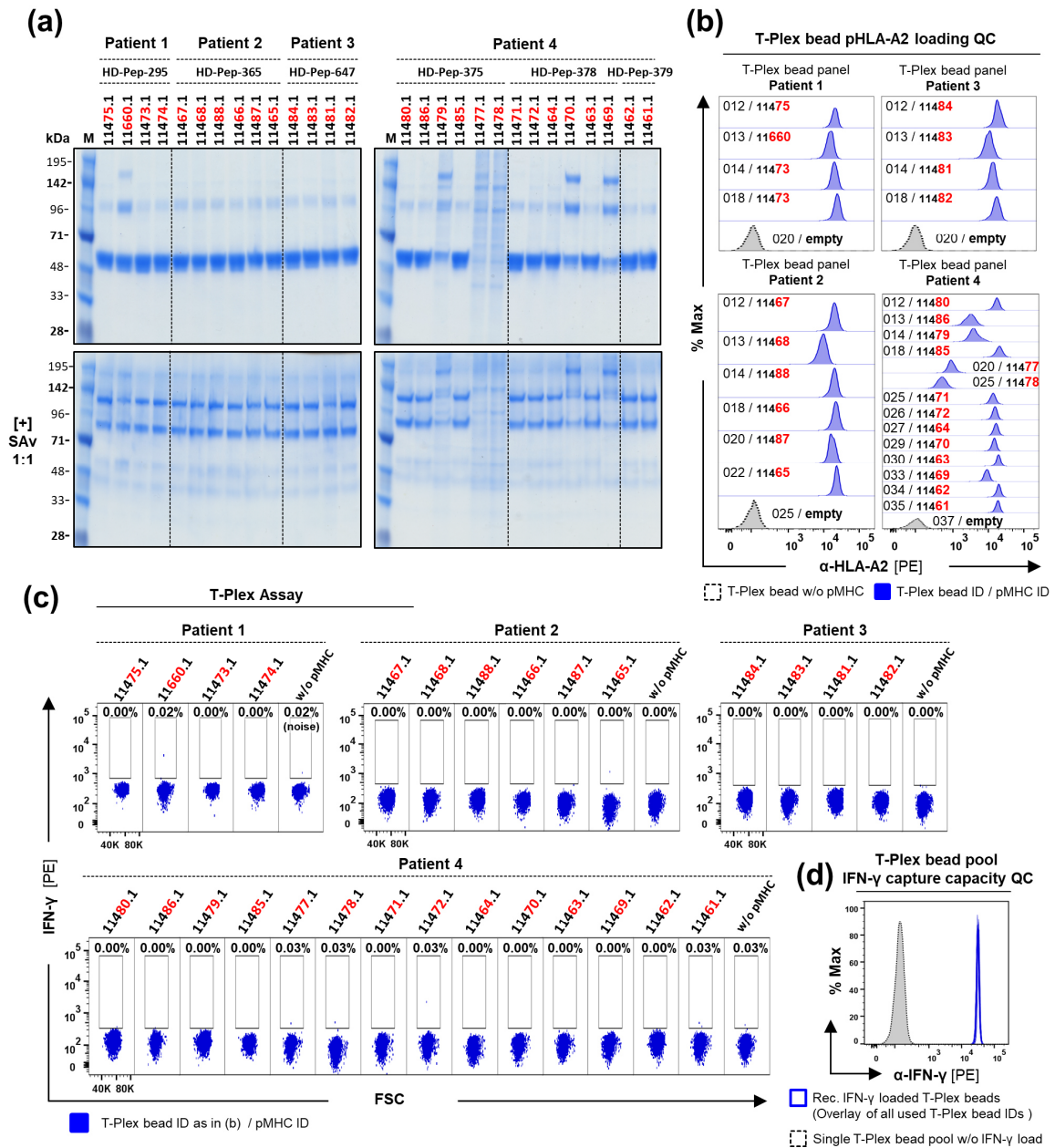


**Figure 4.23 | Analysis of cancer patient-derived peripheral blood by T-Plex beads displaying putative T cell neoepitopes**

**(a)** Successful production of pMHC-I\*Fc representing 14 *in silico* predicted HLA-A2-restricted neoepitope and 14 corresponding WT epitopes derived from four cancer patients. pHLA-A2\*Fc constructs presenting in Table 4.5 listed peptides were produced using the the 293-F TGE system followed by thrombin-based cleavage of the Fc and His-tag-based affinity chromatography of monomeric pHLA-A2 (pHLA-A2\*). Efficient *in vivo* biotinylation was confirmed by equimolar addition of streptavidin (SAv) to pHLA-A2\* molecules prior to 10% SDS-PAGE leading to an observed gel shift.

**(b)** pHLA-A2 loading quality control (QC) of SA v/αIFN-γ T-Plex beads. Color-coded Luminex beads were covalently conjugated with α-IFN-γ capture mAb (clone MD-1) and SA v in a 1:1 ratio (T-Plex beads). The resulting T-Plex beads were loaded with indicated biotinylated pHLA-A2\* constructs followed by α-HLA-A2 mAb-PE (BB7.2) staining.

**(c)** Immunogenicity analysis of *in silico* predicted HLA-A2 restricted neoepitopes by a corresponding T-Plex Assay. Peripheral blood isolated CD8<sup>+</sup> T cells of four cancer patients were co-cultured with T-Plex beads displaying putative neoepitopes (10,000 beads per epitope). Prior to rolling at 60 rpm for 5 h at 37°C, CD8<sup>+</sup> T cells and T-Plex beads were centrifuged. Rows of T-Plex Assay FACS plots represent data analysis from the multiplexed assay reaction. T-Plex beads without pHLA-A2 loading were used to define the baseline signal of IFN-γ-loaded beads (neg. ctrl). After 5 h T-Plex beads were magnetically separated from the T cells and analyzed. The T cell sample was brought back into culture.

**(d)** Confirmed homogenous IFN-γ-capture capacity of all used SA v/αIFN-γ T-Plex beads. IFN-γ-capture capacity was analyzed by incubating all used T-Plex bead pools with 4 ng/mL recombinant IFN-γ (BioLegend) for 2 h at 37°C followed by α-IFN-γ-PE mAb (clone 4S.B3) staining. Shown is the overlay of the fluorescence signal of all used T-Plex beads (blue lines) and one separated T-Plex bead pool lacking previous IFN-γ-loading (dotted line).

#### 4 | Results Part 2 – Development of the T-Plex Assay

In a final step, we aimed to confirm the obtained T-Plex Assay data by using a pMHC-I multimer staining reflecting the same predicted neopeptides. Thus, the biotinylated neopeptide and wt-peptide HLA-A2\* protein batches previously also used for the T-Plex bead assembly were multimerized on the basis of streptavidin-APC to gain pMHC-I multimers. Next, patient-derived CD8<sup>+</sup> T cells, which had been directly cultured after the initial T-Plex Assay run were individually stained with a selected set of neopeptide- and in some cases also wildtype peptide-bearing pMHC-I multimers. At least 10,000 CD8<sup>+</sup> T cells were used per staining. Yet, in accordance with the T-Plex Assay data also the corresponding pMHC-I multimer-based analysis revealed no neopeptide/HLA-A2-specific CD8<sup>+</sup> T cells population for any of the analyzed patients and putative neopeptides (**Fig. 4.24**). Only in case of patient 1 a minor wt-peptide [ALFEAAREVTL]/HLA-A2 [11473.1] specific CD8<sup>+</sup> T cell population was observed, which however was not detected by the corresponding T-Plex Assay shown above and thus may potentially represents a staining artifact.

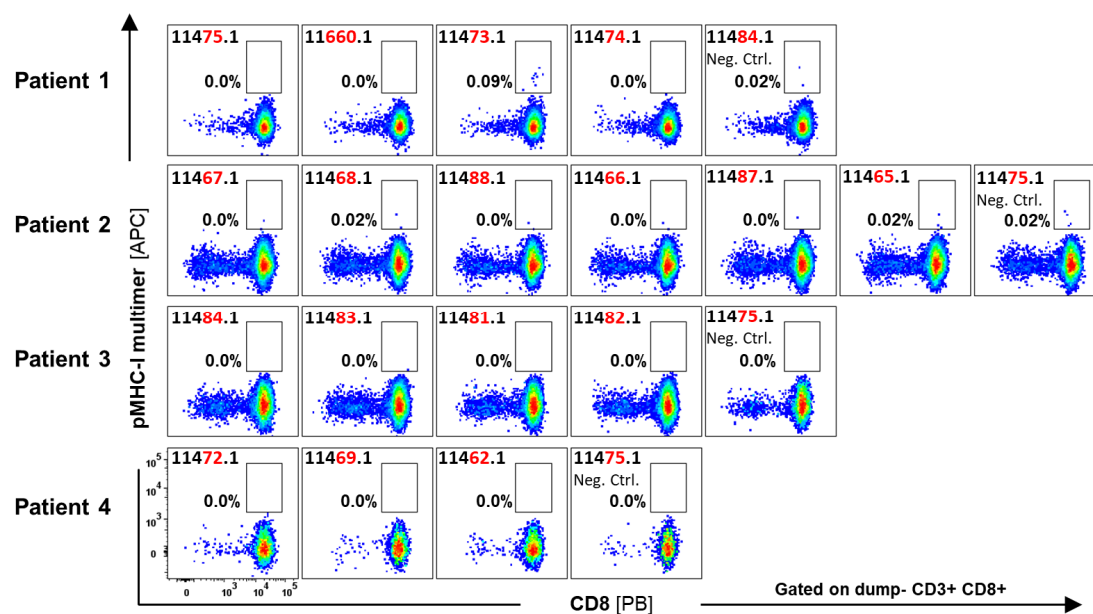


**Figure 4.24 | Neopeptide pMHC-I multimer staining of cancer patient-derived CD8<sup>+</sup> T cells to validate corresponding T-Plex Assay-based analysis**

Peripheral blood CD8<sup>+</sup> T cells of indicated cancer patients were first analyzed by the T-Plex Assay (**Fig. 4.23**) and brought back into culture for 6 days followed by a pMHC-I multimer staining using the same pHLA-A2 constructs as previously used for the T-Plex bead assembly. Neopeptide as well as corresponding wild-type epitope bearing pHLA-A2\* (also see **Table 4.5**) constructs were multimerized on the basis of streptavidin-APC. Due to the limited availability of cell material, only 10,000–25,000 CD8<sup>+</sup> T cells could be labeled with a selected panel of indicated pHLA-A2 multimers. Staining was individually performed per epitope in the presence of dasatinib [50 nM]. A pHLA-A2\* construct displaying an irrelevant epitope for the individual patient served as negative control (neg. ctrl.) staining. The frequencies of pMHC-I multimer<sup>+</sup> cells within the CD8<sup>+</sup> T cell population is shown.

Reasons for the lack of immunogenicity of the predicted neopeptides as indicated by the absence of a corresponding antigen-specific CD8<sup>+</sup> T cells population are manifold. In order for a predicted neopeptide to become an immunogenic neopeptide, the corresponding neopeptide must be first successfully processed and presented by a MHC molecule on the cell surface and second the presented pMHC complex must be recognized by a cognate T cell. The latter includes that the T cell repertoire is not “blind” for that particular neopeptide due to tolerance mechanisms caused by strong similarities between the wild-type peptide and neopeptide (327). In this study we took advantage of the NetMHC 4.0 and NetMHCpan 4.0 algorithm to predict the binding likelihood of the neopeptide and corresponding wt-peptide counterpart for the allele HLA-A\*02:01. Since all patient-derived

neopeptides as well as wt-peptide bearing pHLA-A2\* constructs were successfully expressed, we can assume that all predicted peptide sequences had in fact the capacity to bind and stabilize the HLA-A\*02:01 complex to certain degree. Yet, these algorithms do not allow the prediction of immunogenicity meaning the capacity to elicit a T cell response. A meta-analysis done by Bjerregaard *et al.* showed that out of 1,948 evaluated peptide-HLA combinations (comprising 1,874 unique tested peptides and 27 HLA alleles) representing putative mutation-driven neoepitopes only 53 T cell responses could be actually experimentally confirmed. Thus, the chance to experimentally validate the immunogenicity of a given predicted neopeptide is currently as low as 2.7%. Yet, 96% of all confirmed immunogenic peptides had a %rank score < 2.0 as shown by NetMHCpan 4.0 algorithm-based reanalysis (328), which is the same threshold that we also applied. However, due to the low mutational burden of the analyzed patient cohort as well as our current limitation that we solely focused on the HLA-A\*02:01 allele, we were so far only able to evaluate the immunogenicity of 14 potential neopeptides. To further increase our chance to identify immunogenic neopeptides, we will seek in the near future to establish a broader portfolio of frequent HLA-A, B and C alleles to better cover the individual patient's HLA-I type.

Another issue might be the generally observed, very low frequency of so-called circulating neoantigen-specific T cells present in patient-derived peripheral blood that limits the possibility for direct *ex vivo* detection of these cells. In our study, we were only able to recover 100,000 to 250,000 viable CD8<sup>+</sup> T cells after thawing the cancer patient-derived PBMC cryostocks, which according to the vast majority of reports may only contain 2 – 100 cancer neoepitope-specific T cells. For instance, a former case study interrogating the immunogenicity of predicted neoepitopes in a melanoma patient cohort, encountered a frequency of 0.002 – 0.4% among CD8<sup>+</sup> T cells present in peripheral blood to be specific for neoantigens as detected by pMHC-I multimer analysis (225). More recently, Cafri *et al.* reported frequencies in peripheral blood to be as low as 0.0007% (0.02 – 0.0007%) among a cohort of common metastatic epithelial cancers, which was retrospectively determined in the original blood sample by TCR sequencing after cognate neoantigen-specific T cell pools had been identified beforehand using an *in vitro* stimulation (IVS)-based enrichment method. For the latter, peripheral blood-derived bulk memory T cells (i.e. T<sub>EM</sub>, T<sub>CM</sub>, T<sub>EMRA</sub>) were initially sorted from peripheral blood and subsequently co-cultured for 12 days on long peptide-pulsed or tandem-minigene transfected DCs to enrich for neoepitope-specific T cells. Finally, individual neoepitope-responses were interrogated in various functional assays (i.e. ELISpot or 4-1BB and OX40 expression) upon short-term antigenic restimulation (159). In a similar study, Bobisse *et al.* initially co-cultured peripheral blood bulk CD8<sup>+</sup> T cells derived from various ovarian-cancer patients with irradiated autologous PBMCs (CD8<sup>+</sup> and CD4<sup>+</sup>-depleted) pulsed with a pool of short peptides in order to expand “blindly” for neoepitope-specific T cell pools prior to successful detection of individual T cell responses (294). To overcome a potential failure of detection due to a too low T cells frequency and a too low T-Plex Assay sensitivity, we will therefore also incorporate such an *in vitro* stimulation-based enrichment step using short peptide pools covering putative neoepitope candidates prior to performing a T-Plex Assay read-out with the aim to deconvolute the corresponding T cell responses towards the individual neopeptides.

## 4.6 Successful detection of antigen-specific CD4<sup>+</sup> T cell line by the T-Plex Assay

### 4.6.1 Antigen-specific detection of a CD4<sup>+</sup> T cell line by pMHC-II-pCC-Fc-loaded T-Plex beads.

As a last milestone, we aimed at detecting antigen-specific CD4<sup>+</sup> T cell responses by a suitable T-Plex Assay. To address this aim, we already successfully cloned, produced and validated several pMHC-II-Fc fusion constructs as presented in **Section 3.6**. Moreover, beads conjugated with MTB Hsp65<sub>1-13</sub> /HLA-DR3 molecules had the capacity to stimulate the cognate Th1-differentiated MTB Hsp65<sub>1-13</sub> /HLA-DR3-specific CD4<sup>+</sup> T cell clone RP15.1.1 resulting in IFN- $\gamma$  and TNF- $\alpha$  secretion (**Fig. 3.14**). Consequently, we took advantage of the 2<sup>nd</sup> generation T-Plex beads loaded with cognate or control pMHC-II-pCC-Fc to detect titrated amounts of the MTB/DR3-specific CD4<sup>+</sup> T cell clone spiked into bystander T cells (Sur/A2 CD8<sup>+</sup> T cells) (**Fig. 4.25a**). As shown in **Fig. 4.25a** cognate MTB/DR3-associated T-Plex beads detected reliably the presence of 50,000 to 200 MTB/DR3-specific CD4<sup>+</sup> T cells. However, the resulting fractions of IFN- $\gamma$ <sup>+</sup> T-Plex bead populations were somewhat lower as seen in similar experiments using the HCMV/A2-specific CD8<sup>+</sup> T cell line #416 (**Fig. 4.11**). Notably, the T-Plex Assays shown in **Fig. 4.25** were already performed at a higher rolling speed but without a centrifugation step prior to rolling.

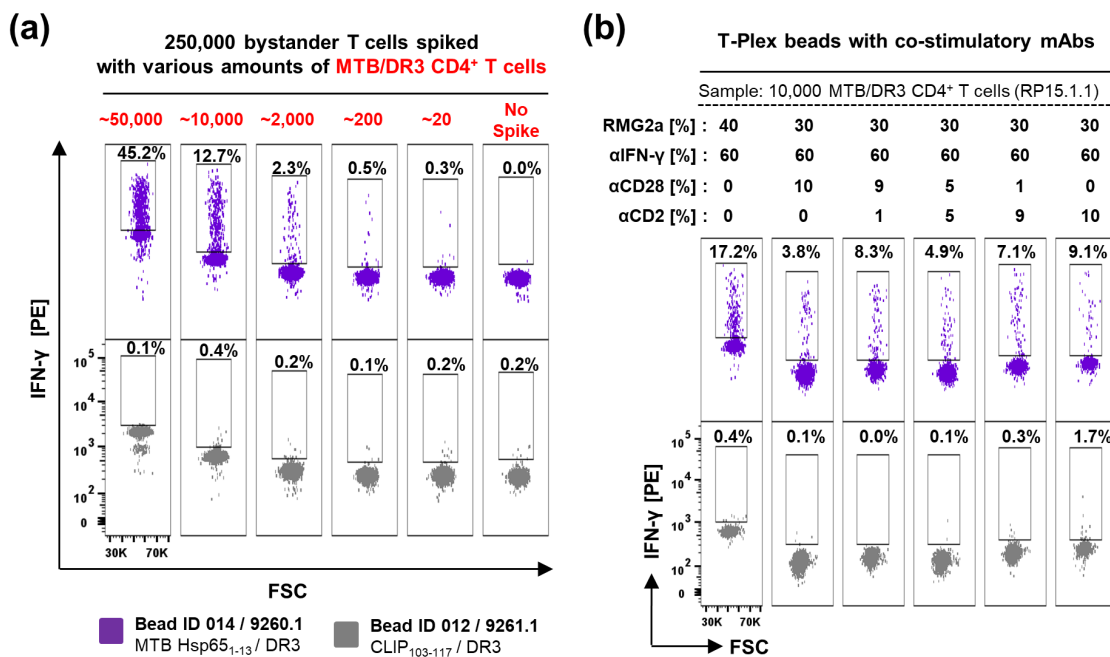


**Figure 4.25 | Antigen-specific detection of the MTB/DR3 CD4<sup>+</sup> T cell line by cognate 2<sup>nd</sup> generation T-Plex beads.**

**(a) Detection of the MTB/DR3 CD4<sup>+</sup> T cell clone RP15.1.1 by a T-Plex Assay.** 2<sup>nd</sup> generation T-Plex beads (60%  $\alpha$ -IFN- $\gamma$  [MD-1] / rat  $\alpha$ -mIgG2a 40% [RMG2a-62]) were loaded with MTB Hsp65<sub>1-13</sub>/HLA-DR3-pCC-Fc [9260.3] (*purple / cognate*) or CLIP<sub>103-117</sub>/DR3-pCC-Fc [9261.3] (*grey / control*). pMHC-II-pCC-Fc-loaded T-Plex beads (2x multiplex / 10,000 beads per T cell epitope) were combined with indicated amounts (*red numbers*) of the MTB Hsp65<sub>1-13</sub> / HLA-DR3-specific CD4<sup>+</sup> T cell clone RP15.1.1 (MTB/DR3) in the presence of 250,000 Survivin<sub>96-104</sub>/A2-specific CD8<sup>+</sup> T cells (bystander T cells). The T-Plex Assay was performed in 500  $\mu$ L tubes, rolling at 60 rpm, 37°C for 5 h. The presence of antigen-specific T cells was indicated by the appearance of an IFN- $\gamma$ <sup>+</sup> subpopulation of cognate T-Plex beads that was above T-Plex control beads (*grey*). Pairs of upper and lower T-Plex Assay FACS plots represent data analysis from the same reaction / bead mix. .

**(b) Performance of T-Plex beads supplemented with co-stimulatory mAbs.** Here, precursor T-Plex beads were generated using covalent conjugation of the indicated ratios of rat  $\alpha$ -mIgG2a (RMG2a-62), IFN- $\gamma$  capture mAb (MD-1),  $\alpha$ -CD28 mAb (15E8) as well as  $\alpha$ -CD2 mAb (RPA-2.10). In a second step, pMHC-II-Fc were loaded to generate fully assembled T-Plex beads and which were finally co-cultured with 10,000 MTB/DR3 CD4<sup>+</sup> T cells as described above.

Moreover, T-Plex beads additionally supplemented with co-stimulatory mAbs rather decreased the detection performance of the MTB/DR3-specific CD4<sup>+</sup> T cells line (**Fig. 4.25b**) than improving it, which was in accordance with previous T-Plex Assay optimization attempts presented in **Fig. 4.15b**. Conclusively, the T-Plex Assay concept-based on 2<sup>nd</sup> generation T-Plex beads can also be applied for the antigen-specific detection of IFN- $\gamma$ -secreting Th1-differentiated CD4<sup>+</sup> T cells.

#### 4.6.2 T-Plex<sup>2</sup> Assay concept – Simultaneous functional profiling of multiple antigen-specific CD4<sup>+</sup> and CD8<sup>+</sup> T cell responses

Unlike the majority of human cytotoxic CD8<sup>+</sup> T cells and Th1-differentiated CD4<sup>+</sup> T cells, other CD4<sup>+</sup> T cell subsets predominantly lack IFN- $\gamma$ -secretion (81) and may be not detected by an IFN- $\gamma$ -capture-based T-Plex Assay. To overcome this problem, we envisioned to detect up to four different prototypic cytokines on the same T-Plex bead reflecting the CD4<sup>+</sup> T cell differentiation profile (**Fig. 4.26a**). A prototypic cytokine for Th2 differentiation is IL-4, whereas Th17 differentiation leads to IL-17 and regulatory T (Treg)-differentiation rather to IL-10 secretion (81). Thus, pMHC-II-Fc-associated T-Plex beads could be theoretically equipped with four different cytokine capture antibodies reflecting the CD4<sup>+</sup> T cell differentiation. In addition, a panel of cytokine detection antibodies conjugated with four different fluorochromes could be used, that are excited by the 488 nm or 405 nm laser of the BD FACS Canto II and are hardly interfering with the channels (APC and APC/Cy7) needed for the read-out of the Luminex bead-classifier colors. The latter would allow to distinguish between the capture of each individual prototypical cytokine.

By taking advantage of the aforementioned concept, one would achieve a multiplex in two dimensions thus referred to as T-Plex<sup>2</sup> Assay. The first dimension of the multiplex assay is encoded by the bead-classifier color and the linked pMHC reflecting the T cell antigen-specificity. The second dimension relies on the conjugated dye of the cytokine detection antibody revealing the activation-dependent secreted cytokine capture and thus reflecting the function of the detected T cell (**Fig. 4.26b**). Alternatively, the sensitivity of the T-Plex Assay might be enhanced using detection of two or more effector molecules secreted by antigen-specific activated CD4<sup>+</sup> or CD8<sup>+</sup> T cells and the subsequent usage of detection antibodies conjugated to the same dye like PE to achieve an overall signal enhancement. Moreover, a panel of cytokine capture and respective detection antibodies conjugated to a T-Plex bead may be used to profile the functional state of antigen-specific CD8<sup>+</sup> T cells. Polyfunctional CD8<sup>+</sup> T cells are mainly characterized by the expression of IFN- $\gamma$ , TNF- $\alpha$  and granzymes B, whereas dysfunctional T cells including subpopulations of tumor-infiltrating CD8<sup>+</sup> T cells might lack this capacity and rather express and secrete IL-10 (329). Taken together, the T-Plex<sup>2</sup> concept would allow the tailored and simultaneous read-out of multiple antigen-specific CD4<sup>+</sup> and CD8<sup>+</sup> T cell responses and would elucidate their associated differentiation and functional status in a single assay.

## 4 | Results Part 2 – Development of the T-Plex Assay

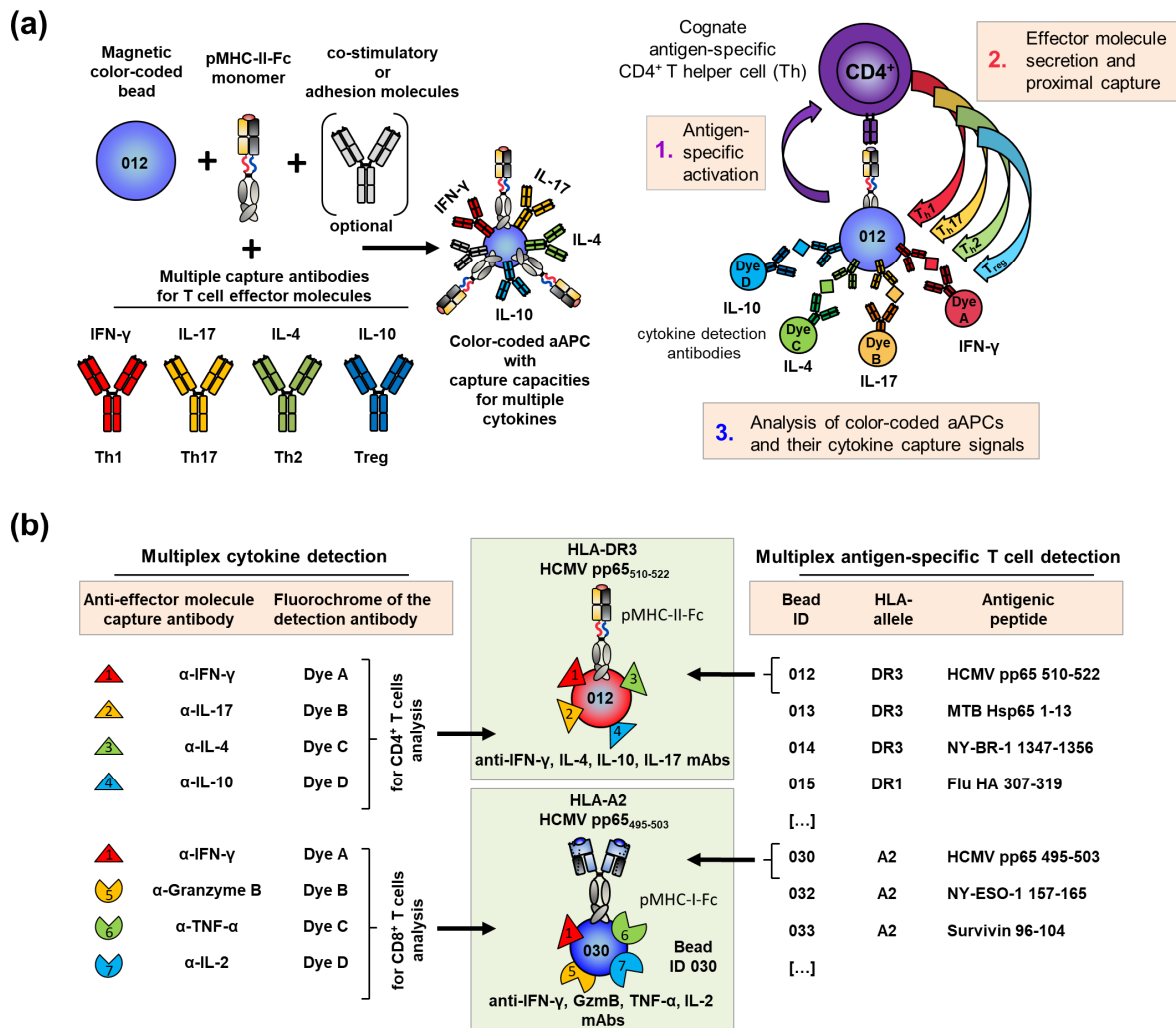


**Figure 4.26 | T-Plex<sup>2</sup> Assay principle – Multiplex-based antigen-specific CD4<sup>+</sup> and CD8<sup>+</sup> T cell detection with parallel functional profiling**

**(a) T-Plex<sup>2</sup> bead core concept and assay principle CD4<sup>+</sup> T cells.** (Left panel) For multiplex-based antigen-specific and functional phenotype profiling of CD4<sup>+</sup> T cell populations, T-Plex<sup>2</sup> beads are assembled by coupling a defined pMHC-II-Fc and other optional co-stimulatory molecules together with multiple prototypic effector cytokine-capture antibodies to color-coded beads (T-Plex<sup>2</sup> beads). (Right panel) As aAPC acting T-Plex<sup>2</sup> beads activate cognate CD4<sup>+</sup> T cells in an antigen-specific manner, which drives secretion of cytokines depending on the functional phenotype and of the activated T cell. A prototypic cytokine for a Th1 CD4<sup>+</sup> T cells is IFN- $\gamma$ , whereas Th2 differentiation rather leads to secretion of IL-4, Th17 differentiation to IL-17 and regulatory T (Treg) differentiation to IL-10. The secreted cytokines are captured proximally on the same bead and can be detected by a detection antibody panel labeled with different fluorochromes (dye A–D) depending on the cytokine.

**(b) Flexible assembly concept of the T-Plex<sup>2</sup> Assay.** Conjugation of different cytokine-capture mAbs combined with cytokine detection mAbs conjugated to different bright fluorochromes allows multiplex detection in two dimensions. The first dimension of the multiplex assay is encoded by the internal color (bead-dye / bead ID) of the pMHC-conjugated Luminex bead and reflects the T cell antigen specificity. The second dimension relies on detecting multiple cytokines on the same T-Plex bead during cognate T cell encounter, which provides information about the differentiation and functional profile of the antigen-specific CD4<sup>+</sup> T cell as well as CD8<sup>+</sup> T cell pools within a single assay reaction. aAPC: artificial antigen-presenting cells

### 4.6.3 Proof-of-principle of a T-Plex<sup>2</sup> Assay for the antigen-specific detection of CD4<sup>+</sup> T cells

In order to demonstrate the T-Plex<sup>2</sup> Assay principle, we took advantage of the MTB Hsp65<sub>1-13</sub>/HLA-DR3-specific CD4<sup>+</sup> T cell clone RP15.1.1. Upon cognate stimulation for 5 h with MTB Hsp65<sub>1-13</sub>/DR3-Fc-loaded beads, the majority (98%) of MTB/DR3-specific CD4<sup>+</sup> T cells expressed TNF- $\alpha$ , whereas only a sub-population also expressed IFN- $\gamma$  (48%) and a minority expressed IL-4 (21%) and IL-2 (5%) (**Fig. 4.27a**).

Consequently, we were interested if the same cytokine-secretion profile could be reflected also by corresponding T-Plex beads. Thus, we replaced the IFN- $\gamma$  capturing mAb of our “standard” 2<sup>nd</sup> generation T-Plex beads by capture antibodies for TNF- $\alpha$ , IL-2 and IL-4 and performed separated T-Plex analysis-based on the individual cytokines using the MTB/DR3-specific CD4<sup>+</sup> T cell clone as test sample (**Fig. 4.27b**). In accordance with the previously mentioned intracellular cytokine data, roughly twice as much cognate TNF- $\alpha$ -capture mAb-based T-Plex beads (64%) were cytokine-loaded compared to T-Plex-beads on the basis of the IFN- $\gamma$ -mAb (33%) and only 20% of the IL-4-capture-based T-Plex beads and ~3% of the IL-2-capture-based T-Plex beads (**Fig. 4.27b**). We concluded that, the sum of individual T-Plex reactions using different cytokine captures reflected the overall cytokine secretion phenotype of the MTB Hsp65<sub>1-13</sub>/DR3-specific CD4<sup>+</sup> T cell clone.

In the next and final step of this study, we aimed at detecting at least three different cytokines on the same T-Plex bead, thus allowing multiplex detection in two dimensions (T-Plex<sup>2</sup> principle). As introduced previously, the first dimension of the T-Plex<sup>2</sup> multiplex assay is encoded by the bead-classifier color (bead ID) and reflects the T cell antigen-specificity, whereas the second dimension relies on the conjugated dye of the cytokine detection antibody indicating the activation-dependent secreted cytokine and thus the function of the detected T cell (**Fig. 4.27c**). During the preparation of the T-Plex<sup>2</sup> beads, we considered that the amount of pMHC complexes on the T-Plex bead should stay constant at roughly 2/5 (40%) of total protein binding capacity of the Luminex bead, whereas the remaining 3/5 (60%) of the surface should be conjugated to the various cytokine capture antibodies including TNF- $\alpha$ , IFN- $\gamma$  and IL-4. Upon co-culture with the MTB/DR3-specific CD4<sup>+</sup> T cell clone, cognate T-Plex<sup>2</sup> were partially loaded with a combination of these cytokines, which could be simultaneously detected in a single multi-dimensional multiplex reaction (**Fig. 4.27c**). Thus, T-Plex<sup>2</sup> beads had the capacity to provide a functional profile of the MTB/DR3-specific CD4<sup>+</sup> T cell clone similar to the ICS data, which represents a good initial proof-of-principle for the T-Plex<sup>2</sup> concept.

However, gaining the capacity to detect multiple cytokines might on the one hand reduce the overall sensitivity of detecting T cells on the other hand. When 20,000 MTB/DR3 CD4<sup>+</sup> T cells were used as test sample, the fraction of overall cytokine positive T-Plex beads reflecting the sensitivity of the T-Plex Assay was highest, if they were conjugated only to a TNF- $\alpha$ -capture mAb (63.7% TNF- $\alpha$  cognate T-Plex beads (**Fig. 4.27b**). This result however dropped to 25–30% cytokine-loaded beads, when next to the TNF- $\alpha$ -mAb two different antibodies against cytokines IL-4 and IFN- $\gamma$  mAbs were conjugated to the same bead (**Fig. 4.27c**). T-Plex<sup>2</sup> beads however, that were equipped to detect TNF- $\alpha$  plus another cytokine (TNF $\alpha$  (+) IFN- $\gamma$  or TNF $\alpha$  (+) IL-4) were overall loaded up to 53% with cytokines and thus performed almost equal to T-Plex beads only conjugated to the TNF- $\alpha$ -capture mAb alone (**Supplementary Fig. S12**). In conclusion the combined conjugation of two prototypic cytokine capture mAbs to the T-Plex beads would be the best option at the moment that would at least allow to distinguish Th1 (TNF- $\alpha$ ) or Th2 (IL-4) differentiated CD4<sup>+</sup> T cells while the assay sensitivity is not reduced of at the same time. Future optimization of the used cytokine capture and detection mAbs and increasing the proportion of pMHC on the bead might resolve this issue to some extent in the future.

#### 4 | Results Part 2 – Development of the T-Plex Assay

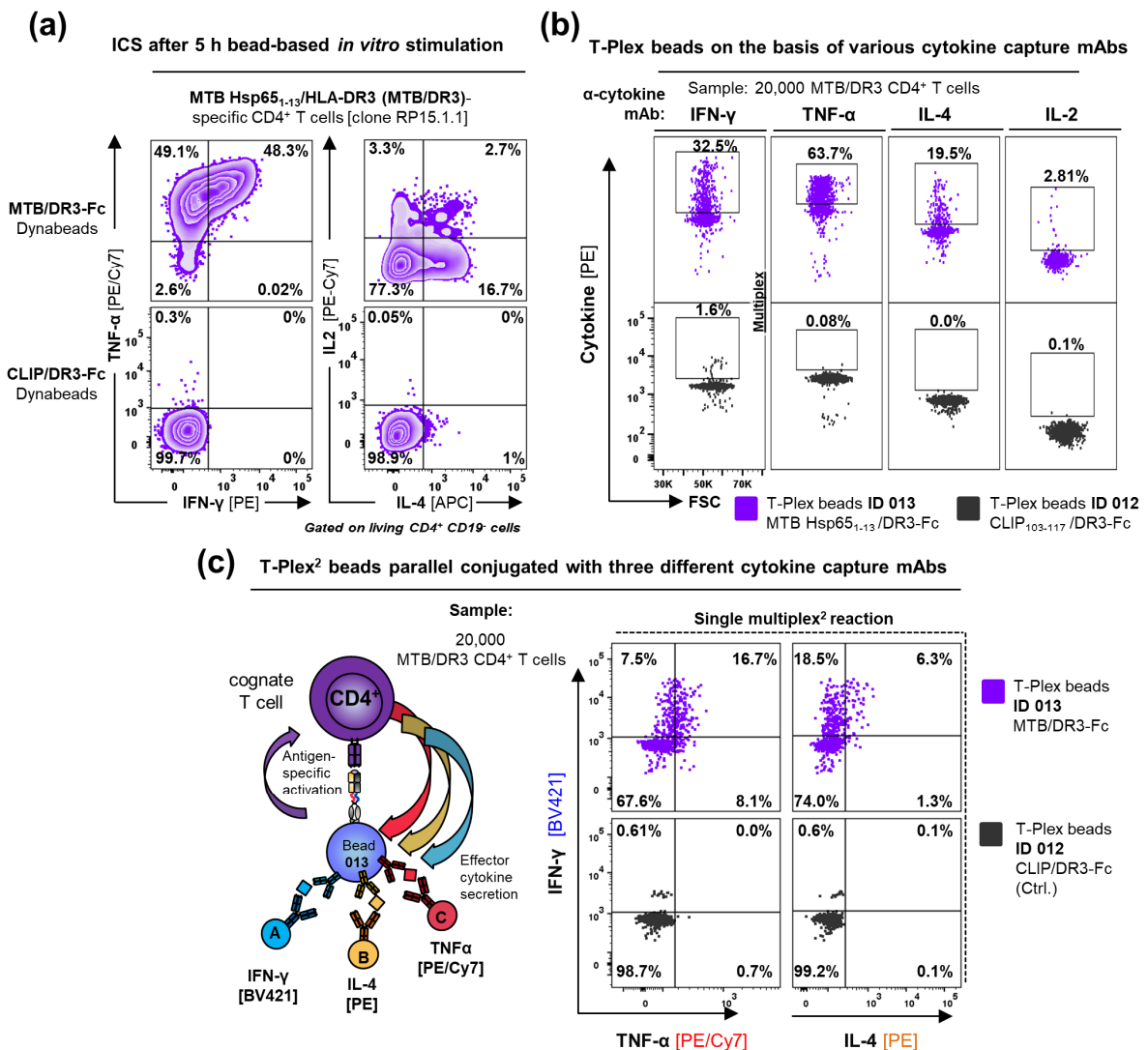


**Figure 4.27 | Proof-of-principle of a T-Plex<sup>2</sup> Assay for the antigen-specific detection of CD4<sup>+</sup> T cells**

**(a) Intracellular cytokine staining (ICS) after 5 h aAPC-based restimulation of the MTB/DR3 CD4<sup>+</sup> T cell line:** Cognate MTB Hsp65<sub>1-13</sub>/HLA-DR3-pCC-Fc (MTB/DR3-Fc) [9260.3] or control CLIP<sub>103-117</sub>/HLA-DR3-pCC-Fc (CLIP/DR3-Fc) [9261.3] coated goat-α-mouse-IgG Dynabeads were co-cultured with equal amounts of MTB Hsp65<sub>1-13</sub>/DR3-specific CD4<sup>+</sup> T cell clone RP15.1.1 (MTB/DR3 T cells) for 5 h at 37°C in a 96-well U-bottom in the presence of brefeldin A and monensin to block cytokine secretion. The frequency of cytokine expressing cells within the CD4<sup>+</sup> T cell population is shown.

**(b) Detection of different cytokines by the T-Plex beads platform:** T-Plex beads were assembled using covalently conjugated α-IFN-γ capture mAb (clone MD-1) and monoclonal α-mIgG2a (RMG2a-62) at a 60% to 40% ratio. Alternatively, the α-IFN-γ mAb was replaced by cytokine capture mAbs binding to IL-2 (MQ1-17H12), IL-4 (8D4-8) or TNF-α (Mab 1). Subsequently, pMHC-II-loaded T-Plex bead pools on the basis of different cytokine mAb were loaded with MTB/DR3-Fc [9260.3] (*purple / cognate*) or CLIP/DR3-Fc [9261.3] (*grey / control*) and were co-cultured with MTB/DR3 T cells. The T-Plex Assay was performed in 500 μL tubes, rolling at 60 rpm, 37°C for 5 h using 10,000 beads per T cell antigen. After the T-Plex reaction, the T-Plex beads were stained with the corresponding cytokine detection mAbs (all in PE) and finally analyzed by FACS. Pairs of upper and lower plots represent data analysis from the same reaction.

**(c) T-Plex<sup>2</sup> Assay proof-of-principle:** T-Plex<sup>2</sup> beads were assembled using covalently conjugated IFN-γ, TNF-α and IL-4 capture mAbs (each 20% of the total Luminex Bead protein binding capacity) and monoclonal α-mIgG2a (2/5 [40%]). pMHC-II-loaded T-Plex<sup>2</sup> beads were incubated with the MTB/DR3 T cells and T-Plex Assay was performed as described above. Next, T-Plex<sup>2</sup> beads were stained with the corresponding cytokine detection mAbs conjugated to different fluorochromes as described in the figure and analyzed by FACS. All four T-Plex Assay FACS plots shown are from the same single T-Plex<sup>2</sup> reaction / bead mix.

## 5 | Discussion

### 5.1 On the route to efficient and high-throughput production strategies of correctly folded pMHC-I-Fc and pMHC-II-Fc molecules

#### 5.1.1 Emergence of novel productions strategies for recombinant soluble pMHC-I molecules

##### 5.1.1.1 The cumbersome conventional pMHC-I production strategy

The first direct flow-cytometric visualization of antigen-specific T cell populations by recombinant soluble pMHC-I multimers has clearly revolutionized ever since many areas of immunological research (203). Yet, conventional pMHC-I multimer production represents until today a cumbersome task, which partially spoils further scientific, diagnostic or therapeutic endeavors. As introduced in **Section 1.5.2.1**, conventional pMHC-I multimer production is a labour intensive multistep process which typically starts upon expression of MHC-I heavy chain ectodomain (HC) and human  $\beta_2$ -microglobulin ( $\beta_2m$ ) in *E. coli* followed by the isolation of respective denatured proteins from inclusion bodies. Partially renatured MHC-I HC,  $\beta_2m$  and a chemically synthesized peptide-ligand are subsequently assembled to a pMHC-I complex following a time-consuming, laborious and error-prone *in vitro* folding step, which may preclude certain HLA-alleles as well as low affinity peptides that fail to form a stable pMHC-I complex *in vitro*. After an initial size exclusion chromatography (SEX), folded pMHC-I are subsequently enzymatically biotinylated using recombinant BirA ligase followed by an final ion-exchange chromatography (IEX) purification step. This conventional production strategy typically results in an overall moderate production efficiency of up to 5  $\mu$ g final pMHC-I per mL of original bacterial culture volume (209) (For an overview of different pMHC-I production strategies see **Table 5.1**). In this regard, Leisner *et al.* demonstrated that selective purification of solely pre-oxidized MHC-I HC isomers by hydrophobic interaction chromatography (HIC) combined with *in vivo* biotinylation of the MHC-I HC by *birA* co-transformation resulted in an improved *in vitro* refolding efficiency as well as roughly ten times higher overall production yields (292, 330).

##### 5.1.1.2 Efficient SCT-Fc molecules production using mammalian TGE systems

An elegant solution of this issue of error-prone *in vitro* refolding of in particular unfavourable low-affinity peptide ligands and MHC-I HC combinations, that might still be biologically relevant, represents engineering and expression of a soluble single-chain trimer (SCT) that ensures full assembly of a peptide ligand, human  $\beta_2$ -microglobulin ( $\beta_2m$ ) and the MHC-I heavy chain (HC) through covalently associated flexible linkers (240). Moreover, it has been previously shown that expression of SCTs lacking the transmembrane and cytoplasmic regions in mammalian cells allows for efficient purification of soluble and already correctly folded SCTs (239, 331). Yet these earlier production strategies relied on the generation of stably transfected mammalian SCT producer cell lines, which combined with the individual cloning procedure for each SCT sums up to an increased rather than reduced workload compared to the conventional pMHC-I production strategy. To this end, we demonstrated in this study a variety of novel strategies for a fast, less labor-intensive and high-throughput-compatible manufacturing of fully-folded, soluble recombinant pMHC-I molecules using mammalian cell transient-gene expression (TGE) systems. As an initial strategy, we took advantage of the disulfide-trapped variant SCT (dt-SCT) design (**Section 1.6**) (223, 245) that was fused to a mIgG2a-Fc (Hinge-CH2-CH3) (dt-SCT-Fc) followed by C-terminal Strep-tag II (STag) (**Section 3.1**). Moreover, we implemented the CHO-S cell transient gene expression system including the usage of ProCHO-4 medium and PEI transfection reagent (266–269) combined with StrepTactin-Sepharose-filled column-based affinity

chromatography (270) for the expression and purification of dt-SCT-Fc constructs. Using this manufacturing process, we were able to successfully produce over 15 soluble dt-SCT-Fc bearing the ectodomain of HLA-A\*02:01 (pHLA-A2-Fc) presenting various published peptide ligands (**Section 3.1 / Table 3.1**). These constructs were manufactured in as little as 7 days and with as little as three hands-on working steps including (1) transfection, (2) affinity chromatography and (3) final dialysis for any tested dt-SCT-Fc construct. The average production efficiency including purification was 11  $\mu\text{g}$  (yield dt-SCT-Fc) / mL (CHO-S TGE volume) across all tested pHLA-A2-Fc constructs with a range of 3–25  $\mu\text{g}/\text{mL}$  (**Table 3.1**). Moreover, the correct folding as well as specificity of four defined pHLA-A2-Fc molecules either presenting the HCMV pp65<sub>495–503</sub>, Flu MP<sub>58–66</sub>, EBV BMLF<sub>259–267</sub> or Survivin<sub>96–104</sub> peptide was confirmed beyond doubt by their capacity to bind to as well as to stimulate cognate CD8<sup>+</sup> T cell lines, when used as staining tools or upon their immobilization on beads, respectively.

**Table 5.1 | Comparison of methods for recombinant soluble pMHC-I molecule production**

Molecular Structure	Peptide linkage	Expression system		<i>In vivo</i> biotinylation	Required <i>In vitro</i> protein refolding	Purification methods	Manufacturing time (days) <sup>(a)</sup>	Production efficiency ( $\mu\text{g}/\text{mL}$ ) <sup>(b)</sup>	Ref.:
<b>In-house established mammalian cell-based pMHC-I production platforms</b>									
dt-SCT-mIgG2-Fc	covalent	CHO-S	transient	No	No	AC (1)	7	3–25	-
dt-SCT-*mIgG2-Fc (* cleavage site)	covalent	293-F	transient	Yes	No	AC (2)	8	10–35	-
	covalent	Expi293-F	transient	Yes	No	AC (2)	8	16–83	-
dt-SCT	covalent	293-F	transient	Yes	No	AC (2)	7	11–23	-
<b>Published mammalian cell-based pMHC-I production platforms</b>									
SCT-mIgG1 (full length)	covalent	J558L	stable	No	No	AC (3)	20–25	0.5	(239)
Peptide + $\beta_2\text{m}$ + MHC-I HC-mIgG1	Non-covalent	J558L	stable	No	No	AC (3)	20–25	1–20	(215)
SCT	covalent	CHO-S	stable	No	No	AC (4)	20	100	(332)
SCT	covalent	Expi293-F	transient	Yes	No	AC (5)	10	200–300	(241)
<b>Published prokaryotic cell-based pMHC-I production platforms</b>									
Peptide + MHC-I HC + $\beta_2\text{m}$	Non-covalent	<i>E. coli</i>	transient	No	Yes	SEC + IEX	10	2–5	(209)
Peptide + MHC-I HC + $\beta_2\text{m}$	Non-covalent	<i>E. coli</i>	transient	yes	Yes	HIC + SEC	7	20–30	(292, 330)
dt-SCT	covalent	<i>E. coli</i>	transient	No	Yes	SEC	N/A	N/A	(242)

(a) Indicated pMHC-I manufacturing duration comprises the average time span starting from the initial cell transfection / transformation of a given expression construct followed by all production steps necessary including transient culture of transfected / transformed cells or stable cell line generation as well as applied protein purification procedure. Not included are DNA oligo synthesis and cloning steps for SCT constructs or chemical peptide synthesis, which in both cases take roughly 2–3 weeks. (b) Production efficiency is described as the final yield of purified and correctly folded pMHC-I complexes divided by the initial transfected / transformed cell culture volume (transient gene expression) or harvested volume of a stably transfected cell line cultured for 4–7 days and subsequently used for protein purification. **AC**: Affinity chromatography based on; **(1)**: StrepTactin-coated Sepharose; **(2)**: HisMag Sepharose Excel (GE HealthCare); **(3)**: 5-iodo-4-hydroxy-3-nitrophenylacetyl-Sepharose; **(4)**: anti-murine MHC-I mAb (clone M1/42 specific for murine H-2) coated Sepharose; **(5)**: Ni-NTA Sepharose filled columns; **SEC**: Size exclusion chromatography; **IEX**: Ion exchange chromatography; **HIC**: Hydrophobic interaction chromatography. N/A: Information not available.

A construct design similar to ours, however, a different manufacturing strategy was described previously by Greten *et al.* in the early 2000s, which also omits the need for *in vitro* protein refolding by taking advantage of a mammalian cell line for recombinant soluble pMHC-I production. Here, the authors fused a defined complete pHLA-A2 (lacking the transmembrane domain) according to the SCT design principle (peptide-linker- $\beta_2\text{m}$ -linker-MHC-I HC) to the variable domain of a mIgG1 full-length heavy chain specific for the hapten 4-hydroxy-3-nitrophenyl acetyl (NP) facilitating an affinity

chromatography based on NP-linked Sepharose. The resulting SCT-mIgG1 construct was subsequently electroporated into the murine plasma cell line J558L, which expresses a murine  $\lambda$  Ig light chain but lacks endogenous Ig heavy chain expression. However, in that production approach Greten *et al.* relied on the subsequent generation of stable transfected J558L cell lines using Geneticin (G418)-based selection of SCT-mIgG1 producing cell clones, which was typically achieved within two weeks. Nevertheless, Greten *et al.* reported a rather low production efficiency of only 0.5  $\mu\text{g}/\text{mL}$  based on supernatants harvested after 3–4 days of culturing stable SCT-mIgG1 producing J558L clones (239). In an alternative approach, the same group fused solely the MHC-I HC ectodomain to the variable HC domain of the  $\alpha$ -NP mAb of mIgG1 isotype (MHC-I-mIgG1). Upon co-transfection of J558L cells with MHC-I-mIgG1 as well as human  $\beta_2\text{m}$  expression vectors, the  $\beta_2\text{m}$ -associated MHC-I-mIgG1 molecules were subsequently purified as described above, resulting in an overall higher production yield of 1–20  $\mu\text{g}/\text{mL}$  culture volume. In a final step, these purified  $\beta_2\text{m}$ -associated MHC-I-mIgG1 molecules were passively loaded with a desired chemically synthesized peptide prior to their experimental usage as peptide-loaded  $\beta_2\text{m}$ -associated MHC-I-mIgG1 dimers (pMHC-I-mIgG1) (213, 215, 216).

Quite recently in 2019, Wooster *et al.* in addition demonstrated the production of a monomeric SCT encoding for murine H-2K<sup>b</sup> presenting the ovalbumin<sub>257–264</sub>-derived peptide SIINFEKL (OVA<sub>257–264</sub>/K<sup>b</sup>) using a sleeping beauty transposon system for the generation of stably secreting CHO-S cell lines. Through transposon-directed delivery combined with puromycin-based selection, the authors achieved the generation of CHO-S cell lines that stably secreted the OVA<sub>257–264</sub>/K<sup>b</sup> within two weeks, which in the following allowed production yields of up to 100  $\mu\text{g}/\text{mL}$  from a 4-day culture. This approach is appealing for the continuous production of recombinant pMHC-I molecules representing very well-known and frequently asked T cell epitopes. Yet, generation of stable transfected cell lines either based on the J558L cell line / electroporation- or CHO-S / transposon-gene delivery system requires multiple hands-on working steps per expression construct, which makes manufacturing of larger panels of different soluble pMHC-I molecules, presenting for instance various cancer patient-derived potential neoepitope candidate peptides, rather laborious as compared to the usage of efficient mammalian TGE systems.

### 5.1.1.3 Further optimization of our dt-SCT-Fc construct design and production strategy

Our produced dt-SCT-Fc molecules have been proven particularly useful throughout the study to drive cognate antigen-specific T cell stimulation based on dt-SCT-Fc coated beads that mimic APC function. However, when used as staining tools these dimeric dt-SCT-Fc molecules displayed an inferior performance for the detection of antigen-specific T cells compared to commercially available pMHC-I multimers, which was in accordance with previous reports comparing peptide-loaded MHC-I-mIgG1 dimers with streptavidin-based pMHC-I multimers (217). Therefore, we revised the dt-SCT-Fc construct design by introducing a modified linker sequence between the C-terminus of the dt-SCT ectodomain domain and the N-terminus of the fused mIgG2a-Fc. This modified linker contained in N- to C-terminal order, an octa-histidine-tag (His<sub>8</sub>-tag), an AviTag for site-specific biotinylation and two consecutive thrombin recognition sites (\*) allowing for optional proteolytic cleavage of the Fc-portion and the subsequent His<sub>8</sub>-tag-based purification of monomeric dt-SCT (**Section 3.4**). This unique dt-SCT-\*Fc design offered the possibility to be incorporated in multiple assay platforms as well as applications depending on the chosen production and purification process. We will hold on to the SCT-Fc fusion concept to reserve the possibility to immobilize dt-SCT-\*Fc on 2<sup>nd</sup> generation T-Plex beads (Luminex beads coated with anti-mIgG2a-Fc mAb and anti-IFN- $\gamma$  mAb) by directly using crude mammalian supernatants derived from very small scale 96-well-based protein productions (~ 800  $\mu\text{L}$ ) without the need of any further protein purification or dialysis steps. Of note, this combined dt-SCT-Fc-production

/ T-Plex Assay concept is potentially very attractive for the screening of very large lists of potential neoepitope candidates derived from patients with a very high mutational burden. Moreover, we reasoned that the Fc-domain confers greater stability to the linked dt-SCT and thus might enhance the overall expression in mammalian production systems, which has been frequently reported for other Fc-fusion proteins (333). As an alternative application, biotinylated monomeric dt-SCT have been successfully used in this study to generate pMHC-I multimers after complexation with streptavidin that displayed quite similar staining performances compared to commercially available pMHC-I pentamers (**Section 3.4**). Moreover, biotinylated monomeric dt-SCT were also applied for a T-Plex Assay using streptavidin / anti-IFN- $\gamma$  mAb-based T-Plex beads (**Section 4.5 & Supplementary Fig. 11**) as well as to drive antigen-specific T cell proliferation upon immobilization of biotinylated monomeric dt-SCT on anti-biotin MACSiBeads (Miltenyi) combined with co-stimulatory mAbs (**Section 3.5**).

For convenient production of biotinylated dt-SCT-\*Fc constructs, we co-transfected a given dt-SCT-\*Fc plasmid together with a plasmid encoding for the *birA* gene bearing an additional C-terminal ER retention signal sequence (leader-BirA<sub>KDEL</sub>) to achieve efficient biotinylation during dt-SCT-\*Fc translation and secretion, which is often referred to as *in vivo* biotinylation (262). For small-scale purification of up to 200  $\mu$ g of highly pure biotinylated monomeric dt-SCT after proteolytic cleavage of the Fc, we further routinely took advantage of magnetic “His Mag Sepharose Excel” (GE HealthCare) allowing for efficient His-tag-based protein affinity chromatography from eukaryotic cell supernatants without the need of prior buffer exchange. Using a 96-well magnet, we were able to purify over 30 expressed and proteolytic digested dt-SCT in parallel within less than 2 hours hands on time, which may be optionally further automatized using a KingFisher<sup>TM</sup> magnetic particle purification system (Thermo Scientific) for instance. In light of this study, we further compared several mammalian TGE systems on the basis of CHO-S cells, ExpiCHO-S, 293-F and Expi293-F cell lines (**Section 3.4.2**) to identify the most efficient system to produce *in vivo* biotinylated dt-SCT-\*Fc. In particular, the used 293-F and Expi293-F TGE systems consistently resulted in very high (>95%) biotinylation efficiencies, whereas usage of the CHO-S as well as ExpiCHO-S TGE systems resulted in an often incomplete dt-SCT-\*Fc biotinylation across various productions. Yet, we have not systematically investigated if, for instance, a higher concentrated biotin supplementation of the respective CHO-S and ExpiCHO-S cell culture medium beyond 4  $\mu$ g/mL biotin might increase the *in vivo* biotinylation efficiency. Production efficiencies across four tested dt-SCT-\*Fc construct comprising pHLA-A2-\*Fc molecules either presenting the HCMV pp65<sub>495–503</sub>, Flu MP<sub>58–66</sub>, EBV BMLF<sub>259–267</sub> or Survivin<sub>96–104</sub> peptide was on average 25  $\mu$ g/mL for the 293-F and 44  $\mu$ g/mL for the Expi293-F TGE system, respectively.

A soluble SCT manufacturing strategy very similar to ours comprising the production of *in vivo* biotinylated SCT in Expi293-F cells, was reported in parallel to this study by Lyu *et al.* in 2019. Here, the authors cloned a soluble SCT monomer (lacking a disulfide tap) of EBV BLRF-1<sub>198–206</sub> [TYPVLEEMF] / HLA-A\*24:02 as well as EBV EBNA3A<sub>246–254</sub> [RYSIFFDYM] / HLA-A\*24:02 that bear a C-terminal AviTag followed by a deca-histidine-tag. To produce *in vivo* biotinylated soluble SCTs, Expi293F cells were co-transfected with the respective SCTs and BirA following a 7-day transient-gene expression. In the following harvested supernatants were subjected to intensive dialysis prior to standard Ni-NTA-Sepharose-filled column affinity chromatography. For these two SCTs the authors reported production efficiencies of 200–300  $\mu$ g/mL (241), which was slightly higher but still in a similar range as our produced HCMV pp65<sub>495–503</sub> [NLVPMVATV] / HLA-A\*02:01 and Survivin<sub>96–104</sub> [LMLGEFLKL] / HLA-A\*02:01 dt-SCT-\*Fc constructs using the Expi293-F system with production efficiencies of 56 and 83  $\mu$ g/mL, respectively (**Supplementary Table S1**). In this regard, Chang *et al.* reported 10-times higher production yields after *in vitro* refolding of HLA-A\*24:02 HC with  $\beta_2m$  and an optimal peptide ligand

(i.e. 45 µg/mL) compared to HLA-A\*02:01 (i.e. 4.4 µg/mL) (334). Thus, our lower production yields might be explained by the slightly different biochemical properties including overall stability of those two different HLA alleles.

#### **5.1.1.4 Advantages and disadvantages of SCTs compared to peptide exchange strategies for high-throughput production of soluble pMHC-I molecules**

Based on the conventional recombinant pMHC-I procedure (**Section 1.5.2.1**), several other techniques have been developed to allow for the production of a stable peptide-receptive MHC-I that can be loaded within hours, and without further purification steps with a peptide of choice, and thus circumvent the need to undertake *in vitro* refolding as well as purification steps for every individual peptide / MHC-I combination. These conditional peptide exchange technologies include pMHC-I complexes that are loaded with a photo-sensitive peptide that is cleaved upon UV-light exposure (217, 335, 336) or that are loaded with a placeholder peptide that solely stabilizes the pMHC-I complex at 4°C but dissociates at elevated temperatures (227), leaving the remaining destabilized MHC-I HC highly receptive for peptide exchange. More recently, Saini *et al.* reported successful production of peptide-receptive MHC-I molecules based on a disulfide-stabilized variant of HLA-A\*02:01, HLA-A\*24:02 and murine H-2K<sup>b</sup> HC bearing two artificial cysteine residues at position 84 and 139, leading to an improved peptide-independent stability and allowing successful *in vitro* refolding of empty MHC-I molecules assisted by dipeptides (226, 337). However, all three approaches allowing for peptide loading of choice require labor-intensive screening of a respective HLA-specific place-holder peptide or dipeptides, respectively, that support successful re-folding *in vitro*. Thus, the feasibility of these approaches has so far only been shown for a limited number MHC-I alleles, which holds particularly true for the more recently reported temperature-induced peptide ligand exchange technology that was only shown for HLA-A\*02:01 as well as murine H-2K<sup>b</sup> as well as for the generation of disulfide-stabilized empty pMHC-I. UV-sensitive conditional ligands have initially been reported for HLA-A\*02:01 (217) and were later expanded to HLA-A\*01:01, HLA-A\*03:01, A\*11:01, B\*07:02 (335), B\*08:01 (338), B\*57:03 (339), as well as 16 frequent Asian HLA-A, B and C variants including A\*24:02, B\*40:01 and C\*07:02 (334). Importantly, the UV-mediated peptide exchange bears the risk of incomplete removal of the photocleavable peptide as well as quick unfolding of the MHC-I heavy chain if peptide exchange for a low-affinity peptide is intended, which might result in an overall potential lack of functionality for the formed pMHC molecules and lower staining performances of the corresponding pMHC-I multimer reagents (217, 337). Moreover, it is worth mentioning that these MHC-I peptide-loading strategies rely on in-house or commercial production of synthetic peptides, which, in case larger libraries are needed, are frequently ordered at less than 70% purity given the costs associated with custom peptide production. However, it has been reported these larger peptide libraries may contain impurities that can affect T cell recognition leading to false-positive results (340, 341).

In contrast, the SCT manufacturing strategy permits a direct quality control of the respective expression plasmid by DNA sequencing analysis to exclude potential cloning of false peptide sequences. Moreover, in particular disulfide-trapped SCTs have been shown to be completely refractory to exogenous peptide exchange, thus also minimizing the risk of being loaded with random endogenous peptide ligands during protein synthesis (242, 244, 245). So far, successful soluble SCT production among the classical HLA-I alleles has been only reported for HLA-A\*02:01, HLA-B\*27:05, (240) and HLA-A\*24:02 (241). Within this study we also focused on HLA-A\*02:01 to reach a proof-of-concept for the implementation of novel production strategies. Currently, we also successfully achieved production of HLA-A\*68:01, HLA-B\*57:01 and HLA-C\*07:01-based on dt-SCT-\*Fc molecules (**data not shown**). Thus, the dt-SCT concept combined with a high-throughput mammalian protein

production system bears great potential in being applicable across many if not all HLA-I alleles allowing for highly personalized production of neoepitope-presenting HLA-I molecules covering ideally all six HLA-I alleles of an individual cancer patient. The latter would also increase the likelihood of identifying truly immunogenic epitopes and corresponding T cell populations (149).

Another key advantage of the dt-SCT design over other production strategies represents its very high stability and its unique capacity to incorporate also low-affinity peptide ligands. The latter is important to be able to test a broad spectrum of potential epitope peptide candidates derived from either shared tumor antigens or unique mutation-derived tumor neoantigens since also many known immunogenic epitopes display low-binding affinity (342). Within this study, we have demonstrated the successful production of dt-SCT bearing several putative neoepitope peptides as well as wild-type counter parts. Among the list of peptides (**Section 4.5 / Table 4.5**) a selected pHLA-A2\*Fc construct bearing the wildtype control peptide [HMEVFNQRL] was still successfully expressed despite the fact that this peptide had a very low predicted binding affinity of  $\sim 4413.99$  nM towards HLA-A\*02:01.

Yet, Kotsiou *et al.* reported the imported finding that mammalian cell-based production of a soluble monomeric but not transmembrane bound dt-SCT bearing a peptide ligand with a suboptimal C-terminal anchor residue was prone to apparent homodimer formation (343). Here, HLA-A\*02:01 in a soluble dt-SCT format displaying either the minor histocompatibility antigens HA-1<sub>137-145</sub> [VLHDDLLEA] or HA-2 (myosin-Ig<sub>41-49</sub>) [YIGEVLSV], respectively, were cloned following the production in retrovirally transduced HEK293T cells. Although both peptides displayed a relatively high binding affinity towards HLA-A\*02:01, which is in case of HA-1<sub>137-145</sub> [VLHDDLLEA] 28.61 nM (%rank 0.40) and for HA-2 (myosin-Ig<sub>41-49</sub>) [YIGEVLSV] 6.97 nM (%rank 0.06%) according to the NetMHC4.0 algorithm (281), respectively, only soluble HA-1<sub>137-145</sub>/HLA-A2 dt-SCT were secreted predominantly as homodimers as shown by SDS-PAGE analysis. Still these homodimers displayed a correct folding according to immunoblotting based on thh anti-HLA-A2 mAb BB7.2 and may consist of dt-SCT in a head-to-head orientation, with the peptide ligand of one molecule sitting in the binding groove of the other pMHC-I molecule and vice versa. The authors reasoned that the unfavourable alanine residue at position 9 of the VLHDDLLEA peptide, which makes only very few contacts with the HLA-A2 F pocket might be the driver for this apparent homodimer formation. In fact, subsequent mutation of position 9 to valine (VLHDDLLEV, 6.08 nM / %rank 0.05) led to a significant reduction of corresponding dt-SCT homodimer formation (343). So far, we have not yet encountered the same homodimerization phenomenon during the production of several neoepitope peptide candidates even if the C-terminal anchor residue was alanine. For instance the pHLA-A2\*-Fc constructs 11461.1 presenting the peptide HLLEGDLDKA was successfully produced and purified as monomer after proteolytic digestion with thrombin (**Section 4.5 / Fig. 4.23a**). Moreover, in case of HLA-A2 we routinely replaced less favourable C-terminal residues by valine to increase the overall production yields of well-known peptide ligands (**Section 3.1 / Table 3.1**). However, we are well aware that also subtle peptide modification might impact affect TCR recognition. A famous example is the cysteine to valine mutation at position 9 of the NY-ESO-1<sub>157-165</sub> peptide [SLLMWITQC]. It has been shown that the mutated version of the peptide [SLLMWITQV] sits slightly deeper in the HLA-A2 F pocket, which leads to a slight repositioning of the central peptide region affecting the recognition of the cloned cognate TCR 1G4. However, in this case TCR recognition was even improved by the C165V mutation leading to an enhanced killing of peptide-pulsed target cells by 1G4-transgenic T cells (344).

### 5.1.1.5 Future directions regarding pMHC-I\*-Fc construct designs

In order to generate pMHC-I multimers for subsequent T cell stainings, we took advantage of BirA-ligase mediated and site-specific biotinylation of pMHC-I [dt-SCT]\*-Fc constructs bearing the biotin acceptor peptide sequence [GLNDIFEAQKIEWHE] known as AviTag™ (258) followed by streptavidin-based multimerization, which is essentially the same pMHC multimerization strategy as originally described by Altman *et al.* in 1996 (203). Moreover, to avoid an *in vitro* biotinylation step, which goes along with the requirement of additional buffer exchange and purification steps as well as purchasing the recombinant BirA ligase enzyme, we co-transfected an endoplasmic reticulum retained version of IgkL-BirA<sub>KDEL</sub> (264) together with desired pMHC-I\*-Fc constructs to allow for direct *in vivo* biotinylation during protein synthesis within the cell. In particular, the 293-F or Expi293-F TGE systems allowed consistently very high if not complete biotinylation throughout the study of all produced pMHC-I\*-Fc upon BirA<sub>KDEL</sub> co-transfection, which was in accordance with previous studies showing very high *in vivo* biotinylation efficiencies for MHC-I HC expression in bacteria (292) and SCT expression in mammalian Expi293-F cells (241), respectively. Currently, we have been using a co-transfection of the pMHC-I\*-Fc vector together in a 1:1 ratio with an IgkL-BirA<sub>KDEL</sub> encoding vector, which typically reduces the production yields by 2-3-fold compared to a production lacking the BirA co-transfection. Thus, in the near future we aim for a one vector system linking the pMHC-I\*-Fc reading frame via a T2A-sequence to the BirA<sub>KDEL</sub> reading frame, which will most likely further improve our production yields.

An interesting alternative represents the usage of the 25-residue version of the so-called streptavidin-binding peptide tag (SBP-tag) [GHVVEGLAGELEQLRARLEHHPQG] (345) instead of a biotinylated AviTag, which has not yet been utilized to generate pMHC-I multimers. The SBP-tag binds tightly ( $K_d = 1.47$  nM) to streptavidin, yet with far lower affinity than the cognate ligand biotin ( $K_d = 50$  fM), which would allow the induced dissociation of streptavidin-bound pMHC-I-SBP-tag molecules upon addition of an excess of biotin. Other reversible pMHC multimer assembly concepts have been reported previously based on a pMHC-I-Strep-tag II / Strep-Tactin-scaffold system (*Streptamers*) (272) or pMHC-I-His<sub>6</sub>-tag / Ni<sup>2+</sup>-NTA-scaffold (NTAmers) (346). Both systems have been proven useful in particular to increase the viability of antigen-specific T cells subjected to a pMHC-I multimer-based flow cytometric or magnetic sorting procedure. After the cell sorting procedure, these reversible pMHC-I multimers can be disassembled by addition of biotin or imidazole, respectively, resulting in a quick dissociation of monomeric pMHC-I from the bound TCR reducing the risk of induction of activation-induced cell death due to long-term pMHC-I-multimer encounter. However, unlike the His-tag or Strep-tag II-based pMHC-I which require their uniquely supplied scaffolds (i.e. StrepTactin / cross-linked Ni<sup>2+</sup>-NTA), a pMHC-I-SBP-tag based molecule would allow the usage of the more broadly available fluorochrome-conjugated streptavidin.

### 5.2.1 Moderately efficient production of soluble peptide-linked MHC-II-Fc constructs using mammalian transient gene expression systems

It is a well-known issue, that the expression of recombinant soluble MHC-II molecules can be more cumbersome compared to the expression of soluble recombinant pMHC-I molecules. In particular, structural differences between pMHC-I and pMHC-II molecule might account for this. The MHC I  $\alpha$ -chain bears the complete peptide binding groove and forms a quite stable complex with  $\beta_2$ -microglobulin and a suitable peptide ligand in solution. In contrast, both the  $\alpha$  and  $\beta$  chain of the MHC-II molecules contribute to the formation of the peptide binding groove and soluble MHC-II  $\alpha$  and  $\beta$  chains lacking their corresponding transmembrane domains hardly form stable heterodimers in the presence of a peptide ligand (347). Thus, successful *in vitro* refolding of bacteria expression-derived denatured

soluble MHC class II  $\alpha$  and  $\beta$  chains has been only achieved for a very small set of murine as well as human MHC II alleles (204). Moreover, even for the *in vitro* refolding of the fairly suitable HLA-DR1 allele overall a very low production efficiency have been reported that typically requires 10 L of bacteria culture to obtain 20 – 100  $\mu\text{g}$  folded pHLA-DR1 (348) (**Table 5.2**). To this end, the usage of eukaryotic protein production systems combined with the expression of truncated MHC-II  $\alpha$ - and  $\beta$ -chain fused to immunoglobulin-Fc domains and/or molecular zippers such as coiled-coil acidic/basic “leucine zipper”, which are stabilizing pMHC-II heterodimer formation, have been the preferred manufacturing strategy (204). We have mostly been following that path in this study and demonstrated the production of soluble heterodimeric pMHC-II-parallel coiled-coil (pCC) “zipper”-Fc constructs presenting either a covalently associated immunogenic peptide ligand (**Section 3.6.1**) or a cleavable placeholder peptide (**Section 3.6.3**) allowing for subsequent exchange of a soluble peptide of interest, quite similar to the study presented by Day *et al.* (235). For pMHC-II-pCC-Fc production, we tested several mammalian transient gene production systems growing in suspension including the ExpiCHO-S, CHO-S/ProCHO-4/PEI and 293-F system (**Table 5.2 & Supplementary Table S3**). Importantly, independent of the used production systems, all produced MTB/HLA-DR3-pCC-Fc molecules, when immobilized on anti-mIgG-Fc beads, displayed the capacity to stimulate the cognate MTB/DR3-restricted T cell line, which proves an overall correct folding in particular of this MTB/HLA-DR3 molecule. The highest production yield for non-biotinylated pMHC-II-pCC-Fc molecules was achieved using the ExpiCHO-S system followed by StrepTactin-based affinity chromatography (3–6  $\mu\text{g}/\text{mL}$ ). Unfortunately, the ExpiCHO system demonstrated only poor *in vivo* biotinylation efficiencies upon co-transfection with BirA ligase and supplementation with 4  $\mu\text{g}/\text{mL}$  biotin. Therefore, the CHO-S/ProCHO-4/PEI or 293-F system was preferentially used for the expression of *in vivo* biotinylated pMHC-II-pCC-Fc molecules followed by  $\text{Ni}^{2+}$ -NTA-based affinity chromatography. However, the usage of the CHO-S/ProCHO-4/PEI and 293-F TGE system resulted only in moderate production efficiencies for *in vivo* biotinylated pMHC-II-pCC-Fc constructs, which were in the range of  $\sim 0.1$ – $0.5$   $\mu\text{g}/\text{mL}$  and  $0.3$ – $2.6$   $\mu\text{g}/\text{mL}$ , respectively. Thus, typically culture volumes of  $>200$  mL were required to obtain a substantial production yield of  $50$ – $100$   $\mu\text{g}$ . Nevertheless, the usage of these mammalian transient gene expression systems represents an overall attractive alternative for the parallel production multiple peptide-tethered MHC-II molecules compared to other production systems, especially those which require time consuming ( $> 2$ – $3$  weeks) generation of stably transfected production cell lines (**Table 5.2**).

In this regard, the generation of stably transfected *Drosophila melanogaster* Schneider S2 cells requires a particularly high workload, while still resulting in overall moderate – low production efficiencies ( $0.1$ – $0.3$   $\mu\text{g}/\text{mL}$ ). A frequently used alternative is the transient expression of soluble of pMHC-II molecules in baculovirus-transduced Sf9 cells or Hi5 cells resulting in significantly higher production yields (**Table 5.2**). However, as a downside these systems require laborious and highly variable production of corresponding baculovirus stocks, whereas the ExpiCHO-S, CHO-S/ProCHO-4/PEI as well as 293-F TGE system only require a simple plasmid preparation step. Very recently in 2019, Serra *et al.* reported another straightforward strategy for soluble pMHC-II production based on lentivirus transduction of CHO-S cells. CHO-S cells displaying high expression levels of an integrated reporter gene (i.e. EGFP) were sorted by flow cytometry and grown in shaker flasks filled with protein-free medium. The culture was fed every two days until day 10 and finally harvested on day 14, followed by various affinity purification steps resulting in typical production yields for soluble peptide-tethered MHC-II  $\alpha\beta$  chains fused to leucine zipper motifs of  $0.6$  up to  $12$   $\mu\text{g}/\text{mL}$  depending on the linked peptide. Moreover, the authors showed that soluble peptide-tethered or “empty” MHC-II  $\alpha\beta$  chains linked to heterodimeric mutated human IgG1-Fc domains that form so-called knob-into-hole (KIH) structures let to an average

4-fold yield increase (i.e. 33–45 µg/mL), when directly compared to the expression of corresponding peptide-tethered MHC-II αβ chains fused to leucine zipper heterodimerization domains. Further, it was shown that the pMHC-II-IgG1-Fc (KIH) design confers greater overall stability in *in vivo* applications using coated nanoparticles (344).

**Table 5.2 | Comparison of methods for recombinant soluble pMHC-II molecule production**

Molecular structure [Type of peptide linkage]	Allotype	Expression system		Enzymatic biotiny- lation	Required <i>In vitro</i> protein refolding	Purifi- cation methods	Manu- facturing time (days) <sup>(a)</sup>	Production efficiency (µg/mL) <sup>(b)</sup>	Ref.:
<b>In-house established mammalian cell-based pMHC-II production platforms</b>									
p-MHC-II β-chain-zipper-mFc + MHC-II α-chain-zipper-mFc [Covalent]	DRB1*03:01	ExpiCHO-S	Transient	No	No	AC (1)	14	3.5–6.0	-
		CHO-S	Transient	<i>In vivo</i>	No	AC (2)	8	0.1–0.5	-
		293-F	Transient	<i>In vivo</i>	No	AC (2)	8	0.3–2.6	-
<b>Published mammalian cell-based pMHC-II production platforms</b>									
p-MHC-II β-chain-Zipper + HLA-II α-chain-Zipper [Covalent]	DRB1*01:01 DRB1*04:01 DRB1*15:01 DRB5*01:01	CHO	Stable (Plasmid)	<i>In vitro</i>	No	AC (3)	~ 45	N/A	(235)
p-MHC-II β-chain-Zipper + HLA-II α-chain-Zipper [Covalent]	DRB1*01:01	CHO-S	Stable (Lentivirus)	<i>In vitro</i>	No	AC (1) + AC (2) + IEX	~ 45	0.6–12	(349)
p-MHC-II β-chain-hlgG1-Fc (HOLE) + MHC-II α-chain-hlgG1-Fc (KNOB) [Covalent]	DRB1*04:01 DRB1*15:01 DRB4*01:01 DRB5*01:01	CHO-S	Stable (Lentivirus)	<i>In vitro</i>	No	AC (4) + IEX	~ 45	33–45	(349)
MHC-II β-chain-hlgG1-Fc (HOLE) + MHC-II α-chain-hlgG1-Fc (KNOB) + peptide [Non-covalent]	DQA1*05:01/ DQB1*02:01	CHO-S	Stable (Lentivirus)	<i>In vivo</i>	No	AC (4) + AC (5)	~ 45	10–30	(349)
<b>Published insect cell-based pMHC-II production platforms</b>									
MHC-II β-chain + MHC-II α-chain + peptide [Non-covalent]	DRB1*01:01	S2 Schneider	Stable (Plasmid)	<i>In vitro</i>	No	AC (3) + SEC	~ 45	0.1–0.3	(348)
p-HLA-II β-chain-Zipper + HLA-II α-chain-Zipper [Covalent]	DRB1*15:01	S2 Schneider	Stable (Plasmid)	<i>In vivo</i>	No	AC (3)	~ 45	N/A	(291)
p-MHC-II β-chain-zipper + MHC-II α-chain-zipper-mFc (bivalent molecule) [Covalent]	DRB1*15:01	S2 Schneider	Stable (Plasmid)	No	No	AC (3) + (4)	~ 45	0.2	(350)
p-HLA-II β-chain-Zipper + α-chain-Zipper [Covalent]	DRB1*15:01	Sf9	Transient (baculovirus)	<i>In vitro</i>	No	AC (3)	7	1.4–2.4	(351)
p-MHC-II β-chain-Zipper + HLA-II α-chain-Zipper (+ calreticulin) [Covalent]	DRB1*04:01	Hi5	Transient (baculovirus)	<i>In vitro</i>	No	AC (3) + + SEC	6	20–40 (50–70)	(352)
<b>Published bacteria-based pMHC-II production platforms</b>									
p-MHC-II β-chain MHC-II α-chain + peptide [Non-covalent]	DRB1*01:01	<i>E. coli</i>	transient	<i>In vitro</i>	Yes	IEX + AC (3) + SEC	~ 10	0.003–0.02	(348)
MHC-II β-chain MHC-II α-chain [Covalent]	DRB1*01:01	<i>E. coli</i>	transient	<i>In vitro</i>	Yes	IEX + AC (3) + SEC	~ 10	N/A	(353)

(a) Indicated pMHC-II manufacturing time comprises the average time span starting from the initial cell transfection / transformation of a given expression construct followed by all production steps necessary including transient culture of transfected / transformed cells or stable cell line generation as well as protein purification procedure. (b) Production efficiency is described as the final yield of purified and correctly folded pMHC-II complexes divided by the initially transfected / transformed cell culture volume (transient gene expression) or harvested volume of established producer cell lines cultured for multiple days (7–14 days) and subsequent protein purification steps. AC: Affinity chromatography based on; (1) immobilized Strep-Tactin; (2) immobilized Ni<sup>2+</sup>-NTA or similar; (3) anti-HLA-DR α-chain mAb L243 or LB3.1 mAb conjugated-Sepharose; (4) immobilized protein A/G; (5) immobilized avidin. IEX: Ion exchange chromatography. SEC: Size exclusion chromatography. N/A: not available/not reported.

Thus, taking advantage of IgG1-Fc (KIH) domains is quite attractive for the pMHC-II fusion construct design in particular when combined with mammalian expression systems. In this regard, we are also currently designing and evaluating novel pMHC-II constructs based on a peptide-tethered  $\beta$ -chain fused to an immunoglobulin CH1-domain followed by a flexible linker sequence bearing AviTag, His<sub>8</sub>-tag as well as a thrombin recognition site and a C-terminal Fc domain (Hinge-CH2-CH3). This Fc-linked pMHC-II  $\beta$ -chain is then combined with the corresponding MHC-II  $\alpha$ -chain fused to the immunoglobulin kappa light chain (CL). We speculate that a direct fusion of the MHC-II  $\alpha\beta$  to the covalently associated CL/CH1 domain might confer additional stability to heterodimeric pMHC-II complex and thus might further increase our production efficiencies.

Moreover, it would be highly interesting to test, if usage of the Expi293-F system would further increase our soluble pMHC-II-pCC-Fc production yields compared to the already used 293-F system. Previous studies have shown, that the Expi293-F system typically reveals 2- to 10-fold higher yield compared to the 293-F system (354), which would be in accordance with our observed 2- to 4-fold increase in yield for the production of pMHC-I (dt-SCT)-\*Fc constructs when the Expi293-F system was used (**Table 5.1**). Alternatively, higher levels of recombinant protein expression might be also achieved by taking advantage of HEK293 cell lines that have been engineered to express the Epstein-Barr virus antigen-1 (EBNA1) such as 293-6E cells together with the pTT5 expression vector carrying an Epstein-Barr virus origin of replication (oriP) that allows maintenance of a high plasmid copy number upon transfection. The latter typically shows an up to 3-fold improvement in recombinant protein yields compared to similar non-oriP vector based systems (355–357).

As an additional future aim, we want to further validate the binding of in-house produced pMHC-II-pCC-Fc molecules based on other alleles than HLA-DR3. So far, we have only validated the cognate binding of the soluble MTB/DR3-pCC-Fc pMHC-II construct towards its cognate T cell line. In the near future peripheral blood of healthy donors expressing HLA-DR1 or HLA-DR4 will be analyzed by corresponding in-house produced pHLA-DR1 / DR4 multimers presenting for instance the well-known tetanus toxin<sub>830–843</sub> [QYIKANSKFIGITE] or Influenza HA<sub>307–319</sub> [PKYVKQNTLKLAT] epitope, whose cognate T cell pools have been frequently observed in healthy donors (358, 359).

### **5.3 The T-Plex Assay – A novel *in vitro* multiplex assay using color-coded beads serving as biosensors for cognate antigen-specific T cell pools**

#### **5.3.1 T-Plex beads – “Off-the-shelf” biosensors for cognate antigen-specific T cell pools**

In this study, we developed, demonstrated and optimized a novel and highly sensitive *in vitro* assay concept for the detection and direct discrimination of multiple functional antigen-specific T cell responses. This multiplex assay concept, which we named T-Plex Assay (TPA), is based on cell-sized (6.5  $\mu\text{m}$  in diameter) spectral color-coded magnetic polystyrene beads (MagPlex<sup>®</sup> microspheres by Luminex) that are coated on their surface defined recombinant pMHC-I or pMHC-II molecules, which converts these beads into color-coded artificial antigen-presenting cells driving antigen-specific T cell activation. In addition, we immobilized antibodies on the same bead surface, most notably an anti-human IFN- $\gamma$  mAb, against common T cell effector cytokines, that are secreted upon T cell activation and allows the barcoded aAPCs to function as a cell contact-dependent biosensor for its cognate antigen-specific T cell population. We have termed these aAPCs with effector cytokine capture capacity T-Plex beads. Being aware of the fact that upon T cell activation by its cognate T-Plex bead secreted

soluble effector molecules might also bind to vicinuous bystander T-Plex beads reflecting other antigen specificities, we implemented an assay procedure that minimizes this “noise signal” on irrelevant T-Plex beads while improving the contact probability between cognate T-Plex beads and T cells. In particular, the usage of a single tube that is simply rotated along its longitudinal axis at high speed has been sufficient to minimize cross-bleeding of soluble effector molecules throughout the co-culture of a given pool of T-Plex bead species reflecting various antigen specificities to be screened. After the co-culture a given T-Plex bead pool is magnetically separated from the T cell sample and analyzed for its effector cytokine load by flow cytometry. Finally, the presence of an antigen-specific T cell population is indirectly indicated by the appearance of an IFN- $\gamma^+$  subpopulation of cognate T-Plex beads that is above T-Plex control beads. For the assembly of the T-Plex beads of choice, we took advantage of our self-implemented soluble pMHC-I and pMHC-II production pipeline as discussed before. Yet, the T-Plex Assay concept may be also applicable to soluble recombinant pMHC-I and pMHC-II molecules produced by alternative production strategies and that are in general also commercially available.

To the best of our knowledge, this is the first time that an assay principle has been reported that is based on bead-based fluorochrome-barcoded aAPC biosensors allowing for the detection of multiple antigen-specific T cell responses within a single reaction. As introduced in **Section 1.5.1.3**, a few predecessor studies have used cell-based fluorochrome-barcoded peptide-pulsed APCs to serve as an indirect biosensor for cognate antigen-specific T cell populations. For instance, Quah *et al.* used various concentrations of up to three fluorescent cell-labeling dyes followed by a peptide pulse to generate a library of individual barcoded cellular APCs, which were subsequently pooled and served as targets upon co-culturing with CD8<sup>+</sup> T cells. Thus, multiple antigen-specific CD8<sup>+</sup> T cell responses could be analyzed in parallel by the corresponding detection of cytolysis of the respective barcoded cognate APC population (177, 178). However, this assay approach displayed an overall lack of sensitivity compared to other conventional assay platform such as ELISpot or pMHC multimer staining and required high amounts of cellular APCs, which are often limited in a clinical setting. In contrast, our synthetic aAPCs-biosensor concept based on already commercially available color-coded xMAP MagPlex<sup>®</sup> microspheres enables a highly standardized and simple manufacturing process, which is completely independent of the availability of cellular HLA-matched APCs and avoids variations associated with peptide loading of living cellular APC and their subsequent labeling with cell tracer dyes. Moreover, our T-Plex beads can be stored and used over an extended period allowing for more reproducible assay results. Furthermore, T-Plex beads represent either an “off-the-shelf” reagent for well-known and frequently investigated antigen-specificities such as viral epitopes and can be rapidly produced as customized reagent in case novel putative antigens shall be screened for their immunogenicity using our described pMHC-I and pMHC-II production pipeline.

### 5.3.2 The T-Plex Assay – An easy-to-use multiplex assay designed for broad laboratory practice

Since their commercialization twenty years ago, the microsphere-based suspension array developed by Luminex Corp., also termed Luminex xMAP (multi-analyte profiling) technology, has been widely used to develop novel assays for the simultaneous detection of multiple soluble analytes in a single reaction. In particular, the “open architecture” of the polystyrene SeroMAP<sup>™</sup> microspheres and superparamagnetic MagPlex<sup>®</sup> microspheres functionalized with carboxyl groups for covalent attachment of various assay capture molecules such as protein antigens, antibodies or nucleic acids have enabled many researches among others to simultaneously quantify humoral antibody responses or cytokine levels (360). Within this study, we have demonstrated how MagPlex<sup>®</sup> microspheres (Luminex beads) can be customized in a way that they can be applied to simultaneously detect multiple

antigen-specific T cell responses *in vitro*, which opens the novel option to use the xMAP technology to interrogate multiple putative T cell epitopes in a high-throughput fashion. Our T-Plex Assay, however, is based on a selected analyte (IFN- $\gamma$  in most cases) capture on color-coded microspheres in a cell contact-dependent manner. This results in a mixture of microspheres of one spectral identifier that displays various degree of analyte capture, which in light of Luminex' xMAP technology design could be seen as an odd assay behavior. The entire Luminex xMAP technology including the analyzer instrument (e.g. Luminex analyzer 100/200™) and its software are by default engineered to (i) measure Luminex microspheres, (ii) identify their spectral identity, (iii) quantify the reporter signal provided by captured analyte of a given microsphere population, and (vi) report this value as median fluorescent intensity in a rapid and highly automated fashion. Consequently, the Luminex analyzer requires homogenous capture of a given soluble analyte on the entire cognate microsphere population to ensure a robust automated data analysis. The latter however, prohibits measurement of a T-Plex Assay, where individual T-Plex beads species within one spectral identity rather displays a heterogeneous capture of IFN- $\gamma$  leading to an appearance of an IFN- $\gamma^+$  and IFN- $\gamma^-$  subpopulations. A simple way out of these instrument- and software-mediated issues represent the usage of conventional flow cytometers and software instead, that are designed for fluorochrome-based multiparametric analysis of cells or particles and allow for the “gating” of individual populations. By applying this approach, we have already incorporated up to 30 different MagPlex® microspheres species within on T-Plex Assay (**Supplementary Fig. S9**). Yet, we envisaged that T cell responses against up to 80 epitopes could be reliably measured by the T-Plex Assay based on commercially available 80 spectral distinct magnetic MagPlex® microspheres, which are suited for the Luminex analyzer 100/200™ instrument and thus may also be well discriminated by the BD FACS Canto II system. In this respect, the T-Plex Assay has one of the highest multiplex capacities across various non-next generation sequencing-based methods for the detection of antigen-specific T cell populations. The frequently applied, two-dimensionally encoded, combinatorial fluorochrome-based pMHC-I multimer staining is typically limited to only 25–27 antigens per staining due to a restricted availability of bright streptavidin-conjugated fluorochromes and background issues associated with quantum dots (185, 186). Moreover, with a multiplex capacity of up to 80 possible antigens, the T-Plex Assay is in the closer range as the pMHC multimer heavy metal-barcoding approach enabling the parallel analysis of up to 120 T cell antigen specificities (188, 199). However, as introduced in **Section 1.5.2.2**, mass-cytometry-based analysis does not permit the recovery of the sample, because the cells are disrupted during the measurement and the limited availability of mass-cytometers as well as high reagent costs strongly limits a wide-spread usage of this technology in general (228), unlike the T-Plex Assay. Therefore, we strongly believe that the T-Plex Assay is highly attractive for routine laboratory practice since only commonly available lab devices such as a cell culture incubator, tube-rolling system and magnets suitable for tubes are required in order to perform a T-Plex Assay. For read-out and data analysis, common flow cytometers such as BD FACS Canto II are sufficient. Moreover, the T-Plex Assay requires typically less than 3 hours hands-on time including pMHC / T-Plex bead library assembly and flow cytometric measurement, which is less than half of the hands-on time required for similar conventional functional T cell assays (**Section 1.5 / Table 1.3**), such as ELISpot or intracellular cytokine staining (171–174).

### 5.3.3 The application scope of the T-Plex Assay and its strength as well as limitations

We have proven that the T-Plex Assay enables a reproducible, sensitive and simultaneous measurement of multiple virus antigen-specific T cell responses using healthy donor-derived T cells with equal sensitivity as alternative and frequently used conventional assays (e.g. pMHC multimer staining). Furthermore, we envision that the T-Plex Assay allows affordable and convenient deciphering of functional T cell responses against a broad range of antigens associated with cancer, infectious diseases and autoimmune diseases. Here, the T-Plex Assay may be used as tool to discover novel immunogenic T cell epitopes that in turn guide vaccine design to boost the immunity against e.g. viral or tumor antigens or to tolerize immune responses against autoantigens. In the same breath, the T-Plex Assay may be applied to monitor the success of vaccination regimes steering pre-defined antigen-specific T cells responses or to monitor the induction of novel T cell responses during cancer immune-checkpoint inhibition therapy. However, since the T-Plex Assay relies on the production of soluble recombinant pMHC-I and pMHC-II, the T-Plex Assay similar to a pMHC multimer staining requires prior information about the HLA haplotype of the cell material.

Moreover, the discovery of novel epitopes using either the T-Plex Assay or pMHC multimers is typically in need of *in silico* prediction of putative peptide ligands, which is far from being unbiased. In particular, since only the most frequent and most characterized MHC alleles as well as high-affinity peptides are focused upon, this procedure can overlook immunogenic peptides that might show a low-binding affinity and less anticipated HLA restriction (119, 132). As an alternative, rather unbiased method, large pools of long peptides (i.e. 25–30 residues) (152) or so-called “tandem-minigens” (153) can be used to screen the immunogenicity of putative novel antigens in an HLA-independent but antigen processing-dependent manner using co-cultures of T cells with cellular APCs. The latter, however, typically require large numbers of autologous APCs and T cells, which are often limited in a clinical setting.

A unique strength of the T-Plex assay principle is the option for a complete sample recovery that allows for continuous culture of the analyzed T cell sample after simple magnetic separation of the T-Plex beads from the sample. The latter in turn opens the possibility to conduct further experiments with the same sample as well as to enrich and expand for identified antigen-specific T cell pools. Such a “sample recycling” strategy can be very useful in case only limiting amounts of clinical samples are available. Among most conventional assays for antigen-specific T cell detection (**Section 1.5 / Table 1.3**) this is reliably only possible, when an ELISpot is performed. As an example, Ott *et al.* used only  $11 \times 10^6$  PBMC from patients with type 1 diabetes to test their response towards 70 individual peptide pools – first directly *ex vivo* using an ELISpot assay – and then again after 12 days culture of the recovered cell material (361). In this way, the chances of gaining information about direct *ex vivo* antigen-specific T cell responses are maximized, while still maintaining the option of learning about initially undetected responses after cell expansion and retesting. In addition, unlike an ELISpot the T-Plex Assay would allow for discrimination of multiple antigen-specific T cell populations at the same time.

As a disadvantage, the current T-Plex Assay only permits the partial enumeration of functional antigen-specific T cell responses. For the optimized T-Plex Assay protocol that includes a co-centrifugation step of T-Plex beads and a given test sample, we consistently observed within a certain window a linear relationship between the absolute amounts of antigen-specific T cells present during the co-culture and the amounts of total cognate T-Plex beads becoming IFN- $\gamma^+$ . For instance within the range of 500 to 3 HCMV/A2-specific T cells, consistently roughly 10-times more IFN- $\gamma^+$  T-Plex were considered IFN- $\gamma^+$  (**Section 4.3.3 / Fig. 4.17**), which would theoretically allow for the indirect enumeration of that

HCMV/A2-specific T cells present within that range. However, as shown in **Section 4.4 / Fig. 4.20** this observation did not hold to be generally true for the detection of other antigen-specific T cell populations such as EBV/A2- or Flu/A2-specific CD8<sup>+</sup> T cells, where 2- to 10-fold less T-Plex beads became IFN- $\gamma$ <sup>+</sup> compared to the actual total amounts of cognate T cells present in the reaction. Therefore, the results obtained by the HCMV/A2-specific T cell lines might be rather the exception, which might be caused by the exceptionally very high affinity of the HCMV pp65<sub>495-503</sub>/HLA-A2-specific T cell receptor (325). In order to further elucidate and understand this discrepancy, we will perform further optimized T-Plex Assays using titrating amounts of our established EBV/A2- and Flu/A2-specific CD8<sup>+</sup> T cell lines in comparison to the already used HCMV/A2-specific T cell lines.

#### 5.3.4 Novel, recently reported alternative methods to detect antigen-specific T cells without the need of next-generation sequencing (NGS)

An alternative assay concept for the detection of antigen-specific T cell populations based on non-barcoded bead-based aAPCs combined with an ELISpot readout termed aAPC-microplate assay (362) was reported recently and parallel to our study by Shen *et al.* Here, the authors immobilized various biotinylated pMHC-I single-chain trimers presenting Hepatitis B virus (HBV) peptide epitopes together with an anti-human CD28 mAb on streptavidin-coated magnetic Dynabeads (4.5  $\mu$ m in diameter) to generate bead-based aAPCs quite similar to our approach. Subsequently, isolated CD8<sup>+</sup> T cells of adult chronic HBV-infected patients were co-cultured initially for two hours at RT with individual aAPCs pools in 96-well plate, which has been pre-coated with an anti-IFN- $\gamma$  capture mAb to allow an ELISpot read-out procedure. After the 2 h, RT initial contact time, the 96-well plate was placed over 96-well magnet and the assay plate was subsequently washed to enrich for antigen-specific T cell populations that within this initial time window bound to the cognate magnetic aAPC. In a final step, the enriched antigen-specific T cell pool were cultured with their cognate aAPCs at 37°C for 24 h to drive their activation resulting in microscopically visible IFN- $\gamma$  spots after ELISpot read-out. The usage of the aAPC-microplate assay allowed sensitive enumeration of low frequency T cell populations which correlated very well with a corresponding pMHC-I multimer staining. Further, this assay approach also overcomes the need of autologous or HLA-match cellular APCs. However, unlike the T-Plex Assay the described aAPC-microplate assay does not allow discrimination of multiple antigen specific T cell responses within one reaction (i.e. one well). Nevertheless, it might be interesting to incorporate this initial antigen-specific enrichment step in the T-Plex Assay procedure. It might be beneficial to incubate magnetic T-Plex beads and T cell sample for 1-2 h at RT or even 4°C to prevent T cell activation followed by magnetic isolation of bound T cells and rolling of antigen-specifically enriched T cells and T-Plex beads in a single tube at 37°C. An advantage of this enrichment step could be an increased assay sensitivity as well as it might facilitate subsequent generation of defined T cell lines based on simple antigen-independent T cell expansion methods (i.e. anti-CD3 / anti-CD28-coated beads or PHA-L addition). However, so far we have not systematically evaluated if magnetic T-Plex beads are suitable for magnetic enrichment of antigen-specific T cells. We currently rather assume that cognate T cells interact only transiently with T-Plex beads during the T-Plex Assay procedure since this cognate T cell population is typically not depleted from the test sample after its magnetic separation from the T-Plex beads after the assay procedure (**Fig. 4.8 & Fig. 4.21**).

In this regard, Peng *et al.* reported very recently by the end of 2019, another elegant bead-based assay platform allowing for enrichment and multiplexed discrimination of multiple antigen-specific T cell populations at the same time. Here, the authors used simple bright-field and fluorescence microscopy to analyze bead-associated T cells as a final readout method. As a core concept they used pMHC-I

multimers coupled to smaller magnetic beads (1  $\mu\text{m}$  in diameter) via DNA linkers serving as barcodes for complementary fluorescently labeled single-stranded (ss)DNA hybridization probes (363). In detail, individual pMHC-I multimers were based on a mutated streptavidin scaffold bearing a single cysteine residue at the C-terminus of each subunit allowing for site-specific attachment of a ssDNA oligo to the modified streptavidin as described before by (364). In order to allow efficient magnetic enrichment and a high avidity interaction with cognate T cells, these ssDNA-oligo-linked pMHC-I multimers were immobilized on streptavidin-coated MyOne T1 Dynabeads (1  $\mu\text{m}$  in diameter) coupled previously to another defined biotinylated ssDNA oligo. This biotinylated bead-coupled ssDNA oligomer encoded firstly for an individual barcode comprising three unique sequences that in turn served as docking sites for complementary fluorochrome-labeled ssDNA oligo probes and secondly for a complementary hybridization site for the ssDNA-oligo-linked pMHC-multimer. Subsequently, the authors demonstrated that a library of up to 27 ( $3^3$ ) neoantigen-loaded pMHC-I multimers conjugated to barcoded bead pools could be successfully applied to enrich for cancer patient-derived neoantigen-specific T cells by magnetic pull-down. Further, they showed that these enriched T cells could be well discriminated in an antigen-specific manner based on the attached bead-associated DNA barcode. For the latter, isolated cells were simply imaged and counted either in a hemocytometer plastic chip or in microfluidic chamber engineered by the authors that was equipped with cell traps allowing for a better analysis of individual bead-associated T cells. For decoding of the 3-position DNA barcode of the respective the pMHC/bead library, sets of dye-labeled ssDNA oligo probes were sequentially hybridized, imaged and displaced in three rounds (one for each position) ending up in a sequential color-code combination that finally assigned the antigen specificity to every imaged bead-associated T cell. In addition, the authors managed to isolate identified, single neoantigen-specific T cells whose TCR could be sequenced after single cell reverse transcriptase (RT)-PCR (363). The latter dramatically reduces the time and cost associated for the identification and isolation of highly personalized neoantigen-specific TCRs, which could be potentially used in a second step for the manufacturing of an adoptive T cell therapy.

#### 5.3.5 Novel NGS-based methods to detect antigen-specific T cells or to dissect putative T cell epitopes on a genome-wide level

Here, we intentionally focused on the development of an easy-to-use aAPC-based multiplex platform to detect multiple functional-responding antigen-specific T cell populations in a single reaction that requires only commonly available instruments and thus allows for a fast implementation in routine laboratory practice. Yet, in parallel to our study, also several highly potent, alternative methods have been developed and reported, that take advantage of next-generation sequencing (NGS) techniques combined with molecular identifiers such as DNA barcodes in order to directly screen for T cell epitopes with theoretically unlimited multiplex capacity.

As introduced in **Section 1.5.2.2**, the pioneering work of Bentzen *et al.* showed for the first time the feasibility of generating a library of fluorescent, DNA-barcoded pMHC-I multimers, which allowed interrogation of over 1000 T cell antigen-specificities in a single sample. In their approach, the library was generated using unique DNA barcodes attached to individual UV-light-mediated synthetic peptide-loaded pMHC-I multimers. T cells that have bound a pMHC-I multimer were subsequently isolated by FACS sorting followed by bulk NGS sequencing that enabled the determination of the relative abundance of different antigen-specific T cell pools in the test sample (189). More recently, Zhang *et al.* further developed and applied this technology in a high-throughput manner to directly identify and isolate neoantigen-specific TCRs. Here, the authors very elegantly used DNA oligonucleotides that

served on the one hand as DNA barcode for the pMHC-I multimer, and on the other hand encoded for the immunogenic peptide itself which was loaded upon *in vitro* transcription and translation on the corresponding pMHC-I via peptide-exchange omitting expensive synthetic peptide synthesis. In addition, following an initial FACS sorting step, Zhang *et al.* used a single cell sequencing approach to simultaneously identify both the TCR  $\alpha\beta$  sequence and the antigen-specificity for each sorted T cell based on the bound pMHC-I multimer and its associated barcode (365). Both studies demonstrated the feasibility to use DNA-barcoded pMHC-I multimers to confirm the immunogenicity of putative neoepitopes in a high-throughput fashion through detection of low-frequency cognate T cell populations.

Soluble pMHC multimer-based screening platforms as discussed above have been typically used to validate the immunogenicity of *in silico* predicted antigens with the intention to detect cognate T cell pools and if possible to isolate their TCR sequence. As an alternative, several groups have designed quite recently various novel expression vector-based reporter systems allowing for a cell-cell contact-dependent high-throughput mapping of T cell epitopes for a given disease-relevant TCR of yet unknown specificity (“orphan TCR”), which omits costly manufacturing of recombinant pMHC multimers. These cell-based platforms for TCR ligand discovery comprise among others, the “signaling and antigen-presenting bifunctional receptor” (SABRs) system (366), the “pMHC-TCR hybrid system” (MCR) (367) and “T-Scan” reporter system (368). The SABR reporter system comprises a lentiviral vector that encodes for the extracellular domain of a covalently linked peptide- $\beta_2m$ -MHC heavy chain trimer (SCT) fused to an intracellular CD3 $\zeta$  signaling domain followed by a CD28 costimulatory domain, which was transduced into Jurkat cells expressing GFP under the control of NFAT (NFAT-GFP-Jurkat cells). In parallel, a TCR isolated from an e.g. tumor-reactive CD8<sup>+</sup> T cell of unknown specificity was transduced in parental Jurkat cells (TCR-Jurkat). TCR-Jurkat cells and a given library of SABR-transduced NFAT-GFP-Jurkat cells reflecting putative T cell epitopes were co-cultured, which allowed for the subsequent FACS sorting of responding GFP<sup>+</sup> NFAT-Jurkat cells expressing the cognate SABR. Sequencing of the epitope portion of the SABR of the isolated GFP<sup>+</sup> Jurkat cells finally provided the sought information about the specificity of the TCR (366). A similar NFAT reporter system, yet designed for the epitope screening of TCRs derived from CD4<sup>+</sup> T cells, represents the “pMHC-TCR hybrid” system also referred to as MCR system. Here, the ectodomain of a peptide-tethered MHC-II  $\alpha\beta$  heterodimer is fused to the constant domains of an  $\alpha\beta$  TCR including its hinge region, transmembrane and intracellular domains. Subsequently, MCR libraries are transduced into reporter cell lines, which are used as target cells for T cells or TCR-transduced cells. This in turn allows for the identification of the sought cognate antigen by the combined action of FACS sorting and sequencing of cells expressing the cognate MCR (367). Finally, the “T-Scan” approach reported recently by Kula *et al.* represents another highly sophisticated, engineered, cell-based reporter system to identify the cognate antigen of a given T cell / TCR without the requirement of prior *in silico* prediction of potential MHC peptide ligands. Here, the authors firstly engineered a MHC-negative HEK293T cell line using the CRISPR/Cas9 system, which in the next step was transduced with an HLA allele of interest. These modified HEK293T cells subsequently received a comprehensive lentivirus-delivered antigen library covering desired antigens (i.e. 90 amino acid fragments) together with a granzyme-B driven reporter construct allowing for high-throughput T cell antigen identification on a human genome- or pathogen genome-wide scale. As an example, the authors impressively screened a self-reactive TCR against a library of 259,345 fragments encoding the entire human proteome (368).

### 5.3.6 Open questions regarding the T-Plex Assay

#### **5.3.6.1 Does the T-Plex Assay work independently of the T cells' individual differentiation and functional status and reliably solely based on cognate pMHC-encounter?**

An open question remains if the T-Plex Assay allows for the detection of a broad spectrum of antigen-specific T cell populations that might display various stages of differentiation (i.e. naïve vs. effector memory) or functional states (i.e. highly responsive with low activation threshold vs. hypo-responsive exhausted / dysfunctional phenotype). For the same reason, we cannot fully estimate to what degree incorporation of molecules acting in a co-stimulatory manner, such as anti-CD28 mAbs, might broaden the range of detection. Co-immobilization of recombinant pMHC and anti-CD28 mAbs on a bead-surface as well as cellular aAPCs that have been molecularly engineered to co-express a cognate antigen and co-stimulatory molecules such as B7.1 (CD80) have been generally defined as the minimum requirement to activate full-fledged T cell effector functions and to induce robust proliferation in the presence of additional cytokines such as IL-2, IL-7 and IL-15 (250, 369). The latter is based on the general dogma that optimal T cell activation requires the integration of multiple signaling events gained by TCR engagement (signal 1) as well as by signals received through co-stimulatory or co-inhibitory receptors (signal 2), as well as cytokine receptors (signal 3) (39–41). Yet, the relative importance of each individual signal 1–3 may highly depend on the cellular and experimental context. In this regard, Lim *et al.* observed that a panel of unique human HTLV-I-specific CD8<sup>+</sup> T cell clones established by pMHC-I multimer-guided single cell sorting showed very similar degrees of high cytotoxicity against peptide-pulsed HLA-A2-transgenic CHO target cells. However, only the minority clones (3 out of 9) secreted IFN- $\gamma$  and proliferated in the presence of target cells pulsed at a high (> 1  $\mu$ M) peptide concentration but not at lower antigen-densities. In contrast, peptide-pulsed CHO cells, transgenic for both HLA-A2 and B7-1 (CD80) or HLA-A2 and LFA-3 (CD58), respectively, induced cognate IFN- $\gamma$  secretion in all T cell clones at 100-times lower antigen-densities (370), suggesting that both engagement of CD2 and CD28 expressed on T cells lower the T cell activation threshold and enhance cytokine production. In direct contrast, we have observed throughout this study that immobilization of recombinant pMHC-I including HCMV/A2, Flu/A2, EBV/A2 and Survivin/A2 as well as pMHC-II including MTB/DR3 on various bead types (diameter 4.5 – 6.5  $\mu$ m) were sufficient to induce IFN- $\gamma$  secretion of corresponding cognate T cell lines in the absence of co-stimulatory mAbs. Addition of either soluble anti-CD28 mAbs during the co-culture of beads and T cells or the additional co-immobilization of pMHC and anti-CD28 and/or anti-CD2 on a given bead surface hardly influenced the activation of these T cell lines nor did a corresponding T-Plex Assay display an improved performance. The T-Plex Assay also allowed for a robust detection of virus-specific CD8<sup>+</sup> T cells (i.e. HCMV/A2, Flu/A2, EBV/A2-specific) present in various healthy donors in the absence of additional co-stimulatory mAbs. However, in all cases our T cell lines as well as healthy donor peripheral blood were cultured for at least 3 days in the presence of IL-15 (among other cytokines), which, together with IL-7, has been shown to reduce T cell activation thresholds (371) and may partially make additional co-stimulatory signals through e.g. CD28 dispensable. To further elucidate this issue, we will perform T-Plex Assays interrogating virus-specific T cells from directly *ex vivo* isolated CD8<sup>+</sup> T cells that have not yet undergone any *in vitro* culturing.

#### **5.3.6.2 What is the true nature of the interaction between cognate T cells and T-Plex beads that facilitate the unique read-out of the T-Plex Assay?**

Another intriguing question is how cognate T cells and T-Plex beads interact during the co-culture in rotating conditions? For instance, do cognate T cells and T-Plex beads undergo a long-lasting stable interaction or rather multiple transient interactions?

One of our last cell-titration experiments (**Fig. 4.17**) indicated that a given HCMV/A2-specific CD8<sup>+</sup> T cell interacted on average with 10 cognate T-Plex beads, which would rather indicate a transient mode of interaction with multiple beads, especially since T-Plex beads have a similar size (6.5  $\mu\text{m}$ ) as T cells. Regardless of the duration of interactions, several biological features of T cell activation may act in favor of the T-Plex Assay. As previously introduced in **Section 1.2.3.4**, it has been shown that a polarized TCR stimulation of CD8<sup>+</sup> T cells as well as CD4<sup>+</sup> T cells by a given APC induces a polarized movement of the microtubule-organizing center (MTOC) towards the APC interaction site within two minutes (60, 70). This so-called “synaptic” route of secretion leads to a polarized release of cytotoxic mediators such as granzymes and perforin, but also other effector molecules such as IL-2 and IFN- $\gamma$  towards the APC (60–62, 66, 68). In turn, this mode of action might favor proximal capture of these cytokines on interacting T-Plex beads and minimize bystander capture of diffusing cytokines on irrelevant T-Plex beads nearby. Other cytokines, e.g. TNF- $\alpha$  and IL-4 have been described to be secreted rather multi-directionally regardless of the APC interaction site (61). Nevertheless, we have not observed severe background issues when these cytokines were used as reporter cytokines for a cognate T-Plex / T cell interaction (**Section 4.6.3 / Fig. 4.27**). Moreover, it has been shown that CD8<sup>+</sup> T cells as well as Th1-differentiated CD4<sup>+</sup> T cells rapidly produce IFN- $\gamma$  (i.e. within 90 minutes) and TNF- $\alpha$  (i.e. within 30 minutes) when their TCR is engaged by a cognate APC, but that cytokine production ceases immediately when the antigenic contact is broken and resumption of stimulation causes rapid reinitiation (372–374). Altogether, these features may contribute to a corresponding cognate T-Plex bead capturing higher amounts of IFN- $\gamma$  in close contact with a given T cell compared to bystander beads nearby, which finally enables the distinction of beads that have been in contact with a cognate T cell compared to beads that have not.

### 5.3.6.3 What are the critical parameters to move beyond an IFN- $\gamma$ -based T-Plex Assay?

In the peripheral blood most circulating memory CD4<sup>+</sup> and CD8<sup>+</sup> T cells produce IFN- $\gamma$ , IL-2 and TNF- $\alpha$  following short-term stimulation (91). Thus, various assays including ELISpot, ICS (**Section 1.5 / Table 1.3**) and our T-Plex Assay that focus on the detection of IFN- $\gamma$  serving as surrogate marker for antigen-specific stimulation have been proven to be quite robust. Yet, as an advancement to an IFN- $\gamma$  capture-based T-Plex Assay, we envision that parallel detection of multiple cytokines per antigen-specific T-Plex bead may broaden the application potential in a concept we termed T-Plex<sup>2</sup> Assay. Following that concept, we aimed to enable the simultaneous read-out of multiple antigen-specific CD4<sup>+</sup> and CD8<sup>+</sup> T cell responses and to learn more about the functional status and / or differentiation profile of a detected T cell at the same time and within a single assay. So far, only the combination of an *in vitro* stimulation followed by an intracellular cytokine staining and finally a multiplex pMHC multimer staining allowed a read-out similar to the T-Plex<sup>2</sup> concept (189). However, antigen-specific (i.e. peptide pulse) or polyclonal (i.e. anti-CD3 mAb) *in vitro* stimulation typically results in a very rapid TCR down-modulation, which in turn spoils the efficiency of a subsequent pMHC multimer staining. Moreover, due the fixation necessary for an ICS, no vital cells can be recovered. To this end, we have developed a T-Plex<sup>2</sup> bead prototype that so far allowed successful detection of up to three cytokine (i.e. IFN- $\gamma$ , TNF- $\alpha$ , IL-4) in an antigen-specific manner. Yet, the current prototype revealed rather poor signal intensities for each individual cytokine capture on the same bead. Thus, further optimization regarding the selection of cytokine capture and detection antibodies will be done in the future in order to overcome this issue. Moreover, it has clearly been shown that for instance IL-2 secretion is more dependent on co-stimulatory signals compared to IFN- $\gamma$  (375). Therefore, also for the future development of the T-Plex<sup>2</sup> Assay, we have to further evaluate the role of costimulatory signals for the

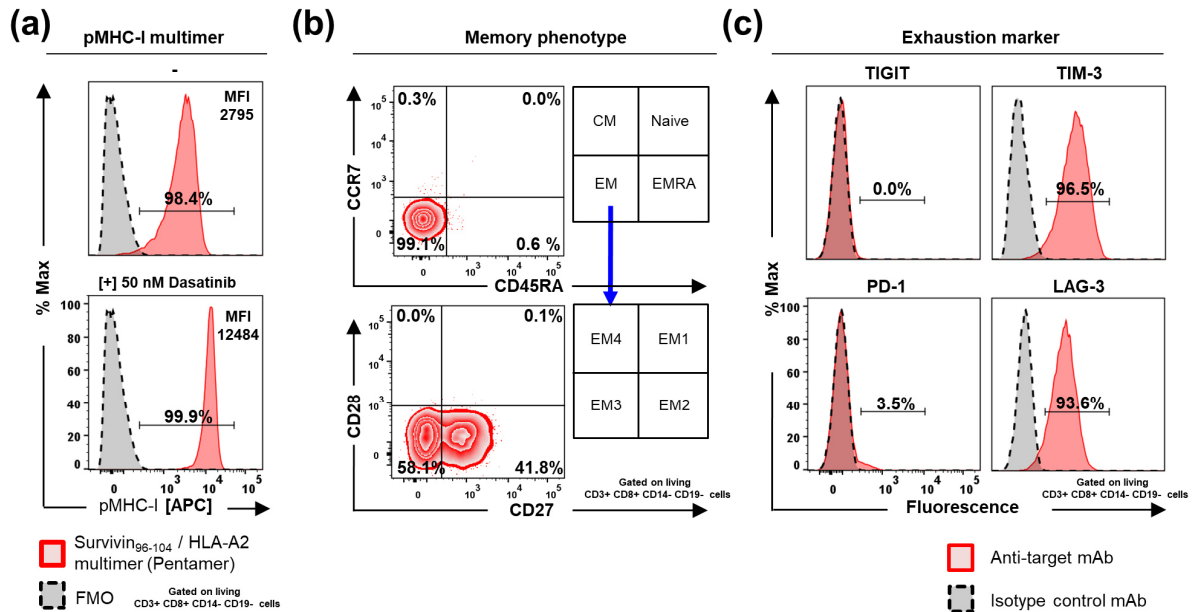
assay performance e.g. through CD28, but also analyze CD27 and LFA-1 (CD18/CD11a) engagement that also play supportive roles in T cell activation (376, 377).

Finally, another interesting, modified T-Plex Assay concept would be the assessment of the cytotoxic function of CD8<sup>+</sup> T cells or a subset of human CD4<sup>+</sup> T cells through the measurement of granzyme B in parallel to IFN- $\gamma$ . Previous studies have already shown the feasibility to perform ELISpot measurements of granzyme B (378, 379). Moreover, Nowacki *et al.* have shown that assessment of granzyme B production of directly *ex vivo* isolated human CD8<sup>+</sup> T cells can discriminate recently activated CD8<sup>+</sup> T cell memory or effector cells from resting memory cells that do not possess preformed lytic granules (379).



## Supplementary Figures

Survivin<sub>96-104</sub>/A2-specific CD8<sup>+</sup> T cell line



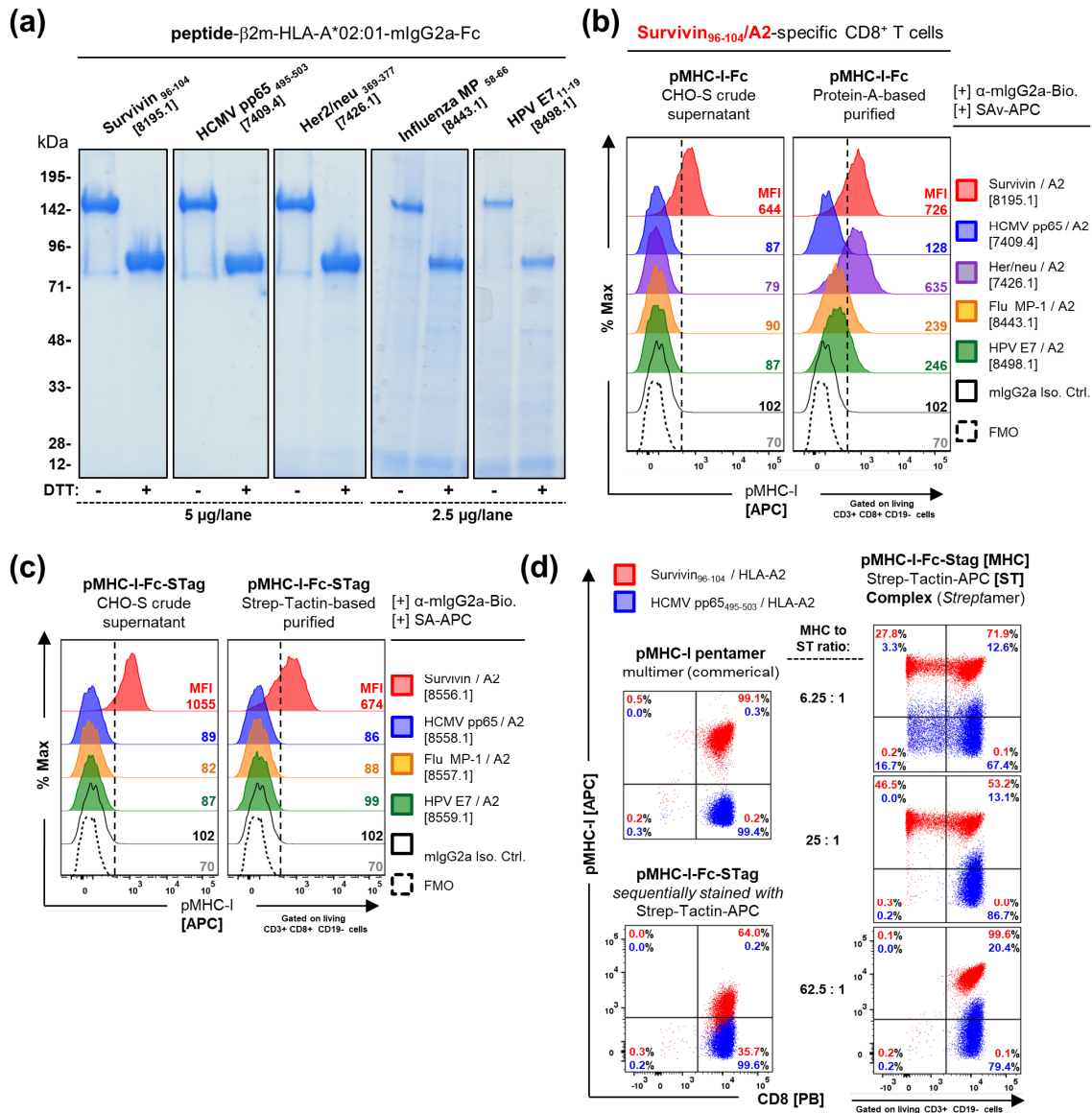
### Supplementary Figure S1 | Characterization of the Survivin/HLA-A2-specific CD8<sup>+</sup> T cell line

**(a) Verification of antigen specificity and cell line purity.** The Survivin<sub>96-104</sub>/HLA-A\*02:01-specific and allogeneic CD8<sup>+</sup> T cell line (Sur/A2 CD8<sup>+</sup> T cells) was stained in the presence or absence of dasatinib [50 nM] with cognate pHLA-A2 pentamer (from ProImmune) at 25 μg/mL followed by lineage marker staining.

**(b) Terminal differentiated effector memory phenotype.** Sur/A2 CD8<sup>+</sup> T cells lack the expression of CCR7 and CD45RA as well as CD28.

**(c) Expression analysis of selected exhaustion markers.**

EM: Effector memory; CM: Central memory; FMO: Fluorescence-minus-one background control; MFI: Median fluorescent intensity;



**Supplementary Figure S2 | Comparative binding analysis of protein A- vs. Strep-Tactin-based purified pMHC-I-Fc constructs and binding performance of complexes consisting of Strep-Tactin and pMHC-I-Fc (Streptamers)**

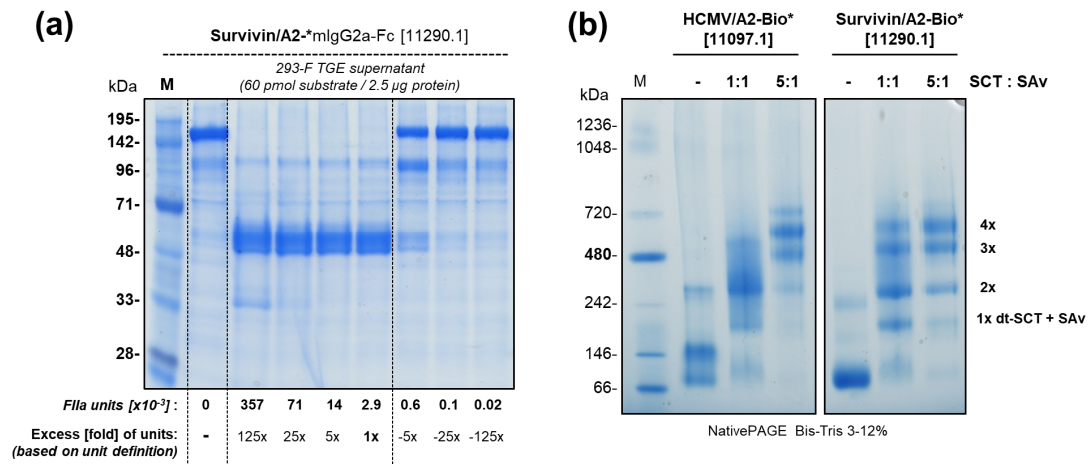
**(a) Protein A-based affinity chromatography of disulfide-trapped (dt) pMHC-I [SCT]-mIgG2a-Fc.** CHO-S supernatant of 6 days transient pMHC-I-Fc expression was purified using protein-A resin filled columns. Elution was performed by acidic pH 3.0 glycine/HCl buffer followed by immediate neutralization and dialysis. Shown are multiple 10% SDS-PAGEs of the final products under non-reducing and reducing conditions (+DTT) after Coomassie staining.

**(b-c) Binding analysis of protein-A- vs. Strep-Tactin-based purified pMHC-I-Fc constructs.**

The Survivin<sub>96-104</sub>/A2-specific CD8<sup>+</sup> T cell line (Sur/A2 CD8<sup>+</sup> T cells) was stained in the presence of dasatinib [50 nM] with cognate [red] or control pMHC-I-Fc [other colors] constructs at 25  $\mu$ g/mL. Binding performance of crude CHO-S supernatants or corresponding protein-A-based (b) or Strep-Tactin-based (c) purified pMHC-I-Fc is shown. Binding was detected by sequential staining with  $\alpha$ -mIgG2a-biotin (clone RMG2a-62) and streptavidin-APC (SAV-APC) parallel to the lineage marker staining. Black lines indicate the baseline of biotinylated mIgG2a-Isotype control and SAV-APC.

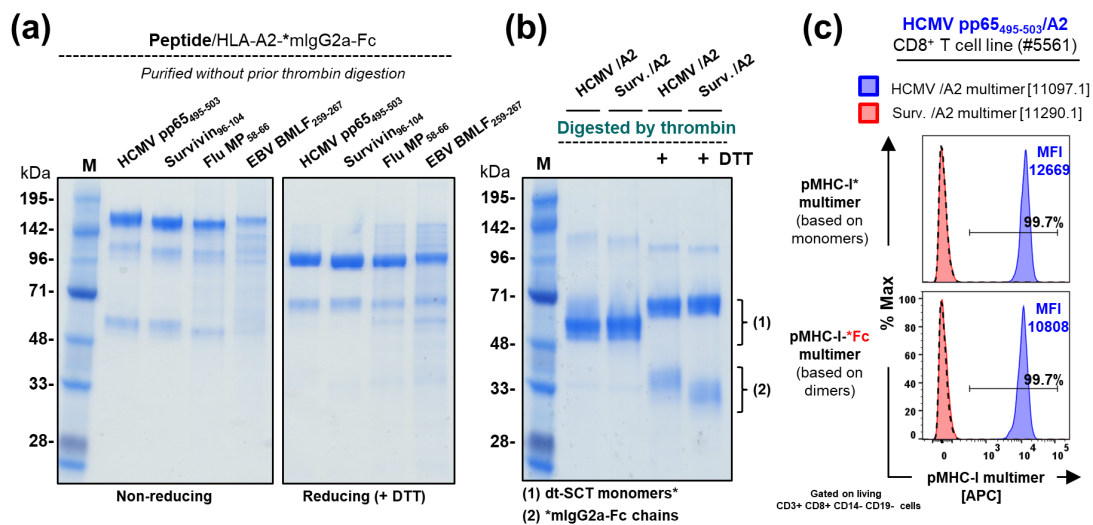
**(d) Titration of the pMHC-I-Fc-STag to Strep-Tactin-APC ratio for complex formation (Streptamer) prior T cell staining.**

Purified pMHC-I-Fc-STag [MHC] was incubated with Strep-Tactin-APC [ST] for complex formation at indicated molar ratios for 30 min on ice followed by staining of Sur/A2 CD8<sup>+</sup> T cells. Molar ratios were calculated based on the molecular weight of a single Strep-Tactin-APC (IBA Lifesciences) molecule and pMHC-I-Fc-STag (both ~165 kDa). This indicated ratio is only a rough approximation, since Strep-Tactin-APC is provided as an undefined polymer. Shown are overlays of Sur/A2 CD8<sup>+</sup> T cells (gated on living CD3<sup>+</sup>) either stained with cognate [red] or control [blue] pMHC-I-Fc-STag or corresponding commercial pMHC-I pentamer. FMO: fluorescence-minus-one background control; MFI: Median fluorescent intensity; [8556.1 = construct ID].



**Supplementary Figure S3 | Assessment of required thrombin units for complete pMHC-I\*Fc cleavage and validation of pMHC-I multimer formation**

**(a) Titration of thrombin (FIIa) units into pMHC-I\*Fc containing 293-F supernatants.** 50 µL 293-F supernatant containing 2.5 µg homodimeric pHLA-A2-\*Fc (160 kDa) according to mIgG-quantification ELISA (data not shown) was incubated for 16 h with various amounts of thrombin units (Novagen) followed by non-reducing 10% SDS-PAGE analysis. The FIIa unit definition is  $4.8 \times 10^{-5}$  units/pmol substrate incubated for 16 h at RT. 2.5 µg of pHLA-A2-\*Fc bearing in total four thrombin cleavage sites (FIIa-CS) per molecule correspond to 60 pmol substrate, which is ideally cleaved by  $2.9 \times 10^3$  units FIIa defined as no / (1x) excess of FIIa units. **(b) Validation of biotinylation and multimer formation.** Purified *in vivo* biotinylated monomeric HCMV/HLA-A2\* [11097.1] and Survivin/HLA-A2\* [11290.1] were incubated with streptavidin (SAv) at an eqimolar ratio (1:1) or at a 5:1 pMHC-I\* (dt-SCT) to SAv ratio and analyzed by NativePAGE.

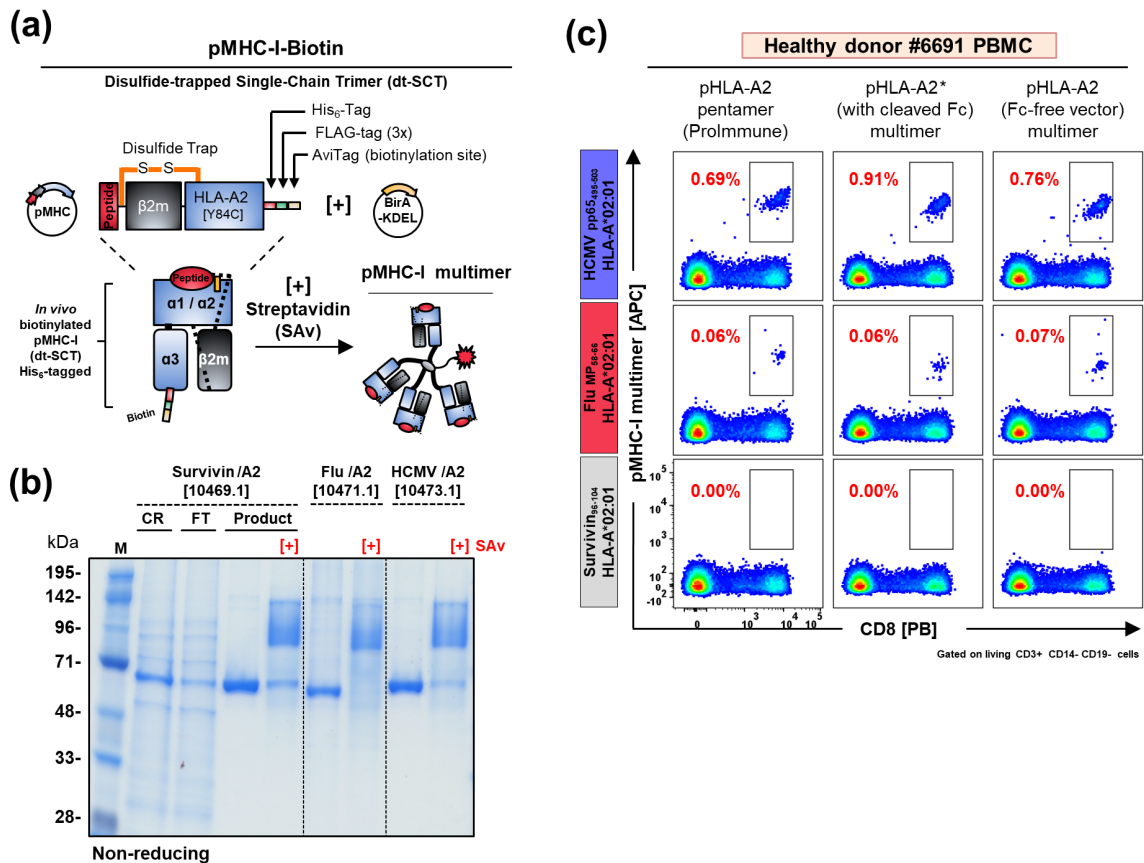


**Supplementary Figure S4 | Purification of biotinylated pMHC-I\*Fc homodimers and usage for pMHC-I multimers**

**(a) Affinity chromatography of biotinylated homodimeric pMHC-I\*Fc.** 293-F supernatants of 6 days transient expression of HCMV/HLA-A2-\*Fc [11097.1], Survivin/HLA-A2-\*Fc [11290.1], Flu/HLA-A2-\*Fc [11291.1] and EBV/HLA-A2-\*Fc [11292.1] were purified using His Mag Sepharose Excel (GE Healthcare). Shown is a 10% SDS-PAGE of the final products under non-reducing and reducing conditions (+ DTT) after Coomassie staining.

**(b) Thrombin-based digestion of purified HCMV/HLA-A2\*Fc [11097.1] and Survivin/HLA-A2\*Fc [11290.1].** 10 µg homodimeric pHLA-A2-\*Fc (160 kDa) bearing in total four thrombin cleavage sites (FIIa-CS) per molecule (in total 250 pmol substrate) was incubated with a 5-fold excess of recommended thrombin catalytic units (Novagen) at 37°C for 16 h followed by 10% SDS-PAGE analysis. Non-reducing SDS-PAGE condition displays the in molecular weight overlapping cleaved \*mIgG2a-Fc (H-CH2-CH3) and cleaved pHLA-A2\* monomers.

**(c) Antigen-specific staining of a cognate T cell line by pMHC-I multimers based on homodimeric biotinylated pMHC-I\*Fc as well as digested monomeric pMHC-I\*.** The HCMV/HLA-A2 specific CD8+ T cell line #5561 was stained either with Fc-bearing HCMV/HLA-A2-\*Fc [11097.1] or Survivin/HLA-A2-\*Fc [11290.1] based pMHC-I multimers or corresponding multimers formed with pHLA-A2\* lacking the Fc. pMHC-I multimer staining was performed at 2.5 µg/mL in the presence of 50 nM dasatinib. pMHC-I multimer signal of the CD8+ / CD3+ T cell population is shown. Dashed line indicates the fluorescence-minus-one background control. MFI: Median fluorescent intensity.

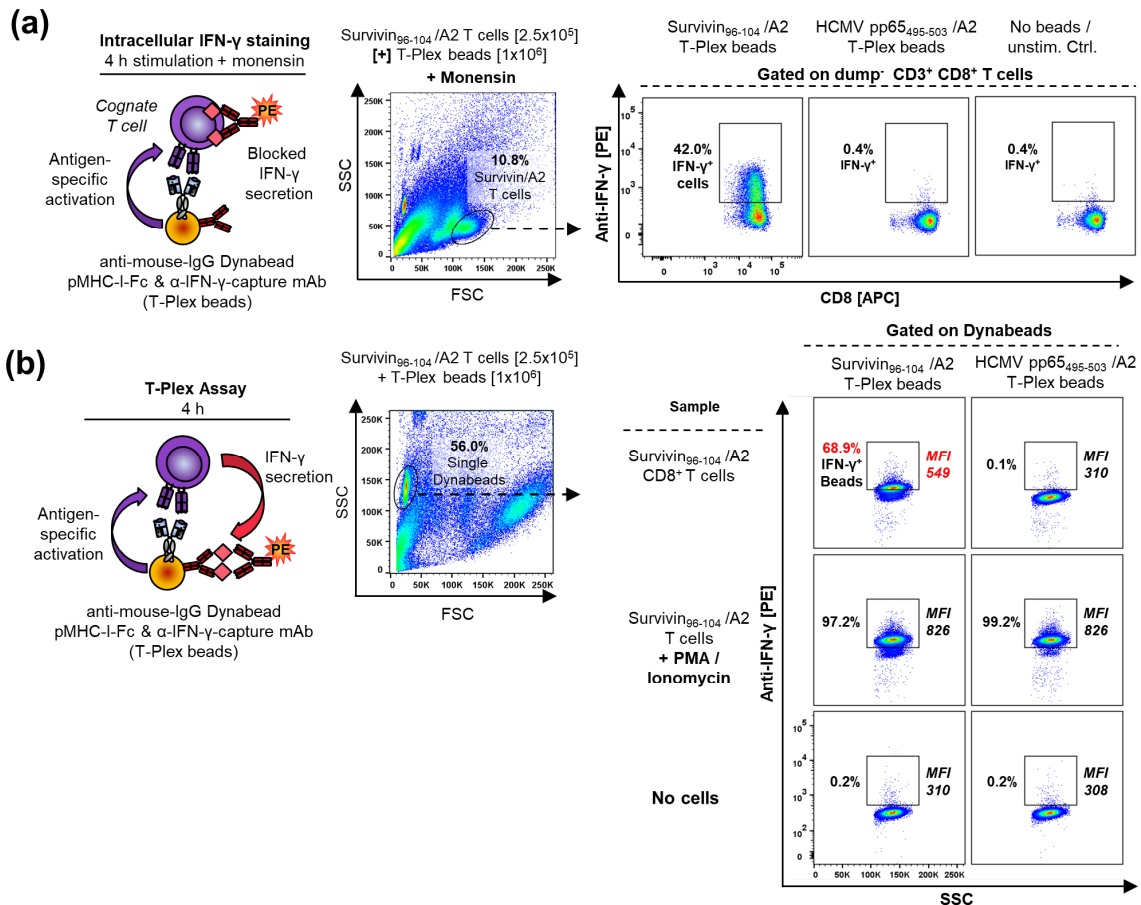


**Supplementary Figure S5 | Successful production of Fc-free biotinylated monomeric pMHC-I (dt-SCT) using the 293-F system and its subsequent binding validation**

**(a) Monomeric pMHC-I biotin-tagged construct** consist of a single polypeptide chain, which comprises the pMHC-I complex as a disulfide-trapped single-chain-trimer (dt-SCT) fused to a His<sub>6</sub>-tag, triple FLAG-tag and a C-terminal AviTag. The monomeric pMHC-I construct is site-specifically biotinylated *in vivo* by co-expression with IgκL-BirA<sub>KDEL</sub> [8521.1]. pMHC-I-biotin monomers can be multimerized by the addition of streptavidin (SAV).

**(b) Affinity chromatography of biotinylated monomeric pMHC-I.** Monomeric dt-SCT Survivin/HLA-A2 [10469.1], Flu/HLA-A2 [10471.1] or HCMV/HLA-A2 [10473.1] were transiently co-expressed with IgκL-BirA<sub>KDEL</sub> [8521.1] using the 293-F system for 6 days. 293-F supernatants (CR) were purified using His Mag Sepharose Excel (GE Healthcare). Biotinylation of monomeric indicated pHLA-A2 constructs was confirmed by a gel-shift upon equimolar addition of SAV prior to SDS-PAGE analysis. Shown is a 10% SDS-PAGE under non-reducing conditions after Coomassie staining.

**(c) Detection of virus-specific T cell populations within healthy donor PBMC by in-house produced pMHC-I multimers.** PBMC of cryopreserved HLA-A2<sup>+</sup> healthy donor #6691 were analyzed by indicated pHLA-A2 pentamers (Prolimmune) as well as own multimers assembled with streptavidin-APC and the pHLA-A2\*-Fc construct backbone with Fc-cleaved off (monomeric HCMV/HLA-A2\* [11097.1], Survivin/HLA-A2\* [11290.1], Flu/HLA-A2\* [11291.1]) or monomeric pHLA-A2 construct backbone Survivin/HLA-A2 [10469.1], Flu/HLA-A2 [10471.1] or HCMV/HLA-A2 [10473.1]. pMHC-I multimer staining was performed at 10 μg/mL in the presence of 50 nM dasatinib. The frequency of multimer<sup>+</sup> cells within the CD3<sup>+</sup> T cell population is shown. M: marker; FT: Flow-through.

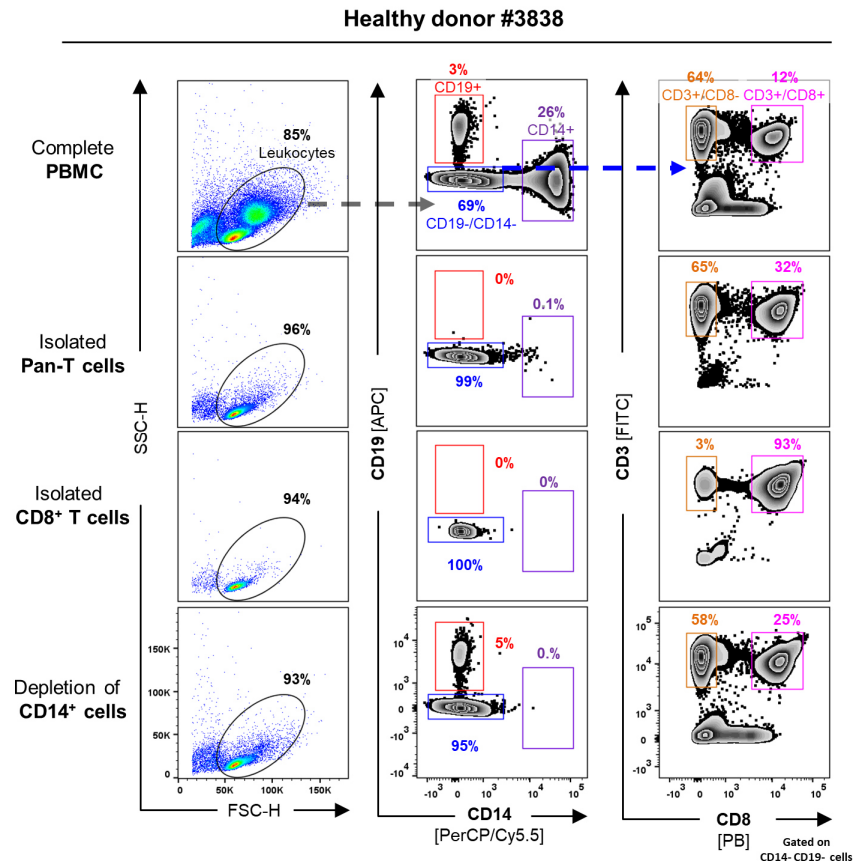


**Supplementary Figure S6 | Dynabead pilot experiment — Detection of an antigen-specific T cell response by analyzing IFN- $\gamma$  load on aAPCs with IFN- $\gamma$  capture capacity**

**(a & b)**  $\alpha$ M-IgG-Dynabeads (M450, 4.5  $\mu$ m) were loaded with  $\alpha$ -IFN- $\gamma$  mAb (clone NIB42) and indicated purified pMHC-I-Fc in a 3 to 2 ratio (T-Plex beads).

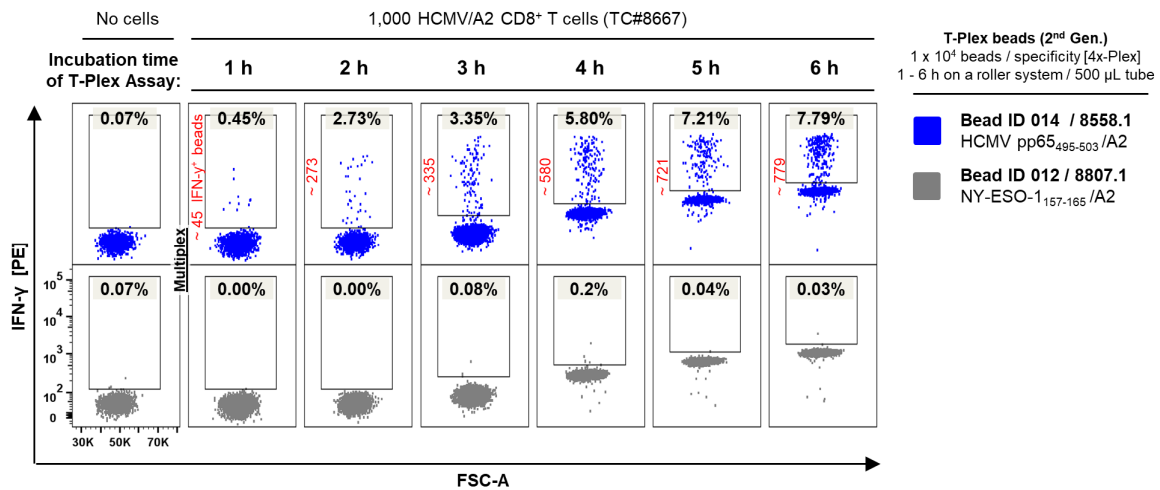
**(a) Detection of a T-Plex bead-based antigen-specific T cell response by ICS.** Survivin<sub>96-104</sub>/A2-specific CD8<sup>+</sup> T cells (Sur/A2 T cells) were separately co-cultured for 4 h with cognate or control T-Plex beads (E:T = 1:4) in individual wells of a 96-well U-bottom in the presence of monensin to ensure intracellular cytokine accumulation. Stimulation of the Sur/A2 CD8<sup>+</sup> T cell line is shown by induction of cytokine expression as analyzed by intracellular staining (ICS).

**(b) Corresponding T-Plex Assay readout.** Sur/A2-specific CD8<sup>+</sup> T cells were co-cultured with T-Plex Dynabeads as in (a) but in the absence of monensin to allow for cytokine secretion. After 4 h incubation the cell/bead mix was stained with  $\alpha$ -IFN- $\gamma$ -PE detection mAb (clone 4S.B3) and analyzed by FACS (BD FACS Canto II). Shown is the fraction and MFI of IFN- $\gamma$ -loaded cognate or control T-Plex beads. To assess the maximal IFN- $\gamma$ -binding capacity of the T-Plex beads, T cells were additionally stimulated using PMA and Ionomycin. MFI: Median fluorescent intensity.



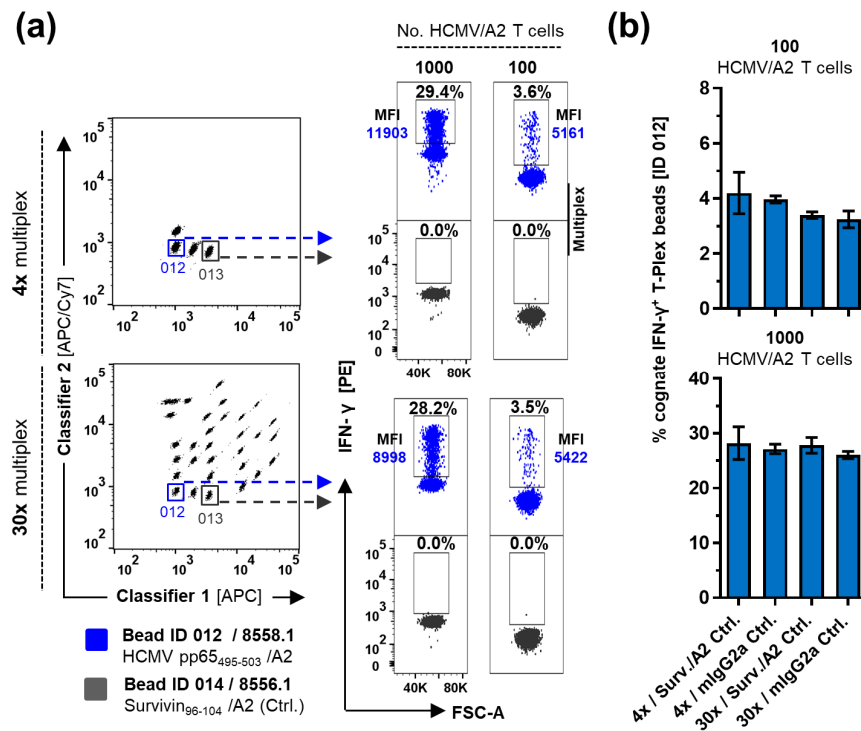
**Supplementary Figure S7 | Healthy donor #3838 after MACS-based sample preparation (Linked to Figure 4.12)**

Shown is the cell composition of total PBMC derived from healthy donor #3838 and after the indicated MACS-based sample preparations



**Supplementary Figure S8 | Time course of the T-Plex Assay**

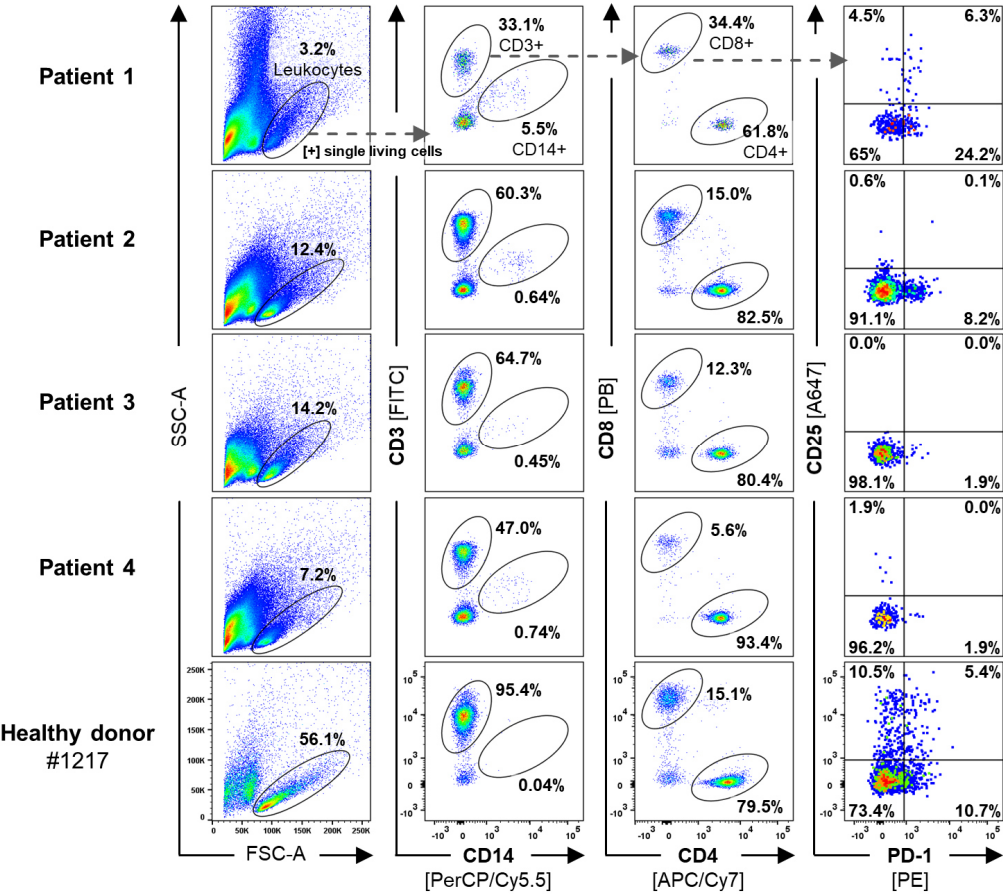
pMHC-I-Fc loaded 2<sup>nd</sup> generation T-Plex beads (10,000 beads per T-Plex bead ID / T cell epitope) were combined with 1,000 cells of the HCMV pp65<sub>495-503</sub>/A2-specific CD8<sup>+</sup> T cell line #8667 (HCMV/A2 T cells). The T-Plex Assay was performed in a 500  $\mu$ L tube rotating at 37°C for 1 – 6 h at 40 rpm as shown in the figure. The presence of a T cell line was indicated by the appearance of an IFN- $\gamma$ <sup>+</sup> subpopulation of cognate T-Plex beads. In this experiment four different color regions (Bead ID: 012, 013, 014, 018) of 2<sup>nd</sup> generation T-Plex beads were loaded with a defined set of pHLA-A2-Fc molecules (construct IDs: 8557.1 / 8558.1 / 8804.1 / 8807.1). Shown is only the IFN- $\gamma$  signal of the cognate HCMV/A2 T-Plex beads ID 14 (blue) and one representative corresponding control bead signal ID-18 (grey). Pairs of upper and lower FACS plots represent data analysis from the same reaction / bead mix (multiplex detection).



**Supplementary Figure S9 | The fraction of IFN-γ<sup>+</sup> T-Plex beads upon cognate T cell interaction is not influenced by the number of irrelevant bystander T-Plex beads**

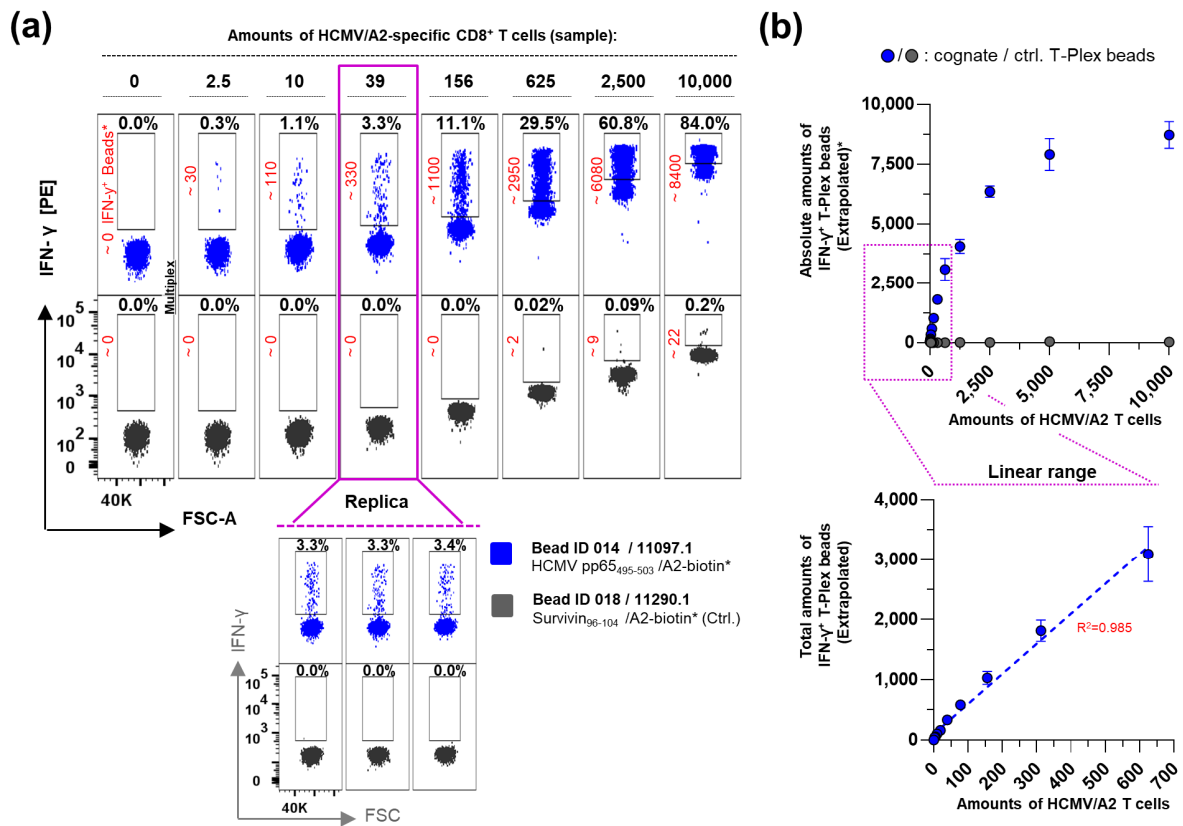
2<sup>nd</sup> generation (IFN-γ-capture mAb (MD-1) / rat α-mlgG2a-Fc mAb (RMG2a-62) T-Plex beads with the position ID 012 were loaded with HCMV pp65<sub>495-503</sub>/HLA-A2-Fc [8558.1] and with combined either 3 (4x multiplex) or 29 (30x multiplex) different T-Plex bead species previously loaded with Survivin<sub>96-104</sub>/HLA-A2-Fc [8556.1], or alternatively with mlgG2a isotype control mAb [MOPC-173] serving as control. T-Plex beads (10,000 beads per T-Plex bead ID) were combined either with 100 or 1,000 cells of the HCMV pp65<sub>495-503</sub>/A2-specific CD8<sup>+</sup> T cell line #5561 (HCMV/A2 T cells) in 0.5 mL tubes. Tubes were shortly centrifuged and rotated for 5 h at 60 rpm and 37°C. All conditions were performed in triplicates. **(a)** Shown is the IFN-γ signal of the cognate HCMV/A2 T-Plex beads ID 12 (blue) loaded with HCMV/A2-Fc and one representative corresponding control-bead signal ID-14 (grey) loaded with Survivin/A2-Fc. Pairs of upper and lower FACS-plots represent data analysis from the same reaction / bead mix. **(b)** Summarizing bar diagrams showing the fraction of cognate IFN-γ-loaded (IFN-γ<sup>+</sup>) T-Plex beads depending on the sample input of HCMV/A2 T cells and indicated T-Plex bead pools.

Supplementary Figures



**Supplementary Figure S10 | | Cancer patient peripheral blood immune cells composition and CD25 and PD-1 expression profile of the CD8<sup>+</sup> T cell population one day after thawing**

Shown is the cell composition of thawed PBMC from cryopreserved stocks from the indicated cancer patients that were rested for 1 day as well as PBMC derived from one healthy donor that have been cultured for 3 days prior to analysis.

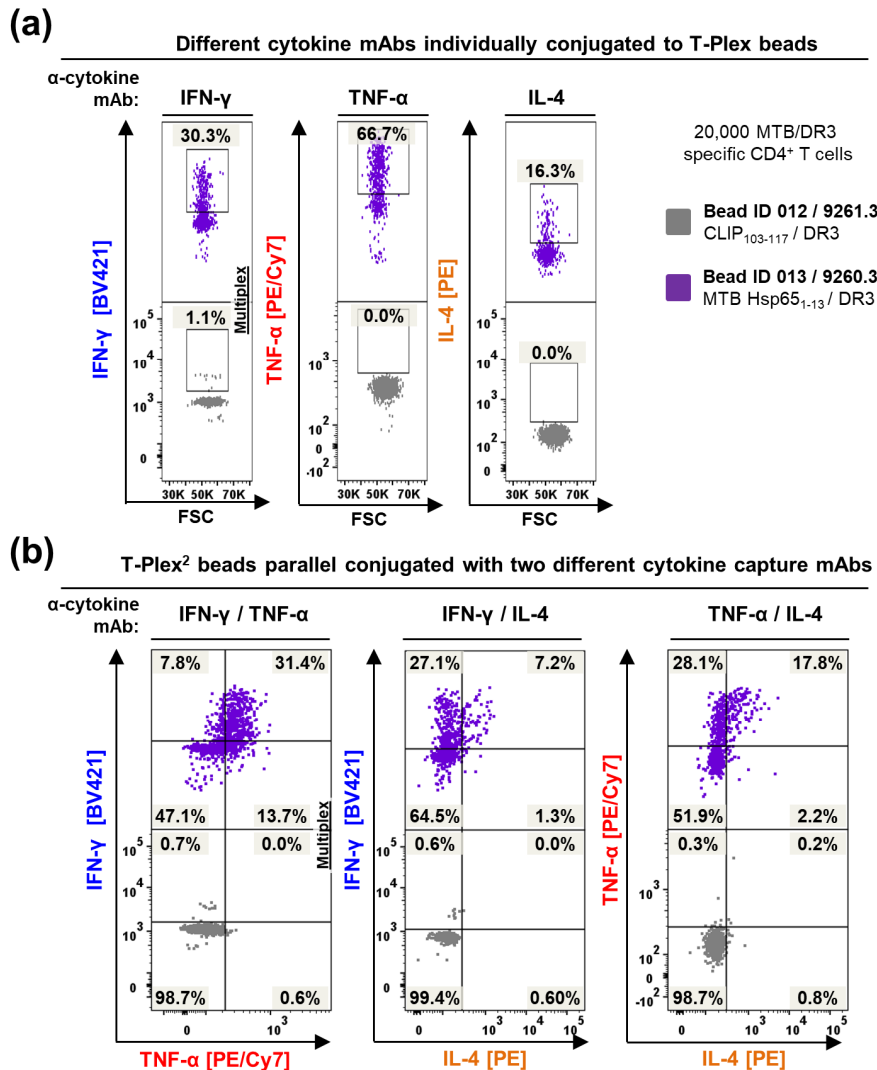


**Supplementary Figure S11 | Highly sensitive detection of HCMV/A2-specific T cells by streptavidin / IFN- $\gamma$ -capture mAb conjugated T-Plex beads loaded with cognate monomeric biotinylated pMHC-I**

**(a) Assessment of diluting amounts of antigen-specific T cells by SA $\nu$ /IFN $\gamma$ -mAb based T-Plex beads.**

Four different Luminex bead species (ID: 012, 013, 014, 018) were covalently conjugated with streptavidin (SA $\nu$ ) and IFN- $\gamma$  capture mAb in a 1:1 ratio and were subsequently loaded either with purified monomeric, Fc-cleaved, biotinylated cognate HCMV/A2\* [11097.1] or irrelevant pHLA-I [11290.1 / 11291.1 / 11292.1]. Assembled T-Plex beads were combined in 0.5 mL tubes with a two-fold serial dilution of HCMV pp65<sub>495-503</sub> / A2-specific CD8<sup>+</sup> T cell line #5561 (HCMV/A2 T cells) ranging from 10,000 to ~2.5 cells. Combined cell sample and T-Plex beads were centrifuged for 5 min at 2500 rpm prior to rolling at 60 rpm for 5 h at 37°C. All conditions were performed in triplicates. Shown is one representative IFN- $\gamma$  signal of the cognate HCMV/A2 T-Plex beads (blue) and one-out-of-three corresponding control bead signals (grey) as well as a selective triplicate of one cell dilution. Pairs of upper and lower FACS-plots represent data analysis from the same reaction. Extrapolated total amounts of IFN- $\gamma$ <sup>+</sup> T-Plex beads are shown in red numbers.

**(b) Corresponding T-Plex Assay linear range assessment and inter experimental reproducibility.** Amounts of total HCMV/A2 T cells derived from counting chamber-based calculations is plotted against extrapolated total amounts IFN- $\gamma$ <sup>+</sup> T-Plex beads. Linear regression is shown through linear points only.



**Supplementary Figure S12 | Detection of an antigen-specific CD4<sup>+</sup> T cell line using T-Plex beads with various cytokine capture capacities**

**(a) Detection of different cytokines by the T-Plex beads platform:** T-Plex beads were assembled using covalently conjugated  $\alpha$ -IFN- $\gamma$  capture mAb (clone MD-1) and monoclonal  $\alpha$ -mIgG2a (RMG2a-62) at a 60% to 40% ratio. Alternatively, the  $\alpha$ -IFN- $\gamma$  mAb was replaced by cytokine capture mAbs binding to IL-4 (8D4-8) or TNF- $\alpha$  (Mab 1). Subsequently, pMHC-II-loaded T-Plex bead pools on the basis of different cytokine mAb were loaded with MTB/DR3-Fc [9260.3] (purple / cognate) or CLIP/DR3-Fc [9261.3] (grey / control) and were co-cultured with 20,000 cells of the MTB Hsp65<sub>1-13</sub>/ DR3-specific CD4<sup>+</sup> T cell clone RP15.1.1 (MTB/DR3 T cells). The T-Plex Assay was performed in 500  $\mu$ L tubes, rolling at 60 rpm, 37°C for 5 h using 10,000 beads per T cell antigen. After the T-Plex reaction, the T-Plex beads were stained with the corresponding cytokine detection mAbs conjugated to the indicated fluorochromes and finally analyzed by a BD FACS Canto II. Pairs of upper and lower plots represent data analysis from the same reaction.

**(b) T-Plex<sup>2</sup> Assay proof-of-principle:** T-Plex<sup>2</sup> beads were assembled using covalently conjugated paired combinations of IFN- $\gamma$ , TNF- $\alpha$  and IL-4 capture mAbs (each 3/10 (30% of the total Luminex Bead protein binding capacity) and monoclonal  $\alpha$ -mIgG2a (2/5 [40%]). pMHC-II-loaded T-Plex<sup>2</sup> beads were incubated with MTB/DR3 T cells and the T-Plex Assay was performed as described above. Next, T-Plex<sup>2</sup> beads were stained with the corresponding cytokine detection mAbs conjugated to different fluorochromes as described in the figure and analyzed by a BD FACS Canto II. Pairs of upper and

## Supplementary Tables

**Supplementary Table S1 | Production efficiencies of *in vivo* biotinylated pHLA-A2-\*Fc constructs across various mammalian TGE systems**

Construct ID:	Structure	Allele	Antigen	TGE System	Purification system	Production efficiency [ $\mu\text{g}$ yield / mL culture vol.]:
11097.1 [+] 8521.1	pMHC-I-His <sub>8</sub> -tag-AviTag-FIIa-CS (2x)-mIgG2a-Fc [+] IgkL-BirA <sub>KDEL</sub> for <i>in vivo</i> biotinylation	HLA-A2	HCMV pp65 495–503	CHO-S / PEI / ProCHO-4	His Mag Sepharose Excel	13.0
11290.1 [+] 8521.1		HLA-A2	Survivin 96–104 / T97M			14.1
11291.1 [+] 8521.1		HLA-A2	Flu A MP 58–66			7.8
11292.1 [+] 8521.1		HLA-A2	EBV BMLF-1 259–267			7.6
11097.1 [+] 8521.1	pMHC-I-His <sub>8</sub> -tag-AviTag-FIIa-CS (2x)-mIgG2a-Fc [+] IgkL-BirA <sub>KDEL</sub> for <i>in vivo</i> biotinylation	HLA-A2	HCMV pp65 495–503	ExpCHO-S system	His Mag Sepharose Excel	58.0
11290.1 [+] 8521.1		HLA-A2	Survivin 96–104 / T97M			74.0
11291.1 [+] 8521.1		HLA-A2	Flu A MP 58–66			32.0
11292.1 [+] 8521.1		HLA-A2	EBV BMLF-1 259–267			13.0
11097.1 [+] 8521.1	pMHC-I-His <sub>8</sub> -tag-AviTag-FIIa-CS (2x)-mIgG2a-Fc [+] IgkL-BirA <sub>KDEL</sub> for <i>in vivo</i> biotinylation	HLA-A2	HCMV pp65 495–503	293-F / 293-Medium 293-free agent	His Mag Sepharose Excel	33.9
11290.1 [+] 8521.1		HLA-A2	Survivin 96–104 / T97M			34.3
11291.1 [+] 8521.1		HLA-A2	Flu A MP 58–66			21.5
11292.1 [+] 8521.1		HLA-A2	EBV BMLF-1 259–267			9.9
11097.1 [+] 8521.1	pMHC-I-His <sub>8</sub> -tag-AviTag-FIIa-CS (2x)-mIgG2a-Fc [+] IgkL-BirA <sub>KDEL</sub> for <i>in vivo</i> biotinylation	HLA-A2	HCMV pp65 495–503	Exp293-F system	His Mag Sepharose Excel	56.0
11290.1 [+] 8521.1		HLA-A2	Survivin 96–104 / T97M			83.0
11291.1 [+] 8521.1		HLA-A2	Flu A MP 58–66			22.0
11292.1 [+] 8521.1		HLA-A2	EBV BMLF-1 259–267			16.0

**Supplementary Table S2 | Production efficiencies of *in vivo* biotinylated monomeric Fc-free pHLA-A2 constructs using the 293-F TGE system**

Construct ID:	Structure	Allele	Antigen	TGE System	Purification system	Production efficiency [ $\mu\text{g}$ yield / mL culture vol.]:
10469.1 [+] 8521.1	pMHC-I-His <sub>8</sub> -tag-FLAG-tag (3x)-AviTag [+] IgkL-BirA <sub>KDEL</sub> for <i>in vivo</i> biotinylation	HLA-A2	Survivin 96–104 / T97M	293-F / 293-Medium 293-free agent	His Mag Sepharose Excel	17.3
10471.1 [+] 8521.1		HLA-A2	Flu A MP 58–66			10.8
10473.1 [+] 8521.1		HLA-A2	HCMV pp65 495–503			23.3

**Supplementary Table S3 | Production efficiencies of various peptide-HLA-II-pCC-Fc constructs across different mammalian TGE systems and purification methods**

Construct ID:	Structure	Allele	Antigen	TGE System	Purification system	Production efficiency [ $\mu\text{g}/\text{mL}$ (culture)]:
8634.1 [+] 8746.1	px-EK-HLA-II $\beta$ -chain-pCC-basic-Fc-His <sub>6</sub> tag [+] HLA-II $\alpha$ -chain-pCC-acidic-Fc-tandem STag	HLA-DR3	CLIP 103–117	ExpiCHO-S TGE System	StrepTactin High Capacity resin-filled column	4.2
9221.1 [+] 8746.1	px-FII-HLA-II $\beta$ -chain-pCC-basic-Fc-His <sub>6</sub> tag [+] HLA-II $\alpha$ -chain-pCC-acidic-Fc-tandem STag	HLA-DR3	CLIP 103–117			3.7
9261.3	px-EK-HLA-II $\beta$ -chain-pCC-basic-Fc-His <sub>6</sub> tag-AviTag T2A HLA-II $\alpha$ -chain-pCC-acidic-Fc-tandem STag	HLA-DR3	CLIP 103–117			6.1
10338.2	px-FII-HLA-II $\beta$ -chain-pCC-basic-Fc-His <sub>6</sub> tag-AviTag T2A HLA-II $\alpha$ -chain-pCC-acidic-Fc-tandem STag	HLA-DR3	CLIP 103–117			5.1
9062.1 [+] 8746.1	pHLA-II $\beta$ -chain-pCC-basic-Fc-His <sub>6</sub> tag [+] HLA-II $\alpha$ -chain-pCC-acidic-Fc-tandem STag	HLA-DR3	MTB Hsp65 1–13			3.5
9260.3	pHLA-II $\beta$ -chain-pCC-basic-Fc-His <sub>6</sub> tag-AviTag T2A HLA-II $\alpha$ -chain-pCC-acidic-Fc-tandem STag	HLA-DR3	MTB Hsp65 1–13			6.0
9221.1 [+] 10092.1 [+] 8521.1	px-FII-HLA-II $\beta$ -chain-pCC-basic-Fc-His <sub>6</sub> tag [+] HLA-II $\alpha$ -chain-pCC-acidic-Fc-AviTag [+] IgkL-BirA <sub>KDEL</sub> for <i>in vivo</i> biotinylation	HLA-DR3	CLIP 103–117	CHO-S / PEI / ProCHO-4	Ni-NTA Superflow resin-filled column	0.1
9062.1 [+] 10092.1 [+] 8521.1	pHLA-II $\beta$ -chain-pCC-basic-Fc-His <sub>6</sub> tag [+] HLA-II $\alpha$ -chain-pCC-acidic-Fc-AviTag [+] IgkL-BirA <sub>KDEL</sub> for <i>in vivo</i> biotinylation	HLA-DR3	MTB Hsp65 1–13			0.1
9260.3 [+] 8521.1	pHLA-II $\beta$ -chain-pCC-basic-Fc-His <sub>6</sub> tag-AviTag T2A HLA-II $\alpha$ -chain-pCC-acidic-Fc-tandem STag [+] IgkL-BirA <sub>KDEL</sub> for <i>in vivo</i> biotinylation	HLA-DR3	MTB Hsp65 1–13			0.3
9261.3 [+] 8521.1	px-EK-HLA-II $\beta$ -chain-pCC-basic-Fc-His <sub>6</sub> -tag/ AviTag T2A HLA-II $\alpha$ -chain-pCC-acidic-Fc-tandem STag [+] IgkL-BirA <sub>KDEL</sub> for <i>in vivo</i> biotinylation	HLA-DR3	CLIP 103–117			0.3
10320'.1 [+] 8521.1	pHLA-II $\beta$ -chain-pCC-basic-Fc-His <sub>6</sub> tag-AviTag T2A HLA-II $\alpha$ -chain-pCC-acidic-Fc-tandem STag [+] IgkL-BirA <sub>KDEL</sub> for <i>in vivo</i> biotinylation	HLA-DR3	HCMV pp65 510–522			0.5
10338.2 [+] 8521.1	px-FII-HLA-II $\beta$ -chain-pCC-basic-Fc-His <sub>6</sub> tag-AviTag T2A HLA-II $\alpha$ -chain-pCC-acidic-Fc-tandem STag [+] IgkL-BirA <sub>KDEL</sub> for <i>in vivo</i> biotinylation	HLA-DR3	CLIP 103–117			0.12
9062.1 [+] 10092.1 [+] 8521.1	pHLA-II $\beta$ -chain-pCC-basic-Fc-His <sub>6</sub> tag [+] HLA-II $\alpha$ -chain-pCC-acidic-Fc-AviTag [+] IgkL-BirA <sub>KDEL</sub> for <i>in vivo</i> biotinylation	HLA-DR3	MTB Hsp65 1–13	293-F / 293 expression medium / 293-free transfection agent	Ni-NTA Superflow resin-filled column	0.3
9221.1 [+] 10092.1 [+] 8521.1	px-FII-HLA-II $\beta$ -chain-pCC-basic-Fc-His <sub>6</sub> tag [+] HLA-II $\alpha$ -chain-pCC-acidic-Fc-AviTag [+] IgkL-BirA <sub>KDEL</sub> for <i>in vivo</i> biotinylation	HLA-DR3	CLIP 103–117			2.6
9066.1 [+] 10092.1 [+] 8521.1	pHLA-II $\beta$ -chain-pCC-basic-Fc-His <sub>6</sub> tag [+] HLA-II $\alpha$ -chain-pCC-acidic-Fc-AviTag [+] IgkL-BirA <sub>KDEL</sub> for <i>in vivo</i> biotinylation	HLA-DR3	HCMV pp65 510–522			0.3
9260.3 [+] 8521.1	pHLA-II $\beta$ -chain-pCC-basic-Fc-His <sub>6</sub> tag-AviTag T2A HLA-II $\alpha$ -chain-pCC-acidic-Fc-tandem STag [+] IgkL-BirA <sub>KDEL</sub> for <i>in vivo</i> biotinylation	HLA-DR3	MTB Hsp65 1–13			0.2

Shown pHLA-II-pCC-Fc constructs were produced and purified using the indicated mammalian cell transient gene expression system (TGE) as described in the material and methods section (**Section 2.3**). The production efficiency has been calculated based on the obtained yield of purified protein [ $\mu\text{g}$ ] of a given construct divided by the TGE culture volume [mL] used for the corresponding purification. HLA-DR3: HLA-DRB1\*03:01 / DRA\*01; pCC-acidic / basic-Fc: parallel coiled-coil basic / acidic heterodimerization domain followed by the murine IgG2a-Fc (Hinge-CH2-CH3); px-FII: peptide ligand followed by a C-terminal linker bearing a thrombin cleavage site. px-EK: peptide ligand followed by C-terminal linker bearing an enterokinase cleavage site

## References

1. Murphy KM, Travers P, Walport M, Janeway C. 2011. *Janeway's Immunobiology*. New York: Garland Science. 8th ed.
2. Vesely MD, Kershaw MH, Schreiber RD, Smyth MJ. 2011. Natural Innate and Adaptive Immunity to Cancer. *Annu. Rev. Immunol.* 29(1):235–71
3. Bendelac A, Savage PB, Teyton L. 2007. The Biology of NKT Cells. *Annu. Rev. Immunol.* 25(1):297–336
4. Chien Y, Meyer C, Bonneville M. 2014.  $\gamma\delta$  T Cells: First Line of Defense and Beyond . *Annu. Rev. Immunol.* 32(1):121–55
5. Pandya PH, Murray ME, Pollok KE, Renbarger JL. 2016. The Immune System in Cancer Pathogenesis: Potential Therapeutic Approaches. *J. Immunol. Res.* 2016:4273943
6. Qi Q, Liu Y, Cheng Y, Glanville J, Zhang D, et al. 2014. Diversity and clonal selection in the human T-cell repertoire. *Proc. Natl. Acad. Sci.* 111(36):13139–44
7. Klein L, Kyewski B, Allen PM, Hogquist KA. 2014. Positive and negative selection of the T cell repertoire: What thymocytes see (and don't see). *Nat. Rev. Immunol.* 14(6):377–91
8. Nemazee D. 2017. Mechanisms of central tolerance for B cells. *Nat. Rev. Immunol.* 17(5):281–94
9. Rossjohn J, Gras S, Miles JJ, Turner SJ, Godfrey DI, McCluskey J. 2015. T Cell Antigen Receptor Recognition of Antigen-Presenting Molecules. *Annu. Rev. Immunol.* 33(1):169–200
10. Roche PA, Furuta K. 2015. The ins and outs of MHC class II-mediated antigen processing and presentation. *Nat. Rev. Immunol.* 15(4):203–16
11. Blum J, Wearsch P, Cresswell P. 2013. Pathways of antigen processing. *Annu. Rev. Immunol.* 31:443–73
12. Romieu-Mourez R, François M, Boivin M, Stagg J, Galipeau J. 2007. Regulation of MHC class II expression and antigen processing in murine and human mesenchymal stromal cells by IFN- $\gamma$ , TGF- $\beta$ , and cell density. *J Immunol.* 179(3):1549–58
13. Geppert T, Lipsky P. 1985. Antigen presentation by interferon- $\gamma$ -treated endothelial cells and fibroblasts: differential ability to function as antigen-presenting cells despite comparable Ia expression. *J Immunol.* 135(6):3750–62
14. Hemon P, Jean-Louis F, Ramgolam K, Brignone C, Viguier M, et al. 2011. MHC Class II Engagement by Its Ligand LAG-3 (CD223) Contributes to Melanoma Resistance to Apoptosis. *J. Immunol.* 186(9):5173–83
15. Wieczorek M, Abualrous ET, Sticht J, Álvaro-Benito M, Stolzenberg S, et al. 2017. Major histocompatibility complex (MHC) class I and MHC class II proteins: Conformational plasticity in antigen presentation. *Front. Immunol.* 8(MAR):1–16
16. Madden DR. 1995. The Three-Dimensional Structure of Peptide-MHC Complexes. *Annu Rev Immunol.* 13:587–622
17. Rammensee HG, Falk K, Rötzschke O. 1993. Peptides Naturally Presented by MHC Class I Molecules. *Annu. Rev. Immunol.* 11(1):213–44
18. Kurts C, Robinson BWS, Knolle PA. 2010. Cross-priming in health and disease. *Nat. Rev. Immunol.* 10(6):403–14
19. Crotzer VL, Blum JS. 2010. Autophagy and adaptive immunity. *Immunology.* 131(1):9–17
20. Yewdell JW. 2011. DRiPs solidify: Progress in understanding endogenous MHC class I antigen processing. *Trends Immunol.* 32(11):548–58
21. Bard J, Goodall E, Greene E, Jonsson E, Dong K, Martin A. 2018. Structure and Function of the 26S Proteasome. *Annu Rev Biochem.* 87:697–724
22. Kincaid EZ, Che JW, York I, Escobar H, Reyes-Vargas E, et al. 2012. Mice completely lacking immunoproteasomes show major changes in antigen presentation. *Nat. Immunol.* 13(2):129–35
23. Seifert U, Bialy L, Ebstein F, Bech-Otschir D, Voigt A, et al. 2010. Immunoproteasomes preserve protein homeostasis upon interferon-induced oxidative stress. *Cell.* 142(4):613–24
24. Gaczynska M, Rock K, AL G. 1993. Gamma-interferon and expression of MHC genes regulate peptide hydrolysis by proteasomes. *Nature.* 365(6443):264–67
25. Sijts EJAM, Kloetzel PM. 2011. The role of the proteasome in the generation of MHC class I ligands and immune responses. *Cell. Mol. Life Sci.* 68(9):1491–1502
26. Kobayashi KS, Van Den Elsen PJ. 2012. NLRC5: A key regulator of MHC class I-dependent immune responses. *Nat. Rev. Immunol.* 12(12):813–20
27. Koopmann JO, Post M, Neefjes JJ, Hämmerling GJ, Momburg F. 1996. Translocation of long peptides by transporters associated with antigen processing (TAP). *Eur. J. Immunol.* 26(8):1720–28
28. Reits E, Griekspoor A, Neijssen J, Groothuis T, Jalink K, et al. 2003. Peptide Diffusion, Protection, and Degradation in Nuclear and Cytoplasmic Compartments before Antigen Presentation by MHC Class I. *Immunity.* 18(1):97–108
29. Bles A, Januliene D, Hofmann T, Koller N, Schmidt C, et al. 2017. Structure of the human MHC-I peptide-loading complex. *Nature.* 551(7681):525–28

## References

30. Wearsch PA, Cresswell P. 2007. Selective loading of high-affinity peptides onto major histocompatibility complex class I molecules by the tapasin-ERp57 heterodimer. *Nat. Immunol.* 8(8):873–81
31. Peaper D, Cresswell P. 2008. The redox activity of ERp57 is not essential for its functions in MHC class I peptide loading. *Proc. Natl. Acad. Sci. U. S. A.* 105(30):10477–82
32. Fiset O, Wingbermühle S, Tampé R, Schäfer L. 2016. Molecular mechanism of peptide editing in the tapasin-MHC I complex. *Sci Rep.* Jan 12(6):19085
33. Trombetta ES, Mellman I. 2005. Cell Biology of Antigen Processing in Vitro and in Vivo. *Annu. Rev. Immunol.* 23(1):975–1028
34. Landsverk OJB, Bakke O, Gregers TF. 2009. MHC II and the endocytic pathway: Regulation by invariant chain. *Scand. J. Immunol.* 70(3):184–93
35. Denzin L, Cresswell P. 1995. HLA-DM induces CLIP dissociation from MHC class II alpha beta dimers and facilitates peptide loading. *Cell.* 82(1):155–65
36. Kropshofer H, Vogt AB, Moldenhauer G, Hammer J, Blum JS, Hämmerling GJ. 1996. Editing of the HLA-DR-peptide repertoire by HLA-DM. *EMBO J.* 15(22):6144–54
37. Brocke P, Garbi N, Momburg F, Hämmerling GJ. 2002. HLA-DM, HLA-DO and tapasin: Functional similarities and differences. *Curr. Opin. Immunol.* 14(1):22–29
38. Mellins ED, Stern LJ. 2014. HLA-DM and HLA-DO, key regulators of MHC-II processing and presentation. *Curr. Opin. Immunol.* 26(1):115–22
39. Malissen B, Bongrand P. 2015. Early T Cell Activation: Integrating Biochemical, Structural, and Biophysical Cues. *Annu. Rev. Immunol.* 33(1):539–61
40. Gaud G, Lesourne R, Love PE. 2018. Regulatory mechanisms in T cell receptor signalling. *Nat. Rev. Immunol.* 18(8):485–97
41. Chen L, Flies DB. 2013. Molecular mechanisms of T cell co-stimulation and co-inhibition. *Nat. Rev. Immunol.* 13(4):227–42
42. Garcia KC, Degano M, Stanfield RL, Brunmark A, Jackson MR, et al. 1996. An alpha beta T Cell Receptor Structure at 2.5 Å and Its Orientation in the TCR-MHC Complex. *Science.* 274(5285):209–19
43. Wang J, Reinherz E. 2012. The structural basis of  $\alpha\beta$  T-lineage immune recognition: TCR docking topologies, mechanotransduction, and co-receptor function. *Immunol. Rev.* 250(1):102–19
44. Wu P, Zhang T, Liu B, Fei P, Cui L, et al. 2019. Mechano-regulation of Peptide-MHC Class I Conformations Determines TCR Antigen Recognition. *Mol. Cell.* 73(5):1015-1027.e7
45. Chakraborty AK, Weiss A. 2014. Insights into the initiation of TCR signaling. *Nat. Immunol.* 15(9):798–807
46. Ward-Kavanagh LK, Lin WW, Šedý JR, Ware CF. 2016. The TNF Receptor Superfamily in Co-stimulating and Co-inhibitory Responses. *Immunity.* 44(5):1005–19
47. Boomer JS, Green JM. 2010. An enigmatic tail of CD28 signaling. *Cold Spring Harb. Perspect. Biol.* 2(8):
48. Zappasodi R, Merghoub T, Wolchok JD. 2018. Emerging Concepts for Immune Checkpoint Blockade-Based Combination Therapies. *Cancer Cell.* 33(4):581–98
49. Curtsinger JM, Mescher MF. 2010. Inflammatory cytokines as a third signal for T cell activation. *Curr. Opin. Immunol.* 22(3):333–40
50. Starbeck-Miller GR, Xue H-H, Harty JT. 2014. IL-12 and type I interferon prolong the division of activated CD8 T cells by maintaining high-affinity IL-2 signaling in vivo. *J. Exp. Med.* 211(1):105–20
51. Osborne LC, Abraham N. 2010. Regulation of memory T cells by  $\gamma\text{c}$  cytokines. *Cytokine.* 50(2):105–13
52. Fooksman DR, Vardhana S, Vasiliver-Shamis G, Liese J, Blair DA, et al. 2009. Functional Anatomy of T Cell Activation and Synapse Formation. *Annu. Rev. Immunol.* 28(1):79–105
53. Xie J, Tato CM, Davis MM. 2013. How the immune system talks to itself: The varied role of synapses. *Immunol. Rev.* 251(1):65–79
54. De La Roche M, Asano Y, Griffiths GM. 2016. Origins of the cytolytic synapse. *Nat. Rev. Immunol.* 16(7):421–32
55. Halle S, Halle O, Förster R. 2017. Mechanisms and Dynamics of T Cell-Mediated Cytotoxicity In Vivo. *Trends Immunol.* 38(6):432–43
56. Monks C, Freiberg B, Kupfer H, Sciaky N, Kupfer A. 1998. Three-dimensional segregation of supramolecular activation clusters in T cells. *Nature.* 395:82–86
57. Varma R, Campi G, Yokosuka T, Saito T, Dustin ML. 2006. T Cell Receptor-Proximal Signals Are Sustained in Peripheral Microclusters and Terminated in the Central Supramolecular Activation Cluster. *Immunity.* 25(1):117–27
58. Dustin ML, Groves JT. 2012. Receptor Signaling Clusters in the Immune Synapse. *Annu. Rev. Biophys.* 41(1):543–56
59. Hammer JA, Wang JC, Saeed M, Pedrosa AT. 2019. Origin, Organization, Dynamics, and Function of Actin and Actomyosin Networks at the T Cell Immunological Synapse. *Annu. Rev. Immunol.* 37(1):201–24
60. Ueda H, Morphew MK, McIntosh JR, Davis MM. 2011. CD4+ T-cell synapses involve multiple distinct stages. *Proc. Natl. Acad. Sci.*

- 108(41):17099–104
61. Huse M, Lillemeier BF, Kuhns MS, Chen DS, Davis MM. 2006. T cells use two directionally distinct pathways for cytokine secretion. *Nat. Immunol.* 7(3):247–55
  62. Depoil D, Zaru R, Guiraud M, Chauveau A, Harriague J, et al. 2005. Immunological synapses are versatile structures enabling selective T cell polarization. *Immunity.* 22(2):185–94
  63. Gunzer M, Schäfer A, Borgmann S, Grabbe S, Zänker KS, et al. 2000. Antigen presentation in extracellular matrix: Interactions of T cells with dendritic cells are dynamic, short lived, and sequential. *Immunity.* 13(3):323–32
  64. Stinchcombe JC, Griffiths GM. 2007. Secretory Mechanisms in Cell-Mediated Cytotoxicity. *Annu. Rev. Cell Dev. Biol.* 23(1):495–517
  65. Lopez JA, Brennan AJ, Whisstock JC, Voskoboinik I, Trapani JA. 2012. Protecting a serial killer: Pathways for perforin trafficking and self-defence ensure sequential target cell death. *Trends Immunol.* 33(8):406–12
  66. Wiedemann A, Depoil D, Faroudi M, Valitutti S. 2006. Cytotoxic T lymphocytes kill multiple targets simultaneously via spatiotemporal uncoupling of lytic and stimulatory synapses. *Proc. Natl. Acad. Sci.* 103(29):10985–90
  67. Purbhoo MA, Irvine DJ, Huppa JB, Davis MM. 2004. T cell killing does not require the formation of a stable mature immunological synapse. *Nat. Immunol.* 5(5):524–30
  68. Faroudi M, Utzny C, Salio M, Cerundolo V, Guiraud M, et al. 2003. Lytic versus stimulatory synapse in cytotoxic T lymphocyte/target cell interaction: Manifestation of a dual activation threshold. *Proc. Natl. Acad. Sci.* 100(24):14145–50
  69. Halle S, Keyser KA, Stahl FR, Busche A, Marquardt A, et al. 2016. In Vivo Killing Capacity of Cytotoxic T Cells Is Limited and Involves Dynamic Interactions and T Cell Cooperativity. *Immunity.* 44(2):233–45
  70. Stinchcombe JC, Majorovits E, Bossi G, Fuller S, Griffiths GM. 2006. Centrosome polarization delivers secretory granules to the immunological synapse. *Nature.* 443(7110):462–65
  71. Steinman RM, Banchereau J. 2007. Taking dendritic cells into medicine. *Nature.* 449(7161):419–26
  72. Hammer GE, Ma A. 2013. Molecular Control of Steady-State Dendritic Cell Maturation and Immune Homeostasis. *Annu. Rev. Immunol.* 31(1):743–91
  73. Eisenbarth SC. 2019. Dendritic cell subsets in T cell programming: location dictates function. *Nat. Rev. Immunol.* 19(2):89–103
  74. Worbs T, Hammerschmidt SI, Förster R. 2017. Dendritic cell migration in health and disease. *Nat. Rev. Immunol.* 17(1):30–48
  75. Joffre OP, Segura E, Savina A, Amigorena S. 2012. Cross-presentation by dendritic cells. *Nat. Rev. Immunol.* 12(8):557–69
  76. Collin M, Bigley V. 2018. Human dendritic cell subsets: an update. *Immunology.* 154(1):3–20
  77. Borst J, Ahrends T, Båbala N, Melief CJM, Kastenmüller W. 2018. CD4+ T cell help in cancer immunology and immunotherapy. *Nat. Rev. Immunol.* 18(10):635–47
  78. Gardner A, Ruffell B. 2016. Dendritic Cells and Cancer Immunity. *Trends Immunol.* 37(12):855–65
  79. Mastelic-Gavillet B, Balint K, Boudousquie C, Gannon PO, Kandalaft LE. 2019. Personalized dendritic cell vaccines—recent breakthroughs and encouraging clinical results. *Front. Immunol.* 10(APR):
  80. Wimmers F, Schreiber G, Sköld AE, Figdor CG, De Vries IJM. 2014. Paradigm shift in dendritic cell-based immunotherapy: From in vitro generated monocyte-derived DCs to naturally circulating DC subsets. *Front. Immunol.* 5(APR):1–12
  81. Zhu J, Yamane H, Paul WE. 2010. Differentiation of Effector CD4 T Cell Populations. *Annu Rev Immunol.* 28:445–89
  82. Crotty S. 2014. T Follicular Helper Cell Differentiation, Function, and Roles in Disease. *Immunity.* 41(4):529–42
  83. Sakaguchi S, Miyara M, Costantino CM, Hafler DA. 2010. FOXP3+ regulatory T cells in the human immune system. *Nat. Rev. Immunol.* 10(7):490–500
  84. Quezada SA, Simpson TR, Peggs KS, Merghoub T, Vider J, et al. 2010. Tumor-reactive CD4+ T cells develop cytotoxic activity and eradicate large established melanoma after transfer into lymphopenic hosts. *J. Exp. Med.* 207(3):637–50
  85. Kreiter S, Vormehr M, van de Roemer N, Diken M, Löwer M, et al. 2015. Mutant MHC class II epitopes drive therapeutic immune responses to cancer. *Nature.* 520(7549):692–96
  86. Marshall NB, Swain SL. 2011. Cytotoxic CD4 T cells in antiviral immunity. *J. Biomed. Biotechnol.* 2011:954602
  87. Mosser DM, Edwards JP. 2008. Exploring the full spectrum of macrophage activation. *Nat. Rev. Immunol.* 8(12):958–69
  88. Vignali DAA, Collison LW, Workman CJ. 2008. How regulatory T cells work. *Nat. Rev. Immunol.* 8(7):523–32
  89. Campbell DJ, Koch MA. 2011. Phenotypical and functional specialization of FOXP3+ regulatory T cells. *Nat. Rev. Immunol.* 11(2):119–30
  90. Zhang N, Bevan MJ. 2011. CD8+ T Cells: Foot Soldiers of the Immune System. *Immunity.* 35(2):161–68

## References

91. Farber DL, Yudanin NA, Restifo NP. 2014. Human memory T cells: Generation, compartmentalization and homeostasis. *Nat. Rev. Immunol.* 14(1):24–35
92. Kumar B V., Connors TJ, Farber DL. 2018. Human T Cell Development, Localization, and Function throughout Life. *Immunity.* 48(2):202–13
93. Peter ME, Hadji A, Murmann AE, Brockway S, Putzbach W, et al. 2015. The role of CD95 and CD95 ligand in cancer. *Cell Death Differ.* 22(4):549–59
94. Castro F, Cardoso AP, Gonçalves RM, Serre K, Oliveira MJ. 2018. Interferon-gamma at the crossroads of tumor immune surveillance or evasion. *Front. Immunol.* 9(MAY):1–19
95. Kalliolias GD, Ivashkiv LB. 2016. TNF biology, pathogenic mechanisms and emerging therapeutic strategies. *Nat. Rev. Rheumatol.* 12(1):49–62
96. Carswell E, Old L, Kassel R, Green S, Fiore N, Williamson B. 1975. An endotoxin-induced serum factor that causes necrosis of tumors. *Proc. Natl. Acad. Sci. U. S. A.* 72(9):3666–70
97. Balkwill F. 2009. Tumour necrosis factor and cancer. *Nat Rev Cancer.* 9(5):361–71
98. Kaech SM, Cui W. 2012. Transcriptional control of effector and memory CD8+ T cell differentiation. *Nat Rev Immunol.* 12(11):749–61
99. Akondy RS, Johnson PLF, Nakaya HI, Edupuganti S, Mulligan MJ, et al. 2015. Initial viral load determines the magnitude of the human CD8 T cell response to yellow fever vaccination. *Proc. Natl. Acad. Sci. U. S. A.* 112(10):3050–55
100. Gattinoni L, Klebanoff C a, Restifo NP. 2012. Paths to stemness: building the ultimate antitumour T cell. *Nat. Rev. Cancer.* 12(10):671–84
101. Gattinoni L, Lugli E, Ji Y, Pos Z, Paulos CM, et al. 2011. A human memory T cell subset with stem cell-like properties. *Nat. Med.* 17(10):1290–97
102. Romero P, Zippelius A, Kurth I, Pittet MJ, Touvrey C, et al. 2007. Four functionally distinct populations of human effector-memory CD8+ T lymphocytes. *J. Immunol.* 178(7):4112–19
103. Moro-García MA, Alonso-Arias R, López-Larrea C. 2012. Molecular mechanisms involved in the aging of the T-cell immune response. *Curr. Genomics.* 13(8):589–602
104. Mueller SN, Mackay LK. 2016. Tissue-resident memory T cells: Local specialists in immune defence. *Nat. Rev. Immunol.* 16(2):79–89
105. McLane LM, Abdel-Hakeem MS, Wherry EJ. 2019. CD8 T Cell Exhaustion During Chronic Viral Infection and Cancer. *Annu. Rev. Immunol.* 37(1):457–95
106. Wherry EJ, Kurachi M. 2015. Molecular and cellular insights into T cell exhaustion. *Nat. Rev. Immunol.* 15(8):486–99
107. Crawford A, Angelosanto JM, Kao C, Doering TA, Odorizzi PM, et al. 2014. Molecular and Transcriptional Basis of CD4+ T Cell Dysfunction during Chronic Infection. *Immunity.* 40(2):289–302
108. Wherry EJ, Ha SJ, Kaech SM, Haining WN, Sarkar S, et al. 2007. Molecular Signature of CD8+ T Cell Exhaustion during Chronic Viral Infection. *Immunity.* 27(4):670–84
109. McKinney EF, Lee JC, Jayne DRW, Lyons PA, Smith KGC. 2015. T-cell exhaustion, co-stimulation and clinical outcome in autoimmunity and infection. *Nature.* 523(7562):612–16
110. Ribas A, Wolchok JD. 2018. Cancer immunotherapy using checkpoint blockade. *Science (80-. ).* 359(6382):1350–55
111. Rosenthal R, McGranahan N, Herrero J, Swanton C. 2017. Deciphering Genetic Intratumor Heterogeneity and Its Impact on Cancer Evolution. *Annu. Rev. Cancer Biol.* 1(1):223–40
112. Schreiber RD, Old LJ, Smyth MJ. 2011. Cancer immunoediting: Integrating the role of immunity in cancer suppression and promotion. *Science (80-. ).* 331(March):78
113. Reuschenbach M, Von Knebel Doeberitz M, Wentzensen N. 2009. A systematic review of humoral immune responses against tumor antigens. *Cancer Immunol. Immunother.* 58(10):1535–44
114. Fridman WH, Zitvogel L, Sautès-Fridman C, Kroemer G. 2017. The immune contexture in cancer prognosis and treatment. *Nat. Rev. Clin. Oncol.* 14(12):717–34
115. Chen DS, Mellman I. 2013. Oncology meets immunology: The cancer-immunity cycle. *Immunity.* 39(1):1–10
116. Rosenberg SA, Restifo NP. 2015. Adoptive cell transfer as personalized immunotherapy for human cancer. *Science.* 348(6230):62–68
117. June CH, O'Connor RS, Kawalekar OU, Ghassemi S, Milone MC. 2018. CAR T cell immunotherapy for human cancer. *Science.* 359(6382):1361–65
118. Hollingsworth RE, Jansen K. 2019. Turning the corner on therapeutic cancer vaccines. *npj Vaccines.* 4(1):1–10
119. Schumacher TN, Scheper W, Kvistborg P. 2018. Cancer Neoantigens. *Annu. Rev. Immunol.* 37(1):173–200
120. Mahoney KM, Rennert PD, Freeman GJ. 2015. Combination cancer immunotherapy and new immunomodulatory targets. *Nat. Rev. Drug Discov.* 14(8):561–84
121. Coulie PG, Van Den Eynde BJ, Van Der Bruggen P, Boon T. 2014. Tumour antigens recognized by

- T lymphocytes: At the core of cancer immunotherapy. *Nat. Rev. Cancer.* 14(2):135–46
122. Ilyas S, Yang JC. 2015. Landscape of Tumor Antigens in T Cell Immunotherapy. *J. Immunol.* 195(11):5117–22
  123. Novellino L, Castelli C, Parmiani G. 2005. A listing of human tumor antigens recognized by T cells: March 2004 update. *Cancer Immunol. Immunother.* 54(3):187–207
  124. Caballero OL, Chen YT. 2009. Cancer/testis (CT) antigens: Potential targets for immunotherapy. *Cancer Sci.* 100(11):2014–21
  125. De Vries TJ, Fourkour A, Wobbes T, Verkroost G, Ruiter DJ, Van Muijen GNP. 1997. Heterogeneous expression of immunotherapy candidate proteins gp100, MART-1, and tyrosinase in human melanoma cell lines and in human melanocytic lesions. *Cancer Res.* 57(15):3223–29
  126. Rosenfeld C, Cheever M, Gaiger A. 2003. WT1 in acute leukemia, chronic myelogenous leukemia and myelodysplastic syndrome: therapeutic potential of WT1 targeted therapies. *Leukemia.* 17(7):1301–12
  127. Gotter J, Brors B, Hergenroth M, Kyewski B. 2004. Medullary Epithelial Cells of the Human Thymus Express a Highly Diverse Selection of Tissue-specific Genes Colocalized in Chromosomal Clusters. *J. Exp. Med.* 199(2):155–66
  128. Robbins PF, Kassim SH, Tran TLN, Crystal JS, Morgan RA, et al. 2015. A pilot trial using lymphocytes genetically engineered with an NY-ESO-1-reactive T-cell receptor: Long-term follow-up and correlates with response. *Clin. Cancer Res.* 21(5):1019–27
  129. Morgan R a, Chinnasamy N, Abate-Daga D, Gros A, Robbins PF, et al. 2013. Cancer regression and neurological toxicity following anti-MAGE-A3 TCR gene therapy. *J. Immunother.* 36(2):133–51
  130. Linette GP, Stadtmauer E a., Maus M V., Rapoport AP, Levine BL, et al. 2013. Cardiovascular toxicity and titin cross-reactivity of affinity-enhanced T cells in myeloma and melanoma. *Blood.* 122(6):863–71
  131. Yang A, Farmer E, Wu TC, Hung CF. 2016. Perspectives for therapeutic HPV vaccine development. *J. Biomed. Sci.* 23(1):1–19
  132. Garcia-Garijo A, Fajardo CA, Gros A. 2019. Determinants for Neoantigen Identification. *Front. Immunol.* 10(June):1–19
  133. Snyder A, Makarov V, Merghoub T, Yuan J, Zaretsky JM, et al. 2014. Genetic Basis for Clinical Response to CTLA-4 Blockade in Melanoma. *N. Engl. J. Med.* 371(23):2189–99
  134. Rizvi NA, Hellmann MD, Snyder A, Kvistborg P, Makarov V, et al. 2015. Mutational landscape determines sensitivity to PD-1 blockade in non – small cell lung cancer. *Science.* 348(6230):124–28
  135. McGranahan N, Furness A, Rosenthal R, Ramskov S, Lyngaa R, et al. 2016. Clonal neoantigens elicit T cell immunoreactivity and sensitivity to immune checkpoint blockade. *Science.* 351(6280):1463–70
  136. van Rooij N, van Buuren M, Philips D, Velds A, Toebes M, et al. 2013. Tumor exome analysis reveals neoantigen-specific T-cell reactivity in an ipilimumab-responsive melanoma. *J Clin Oncol.* 31(32):e439-42.
  137. Ott PA, Hu Z, Keskin DB, Shukla SA, Sun J, et al. 2017. An immunogenic personal neoantigen vaccine for patients with melanoma. *Nature.* 547(7662):217–21
  138. Sahin U, Derhovanessian E, Miller M, Kloke B, Simon P, et al. 2017. Personalized RNA mutanome vaccines mobilize poly-specific therapeutic immunity against cancer. *Nature.* 547(7662):222–26
  139. Carreno B, Magrini V, Becker-Hapak M, Kaabinejadian S, Hundal J, et al. 2015. A dendritic cell vaccine increases the breadth and diversity of melanoma neoantigen-specific T cells. *Science.* 348(3236):803–8
  140. Tran E, Turcotte S, Gros A, Robbins PF, Lu Y, et al. 2014. Cancer immunotherapy based on mutation-specific CD4+ T cells in a patient with epithelial cancer. *Science.* 9(May):641–45
  141. Tran E, Robbins PF, Lu Y-C, Prickett TD, Gartner JJ, et al. 2016. T-Cell Transfer Therapy Targeting Mutant KRAS in Cancer. *N. Engl. J. Med.* 375(23):2255–62
  142. Zacharakis N, Chinnasamy H, Black M, Xu H, Lu YC, et al. 2018. Immune recognition of somatic mutations leading to complete durable regression in metastatic breast cancer. *Nat. Med.* 24(6):724–30
  143. Malekzadeh P, Pasetto A, Robbins PF, Parkhurst MR, Paria BC, et al. 2019. Neoantigen screening identifies broad TP53 mutant immunogenicity in patients with epithelial cancers. *J. Clin. Invest.* 129(3):1109–14
  144. Wolfel T, Hauer M, Schneider J, Serrano M, Wolfel C, et al. 1995. A p16INK4a-insensitive CDK4 mutant targeted by cytolytic T lymphocytes in a human melanoma. *Science.* 269(5228):1281–84
  145. Veatch JR, Lee SM, Fitzgibbon M, Chow IT, Jesernig B, et al. 2018. Tumor-infiltrating BRAFV600E-specific CD4+ T cells correlated with complete clinical response in melanoma. *J. Clin. Invest.* 128(4):1563–68
  146. Schumacher T, Bunse L, Pusch S, Sahm F, Wiestler B, et al. 2014. A vaccine targeting mutant IDH1 induces antitumour immunity. *Nature*
  147. Stratton MR, Campbell PJ, Futreal PA. 2009. The

## References

- cancer genome. *Nature*. 458(7239):719–24
148. Alexandrov LB, Nik-Zainal S, Wedge DC, Aparicio S a JR, Behjati S, et al. 2013. Signatures of mutational processes in human cancer. *Nature*. 500(7463):415–21
  149. Karpanen T, Olweus J. 2017. The potential of donor T-cell repertoires in neoantigen-targeted cancer immunotherapy. *Front. Immunol.* 8(DEC):1–8
  150. Robbins PF, Lu YC, El-Gamil M, Li YF, Gross C, et al. 2013. Mining exomic sequencing data to identify mutated antigens recognized by adoptively transferred tumor-reactive T cells. *Nat. Med.* 19(6):747–52
  151. Bassani-Sternberg M, Bräunlein E, Klar R, Engleitner T, Sinitcyn P, et al. 2016. Direct identification of clinically relevant neoepitopes presented on native human melanoma tissue by mass spectrometry. *Nat. Commun.* 7(May):
  152. Linnemann C, Buuren MM Van, Bies L, Verdegaal EME, Schotte R, et al. 2015. High-throughput epitope discovery reveals frequent recognition of neo-antigens by CD4 + T cells in human melanoma. *Nat. Med.* 21(1):81–85
  153. Lu YC, Yao X, Crystal JS, Li YF, El-Gamil M, et al. 2014. Efficient identification of mutated cancer antigens recognized by T cells associated with durable tumor regressions. *Clin. Cancer Res.* 20(13):3401–10
  154. Saini SK, Rekers N, Hadrup SR. 2017. Novel tools to assist neoepitope targeting in personalized cancer immunotherapy. *Ann. Oncol.* 28(October):xii3–10
  155. Bacher P, Scheffold A. 2013. Flow-Cytometric Analysis of Rare Antigen-Specific T Cells. *Cytom. A.* 83(8):692–701
  156. Bentzen A, Hadrup S. 2017. Evolution of MHC-based technologies used for detection of antigen-responsive T cells. *Cancer Immunol. Immunother.* 66(5):657–66
  157. Dey S, Kamil Reza K, Wuethrich A, Korbie D, Ibn Sina AA, Trau M. 2019. Tracking antigen specific T-cells: Technological advancement and limitations. *Biotechnol. Adv.* 37(1):145–53
  158. Tischer S, Dieks D, Sukdolak C, Bunse C, Figueiredo C, et al. 2014. Evaluation of suitable target antigens and immunoassays for high-accuracy immune monitoring of cytomegalovirus and Epstein-Barr virus-specific T cells as targets of interest in immunotherapeutic approaches. *J. Immunol. Methods.* 408:101–13
  159. Cafri G, Yossef R, Pasetto A, Deniger DC, Lu YC, et al. 2019. Memory T cells targeting oncogenic mutations detected in peripheral blood of epithelial cancer patients. *Nat. Commun.* 10(1):1–9
  160. Yu W, Jiang N, Ebert PJR, Kidd BA, Müller S, et al. 2015. Clonal Deletion Prunes but Does Not Eliminate Self-Specific  $\alpha\beta$  CD8+ T Lymphocytes. *Immunity.* 42(5):929–41
  161. Jenkins MK, Chu HH, McLachlan JB, Moon JJ. 2010. On the Composition of the Preimmune Repertoire of T Cells Specific for Peptide–Major Histocompatibility Complex Ligands. *Annu. Rev. Immunol.* 28(1):275–94
  162. Davis MM, Altman JD, Newell EW. 2011. Interrogating the repertoire: broadening the scope of peptide-MHC multimer analysis. *Nat. Rev. Immunol.* 11(8):551–58
  163. Gros A, Parkhurst MR, Tran E, Pasetto A, Robbins PF, et al. 2016. Prospective identification of neoantigen-specific lymphocytes in the peripheral blood of melanoma patients. *Nat. Med.* 22(4):433–38
  164. Gros A, Robbins PF, Yao X, Li YF, Turcotte S, et al. 2014. PD-1 identifies the patient-specific CD8+ tumor-reactive repertoire infiltrating human tumors. *J. Clin. Invest.* 124(5):2246–59
  165. De Simone M, Rossetti G, Pagani M. 2018. Single cell T cell receptor sequencing: Techniques and future challenges. *Front. Immunol.* 9(JUL):1–7
  166. Thorsson V, Gibbs DL, Brown SD, Wolf D, Bortone DS, et al. 2018. The Immune Landscape of Cancer. *Immunity.* 48(4):812–830.e14
  167. Glanville J, Huang H, Nau A, Hatton O, Wagar LE, et al. 2017. Identifying specificity groups in the T cell receptor repertoire. *Nature.* 547(7661):94–98
  168. Han A, Glanville J, Hansmann L, Davis MM. 2014. Linking T-cell receptor sequence to functional phenotype at the single-cell level. *Nat. Biotechnol.* 32(7):684–92
  169. Danilova L, Anagnostou V, Caushi JX, Sidhom J-W, Guo H, et al. 2018. The Mutation-Associated Neoantigen Functional Expansion of Specific T Cells (MANAFEST) Assay: A Sensitive Platform for Monitoring Antitumor Immunity. *Cancer Immunol. Res.* 6(8):888–99
  170. Scheper W, Kelderman S, Fanchi LF, Linnemann C, Bendle G, et al. 2019. Low and variable tumor reactivity of the intratumoral TCR repertoire in human cancers. *Nat. Med.* 25(1):89–94
  171. Moodie Z, Price L, Gouttefangeas C, Mander A, Janetzki S, et al. 2010. Response definition criteria for ELISPOT assays revisited. *Cancer Immunol. Immunother.* 59(10):1489–1501
  172. Lehmann P, Zhang W. 2012. Unique strengths of ELISPOT for T cell diagnostics. *Methods Mol. Biol.* 792:3–23
  173. Cox JH, Ferrari G, Janetzki S. 2006. Measurement of cytokine release at the single cell level using the ELISPOT assay. *Methods.* 38:274–82
  174. Lamoreaux L, Roederer M, Koup R. 2006. Intracellular cytokine optimization and standard operating procedure. *Nat. Protoc.* 1(3):1507–16

175. Campbell JDM, Foerster A, Lasmanowicz V, Niemöller M, Scheffold A, et al. 2010. Rapid detection, enrichment and propagation of specific T cell subsets based on cytokine secretion. *Clin. Exp. Immunol.* 163(1):1–10
176. Brosterhus H, Brings S, Leyendeckers H, Manz RA, Radbruch A, et al. 1999. Enrichment and detection of live antigen-specific CD4 + and CD8 + T cells based on cytokine secretion. *Eur. J. Immunol.* 29:4053–59
177. Quah BJC, Wijesundara DK, Ranasinghe C, Parish CR. 2012. Fluorescent target array killing assay: A multiplex cytotoxic T-cell assay to measure detailed T-cell antigen specificity and avidity in vivo. *Cytom. Part A.* 81 A(8):679–90
178. Quah BJC, Wijesundara DK, Ranasinghe C, Parish CR. 2013. Fluorescent target array T helper assay: A multiplex flow cytometry assay to measure antigen-specific CD4+ T cell-mediated B cell help in vivo. *J. Immunol. Methods.* 387(1–2):181–90
179. Tong L, Schuhmacher C, Assenmacher M, Zänker K, Jähn P. 2014. Multiplex and functional detection of antigen-specific human T cells by ITRA — Indirect T cell recognition assay. *J. Immunol. Methods.* 404:13–23
180. Soen Y, Chen DS, Kraft DL, Davis MM, Brown PO. 2003. Detection and Characterization of Cellular Immune Responses Using Peptide – MHC Microarrays. *PLoS Biol.* 1(3):E65
181. Chen DS, Soen Y, Stuge TB, Lee PP, Weber JS, et al. 2005. Marked differences in human melanoma antigen-specific T cell responsiveness after vaccination using a functional microarray. *PLoS Med.* 2(10):e265
182. Stone JD, Demkowicz WE, Stern LJ. 2005. HLA-restricted epitope identification and detection of functional T cell responses by using MHC-peptide and costimulatory microarrays. *Proc. Natl. Acad. Sci.* 102(10):3744–49
183. Brooks SE, Bonney SA, Lee C, Publicover A, Khan G, et al. 2015. Application of the pMHC array to characterise tumour antigen specific T cell populations in leukaemia patients at disease diagnosis. *PLoS One.* 10(10):1–19
184. Schmidt J, Dojcinovic D, Guillaume P, Luescher I. 2013. Analysis, isolation, and activation of antigen-specific CD4+ and CD8+ T cells by soluble MHC-peptide complexes. *Front. Immunol.* 4(JUL):1–14
185. Hadrup SR, Bakker AH, Shu CJ, Andersen RS, van Veluw J, et al. 2009. Parallel detection of antigen-specific T-cell responses by multidimensional encoding of MHC multimers. *Nat. Methods.* 6(7):520–26
186. Andersen RS, Kvistborg P, Mørch Frøsig T, Pedersen NW, Lyngaa R, et al. 2012. Parallel detection of antigen-specific t cell responses by combinatorial encoding of MHC multimers. *Nat. Protoc.* 7(5):891–902
187. Newell EW, Klein LO, Yu W, Davis MM. 2009. Simultaneous detection of many T-cell specificities using combinatorial tetramer staining. *Nat. Methods.* 6(7):497–99
188. Newell EW, Sigal N, Nair N, Kidd B a, Greenberg HB, Davis MM. 2013. Combinatorial tetramer staining and mass cytometry analysis facilitate T-cell epitope mapping and characterization. *Nat. Biotechnol.* 31(7):623–29
189. Bentzen AK, Marquard AM, Lyngaa R, Saini SK, Ramskov S, et al. 2016. Large-scale detection of antigen-specific T cells using peptide-MHC-I multimers labeled with DNA barcodes. *Nat. Biotechnol.* 34(10):1037–45
190. Thorn R, Palmer J, Manson L. 1974. A simplified <sup>51</sup>Cr-release assay for killer cells. *J Immunol Methods.* 4(2):301–15
191. Quah BJC, Warren HS, Parish CR. 2007. Monitoring lymphocyte proliferation in vitro and in vivo with the intracellular fluorescent dye carboxyfluorescein diacetate succinimidyl ester. *Nat. Protoc.* 2(9):2049–56
192. Czerkinsky C, Nilsson L, Nygren H, Ouchterlony O, Tarkowski A. 1983. A solid-phase enzyme-linked immunospot (ELISPOT) assay for enumeration of specific antibody-secreting cells. *J. Immunol. Methods.* 65(1–2):109–21
193. Betts MR, Brenchley JM, Price DA, De Rosa SC, Douek DC, et al. 2003. Sensitive and viable identification of antigen-specific CD8+ T cells by a flow cytometric assay for degranulation. *J. Immunol. Methods.* 281(1–2):65–78
194. Zaunders JJ, Munier ML, Seddiki N, Pett S, Ip S, et al. 2009. High Levels of Human Antigen-Specific CD4+ T Cells in Peripheral Blood Revealed by Stimulated Coexpression of CD25 and CD134 (OX40). *J. Immunol.* 183(4):2827–36
195. Bacher P, Schink C, Teutschbein J, Kniemeyer O, Assenmacher M, et al. 2013. Antigen-Reactive T Cell Enrichment for Direct, High-Resolution Analysis of the Human Naive and Memory Th Cell Repertoire. *J. Immunol.* 190(8):3967–76
196. Wöfl M, Kuball J, Eyrich M, Schlegel PG, Greenberg PD. 2008. Use of CD137 to study the full repertoire of CD8+ T cells without the need to know epitope specificities. *Cytom. Part A.* 73(11):1043–49
197. Parkhurst M, Gros A, Pasetto A, Prickett T, Crystal JS, et al. 2017. Isolation of T-cell receptors specifically reactive with mutated tumor-associated antigens from tumor-infiltrating lymphocytes based on CD137 expression. *Clin. Cancer Res.* 23(10):2491–2505
198. Yossef R, Tran E, Deniger DC, Gros A, Pasetto A, et al. 2018. Enhanced detection of neoantigen-reactive T cells targeting unique and shared oncogenes for personalized cancer immunotherapy. *JCI Insight.* 3(19):
199. Simoni Y, Becht E, Fehlings M, Loh CY, Koo SL, et al. 2018. Bystander CD8 + T cells are abundant

## References

- and phenotypically distinct in human tumour infiltrates. *Nature*. 557(7706):575–79
200. Tong L, Schuhmacher C, Assenmacher M, Zänker K, Jähn P. 2014. Multiplex and functional detection of antigen-specific human T cells by ITRA-Indirect T cell recognition assay. *J. Immunol. Methods*. 404(1):13–23
  201. Matsui K, Boniface J, Reay P, Schild H, Fazekas, de St Groth B Davis M. 1991. Low affinity interaction of peptide-MHC complexes with T cell receptors. *Science*. 254(5039):1788–91
  202. Boniface JJ, Rabinowitz JD, Wulfiging C, Hampi J, Reich Z, et al. 1998. Initiation of signal transduction through the T cell receptor requires the multivalent engagement of peptide/MHC ligands. *Immunity*. 9(6):891
  203. Altman JD, Moss PAH, Goulder PJR, Barouch DH, McHeyzer-Williams MG, et al. 1996. Phenotypic analysis of antigen-specific T lymphocytes. *Science*. 274(5284):94–96
  204. Vollers SS, Stern LJ. 2008. Class II major histocompatibility complex tetramer staining : progress , problems , and prospects. *Immunology*. 123:305–13
  205. Dolton G, Tungatt K, Lloyd A, Bianchi V, Theaker SM, et al. 2015. More Tricks with Tetramers: A Practical Guide to Staining T cells with peptide-MHC Multimers. *Immunology*. 146:11–22
  206. Lissina A, Ladell K, Skowera A, Clement M, Edwards E, et al. 2009. Protein kinase inhibitors substantially improve the physical detection of T-cells with peptide-MHC tetramers. *J. Immunol. Methods*. 340(1):11–24
  207. Moon JJ, Chu HH, Pepper M, McSorley SJ, Jameson SC, et al. 2007. Naive CD4+ T Cell Frequency Varies for Different Epitopes and Predicts Repertoire Diversity and Response Magnitude. *Immunity*. 27(2):203–13
  208. Bacher P, Scheffold A. 2015. New technologies for monitoring human antigen-specific T cells and regulatory T cells by flow-cytometry. *Curr. Opin. Pharmacol.* 23:17–24
  209. Altman JD, Davis MM. 2016. MHC-peptide tetramers to visualize antigen-specific T cells. *Curr. Protoc. Immunol.* 115:17.3.1-17.3.44
  210. Dolton G, Lissina A, Skowera A, Ladell K, Tungatt K, et al. 2014. Comparison of peptide-major histocompatibility complex tetramers and dextramers for the identification of antigen-specific T cells. *Clin. Exp. Immunol.* 177(1):47–63
  211. Chattopadhyay PK, Price DA, Harper TF, Betts MR, Yu J, et al. 2006. Quantum dot semiconductor nanocrystals for immunophenotyping by polychromatic flow cytometry. *Nat. Med.* 12(8):972–77
  212. Huang J, Zeng X, Sigal N, Lund PJ, Su LF, et al. 2016. Detection, phenotyping, and quantification of antigen-specific T cells using a peptide-MHC dodecamer. *Proc. Natl. Acad. Sci.* 113(13):E1890–97
  213. Greten T, Slansky J, Kubota R, Soldan S, Jaffee E, et al. 1998. Direct visualization of antigen-specific T cells: HTLV-1 Tax11-19- specific CD8(+) T cells are activated in peripheral blood and accumulate in cerebrospinal fluid from HAM/TSP patients. *Proc. Natl. Acad. Sci. U. S. A.* 95(13):7568–73
  214. Porto JDAL, Johansen TE, Parfiit DJO, Tuvesont D, Gether U, et al. 1993. A soluble divalent class I major histocompatibility complex molecule inhibits alloreactive T cells at nanomolar concentrations. *Proc. Natl. Acad. Sci. U. S. A.* 90(14):6671–75
  215. Schneck J, Slansky J, O’Herrin S, Greten T. 2001. Monitoring Antigen-Specific T Cells Using MHC-Ig Dimers. *Curr Protoc Immunol.*, pp. 1–17
  216. Oelke M, Maus M V, Didiano D, June CH, Mackensen A, Schneck JP. 2003. Ex vivo induction and expansion of antigen-specific cytotoxic T cells by HLA-Ig-coated artificial antigen-presenting cells. *Nat. Med.* 9(5):619–24
  217. Toebe M, Coccoris M, Bins A, Rodenko B, Gomez R, et al. 2006. Design and use of conditional MHC class I ligands. *Nat. Med.* 12(2):246–51
  218. Oelke M, Schneck JP. 2004. HLA-Ig-based artificial antigen-presenting cells: Setting the terms of engagement. *Clin. Immunol.* 110(3):243–51
  219. Oelke M, Schneck JP. 2010. Overview of a HLA-Ig based “lego-like system” for T cell monitoring, modulation and expansion. *Immunol. Res.* 47(1–3):248–56
  220. Schumacher T, Heemels M, Neefjes J, Kast W, Melief C, Ploegh H. 1990. Direct binding of peptide to empty MHC class I molecules on intact cells and in vitro. *Cell*. 62(3):563–67
  221. Kozono H, White J, Clements J, Marrack P, Kappler J. 1994. Production of soluble MHC class II proteins with covalently bound single peptides. *Nature*. 369(6476):151–54
  222. Crawford F, Kozono H, White J, Marrack P, Kappler J. 1998. Detection of antigen-specific T cells with multivalent soluble class II MHC covalent peptide complexes. *Immunity*. 8(6):675–82
  223. Yu YYL, Netuschil N, Lybarger L, Connolly JM, Hansen TH. 2002. Cutting edge: single-chain trimers of MHC class I molecules form stable structures that potently stimulate antigen-specific T cells and B cells. *J. Immunol.* 168(7):3145–49
  224. Bakker A, Schumacher T. 2005. MHC multimer technology: current status and future prospects. *Curr. Opin. Immunol.* 17(4):428–33
  225. Cohen CJ, Gartner JJ, Horovitz-Fried M, Shamalov K, Trebska-McGowan K, et al. 2015. Isolation of neoantigen-specific T cells from

- tumor and peripheral lymphocytes. *J. Clin. Invest.* 125(10):3981–91
226. Saini SK, Schuster H, Ramnarayan VR, Rammensee H-G, Stevanović S, Springer S. 2015. Dipeptides catalyze rapid peptide exchange on MHC class I molecules. *Proc. Natl. Acad. Sci.* 112(1):202–7
227. Luimstra JJ, Garstka MA, Roex MCJ, Redeker A, Janssen GMC, et al. 2018. A flexible MHC class I multimer loading system for large-scale detection of antigen-specific T cells. *J. Exp. Med.* 215(5):1493–1504
228. Spitzer MH, Nolan GP. 2016. Mass Cytometry: Single Cells, Many Features. *Cell.* 165(4):780–91
229. Nielsen M, Lund O, Buus S, Lundegaard C. 2010. MHC Class II epitope predictive algorithms. *Immunology.* 130(3):319–28
230. Uchtenhagen H, Rims C, Blahnik G, Chow I, Kwok WW, et al. 2016. Efficient ex vivo analysis of CD4+ T-cell responses using combinatorial HLA class II tetramer staining. *Nat. Commun.* 7:1–12
231. Arnold PY, Vignali KM, Miller TB, La NL, Cauley LS, et al. 2002. Reliable generation and use of MHC class II:gamma2aFc multimers for the identification of antigen-specific CD4(+) T cells. *J Immunol Methods.* 271(1–2):137–51
232. Novak EJ, Liu AW, Nepom GT, Kwok WW. 1999. MHC class II tetramers identify peptide-specific human CD4+ T cells proliferating in response to influenza A antigen. *J. Clin. Invest.* 104(12):63–67
233. Sabatino JJ, Huang J, Zhu C, Evavold BD. 2011. High prevalence of low affinity peptide–MHC II tetramer–negative effectors during polyclonal CD4 + T cell responses. *J. Exp. Med.* 208(1):81–90
234. Ayyoub M, Dojcinovic D, Pignon P, Raimbaud I, Schmidt J, et al. 2010. Monitoring of NY-ESO-1 specific CD4+ T cells using molecularly defined MHC class II/His-tag-peptide tetramers. *Proc. Natl. Acad. Sci.* 107(16):7437–42
235. Day CL, Seth NP, Lucas M, Appel H, Gauthier L, et al. 2003. Ex vivo analysis of human memory CD4 T cells specific for hepatitis C virus using MHC class II tetramers. *J. Clin. Invest.* 112(6):831–42
236. Braendstrup P, Justesen S, Osterbye T, Nielsen LLB, Mallone R, et al. 2013. MHC class II tetramers made from isolated recombinant  $\alpha$  and  $\beta$  chains refolded with affinity-tagged peptides. *PLoS One.* 8(9):e73648
237. Landais E, Romagnoli P a, Corper AL, Shires J, Altman JD, et al. 2009. New design of MHC class II tetramers to accommodate fundamental principles of antigen presentation. *J. Immunol.* 183(12):7949–57
238. Horst D, Verweij MC, Davison AJ, Rensing ME, Wiertz EJHJ. 2011. Viral evasion of T cell immunity: Ancient mechanisms offering new applications. *Curr. Opin. Immunol.* 23(1):96–103
239. Greten TF, Korangy F, Neumann G, Wedemeyer H, Schlote K, et al. 2002. Peptide – B2-microglobulin – MHC fusion molecules bind antigen-specific T cells and can be used for multivalent MHC – Ig complexes. *J. Immunol. Methods.* 271:125–35
240. Hansen T, Yu YYL, Fremont DH. 2009. Preparation of stable single-chain trimers engineered with peptide,  $\beta$ 2 microglobulin, and MHC heavy chain. *Curr. Protoc. Immunol.* Chapter 17(Unit 17.5):
241. Lyu F, Ozawa T, Hamana H, Kobayashi E, Muraguchi A, Kishi H. 2019. A novel and simple method to produce large amounts of recombinant soluble peptide/major histocompatibility complex monomers for analysis of antigen-specific human T cell receptors. *N. Biotechnol.* 49(July 2018):169–77
242. Mitaksov V, Truscott SM, Lybarger L, Connolly JM, Hansen TH, Fremont DHH. 2007. Structural Engineering of pMHC Reagents for T Cell Vaccines and Diagnostics. *Chem. Biol.* 14(8):909–22
243. Lybarger L, Yu YYL, Miley MJ, Fremont DH, Myers N, et al. 2003. Enhanced Immune Presentation of a Single-chain Major Histocompatibility Complex Class I Molecule Engineered to Optimize Linkage of a C-terminally Extended Peptide. *J Biol Chem.* 278(29):27105–11
244. Truscott SM, Wang X, Lybarger L, Biddison WE, McBerry C, et al. 2008. Human major histocompatibility complex (MHC) class I molecules with disulfide traps secure disease-related antigenic peptides and exclude competitor peptides. *J. Biol. Chem.* 283(12):7480–90
245. Truscott SM, Lybarger L, Martinko JM, Mitaksov VE, Kranz DM, et al. 2007. Disulfide bond engineering to trap peptides in the MHC class I binding groove. *J Immunol.* 178(10):6280–89
246. Obermann S, Petrykowska S, Manns MP, Korangy F, Greten TF. 2007. Peptide-b2-microglobulin-major histocompatibility complex expressing cells are potent antigen-presenting cells that can generate specific T cells. *Immunology.* 122(1):90–97
247. Kotsiou E, Brzostek J, Gould KG. 2011. Properties and applications of single-chain major histocompatibility complex class I molecules. *Antioxid. Redox Signal.* 15(3):645–55
248. Hansen TH, Connolly JM, Gould KG, Fremont DH. 2010. Basic and translational applications of engineered MHC class I proteins. *Trends Immunol.* 31(10):363–69
249. Steenblock ER, Wrzesinski SH, Flavell RA, Fahmy TM. 2009. Antigen presentation on artificial acellular substrates: modular systems for

## References

- flexible, adaptable immunotherapy. *Expert Opin. Biol. Ther.* 9(4):451–64
250. Schluck M, Hammink R, Figdor CG, Verdoes M, Weiden J. 2019. Biomaterial-Based Activation and Expansion of Tumor-Specific T Cells. *Front. Immunol.* 10(May):
251. Verreck FAW, Fargeas CA, Hammerling GJ. 2001. Conformational alterations during biosynthesis of HLA-DR3 molecules controlled by invariant chain and HLA-DM. *Eur. J. Immunol.* 31(4):1029–36
252. Salter RD, Cresswell P. 1986. Impaired assembly and transport of HLA-A and -B antigens in mutant TxB cell hybrid a HLA -A HLA-B. *Embo.* 5(5):943–49
253. Leisegang M, Wilde S, Spranger S, Milosevic S, Frankenberger B, et al. 2010. MHC-restricted fratricide of human lymphocytes expressing survivin-specific transgenic T cell receptors. *J. Clin. Invest.* 120(11):3869–77
254. Tan MCAA, Mommaas AM, Drijfhout JW, Jordens R, Onderwater JJM, et al. 1997. Mannose receptor-mediated uptake of antigens strongly enhances HLA class II-restricted antigen presentation by cultured dendritic cells. *Eur. J. Immunol.* 27(9):2426–35
255. Geluk A, Van Meijgaarden KE, Janson AA, Drijfhout JW, Meloen RH, et al. 1992. Functional analysis of DR17(DR3)-restricted mycobacterial T cell epitopes reveals DR17-binding motif and enables the design of allele-specific competitor peptides. *J. Immunol.* 149(9):2864–71
256. Rölle A, Meyer M, Calderazzo S, Jäger D, Momburg F. 2018. Distinct HLA-E Peptide Complexes Modify Antibody-Driven Effector Functions of Adaptive NK Cells. *Cell Rep.* 24:1967–76
257. Kim B, Oakley MG. 2002. A General Method for Selection and Screening of Coiled Coils on the Basis of Relative Helix Orientation. *J Am Chem Soc*, pp. 8237–44
258. Beckett D, Kovaleva E, Schatz PJ. 1999. A minimal peptide substrate in biotin holoenzyme synthetase-catalyzed biotinylation. *Protein Sci.* 8:921–29
259. Kim JH, Lee SR, Li LH, Park HJ, Park JH, et al. 2011. High cleavage efficiency of a 2A peptide derived from porcine teschovirus-1 in human cell lines, zebrafish and mice. *PLoS One.* 6(4):1–8
260. Donnelly MLL, Hughes LE, Luke G, Mendoza H, Ten Dam E, et al. 2001. The “cleavage” activities of foot-and-mouth disease virus 2A site-directed mutants and naturally occurring “2A-like” sequences. *J. Gen. Virol.* 82(5):1027–41
261. Wooldridge L, Lissina A, Vernazza J, Gostick E, Laugel B, et al. 2007. Enhanced immunogenicity of CTL antigens through mutation of the CD8 binding MHC class I invariant region. *Eur. J. Immunol.* 37(5):1323–33
262. Parrott MB, Barry MA. 2000. Metabolic Biotinylation of Recombinant Proteins in Mammalian Cells and in Mice. *Mol Ther.* 1(1):96–104
263. Barat B, Wu AM. 2007. Metabolic biotinylation of recombinant antibody by biotin ligase retained in the endoplasmic reticulum. *Biomol Eng.* 24(3):283–91
264. Munro S, Pelham HRB. 1987. A C-terminal signal prevents secretion of luminal ER proteins. *Cell.* 48(5):P899-907
265. Recipe: Polyethylenimine (PEI), linear (1 mg/mL). 2008. *Cold Spring Harb Protoc*
266. Rajendra Y, Kiseljak D, Baldi L, Hacker DL, Wurm FM. 2011. A simple high-yielding process for transient gene expression in CHO cells. *J. Biotechnol.* 153(1–2):22–26
267. Rajendra Y, Kiseljak D, Baldi L, Hacker DL, Wurm FM. 2012. Reduced glutamine concentration improves protein production in growth-arrested CHO-DG44 and HEK-293E cells. *Biotechnol. Lett.* 34(4):619–26
268. Wulhfard S, Baldi L, Hacker D, Wurm F. 2010. Valproic acid enhances recombinant mRNA and protein levels in transiently transfected Chinese hamster ovary cells. *J Biotechnol.* 148(2–3):128–32
269. Wulhfard S, Bouchet S, Cevey J, Jesus M De, Hacker DL, Wurm FM. 2008. Mild Hypothermia Improves Transient Gene Expression Yields Several Fold in Chinese Hamster Ovary Cells. *Biotechnol Prog.* 24(2):458–65
270. Schmidt T, Skerra A. 2015. The Strep-tag system for one-step affinity purification of proteins from mammalian cell culture. *Methods Mol Biol.* 1286:83–95
271. Herzenberg LA, Tung J, Moore WA, Herzenberg LA, Parks DR. 2006. Interpreting flow cytometry data: A guide for the perplexed. *Nat. Immunol.* 7(7):681–85
272. Knabel M, Franz TJ, Schiemann M, Wulf A, Villmow B, et al. 2002. Reversible MHC multimer staining for functional isolation of T-cell populations and effective adoptive transfer. *Nat. Med.* 8(6):631–37
273. Wills MR, Carmichael AJ, Mynard K, Jin X, Weekes MP, et al. 1996. The human cytotoxic T-lymphocyte (CTL) response to cytomegalovirus is dominated by structural protein pp65: frequency, specificity, and T-cell receptor usage of pp65-specific CTL. *J. Virol.* 70(11):7569–79
274. Morrison J, Elvin J, Latron F, Gotch F, Moots R, et al. 1992. Identification of the nonamer peptide from influenza A matrix protein and the role of pockets of HLA-A2 in its recognition by cytotoxic T lymphocytes. *Eur J Immunol.* 22(4):903–7
275. Steven NM, Annels NE, Kumar A, Leese AM, Kurilla MG, Rickinson AB. 1997. Immediate Early

- and Early Lytic Cycle Proteins Are Frequent Targets of the Epstein-Barr Virus-induced Cytotoxic T Cell Response. *J. Exp. Med.* 185(9):1605–18
276. Andersen MH, Pedersen L, Capeller B, Bröcker EB, Becker JC, Straten P. 2001. Spontaneous cytotoxic T-cell responses against survivin-derived MHC class I-restricted T-cell epitopes in situ as well as ex vivo in cancer patients. *Cancer Res.* 61(16):5964–68
277. Jäger E, Chen YT, Drijfhout JW, Karbach J, Ringhoffer M, et al. 1998. Simultaneous humoral and cellular immune response against cancer-testis antigen NY-ESO-1: definition of human histocompatibility leukocyte antigen (HLA)-A2-binding peptide epitopes. *J. Exp. Med.* 187(2):265–70
278. Bronke C, Palmer NM, Westerlaken GHA, Toebes M, Van Schijndel GMW, et al. 2005. Direct Ex Vivo detection of HLA-DR3-restricted cytomegalovirus- and Mycobacterium tuberculosis-specific CD4+ T cells. *Hum. Immunol.* 66(9):950–61
279. Chou CL, Mirshahidi S, Su KW, Kim AR, Narayan K, et al. 2008. Short peptide sequences mimic HLA-DM functions. *Mol. Immunol.* 45(7):1935–43
280. Koşaloğlu Z, Zörnig I, Halama N, Kaiser I, Buchhalter I, et al. 2016. Identification of immunotherapeutic targets by genomic profiling of rectal NET metastases. *Oncimmunology.* 5(11):
281. Andreatta M, Nielsen M. 2016. Gapped sequence alignment using artificial neural networks: Application to the MHC class I system. *Bioinformatics.* 32(4):511–17
282. Jurtz V, Paul S, Andreatta M, Marcatili P, Peters B, Nielsen M. 2017. NetMHCpan-4.0: Improved Peptide–MHC Class I Interaction Predictions Integrating Eluted Ligand and Peptide Binding Affinity Data. *J. Immunol.* 199(9):3360–68
283. Brodsky F, Parham P, Barnstable C, Crumpton M, Bodmer W. 1979. Monoclonal antibodies for analysis of the HLA system. *Immunol Rev.* 47:3–61
284. Almagro Armenteros JJ, Tsirigos KD, Sønderby CK, Petersen TN, Winther O, et al. 2019. SignalP 5.0 improves signal peptide predictions using deep neural networks. *Nat. Biotechnol.* 37(4):420–23
285. Neudorfer J, Schmidt B, Huster KM, Anderl F, Schiemann M, et al. 2007. Reversible HLA multimers (Streptamers) for the isolation of human cytotoxic T lymphocytes functionally active against tumor- and virus-derived antigens. *J. Immunol. Methods.* 320(1–2):119–31
286. Strønen E, Toebes M, Kelderman S, Buuren MM Van, Yang W, et al. 2016. Targeting of cancer neoantigens with donor-derived T cell receptor repertoires. *Science.* 352(6291):1337–41
287. Somasundaram R, Swoboda R, Caputo L, Otvos L, Weber B, et al. 2006. Human leukocyte antigen-A2-restricted CTL responses to mutated BRAF peptides in melanoma patients. *Cancer Res.* 66(6):3287–93
288. Perica K, Tu A, Richter A, Bieler JG, Edidin M, Schneck JP. 2014. Magnetic field-induced T cell receptor clustering by nanoparticles enhances T cell activation and stimulates antitumor activity. *ACS Nano.* 8(3):2252–60
289. Altieri DC. 2003. Validating survivin as a cancer therapeutic target. *Nat. Rev. Cancer.* 3(1):46–54
290. Toebes M, Rodenko B, Ovaa H, Schumacher TNM. 2009. Generation of peptide MHC class I monomers and multimers through ligand exchange. *Curr. Protoc. Immunol.* 0702(SUPPL. 87):1–30
291. Yang J, Jaramillo A, Shi R, Kwok WW, Mohanakumar T. 2004. In vivo biotinylation of the major histocompatibility complex (MHC) class II/peptide complex by coexpression of BirA enzyme for the generation of MHC class II/tetramers. *Hum. Immunol.* 65(7):692–99
292. Leisner C, Loeth N, Lamberth K, Justesen S, Sylvester-Hvid C, et al. 2008. One-pot, mix-and-read peptide-MHC tetramers. *PLoS One.* 3(2):
293. Tykvart J, Šácha P, Bařinka C, Knedlík T, Starková J, et al. 2012. Efficient and versatile one-step affinity purification of in vivo biotinylated proteins: Expression, characterization and structure analysis of recombinant human glutamate carboxypeptidase II. *Protein Expr. Purif.* 82(1):106–15
294. Bobisse S, Genolet R, Roberti A, Tanyi JL, Racle J, et al. 2018. Sensitive and frequent identification of high avidity neo-epitope specific CD8 + T cells in immunotherapy-naive ovarian cancer. *Nat. Commun.* 9(1):1–10
295. Bruns H, Bessell C, Varela JC, Haupt C, Fang J, et al. 2015. CD47 enhances in vivo functionality of artificial antigen-presenting cells. *Clin. Cancer Res.* 21(9):2075–83
296. Moro M, Cecconi V, Martinoli C, Dallegno E, Giabbai B, et al. 2005. Generation of functional HLA-DR \* 1101 tetramers receptive for loading with pathogen or tumour derived synthetic peptides. *BMC Immunol.* 15:1–15
297. Gaseitsiwe S, Maeurer M. 2009. Identification of MHC class II binding peptides: microarray and soluble MHC class II molecules. *Methods Mol Biol.* 521:417–26
298. Gaseitsiwe S, Valentini D, Mahdavi S, Reilly M, Ehrnst A, Maeurer M. 2010. Peptide microarray-based identification of Mycobacterium tuberculosis epitope binding to HLA-DRB1\*0101, DRB1\*1501, and DRB1\*0401. *Clin. Vaccine Immunol.* 17(1):168–75
299. Beyer M, Nesterov A, Block I, König K,

## References

- Felgenhauer T, et al. 2007. Combinatorial synthesis of peptide arrays onto a microchip. *Science*. 318(December):1888
300. Burkholder B, Huang RY, Burgess R, Luo S, Jones VS, et al. 2014. Tumor-induced perturbations of cytokines and immune cell networks. *Biochim. Biophys. Acta - Rev. Cancer*. 1845(2):182–201
301. Fridman WH, Pagès F, Sautès-Fridman C, Galon J. 2012. The immune contexture in human tumours: impact on clinical outcome. *Nat. Rev. Cancer*. 12(4):298–306
302. Gnjatich S, Ritter E, Buchler MW, Giese NA, Brors B, et al. 2010. Seromic profiling of ovarian and pancreatic cancer. *Proc. Natl. Acad. Sci.* 107(11):5088–93
303. Michels J, Becker N, Suciu S, Kaiser I, Benner A, et al. 2018. Multiplex bead-based measurement of humoral immune responses against tumor-associated antigens in stage II melanoma patients of the EORTC18961 trial. *Oncoimmunology*. 7(6):1–9
304. Angeloni S, Das S, Dunbar S, Stone V, Swift S. 2018. *The Luminex xMAP® Cookbook 4th Edition*
305. Jun BH, Kang H, Lee YS, Jeong DH. 2012. Fluorescence-based multiplex protein detection using optically encoded microbeads. *Molecules*. 17(3):2474–90
306. Sosale NG, Spinler KR, Alvey C, Discher DE. 2015. Macrophage engulfment of a cell or nanoparticle is regulated by unavoidable opsonization, a species-specific 'Marker of Self' CD47, and target physical properties. *Curr Opin Immunol*. 35:107–12
307. Nimmerjahn F, Ravetch J V. 2006. Fcγ receptors: Old friends and new family members. *Immunity*. 24(1):19–28
308. Fahmy T, Bieler J, Edidin M, Schneck J. 2001. Increased TCR Avidity after T Cell Activation A Mechanism for Sensing Low-Density Antigen. *Immunity*. 14(2):135–43
309. Kumar R, Ferez M, Swamy M, Arechaga I, Rejas MT, et al. 2011. Increased Sensitivity of Antigen-Experienced T Cells through the Enrichment of Oligomeric T Cell Receptor Complexes. *Immunity*. 35(3):375–87
310. Sharma SK, Alexander-Miller MA. 2011. Increased sensitivity to antigen in high avidity CD8+ T cells results from augmented membrane proximal T-cell receptor signal transduction. *Immunology*. 133(3):307–17
311. Borger JG, Zamoyska R, Gakamsky DM. 2014. Proximity of TCR and its CD8 coreceptor controls sensitivity of T cells. *Immunol. Lett.* 157(1–2):16–22
312. Anikeeva N, Fischer NO, Blanchette CD, Sykulev Y. 2019. Extent of MHC Clustering Regulates Selectivity and Effectiveness of T Cell Responses. *J. Immunol.* 202(2):591–97
313. Maecker HT, Hassler J, Payne JK, Summers A, Comatas K, et al. 2008. Precision and linearity targets for validation of an IFNγ ELISPOT, cytokine flow cytometry, and tetramer assay using CMV peptides. *BMC Immunol.* 9:1–9
314. Xu Y, Theobald V, Sung C, DePalma K, Atwater L, et al. 2008. Validation of a HLA-A2 tetramer flow cytometric method, IFNγ real time RT-PCR, and IFNγ ELISPOT for detection of immunologic response to gp100 and MelanA/MART-1 in melanoma patients. *J. Transl. Med.* 6:0–1
315. Karlsson AC, Martin JN, Younger SR, Bredt BM, Epling L, et al. 2003. Comparison of the ELISPOT and cytokine flow cytometry assays for the enumeration of antigen-specific T cells. *J. Immunol. Methods*. 283(1–2):141–53
316. Barclay AN, van den Berg TK. 2014. The Interaction Between Signal Regulatory Protein Alpha (SIRPα) and CD47: Structure, Function, and Therapeutic Target. *Annu. Rev. Immunol.* 32(1):25–50
317. Rodriguez PL, Harada T, Christian DA, Pantano DA, Tsai RK, Discher DE. 2013. Minimal "Self" Peptides That Inhibit Phagocytic Clearance and Enhance Delivery of Nanoparticles. *Science*. 339(6122):971–75
318. Tsai RK, Discher DE. 2008. Inhibition of "self" engulfment through deactivation of myosin-II at the phagocytic synapse between human cells. *J. Cell Biol.* 180(5):989–1003
319. Taylor PR, Martinez-Pomares L, Stacey M, Lin H-H, Brown GD, Gordon S. 2005. Macrophage Receptors and Immune Recognition. *Annu. Rev. Immunol.* 23(1):901–44
320. Acuto O, Michel F. 2003. CD28-mediated costimulation: A quantitative support for TCR signalling. *Nat. Rev. Immunol.* 3(12):939–51
321. Krosgaard M, Davis MM. 2005. How T cells 'see' antigen. *Nat. Immunol.* 6(3):239–45
322. Dushek O, Aleksic M, Wheeler RJ, Zhang H, Cordoba S, et al. 2011. Antigen Potency and Maximal Efficacy Reveal a Mechanism of Efficient T Cell Activation. *Sci Signal.* 4(176):1–9
323. Bachmann MF, Barner M, Kopf M. 1999. CD2 sets quantitative thresholds in T cell activation. *J. Exp. Med.* 190(10):1383–92
324. Boldajipour B, Nelson A, Krummel MF. 2016. Tumor-infiltrating lymphocytes are dynamically desensitized to antigen but are maintained by homeostatic cytokine. *JCI Insight.* 1(20):
325. Miyama T, Kawase T, Kitaura K, Chishaki R, Shibata M, et al. 2017. Highly functional T-cell receptor repertoires are abundant in stem memory T cells and highly shared among individuals. *Sci. Rep.* 7(1):1–13
326. Schumacher TN, Schreiber RD. 2015. Neoantigens in cancer immunotherapy. *Science*. 348(6230):69–74

327. Duan F, Duitama J, Al Seesi S, Ayres CM, Corcelli SA, et al. 2014. Genomic and bioinformatic profiling of mutational neoepitopes reveals new rules to predict anticancer immunogenicity. *J. Exp. Med.* 211(11):2231–48
328. Bjerregaard AM, Nielsen M, Jurtz V, Barra CM, Hadrup SR, et al. 2017. An analysis of natural T cell responses to predicted tumor neoepitopes. *Front. Immunol.* 8(NOV):1–9
329. Wang C, Singer M, Anderson AC. 2017. Molecular Dissection of CD8+ T-Cell Dysfunction. *Trends Immunol.* 38(8):567–76
330. Ferré H, Ruffet E, Blicher T, Sylvester-Hvid C, Nielsen L, et al. 2003. Purification of correctly oxidized MHC class I heavy-chain molecules under denaturing conditions: A novel strategy exploiting disulfide assisted protein folding. *Protein Sci.* 12(3):551–59
331. Choudhuri K, Parker M, Milicic A, Cole DK, Shaw MK, et al. 2009. Peptide-Major Histocompatibility Complex Dimensions Control Proximal Kinase-Phosphatase Balance during. *J. Biol. Chem.* 284(38):26096–105
332. Wooster AL, Anderson TS, Lowe DB. 2019. Expression and characterization of soluble epitope-defined major histocompatibility complex (MHC) from stable eukaryotic cell lines. *J. Immunol. Methods.* 464:22–30
333. Zhang J, Carter J, Siu S, W. O'Neill J, H. Gates A, et al. 2010. Fusion Partners as a Tool for the Expression of Difficult Proteins in Mammalian Cells. *Curr. Pharm. Biotechnol.* 11(3):241–45
334. Chang CXL, Tan AT, Or MY, Toh KY, Lim PY, et al. 2013. Conditional ligands for Asian HLA variants facilitate the definition of CD8+ T-cell responses in acute and chronic viral diseases. *Eur. J. Immunol.* 43(4):1109–20
335. Bakker AH, Hoppes R, Linnemann C, Toebes M, Rodenko B, et al. 2008. Conditional MHC class I ligands and peptide exchange technology for the human MHC gene products HLA-A1, -A3, -A11, and -B7. *Proc. Natl. Acad. Sci.* 105(10):3825–30
336. Rodenko B, Toebes M, Hadrup SR, van Esch WJE, Molenaar AM, et al. 2006. Generation of peptide-MHC class I complexes through UV-mediated ligand exchange. *Nat. Protoc.* 1(3):1120–32
337. Saini SK, Tamhane T, Anjanappa R, Saikia A, Ramskov S, et al. 2019. Empty peptide-receptive MHC class I molecules for efficient detection of antigen-specific T cells. *Sci. Immunol.* 4(37):
338. Frøsig TM, Yap J, Seremet T, Lyngaa R, Svane IM, et al. 2015. Design and validation of conditional ligands for HLA-B\*08:01, HLA-B\*15:01, HLA-B\*35:01, and HLA-B\*44:05. *Cytom. Part A.* 87(10):967–75
339. Brackenridge S, Evans EJ, Toebes M, Goonetilleke N, Liu MKP, et al. 2011. An Early HIV Mutation within an HLA-B\*57-Restricted T Cell Epitope Abrogates Binding to the Killer Inhibitory Receptor 3DL1. *J. Virol.* 85(11):5415–22
340. De Graaf MT, De Beukelaar JW, Burgers PC, Luider TM, Kraan J, et al. 2008. Contamination of synthetic HuD protein spanning peptide pools with a CMV-encoded peptide. *Cytom. Part A.* 73(11):1079–85
341. Currier JR, Galley LM, Wenschuh H, Morafo V, Ratto-Kim S, et al. 2008. Peptide impurities in commercial synthetic peptides and their implications for vaccine trial assessment. *Clin. Vaccine Immunol.* 15(2):267–76
342. Gfeller D, Bassani-Sternberg M. 2018. Predicting antigen presentation-What could we learn from a million peptides? *Front. Immunol.* 9(JUL):1–17
343. Kotsiou E, Brzostek J, Lenart I, Antoniou A, Dyson J, Gould K. 2011. Dimerization of soluble disulfide trap single-chain major histocompatibility complex class I molecules dependent on peptide binding affinity. *Antioxid Redox Signal.* 15(3):635–44
344. Chen J-L, Stewart-Jones G, Bossi G, Lissin NM, Wooldridge L, et al. 2005. Structural and kinetic basis for heightened immunogenicity of T cell vaccines. *J. Exp. Med.* 201(8):1243–55
345. Barrette-Ng IH, Wu SC, Tjia WM, Wong SL, Ng KKS. 2013. The structure of the SBP-Tag-streptavidin complex reveals a novel helical scaffold bridging binding pockets on separate subunits. *Acta Crystallogr. Sect. D Biol. Crystallogr.* 69(5):879–87
346. Schmidt J, Guillaume P, Irving M, Baumgaertner P, Speiser D, Luescher IF. 2011. Reversible Major Histocompatibility Complex I-Peptide Multimers Containing Ni<sup>2+</sup>-Nitrilotriacetic Acid Peptides and Histidine Tags Improve Analysis and Sorting of CD8+ T Cells. *J. Biol. Chem.* 286(48):41723–35
347. Cosson P, Bonifacio JS. 1992. Role of transmembrane domain interactions in the assembly of class II MHC molecules. *Science (80-. ).* 258(5082):659–62
348. Cameron TO, Norris PJ, Patel A, Moulon C, Rosenberg ES, et al. 2002. Labeling antigen-specific CD4+ T cells with class II MHC oligomers. *J. Immunol. Methods.* 268(1):51–69
349. Serra P, Garabatos N, Singha S, Fandos C, Garnica J, et al. 2019. Increased yields and biological potency of knob-into-hole-based soluble MHC class II molecules. *Nat. Commun.* 10(1):1–14
350. Appel H, Gauthier L, Pyrdol J, Wucherpfennig KW. 2000. Kinetics of T-cell receptor binding by bivalent HLA-DR-peptide complexes that activate antigen-specific human T-cells. *J. Biol. Chem.* 275(1):312–21
351. Gauthier L, Smith K, Pyrdol J, Kalandadze A, Strominger J, et al. 1998. Expression and crystallization of the complex of HLA-DR2 ( DRA

## References

- , DRB1 \* 1501 ) and an immunodominant peptide of human myelin. *Proc. Natl. Acad. Sci.* 95(20):11828–33
352. Fourneau JM, Cohen H, Van Endert PM. 2004. A chaperone-assisted high yield system for the production of HLA-DR4 tetramers in insect cells. *J. Immunol. Methods.* 285(2):253–64
353. Cunliffe SL, Wyer JR, Sutton JK, Lucas M, Harcourt G, et al. 2002. Optimization of peptide linker length in production of MHC class II/peptide tetrameric complexes increases yield and stability, and allows identification of antigen-specific CD4+ T cells in peripheral blood mononuclear cells. *Eur. J. Immunol.* 32(12):3366–75
354. Chiou H, Vasu S, Liu C, Cisneros I, Jones M, Zmuda J. 2014. Scalable transient protein expression. *Methods Mol Biol.* 1104:35–55
355. Durocher Y, Perret S, Kamen A. 2002. High-level and high-throughput recombinant protein production by transient transfection of suspension-growing human 293-EBNA1 cells. *Nucleic Acids Res.* 30(2):E9
356. Tom R, Bisson L, Durocher Y. 2008. Transfection of HEK293-EBNA1 cells in suspension with 293fectin for production of recombinant proteins. *Cold Spring Harb. Protoc.* 3(3):3–6
357. Tom R, Bisson L, Durocher Y. 2008. Transfection of HEK293-EBNA1 cells in suspension with linear PEI for production of recombinant proteins. *Cold Spring Harb. Protoc.* 3(3):1–5
358. Scriba TJ, Purbhoo M, Day CL, Robinson N, Fidler S, et al. 2005. Ultrasensitive Detection and Phenotyping of CD4+ T Cells with Optimized HLA Class II Tetramer Staining. *J. Immunol.* 175(10):6334–43
359. Ye M, Kasey S, Khurana S, Nguyen NT, Schubert S, et al. 2004. MHC class II tetramers containing influenza hemagglutinin and EBV EBNA1 epitopes detect reliably specific CD4+ T cells in healthy volunteers. *Hum. Immunol.* 65(5):507–13
360. Graham H, Chandler DJ, Dunbar SA. 2019. The genesis and evolution of bead-based multiplexing. *Methods.* 158(October 2018):2–11
361. Ott PA, Herzog BA, Quast S, Hofstetter HH, Boehm BO, et al. 2005. Islet-cell antigen-reactive T cells show different expansion rates and Th1/Th2 differentiation in type 1 diabetic patients and healthy controls. *Clin. Immunol.* 115(1 SPEC. ISS.):102–14
362. Shen C, Xu T, Wu Y, Li X, Xia L, et al. 2017. Frequency and reactivity of antigen-specific T cells were concurrently measured through the combination of artificial antigen-presenting cell, MACS and ELISPOT. *Sci. Rep.* 7(1):1–14
363. Peng S, Zaretsky JM, Ng AHC, Chour W, Bethune MT, et al. 2019. Sensitive Detection and Analysis of Neoantigen-Specific T Cell Populations from Tumors and Blood. *Cell Rep.* 28(10):2728–2738.e7
364. Kwong G, Radu C, Hwang K, Shu C, Ma C, et al. 2009. Modular Nucleic Acid Assembled p / MHC Microarrays for Multiplexed Sorting of Antigen-Specific T Cells. *J. Am Chem Soc.* 131(28):pp9695-9703
365. Zhang SQ, Ma KY, Schonnesen AA, Zhang M, He C, et al. 2018. High-throughput determination of the antigen specificities of T cell receptors in single cells. *Nat. Biotechnol.* 36(12):1156–59
366. Joglekar A V., Leonard MT, Jeppson JD, Swift M, Li G, et al. 2019. T cell antigen discovery via signaling and antigen-presenting bifunctional receptors. *Nat. Methods.* 16(2):191–98
367. Kisielow J, Obermair FJ, Kopf M. 2019. Deciphering CD4 + T cell specificity using novel MHC–TCR chimeric receptors. *Nat. Immunol.* 20(5):652–62
368. Kula T, Dezfulian MH, Wang CI, Abdelfattah NS, Hartman ZC, et al. 2019. T-Scan: A Genome-wide Method for the Systematic Discovery of T Cell Epitopes. *Cell.* 178(4):1016-1028.e13
369. Perica K, Kosmides AK, Schneck JP. 2015. Linking form to function: Biophysical aspects of artificial antigen presenting cell design. *Biochim. Biophys. Acta - Mol. Cell Res.* 1853(4):781–90
370. Lim D-G, Bieganowska Bourcier K, Freeman GJ, Hafler DA. 2000. Examination of CD8 + T Cell Function in Humans Using MHC Class I Tetramers: Similar Cytotoxicity but Variable Proliferation and Cytokine Production Among Different Clonal CD8 + T Cells Specific to a Single Viral Epitope. *J. Immunol.* 165(11):6214–20
371. Deshpande P, Cavanagh MM, Le Saux S, Singh K, Weyand CM, Goronzy JJ. 2013. IL-7– and IL-15– Mediated TCR Sensitization Enables T Cell Responses to Self-Antigens. *J. Immunol.* 190(4):1416–23
372. Silfka MK, Rodriguez F, Whitton JL. 1999. Rapid on/off cycling of cytokine production by virus-specific CD8+ T cells. *Nature.* 401(6748):76–79
373. Badovinac VP, Corbin GA, Harty JT. 2000. Cutting Edge: OFF Cycling of TNF Production by Antigen-Specific CD8 + T Cells Is Antigen Independent . *J. Immunol.* 165(10):5387–91
374. Helmstetter C, Flossdorf M, Peine M, Kupz A, Zhu J, et al. 2015. Individual T Helper Cells Have a Quantitative Cytokine Memory. *Immunity.* 42(1):108–22
375. Hombach A, Sent D, Schneider C, Heuser C, Koch D, et al. 2001. T-cell activation by recombinant receptors: CD28 costimulation is required for interleukin 2 secretion and receptor-mediated T-cell proliferation but does not affect receptor-mediated target cell lysis. *Cancer Res.* 61(5):1976–82
376. Benard E, Nunès JA, Limozin L, Sengupta K. 2018. T cells on engineered substrates: The impact of TCR clustering is enhanced by LFA-1

- engagement. *Front. Immunol.* 9(SEP):1–12
377. Feau S, Garcia Z, Arens R, Yagita H, Borst J, Schoenberger SP. 2012. The CD4+ T-cell help signal is transmitted from APC to CD8 + T-cells via CD27-CD70 interactions. *Nat. Commun.* 3:948–49
378. Shafer-Weaver K, Sayers T, Strobl S, Derby E, Ulderich T, et al. 2003. The Granzyme B ELISPOT assay: An alternative to the <sup>51</sup>Cr-release assay for monitoring cell-mediated cytotoxicity. *J. Transl. Med.* 1:1–9
379. Nowacki TM, Kuerten S, Zhang W, Shive CL, Kreher CR, et al. 2007. Granzyme B production distinguishes recently activated CD8+ memory cells from resting memory cells. *Cell. Immunol.* 247(1):36–48



## Appendix – Protein sequences of produced soluble pMHC molecules

### (i) Produced and used soluble pMHC-I [dt-SCT]-mIgG2a-Fc constructs:

Construct ID:	Allele:	Antigen:	Peptide sequence:
7409.4	HLA-A*02:01 [Y84C]	HCMV pp65 495–503	NLVPMVATV
7426.1		HER-2/neu 369–377	KIFGSLAFL
8195.1		Survivin 96–104 / T97M	LMLGEFLKL
8443.1		Flu A MP 58–66	GILGFVFTL
8498.1		HPV-16 E7 11–19 / T19V	YMLDLQPEV

#### Exemplary protein sequence of construct 7409.4:

MAKANLLVLLCALAAADA | NLVPMVATVCGSGGGGAPGSGGGSIQRTPKIQVYSRHPAENGKSNFLNCYVSGFH  
 PSDIEVDLLKNGERIEKVEHSDLSFSKDWSFYLLYYTEFTPTTEKDEYACRVNHVTL SQPKIVKWRDRMRSASGGG  
 GSGGGGSGGGGASGGGGDLGSHSMRYFFTSVSRPGRGEPRFIAVG YVDDTQFVRFSDAASQRMEPRAPWIEQE  
 GPEYWDGETRKVKAHSQTHRVDLGLTRG CYNQSEAGSHTVQRMYGCDVGS DWRFLRGYHQYAYDGKDY IALKEDL  
 RSWTAADMAAQTTKHKWEAAHVAEQLRAYLEGTCVEWLRRLYLENGKETLQRTDAPKTHMTHHAVSDHEATLRCWA  
 LSFYPAEITLTWQRDGEDQTQDTEL VETRPAGDGT FQKWA AVVVPSGQEQR YTCHVQHEGLPKPLTLRWE PSSQP  
 TIPGDP EPRGPTIKPSP PCKCPAPNLLGGPSVFI FPPKIKDVLMI SLSPMVTCVVVDVSEDDPDVQISW FVNNVE  
 VLTAQTQTHREDYNSTLRVVSALPIQH QDWMGKFEFKCKVNNKALPAPIERTISK PKG SVRAPQVYVLP PPEEEM  
 TKKQVTLTCMVTDFMPEDIYVEWTNNGKTELNYKNTEPVLDS DGSYFMYSKLRVEKKNWVERNSYSCSVVHEGLH  
 NHHTTKSFSRTPGK\*

**Legend:** Leader sequence (modified hemagglutinin leader) | Peptide-linker #1-β<sub>2</sub>m-linker #2-HLA-A\*02:01 [Y84C] ectodomain-linker #3-mouse IgG2a-Fc [C224S] (Hinge-CH2-CH3)

### (ii) Produced and used soluble pMHC-I [dt-SCT]-CH1-mIgG2a-Fc constructs:

Construct ID:	Allele:	Antigen:	Peptide sequence:
8414.1	HLA-A*02:01 [Y84C]	HCMV pp65 495–503	NLVPMVATV
8415.2		Survivin 96–104 / T97M	LMLGEFLKL

#### Exemplary protein sequence of construct 8414.1:

MAKANLLVLLCALAAADA | NLVPMVATVCGSGGGGAPGSGGGSIQRTPKIQVYSRHPAENGKSNFLNCYVSGFH  
 PSDIEVDLLKNGERIEKVEHSDLSFSKDWSFYLLYYTEFTPTTEKDEYACRVNHVTL SQPKIVKWRDRMRSASGGG  
 GSGGGGSGGGGASGGGGDLGSHSMRYFFTSVSRPGRGEPRFIAVG YVDDTQFVRFSDAASQRMEPRAPWIEQE  
 GPEYWDGETRKVKAHSQTHRVDLGLTRG CYNQSEAGSHTVQRMYGCDVGS DWRFLRGYHQYAYDGKDY IALKEDL  
 RSWTAADMAAQTTKHKWEAAHVAEQLRAYLEGTCVEWLRRLYLENGKETLQRTDAPKTHMTHHAVSDHEATLRCWA  
 LSFYPAEITLTWQRDGEDQTQDTEL VETRPAGDGT FQKWA AVVVPSGQEQR YTCHVQHEGLPKPLTLRWE PSSQP  
 TIPGDL TVSSAKTTAPSVYPLAPVCGD TTGSSVTLGCLVKGYFPEPVTLTWN SGLSSGVHTFP AVLQSDLYTLS  
 SSVTVTSSTWPSQSITCNVAHPASSTKV DKKI GDEPRGPTIKPSP PCKCPAPNLLGGPSVFI FPPKIKDVLMI S  
 LSPMVTCVVVDVSEDDPDVQISW FVNNVEVLTAQTQTHREDYNSTLRVVSALPIQH QDWMGKFEFKCKVNNKALP  
 APIERTISK PKG SVRAPQVYVLP PPEEEMTKKQVTLTCMVTDFMPEDIYVEWTNNGKTELNYKNTEPVLDS DGSY  
 FMYSKLRVEKKNWVERNSYSCSVVHEGLHNNHHTTKSFSRTPGK\*

**Legend:** Leader sequence (modified hemagglutinin leader) | Peptide-linker #1-β<sub>2</sub>m-linker #2-HLA-A\*02:01 [Y84C] ectodomain-adaptor-CH1-adaptor-Hinge-CH2-CH3 of mouse IgG2a [C224S]

**(iii) Produced and used soluble pMHC-I [dt-SCT]-mIgG2a-Fc-Strep-tag II constructs:**

Construct ID:	Allele:	Antigen:	Peptide sequence:
8556.1	HLA-A*02:01 [Y84C]	Survivin 96–104 / T97M	LMLGEFLKL
8557.1		Flu A MP 58–66	GILGFVFTL
<b>8558.1</b>		HCMV pp65 495–503	NLVPMVATV
8559.1		HPV–16 E7 11-19 / T19V	YMLDLQPEV
8803.1		MART-1 26–35 / A27L	ELAGIGILTV
8804.1		EBV BMLF-1 259–267	GLCTLVAML
8805.7		MUC-1 927–935	STAPPVHNV
8806.1		TP53 264–272	LLGRNSFEV
8807.1		NY-ESO-1 157–165 / C165V	SLLMWITQV
8808.1		NY-BR-1 960–968	SLSKILDTV
8809.1		CEA 605–613	YLSGANLNL
8810.2		HIV p17 gag 77–85	SLYNTVATL
8811.2		HER-2/neu 369–377	KIFGSLAFL
8812.1		KRAS 5–14	KLVVVGAGGV
8814.3		KRAS 5–14 / G12V	KLVVVGAVGV
8815.1		KRAS 5–14 / G12D	KLVVVGADGV
8826.3		KRAS 5–14 / G13D	KLVVVGAGDV
8816.2		BRAF 597–605/ S605V	LATVKSRWV
8817.2		BRAF 597–605/ V600E / S605V	LATEKSRWV
8818.1		c-Met 630–638	YVDPVITSI
8819.1		hTERT 540–548	ILAKFLHWL
8820.3		HPV-16 E7 11–19	YMLDLQPET
9670.1 <sup>#</sup>		HLA-A*02:01	Survivin 96–104 / T97M
9672.1 <sup>#</sup>	[Y84C, Q115E]	HCMV pp65 495–503	NLVPMVATV

Note #: Indicated constructs share the same overall structure as 8558.1 but with an additional Q115E point mutation within the HLA-A2  $\alpha$ 2-domain according to (261).

**Exemplary protein sequence of construct 8558.1:**

MAKANLLVLLCALAAADA | **NLVPMVATV**CGSGGGGAPGSGGGSIQRTPKIQVYSRHPAENGKSNFLNCYVSGFH  
**PSDIEVDLLKNGERIEKVEHSDLSFSKDWSFYLLYYTEFTPTTEKDEYACRVNHVTL**SQPKIVKWDRDMRSASGGG  
GSGGGGSGGGGSASGGGGDLGSHSMRYFFTSVSRPGRGEPFRFIAVGYVDDTQFVRFSDAASQRMEPRAPWIEQE  
GPEYWDGETRQVKAHSQTHRVDLGTLRG**CYNQ**SEAGSHTVQRMYGCDVGS DWRFLRGYHQYAYDGKDYIALKEDL  
RSWTAADMAAQTTKHKWAAHVAEQLRAYLEGTCVEWLRRLYLENGKETLQRTDAPKTHMTHHAVSDHEATLRCWA  
LSFYPAEITLTWQRDGEDQTQDTELVETRPAGDGT**FQK**WAAVVVPSGQEQR**Y**TCHVQHEGLPKPLTLRWEPPSSQP  
**TIP**TSQLTSEPRGPTIK**SP**PPCKCPAPNLLGGPSVFI**F**PPKIKDVLMI**SL**SPMVT**CV**VVDVSEDDDPD**VQ**ISW**FVN**  
NVEVLTAQTQTHRE**DYQ**STLRVVSALPIQHQDWM**S**GKE**F**KCKVNNKALPAPIERTIS**K**PKGSVRAPQ**V**YVLP**PP**E  
EEMTKKQVTLTCMVTDFMPED**I**YVEWTNNGKTELNYK**NT**EPVLDSDGSY**F**MY**S**KLRVEKKNW**V**ERN**S**Y**S**CS**V**V**H**E  
GLHNHHTTKS**F**S**R**TPG**KD**PG**WS**H**PQ**FE**KSR**^**GFV**\*

**Legend:** Leader sequence (modified hemagglutinin leader) | **Peptide**-linker #1- $\beta$ 2m-linker #2-**HLA-A\*02:01 [Y84C] ectodomain**-linker #3-mouse IgG2a-Fc [**C224S**, **N297Q**] (Hinge-CH2-CH3)-**Strep-tag II** (flanked by adapter sites)

(iv) Produced and used soluble heterodimeric pMHC-I [dt-SCT] pCC-mIgG2a-Fc constructs:

Construct ID:	Allele:	Antigen:	Peptide sequence:
9237.1	HLA-A*02:01	Survivin 96–104 / T97M	LMLGEFLKL
10347.7	[Y84C]	HCMV pp65 495–503	NLVPMVATV

Exemplary protein sequence of construct **10347.7**:

MAKANLLVLLCALAAADA | **NLVPMVATV**CGSGGGGAPGSGGGSIQRTPKIQVYSRHPAENGKSNFLNCYVSGFH  
 PSDIEVDLLKNGERIEKVEHSDLSFSKDWSFYLLYYTEFTPTTEKDEYACRVNHVTLTSLQPKIVKWDRDRMSASGGG  
 GSGGGGSGGGGASGGGGDLGSHSMRYFFTSVSRPGRGEPRIAVGYVDDTQFVRFSDAASQRMEPRAPWIEQE  
 GPEYWDGETRKKVAHSQTHRVDLGLTRG**CYNQ**SEAGSHTVQRMYGCDVGSWDRFLRGYHQYAYDGKDYIALKEDL  
 RSWTAADMAAQTTKHKWAAHVAEQLRAYLEGTCVEWLRRLYLENGKETLQRTDAPKTHMTHHAVSDHEATLRCWA  
 LSFYPAEITLTWQRDGEDQTDTELVEVTRPAGDGTFOKWAAVVVPSTGQEQRYTCHVQHEGLPKPLTLRWEPSQP  
 TIPIASGNSGGGGSKQLKKKQLQALKKKNAQLKWKLQALKKKLAQASEPRGPPTIKPSPPCKCPAPNLLGGPSVFI  
 FPPKIKDVLMIISLSPMVTVCVVVDVSEDDPDVQISWVFNNEVLTAAQTQTHREDYQSTLRVVSALPIQHODWMSGKE  
 FKCKVNNKALPAPIERTISKPKGVRAPQVYVLPPEEEMTKKQVTLTCMVTDMPEDIYVEWTNNGKTELNYKN  
 TEPVLDSDGSYFMYSKLRVEKKNWVERNSYSCSVVHEGLHNHHTTKSFSTRTPGK**DPGLNDIFEAQKIEWHEHHHH**  
**HHS**GSGEGRG**SLLT**CGDVEENPG | MAKANLLVLLCALAAADA | **NLVPMVATV**CGSGGGGAPGSGGGSIQRTPKI  
 QVYSRHPAENGKSNFLNCYVSGFHPSDIEVDLLKNGERIEKVEHSDLSFSKDWSFYLLYYTEFTPTTEKDEYACRV  
 NHVTLTSLQPKIVKWDRDRMSASGGGGGSGGGGSGGGGASGGGGDLGSHSMRYFFTSVSRPGRGEPRIAVGYVDDT  
 QFVRFSDAASQRMEPRAPWIEQEGPEYWDGETRKKVAHSQTHRVDLGLTRG**CYNQ**SEAGSHTVQRMYGCDVGS  
 WDRFLRGYHQYAYDGKDYIALKEDLRSWTAADMAAQTTKHKWAAHVAEQLRAYLEGTCVEWLRRLYLENGKETLQ  
 TDAPKTHMTHHAVSDHEATLRCWALSFYPAEITLTWQRDGEDQTDTELVEVTRPAGDGTFOKWAAVVVPSTGQEQ  
 RYTCHVQHEGLPKPLTLRWEPSQPPTIPIASGNSGGGGSKQLEKELQALEKENAQLEWELQALEKELAQASEPRGP  
 TIKPSPPCKCPAPNLLGGPSVFIFFPKIKDVLMIISLSPMVTVCVVVDVSEDDPDVQISWVFNNEVLTAAQTQTHRE  
 DYQSTLRVVSALPIQHODWMSGKEFKCKVNNKALPAPIERTISKPKGVRAPQVYVLPPEEEMTKKQVTLTCMV  
 TDFMPEDIYVEWTNNGKTELNYKNTEPVLDSDGSYFMYSKLRVEKKNWVERNSYSCSVVHEGLHNHHTTKSFSTR  
 TPGK**DPGWSHPQFEK**SSGGGGGSGGGGSGGGGSS**WSHPQFEK**V\*

**Legend:** Leader sequence (modified hemagglutinin leader) | **Peptide**-linker #1- $\beta$ 2m-linker #2-HLA-A\*02:01 **[Y84C]** ectodomain-linker #3 containing **pCC-basic**-mouse IgG2a-Fc **[C224S, N297Q]** (Hinge-CH2-CH3)-**AviTag**-His<sub>6</sub> tag-**T2A** sequence | Leader sequence | **Peptide**-linker #1- $\beta$ 2m-linker #2-HLA-A\*02:01 **[Y84C]** ectodomain-linker #3 containing **pCC-acidic**-mouse IgG2a-Fc-Tandem Strep-tag II

**(v) Produced and used soluble homodimeric pMHC-I [dt-SCT]-\*mIgG2a-Fc constructs:**

Construct ID*:	Allele:	Antigen:	Peptide sequence:
11097.1	HLA-A*02:01 [Y84C]	HCMV pp65 495–503	NLVPMVATV
11290.1		Survivin 96–104 / T97M	LMLGEFLKL
11291.1		Flu A MP 58–66	GILGFVFTL
11292.1		EBV BMLF-1 259–267	GLCTLVAML

Note\*: Constructs presented in Table 4.5 (Section 4.5) follow the same construct design as 11097.1.

**Exemplary protein sequence of construct 11097.1:**

MAKANLLVLLCALAAAEA | **NLVPMVATV** **CGSGGGGAPGSGGGS** **IQRTPKIQVYSRHPAENGKSNFLNCYVSGFH**  
**PSDIEVDLLKNGERIEKVEHSDLSFSKDWSFYLLYYTEFTPTTEKDEYACRVNHVTL** **SQPKIVKWRDRM** **SGGSGGG**  
**GSGGGGSGGGGS** **ASGGGG** **GSHSMRYFFTSVSRPGRGEPRIA** **AVGYVDDTQFVRFDS** **DAASQRMEPRAPWIEQEGPE**  
**YWDGETRQVKAHSQTHRVDLGLTRG** **CYNQSEAGSHTVQRM** **YCDVGS** **DWRFLRGYHQYAYDGKDY** **IALKEDLR** **SW**  
**TAADMAAQTTKHKWEAAHVAEQLRAYLEGTCVEWLR** **RYLENGKETLQRTDAPKTHMTHHAVSDHEATLRCWALS** **F**  
**YPAEITLTWQRDGEDQTDTELVETRPAGDGT** **FQKWA** **AVVVP** **SGQEQR** **YTCHVQHEGLPKPLTLR** **WEPSSQPTIP**  
**TSQLASTGQLHHHHHHHQL** **GLNDIFEAQKIEWHEL** **VPRSLVPRS** **TS** **EPRGPTIKP** **SPPCKCPAPNLLGGPSVFI**  
**FPPKIKDVLMI** **SLSPMVT** **CVVVDVSEDDPDVQIS** **WVFN** **VEVLT** **AQTQ** **THRE** **DYQ** **STLR** **VVSALPI** **QH** **QD** **WMSGK**  
**EFKCKVNNKALPAPIERTISKPKG** **SVRAPQ** **VYVLP** **PPPEEMTKQ** **VTL** **TCM** **VTDF** **MPEDI** **Y** **VEW** **TN** **NGK** **TEL** **NYK**  
**NTEPVLDS** **DGSY** **FMYSKLR** **VEKKN** **WVERNS** **YSCSV** **VHEGL** **HNHHT** **TKS** **FS** **RTP** **PGK** **DPC** **W** **SH** **PQ** **FEK** **SR** **GPV**\*

**Legend:** Leader sequence (modified hemagglutinin leader) | **Peptide**-linker #1- $\beta$ <sub>2</sub>m-linker #2-**HLA-A\*02:01 [Y84C]** ectodomain-linker #3 containing His<sub>8</sub>tag-**AviTag**-**Thrombin recognition site (2x)**-mouse IgG2a-Fc [**C224S**, **N297Q**] (Hinge-CH2-CH3)-**Strep-Tag II** (flanked by restriction sides)

**(vi) Produced and used soluble monomeric pMHC-I [dt-SCT] constructs:**

Construct ID:	Allele:	Antigen:	Peptide sequence:
10469.1	HLA-A*02:01 [Y84C]	Survivin 96–104 / T97M	LMLGEFLKL
10471.1		Flu A MP 58–66	GILGFVFTL
10473.1		HCMV pp65 495–503	NLVPMVATV

**Exemplary protein sequence of construct 10473.1:**

MAKANLLVLLCALAAADA | **NLVPMVATV** **CGSGGGGAPGSGGGS** **IQRTPKIQVYSRHPAENGKSNFLNCYVSGFH**  
**PSDIEVDLLKNGERIEKVEHSDLSFSKDWSFYLLYYTEFTPTTEKDEYACRVNHVTL** **SQPKIVKWRDRM** **RSASGGG**  
**GSGGGGSGGGGS** **ASGGGGDL** **GSHSMRYFFTSVSRPGRGEPRIA** **AVGYVDDTQFVRFDS** **DAASQRMEPRAPWIEQ**  
**GPEYWDGETRQVKAHSQTHRVDLGLTRG** **CYNQSEAGSHTVQRM** **YCDVGS** **DWRFLRGYHQYAYDGKDY** **IALKEDL**  
**RSWTAADMAAQTTKHKWEAAHVAEQLRAYLEGTCVEWLR** **RYLENGKETLQRTDAPKTHMTHHAVSDHEATLRCWA**  
**LSFYPAEITLTWQRDGEDQTDTELVETRPAGDGT** **FQKWA** **AVVVP** **SGQEQR** **YTCHVQHEGLPKPLTLR** **WEPSSQ**  
**TI** **PGDPKLLQ** **ASGGGGSGGGGSGGGGS** **ASGGGGDLGS** **HHHHH** **GIQ** **DYKDDDDK** **ADYKDDDDK** **ALDYKDDDDK** **AL**  
**EVLFQGPALHPMAG** **GLNDIFEAQKIEWHE** **VD**\*

**Legend:** Leader sequence (modified hemagglutinin leader) | **Peptide**-linker #1- $\beta$ <sub>2</sub>m-linker #2-**HLA-A\*02:01 [Y84C]** ectodomain-linker #3 containing His<sub>6</sub>tag-**FLAGtag (3x)**-**AviTag**

(vii) Produced and used soluble heterodimeric pMHC-II-pCC-Fc constructs:

Construct ID:	Structure	Allele	Antigen	Peptide
8634.1 [+] 8746.1	px-EK-HLA-II $\beta$ -chain-pCC-basic-Fc-His <sub>6</sub> tag [+] HLA-II $\alpha$ -chain-pCC-acidic-Fc-tandem STag	HLA-DR3	CLIP 103–117	PVSKMRMATPLLMQA
9062.1 [+] 8746.1	pHLA-II $\beta$ -chain-pCC-basic-Fc-His <sub>6</sub> tag [+] HLA-II $\alpha$ -chain-pCC-acidic-Fc-tandem STag	HLA-DR3	MTB Hsp65 1–13	MAKTIAYDEEARR
9062.1 [+] 10092.1	pHLA-II $\beta$ -chain-pCC-basic-Fc-His <sub>6</sub> tag [+] HLA-II $\alpha$ -chain-pCC-acidic-Fc-AviTag	HLA-DR3	MTB Hsp65 1–13	MAKTIAYDEEARR
9066.1 [+] 10092.1	pHLA-II $\beta$ -chain-pCC-basic-Fc-His <sub>6</sub> tag [+] HLA-II $\alpha$ -chain-pCC-acidic-Fc-AviTag	HLA-DR3	HCMV pp65 510–522	YQEFFWDANDIYR
9221.1 [+] 8744.1	px-FII-HLA-II $\beta$ -chain-pCC-basic-Fc-His <sub>6</sub> tag [+] HLA-II $\alpha$ -chain-pCC-acidic-Fc-tandem STag	HLA-DR3	CLIP 103–117	PVSKMRMATPLLMQA
9221.1 [+] 10092.1	px-FII-HLA-II $\beta$ -chain-pCC-basic-Fc-His <sub>6</sub> tag [+] HLA-II $\alpha$ -chain-pCC-acidic-Fc-AviTag	HLA-DR3	CLIP 103–117	PVSKMRMATPLLMQA
9260.3	pHLA-II $\beta$ -chain-pCC-basic-Fc-His <sub>6</sub> tag-AviTag T2A HLA-II $\alpha$ -chain-pCC-acidic-Fc-tandem STag	HLA-DR3	MTB Hsp65 1–13	MAKTIAYDEEARR
9261.3	px-EK-HLA-II $\beta$ -chain-pCC-basic-Fc-His <sub>6</sub> tag-AviTag T2A HLA-II $\alpha$ -chain-pCC-acidic-Fc-tandem STag	HLA-DR3	CLIP 103–117	PVSKMRMATPLLMQA
10320'.1	pHLA-II $\beta$ -chain-pCC-basic-Fc-His <sub>6</sub> tag-AviTag T2A HLA-II $\alpha$ -chain-pCC-acidic-Fc-tandem STag	HLA-DR3	HCMV pp65 510–522	YQEFFWDANDIYR
10338.2	px-FII-HLA-II $\beta$ -chain-pCC-basic-Fc-His <sub>6</sub> tag-AviTag T2A HLA-II $\alpha$ -chain-pCC-acidic-Fc-tandem STag	HLA-DR3	CLIP 103–117	PVSKMRMATPLLMQA

HLA-DR3: HLA-DRB1\*03:01 / DRA\*01; pCC-acidic / basic-Fc: parallel coiled-coil basic / acidic heterodimerization domain followed by the murine IgG2a-Fc (Hinge-CH2-CH3); px-FII: peptide ligand followed by a C-terminal linker bearing a thrombin cleavage site. px-EK: peptide ligand followed by C-terminal linker bearing an enterokinase cleavage site.

Protein sequence of construct **8634.1**:

MKWVTFISLLFLFSSAYS | PVSKMRMATPLLMQAGGGGSDDDDKSGGGSGGDTRPRFLEYSTSECHFFNGTERVRYLDRYFHNQEENVRFDSDVGEFRAVTELGPRDAEYWNQKDLLEQKRGRVDNYCRHNYGVVESFTVQRRVHPKVTVPYPSKTQPLQHHNLLVCSVSGFYPGSIEVRWFRNGQEEKTGVVNSTGLIHNGDWTFTQTLVMLETVPRSGEVYTCQVEHPSVTSPLTVEWRARSESAQS KNSGGGGSKQLKKKLQALKKKNAQLKWKLQALKKKLAQASEPRGPTIKPSPPCKCPAPNLLGGPSVFI FPPKIKDVLMI SLSPMVTCVVVDVSEDDPDVQI SWFVNNVEVLTAQTQTHREDYQSTLRVVSALPIQHQDWMMSGKEFKCKVNNKALPAPIERTISKPKG SVRAPQVYVLPPEEEMTKKQVTLTCMVTDFMPEDIYVEWTNNGKTELNYKNTEPVLDS DGSYFMYSKLRVEKKNWVERNSYSCSVVHEGLHNNHHTTKSFSRTPGKDPGHHHHHSS\*

**Legend:** Leader sequence (human serum albumin) | Peptide-linker #1 containing an enterokinase cleavage site-HLA-DRB1\*03:01  $\beta$ -chain ectodomain-linker #2 containing pCC-basic-mouse IgG2a-Fc [C224S, N297Q] (Hinge-CH2-CH3)-His<sub>6</sub>tag

Protein sequence of construct **8746.1**:

MAISGVPVLGFFIIAVLMSAQESWA | IKEEHVIIQAEFYLNPDQSGEFMFDFDGDEIFHVDMAKKETVWRLEEFGRFASFEAQ GALANIAVDKANLEIMTKRSNYTPITNVPPEVTVLTNSPVELREPNVLI CFIDKFTPPVVNVTWLRN GPKVTLTGVS ETVFLPREDHFLFRKFHYLPFLPSTEDVDYDCRVEHWGLDEPLLKHWEFDAPSLPETTE NSGGGGSKQLEKELQALEKENAQLLEWELQALEKELAQASEPRGPTIKPSPPCKCPAPNLLGGPSVFI FPPKIKDVLMI SLSPMVTCVVVDVSEDDPDVQI SWFVNNVEVLTAQTQTHREDYQSTLRVVSALPIQHQDWMMSGKEFKCKVNNKALPAPIERTISKPKG SVRAPQVYVLPPEEEMTKKQVTLTCMVTDFMPEDIYVEWTNNGKTELNYKNTEPVLDS DGSYFMYSKLRVEKKNWVERNSYSCSVVHEGLHNNHHTTKSFSRTPGKDPGWSHPQFEKSSGGGGSGGGGSSWSHPQFEKSS\*

**Legend:** HLA-DRA\*01 leader sequence | HLA-DRA\*01:01  $\alpha$ -chain ectodomain-linker #1 containing pCC-acidic-mouse IgG2a-Fc [C224S, N297Q] (Hinge-CH2-CH3)-Tandem Strep-tag II

## Appendix – Protein sequences of produced soluble pMHC molecules

### Exemplary protein sequence of construct **9062.1**:

MKWVTFISLLFLFSSAYS | **MAKTIAYDEEAR**SGGGGSGGGGSGGGGSGGDTRPRFLEYSTSECHFFNGTERVRYLDRYFHNQEENVRFDSDVGEFRAVTELGPRDAEYWNQKDLLEQKRGRVDNYCRHNYGVVESFTVQRRVHPKVTVYPSKTQPLQHHNLLVCSVSGFYPGSIEVRWFRNGQEEKTGVVSTGLIHNGDWTFFQTLVMLETVPRSGEVYTCQVEHPSVTSPLTVEWRARSESAQS **KNSGGGGSKQLKKKLQALKKKNAQLKWKLQALKKKLAQ**ASEPRGPTIKPSPCKCPAPNLLGGPSVFI FPPKIKDVLMI SLSPMVT CVVVDVSEDDPDVQISWFVNNVEVLTAQTQTHREDYQSTLRVVSALPIQHQDWMMSGKEFKCKVNNKALPAPIERTISKPKGSVRAPQVYVLPPEEEMTKKQVTLTCMVTDFMPEDIYVEWTNNGKTELNYKNTEPVLDSGYSYFMYSKLRVEKKNWVERNSYSCSVVHEGLHNHHTTKSFSRTPGK **DPGHHHHHSS\***

**Legend:** Leader sequence (human serum albumin) | **Peptide-linker #1**- HLA-DRB1\*03:01  $\beta$ -chain ectodomain-linker #2 containing **pCC-basic**-mouse IgG2a-Fc [**C224S**, **N297Q**] (Hinge-CH2-CH3)-His<sub>6</sub>tag

### Protein sequence of construct **9221.1**:

MKWVTFISLLFLFSSAYS | **PVSKMRMATPLLMQA**SGGGS **LVPRGS**GGSGSGGDTRPRFLEYSTSECHFFNGTERVRYLDRYFHNQEENVRFDSDVGEFRAVTELGPRDAEYWNQKDLLEQKRGRVDNYCRHNYGVVESFTVQRRVHPKVTVYPSKTQPLQHHNLLVCSVSGFYPGSIEVRWFRNGQEEKTGVVSTGLIHNGDWTFFQTLVMLETVPRSGEVYTCQVEHPSVTSPLTVEWRARSESAQS **KNSGGGGSKQLKKKLQALKKKNAQLKWKLQALKKKLAQ**ASEPRGPTIKPSPCKCPAPNLLGGPSVFI FPPKIKDVLMI SLSPMVT CVVVDVSEDDPDVQISWFVNNVEVLTAQTQTHREDYQSTLRVVSALPIQHQDWMMSGKEFKCKVNNKALPAPIERTISKPKGSVRAPQVYVLPPEEEMTKKQVTLTCMVTDFMPEDIYVEWTNNGKTELNYKNTEPVLDSGYSYFMYSKLRVEKKNWVERNSYSCSVVHEGLHNHHTTKSFSRTPGK **DPGHHHHHSS\***

**Legend:** Leader sequence (human serum albumin) | **Peptide-linker #1** containing an **Thrombin cleavage site**-HLA-DRB1\*03:01  $\beta$ -chain ectodomain-linker #2 containing **pCC-basic**-mouse IgG2a-Fc [**C224S**, **N297Q**] (Hinge-CH2-CH3)-His<sub>6</sub>tag

### Protein sequence of construct **10092.1**:

MAISGVPVLGFFIIAIVLMSAQESWA | IKEEHV I IQAEFYLNPDQSGEFMFDFDGD E I FHVDMAKKETVWRLEEFGRFASFEAQGALANIAVDKANLEIMTKRSNYTPITNVPPEVTVLTNSPVELREPNVLCFIDKFTPPVNVNVTWLRN GKPVT TGVSETVFLPREDLHFRKFHYLPFLPSTEDVYDCRVEHWGLDEPLLKHWEFDAPSPLPETTE **NSSGGGGSKQLEKELQALEKENAQLEWELQALEKELAQ**ASEPRGPTIKPSPCKCPAPNLLGGPSVFI FPPKIKDVLMI SLSPMVT CVVVDVSEDDPDVQISWFVNNVEVLTAQTQTHREDYQSTLRVVSALPIQHQDWMMSGKEFKCKVNNKALPAPIERTISKPKGSVRAPQVYVLPPEEEMTKKQVTLTCMVTDFMPEDIYVEWTNNGKTELNYKNTEPVLDSGYSYFMYSKLRVEKKNWVERNSYSCSVVHEGLHNHHTTKSFSRTPGK **DPGLNDIFEAQKIEWHEV\***

**Legend:** HLA-DRA\*01 leader sequence | HLA-DRA\*01:01  $\alpha$ -chain ectodomain-linker #1 containing **pCC-acidic**-mouse IgG2a-Fc [**C224S**, **N297Q**] (Hinge-CH2-CH3)-**AviTag**

**Protein sequence of construct 9260.3:**

MKWVTFISLLFLFSSAYS | **MAKTIAYDEEAR**SGGGGSGGGGSGGGGSGGDTRPRFLEYSTSECHFFNGTERVR  
YLDRYFHNQEENVRFDSDVGEFRAVTELRPDAEYWNQKDLLEQKRGRVDNYCRHNYGVVESFTVQRRVHPKVT  
VYPSKTQPLQHHNLLVCSVSGFYPGSIEVRWFRNGQEEKTGVVSTGLIHNGDWTFFQTLVMLETVPRSGEVYTCQV  
EHPSVTSPLTVEWRARSESAQS **KNSGGGGS****KQLKQKLLQALKKKNAQLKWKLLQALKKKLAQ**ASEPRGPTIKP**S**PPC  
KCPAPNLLGGPSVFI FPPKIKDVLMI SLSPMVT CVVVDVSEDDPDVQI SWFVNNVEVLTAQTQTHREDY**Q**STLRV  
VSALPIQHQDWMSGKEFKCKVNNKALPAPIERTISPKPGSVRAPQVYVLPPEEEMTKKQVTLTCMVTDFMPEDI  
YVEWTNNGKTELNYKNTEPVLDSGYSYFMYSKLRVEKKNWVERNSYSCSVVHEGLHNHHTTKSFSRTPGK**DPGLN**  
**DIFEAQKIEWHEHHHHHHS****GSEGRGSLTTCGDVEENPG** | **P**MAISGVPVLGFFIIAVLMSAQESWA | IKEEHV I IQ  
AEFYLNPDQSGEFMFDFDGDDEIFHVDMAKKETVWRLEEFGRFASFQAQALANIAVDKANLEIMTKRSNYTPITN  
VPPEVTVLNSPVELREPNVLICFIDKFTPPVNVNVTWLRNGKPVTTGVSETVFLPREDHLFRKFHYLPFLPSTED  
VYDCRVEHWGLDEPLLKHWEFDAPSPLPETTE**ENSGGGGS****KQLEKELQALEKENAQLEWELQALEKELAQ**ASEPRG  
PTIKP**S**PPCKCPAPNLLGGPSVFI FPPKIKDVLMI SLSPMVT CVVVDVSEDDPDVQI SWFVNNVEVLTAQTQTHR  
EDY**Q**STLRVVSALPIQHQDWMSGKEFKCKVNNKALPAPIERTISPKPGSVRAPQVYVLPPEEEMTKKQVTLTCM  
VTDFMPEDIYVEWTNNGKTELNYKNTEPVLDSGYSYFMYSKLRVEKKNWVERNSYSCSVVHEGLHNHHTTKSFSR  
TPGK**DPGW****SHPOFEK**SSGGGSGGGGSGGGGSS**WSHPQFEK**V\*

**Legend:** Leader sequence (human serum albumin) | **Peptide**-linker #1-HLA-DRB1\*03:01  $\beta$ -chain  
ectodomain-linker #2 containing **pCC-basic**-mouse IgG2a-Fc [**C224S**, **N297Q**] (Hinge-CH2-CH3)-  
**AviTag**-His<sub>6</sub> tag- **T2A sequence** | HLA-DRA\*01 leader sequence | HLA-DRA\*01:01  $\alpha$ -chain ectodomain-  
linker #1\* containing **pCC-acidic**-mouse IgG2a-Fc-Tandem Strep-tag II

**Protein sequence of construct 9261.3:**

MKWVTFISLLFLFSSAYS | **PVSKMRMATPLLMQA**GGGGS**DDDDK**SGGGSGGDTRPRFLEYSTSECHFFNGTERVR  
YLDRYFHNQEENVRFDSDVGEFRAVTELRPDAEYWNQKDLLEQKRGRVDNYCRHNYGVVESFTVQRRVHPKVT  
VYPSKTQPLQHHNLLVCSVSGFYPGSIEVRWFRNGQEEKTGVVSTGLIHNGDWTFFQTLVMLETVPRSGEVYTCQV  
EHPSVTSPLTVEWRARSESAQS **KNSGGGGS****KQLKQKLLQALKKKNAQLKWKLLQALKKKLAQ**ASEPRGPTIKP**S**PPC  
KCPAPNLLGGPSVFI FPPKIKDVLMI SLSPMVT CVVVDVSEDDPDVQI SWFVNNVEVLTAQTQTHREDY**Q**STLRV  
VSALPIQHQDWMSGKEFKCKVNNKALPAPIERTISPKPGSVRAPQVYVLPPEEEMTKKQVTLTCMVTDFMPEDI  
YVEWTNNGKTELNYKNTEPVLDSGYSYFMYSKLRVEKKNWVERNSYSCSVVHEGLHNHHTTKSFSRTPGK**DPGLN**  
**DIFEAQKIEWHEHHHHHHS****GSEGRGSLTTCGDVEENPG** | **P**MAISGVPVLGFFIIAVLMSAQESWA | IKEEHV I IQ  
AEFYLNPDQSGEFMFDFDGDDEIFHVDMAKKETVWRLEEFGRFASFQAQALANIAVDKANLEIMTKRSNYTPITN  
VPPEVTVLNSPVELREPNVLICFIDKFTPPVNVNVTWLRNGKPVTTGVSETVFLPREDHLFRKFHYLPFLPSTED  
VYDCRVEHWGLDEPLLKHWEFDAPSPLPETTE**ENSGGGGS****KQLEKELQALEKENAQLEWELQALEKELAQ**ASEPRG  
PTIKP**S**PPCKCPAPNLLGGPSVFI FPPKIKDVLMI SLSPMVT CVVVDVSEDDPDVQI SWFVNNVEVLTAQTQTHR  
EDY**Q**STLRVVSALPIQHQDWMSGKEFKCKVNNKALPAPIERTISPKPGSVRAPQVYVLPPEEEMTKKQVTLTCM  
VTDFMPEDIYVEWTNNGKTELNYKNTEPVLDSGYSYFMYSKLRVEKKNWVERNSYSCSVVHEGLHNHHTTKSFSR  
TPGK**DPGW****SHPOFEK**SSGGGSGGGGSGGGGSS**WSHPQFEK**V\*

**Legend:** Leader sequence (human serum albumin) | **Peptide**-linker #1 containing an **enterokinase**  
**cleavage site**-HLA-DRB1\*03:01  $\beta$ -chain ectodomain-linker #2 containing **pCC-basic**-mouse IgG2a-Fc  
[**C224S**, **N297Q**] (Hinge-CH2-CH3)-**AviTag**-His<sub>6</sub> tag- **T2A sequence** | HLA-DRA\*01 leader sequence |  
HLA-DRA\*01:01  $\alpha$ -chain ectodomain-linker #1\* containing **pCC-acidic**-mouse IgG2a-Fc-Tandem  
Strep-tag II

Appendix – Protein sequences of produced soluble pMHC molecules

**Protein sequence of construct 10338.2:**

MKWVTFISLLFLFSSAYS | PVSKMRMATPLLMQA<sup>AGSSGS</sup>LVPRGS<sup>GGSSGS</sup>GDTRPRFLEYSTSECHFFNGTERV  
RYLDRYFHNQEENVRFDSDVGEFRAVTELGPRDAEYWNSSQKDLLEQKRGRVDNYCRHNYGVVESFTVQRRVHPKV  
TVYPSKTQPLQHNNLLVCSVSGFYPGSIEVRWFRNGQEKTGVVSTGLIHNGDWTFTQTLVMLETVPRSGEVYTCQ  
VEHPSVTSPLTVEWRARSESAQS<sup>KNSGGGGS</sup>SKQLKKKLQALKKKNAQLKWKLQALKKKLAQ<sup>ASE</sup>PRGPTIKP<sup>SPP</sup>  
CKCPAPNLLGGPSVFI<sup>FPPKIKDVLMI</sup>SLSPMVT<sup>CVVVDVSEDDPDVQISWFVNNVEVLT</sup>AQTQTHREDY<sup>QSTLR</sup>  
VVSALPIQHQDWMMSGKEFKCKVNNKALPAPIERTISKPKGSVRAPQVYVLPPEEEMTKKQVTLTCMVTDFMPED  
IYVEWTNNGKTELNYKNTEPVLDSGYSFYMSKLRVEKKNWVERNSYSCSVVHEGLHNHHTTKSFSRTPGK<sup>DPGL</sup>  
**NDIFEAQKIEWHEHHHHHGS**GEGRGS<sup>SLLTCGDVEENPG</sup> | PMAISGVPVLGFFIIAVLMSAQESWA | IKEEHVII  
QAEFYLNPDQSGEFMFDFDGDDEIFHVDMAKKETVWRLEEFGRFASFEAQGALANIAVDKANLEIMTKRSNYTPIT  
NVPPEVTVLTNSPVELREPNVLCIFIDKFTPPVNVNVTWLRNGKPVTTGVSETVFLPREDHLFRKFHYLPFLPSTE  
DVYDCRVEHWGLDEPLLKHWEFDAPSPLPETT<sup>ENS</sup>GGGG<sup>SKQLEKELQALEKENAQLEWELQALEKELAQASE</sup>PR  
GPTIKP<sup>SPPCKCPAPNLLGGPSVFI</sup>FPPKIKDVLMI<sup>SLSPMVT</sup>CVVVDVSEDDPDVQISWFVNNVEVLT<sup>AQTQTH</sup>  
REDY<sup>QSTLR</sup>VVSALPIQHQDWMMSGKEFKCKVNNKALPAPIERTISKPKGSVRAPQVYVLPPEEEMTKKQVTLTC  
MVTDFMPEDIYVEWTNNGKTELNYKNTEPVLDSGYSFYMSKLRVEKKNWVERNSYSCSVVHEGLHNHHTTKSFS  
RTPGK<sup>DPGWSHPQFEK</sup>SSGGGGSSGGGGSS<sup>WSHPQFEK</sup>V\*

**Legend:** Leader sequence (human serum albumin) | Peptide-linker #1 containing an Thrombin cleavage site-HLA-DRB1\*03:01 β-chain ectodomain-linker #2 containing pCC-basic-mouse IgG2a-Fc [C224S, N297Q] (Hinge-CH2-CH3)-AviTag-His<sub>6</sub>tag-T2A sequence- HLA-DRA\*01 leader sequence | HLA-DRA\*01:01 α-chain ectodomain-linker #1\* containing pCC-acidic-mouse IgG2a-Fc-Tandem Strep-tag II

**(viii) Produced and used soluble heterodimeric HLA-DM-pCC-Fc constructs:**

**Protein sequence of construct 8635.1:**

MITFLPLLLGLSLGCTGA | GGFVAHVESTCLLDDAGTPKDFTYCI<sup>SFNKDLLTCWDPEENKMAPCE</sup>FVNLNSLAN  
VLSQHLNQKDTLMQRLRNGLQNCATHTQPFWGS<sup>LTNRTRPPSVQVAKTTPFNTREP</sup>VMLACYVWGFYPAEVTITW  
RKNGKLVMPHSSAHKTAQPNGDWTYQTL<sup>SHLALTPSYGDTYTCVVEHIGAPEPILRDWTPGLSPMQTL</sup><sup>KNSGGGG</sup>  
<sup>SKQLKKKLQALKKKNAQLKWKLQALKKKLAQASE</sup>PKS<sup>SDKTH</sup>TCPPCPAPELLGGPSVFLFPPKPKDTLMISRTF  
EVT<sup>CVVVDVSHEDPEVKFNWYVDGVEVHNAKTKPREEQYQSTYR</sup>VVSVLTVLHQDWLNGKEYKCKVSNKALPAPI  
EKTISKAKGQPREPQVYTLPPSRDELTKNQVSLTCLVKGFYPSDIAVEWESNGQPENNYKTTTPVLDSDGSFFLY  
SKLTVDKSRWQQGNV<sup>FSCSVMHEALHNHYTQKSL</sup>SLSPGK<sup>DPG</sup><sup>HHHHHSS</sup>\*

**Legend:** HLA-DM β-chain leader sequence | HLA-DM β-chain ectodomain-linker #1 containing pCC-basic-human IgG1-Fc [C220S, N297Q] (Hinge-CH2-CH3)-His<sub>6</sub>tag

**Protein sequence of construct 8744.1:**

MGHEQNQGAALLQMLPLLWLLPHSWA | VPEAPTPMWPDDLQNH<sup>TFLHTVYQC</sup>DGSPSVGLSEAYDEDQLFFDFD  
QNTRVPRLP<sup>EFADWAQEQGDAPAILFDKEFCEWMIQQIGPKLDGKIPVSRGFPIAEVFTL</sup>KPLEFGKPNLTVCFV  
SNLFPMLTVNWQHHSVPVEGFGPTFVSAVDGLSFQAFSYLNFTPEPSDIFSCIVTHEIDRYTAIAYWVPRNALP  
SDLLENV<sup>LNSGGGGS</sup>SKQLEKELQALEKENAQLEWELQALEKELAQ<sup>ASE</sup>PKS<sup>SDKTH</sup>TCPPCPAPELLGGPSVFLF  
PPKPKDTLMISRTPEVT<sup>CVVVDVSHEDPEVKFNWYVDGVEVHNAKTKPREEQYQSTYR</sup>VVSVLTVLHQDWLNGKE  
YKCKVSNKALPAPIEKTISKAKGQPREPQVYTLPPSRDELTKNQVSLTCLVKGFYPSDIAVEWESNGQPENNYKT  
TPVLDSDGSFFLYSKLTVDKSRWQQGNV<sup>FSCSVMHEALHNHYTQKSL</sup>SLSPGK<sup>DPGWSHPQFEK</sup>SSGGGGSSGGG  
GSGGGGGSS<sup>WSHPQFEKSS</sup>\*

**Legend:** HLA-DM α-chain leader sequence | HLA-DM α-chain ectodomain-linker #1 containing pCC-acidic-human IgG1-Fc [C220S, N297Q] (Hinge-CH2-CH3)-Tandem Strep-tag II